The fabrication and characterisation of novel Floreon-based electrospun membranes for periodontal treatment

Submitted in fulfilment of the requirement for the Degree of

Doctor of Philosophy (PhD)

Ali Mansour A. Alqahtani

SCHOOL OF CLINICAL DENTISTRY

UNIVERSITY OF SHEFFIELD

UNITED KINGDOM

DECEMBER 2022

Acknowledgments

Foremost, I would like to convey my sincere gratitude and appreciation to my esteemed supervisors, Dr. Ilida Ortega Asencio and Dr. Robert D Moorehead, for their invaluable guidance, expert advice, and unwavering support throughout the duration of this project. Their sage supervision and insightful feedback have been instrumental in making this work possible, and I am deeply grateful for their contributions to my scientific growth and proficiency in laboratory practices.

I am deeply grateful to prof. Cheryl Miller and Dr. Helen Colley, for providing me with normal oral fibroblasts and rat mesenchymal stromal cells. Besides, My gratitude goes to Dr. Christopher J Hill, Dr. Craig Robertson, Dr. Oday Hussein, Mr. Linden Drezet and Mr. Sylwester Mikula, for welcoming me into their laboratory and for their significant contributions to the many scaffold characterisation experiments., as this project would not have been done without their continuous support and unconditional help.

I would like to express my gratitude to the Saudi Arabian Cultural Bureau in London and King Khalid University for their invaluable support and assistance during my studies. Without their administrative and financial support, pursuing a PhD would have been an insurmountable challenge. I am truly grateful for the opportunity they provided me.

I would also like to acknowledge the hard work and contributions of the research, technical, and support staff at the University of Sheffield. Their expertise and dedication played a crucial role in enabling me to conduct my research effectively.

My family has been my constant source of support, and I cannot thank them enough for their unceasing prayers and encouragement. I am especially grateful to my wife, Fadia, and my children, Alin and Mansour, for their unconditional love, motivation, and inspiration that kept me going during the toughest times.

I also extend my heartfelt thanks to my siblings for their unwavering support and encouragement throughout my academic journey.

Lastly, I want to express my deepest gratitude to my parents, Prof. Mansour Alqahtani and Mrs. Fatima Alqahtani. They have been my pillars of strength and support, providing emotional and financial assistance, instilling in me values and principles that were essential to my success, and praying for me throughout. I owe everything I have achieved in life to them, and I am honored and privileged to be their son.

Above all, I give all praise and thanks to Allah Almighty for countless blessings on me.

Ali Mansour Alqahtani

Abstract

Guided bone regeneration (GBR) is a dental procedure used for treating periodontal disease. GBR uses barrier membranes to facilitate the growth of hard or soft tissues, specific to the site and nature of the injury. Current GBR membranes are limited by space maintenance, early/late absorption, poor mechanical properties, and the need for a second operation to remove non-resorbable membranes. Therefore, it is essential to develop new manufacturing techniques and alternative materials for the next generation of GBR membranes. A biological and sustainable polyester blend called Floreon has been previously explored as a suitable material for bone tissue engineering. In this study, a biofunctional GBR bilayered membrane was designed for periodontal disease using Floreon for the first time. The objectives were to ensure membrane adherence to the relevant bone cells to facilitate new bone formation, determine membrane suitability as a cell barrier, and test the membrane mechanical performance.

Floreon membranes were characterised and compared with traditional PLA membranes. Promising results were obtained using the combination of electrospinning and spin-coating for manufacturing the final bilayer, which showed improved mechanical properties with increased maximum tensile strength. Relevant physical properties such as porosity, wettability and crystallinity, were found to be superior in Floreon membranes. Furthermore, the addition of bioceramics enhanced their thermal stability. Bioceramics increased the crystallinity and crystallisation temperature (Tc) of the membrane, thereby strengthening the interfacial interaction with the polymer. The tensile properties of the membrane under stress exhibited increased stiffness when 10 weight percent of bioceramics were incorporated. Degradation studies in simulated body fluid (SBF) solution showed that bioceramics did not affect the structural integrity of microfibers, but the hydrophilicity of the membrane was altered. Apatite layers were discovered on the membranes, facilitating cell attachment, adhesion, and dissemination. Changes in pH were also observed during the immersion period, which had an effect on cell behaviour. Furthermore, the addition of bioceramics allowed mesenchymal stromal cells to successfully adhere, proliferate faster, migrate more, and produce more total protein and DNA, demonstrating the biocompatibility of the Floreon membranes.

In conclusion, a robust and reproducible bilayer membrane with excellent mechanical behaviour, as well as key morphological and physical properties, was successfully manufactured using Floreon. The porous part of the bilayer presented enhanced mesenchymal stromal cell adhesion and migration, and the non-porous part of the membrane showed barrier layer function, avoiding fibroblast invasion. The study's findings suggest that Floreon is a promising material to be used as a GBR alternative for addressing periodontal issues in the future.

Outputs

Conference Presentations

1. The Tissue and Cell Conference (CDT), Birmingham, United Kingdome, "A bioactive functionally graded Guided tissue regeneration membrane" 13-15th June 2022.

2. The UK Society for Biomaterials (UKSB2022) annual conferences, Sheffield, United Kingdome, " Periodontal treatments using a novel functionally ceramic-modified polyester blends membrane, 27-28th June 2022.

3. The 6th world congress of the Tissue Engineering and Regenerative Medicine International Society (TERMIS2021), online, " The use of ceramic-modified polyester blends for the manufacture of a multi-functional bilayer membrane for the regeneration of periodontal tissue" 15 –19th November 2021.

4. The white rose biomaterials and tissue engineering group (BITEG- 2021) annual meeting, Sheffield, "Fabrication and characterisation of electrospun membranes based on ceramic-modified biopolymer blend for periodontal therapy" 20th December 2021.

5. The white rose biomaterials and tissue engineering group (BITEG- 2019) annual meeting, York, "Optimising mechanical and osteogenic properties of ceramic-modified polyester blends via the use of advanced manufacturing techniques" 16th December 2019.

Manuscripts in Process

Ali M. Alqahtani, Robert Moorehead, Ilida Ortega Asencio. The use of ceramic-modified polyester blends for the manufacture Of a multi-functional bilayer membrane for the regeneration of Periodontal tissue. (in preparation)

Contents

Abbreviations

%	Percentage
ºC	Degree Celsius
BMP	Bone morphogenic protein
Ca	Calcium
$CaSiO_3$	Calcium Silicate
CO	Carbon monoxide
conc	Concentration
DiH2O	Distilled water
DSC	Differential scanning calorimetry
Eq	Equation
EtOH	Ethanol
FGF	Fibroblast growth factor
FTIR	Fourier transform infrared spectroscopy
GBR	Guided Bone Regeneration
gm or g	Gram
GTR	Guided Tissue Regeneration
H&E	Hematoxylin and eosin
HA	Hydroxyapatite
hrs	Hours
IGF	Insulin–like growth factor
mg	Milligram
min	Minutes
MIP	Mercury intrusion porosimetry
mm	Millimeter
MPa	Mega Pascal
MSCs	Mesenchymal stem cells
Mw	Molecular weight
Na	Sodium
NOFs	Normal oral fibroblast cells
-OH	Hydroxyl
PBS	Phosphate buffered saline
PCL	Poly-ε-caprolactone
PDGF	Platelet derived growth factor
PDL	Periodontal ligaments
PGA	Polyglycolic acid

PLA	Polylactic acid
PO_4	Phosphate
SBF	Simulated body fluid
SD	Standard deviation
SEM	Scanning electron microscopy
T_C	Crystallisation temperature
TCP	Tri calcium phosphate
TEM	Transmission Electron Microscopy
T_g	Glass transition temperature
TGA	Thermogravimetric Analysis
T_m	Melting temperature
XRD	X-ray diffraction
βTCP	Beta tricalcium phosphate

List of Figures

List of Tables

CHAPTER 1:

INTRODUCTION

Chapter 1: Introduction

Periodontitis is a challenging and commonly occurring human disease whose negative effects are widely known. The condition destroys the periodontium, the part of the mouth that supports the teeth. The periodontium is a complex structure, consisting of the gingiva, periodontal ligament, alveolar bone, and cementum. To treat this condition, medical practitioners use conventional methods like surgical cleaning, scaling, and root-planing. Through these procedures, dental plaque and calculus can be removed. However, the periodontal tissue does not return to its original state. Periodontitis can also cause the bone height to reduce significantly, as well as gingival recession, which can lead to functional and aesthetic issues. Another method often used to treat periodontitis is based on the use of graft materials or bone fillers in conjunction with a membrane so that it can be a barrier for the soft tissue at the site of the bone defect. This method is known as guided bone regeneration (GBR).

GBR works by blocking the non-osteogenic soft tissue cells from invading the bone area (as soft tissue grows at a faster speed than bone tissue). The wound defect area is thus protected by placing a membrane over the defect of the bone, allowing the osteogenic cells to repopulate the bone area. GBR has evolved over the years to emerge as one of the ways to treat periodontal issues and for the regeneration of the tissues lost due to the disease. The associated results, however, remain clinically humble and new strategies should be explored to allow GBR approaches to achieve their greatest potential. On the one hand, currently used GBR membranes do not present strong osteogenic capabilities, acting as mere barriers rather than encouraging healing; secondly, clinically utilised scaffolds present modest mechanical properties, resulting in poor space maintenance during regeneration. There is therefore a need to develop new membranes with improved mechanical properties capable of withstanding collapse at the defect site and facilitating tissue regeneration.

One potential route to dealing with the above-mentioned drawbacks is to use new polyester polymer blends in combination with ceramic materials. The addition of highly porous bio-ceramic materials to polyesters has been extensively investigated in tissue regeneration studies, specifically for bone healing applications. These materials include more than one component and incorporate a polymer phase with hardness and tensile quality as well as an inorganic phase with some degree of biological activity, which improves its physical characteristics as well as the degradation rate and biological performance. How to incorporate ceramic components within

polymer blends is challenging. However, fibre technology (electrospinning-based approaches) can be useful in terms of exploring ceramic-polymer blend materials.

Electrospinning technology is a versatile fabrication method commonly used in tissue engineering. This technique has the potential to be used to manufacture nanofibrous scaffolds for GBR. These scaffolds are three-dimensional, non-woven, and highly porous. Fibrous scaffolds are efficient as they have a similar structural morphology to the structure found in the ECM (extracellular matrix) and also a high surface area to volume ratio, which can be useful for tissue engineering applications.

Polyesters are frequently utilised in tissue engineering due to their established non-toxic, biocompatible, and biodegradable characteristics. Recently, Floreon Ltd. collaborated with researchers at Sheffield to investigate the biomedical potential of novel blends of polyesters that exhibit superior mechanical properties compared to their commercially available counterparts. These blends also offer improved processability and customisable properties, as reported by Lee *et al.* (2016), Floreon (2017), and Floreon (2018). Although these blends were initially developed for packaging applications, the team reported the potential use of these materials for bone tissue engineering applications (Ramos-Rodriguez *et al.*, 2022). To the best of current knowledge, this is the first instance where these blends have been explored for dental applications.

The present study aims to develop a multifunctional bi-layered device, composed of two distinct layers, with the ultimate objective of promoting new bone formation and preserving the bone socket. The core layer (i), fabricated using electrospinning technology, is constructed from Floreon reinforced with appropriate bioceramic materials. The hypothesis posits that this membrane will have the ability to retain the bone socket and promote the adhesion of osteoblasts, thereby facilitating the formation of new bone. The outermost layer (ii) of the device, which is a smooth surface layer of Floreon, is produced using two distinct techniques: spin-coating or solvent casting. This second layer will act as a physical barrier, preventing non-osteoblast interference, while also ensuring superior mechanical performance. The membranes will subsequently undergo thorough characterisation in terms of their physicochemical, morphological, bioactivity, degradation, mechanical properties, and biocompatibility.

CHAPTER 2:

LITERATURE REVIEW

Chapter 2: Literature review

2.1 The healthy periodontium

The periodontium is considered a segment of the oral cavity that supports the teeth by connecting them to the bone and preserving the oral mucosa's functional integrity. It is, therefore, necessary to know the primary structure of the mucogingival complex. This helps to have a good pathogenic process perception and the modalities of treatment available when working on periodontal problems. The anatomy comprises the following four crucial components: gingiva, periodontal ligaments, alveolar bone and cementum (Palumbo, 2011; Newman *et al.*, 2018).

2.1.1 Gingiva

The part in charge of covering the bone and offering structural aid to teeth and their cervical segment is denominated gingiva (or gums) (Figure 2-1). Gingiva is also a part of the oral cavity's mucosa where the shape of the structure depends on the pattern of tooth eruption. The dentogingival complex refers to the functional unit comprising of junctional epithelial attachment and connective tissue attachment of the gingiva, both of which provide biological protection and are firmly attached to the hard dental tissue via hemidesmosomes (Lemmons and Beebe, 2019; El Chaar and Abitbol, 2023).

In a person with good health, the gums are rigid, sharp-edged, and possess a pale-red coloration. Their colour, however, is reliant upon the regional concentration of proteins such as melanin in the epithelium. The gradient of these proteins controls the intensity of colour in the gingival tissue. Keratinisation and the fibrousness of the underlying connective tissue are also involved in the colour changes of melanin in this tissue. The marginal and attached gingiva are the regions in which the gums are divided into. The segment of the gingiva that is known as free or unattached gingiva, which is the terminal edge of the gums that surrounds the teeth, is normally about 1 mm wide. which can be separated with ease through the inclusion of a periodontal probe for the purpose of measuring the deepness of the periodontal pocket. On the other hand, the attached gingiva is firmly adhered to the bone that lies underneath and is positioned upwards (Lemmons and Beebe, 2019; El Chaar and Abitbol, 2023).

Another essential section, where the alveolar mucosa joins with the gums, is the "mucogingival junction." Interdental gingiva represents the part of the gingiva that can be found in between the teeth, hence the name. The aforementioned interdental gingiva works as a link between the facial and lingual gingiva parts. Many food particles and detritus build up in this area, and it's an

important site for pathogen pooling and gum lesion initiation (Palumbo, 2011). The main cells that have a critical function in the starting up of gingival lesion regeneration include Merkel's cells, Langerhans' cells, and other immune response cells that can be found in great quantities throughout the gingival epithelium. Throughout all of these sections, there exists another important process to be mentioned: the arrangement of gum fibres destined to maintain the structural cohesion of the mucous membranes located in the mouth, in addition to maintaining the gingival margin around the neck of the tooth (Newman *et al.*, 2018; El Chaar and Abitbol, 2023).
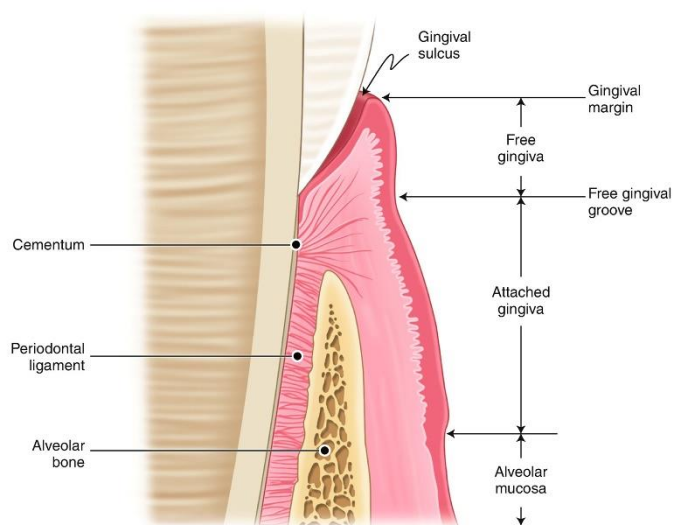
Figure 2-1 Illustrative diagram of a vertical section through a cervical third of tooth structure and periodontal tissues. Image Reprinted from (Bottino et al., 2012) with permission from Elsevier.

2.1.2 Periodontal ligaments (PDL)

The periodontal ligament (PDL) is another crucial part of the tooth-supporting structure. It surrounds the cementum of the tooth roots and joins them to the opposite bone socket wall. (Figure 2-1). In addition to playing a significant and necessary role in maintaining the tooth in the alveolar bone, the periodontal ligament absorbs the pressures caused by chewing and transfers them to the alveolar bone that surrounds the tooth. Additionally, it facilitates the lymphatic and vascular drainage required to nourish the cementum, bone, and gingiva. These fibre structures are mainly composed of collagen, but the PDL also contains fibres whose main constituent is oxytalan, which run in the same direction as the surface of the root and sporadically embed themselves into the cementum (Newman *et al.*, 2018; Stepaniuk, 2019). These structures make

up a mesh of conjoined fibres instead of an elastic cable structure. Following a periodontal disease, an additional group of transseptal fibres are able to rebuild themselves even after the alveolar bone structure receives significant damage. The fibres of the alveolar crest prevent tooth extrusion and are able to withstand the tooth's lateral motion vector. The width of the periodontal ligaments ranges from 0.15 to 0.38 mm. The PDL, like other connective tissues with elastic fibres, consists of a fibre-based inner matrix in a lattice of ground hunk composed of cells, capillaries, and neural tissue. (Newman *et al.*, 2018; Stepaniuk, 2019).

2.1.3 Alveolar bone

One of the most diverse and adaptive tissues, both in structure and function, that exists in humans is bone. It functions as the most important mechanical support structure for the whole organism. To offer protection and provide support for teeth is the alveolar bone's main purpose (Figure 2-1). The presence of teeth will determine if alveolar bone develops or not. Alveolar ridge resorption occurs after tooth extraction and will not regrow in the absence of teeth. The alveolar bone is constantly under remodelling in function of its perceived stimuli. The external surfaces of the alveolar structures are made up of compacted bone that covers the cancellous bone structure (Newman *et al.*, 2018; Stepaniuk, 2019; El Chaar and Abitbol, 2023).

Many small channels exist in the inner layer of the alveolar ridge that allow for nerves and capillaries to enter the periodontal ligament area. The "bundle bone" is a thin slab of bone cells through which the fibres are inserted, and it possesses many characteristics in common with root cementum regarding its structure and functional purpose. The compact bone, also known as the cortical bone of the external alveolar regions, varies in thickness across its expanse over the maxillary teeth. The cortical plate is thicker on the buccal and palatal sides of the molars, whereas it is fairly thin and smooth over the incisors, canines, and premolars. The cortical plate in the mandible is thicker in contrast to the maxilla on both buccal and lingual aspects, especially over the posterior region compared to the anterior region on the buccal aspect. The alveolar bone, like other types of bone, is made up of bone cells and bone matrix (Rose *et al.*, 2004; El Chaar and Abitbol, 2023).

2.1.3.1 Bone Matrix

The mineralised matrix of bone is made up of organic components, making up 33% of its total weight, and inorganic components, making up the remaining 67%. (Table 2-1) (Murugan and Ramakrishna, 2005; Ten Cate and Nanci, 2013). The latter is mainly made up of primarily crystalline hydroxyapatite (HA), which is able to provide structural hardness and strength to the

bone. The organic component of the bone matrix, namely, "osteoid", is composed of collagen and non-collagenous proteins, of which type I collagen is the main structural protein, which comprises 90% of all the organic matrix. Collagen (type I) offers mechanical cohesiveness to the connective tissue. It also gives bone its flexibility and elasticity by protecting it from forces that could damage its structure.

Non-collagenous proteins represent the last 10% of the content of the organic matrix and consist of four essential groups: several growth factors; vitamin K-dependent proteins; glycoproteins; and proteoglycans. Proteoglycan consists mainly of hyaluronic acid (HA) and chondroitin sulphate, which provide flexibility to compression of the bone structure and are responsible for attaching growth factors. Furthermore, compounds such as bone sialoprotein, osteopontin, and osteonectin are in charge of the adherence of osseous cells to the matrix and of sticking fibrous proteins, like collagen, to the hydroxyapatite crystalline constructs. Vitamin K-dependent proteins, which include osteocalcin (OC), chelate calcium and enable the growth of osteoclasts during remodelling of bone structure; elimination of pluripotent cells is carried out through the help of proteins such as protein S. Bone morphogenetic proteins (BMPs), which can induce the differentiation of bone marrow mesenchymal stem cells into osteoblasts, are an example of growth factors that can have various effects on different cell types. (Pawlina and Ross, 2018).

Table 2-1 Composition of bone matrix: [adapted from (Murugan and Ramakrishna, 2005)]

Inorganic components	(Wt%)	Organic components	(Wt%)
Hydroxyapatite	~ 60	Collagen	~ 20
Carbonate	~ 4	Water	~ 9
Citrate	~ 0.9	Non-collagenous proteins	~ 3
Sodium	~ 0.7	Others: Polysaccharides, lipids, cytokines	~ 1
Magnesium	~ 0.5		
Others: Cl^-, F^-, K^+, Sr^{2+}, Pb^{2+}, Zn^{2+}, Cu^{2+}, Fe^{2+}	~ 0.9		

2.1.3.2 Bone Cells

There are five cell types that have been identified in bone structures. These are: bone lining cells, osteocytes, osteoblasts, osteoprogenitors, and osteoclasts (Figure 2-2). These cells, with the exception of osteoclasts, have their origin in mesenchymal stem cells that then become osteoprogenitor cells, osteoblasts, and finally, osteocytes and lining cells (Wu *et al.*, 2017). In contrast, osteoclasts, the cells actively responsible for bone resorption, originate from the monocyte-macrophage lineage of the mononuclear hematopoietic system (Pawlina and Ross, 2018).

Osteoprogenitor cells can renew themselves, and they are able to differentiate into osteoblasts, the main cells in charge of secreting matrix proteins, as well as the addition of calcium to unmineralised osseous structure or osteoid. As these differentiated cells continue to gradually excrete these proteins, they finally encase themselves in a calcified matrix and transform into osteocytes (Wu *et al.*, 2017).

The most important function that is carried out by osteocytes is the maintenance of the bone structure, cohesion, and durability by perceiving the physical, biological, and chemical signals of the environment and responding to these stimuli by transducing these signals to other cells that are a critical part of bone remodelling. Failure of the aforementioned system can result in osteosclerosis and, ultimately, death (Ten Cate and Nanci, 2013).

Cells responsible for covering non-remodeled bone surfaces, bone lining cells, play a very important part in the process of phosphate and calcium metabolism, therefore maintaining the bone surface from the activity of osteoclasts' resorption. These are also likely to play a role in the remodelling of bone structure. Osteoclasts are cells in charge of degrading mineralised bone matrix during bone remodelling through the secretion of hydrolytic enzymes and specific protease secretions that dissolve both the organic matrix, often the first type of collagen, as well as the inorganic bone components. Since the bone-resorption site is a high-calcium environment, osteoclasts can maintain normal intracellular calcium levels by expelling breakdown products via membrane vesicle transcytosis (Berkovitz, Holland and Moxham, 2017; Pawlina and Ross, 2018).
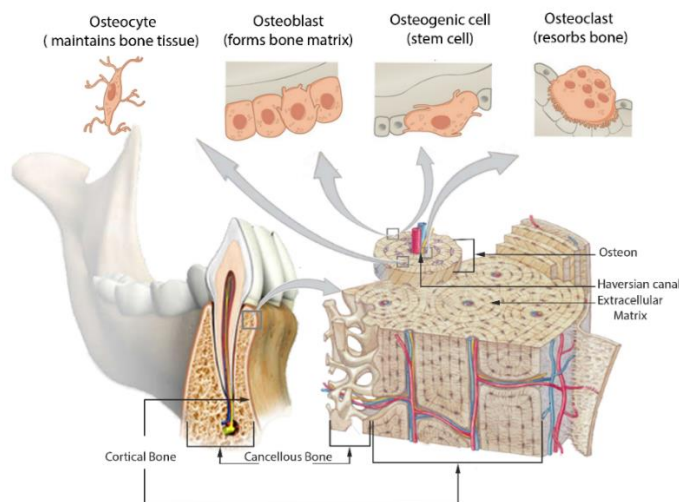
Figure 2-2 The structure of alveolar bone and different Types of bone cells, Images adapted from (OpenStax College - Anatomy & Physiology, 2013) *via Wikimedia Commons with permission to use and modify.*

2.1.4 Cementum

Cementum is a specialised calcified tissue that protects a tooth's root and connects the teeth to the alveolar bone by anchoring the ligament (PDL) (Figure 2-1). Similarly to alveolar bone cells, cementum cells are named Cementocytes for the cementum maintenance in which it serves as a circulatory passage and interacts with adjacent cell processes; Cementoblasts for the synthesis of the organic matrix of cementum; and Cementoclasts for the resorption of cementocytes. There are two forms of cementum, cellular and acellular; cellular cementum covers only the apical third of the root, while acellular cementum covers the remaining two-thirds (Palumbo, 2011; Newman *et al.*, 2018; El Chaar and Abitbol, 2023).

2.2 Periodontal diseases

Periodontitis is a disease that causes inflammation due to the accumulation of bacteria on the tooth surface (i.e., plaque). This creates calculus in which other pathogens can thrive. These pathogens can deploy collagenase, which can destroy several different parts of the periodontium with the purpose of gaining access to deeper sections of the tooth (Kwon, Lamster and Levin, 2021). When the plaque builds up, the organism activates its immune defences, including the release of white blood cells (neutrophils), which frequently leads to local inflammation of the affected site as these cells attempt to cover the pathogens (Hao *et al.*, 2015). In order to fight infection, the human body often produces cytokines. The inordinate release of these chemical

mediators may also become deleterious for the patient and ultimately disrupt the attachment between alveolar bone structure and connective tissue (Page, 1991; Kwon, Lamster and Levin, 2021). After this immune response is mobilised to the gums, it is unlikely to elicit the breakdown of the bone or the coupling apparatus. However, it can still increase the levels of blood housed in the gingiva. This condition is called gingivitis. This condition does not necessarily evolve into periodontitis, but the longer it is left untreated, the higher the chances of it evolving negatively (Obiechina, 2011). Figure 2-3 Figure 2.1 compares X-ray radiographs of healthy and infected periodontium, illustrating resorption of the alveolar bone and root surface exposure, both of which are consequences of periodontitis.

Figure 2-3 X-rays of (a) healthy teeth and periodontium and (b) diseased periodontium, showing recession of the alveolar bone and loss of tooth-bone contact tissue (LAYPORT, 2010).

Furthermore, direct associations have been made that posit that periodontitis is the precursor of other ailments, such as hypertension and peripheral arterial disease (Tsioufis *et al.*, 2011; Chang and Lim, 2012). Other diseases that involve periodontitis as a source are frequently maladies that are bone-related, such as rheumatoid arthritis and osteoporosis. However, other ailments like preterm and low-weight babies also exist (De Smit *et al.*, 2011; Persson *et al.*, 2011; Könönen, Gursoy and Gursoy, 2019). According to Chang and Lim, (2012), diabetes is a widely accepted risk factor for periodontitis. There is evidence that periodontal disease can develop even in those with well-controlled diabetes, indicating that the damage caused by periodontitis to diabetic patients may be irreversible (Iacopino, 2001; Könönen, Gursoy and Gursoy, 2019).

2.3 Treatment modalities of periodontal diseases

This section will describe other techniques that are currently available and can be of great use in dealing with periodontitis, along with their potential disadvantages, even though the focus of this literature review is the analysis of periodontal regenerative treatment through the use of bone graft materials and membranes. Many methodologies are currently available to deal with periodontal inflammatory diseases, which include antibiotics, gingival curettage, scaling and root planing (SRP), open flap and root debridement, and, more recently, the use of growth factors (Bottino *et al.*, 2012; Kinane, Stathopoulou and Papapanou, 2017). These methods will be analysed first, highlighting their limitations and disadvantages, before considering further techniques for regeneration of bone tissue.

2.3.1 Plaque removal and root planing (Non-surgical treatment)

The removal of pathogenic debris (plaque) is paramount during the treatment of patients with periodontal diseases. The elimination of accumulated bacterial plaque and calculus, which are mainly located supra-gingival and sub-gingival through the use of conventional techniques of scaling and root planing, which may include flap intervention, is of great utility. A reduction in the gingival pocket probing depth can be achieved using the scaling technique, which may be beneficial in the treatment of periodontal diseases (Becker *et al.*, 2001). It is important to mention that research has shown that the perceived utility of non-surgical subgingival root planing may not be a useful method with regard to the complete elimination of the bacterial plaque and calculus as provided by the surgical subgingival root planing process (Sherman *et al.*, 1990; Kinane, Stathopoulou and Papapanou, 2017). When it comes to root planing, part of the cementum is eliminated along with all of the debris of calculus on the root surface until it recovers its original form. These methods help build better conditions for the correct development of oral mucosa as well as reduce overall symptoms of gum inflammation, such as bleeding and gingivitis (Deas *et al.*, 2016).

2.3.2 Surgical treatment

Periodontal therapy is targeted towards avoiding the worsening of the ailment as well as recuperating the lost tissues and maintaining efficient therapeutic objectives. Several distinct techniques have been utilised in the past. These methods include gingivectomy, subgingival curettage, and flap procedures, which may include further bone recontouring. Wang and Greenwell analysed periodontal treatment and found that a number of surgical methods that were modified resulted in much higher adherence rates (Wang and Greenwell, 2001; Deas *et al.*, 2016).

Gingivectomy: This method is meant to remove suprabony pockets provided that the attached gingiva is sufficient to eliminate gingival hyperplasia. It can also be useful for other aesthetic procedures, such as crown lengthening (Wang and Greenwell, 2001).

Open flap debridement: The function of this procedure is to provide exposure to root debridement in order to obtain a reduction in pocket and enable optimum coverage of the flap for regenerative therapy tools (Wang and Greenwell, 2001).

Modified Widman Flap This technique is quite similar to open flap debridement; however, it differs in that it aims to remove the tissue damaged by inflammatory processes. It is also regarded as more conservative and is typically used when appearance is of paramount importance (Wang and Greenwell, 2001).

Modern objectives in the treatment of the periodontium are to obtain access to the surface of the root, create better gingival contours, and make oral hygiene easier by lengthening the regular clinical crown in order to facilitate restorative procedures and, in the process, make them more efficient at regaining the damaged tissue. The ultimate goal of periodontal surgical methods is to regenerate the damaged and lost periodontium, which will expand in the future as a treatment method, although the aim of these treatments will be almost entirely tissue regenerative (Wang and Greenwell, 2001). It has been shown that a combination of surgical options, bone grafts, and several other substitute types of bone (such as bioactive glass, endogenous bone, and hydroxyapatite) can be effective in regenerating damaged tissue (Gestrelius, Lyngstadaas and Hammarström, 2000; Lee *et al.*, 2019).

2.3.3 Regenerative therapy

Current periodontal treatment approaches are targeted at minimising and/or removing inflamed tissues induced by bacterial plaque, repairing deficiencies or structural abnormalities, and regenerating new tissues in the region of lost tissues (Taba Jr *et al.*, 2005; Sculean, Nikolidakis and Schwarz, 2008; Liang, Luan and Liu, 2020) . Various methods mentioned previously are only able to stop the progress of the problem, but are unable to reverse the damage or replace the lost tissue (Needleman *et al.*, 2002). Bone grafting, Enamel Matrix Derivative (EMD) and guided regeneration therapy are now used in the development of tissues that have been infected by periodontal diseases. To a certain degree, the overall structure and function of the damaged tissue can be restored(Liang, Luan and Liu, 2020).

2.4 Historical viewpoint on approaches to periodontal regeneration:

The concept of placing a physical barrier along the tooth root surface after periodontal surgery to prevent epithelial downgrowth was first proposed in the 1970s (Lee *et al.*, 2019), (Figure 2-4).
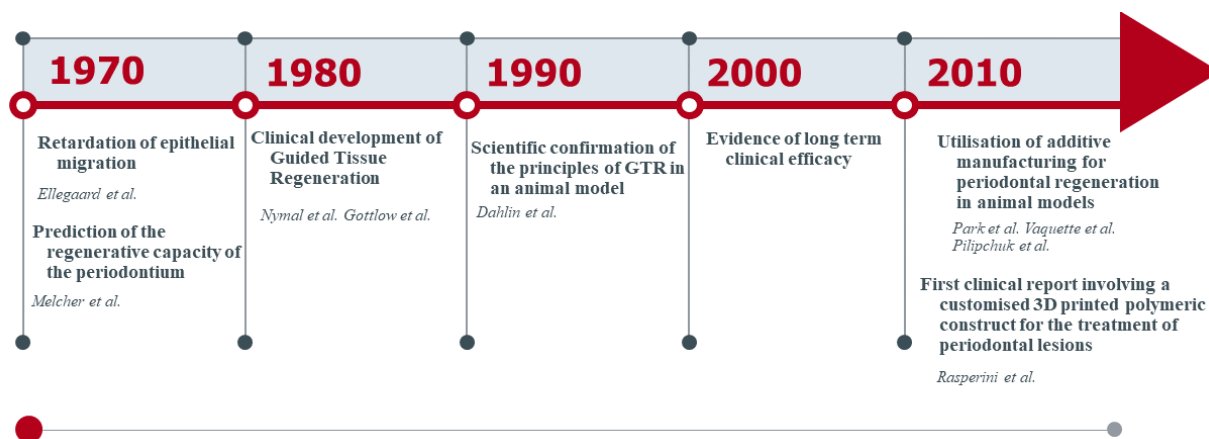
Figure 2-4 Timeline of periodontal regeneration approaches: from the original idea involving a free palatal graft for inhibiting epithelial migration to the most current developments involving additively engineered polymeric multiphasic scaffolds for periodontal tissue engineering.

Indeed, physicians had previously hypothesised that the collapse of gingival tissues into periodontal defects seriously impeded bone resorption (Melcher, 1976; Giannobile, 2014). Several early experiments suggested the placing of a harvested free palatal graft over the periodontal defect in order to delay or at least obstruct the downgrowth of epithelium around the tooth root surface (Lee *et al.*, 2019). Another popular procedure included the insertion of bone grafts (allogenic, autologous, or synthetic) obtained from the patient inside the periodontal defect to regenerate the missing bone (Dhruvakumar, Arun Kumar and Ayilavarapu, 2019). However, neither of these methods is successful for periodontal recovery, and only periodontal healing is observed in the context of a fresh junctional epithelium. After researching the clinical and laboratory evidence, it can be hypothesised that the lack of compartmentalisation between the periodontal defect and the underlying soft tissue was the cause of low regeneration rates. The problem of selective periodontal defect repopulation by tissues capable of fostering periodontal regeneration was presented in a series of pioneering papers by Nyman *et al.*, which contributed to the development of the principle of guided tissue regeneration (GTR) (Nyman *et al.*, 1990; Lee *et al.*, 2019).

2.4.1 Bone graft procedure

Bone grafts have been an option for a long time to successfully deal with the effects of periodontal disease, such as bone loss and damage. A bone graft is meant to fill the space that originated from the damaged tissue with a material that possesses certain qualities and characteristics (Figure 2-5). There are several types currently available, such as allografts, xenografts, alloplastic, and autograft materials. These kinds of graft materials are able to facilitate natural osseous repair through some mechanisms that have already been properly characterised (McAllister and Haghighat, 2007; Dhruvakumar, Arun Kumar and Ayilavarapu, 2019; Zhao *et al.*, 2021):

Osteogenesis: The graft possesses cells that function as seeds for the continuous growth of the tissue by forming a bone matrix.

Osteoinduction: The graft can release factors and biochemical signals that stimulate the formation of new bone by cells.

•**Osteoconduction**: The graft works as a scaffold on which the host bone develops.

Diverse graft materials can be categorised into four general types that are shown in Table 2-2.
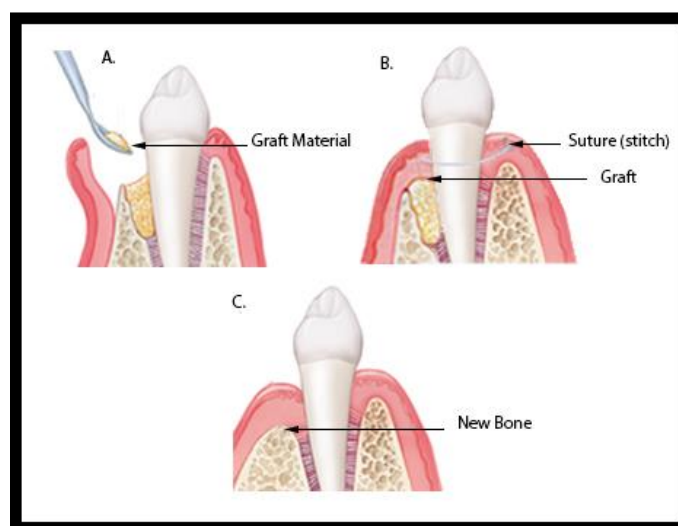
Figure 2-5 A schematic diagram of the management of periodontal defects by a bone graft technique. A) Placing the graft. First, a gum flap is created. Growth factors may then be applied to the root. Graft material is packed into the area where bone was lost. B) Closing up. The gum is closed and sewn together. C) After the area heals. Stitches dissolve or are removed.

Table 2-2 Bone graft classification by material source. adapted from (McAllister and Haghighat, 2007; Zhao *et al.*, 2021).

Type	Source		Benefit	Risk
Autograft	**Patient**		• Osteogenic, osteoinductive and osteoconductive • No immunological rejection living cells and matrices	• Morbidity at donor sites • Amount of bone volume is limited • Rapid absorption
Allograft	**Other human**	Demineralised freeze-dried bone allograft (DFDBA)	• Osteoinudctive and osteoconductive	• Potential of infection and immunological rejection
		Freeze-dried bone allograft (DFDBA)	• Osteoinudctive and osteoconductive	• Potential of infection and immunological rejection
Xenograft	**Other species** (mostly bovine)		• Osteoconductive	• Potential of infection and immunological rejection • Slow resorption or non-resorbable
Alloplast	**Synthetic**	Sintered hydroxyapatite (HA)	• Osteoconductive	• Slow resorption or non-resorbable
		b-tricalcium phosphate (TCP)	• Osteoconductive	• Rapid resorption
		Natural products (Coral, chitosan etc.)	• Osteoconductive, low immunological rejection	• Slow resorption or non-resorbable

In the past, research publications have reported that at least 3.0 mm of bone height can be acquired, regardless of which material the graft is made of (Mellonig, 1992; Zhao *et al.*, 2021). Probably the best option for osteogenesis, osteoconduction, and osteoinduction is autologous bone since it shares all of its properties with the surrounding bone. In this type, a part of the bone structure is extracted from a normal and un-damaged area of the patient who is getting the graft.

The structure that is compatible and inherent to this type makes it very advantageous since it has the same vital bone structures in critical regions and includes nutrients, proteins, and cells as those found in the affected site. However, the autoimmune grafts come with some disadvantages, such as increasing the patient's pain at the same site of the excision. In addition, only small amounts of bone can be extracted without incurring permanent damage to the patient.

Due to these drawbacks, several xenografts, bone grafts, as well as allogeneic materials have been designed and approved for commercial use (Miron and Zhang, 2012). It is important to note that clinicians must take into account the risks associated with these materials, such as infection, resorption, and immune responses. Currently, two types of allografts are available: freeze-dried bone allograft (FDBA) and demineralised freeze-dried bone allograft (DFDBA). These grafts are pre-treated chemically; they keep their osteoinductive capabilities due to the conservation of certain proteins, such as BMPs and TGF-s. These proteins work as powerful growth stimulants and induce the mobilisation of cells from the mesenchyme into the implant. The overall process of demineralisation enhances the excretion of these highly important factors into the extracellular medium (Urist, 1965; Zhao *et al.*, 2021).

The grafts that are extracted from animals, mainly farm cattle, are called xenografts. They go through chemical treatment in order to remove their inherent antigens, in order to avoid the human body's natural immune response. The greatest advantage in using these products lies in the fact that the general structure of the graft can be maintained, and this is because of the prolonged amounts of time required for these materials to be resorbed. These materials are capable of osteoconductivity and little else. However, the overall safeness and efficacy of them has been proved to be clinically relevant (Richardson *et al.*, 1999; Zhao *et al.*, 2021).

Due to the risks related to these types of grafts, scientists have also conducted investigations into the use of synthetic alternatives, which include composite grafts, polymer and inorganic materials, to repair osseous tissue (Rezwan *et al.*, 2006). In particular, materials like hydroxyapatite and β-tricalcium phosphate (β -TCP) have become of increasing clinical importance when studying periodontal diseases. Furthermore, even though synthetic materials lack osteogenic and osteoconductive capabilities, their osteoconductive properties make them excellent options for bone regeneration. Recently, in a study by Schmidlin *et al.*, (2013), it was found that polylactide-coated TCP was sufficient to repair problems in the rabbit's bone structure, all of this while retaining its biocompatibility.

Certain products of natural origin, such as coral, have been shown to be able to be used as bone grafts due to their similarity to human bone structure (Damien and Revell, 2004). Similarly

to synthetic materials, numerous natural products have been proven safe for human use and are very cost-efficient. However, they are still only osteoconductive (Zhao *et al.*, 2021).

Growth Factors

The purpose of the proteins involved in bone regeneration has been a focal point in this discussion, mainly due to the importance of growth factors in cellular growth and proliferation. These so-called "growth factors" are polypeptides that regulate cell proliferation, migration, and adherence. Growth factors can be divided into platelet-derived growth factors (PDGF), fibroblast growth factor (FGF), insulin-like growth factor (IGF), transforming growth factors (TGF), and bone morphogenic proteins (BMP) (Javed *et al.*, 2011; Malli Sureshbabu *et al.*, 2019). These factors can be found in high concentrations in places like the bone and cementum. These growth factors can work either on their own or in tandem with others, in which case their united influence has been demonstrated to facilitate the renewal and repair of the periodontium (Darby and Morris, 2013). Among the many growth factors (GFs), PDGF has been studied the most thoroughly (Javed *et al.*, 2011). Periodontal application of these proteins has shown consistently positive results, which are amplified by the presence of other agents. However, the use of GF's has not yet been implemented widely in clinical practise (Bosshardt and Sculean, 2009; Malli Sureshbabu *et al.*, 2019).

i) Platelet Derived Growth Factor (PDGF).

These growth factors can be found nearly anywhere in the body and have been demonstrated to augment the periodontal regeneration rate in humans in time-dependent studies. These proteins exercise their influence by controlling the rates at which PDL cells differentiate, proliferate, and adhere to surfaces. This has been shown in several studies conducted on beagle bred dogs and non-human primates based on periodontal disease models (Nevins *et al*., 2005; Javed *et al*., 2011). This translated structure is a naturally occurring protein that is abundantly present in the bone matrix and has been found to be an important outcome in cell replication, migration, and surface coverage. Additionally, it is responsible for the creation of extracellular matrix components and endogenous injury treatment. Javed *et al*., (2011) carried out a review in which it was determined that PDGF is a critical component in the promotion of GBR in the oral tissues, specifically around teeth and implants. PDGF also greatly enhances the proliferation of oral cavity tissues, such as gingival, periodontal ligament, cementogenesis and fibroblasts (Javed *et al.*, 2011; Malli Sureshbabu *et al.*, 2019).

ii) Fibroblast Growth Factor (FGF)

These growth factors belong to the family of heparin growth factors, and they possess a myriad of physiological functions, mainly facilitating the formation of new bone structures as well as overall structural regeneration which are of immense help during the early stages of healing (Yun *et al*., 2010; Ramseier *et al*., 2012). *In-vivo* studies on the ability of FGF to regenerate lost or damaged tissue during periodontal disease have been carried out on beagle dogs, and the measured results indicate that FGF might have a critical role in the repair of and growth of cementum, as well as assisting with alveolar bone development. However, this research is far from conclusive, and further experiments under different circumstances are still required to fully correlate these effects with FGF (Javed *et al.*, 2011; Malli Sureshbabu *et al.*, 2019).

iii) Insulin-Like Growth Factors (IGF)

IGFs are produced by the effect of growth hormones and have an important role in restructuring bone. However, exactly how they carry out this function is, as of yet, still unknown (Chen *et al.*, 2006; Malli Sureshbabu *et al.*, 2019).

iv) Bone Morphogenic Proteins (BMPs)

BMPs, of which there are several known types including BMP2 and BMP7, are the primary contributors in the development of both hard and soft, osseous tissues. Their ability to enhance bone cell growth (osteoinduction properties) is influenced by the BMP gradient as well as the presence of other growth factors that operate in tandem with BMP (Wikesjö *et al.*, 2009; Malli Sureshbabu *et al.*, 2019).

Enamel Matrix Derivative (EMD)

EMD is one of the most promising approaches for periodontal tissue regeneration among the many methods currently used to treat periodontal disease.The periodontal regeneration (PR) field was deeply changed after the discovery of EMD. Periodontal regeneration and repair after the effect of EMD application is believed to happen by imitating the events that take place during regular periodontal tissue development. EMD is encountered in large concentrations during the development of the crown part of tooth development. Enamel matrix protein (EMD) is mainly composed of amelogenins (90%) and other (10%) kinds of proteins, such as enamelin, proteolytic enzymes, ameloblastin, and tuftelin. These proteins are recognised for their function in the mineralisation of enamel, so it is reasonable for the orientation and maturation of crystal enamel

during crown development (Grandin, Gemperli and Dard, 2011). Acellular cementum provides firm attachment of periodontal ligament fibres to the surface of the tooth's root, and this process is critical for periodontal regeneration (Yan *et al.*, 2014; Malli Sureshbabu *et al.*, 2019).

Nowadays, the effective use of EMD in periodontal regeneration has been backed by the tasks occupied by cementum cells in repairing the periodontium wound. EMDs are truly fascinating and unique constructs, and they must become the focus of more researchers working with proteomics, substrate tissue engineering, and regeneration, renewal, and strengthening of tissues (Grandin, Gemperli and Dard, 2011; Malli Sureshbabu *et al.*, 2019).

2.4.2 Guided regeneration therapy

The key aim of periodontal regeneration is to establish new cementum with periodontal ligament (PDL) fibres attached to the alveolar bone and promote new bone growth. Currently, there are two surgical approaches that have been used for regenerating periodontal tissues. These are guided tissue regeneration (GTR) and guided bone regeneration (GBR) (Behring *et al.*, 2008; Koo *et al.*, 2008; Sculean, Nikolidakis and Schwarz, 2008). The concept of guided tissue/bone regeneration began in the late 80s and was developed by Nyman *et al.*(1990) based on Melcher's theory. This theory hypotheses that when cells with regenerative capabilities are associated with damaged tissues, they can actually be used to aid in the regeneration of that tissue (Nyman *et al.*, 1990). The hypothesis has been successfully proven in various animal experiments, and the principle of guided tissue regeneration (GTR) has been confirmed (Koo *et al.*, 2008; Sculean, Nikolidakis and Schwarz, 2008; Lee *et al.*, 2019).

GTR refers to the procedure of regenerating periodontal tissue through the use of an occlusive barrier membrane between gingival (epithelial) and alveolar bone/PDL tissue. In this operation, an occlusive membrane will be inserted onto the surgical site in order to inhibit the migration of connective and epithelial tissue through the surgical site (Koo *et al.*, 2008; Sculean, Nikolidakis and Schwarz, 2008; Lee *et al.*, 2019). Progenitor cells that existed in the lining of the residual periodontal ligament, corresponding alveolar bone, or blood can then re-colonise the root region and divide into new periodontal supporting components (Koo *et al.*, 2008). The guided bone regeneration (GBR) approach is often used to repair defective alveolar ridges before or in conjunction with the placement of a dental implant at extraction sites. In GBR, a bone defect is protected by a membrane to stop fibre tissue intrusion into the site of the graft and to promote

the development of a new bone. Intrabony abnormalities and furcations are also treated with GBR (Koo *et al.*, 2008; Sculean, Nikolidakis and Schwarz, 2008; Lee *et al.*, 2019).

In order to promote the development of healthy bone structures surrounding bone defects, GBR permeable membranes can be utilised (Figure 2-6). GBR membranes can also be used in order to preserve the socket area that may be around the tooth due to the presence of periodontal disease, and can even be used to regenerate bone structure at the tooth site after it has been misplaced or extracted (Agrawal, Parr and Lin, 2000).

The efficacy of this therapeutic approach was later verified by Gottlow *et al.*, who effectively extended it to a large group of patients (Gottlow *et al.*, 1984, 1986). Subsequently, the theoretical and biological basis of GBR has been confirmed during the last three decades in several studies (Needleman *et al.*, 2006), and the effectiveness of the procedure has been shown in a multitude of clinical trials (Cortellini, Prato and Tonetti, 1996) and recorded in comprehensive reviews (Murphy and Gunsolley, 2003; Lee *et al.*, 2019).
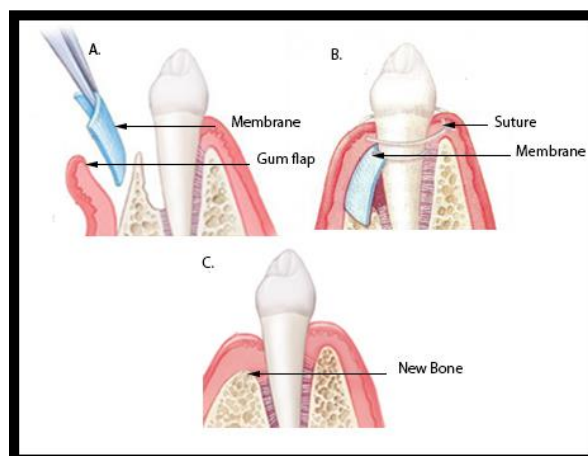
Figure 2-6 Schematic of GTR is a technique used to repair periodontal defects. A) The gum is opened with a procedure known as a flap. Then a membrane (with or without the bone graft material) is placed over the damaged bone. B) Closing up. The gum is closed and sewn together. C) After the area heals. Stitches dissolve or are removed.

Guided regeneration has been shown to have many benefits when it comes to tissue regeneration over more conventional surgery approaches such as open-flap debridement, which is usually used to address intrabony defects and mild to moderate furcations (Murphy and Gunsolley, 2003; Lee *et al.*, 2019).

The concept behind bone augmentation protocols mainly relates to the enhancement in function and aesthetics and can also be used to improve the functions of fixed dental prosthetics, including dental implants and fixed dentures. This procedure greatly helps in correcting contour deficiencies associated with the replacement of artificial teeth as well as offering a friendlier solution to altered speech patterns due to the uncovered areas frequently left between gingival tissues and the restoration (Buser *et al.*, 1993; Lee *et al.*, 2019).

2.4.2.1 Biologic principles for guided regeneration therapy

In order to successfully develop an engineered tissue, the following essential elements are required: properly defined levels and patterns of regulatory signals; an abundance of progenitor cells; a sufficient blood supply; and an appropriate biomaterial scaffold (Slavkin and Bartold, 2006). Whereas cells serve as the processing facility for the formation of newly formed tissue and the differentiation of cells. Cells require external stimuli in order to stimulate growth and matrix synthesis. These can be provided by growth factors or morphogens. New vascular networks are promoted as a result of angiogenic signals, which supply nutrients for tissue growth and maintenance. The three-dimensional architecture of scaffolds aids in directing cell regeneration (Taba Jr *et al.*, 2005; Lee *et al.*, 2019).

The healing process for periodontal surgery wounds follows the same three stages as any other incisional wound. Initially, a fibrin clot is shaped along the flap's margin and the root surface. Then, a connective tissue matrix attached to the root surface takes the place of the fibrin clot (Wikesjö *et al.*, 1991). By keeping the fibrin attached, a new connective tissue bond can form on the root's outer surface. However, a long-bonding epithelial connection forms if the limit of the fibrin clot's tensile strength is surpassed (Wikesjö, Nilvéus and Selvig, 1992; Lee *et al.*, 2019; Nuñez *et al.*, 2019).

In general, the method of periodontal healing is more complicated than other wounds by considerations such as the involvement of various specific cell types and complexity of attachments; avascular root surfaces; different microbial flora; and stromal-cellular interfaces (Pitaru, McCulloch and Narayanan, 1994). The first biological reaction that happens after the installation of the barrier membrane is the action of the tissue-membrane interface to absorb the plasma protein. Hence, the related growth factors and progenitor cells, which play an important role in tissue repair, are attracted to the surface of the membrane with the help of proteins (McClellan and Franses, 2005). In order to provide nourishment to the new tissue in the barrier membrane, which protects defects, much of the vascular supply comes from blood vessels that

originate in the marrow (Schenk *et al.*, 1994). This further explains why it is vital to plan multiple perforations in cortical bone (also called intramarrow penetration), as this assists in the production of an excess of angiogenic and osteogenic cells as a means of creating new blood vessels and constructing new bone tissue. This serves two objectives: first, it induces bleeding or blood clotting around the grafts in order to induce bone formation around the grafts, and second, it increases the number of factors that raise the likelihood of bone growth (Buser *et al.*, 1993; Lee *et al.*, 2019; Nuñez *et al.*, 2019).

There is also controversy about the effector cells in periodontal regeneration. Some reports indicate that PDL cells have the potential to behave as osteoblasts or cementoblasts when they are supplied with growth factors and allowed to proliferate. Other data indicates that PDL cells have the ability to regulate mineral formation, so this will help avoid ankylosis when undergoing regeneration (Lang *et al.*, 1995). In other studies, PDL cells *in vivo* and *in vitro* have been reported to exhibit minimal osteoblastic properties (Pitaru, McCulloch and Narayanan, 1994; Lang *et al.*, 1995). However, other studies argue that osteoblasts, and not PDL cells, are responsible for generating cementum-like material (Melcher, 1976; Boyko, Melcher and Brunette, 1981; Lin, McCulloch and Cho, 1994). Such variations can be attributable to PDL cell heterogeneity, differing study designs, and/or loss of cell properties defined *in vitro* research. In summary, the majority of evidence points to PDL cells as the main source. Some reports also point to bone cells as the origin of regenerative cells (Wang and MacNeil, 1998; Lee *et al.*, 2019; Nuñez *et al.*, 2019).

2.4.2.2   Requirements of GTR/GBR membranes

GTR and GBR membranes need to fulfil specific requirements to be most effective and successful (Gao *et al.*, 2022). These requirements can be summarised as follows:

Cell exclusion: A growth guide membrane can be used to separate several types of unwanted tissue (e.g. epithelial cells) as well as get access to the site of interest (Basile *et al.*, 2015).

Framework: A more rigid framework is frequently necessary when clinical cases need more space maintenance in order to prevent membrane compression into the defect site. Bone grafts can provide this support (Karring, 2000; Gao *et al.*, 2022).

Porosity: In order to achieve appropriate cell growth and proliferate , the cells must have an underlying high-pore structure (Bottino *et al.*, 2012).

Degradation: it is important to provide a degradation profile that suits the tissue regeneration, which takes approximately four to six weeks. Ideally, the membrane should fully degrade after it fulfils its purpose without leaving any residual materials (Sheikh *et al.*, 2016).

Stabilisation: to prevent mechanical disturbances from the outside and overhanging of flap movement during the process of healing. Mini screws or sutures, can be used to keep the membrane in place (Gao *et al.*, 2022).

Clinical manageability: the membrane and the barrier need to possess physical characteristics that enable their handling by the clinician (K.-H. Kim *et al.*, 2005).

Biocompatibility: inflammation should be avoided at all costs in order to avoid increased morbidity and costs (Laycock, B., Nikolić, M., Colwell, J.M., Gauthier, E., Halley, P., Bottle, S. and George, 2017; Gao *et al.*, 2022).

Owing to the large number of scaffolds that can be made from a wide range of materials, these materials have differing degrees of degradation and integrity. These scaffolds can often induce immune reactions in the hosts (Brydone, Meek and Maclaine, 2010). The following section discusses commercial membranes, whether non-absorbable or absorbable, in guided regeneration therapy.

2.5 Types of commercial membranes used in guided regeneration therapy

Barriers used in bone/tissue regeneration procedures have varying degrees of deterioration and properties and, therefore, have generally been divided into resorbable or non-absorbable membranes. Gottlow, (1993) was the first to divide these membranes into two generations depending on when they were created and developed; the first generation consists of nonresorbable membranes, while the second generation contains all resorbable membranes. Before Elgali *et al.*, (2017) reviewed this classification and added a new group, Third generation, its membranes rely on naturally derived sources combined with bone grafts and alternative materials to provide structural support to the defect site and to promote the intrinsic regenerative potential of the host tissue (Elgali *et al.*, 2017; Lee *et al.*, 2019; Nuñez *et al.*, 2019).

The following sections discuss the various commercially available periodontal membranes classified as non-resorbable or resorbable materials and are summarised in Table 2-3.

Table 2-4 Overleaf includes a list of the main biomaterials used in bone tissue engineering, in addition to their main characteristics.

2.5.1 First-generation membranes: non-resorbable guided membranes

In the 1960s and 1970s, the first generation of barrier membranes were developed with the goal of achieving a sufficient mix of physical qualities that would match those of the replaced tissue while also eliciting a low toxic response in the host (Lee *et al.*, 2019; Nuñez *et al.*, 2019).

In the initial GTR experiments, an occlusive membrane consisting of a bacterial filter made from cellulose acetate (Millipore) was utilised. These experiments were conducted by Nyman et al. in 1982 (Nyman *et al.*, 1982). Due to its toxicity, this form of membrane was not appropriate for clinical applications despite serving its goal. In later trials conducted in the 1990s, membranes of expanded polytetrafluoroethylene (e-PTFE) created specifically for periodontal regeneration were applied (Gore Tex Periodontal Material) (Aaboe, Pinholt and Hjorting-Hansen, 1995; Elgali *et al.*, 2017; Lee *et al.*, 2019).

E-PTFE has a dual-layered structure with pores measuring 5–20 microns in diameter. One side of this membrane is 1 mm thick and has an open microstructure that is 90% porous, preventing epithelial penetration; the other side is 0.15 mm thick and has a porous structure that is 30% thick, allowing space for new bone production (Liu and Kerns, 2014). Several investigations have shown that e-PTFE is effective, as described by Liu, J. and Kerns, D.G. (Liu

and Kerns, 2014) However, due to their very porous structural design, they have a high rate of exposure, which is seen as a major disadvantage, in addition to the need for additional surgery to remove them from the location of the newly created tissue.

A high-density PTFE membrane with hole sizes of less than 0.3 microns was created to counteract the drawbacks of e-PPTFE (Madhuri, 2016). In spite of the advantage of non-sticking of tissues to the membrane, which made its removal easy and simple, in addition to its ability to properly regenerate the bones even in exposed cases due to its modified transparency, However, the d-PTFE has limited flexibility, causing it to collapse into the site of the defect (Liu and Kerns, 2014).

Titanium-reinforced e-PTFE and d-PTFE membranes were produced in order to address the lack of mechanical stiffness that appeared in the initial e-PTFE and d-PTFE membranes (Canullo and Malagnino, 2008; Fontana *et al.*, 2008). However, the requirement for a second surgery to remove the membrane is the most significant disadvantage, similar to other non-resorbable membranes, as well as the rigidity of titanium mesh can create some difficulties during removal due to the need for orthopaedic fixation devices such as orthopaedic screws, etc. Ti-mesh also appears frequently, which restricts its applications, particularly in aesthetic applications. (Sam and Pillai, 2014).

2.5.2 Second-generation membranes: resorbable guided membranes

Regarding the several applications of GTR and GBR, an absorbable membrane has been proposed as a replacement to the membrane discussed in the previous section in order to minimise its limitations, most notably the requirement for extra surgery to remove the membrane. Based on the origin of the material used to produce the membrane, absorbable membranes are classified into two main groups: natural membranes and synthetic membranes (Elgali *et al.*, 2017; Lee *et al.*, 2019).

2.5.2.1   Natural resorbable membranes

Numerous natural polymers have been shown to be useful in tissue engineering, which include polysaccharides (cellulose, alginate, starch, hyaluronic acid derivatives, chitin/chitosan), and proteins (soy, fibrin gels, collagen, silk) (Rezwan *et al.*, 2006; Peter, Ganesh, *et al.*, 2010). Natural polymers are also strongly coordinated and may include extracellular substances known as ligands that are essential for binding with cell receptors that can support cell adhesion and function. However On either side, their medicinal use is constrained by their shortage and the complexity of their processing into scaffolds. In addition, they can induce an immune reaction

since natural polymers can lead to cells growing at different developmental stages. Moreover, the rate of degradation varies between patients due to the enzymatic processes involved (Cheung *et al.*, 2007; Elgali *et al.*, 2017; Lee *et al.*, 2019).

Collagen and chitosan appear to be the two main components of most natural membranes, which are naturally derived from many animal sources. Perhaps the most notable one is the use of bovine achilles tendon (Cytoplast®), human skin (Alloderm®), or porcine skin (Bio-Gide®) to produce tissue-derived membranes based on collagen (Felipe *et al.*, 2007; Bottino *et al.*, 2009).

The presence of collagen in these membranes is a significant biological feature, as it contributes to many biological activities. Besides being biocompatible, biodegradable, and hemostatic, it also helps in attracting the gingival fibroblast and periodontal ligament (PDL) in addition to augmentation of the soft tissue. Using collagen type I, most of the commercially available collagen membranes are produced and developed, as well as a mixture of collagen types I and III (Liu and Kerns, 2014). *In vivo* experiments found that the collagen-dependent membrane showed some drawbacks, such as its modest efficiency, especially during degradation. Moreover, it may cause ethical and religious issues as well as be a cause of disease transmission (Behring *et al.*, 2008). Many biophysical characteristics and collagen framework stabilisation can be improved by a number of methods that depend mainly on mechanical and chemical cross-linking, such as adding substances such as glutaraldehyde (GA), diphenyl-phosphoryl azide (DPPA), hexamethylene diisocyanate (HMDIC), and formaldehyde (FA), genipin (Gp), in addition to using ultraviolet light and irradiation (Sundararaghavan *et al.*, 2008; Bottino *et al.*, 2010; Lee *et al.*, 2019).

Collagen structural integrity and mechanical properties are affected by the rehydration protocol, i.e., inserting a cross-linking agent that is natural, genipin into the AlloDerm® (Bottino *et al.*, 2010). Studies have shown that extending the exposure time for genipin (GP) to 6 hours from 30 minutes significantly improves tensile strength in comparison with controls. Also, according to other studies, crosslinking is effective for controlling prolonged biological degradation, decreasing tissue amalgamation, and vascular depression, as well as for decreasing epithelial migration (Schwarz *et al.*, 2006). A biocompatible reaction of the membrane made of silk fibroin by osteoblast was also observed, which could be used for GBR as an alternate barrier membrane(Yoo *et al.*, 2016).

2.5.2.2 Synthetic resorbable membranes

Synthetic polymers have several advantages over natural polymers, including the ability to have their properties tuned, an infinite variety of forms, and well-established structures. The support that is provided by synthetic biomaterials can make it possible to restore the structural integrity and functional capacity of diseased or damaged tissues (Reddy *et al.*, 2021). Synthetic polymers can be modified in terms of their molecular weight, molecular structure, and physical and chemical properties simply unlike polymers derived from natural sources, through the addition of certain functional groups and side chains, synthetic polymers may be self-cross-linked or cross-linked with enzymes or other bioactive molecules (Place *et al.*, 2009; Geckil *et al.*, 2010; Zhu, 2010).

Synthetic biomaterials have the limitation of lacking cell attachment sites and requiring chemical alterations to improve cell adherence (Kluge and Mauck, 2011). Physicochemical and mechanical properties of several commercially available synthetic polymers are close to those of biological tissues (Cascone *et al.*, 2001). The mechanical and physical properties, such as stiffness, Elastic modulus, and degradation rate, are repeatable and predictable throughout a wide spectrum (Kluge and Mauck, 2011; Elgali *et al.*, 2017; Lee *et al.*, 2019).

The most commonly investigated synthetic degradable materials are poly(-hydroxy esters), which include PCL, PGA, PLA, and their copolymer PLGA, and poly(ethers), which include PEO and PEG, PVA, and PU. These are perhaps the most common examples, however there are now many other synthetic materials being studied (Cascone *et al.*, 2001; Kluge and Mauck, 2011; Reddy *et al.*, 2021). These polymers all have varying degrees of biodegradability, biocompatibility, and mechanical qualities; nevertheless, there is not a single polymer that possesses all three of these essential properties at the optimal amount (Ciardelli *et al.*, 2005).

- **PGA-based membranes**

Polyglycolic acid is organically created through polycondensation of glycolic acid or ring-opening polymerisation (ROP) of glycolide. PGA has a very high fusion point at around 226°. PGA can be processed through hydrolysis, and its by-products can be processed by the Krebs cycle and then eliminated. It is generally used as a suture, but it can also be used as a PLA co-polymer. (Liu, Slamovich and Webster, 2005). Resolut® is another commercially available product consisting of two layers: a PLGA compact layer that prevents epithelial cell penetration, and a porous network of polyglycolide fibers that promotes tissue integration. Histological studies showed similar effectiveness to non-resorbable membranes and complete resorption 5–6

months after placement (Pontoriero, Wennström and Lindhe, 1999; Donos, Kostopoulos and Karring, 2002).

Fibers of polyglactin 910, a copolymer of glycolide and L-lactide (9:1 wt/wt), were used to produce a woven mesh (Vicryl Periodontal Mesh®). The polyglactin 910 is inert (no reactions in the surrounding tissue during its adsorption were observed), not antigenic, and preserves its physico-mechanical properties during the first 3–4 weeks (De Sanctis and Zucchelli, 1996). Although animal studies indicated a lack of tissue integration and recession formation, clinical evaluation suggested a similar effectiveness as compared to that of other GBR membranes (Gottlow, 1993; Araujo, Berglundh and Lindhe, 1998; Pontoriero, Wennström and Lindhe, 1999; Donos, Kostopoulos and Karring, 2002).

- **PCL-based Membranes**

Poly-ε-caprolactone is a polymer with some crystal-like properties that melts at about 60 °C. It possesses a relatively slow degradation rate, which makes it better suited for long-term applications like drug delivery systems. A plethora of studies have evaluated this approach and determined that PCL is an effective delivery polymer. Additionally, its physical properties can be modified through the addition of materials like PGA or PLA. It also possesses applications in osseous scaffolding (Marra *et al.*, 1999; Li *et al.*, 2003; Sinha *et al.*, 2004). Membranes based on copolymers of lactic acid and e-caprolactone have been produced, showing a lower degradation time as compared to pure PLA membranes. PCL is characterised by higher hydrophobicity and lower water solubility than PLA, PGA and their copolymers. A commercial product, called Vivosorb®, consisting of poly(DL-lactide-ecaprolactone), was found to be biocompatible, noncytotoxic, occlusive and space maintaining (Meek *et al.*, 2004).

- **PLA-based Membranes**

Polylactic acid is synthetised similarly to PGA, through ring-opening polymerisation of its lactic acid (HOCHCH3COOH) (Conn *et al*., 1995). Its structure can be seen in Figure 2-7.

$$HO - CH_3 - (O - CH_3)_n - O - CH_3 - OH$$
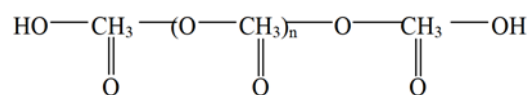
Figure 2-7 Chemical structure of PLA, where (n) denotes the central repeat unit [modified from (Conn et al., 1995; Garlotta, 2001)].

PLA is one of the best biopolymers due to its biocompatibility and ease of biological degradation. Because of its properties, it has been used in various biomedical and clinical applications (Rokkanen *et al.*, 2000; Georgiou *et al.*, 2007; Gupta, Revagade and Hilborn, 2007). PLA exists in three optical isomers, specifically in its L-lactide form as (PLLA) and its D-lactide form as (PDLA). Additionally, it has a hybrid form (PDLLA) (Kim *et al*., 2003). Because of its nature as an amorphous crystal, PDLLA degrades quicker than other forms of PLLA, in less than half a year (Merolli *et al*., 2001; Chen *et al*., 2008).

The Guidor® Matrix Barrier is a bioresorbable membrane, first used for the regeneration of tissues in periodontology, consisting of polylactic acid treated with acetyltributylcitrate to achieve flexibility to guarantee close barrier adaptation to the bone defect. The Guidor® Matrix Barrier has a matrix with two differently perforated layers. The external layer, allowing integration of the overlying gingival flap, presents large pores (rectangular shape) to promote tissue integration and to enable gingival connective tissue to penetrate quickly into the matrix. The inner layer presents small pores (circular shape), able to retard tissue penetration while allowing nutrient permeation. The two layers are separated by many inner spacers, forming an interspace into which tissue can grow. According to the manufacturer, the barrier structure is not affected by the material degradation for at least the first 6 weeks, and a complete resorption takes place after one year due to hydrolysis (Gottlow, 1993; Araujo, Berglundh and Lindhe, 1998).

Atrisorb® membrane is the first liquid product adapted directly at the surgical site: it consists of poly-DL-lactide acid dissolved in N-methyl-2- pyrrolidone. An irregular membrane is produced after polymer exposure to 0.9% saline solution for 4–6 min in a special cassette, in which it is possible to cut it into the desired shape. Membrane thickness is 600–750 µm, and it is positioned into the defect site by applying a moderate pressure. A histological complete

resorption was observed 6–12 months after implantation (Hou *et al.*, 2004). Clinical studies reported its efficacy in the treatment of periodontal defects (Camargo *et al.*, 2002).

The Epi-Guide® Bioresorbable Barrier Matrix is a porous membrane consisting of D-L polylactic acid with a unique three-layer technology, used as an adjunct to periodontal restorative surgery. The Epi-Guide maintains its structure and functions for 5 months after implantation, with a complete bioresorption after one year (Takata, Miyauchi and Wang, 2001). The layer in contact with the gingiva is porous to promote fibroblast infiltration and attachment. On the contrary, the layer in contact with bone defects has a limited porosity that supports fluid uptake, helps adherence to the tooth surface, and inhibits fibroblast movement (Takata, Miyauchi and Wang, 2001; Bilir *et al.*, 2007).

For successful periodontal tissue regeneration, the materials used must be compatible with living tissue and favourable in terms of mechanical properties. These specifications cannot be fulfilled by conventional single-component polymer materials. As a result, designing and preparing multicomponent polymer structures represents a promising approach for developing multifunctional biomaterials (Christenson et al., 2007).

2.5.3 Third-generation membranes

By reviewing the previous absorbable and non-absorbable membranes, interests should arise in developing a new membrane which has a more advanced role as a barrier membrane and has an additional function such as releasing beneficial agents such as bioceramic, antibiotics, growth factors, and adhesion factors into the wound. The substance-releasing membrane should have a proper release time according to the environment of the graft site (Bottino et al., 2012).

2.5.3.1   Resorbable Membranes Based on Polymer Composites:

- **Polymer Blends**

Polymer membranes must meet a few key criteria for successful guided bone and tissue regeneration (GBR and GTR, respectively), appropriated mechanical and physical properties, a suitable degradation profile, as well as the necessary strength to provide an effective barrier function and resist decomposition (Zupancic *et al.*, 2015). Due to a variety of requirements, a single polymer fails to meet all critical criteria. For instance, naturally occurring polymers cannot provide the required mechanical strength and suitable degradation profiles, while synthetic polymers are unable to interact with biological tissues. On the other hand, polyester membranes turn rigid and brittle after introduction to phosphate buffered saline or artificial saliva solution (Owen *et al.*, 2010).

Therefore, the issue of developing membranes with the necessary mechanical properties, the expected rate of decomposition, as well as a structure similar to the natural extracellular matrix (ECM) remains topical (Zhang *et al.*, 2016). A potential solution is to combine two or more polymers in order to offset their disadvantages and find a mutually reinforcing effect.

- **Natural Polymer and Synthetic Polymer Blends**

Natural polymers are known for their increased biocompatibility and bioactive properties compared to synthetic counterparts. For instance, gelatin shows multiple integrin-binding sites to promote cellular adhesion and differentiation (Shi *et al.*, 2014; Xue, He, Liang, *et al.*, 2014). Mixing polymers of natural and synthetic origin should provide opportunities for taking advantage of both of them. For example, a material based on an amalgamation of gelatin with PCL has excellent biocompatibility as well as the essential mechanical, physical, and chemical qualities. Its unique properties allow it to be used in cartilage tissue engineering (Xue *et al.*, 2013; Zheng *et al.*, 2014), neural tissue engineering (Gupta *et al.*, 2009), as well as GBR and GTR (Ji *et al.*, 2013; Shi *et al.*, 2014; Xue, He, Liang, *et al.*, 2014). That being said, chemical segregation between PCL molecules and gelatin is a factor inhibiting the development of composites with the required characteristics.

It has been found that acetic acid can favourably affect the rate and strength of miscibility between PCL and gelatin. For this reason, it is effective for implementation when homogeneous nanofibers with improved performance are required (Feng *et al.*, 2012; Xue, He, Liu, *et al.*, 2014).

The biodegradation period of such membranes is also appropriate for tissue regeneration (Xue, He, Liu, *et al.*, 2014).

The PLLA/chitosan multilayer membrane proposed by Ku *et al.* (2009) has shown excellent potential for utilisation in GBR and GTR. The membrane has external chitosan netting that promotes the adhesion of cells from nanoporous PLLA located in the middle layer. This layered structure allows for improved mechanical strength and integrity preservation for up to eight weeks.

- **Natural Polymers Blends:**

Despite its natural origin, the bioactivity and mechanical properties of chitosan are inferior to those of protein polymers. In order to improve its properties, chitosan is often blended with other polymers. Due to the presence of free carboxyl groups in the structure of gelatin, it successfully blends with chitosan and forms a stable hydrogen bond with it. The ability of gelatin/chitosan membranes to maintain cellular adhesion and proliferation is better than that of gelatin and chitosan on their own (S. Kim *et al.*, 2005). Moreover, the enhancement by proanthocyanidin gives the gelatin/chitosan bond greater stability and improves its mechanical properties compared to membranes constructed from gelatin or chitosan and gelatin blend (S. Kim *et al.*, 2005). An example of the successful integration of natural polymers is a three-layer membrane with a chitosan interlayer sandwiched between two collagen membranes featuring 20 wt % HA (Teng *et al.*, 2008). Hunter and Ma,(2013) have shown that membranes based on hydroxyapatite/chitosan/gelatin can promote the growth of bone marrow mesenchymal stem cells (hBMSC) whilst improving the pace of osteogenic differentiation. Research data assures that gelatin/chitosan or collagen/chitosan membranes possess adequate mechanical and structural properties to be implemented as a barrier membrane. Therefore, they demonstrate the potential to be used in bone and tissue regeneration.

- **Synthetic Polymer Blends**

PLA, PLGA, PCL, and some other aliphatic polyesters are essential components for the production of fibrous scaffolds required for drug delivery systems and tissue regeneration (Jiao and Cui, 2007). At the same time, PLGA is characterised by reduced mechanical strength, which makes it impossible to maintain the scaffolding structure during *in vitro* and *in vivo* clinical trials. When PLGA was reinforced with other polymers such as PCL, applied in an equal ratio, the compressive strength of the PCL/PLGA scaffolding was far superior to the strength ensured by

PLGA alone (Kim *et al.*, 2009). Cytological investigations have demonstrated that penetration of human embryonic kidney 293T cells can be prevented by using PDLLA/PLGA electrospinning devices with an appropriate degradation rate and effective cell occlusion for the purpose of GTR. In addition, implantation of a subcutaneous implant in rats demonstrated that PDLLA/PLGA membranes with a composite ratio of 70/30 and 50/50 are able to double as a physical barrier that stops cellular infiltration for a duration of 13 weeks (Zhang *et al.*, 2016). This data suggests that PDLLA/PLGA membranes can become an effective barrier membrane for tissue regeneration purposes (Zhang *et al.*, 2016). Along with this, composite membranes fabricated from PLA/PCL, PLGA/PCL, and other synthetic compounds may be deemed as a promising technology for GBR and GTR (Kim *et al.*, 2009; Vaquette and Cooper-White, 2013; Xu, Cui and Chang, 2013).

Floreon™ blend

Floreon is a new sustainable polymer blend created by Floreon-Transforming Packaging Limited in collaboration with the University of Sheffield and certified by the EN13432 standard (Floreon 3D, 2014; Floreon, 2018). Based on PLA, Floreon is composed of renewable components, which is likely to improve its mechanical and chemical properties (Floreon 3D, 2014; Floreon, 2018).

In comparison to pure PLA, Floreon exhibits a remarkable four-fold increase in strength and is less susceptible to cracking and breakage during the manufacturing process and testing phases, as demonstrated by Floreon 3D (2014) and Floreon (2018). The compound has a maximum tensile strength of about 1.6 GPa while the elongation at break (fracture strain) is 14% (*Floreon 3D*, 2014; *Floreon*, 2018; Standardization, 2018). Moreover, in comparison to PLA, Floreon exhibits enhanced thermal performance. It has a melting point of 210 °C (Floreon 3D, 2014; Floreon, 2018; Lee, Sapuan and Hassan, 2018), a crystallisation temperature of 85 °C (Lee, Sapuan and Hassan, 2018), and a glass transition temperature of 65 °C. Floreon is extruded at temperatures between 170 and 180 °C. However, since its destruction threshold is 250 °C (Floreon 3D, 2014; Lee, Sapuan and Hassan, 2018), technological processes should not exceed 220 °C. In order to prevent moisture absorption, the material is dried at 65–90 °C after crystallisation (Floreon 3D, 2014). Floreon may undergo thermoforming, compounding, and injection moulding processes in addition to extrusion (including film extrusion).

There are currently eight Floreon variants labelled in the range FL100-FL800 (Floreon 3D, 2014; Floreon, 2018). Due to its resilience to ultraviolet radiation, the Floreon blend is more effective than PLA for 3D printing and lithographic printing (Floreon 3D, 2014; Floreon, 2018).

Although the Floreon was originally designed for the packaging industry, it has recently been investigated as a scaffold for musculoskeletal applications. The conclusion drawn is that the Floreon blend showed great promise for use in bone tissue regeneration (Ramos-Rodriguez *et al.*, 2022).

- **Bio-ceramic/polymer composites**

The incorporation of polymer composites, bioceramic components, and the structural mimicry of bone extracellular matrix (ECM) can be advantageous for the development of biomaterials that are used for guided bone regeneration (GBR) and guided tissue regeneration (GTR) (Bottino *et al.*, 2012). Hydroxyapatite (HA) (Bottino, Thomas and Janowski, 2011), carbonated hydroxyapatite (CHA) (Liao *et al.*, 2005), bioactive glass (BG) (Rowe *et al.*, 2016), β-calcium phosphate (β-TCP) and other bioceramics have been widely used in bone tissue engineering and shown to have excellent biocompatibility and osteoconduction properties (Shim *et al.*, 2013, 2014).

The use of bioactive ceramics in GTR and GBR has a positive impact on mineralisation and cell activity boost on polymer membranes, which suggests the required osteoconductivity and osteoinductivity (Yang *et al.*, 2009; Mota *et al.*, 2012; Leal *et al.*, 2013; Zhao *et al.*, 2015; Rowe *et al.*, 2016). On top of that, bioactive compounds are capable of affecting mechanical properties in a beneficial way (Li *et al.*, 2015). While pure PLGA has a tensile strength of 0.49 MPa, the inclusion of 10–30 wt % nanoapatite into a membrane helps lift it to 0.61 MPa (Jamuna-Thevi *et al.*, 2014). At the same time, the introduction of bioceramics is able to neutralise the acidic derivatives of PLA, chitosan, and other polymers formed due to their decomposition in an alkaline medium (Peter, Binulal, *et al.*, 2010; Mota *et al.*, 2012; Qasim *et al.*, 2015). According to Khan *et al.*, (2008), composite membranes have the ability to effectively and biomimicking preserve the structural and biological functions of damaged dense tissues.

Because hydroxyapatite is osteoinductive, it accelerates bone regeneration and allows the bio-ceramics component to connect directly to the regenerated bone, bypassing connective tissue. The composite has found wide application in orthopaedic surgery and dentistry dealing with hard

tissue restoration (Porter *et al.*, 2004; Rezwan *et al.*, 2006; Bianco *et al.*, 2007). Inorganic-organic composites that emulate the structure of human bone offer increased toughness inherent in polymeric materials and the compressive strength characteristic of inorganic components. Their beneficial nature makes it possible to create bioactive materials with improved mechanical properties and degradation profiles. Such composites are stable enough since the alkalinity of the inorganic fraction (for example, hydroxyapatite) balances the acidic substances formed during the autocatalytic decomposition of polymers (such as PLA) (Ferraz, Monteiro and Manuel, 2004). Fabricated PCL/nHA nanocomposites possess properties characteristic of HA ceramics and simultaneously provide the qualities of synthetic polymer PCL, namely, osteoconductivity and biocompatibility (Rezwan *et al.*, 2006; Bianco *et al.*, 2009). Studies of poly (lactic acid) (PLA) nanofibers containing hydroxyapatite filler showed that HA contributes to the improvement of the mechanical and thermal features of the nanofibers (Sonseca *et al.*, 2012). In addition, testing of the β-chitin-HA composite membrane made it possible to detect inclusions of apatite on the surface of β-chitin membranes. This finding indicates increased biocompatibility and provides a suitable foundation for successful cell attachment, adhesion, and proliferation (Madhumathi *et al.*, 2009).

Bioactive glasses (BSs) are osteoconductive and osteoinductive silica biomaterials with a SiO2-CaO-P2O5 structural grid. The introduction of BG stimulates osteogenesis and angiogenesis both *in vitro* and *in vivo* (Xynos *et al.*, 2001; Gorustovich, Roether and Boccaccini, 2010), and also generates high-performance collagen composites in imitation of bone mineralisation. In particular, it is involved in the release of Ca, P, and Si and the subsequent deposition of Ca and P as well as amorphous Ca-P crystals on the implant surface. The following chemical dehydration reactions convert these crystals to hydroxycarbonate apatite (HCA) (Izquierdo-Barba *et al.*, 2008). In a similar way, wollastonite ($CaSiO_3$) gives up Si and Ca ions, which induce the acceleration of osteogenic differentiation and cell multiplication. Simultaneously, this can lead to deposits of bone-like apatite on the surface of the implant after it has been introduced to simulated body fluids (SBF) (X. Li and Chang, 2005; Wang *et al.*, 2015). Wollastonite exhibits the capability of increased structural mechanical strength, angiogenesis, and bone regenerative capacity. Despite this, it should be subject to further research to identify the bioactivity, osteogenic capacity, and immunogenicity of polymer composites when implanted in humans. These studies are driving the development of polymer/bioceramic based composites offering the advantages of both components (Ramos-Rodriguez *et al.*, 2022).

Table 2-3 List of some commonly used barrier membranes for GTR/GBR therapy.

Resorbability	Barrier membrane	Composition	Main characterisation	Comments	Ref.
(a) Nonresorbable	Gore-Tex®	Expanded polytetrafluoroethylene (e-PTFE)	- Good space maintainer. - Relatively stiff - Handling	-Longest clinical experience	(Becker *et al.*, 1991; Villar and Cochran, 2010)
	Cytoplast® TXT-200	High-density polytetrafluoroethylene (d-PTFE)	- Pores with submicron (0.2 μm) size - Density precludes colonisation of the host flora and prevents the infection.	-Avoids a second surgery	(Bartee, 1995; Barber *et al.*, 2007)
	Gore-Tex-TI®	Titanium reinforced expanded polytetrafluoroethylene (Ti-e-PTFE)	- Most stable space maintainer, requires no filler material	- Titanium should not be exposed - For recession, ridge augmentation	(Jovanovic and Nevins, 1995; Lindfors *et al.*, 2010)
(b) Resorbable: natural	Bio-Gide®	Collagen derived from porcine skin (types I and III)	- Barrier function At least 6 weeks bioactive	- Usually employed in combination with filler substances	(Zhao *et al.*, 2000; Taguchi *et al.*, 2005; Gielkens *et al.*, 2008; Zwahlen *et al.*, 2009)
	BioMend Extend®	Collagen type I derived from bovine tendon	- Resorption: 4–8 weeks - Collagen complexed with formaldehyde	- Collagen network extends the resorption time	(Maksoud, 2001; Sela *et al.*, 2003)
(c) Resorbable: synthetic	Guidor	Poly-DL-lactid/ Poly-L-lactid + acetyltributylcitrate	- Double-layered membrane. - Outer: large pores - Inner: finer pores	- No commercially available	(Gottlow, 1993; Miller *et al.*, 1996; Araujo, Berglundh and Lindhe, 1998)

Resolut	Poly-DL-lactid/Co-glycolid	- Resorption: 10 weeks - Functional integrity - Good space maintainer	- Good tissue integration - Separate suture material	(Pontoriero, Wennström and Lindhe, 1999; Zhao *et al.*, 2000; Donos, Kostopoulos and Karring, 2002)
Vicryl	Polyglactin 910: Polyglicolid/polylactid 9:1	- Relatively soft - Well adaptable - Resorption:4-12 weeks	- Woven membrane. - Four prefabricated shapes	(De Sanctis and Zucchelli, 1996; Zhao *et al.*, 2000; Thoma *et al.*, 2009)
Atrisorb	Poly-DL-lactide and solvent (N-methyl-2-pyrrolidone)	- Soft Well-adaptable - Interesting resorptive characteristics	- Customised membrane fabrication with "Barrier Kit"	(Camargo *et al.*, 2002; Hou *et al.*, 2004)
Epi-Guide	Poly-DL-lactic acid	- 3-layer technology. - Bioresorption: after 6–12 months	- Self-supporting, can be used without support from bone grafting materials.	(Takata, Miyauchi and Wang, 2001; Bilir *et al.*, 2007)
Vivosorb	Poly(DL-lactide-□-caprolactone) (PLCL).	- Anti-adhesive barrier. - Maintains its mechanical properties for up to eight weeks.	- Commercially available as a nerve guide	(Meek *et al.*, 2004)

Table 2-4 Types of biomaterials used in guided regeneration therapy.

Class	Example	Advantages	Disadvantages	Ref.
Polymers- Natural proteins	**Collagen, fibrin, alginate, silk fibroin, Hyaluronic Acid**	• Biocompatible • Biodegradable without inflammation bioactive	• Poor mechanical strength • Rapid resorption	(Sela *et al.*, 2003; Taguchi *et al.*, 2005; Thomas *et al.*, 2007; Wikesjö *et al.*, 2009)
Polymers- Natural Polysaccharides	**Chitosan**	• Biodegradable • Biocompatible • Has an antibacterial and bioadhesive properties • Promote wound healing	• Poor mechanical strength • Rapid resorption	(Thein-Han and Kitiyanant, 2007; Alizadeh *et al.*, 2013; Pighinelli and Kucharska, 2013)
Polymers- Synthetic	**Polyglycolic acid (PGA)**	• Versatile • Reproducible • Thermoplastic so it can be shaped easily	• Inflammatory or immune reaction due to acid release in enzymatic biodegradation • Mechanical stability is of limited duration • Less biocompatible than natural • Not bioactive • Rapid resorption • Low solubility in organic solvent	(Agrawal *et al.*, 2000; Nair and Laurencin, 2007; Place *et al.*, 2009; Bhattarai *et al.*, 2018)
	poly-L-lactide acid (PLLA)	• Degrades slower and dissolves easier than PGA • Reproducible	• The potential to cause immune and foreign-body reactions because it does nor degrade completely • The mechanical stability is of limited duration	
	poly-ε-caprolactone (PCL)	• Slow degradation rate • Reproducible • Good workability	• Inflammatory or immune reaction • Mechanical stability is of limited duration	

Class	Example	Advantages	Disadvantage	Ref.
Polymers-Synthetic	**Hydrogel**	• Modified easily • Biocompatible • Biodegradable	• Contracted • Lack stiffness	(Agrawal *et al.*, 2000; Nair and Laurencin, 2007; Place *et al.*, 2009; Bhattarai *et al.*, 2018)
Metal	**Titanium mesh**	• High mechanical strength and fracture toughness • Biocompatible	• Corrosion may release toxic particles affecting the biocompatibility and induce an inflammatory reaction • Poor stimulation of new bone formation due to the elastic moduli which does not correspond with natural bone	(Jovanovic and Nevins, 1995; Kedem *et al.*, 2005; Fontana *et al.*, 2008)
Ceramic	**HA**	• Biocompatible. • Osteoconductive • Similar to the chemical structure of inorganic phase of bone.	• Slow biodegradation • Difficult to shape due to hardness, fragility, and brittleness	(Sun, Zhou and Lee, 2011; Sulaiman *et al.*, 2013)
	TCP	Same to above	• Rigid and fragile • Faster resorption rate	(Cao and Kuboyama, 2010; Sulaiman *et al.*, 2013)
	Bioglass	• Biocompatible • Osteoconductive • Bioactive • Promote angiogenesis • Enhance cell adhesion and proteins adsorption • Easy to control the chemical composition • Controlled degradation rate	• Brittleness • Low resistance to crack due to low strength and fracture toughness	(Fabbri *et al.*, 2010; Abdollahi, Ma and Cerruti, 2013)

Class	Example	Advantages	Disadvantage	Ref.
Composite	**PGA/β-TCP**	• Better ability for osteogenesis, mineralisation and biodegradation than HA	• Lack of osteoinductivity	(Cao and Kuboyama, 2010)
	Bioglass 45S5 and poly (D, L-lactide) polymer	Improved mechanical properties and resorption rate	Reaction with polymer changes the bioglass surface properties and compromised its bioactivity	(Fabbri *et al.*, 2010)
	Poly (b-hydroxybutyrate co-b-hydroxyvalerate) (PHBV) microsphere and poly (L-lactic-coglycolic acid) (PLGA).	• Supports drugs and growth factors delivery	• Changes in the surface topography and decrease porosity due to dehydration shrinkage	(Huang *et al.*, 2010)
	hyaluronic acid-gelatine	• Good mechanical property Biocompatible • High porosity • Hydrophilic	• Suboptimal cell adhesion due to negative cell-scaffold interaction	(Linh, Min and Lee, 2013)
	Nano HA/polymer	• Promote better cell adhesion and distribution • No significant nflammatory response • Biocompatible Improved mechanical properties	Unknown mechanism of cellular proliferation and differentiation	(Basile *et al.*, 2015)

2.6 Multiphasic scaffolds of periodontal tissues regeneration

A multiphasic scaffold is defined by the differences in its architecture (porosity, pore organisation, etc.) and its chemical composition, which usually mimics to some degree the structure or cellular and biochemical composition of the native tissue. Multiphasic scaffolds are designed to impart biomimetic functionality to tissue-engineered bone and soft tissue grafts have been recognised for some time as having the potential to facilitate clinical translation in the field of orthopaedic tissue engineering, and more recently in the field of periodontal tissue regeneration (Zhang *et al.*, 2019).

In recent years, guided tissue regeneration and guided bone regeneration (GTR and GBR) approaches have been widely used to manage periodontitis. These membranes have separate functions on each side. The occlusive periodontal membrane acts as a barrier to inhibit the ingrowth of epithelial and undesirable tissues into the defective area during periodontal wound healing, whereas the opposite side promotes regeneration of periodontal tissues (Retzepi and Donos, 2010; Zhang *et al.*, 2019). GTR/GBR membranes must have certain features, particularly those utilised in large-area repair, such as mechanical stability, osteoconductivity, and a balance between membrane degradation and tissue regeneration, all of which are required for the membranes to function (Zhang *et al.*, 2019). In a number of studies, bilayer GTR/GBR membranes have been utilised as a treatment for periodontal diseases; here are a few examples from the last few years.

The Yoshimoto group has recently developed bilayer membranes based on PLGA or PCL (Yoshimoto *et al.*, 2018; Abe *et al.*, 2020). These membranes consisted of a solid layer and a porous layer that, respectively, served as a barrier and provided cell support. By changing the freeze-drying temperature, they were able to control the thickness of each layer. These membranes were found to be more functional than monolayer membranes, with evidence suggesting that their porous structure aided in the osteogenic differentiation and proliferation of mesenchymal stem cells. *In vivo* studies also demonstrated that the PLGA bilayer membrane promoted bone regeneration with significantly increased bone formation compared to that with a monolayer membrane (Yoshimoto *et al.*, 2018).

Requicha *et al.*, (2016), in a related method, created a biphasic scaffold made of a porous fibrous PCL/starch scaffold for enabling bone ingrowth and an occlusive membrane developed using the same matter. In this technique also, the occlusive membrane was devised to sustain periodontal ligament regeneration by inhibiting epithelial and gingival tissue invasion of the periodontal defect, hence carefully choosing osteoblast and periodontal fibroblast ingrowth as per the GTR law. After doing *in vitro* analyses, Requicha *et al.*, (2014) and Requicha *et al.*, (2016) discovered a high potential for osteogenesis, which is a key aspect of periodontal regeneration.

Park *et al.*, (2010) suggested an approach that involves computer-assisted design and manufacturing (CAD/CAM), using two dissimilar sacrificial instruments to 3D print a mould with the negative imprint of the scaffold design. This method directly uses additive manufacturing technology to create a biphasic scaffold consisting of bone and ligament compartments (Park *et al.*, 2010). Later, polymer solutions specific to each compartment (polyglycolic acid and polycaprolactone for bone and ligament compartments, respectively) were tossed into these moulds. Consequently, the solvent evaporated before getting rid of the sacrificial material. The resultant porous scaffold had defined dimensions and shape and a definite internal pore architecture. In the process of developing the two compartments independently, they were consequently gathered by utilising a thin PCL film, hence developing into a biphasic scaffold (Park *et al.*, 2010). The researchers used fibrin to deliver BMP-7-transfected human gingival fibroblasts and human periodontal fibroblasts into the bone and periodontal ligament compartments, correspondingly. The usefulness of the cellularised biphasic scaffold was monitored by means of a murine ectopic model while a human dentin block was placed in the periodontal ligament compartment. This process showed that the presence of periodontal cells to a high degree enabled the attachment of a freshly developed ligament onto the dentine slice together with the sedimentation of cementum-like tissue 6 weeks before implantation (Park *et al.*, 2010).

Focusing on guided bone regeneration, which is the focal point of this project, Zhang *et al.*, (2019) have recently studied the most commonly utilised GBR membrane, known as Bio-Gide, which is among the most commonly used commercial biodegradable membranes, and has a wide range of advantages. Bio-Gide possesses a bilayer makeup in which one of the sides is structured to be compact and soft to inhibit epithelium and connective tissue interference on the other side of bone defects, and the opposite side is permeable and coarse to enable the bond of osteoblasts next to the bone defect.

The aforementioned experts described a unique form of multifunctional GBR membrane with similar design characteristics as those of the Bio-Gide membrane but including extra roles that the Bio-Gide membrane cannot accomplish. The unique GBR membrane is made up of a compact nacre-like coating and a permeable membrane. The function of the nacre-like layer is to give great mechanical properties and also to inhibit non-osteoblast interference. Conversely, the porous layer has been designed with the aim of necessitating osteoblast adhesion. For a number of reasons, they asserted that their multifunctional nanocomposite membrane was better than the other GBR membranes. These reasons include: biocompatibility combination with the facial surface, high mechanical performance, sufficient rate of degradation, and efficacious bacteriostasis. For these

reasons, this type of nanocomposite membrane qualifies to be considered as a perfect bioactive GBR membrane for medical use (Eltom, Zhong and Muhammad, 2019; Zhang *et al.*, 2019).

By combining the electrospinning technique with emulsion templating, a bilayer barrier membrane (BM) made of a biodegradable synthetic polymer, PCL, was effectively developed by (Aldemir Dikici *et al.*, 2019). Some of the qualities exhibited by the resultant BM included the absence of delamination, a qualitatively resistant structure to twisting and elongation, and simplicity in handling. The electrospun layer of the BM has been proven to possess the ability to act as a barrier, offering protection to the bone defect against soft tissue interference. On the other hand, the interconnected PCL polyHIPE layer has exhibited pivotal characteristics to be the bone-enhancing layer, supplying crucial needs including boosting collagen and mineral deposition and enhancing cellular infiltration and cell compatibility (Aldemir Dikici *et al.*, 2019).

2.7   Scaffold manufacturing technologies

Based on the characteristics needed and the type of material used, one of several techniques can be used, many of which have been created with the specific purpose of creating porous scaffolds in order to be used in many applications. There are a variety of processes available, ranging from quick and inexpensive processes that result in a relatively low quality scaffold to complicated and time-consuming methods that result in high quality structures.

2.7.1 Solid free-form fabrication technique

SFFT is a manufacturing technique also recognised as rapid prototyping (RP), which also refers to a type of fabrication process called additive manufacturing (Yuan, Zhou and Chen, 2017).In which components are printed by depositing one cross-section layer over the other layer and assembled using a three-dimensional computer-aided design (CAD) model (Liu and Ma, 2004). Three-dimensional scaffolds with complex geometries and dimensionally accurate structures can be manufactured using data obtained from medical scans and then adjusted to meet the needs of each individual patient (Liu and Ma, 2004; Yuan, Zhou and Chen, 2017).

This process is accomplished through several phases. The first phase is based on creating a computer-aided design (CAD) model, which is then sent to a file that can be manipulated with a stereolithography apparatus. Automatically, the STL file is divided into horisontal layers throughout the pre-production phase. Then, printing continues in this layered process. The final structure needs to be hardened and its surface treated before being used (Yuan, Zhou and Chen, 2017). Through the use of sophisticated scanning techniques like magnetic resonance imaging (MRI) or computer tomography (CT) (Yuan, Zhou and Chen, 2017). These highly detailed 3D images can then be used

to make the creation of precise (Rezwan *et al.*, 2006), integrated scaffolds (Leong, Cheah and Chua, 2003) and significantly reproducible (Yuan, Zhou and Chen, 2017).This is particularly useful when making highly porous structures at about 90% or more of the total volume of the scaffold (Cao *et al.*, 2010).

Scaffolds with sophisticated and controlled macro-and microporous structures can be provided by SFFT, potentially both within the same structure (Rezwan et al., 2006). Table 2-5 compares the various SFFT types, which have been evaluated by different research groups (Leong, Cheah and Chua, 2003; Stevens *et al.*, 2008; Lee, Kim and Cho, 2010; Yuan, Zhou and Chen, 2017). This list includes their inherent advantages and disadvantages. SFFT is a modern development. It helps in creating solutions rather quickly, but not all types of SFFT can be used for scaffold manufacturing (Leong, Cheah and Chua, 2003; Stevens *et al.*, 2008; Lee, Kim and Cho, 2010; Yuan, Zhou and Chen, 2017).

Table 2-5 Different types of SFFT with their advantages and disadvantages.

Techniques	Materials	Advantages	Disadvantages	Ref.
Stereolithography (SL)	PEG, PEGDA, PPF, PCL, PDLLA	High accuracy, complex 3D structure including agents and cells, easy removal of photopolymer by heating	Photo-polymerisation of materials, photocurable materials, expensive materials and equipment	(Leong, Cheah and Chua, 2003; Stevens *et al.*, 2008; Lee, Kim and Cho, 2010; Yuan, Zhou and Chen, 2017)
Fused deposition 68odelling (FDM)	Thermoplastic polymers and their composites (PVA, ABSP400)	High porosity, complete pore interconnectivity, possibility of controlling porosity and size of pores, macro shape control, good compressive strength, solvent-free	High processing temperature, limited material range, inconsistency in pores,	
Selective laser sintering (SLS)	Polymer ceramics (PCL, Hap, TCP)	Complex structure, possibility of controlling porosity and size of pores independently, wide range of powder materials, solvent-free, any secondary binder system	High processing temperature, using only thermally stable polymers, limited to small pore size	

3D printing (3D-P)	Ceramics, polymers, metals	Easy process, high porosity, complete pore interconnectivity, possibility of controlling porosity and size of pores independently, macro shape control, wide range of materials	Use of toxic organic solvent, lack of mechanical strength, limited to small pore size	

2.7.2 Three-dimensional bioprinting technique

Bioprinting is an additive manufacturing technique in which several biological materials are incorporated with extreme precision to create structures that mimic living tissues. This process offers the option of scaling it down or up depending on the patient's needs. Furthermore, it allows for the distribution of cellular components, like growth factors and proteins, as well as cells themselves and drug particles. These positive circumstances have led to the creation of solutions that include many clinically relevant applications such as drug examination, high-throughput assays, tissue engineering, various medical applications for tissue regeneration, and cancer research (Ozbolat, Peng and Ozbolat, 2016).

In particular, the printing of blood vessels and organs has been a difficult endeavour, even with modern techniques, due to the necessity to couple a variety of cell types, the limited amount of structural support available, as well as the coupled capillary network normally associated with functional organs (Ozbolat and Yu, 2013).

Research has kept advancing, though, and a few simple capillaries and tissues have been printed, such as blood vessels, skin, and cartilage without blood supply (Aljohani *et al.*, 2018). There have been some attempts to print bone, especially bone that includes its natural components, such as nerve and muscle tissue. Unfortunately, research is still needed since these structures are still functionally inferior to naturally-occurring ones (Datta *et al.*, 2017).

2.7.3 Gas-foaming technique

With this technique, there is no longer a need to use solvents that are normally present in the previously mentioned methods. This method creates a porous network through the dispersion of gas bubbles that, when the material is hardened, act as pores, as illustrated in Figure 2-8. A heated mould is used to heat the polymer material, which is usually made of polylactic-co-glycolic acid, which is then moulded by compressing it to make rigid discs. After this, these moulded structures are pumped with high pressure (5.5 MPa) CO2 for 3 days at 25°C. Afterward, gas pressure is reduced to atmospheric levels and, therefore, gas solubility is reduced. This process makes CO2 gas create inner clumps, which then create the pores needed for the proper function of the implant. This method allows for the total number of porosities to reach up to 93% and sizes of about 100mm. It is not trivial, however, to control pore size and interconnectivity with this technique (Liao *et al.*, 2002; Dehghani and Annabi, 2011).
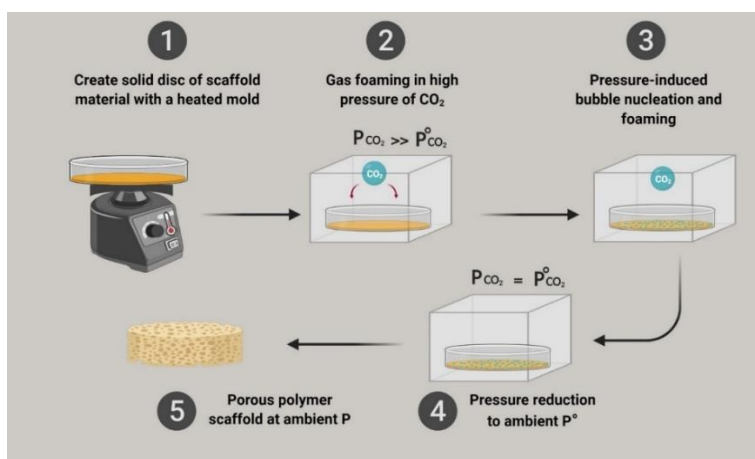
Figure 2-8 Schematic illustration of the gas-foaming technique, [source: (Puppi et al., 2010), redesigned with copyright permission from Elsevier licence number: 4724150945567, dated Dec 08, 2019].

2.7.4 Thermally induced phase separation technique

A procedure that allows for the fabrication of highly-porous anisotropic scaffolds is called Thermally Induced Phase Separation (TIPS). These polymer scaffolds can be controlled with ease but have a low ability to be applied to affected tissues such as ligaments, muscles, nerves, intestines, and osseous structures (Liang *et al.*, 2013). Depending on the concentration of polymer used, certain characteristics will change, such as mechanical properties, pore shape, biological activity, and the rate of resorption. Furthermore, these properties will change depending on the volume of the phase separation (Liu and Ma, 2004). A polymer phase fraction can be achieved by dissolving a polymer

at a high degree of temperature in a certain solvent, then cooling the homogenous polymer/solvent solution to obtain a polymer porous scaffold. After this process is completed, a microporous scaffold can be obtained immediately after the solvent has evaporated, as schematically shown in Figure 2-9 (Liang *et al.*, 2013).
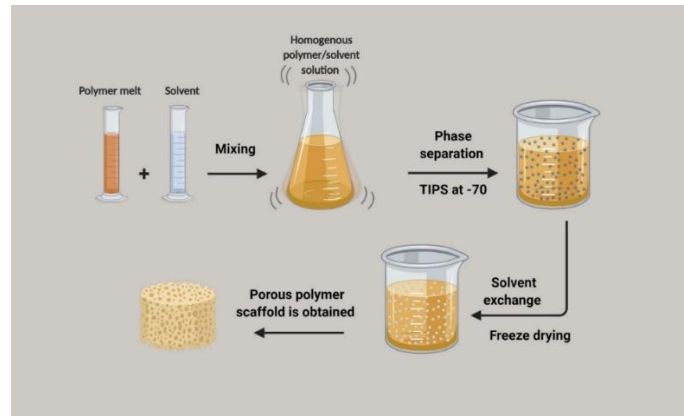
Figure 2-9 Schematic representation of the porous scaffold fabrication process with the Thermally Induced Phase Separation (TIPS), [source: (Puppi et al., 2010), redesigned with copyright permission from Elsevier licence number: 4724150945567, dated Dec 08, 2019].

2.7.5 Emulsion freeze-drying technique

This technique is based on the phase fraction through the use of different physical properties of the fibre by emulsifying the solution and then drying it at a very low temperature (Mikos and Temenoff, 2000), and producing a scaffold that has abundant pores, as illustrated in Figure 2-10.

The first step in this process is the creation of the emulsion by homogenising a polymer in a carbon-based solvent and water. This emulsion must be quickly frozen and the formed phases (solvent and water) are then eliminated by freeze-drying the sample. The resulting polymer scaffolds will have pores of between 20 and 200 µm (Liu and Ma, 2004). This method could be combined with the third method that was mentioned, as well as adding crystal-forming polar compounds like sucrose or NaCl, in order to further increase porosity. Once the sample has been dried, these particles can be cleared with the use of water (Alizadeh *et al.*, 2013).
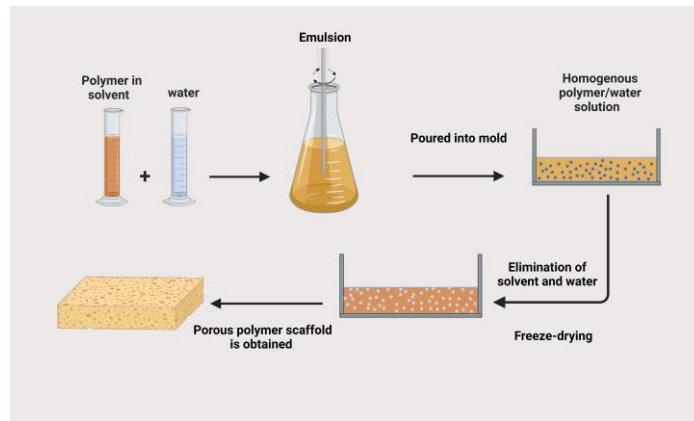
Figure 2-10 Schematic illustration of the freeze-drying process, [source: (Puppi et al., 2010), redesigned with copyright permission from Elsevier licence number: 4724150945567, dated Dec 08, 2019].

2.7.6 Solvent casting and particulate leaching technique

Another common method for making scaffolds is solvent casing. This process starts with the deconstruction of a polymer in a carbon-based solvent, as schematically shown in Figure 2-11. The aforementioned method uses "porogens", a group of chemical compounds that can be distributed into a structure during the manufacturing process and then taken away through the use of water, leaving behind a porous structure. These porogens can create a coupled polymer-porogen structure when added to the overall solution. As soon as the polymer reaches its final form and starts hardening, and the original solvent evaporates away, water is then used to dissolve porogens, which is often a high polarity compound, such as NaCl. Although it is hard to control the final inner structure of the scaffold since it is difficult to predict and control where the porogen particles will be distributed and then dissolved, a 3-dimensional porous polymer scaffold was obtained (Liao *et al.*, 2002; Johnson *et al.*, 2010).
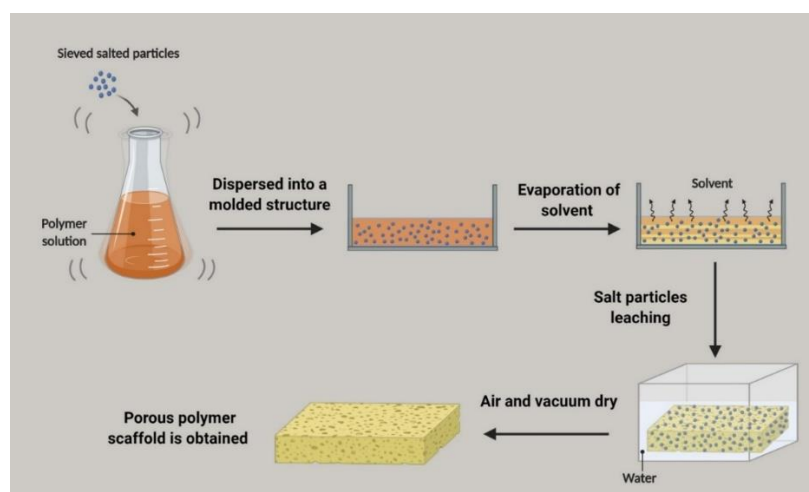
Figure 2-11 Schematic illustration of the solvent casting and particulate leaching technique,[source: (Puppi et al., 2010), redesigned with copyright permission from Elsevier licence number: 4724150945567, dated Dec 08, 2019].

2.7.7 Spin-coating technique

The spin coating technique is a widely used method for depositing thin films of materials onto a flat substrate. In this technique, a liquid solution containing the scaffold material is dispensed onto the substrate, which is then rotated at high speeds (typically in the range of 1000 to 4000 rpm).The centrifugal force generated by the spinning substrate causes the solution to spread out evenly over the substrate, forming a thin film. The speed and duration of the spinning process can be controlled to achieve a desired thickness and uniformity of the film.

In Figure 2-12, a schematic outline of the spin coating process is shown. The figure depicts the substrate, the spin coater, and the solution being applied to the substrate. As the substrate is spun, the centrifugal force pulls the solution towards the edges, creating a thin and uniform film on the substrate.

The advantages of the spin coating technique include its simplicity and cost-effectiveness, as well as its ability to produce films with precise control over their thickness and uniformity. This technique can also be easily combined with other techniques to create complex multilayered structures, such as for periodontal tissue regeneration.
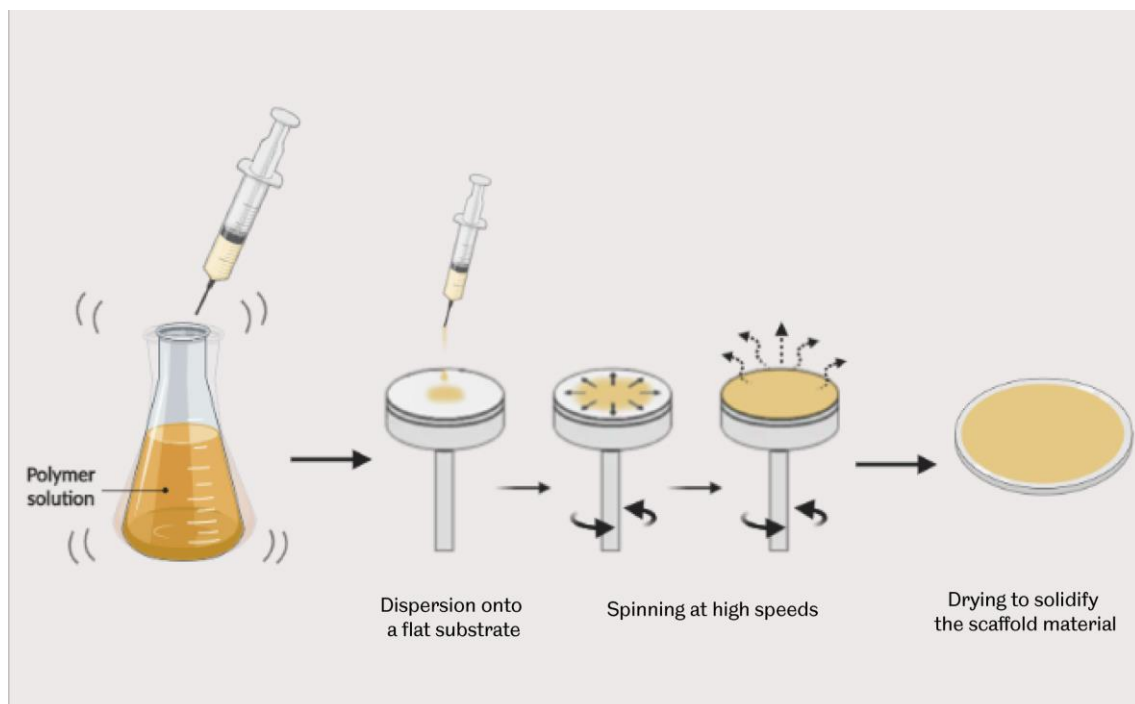
Figure 2-12 Schematic illustration of the spin coating technique, illustrating the steps involved in fabricating a scaffold.

2.7.8 Limitations of the preceding manufacturing techniques

In practice, the techniques used to manufacture scaffolds are divided into solid free-form fabrication and conventional methods. Each of them produces various scaffolds with distinctive characteristics (Roseti *et al.*, 2017). Even though SFFT provides a plethora of potential opportunities for tissue engineering and possesses undeniable advantages, there are some inherent drawbacks that must be considered. Firstly, each method uses a very specific fabrication material. SLS uses a fine powder, whereas the use of thermoplastics is more efficient for FDM. Even when the selected material is appropriate, if it is difficult to prepare, it can make the whole process much more challenging. Secondly, the fact that a material can be successfully printed does not guarantee its proper function, since successful scaffolds also require constructs to maintain their integrity throughout their layers. The material must be able to support itself after its fabrication, maintaining its integrity layer by layer. Thirdly, in the case of the printing of biological tissues, novel material solidification techniques that are used to preserve the fabricated scaffold integrity should be developed (An *et al.*, 2015). Lastly, when using materials that are cell-loaded, the flexibility of print parameters such as shear stress or temperature is restricted. This happens since cell environments are ever changing, and doing so would be deleterious for cell survival (Nair *et al.*, 2009).

While conventional techniques of scaffolding fabrication include the construction of porous polymer structures such as substrates for cell adhesion, it is difficult to obtain complex structures with tunable microscale and macroscale using conventional methods (Abdelaal and Darwish, 2013). In addition, some of these methods are manual-based. Therefore, they are labour-intensive and difficult to reproduce. Another limitation is the need for organic solvents and porogens, which are cytotoxic and their residues may cause inflammatory responses (Hutmacher, 2000). Benefits and limitations of conventional and Solid Free-Form manufacturing techniques are discussed and summarised in Table 2-6 (Kumbar *et al.*, 2008; Eltom, Zhong and Muhammad, 2019).

Table 2-6 Comparison of different scaffold fabrication techniques: advantages and disadvantages, adapted from (Kumbar et al., 2008; Eltom, Zhong and Muhammad, 2019).

Manufacturing Method	Benefits	Potential Limitations
Gas Foaming	• Eliminates use of chemical solvents	• High pressures involved prohibits inclusion of cells and bioactive molecules directly into scaffolds • Temperature labile materials may be denatured during compression moulding step • Difficult to control pore sizes and ensure interconnectivity
Emulsification Freeze-Drying	• Does not require use of solid porogen	• Requires use of organic solvents • Small pore size and • Porosity often irregular • Long processing time
Phase Separation	• Eliminates leaching step of porogen • Can be combined with other techniques easily	• Small pore sizes limit use • Use of organic solvents inhibits use of bioactive molecules or cells during scaffold fabrication
3D Printing - SLA - Inkjet - SLS - Laser-assisted - FDM - Microvalve - Microextrusion	• Complex 3D shapes with high resolution, controlled pore size & morphology and controlled internal structures can be fabricated. Improved capacity to incorporate vascular structures into constructs • Depending on technique used, cells may be included in high concentration directly in scaffold materials.	• Some techniques are limited by printable materials • Set up costs can be expensive for machinery
Solvent casting/ particulate leaching	• Relatively simple technique that allows creation of scaffolds with regular porosity, controlled composition and pore size.	• Use of organic solvents precludes cells and biomolecules being included directly in scaffolds • Can be difficult to control pore shape and interconnectivity • Limited thickness of structures and mechanical properties achievable
Spin-coating	• Simple and cost-effective method. • Precise control over the thickness and uniformity of the film.	• Requires optimization of parameters such as the spinning speed and duration for each specific material and substrate combination.

Electrospinning	• Essential technique for developing nanofibrous scaffolds for the TE • Homogeneous mixture made of fibres with high tensile strength. • Simple instrument • Continuous process • Cost effective compared to other existing methods • Scalable • Ability to fabricate fibre diameters few nm to several microns.	• Used solvents can be toxic. • Jet instability • Packaging, shipping, handling

2.8 Electrospinning for bone regeneration

Over the last ten years, electrospinning technology has become one of the most interesting methods for creating scaffolds used for tissue engineering. The creation of these nanofiber scaffolds has become the focus of research for many investigators due to their many unique properties, especially those which are clinically relevant. In particular, this method is used in order to manufacture nanofibers used in different applications in dentistry like tooth restoration, repair of oral mouth tissue, preventing tooth decay, and restoring other dental and periodontal tissues, such as the repair of dentin, endodontium, oral mucosa, periodontal tissue, as well as alveolar bone regeneration (Zafar *et al.*, 2016).

A type of material that has received a lot of attention recently has been biodegradable polymers, especially in biomedical areas such as bio-prosthetics, tissue engineering, and the application of drug delivery systems. Aliphatic polyesters are one of the most significant types of synthetic biodegradable polymers, owing in particular to their advantageous characteristics of biocompatibility and biodegradability. The main allure of these polymers (polyesters) is their biological compatibility and their ability to be degraded within the organ (Bikiaris *et al.*, 2007).

2.8.1 Set up conditions for electrospinning

Electrostatic spinning, most commonly known as electrospinning, has been a focal point of research for the last 20 years due to the various potential uses of the created microfibres in both nanotechnologies and nanoscience (Ramakrishna *et al.*, 2006). Notable characteristics, such as high permeability, large surface-to-volume ratio, and excellent pore interconnection, have made electrospun microfibres ideal for normal cell functions, such as nutrient and cell transportation (Agarwal, Wendorff and Greiner, 2009; Jang, Castano and Kim, 2009).

Additionally, the nanofibrous scaffolds manufactured through this method can provide excellent extracellular conditions, such as coupling, migration, and cell proliferation, especially for those cells in charge of hard tissue repair. Along with the simplicity of setup and cost efficiency, the opportunity to create microfibres with a large variety of physical and chemical properties is its own merit. This machine consists of a syringe needle, a grounded collector (metal plate), a high-voltage electrical source, and a syringe pump (Figure 2-13). The electrical source must carry around 10 to 30 kilovolts and is applied to solutions that are ejected via the syringe needle. When the electrical charge reaches the starting point, the surface tension of the charged solution begins to change, causing a deformation of the solution droplet into a conical droplet known as the Taylor cone. While the electrical force overcomes the surface tension of the charged solution, thin charged jets are ejected from the tip of the metallic needle in a nearly straight line towards the electrically inverse electrode. As the material is being extruded, the solvent is being evaporated away, resulting in the construction of continuous dry polymer fibres, which leads to the formation of a non-woven surface of the obtained fibres. The grounded collector surface is generally placed about 20 cm from the syringe's tip (Jiang *et al.*, 2015).
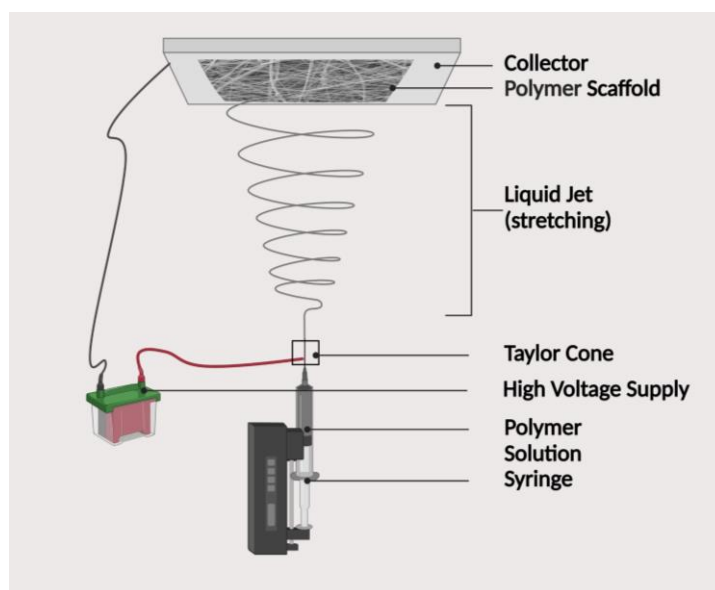
Figure 2-13 Example of electrospinning apparatus, source: (Puppi et al., 2010), redesigned with copyright permission from Elsevier licence number: 4724150945567, dated Dec 08, 2019

2.8.2 Electrospinning process: key variables

Many different variables must be taken into account which could alter the morphology of electrospun materials. which can be divided into the following:

- Properties of the polymer solution
- Electrospinning parameters

2.8.2.1 Solution parameters

The choice of a polymer and a solvating substance must be directed by their physical and molecular properties, such as atomic weights and concentrations of polymer. The choice of a polymer should always take into consideration the wanted structure and its characteristics, while the chosen solvating agent must adhere to the polymer's physicochemical properties (Shenoy *et al*., 2005). Furthermore, the selection of a solvent will affect the properties of the solution, such as surface tension, rate of evaporation, and conductivity. Whereas the polymer's molecular weight mainly influences the relaxation time of the polymer solution as well as its other physical properties such as viscosity. The number of crosslinks of each polymer chain can be controlled by the concentration of the polymer as well as its molecular weight, which also determines the ability of the overall polymeric solution to be processed into a nanofiber scaffold (Shenoy *et al*., 2005). The polymer's concentration is extremely important. The more saturated the solution is with the polymer, the less time it will take for the solvent to evaporate. Lastly, it is possible to add numerous chemical compounds to the solution in order to change some of its properties without needing to choose another polymer material, making the available choices per polymer more numerous (Shenoy *et al*., 2005).

2.8.2.2 Processing parameters

Many factors, such as electrical voltage delivered to the nozzle tip, the distance between the tip and the collecting screen (spinning distance) , solution flow rate, temperature ,humidity, type of the collector, and overall parameters of the used apparatus can influence the process of electrospinning, which leads to a significant change in the shape and function of the microfibres .

The flow rate is what dictates the amount of solution needed for electrospinning. A stable Taylor cone must be maintained at a certain voltage, which requires a corresponding flow rate for a certain voltage (Yuan *et al.*, 2004). When this ratio is low, this is obvious as there is a smaller amount of solution that is drawn away from the tip of the needle, whereas the jet of extruded material starts originating within the needle. On the other hand, at high polymer flow rates, larger droplets of solution will drop from the tip of the needle due to insufficient time for the electrospinning process.

It has been determined that the bead size as well as the diameter of the spun fibre both have a positive correlation to the flow rate of the solution. Basically, in order to produce an electrically charged jet of solution out of the Taylor cone, the applied voltage should be more than 6 kilovolts. It is important to know, however, that if the electrical voltage is increased, more solution will be extruded due to the repulsive electrostatic force that has overcome the surface tension of the charged solution (Ramakrishna, 2005).

Another factor that can adversely affect the electric field strength that is needed is the distance between the nozzle tip and the grounded collector. This distance will also determine the amount of time needed for the solvent to evaporate away. Additionally, the proportion of solvent evaporation is also dependent on the chosen solvent/polymer and its concentration as well as environmental factors. Things like temperature and humidity during the electrospinning affect the speed of the solvent evaporation rate in order to get completely dry microfibres. In the absence of sufficient time for the solvent to evaporate, the excess solvent can cause the fibres to fuse into junctions that lead to bonding between layers with each other. Lastly, the overall structure alignment of these fibres can be modified by changing the shape of the grounded collector; For instance, using a rotated target drum can provide a scaffold with a preferential fibre alignment in a specific direction (Wang, Ding and Li, 2013; Braghirolli, Steffens and Pranke, 2014). Table 2-7 summarises a number of the most important parameters discussed above that have an impact on the electrospinning process.

Table 2-7 Effect of changes in the electrospinning process parameters on the resultant fibre morphology. Adapted from (Pham, Sharma and Mikos, 2006a; Sill and von Recum, 2008).

Parameter	Effect on Fibre Morphology
Viscosity/Concentration	Fibre diameters increase with increasing concentration/viscosity (within optimal range).
Conductivity/Solution charge density	Increasing the conductivity encourage the production of uniform bead-free fibres. In general, increasing conductivity produces smaller fibres.
Polymer molecular weight	At constant viscosity, increasing molecular weight reduces the number of beads and droplets.
Flow Rate	Lower flow rates produce fibres with smaller diameters.
Field strength/Voltage	At too high voltage, beading will be observed. At increased flow rates, fibre diameter decreases.
Distance between tip and collector	A minimum distance is required to obtain dry fibres. At distances either too close or too far, beading can be observed.

2.9   Characterisation of Electrospun Nanofibers

2.9.1 Geometrical characterisation

The geometrical features of electrospun microfibres, which include fibre orientation, fibre diameter, fibre distribution, and morphology (for example, surface structure, roughness, and form), can be analysed and evaluated with the use of instruments such as scanning electron microscopy (SEM), transmission electron microscopy, field emission scanning microscopy (Templeton et al., 2000), and atomic force microscopy (Li et al., 2002). Among these tools, SEM is the most extensively utilised since it is simple to use and widely available. The scanning electron microscope (SEM) is the method of choice for determining the fundamental parameters of processed fibrous films, such as the diameter of the fibres. Fibrous structures often develop imperfections during the electrospinning process, which can be shown by SEM (Jacobs, Anandjiwala and Maaza, 2010).

2.9.2 Chemical characterisation

Various techniques can be employed to investigate the molecular structure of electrospun fibrous scaffolds, such as Fourier Transform Infrared (FTIR) and Nuclear Magnetic Resonance (NMR) (Huang et al., 2000; Bottino, Thomas and Janowski, 2011). Fibrous structures can be regarded as super-molecular structures that reflect the arrangement of macro-molecules, which can be analyzed in detail using techniques such as wide-angle X-ray diffraction, optical birefringence (Chen et al., 2001), differential scanning calorimetry (DSC) (Zussman, Yarin and Weihs, 2002), and X-ray scattering. For instance, DSC was utilized to investigate the thermal behavior of PLA/HA fiber mats, where the incorporation of HA particles was found to have a nucleating effect that enhanced the thermal stability of the fibrous structure, as revealed by the characterization results (Sonseca et al., 2012).

2.9.3 Degradation characteristics

Scaffolds made of biodegradable materials are commonly utilised to provide structural support for tissues undergoing regeneration. Degradable biomaterials are created for use in tissue engineering so that healthy tissue can grow again and then break down when they are no longer needed. Therefore, their rate of breakdown (or their degradation profiles) should coincide with the rate at which the tissue is repaired. As a result, the degrading characteristics of polymeric nanofibers must be thoroughly investigated, as they are the most important aspect for achieving tissue engineering success. Throughout most cases, the rate of polymer degradation corresponds to the material's structure and content (Li, Mauck and Tuan, 2005).

As an example, hydrolytic degradation is more likely when the surface area to volume ratio is high. Consequently, its rate of degradation increases relative to that of microfibers (Li, Mauck and Tuan, 2005). Degradation rates of small-diameter fibres can be further reduced by increasing crystallinity and chain orientation (Dong *et al.*, 2010). Furthermore, the diffusion rate of fibre-composed breakdown byproducts increases noticeably when the surface area increases and the fibre diameter falls. Accordingly, the rate of hydrolytic degradation is reduced (Dong *et al.*, 2010). Several different solutions and methods are available for assessing and analysing the degrading qualities, including simulated bodily fluid (SBF), artificial saliva, and phosphate buffer solution (PBS). Typically, the ion concentration in SBF and synthetic saliva would be the same as that in blood plasma (Tang *et al.*, 2016).

2.9.4 Bioactivity characteristics

There are different needs for the materials used to encourage bone healing. When implanted into live tissue, one of the most important things is for the material to take on a bone-like appetite on its surface. Consequently, a variety of materials have been analysed and tested to ascertain apatite formation in artificial body fluids with ion concentrations that are similar to human blood plasma (Kokubo, 1991).

2.9.5 Mechanical characterisation

Scaffolds for tissue engineering must be able to withstand continuous mechanical loading, so mechanical qualities are particularly important for *in vivo* applications. Evaluation of the mechanical properties of electrospun nanofibers can be performed using conventional methods such as tensile testing (Leal *et al.*, 2013).

2.9.6 *In-vitro* cellular response

The material used to construct a scaffold for biomedical applications must be non-toxic. All biomaterials and medical devices are required to complete a nonclinical safety evaluation (*in vitro* experiments on human and animal cell lines, *in vivo* tests on animals) before being used in a human clinical trial. (Iso and STANDARD, 2009; Plan, 2011; EU-Commission, 2012)

The nonclinical safety evaluation is the first phase in the process of establishing the biocompatibility of a medical material or device. This evaluation is a lengthy and complicated procedure; even the term "biocompatibility" needs to be used with caution and a proper grasp of the biomaterial-tissue system (Williams, 2014). Nevertheless, many easy, rapid, and cost-effective cytotoxicity assays can assist establish if the biomaterial has potentially detrimental biological features or contains toxic chemicals.(Liu *et al.*, 2018)

There is a large variety of testing methods available to choose from in order to assess the level of cell viability present within the scaffolds. Various cellular processes, such as mitochondrial enzyme activity, cell membrane permeability, ATP synthesis, and cellular uptake activity, determine their classification.For this study, viability was determined using the PB assay, which measures mitochondrial enzyme activity. It is a resazurin-based chemical that undergoes a measurable colour change when reduced by mitochondrial enzymes in living cells. This change can be measured using a fluorometric or spectrophotometric technique (Boncler *et al.*, 2014). The Live/Dead® assay with calcein-AM and ethidium homodimer-1 staining was employed in this investigation to assess cell viability in scaffolds. This assay has been widely used for this purpose (Catelas *et al.*, 2006; Haschtmann *et al.*, 2006). Ca-AM and EthD-1 dyes can be combined quickly and easily to provide direct staining of both living and dead cells in a scaffold or tissue. Within living cells, the Ca-AM is hydrolysed into calcein via enzymatic processes, which results in the cells acquiring a brilliant fluorescent green colour. In contrast, the EthD-1 can only enter cells with a damaged membrane and stains nucleic acid bright red (Melamed, Kamentsky and Boyse, 1969).

Proliferation of cells refers to the rise in the total number of cells and is essential for tissue growth. It is the outcome of both cell division and growth. To maintain a balance between cellular size and population size, both processes are tightly controlled in healthy organisms. Cell proliferation assays are useful for studying the impact of medications or other treatments on a cell population in an experimental setting (Guo *et al.*, 2022). In this study, the total protein content of the scaffold was measured using the bicinchoninic acid (BSA) assay, and the quantity of double-stranded DNA (dsDNA) was measured using the picogreen assay to assess cell proliferation. Using an alkaline phosphatase (ALP) assay, the osteogenic differentiation of mesenchymal stem cells (MSCs) on scaffold was evaluated. In section 12, all of these tests were detailed in detail.

2.10 Summary of Literature

The purpose of the literature review section is to provide a synopsis of the research undertaken in the field of BTE, with an emphasis on the regeneration of alveolar bone tissue. The following is a summary of the most important findings from the literature review: (1) The best method for restoring damaged tissues caused by periodontal diseases is guided regeneration therapy; (2) In order for GBR to be effective, barrier membranes must be well-designed incorporating relevant materials and tackling key properties through specific manufacturing routes; (3) Composite materials have the potential to be the most effective choice when it comes to barrier membranes; (4) The use of bioactive ceramics into GTR/GBR membranes has a beneficial effect on enhancing both

mechanical performance and osteogenic capability; (5) Electrospinning can be utilised to create fibrous membranes that stimulate osteoblastic cell activity and bone repair; (6) There are numerous processes for manufacturing smooth membranes, such as solvent casting and spin coating. These membranes have been shown to effectively act as a physical barrier, preventing epithelial cells and connective tissue from growing into bone defect sites.

Following the limitations mentioned in the literature review leads to two main areas of concern. The first is that conventional GBR membranes lack strong osteogenic capabilities, thus they only operate as barriers rather than promote healing, and the second is that clinically used scaffolds feature modest mechanical qualities, leading to poor space maintenance during regeneration. Therefore, novel membranes with enhanced mechanical and osteogenic properties are needed to prevent collapse at the defect site and promote tissue regeneration.

2.11 Thesis aim and objectives

The primary aim of the study was to develop, characterise, and test *in vitro* a new ceramic-modified bilayer membrane for guided tissue/bone regeneration applications to aid in periodontal disease. Periodontitis is a chronic inflammatory pathology that can jeopardise the integrity of tooth support and ultimately, lead to tooth loss. To date, flap debridement and/or flap curettage and periodontal regenerative therapy with membranes and bone grafting materials have been employed with distinct levels of clinical success. Current resorbable and non-resorbable membranes act as a physical barrier to avoid connective and epithelial tissue down-growth into the defect, favouring the regeneration of periodontal tissues. As reported in the previous chapter, membranes based on biodegradable synthetic polymers avoid a second surgical operation, however they show drawbacks concerning their capacity for space maintenance, early/late absorption, mechanical properties, and bacterial infection during degradation.

In this work, a multifunctional bi-layered membrane using a new sustainable polyester blend (Floreon) and relevant bioceramic materials was proposed to improve resorbable membrane properties and enhance bone regeneration efficiency (Figure 2-14). The bilayer membrane will be manufactured using a combination of advanced and conventional fabrication routes, including casting, electrospinning, and spin-coating.
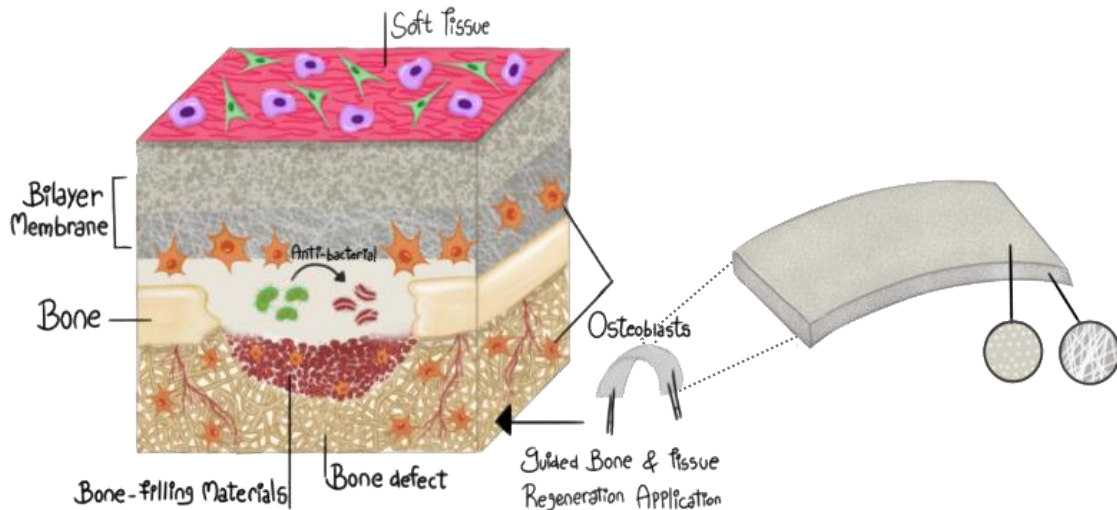
Figure 2-14 Functionalised bi-layered bioabsorbable membrane consisting of a compact and a porous layer.

Thesis objectives

1- Development of the porous layer: nanofiber membranes using the electrospinning technique, based on a Floreon blend reinforced with 5%, 10%, and 25% concentrations of Hydroxyapatite (HA) and Calcium Silicate (CaSiO$_3$). Various compositions are studied to find those with suitable mechanical and biological properties for the application.

    a) Manufacturing porous membranes to be used as core layers.

    b) Constructing Polymer-Ceramic Composites.

    c) Evaluation of geometry, physical, chemical, and mechanical characteristics.

    d) Assessment of bioactivity and degradation properties.

    e) Evaluation of their biocompatibility using Mesenchymal stromal cells (MSCs).

2- Developing a compact surface layer of pure Floreon using two different techniques: spin coating and solvent casting. This acts as a physical barrier to ensure its superior mechanical performance and prevent non-osteoblast interference.

    a) Manufacturing smooth films to serve as surface (top) layers.

    b) Evaluation of geometry, physical, chemical, and mechanical characteristics.

    c) Assessment of bioactivity and degradation properties.

    d) Evaluation of their biocompatibility using normal oral fibroblasts (NOFs).

3- Combining the surface and core layers to create a multifunctional, bi-layered device..

a) The production of composite membranes included (i) an electrospun Floreon core layer reinforced with suitable bioceramic materials and (ii) a spin-coated or solvent-cast Floreon top layer.

b) Evaluate the manufactured bilayer structure geometrically and mechanically.

c) Conducting histological analysis to assess the relative cell attachment on both layers.

CHAPTER 3:

MATERIALS AND METHODS

Chapter 3: Materials and Methods

This chapter describes in detail the materials and methodologies used to fabricate the electrospun membranes, as well as solvent-cast and spin-coated scaffolds. Detailed characterisation of the manufactured constructs was also conducted. The geometrical properties were assessed by optical imaging and scanning electron microscopy (SEM), chemical properties by Fourier transform infrared (FTIR) and X-ray diffraction (XRD) as well as physical properties by mechanical testing of specimens in tensile conditions, thermogravimetric analysis (TGA) and differential scanning calorimetry (DSC).

Biological characterisation was also performed to assess cellular viability and proliferation over time. *In-vitro* bioactivity and degradation of each scaffold were carried out using corrected simulated body fluid (SBF) (Kokubo *et al.*, 1990), by monitoring the changes in pH profile, weight, SEM observation, FTIR chemical alterations, and DSC physical alterations.

Finally, the ability to fabricate a bilayer membrane was evaluated geometrically using optical imaging and scanning electron microscopy (SEM). Histology on the cultured first prototype bilayer scaffolds was also conducted to visualise cellular attachment and distribution as well as to ensure the true barrier nature of low-porosity, non-fibrous membranes (fabricated using spin-coating).

The following flowchart (Figure 3-1) summaries the tests carried out to assess the characteristics of the prepared membranes.
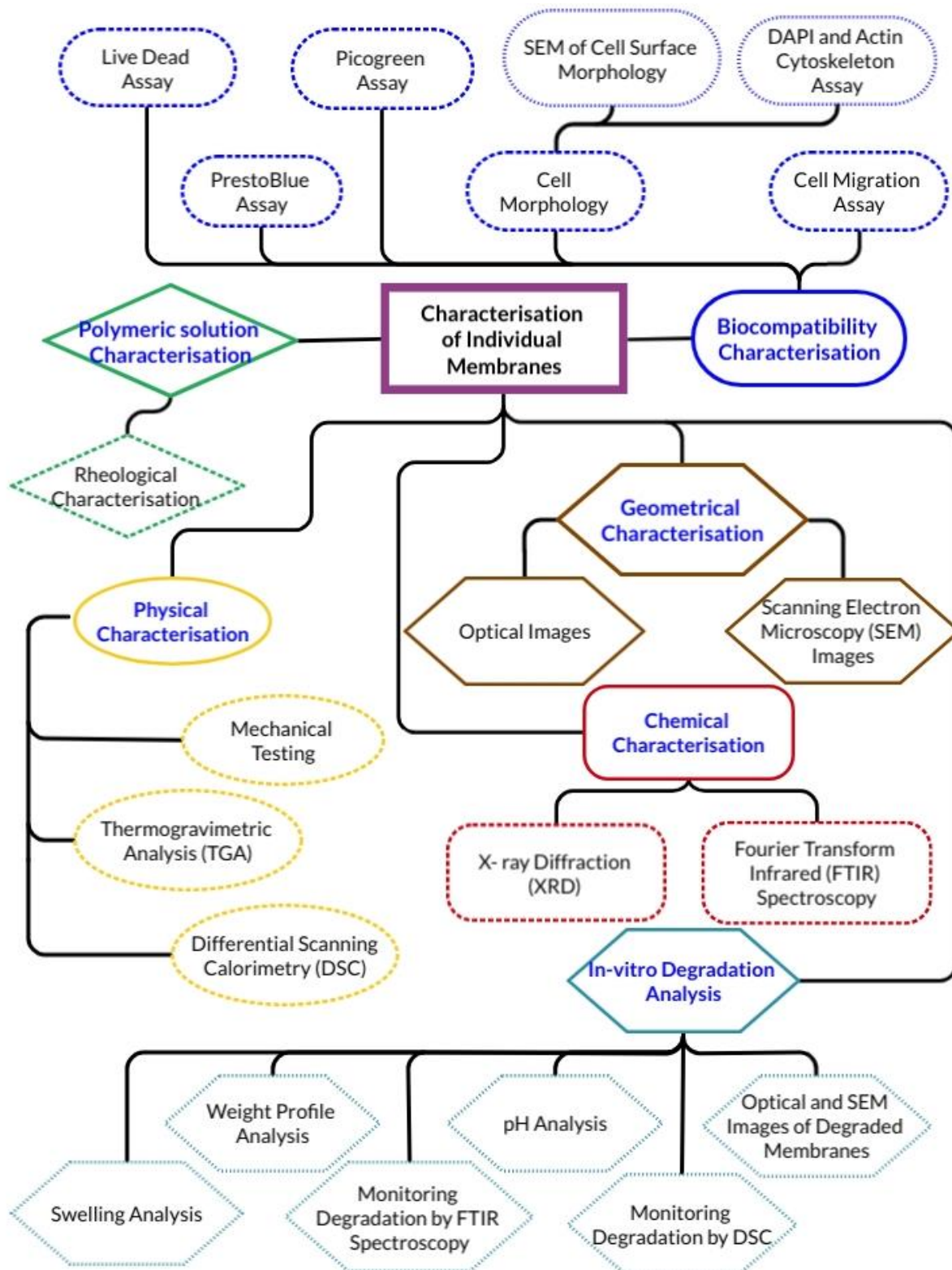
Figure 3-1 a flowchart illustrating the characteristics tests performed on each membrane.

3.1 Materials

The following represents the base materials used in this study: which includes a Floreon blend to prepare the surface layer, while hydroxyapatite and calcium silicate particles were added to the main layer of functionally graded membranes. PLA was used as a control material in both layers. Dichloromethane (DCM) and Dimethylformamide (DMF) solvents were used to prepare the polymeric solutions. All cell culture chemicals and supplies were acquired from Merck and Sigma Aldrich®, UK.

3.1.1 Polymers

To prepare the electrospinning solutions as well as solutions for spin coating and solvent casting, a polyester blend (Floreon) was used. Floreon consists of 80% Poly (L-lactic acid) (PLLA) (Sigma-Aldrich, Poole, UK) with an average molecular weight (60,000 Mw), 5% Polycaprolactone Diol CAPA® 6250 (25,000MW) and 15% Polycaprolactone Diol CAPA® 6800 (80,000 MW). Both were purchased from Silvergate Masterbatch, Wrexham, UK. Pure PLA (60,000 MW) has also been used as a control group.

3.1.2 Bioceramics particles

Two different types of micron-size bioceramic powders were used in the study; details are highlighted below.

- Hydroxyapatite: Medical-grade Hydroxyapatite (HA) was obtained from Plasma Biotal Limited (Plasma Science Group) Derbyshire, United Kingdom; CAPTAL®S BM, Hydroxyapatite (sintered powder), Batch No. 192/0132, Lot 1. The particle size of the HA used was 3.39 ± 1 µm.
- Calcium silicate derivatives (wollastonite) were purchased from NYCO Minerals, Inc., Willsboro-Lewis, New York, NY, USA. It is valuable as a filler in the form of acicular (needle-like) particles with aspect ratios of 5–20 and particle sizes (lengths) of 2–40 μm.

3.1.3 Solvents

Solvents used to prepare polymeric solutions were as follows: Dichloromethane (DCM) CAS NO.75-09-2. and Dimethylformamide (DMF) CAS NO.68-12-2 (both supplied by Fisher Scientific Loughborough, UK).

All polymers, solvents, and ceramic particles were used in this study are listed in detail in Table 3-1. Refer to the next section.

3.2 Membrane Synthesis

A schematic representation of the procedures followed to produce smooth and fibrous membranes using the electrospinning, solvent-casting, and spin-coating methods is shown in Figure 3-2; these same methods were later combined to fabricate bilayer films. The following headings provide a more in-depth explanation of these techniques.
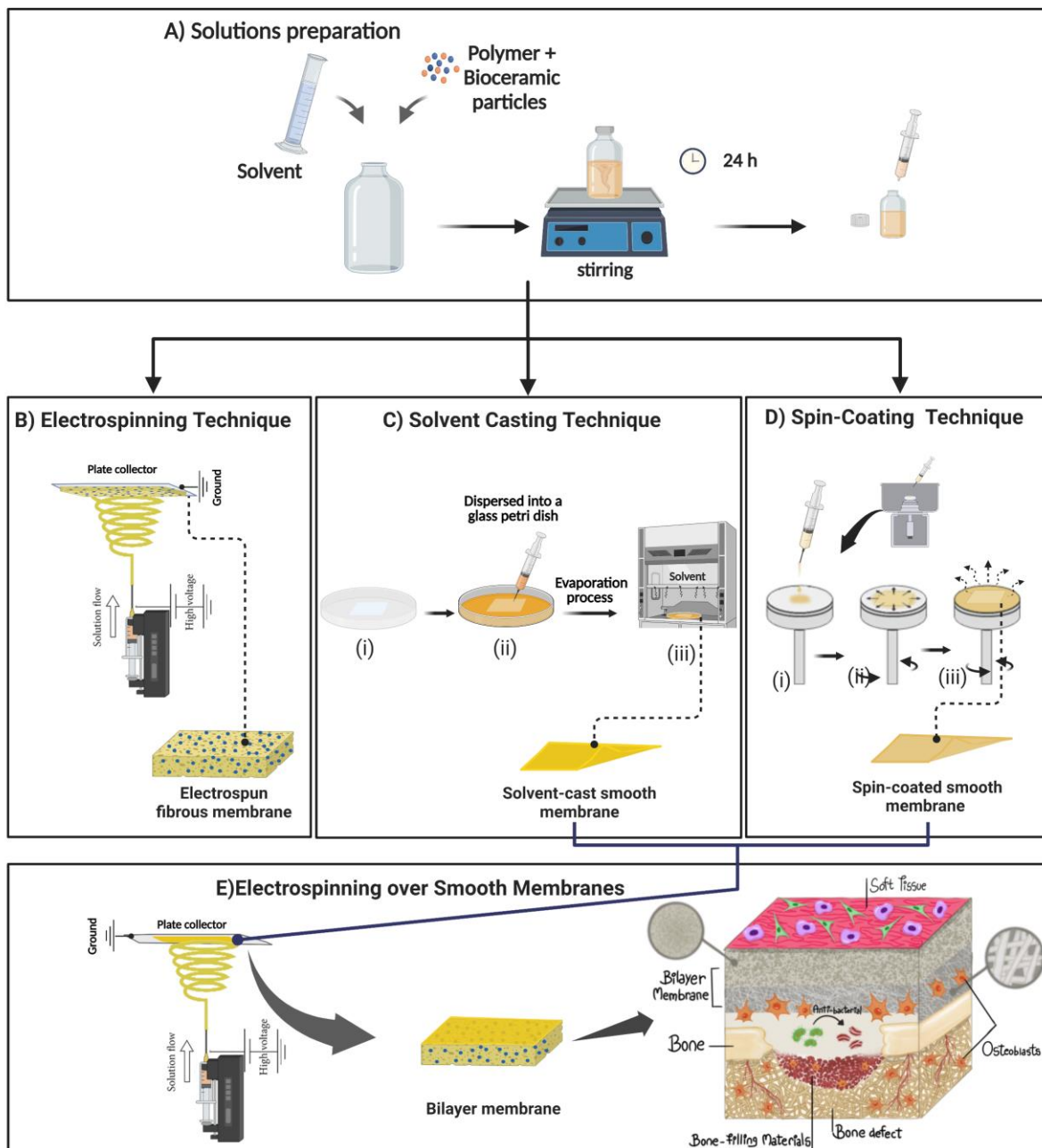
Figure 3-2 Schematic representation of the envisioned tissue engineering strategy based on the use of a double-layer scaffold with two different target functionalities, starting with the preparation of the polymeric solution(A), each according to the type of membrane and the method used. (B) A base-layer composite

membrane consisting of a porous layer prepared by electrospinning of Floreon with the inclusion of bioceramic particles, this being HA and $CaSiO_3$ ceramics. (C) A top-layer membrane with a smooth surface was fabricated in one step by spin-coating of a plain Floreon; A schematic model describing the film formation during the spin-coating process(i), after the initial spin-off stage where the solvent is evaporated (ii), the thin film is formed (iii). (D) A top-layer membrane with a smooth surface was fabricated with a solvent casting technique by self-evaporating a mixed dispersion containing a plain Floreon; the model illustrates the manufacturing process of the cast film, beginning with the preparation of the Petri dish by placing the square microscope slide (i), followed by the pouring of the solution (ii); the dish is then left inside the hood to evaporate the solvent, revealing the finished, smooth film (iii). (E) (i) A diagram showing the steps needed to make bilayer films by electrospinning a polymer/ceramic solution over smooth films made by either solvent casting or spin coating. (ii) Schematic illustration of the main functions of the membrane for GBR application.

3.2.1 Solutions preparation

In order to prepare the Floreon solutions, PLA, PCL-CAPA® 6250, and PCL-CAPA® 6800 were dissolved in a mixture of DCM/DMF (3:1) according to the weights and volumes stated in Table 3-1 in a glass container that had a magnetic stirrer. Once the Floreon solutions appeared to have dissolved, the ceramic fillers (HA and $CaSiO_3$) were added to the solutions to form the range of the desired volume ratios (Table 3-1). The Floreon/filler solutions were then sealed with Parafilm (Bemis NA, Neenah, USA) to prevent solvent evaporation and left to stir overnight at room temperature to obtain homogenous mixtures before being used.

Table 3-1 shows the different combinations in which the materials were generated in this study. The intention behind the design of composites with different bioceramic concentrations was to evaluate various combinations to identify suitable blends for manufacturing the regenerated membranes. In all of the experiments conducted for this work, PLA membranes and PLA membranes with 10% wt bioceramics were used as controls.

Table 3-1 Material compositions used in the study.

Type of membranes	Composite name	Raw materials 10 wt%					Solvents 90 wt%	
		PLA (g)	PCL CAPA® 6250 (g)	PCL CAPA® 6800 (g)	Calcium silicate (CaSiO$_3$) (g)	Hydroxyapatite (HA) (g)	DCM (ml)	DMF (ml)
Fibrous membranes	Pure PLA	2	-	-	-	-	13.5	4.5
	PLA + HA (10 *wt%*)	1.8	-	-	-	0.2		
	PLA + CaSiO$_3$ (10 *wt%*)	1.8	-	-	0.2	-		
	Pure Floreon	1.60	0.1	0.30	-	-		
	Floreon + HA (5 *wt%*)	1.52	0.095	0.285	-	0.1		
	Floreon + CaSiO$_3$ (5 *wt%*)	1.52	0.095	0.285	0.1	-		
	Floreon + HA (10 *wt%*)	1.44	0.09	0.27	-	0.2		
	Floreon + CaSiO$_3$ (10 *wt%*)	1.44	0.09	0.27	0.2	-		
	Floreon + HA (20 *wt%*)	1.28	0.08	0.24	-	0.4		
	Floreon + CaSiO$_3$ (20 *wt%*)	1.28	0.08	0.24	0.4	-		
Smooth membranes	Pure PLA	2	-	-	-	-	18	-
	Pure Floreon	1.60	0.1	0.30	-	-		

3.2.2 Fabrication of electrospun membranes

Electrospinning experiments were performed using a vertically placed electrospinning setup. The prepared electrospinning solution was utilised within 24 hours of preparation. The solution was loaded into a 1 ml syringe (Becton Dickinson, UK), and then any air in the syringe was removed. A blunt-tipped, 2.54 cm tip crimp-sealed 20-gauge needle (Fisnar, New Jersey, USA) was then fitted to the syringe. The syringe and needle were placed in the syringe pump (PHD2000, Harvard Apparatus, UK), and they were connected to the circuit. The solution was electrospun between 18-21 kV at a flow rate of 1 ml.h-1. The needle tip-collector plate separation distance was 20 cm. This system was encased within a fume hood, and a break fail-safe was coupled to the system in order to prevent it from working when the fume hood is open, as shown in Figure 3-4 (A).

3.2.3 Fabrication of solvent cast membranes

The solvent casting technique is used as one of the approaches for the manufacture of smooth films (Figure 3-2 (C) and Figure 3-4 (C-E)). In order to achieve this, a polymeric solution was first prepared by mixing plain Floreon with DCM according to the method and weights mentioned in Section 3.2.1. After 24 hours of stirring, 5 ml of the polymeric solution was poured into glass Petri dishes, covered with an inverted funnel, and allowed to sit overnight to allow the DCM solvent to slowly evaporate. To obtain membranes of uniform thickness, a 60×60 mm square glass microscope slide was placed in each Petri dish. The films were then peeled from the plates and dried in a vacuum oven (Figure 3-3) (Technico™, Fisher Scientific Loughborough, UK) at 60 °C for 24 hours to confirm that all the solvent had been evaporated. The drying in the vacuum oven was carried out in the Chemistry Department at the University of Sheffield.

3.2.4 Fabrication of spin coated membranes

For the spin-coated film with a smooth surface, the same solution as in the prior approach was utilised. Figure 3-2 (D) shows a schematic of the film formation phases that occur during the spin-coating procedure, in which 5 ml of the prepared plain Floreon solution is poured onto a 60 mm x 60 mm square glass microscope slide placed on the spin-coater chuck that is then rotated at speeds ranging from 1000 to 4000 rpm. The spin time had no major impact on the thickness of the film, so it was set at 30 seconds. Due to the high volatility of DCM, most of the solvent evaporated during the spinning process. The films were then peeled from the plates and dried in a vacuum oven (Figure 3-3) (Technico™, Fisher Scientific Loughborough, UK) at 60 °C for 24 hours to confirm that all the solvent had been evaporated. The drying in the vacuum oven was carried out in the Chemistry Department at the University of Sheffield.

Figure 3-3 Technico™ Vacuum Oven used for drying samples.

3.2.5 Fabrication of bilayer membrane

Fabricating a bilayer membrane using spin-coated and electrospun films is depicted in Figure 3-2 (E) and Figure 3-4 (H-J). First, the smooth film was adhered to the collecting plate with double-sided adhesive tape. Next, the areas surrounding the membrane were covered with a barrier plastic sheet in order to direct the attraction of the polymer fibres to the placed film (as shown in Figure 3-4 (H). Afterwards, 2 ml of the spinning solution was electrospun onto the substrate's surface. The detailed technical parameters for spinning were previously described in Section 3.2.2.

All membranes that were used in the following experiments were then kept inside the hood to dry for 24 hours. After the drying period, the as-produced membranes Figure 3-4 (B, E, G and J) were wrapped in aluminum foil and stored in a desiccator until further use.
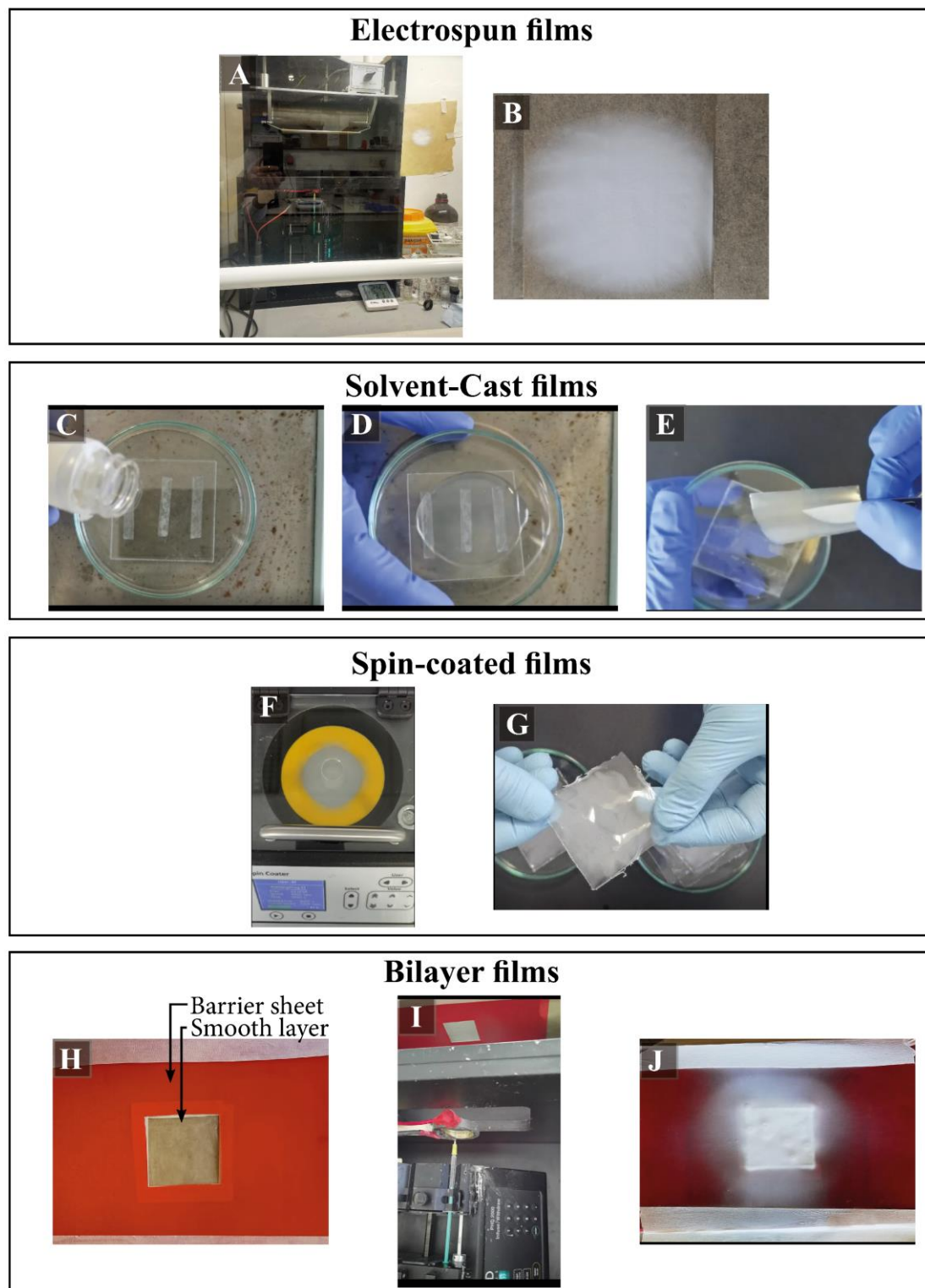
Figure 3-4 The manufacturing techniques utilised in the project during and following the fabrication of fibrous (A,B), solvent (C-E), spin-coated (F, G), and bilayer (H-J) films.

3.3   Membrane Characterisation

3.3.1   Optical microscope

The visual appeal of membranes was evaluated using a Nikon (S5600-DSLR) equipped with a macro lens after the manufacturing process and at various times during the degradation study. The scale bar was set using ImageJ 1.52 GB software (National Institutes of Health, US).

3.3.2   Scanning electron microscopy (SEM)

The morphology and particle size of the HA and $CaSiO_3$ powders, as well as the morphology of the films, were studied using a scanning electron microscope (TESCAN VEGA3 LMU) (Figure 3-5), at a voltage of 20 kV for bioceramic powders and 15 kV for fabricated films.

All of the samples were cut and mounted on aluminium stubs with double-sided carbon conductive adhesive tape. Using a Quorum Q150T ES sputter coater, a thin layer of gold was sputter coated onto the specimens. The coating process took no longer than 4 minutes at a current of 25 mA (stopping at 20 nm thickness). Using ImageJ software, the average diameter of at least 50 fibres in three separate SEM images was calculated for each specimen. Moreover, scanning electron microscopy was utilised to evaluate membranes used for bioactivity studies in order to check for the presence of an apatite layer on the fibres' outer surface following soaking in SBF (section 3.3.12).

Figure 3-5 Scanning electron Microscopy unit used for imaging samples. (TESCAN VEGA3 LMU).

3.3.3 Transmission electron microscopy (TEM)

A high-resolution Transmission Electron Microscope (TEM) operated at 200 keV was used to analyse the morphology and particle size of the bioceramic particles and ceramic-containing electrospun fibres. The powders were ground using a pestle and mortar. A small quantity of powder was added to 1 ml of distilled water in an Eppendorf tube, which was sonicated for 1 minute to break up any aggregates. Two to three drops of the solution were pipetted onto a carbon grid (Agar Scientific, Standsted, UK) using a 1 ml Pasteur pipette and dried at room temperature. The TEM used for this work was the FEI Tecnai Spirit BioTWIN TEM (Philips, Eindhoven, Netherlands) with a Gatan Orius 1000B CCD camera and Gatan Digital Micrograph software (Figure 3-6).

Figure 3-6 Transmission electron Microscopy unit used for imaging samples. (FEI Tecnai Spirit BioTWIN).

3.3.4 Porosity

Porosity is a fundamental characteristic of scaffolds, as it can greatly influence their mechanical, physical and biological properties. Various methods have been employed to measure porosity, but mercury porosimetry is a widely accepted technique due to its ability to determine the total porosity, as well as the average pore diameter and pore size distribution. In this study, the porosity of electrospun scaffolds was investigated using mercury porosimetry, which involves filling the sample cell with scaffolds and infusing them with mercury under increasing pressure to force the mercury into the scaffold pores. Mercury, due to its high surface tension and inability to penetrate pores via capillary action, is an ideal material for pore investigation.(Loh and Choong, 2013; Hekmati et al., 2014). Assuming the pores are all cylindrical and equally accessible to mercury, the applied pressure can be converted into pore diameter using the Washburn equation:

$$D = (-4\ \gamma \cos \theta)/(P\ ) \qquad\qquad\qquad \textbf{Equation 3-1}$$

Where D is the pore diameter, P is the applied pressure, γ is the surface tension of mercury (480 erg cm-2, 0.48 N m-1) and θ is the contact angle between mercury and the pore wall, which is taken to be 140° (Kwon, Kidoaki and Matsuda, 2005; Pham, Sharma and Mikos, 2006b; Hekmati *et al*., 2014). Mercury porosimetry measurements were performed at the Royce Discovery Centre, the University of Sheffield using an AutoPore 9620 porosimeter (Figure 3-7). For each type of scaffold, measurements were taken on a single sample weighing about 200 mg.

Although the Image J software has been used in previous studies to measure porosity in various materials, it was not employed in this study due to its limited precision. Instead, mercury intrusion porosimetry was used due to its high accuracy and reliability in determining porosity. Recent studies have also shown the effectiveness of this technique in measuring porosity of various materials, including porous ceramics (Zeng *et al.*, 2020), polymers (Alvarez-Fernandez *et al.*, 2020) and metal-organic frameworks (Feng *et al.*, 2021). Moreover, the mercury porosimetry technique provides more detailed information on pore size distribution and pore diameter than the Image J software method.

Figure 3-7 AutoPore 9620 porosimeter which was used for measuring the samples porosity based on the mercury porosimetry technique.

3.3.5 Contact angle (Wettability) measurements

The hydrophobicity and hydrophilicity of the polymer films were investigated by utilising a Drop Shape Analysis DSA 100S System (KRÜSS, Germany) (Figure 3-8) in conjunction with the Drop Shape Analysis software developed by KRUSS. samples of polymeric membranes were placed on the platform, and a 10 µL droplet of water was injected onto the film. After that, an image of the droplet was captured using a camera, and the contact angle of the water was calculated. If the obtained values were $\theta < 90°$, the film was classified as hydrophilic, and if they were $\theta > 90°$, as hydrophobic. Each film had three water drops measured: one in the centre and one on each side. Three samples per material were evaluated to determine an average value.
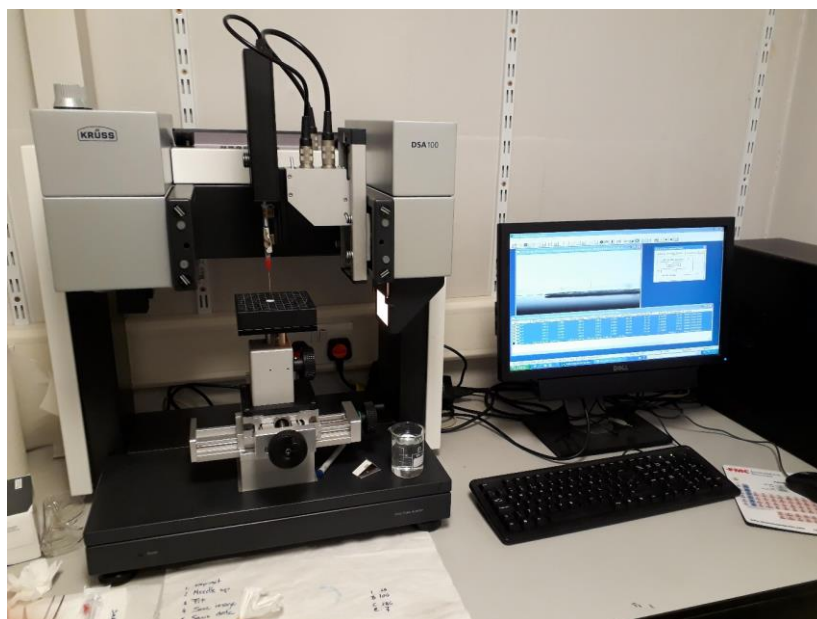
Figure 3-8 Drop Shape Analysis DSA 100S instrument used to measure sample wettability. (KRÜSS, Germany)

3.3.6 X-ray diffraction (XRD)

XRD is a non-destructive analytical technique that enables the analysis of the crystallographic structure of a material. HA, $CaSiO_3$ powders as well as prepared films were characterised using XRD, to determine the crystalline phases present and to estimate the percentage crystallinity. The samples were placed on a zero-background silicon wafer in a sample holder. X-ray diffraction data were collected using Cu-Kα radiation on a BRUKER D8 ADVANCE diffractometer (Bruker AXS GmbH, Karlsruhe, Germany) (Figure 3-9), equipped with a high-resolution energy dispersive Lynxeye XE detector. Data was collected using a coupled 2theta scan from 6 - 90 ° 2theta with an increment of 0.02 ° using 2 s per increment. The total collection time was 2.5 hours per sample. Data were analysed using DIFFRAC plus XRD Commander software, version 5.1.0.5 (32 Bit) Bruker AXS 2010-2019 (Bruker AXS GmbH, Karlsruhe, Germany). The XRD analysis was carried out in the Chemistry Department at the University of Sheffield.

Figure 3-9 Bruker AXS D8 Discover X-ray Diffractometer (XRD) used for sample analysis (Bruker AXS GmbH, Karlsruhe, Germany).

3.3.7 Fourier Transform Infrared (FTIR) spectroscopy

FTIR is an analytical technique that measures the infrared radiation absorption by a material versus its wavelength. The molecular structure of the material is characterised by the wavelength of the light absorbed, which causes vibrations of the molecules. FTIR is also useful for quantitative analysis, as the band intensities that appear in the spectrum due to the vibration of molecules in a material are directly proportional to the concentration of that molecule (Vlachos *et al.*, 2006).

FTIR spectra of the HA, CaSiO$_3$ powders and polymeric films were obtained by a Perkin Elmer FTIR spectrometer (Figure 3-10). The spectra were measured at 4 cm-1 resolution, and a total of 128 scans were obtained in the spectral range 4000 – 400 cm-1. A background spectrum of a carbon sample was obtained before obtaining sample spectra.

Figure 3-10 Perkin Elmer FTIR Spectrometer used for samples analysis.

3.3.8 Thermogravimetric analysis (TGA)

Thermogravimetric analysis (TGA) was used to characterise the thermal stability and decomposition mechanism of manufactured scaffolds, as well as to explain the effect of additives and chemical alterations on fibres and the thermal behaviour of polymer blends.

TGA measures weight variations in a material as a function of time or temperature. TGA data are typically displayed as a TGA curve, with weight (mg) or weight percent (%) (Y-axis) plotted against time or temperature (X-axis), whereas the first order derivative curve of TGA refers to the temperatures at which the highest weight decline occurs (Hatakeyama and Quinn, 1999; Price, Hourston and Dumont, 2000).

TGA measurements were carried out using a Perkin Elmer Pyris-1 instrument (Figure 3-11) before and after the degradation period for all electrospun, solvent-cast, and spin-coated membranes. The process was under a nitrogen atmosphere. The samples were heated at a rate of 10 °C min-1 from 30 to 600 °C. Two samples of each film (n=2) were evaluated, and then the average was calculated. All findings were plotted as temperature (°C) versus weight loss (%), and curves were then analysed using the Pyris software (PerkinElmer, Inc., USA). TGA was conducted by Dr. Oday at the University of Sheffield's Royce Discovery Centre.

Figure 3-11 Perkin Elmer Pyris-1 TGA Instrument used for samples analysis.

3.3.9 Differential Scanning calorimetry (DSC)

Differential Scanning Calorimetry (DSC) was required to assess the thermal behaviour of electrospun, solvent-cast, and spin-coated membranes. A PerkinElmer DSC 4000 (PerkinElmer Inc., USA) (Figure 3-12) was used with 50 mL/min of nitrogen used as a purge gas. The testing procedure was as follows: samples were cut into small pieces weighing approximately 2 mg to facilitate placement in an aluminum pan. The samples were heated between 30 and 200 °C at a rate of 10 °C.min-1. The glass transition temperature (Tg), the cold-crystallisation temperature (Tcc), and the melting temperature (Tm) were then determined using the Pyris software (PerkinElmer, Inc., USA). DSC was conducted by Dr. Oday at the University of Sheffield's Royce Discovery Centre.
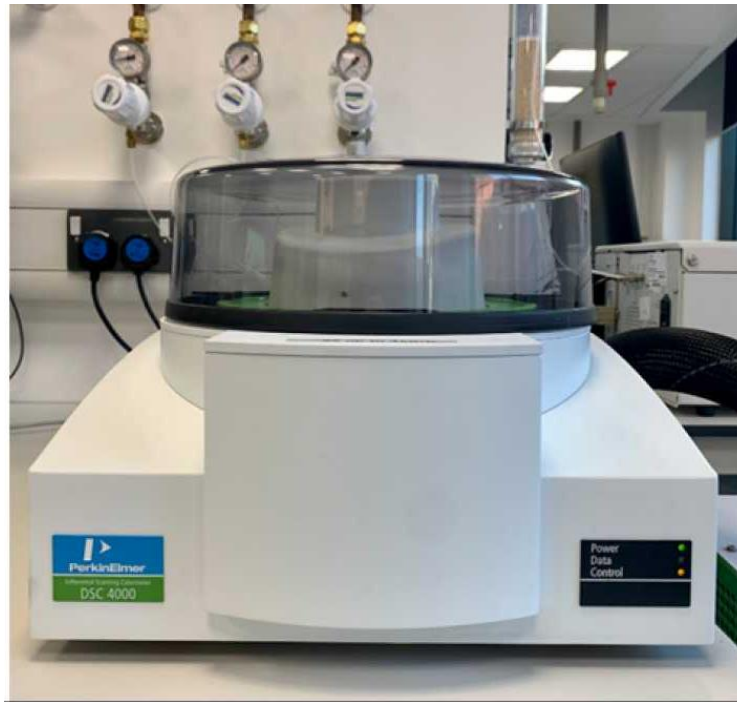
Figure 3-12 PERKIN ELMER DSC 4000 used for samples analysis.

3.3.10   Rheology

Rheological characterisation tests were performed using a stress-controlled rotational rheometer (Anton Paar MCR301) (Figure 3-13) with a 5-bar airline pressure. This was done in the different polymer solutions to obtain their storage and loss modulus using an oscillation strain sweep assay. A 25-mm parallel-plate geometry was used, and all tests were performed at 25 °C. At a constant stress of 1 Pa, oscillatory frequency sweep tests were conducted with an increase in angular frequency from 1 to 1000 rad/s.

Figure 3-13 Anton Paar MCR301 rotational rheometer used for sample analysis.

3.3.11 Mechanical testing

The mechanical properties of the electrospun, solvent-cast, and spin-coated membranes were measured using uniaxial tensile testing. The experiment was carried out using a universal testing machine (Lloyd LRX, UK) (Figure 3-13) with a 50 N cell load operating at a displacement rate of 1 mm min-1. The fabricated scaffolds were cut into a rectangular shape with dimensions of 50 ± 2 mm in length and 10 ± 0.2 mm in width (n = 6). Prior to testing, the strips were measured using a micrometre (MITUTOYO, Digimatic, 25 mm Max Measuring Range, 0.001 mm Graduations). From the data collected, the Young's modulus, the Ultimatete tensile strength (UTS), and the strain at the UTS were collected for all the samples using LLOYD NEXYGEN 4.1 software. Tensile testing was thus performed to a reduced size version of the BS ISO 13934-1 standard for fabric textiles (Institution, 1999, 2013).

Figure 3-14 The universal testing machine used for measuring samples tensile properties.

3.3.12 Degradation and Bioactivity Analysis

For the *In-vitro* bioactivity and biodegradation studies, simulated body fluid (SBF) was created to mimic the pH and ionic strength of human blood plasma. The SBF was prepared by dissolving NaCl, NaHCO$_3$, KCl, K$_2$HPO$_4$·3H$_2$O, MgCl2·6H$_2$O, CaCl$_2$, Na$_2$SO$_4$ and (HOCH$_2$)$_3$CNH$_2$ in distilled water and adjusting the pH of the final fluid to 7.4 using 1M HCl. (Kokubo *et al.*, 1990; Kokubo and Takadama, 2006). Reagents used for preparation of SBF were of analytical grade and supplied by Sigma Aldrich®. UK, listed with proper quantity in the Table 3-2. The final concentration of the ions in the prepared SBF is shown in

Table 3-3.

Specimens of all manufactured membranes were cut to 15 mm in diameter using a Cork borer (0.56″) for analysis of bioactivity, biodegradability, and water adsorption. Various techniques, including scanning electron microscopy (SEM), differential scanning calorimetry (DSC), Fourier transform infrared spectroscopy (FTIR), and optical and gravimetric analysis, were used to characterise the samples during the degradation period. Before conducting the experiment, three specimens of each membrane type were placed in a 12-well plate, sterilised with 70% ethanol, and washed with PBS (Figure 3-15 -A). 3 mL of prepared SBF was added to each sample and replaced weekly to maintain a pH level of 7.04. Samples were placed in an incubator with stirring (Figure 3-15 -C) at 37 °C, weighed every 4 weeks for up to 24 weeks, and were then vacuum dried to calculate the mass of the dried samples. Weight loss (%) was calculated by the following equation:

Weight loss (%)= 100 (M$_1$dry- M$_2$dry) x M$_1$dry   **Equation 3-2**

In which M$_1$ is the recorded mass at week 0, and M$_2$ dry is the vacuum-dried mass after a certain time point. An average of 3 samples was taken to determine the cumulative weight loss percentage of the films during degradation (H. Li and Chang, 2005).

In a separate glass specimen bottle (Fisher brand™, UK), 15mL of SBF was added to each sample, and the pH was recorded (Hanna Instruments PH211 pH Meter). The pH was then taken every 2 weeks up to 24 weeks to observe the change in pH (Figure 3-15 -B). The *In-vitro* bioactivity of these specimens was evaluated using SEM imaging to distinguish changes in the surface morphology of nanofibers after soaking in SBF.

Table 3-2 Chemical reagents and amounts used for synthesising SBF for Bioactivity assay (Kokubo and Takadama, 2006).

Order	Compounds	Chemical	Quantity (g/ ml)
1	Sodium Chloride	NaCl	8.035
2	Sodium Bicarbonate	$NaHCO_3$	0.355
3	Potassium Chloride	KCL	0.225
4	Potassium Hydrogen Phosphate Trihydrate	$(K_2HPO_4 \cdot 3H_2O)$	0.231
5	Magnesium Chloride Hexahydrate	$MgCl2 \cdot 6H_2O$	0.311
6	Hydrochloric acid 1.0M(mol/l)- HCl	HCl	39ml
7	Calcium Fluoride	$CaCl_2$	0.292
8	Sodium sulphate anhydrous	$Na_2 SO_4$	0.072
9	Tris-hydroxymethyl aminomethane	$(HOCH_2)_3CNH_2$	6.118

Table 3-3 Concentration of ions (mmol/L) in the prepared SBF compared to human blood plasma (Kokubo et al., 1990).

	Simulated Body Fluid (SBF)	Human blood Plasma
Ca^{2+}	2.5	2.5
Cl^-	147.8	103
HCO_3^-	4.2	27
HPO_4^{2-}	1	1
K^+	5	5
Mg^{2+}	1.5	1.5
Na^+	142	142
SO_4^{2-}	0.5	0.5
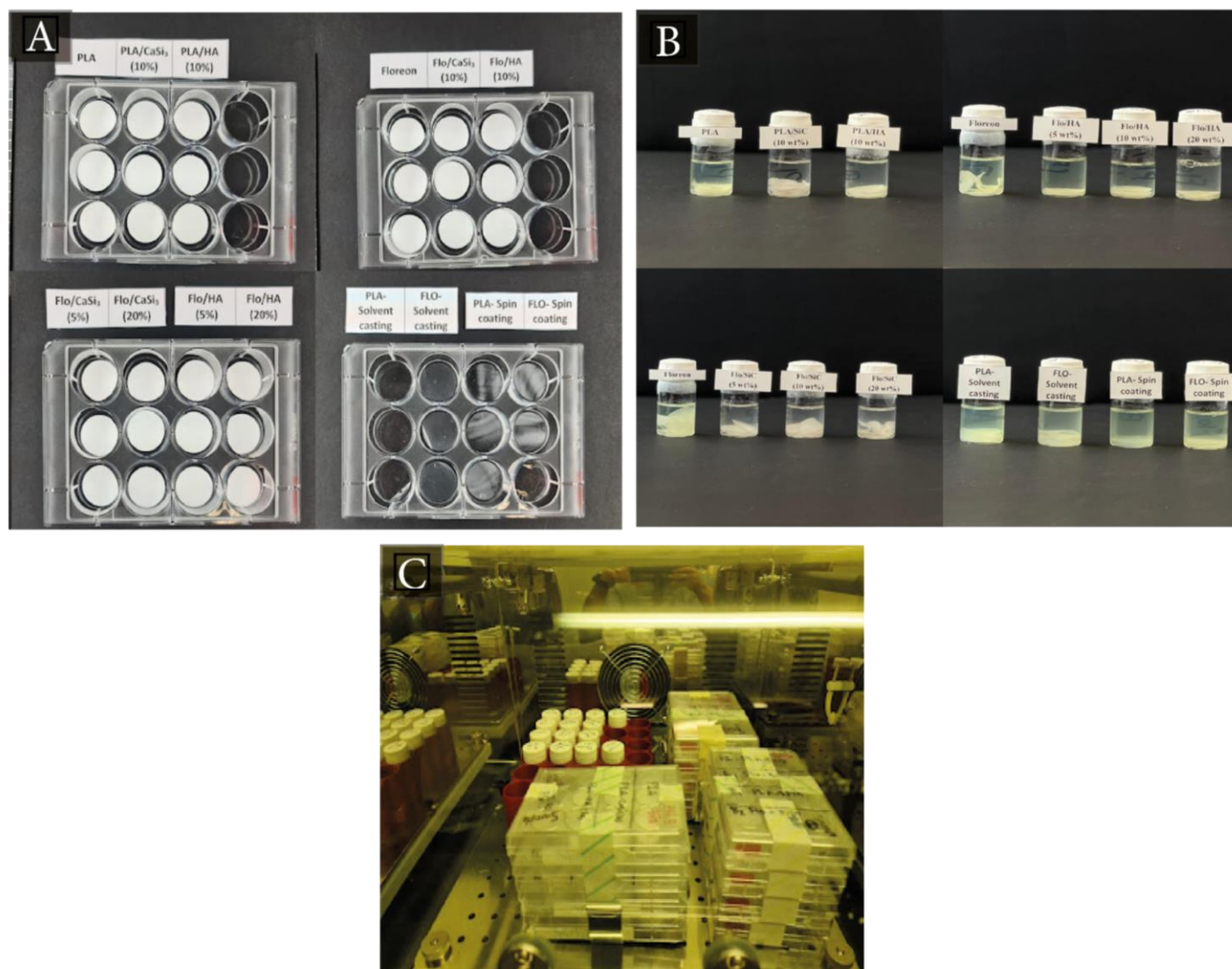
Figure 3-15 Degradation and Bioactivity Analysis preformed for all membrane; Image showing samples preparation at week 0 for Degradation (a) and Bioactivity (b) analysis, (c) showing the stirring incubator that was used in this study

3.4 Biological characterisation

3.4.1 Scaffold preparation for tissue culture

All prepared solvent-cast, spin-coated, and electrospun membranes were evaluated. Prior to cell seeding, 10-mm diameter scaffolds were punched out and sterilised in 70% ethanol for 1 hour, washed twice with PBS (Sigma-Aldrich, Poole, UK) for 15 minutes, and then soaked in basal medium (non-supplemented DMEM, Sigma Aldrich, UK) for 3 hours at 37 ℃ to enhance their hydrophilic properties (Dewey *et al.*, 2021).

3.4.2 Cell Culture

All cell culture procedures were performed inside a standard Class-II laminar flow cabinet (Walker Safety Cabinets Ltd., Glossop, UK). T-75 flasks (Fisher Scientific, Loughborough, UK) were used to expand cells using either DMEM [Dulbecco's modified Eagle's Medium] (Sigma-Aldrich,Poole, UK) or α-MEM [Minimum Essential medium] (Sigma-Aldrich,Poole, UK) for expansion of cells, which were stored in a humidified incubator with an atmosphere of 37 °C, 5% CO_2, 95% air, and 95% humidity (Galaxy R Plus CO_2 incubator, Scientific Laboratory Supplies, Nottingham, UK) . The media were changed regularly every 2–3 days, along with periodic observations of cell morphology and density, until the cells reached confluence, at which point they were passaged. Before passaging cells, media was removed and flasks were washed twice with 5 ml of sterile modified Dulbecco's PBS ((Sigma-Aldrich, Poole, UK) without calcium and magnesium to dislodge loosely attached cells and remove fraction. Following addition of 3 ml of EDTA-trypsin solution [0.05% wt/vol porcine trypsin and 0.02% wt/vol tetra sodium EDTA in Hanks balanced salt solution containing phenol red stored at -20 °C (Sigma-Aldrich, Poole, UK)], the flask was incubated at 37 °C for 5–10 minutes to detach cells. In order to neutralise the trypsin-EDTA reaction, the detached cells were diluted with 10 ml of pre-warmed fresh medium and centrifuged for 5 minutes at 1000 rpm to obtain a cell pellet in universal tubes. This suspension's supernatant was discarded carefully, and the cell pellet was resuspended in 10 ml of fresh growth medium before being reseeded in appropriate medium for each cell line and seeded at 3 x 105 cells in T-75 or 5 x 105 in T-175 tissue culture flasks.

3.4.2.1 Primary cells

- **Normal oral fibroblasts**

Normal oral fibroblasts (NOF) were provided by Dr. Helen Colley at the School of Clinical Dentistry. NOF were obtained from buccal/gingival oral mucosa during conventional dental surgeries (waste tissue collection, but no malignancy excisions) with signed informed permission (ethical approval number 09/H1308/66) as previously reported (Hearnden *et al.*, 2009). The isolation procedure was detailed by Hearnden et al. (2009). NOF-343 was utilised between passages 3–7 (Hearnden *et al.*, 2009).

- **Rat mesenchymal stromal cells**

Rat Mesenchymal Stromal Cells (rBM-MSCs) were provided by Prof. Cheryl Miller's group at the School of Clinical Dentistry. To isolate Mesenchymal stromal cells (MSCs), the bone marrow of 4 to 5 week-old male Wistar rats was obtained from the Field Laboratory (University of Sheffield) using the method described by the same group (Santocildes-Romero *et al.*, 2015), in which they followed the protocol described by Maniatopoulos, Sodek and Melcher, (1988). According to Xu *et al.*, (2012), the rBMSCs used in this study were from passages 3–6. Table 3-4 provides a summary of the primary cells used in this project and their source.

Table 3-4 Details of cell type used in this project.

Cell type	Details	Source
NOF	Normal oral fibroblast from patients 343	Charles Clifford Dental Hospital, The University of Sheffield, UK
rBM-MSCs	Male Wistar rats, 4-5 weeks of age	The Field Laboratory, Dental School, University of Sheffield

3.4.3 Culture media

Primary cells, including NOF and R-MSC, were utilised for this study (section 3.4.2.1). They were cultured in DMEM and -MEM, respectively, for their expansion. Which were supplemented with 10% (v/v) Foetal Bovine Serum (FBS), 1% (v/v) Penicillin/ Streptomycin and 1% (v/v) L-Glutamine (Sigma-Aldrich, Poole, UK); and utilised for cell growth in a humidified environment with 5% CO_2 at 37 °c as a basal medium (section 3.4.2). Types of culture media used in this project and their sources are summarised in Table 3-5.

Table 3-5 The two kinds of culture media used in this study.

Cell type	Growth Media	Additives	Source
NOF 343	Dulbecco's Modified Eagle's Medium (DMEM)	10% (v/v) Foetal Bovine Serum (FBS)	(Sigma-Aldrich, Poole, UK)
rBM-MSCs	Minimum Essential Medium Eagle (MEME) (Sigma Aldrich)	1% (v/v) Penicillin/ Streptomycin 1% (v/v) L-Glutamine	

3.4.4 Counting cells

The cells were counted using a modified Neubauer haemocytometer (Weber Scientific International, UK). In order to obtain the total cell number, the following equation was used, based on the number of cells in four 1 mm^2 squares (1 x104 ml volume) of the grid:

$$\textbf{Concentration of cells per mL} = \frac{\textbf{Number of cells x 10.000}}{\textbf{Number of squares x dilution factor}} \qquad \textbf{Equation 3-3}$$

3.4.5 Freezing cells for long-term preservation

In order to store cells for a long period, after the cells were passaged (as described in section 3.4.2), they were resuspended at a concentration of 1x106 cells/mL in freezing medium (consisting of 90% foetal bovine serum (v/v) and 10% dimethyl sulfoxide (v/v) (Sigma-Aldrich, Poole, UK). For the purpose of cryopreservation, one millilitre of this solution was filled into a cryovial (Greiner bio-one, Gloucestershire, UK) before being placed in a Mr. Frosty™ freezing container with 250 ml isopropanol. achieving a cooling rate of 1°C per minute to -80 °C before long-term storage in liquid nitrogen (196°C) for best cell preservation.

3.4.6 Recovery of frozen cells

When needed, the cryovials were thawed in a 37°C water path and then immediately re-suspended in appropriate supplemented cell culture media and centrifuged at 1000 rpm for 5 minutes. After the DMSO was removed, the pellet was resuspended in media and cultured into a 75 cm^2 tissue culture flask.

3.4.7 Cell seeding and proliferation on monolayer membrane

Membranes made with different techniques (described in Sections 3.2.2 and 3.2.3) were sterilised and soaked in a basal medium using the procedure described in section 3.4.1.

15-mm diameter circle membranes were placed in a sterile 24-well plate, and then stainless steel rings (Medical Workshop, University of Sheffield) were placed on top of the scaffolds so that the edge of the ring base completely surrounded the circle film. The samples were covered with a growth media (section 3.4.3) by pouring 500 µl of media inside the steel ring and another 500 µl around the ring. Afterward, the cell suspension following cell count was poured into the steel ring's centre. After a 24-h incubation period, the rings were carefully removed and then replaced with fresh media. Every two to three days, the media was changed. To start growing cells on the scaffolds, the cells were resuspended, counted with a hemocytometer, and then pipetted on at a density of 4000 cells/cm^2. Cell-seeded membranes were then evaluated at certain time points for cell viability, biocompatibility, or further investigation into their properties, based on the study design.

3.4.8 Co-Culture between rB-MSCs and Fibroblasts on Bi-Layer membrane

After preparing a bilayer film as described in section 3.2.5, scaffolds were then cut into 20 mm diameter circles to fit into the wells of standard 12-well culture plates under sterile conditions (section 3.4.1) with the fibrous layers facing upwards.

Once the metal rings were placed (Figure 3-16-A), r-MSC cells in relevant cell culture media were seeded on top at a density of 4000 cells/cm^2. Seeded films were incubated for 12 hours to improve cell attachment. After incubation, the rings were carefully removed and the bilayer membranes were gently attached to the Cell-crowns insert (Scaffdex, part no: Z742383, Sigma-Aldrich, Poole, UK) with the fibrous layers facing downwards (Figure 3-16-B). The inserts with bilayer membranes attached were placed into 12-well plates with sterile forceps. On the smooth layer, NOF cells were pipetted in the insert's centre at a density of 4000 cells/cm^2. The relevant cell culture media was gently pipetted into and around the insert as shown in Figure 3-16 – C and D. Then, during the incubation period, the media was carefully changed every 2-3 days. Further investigations on these membranes were conducted.
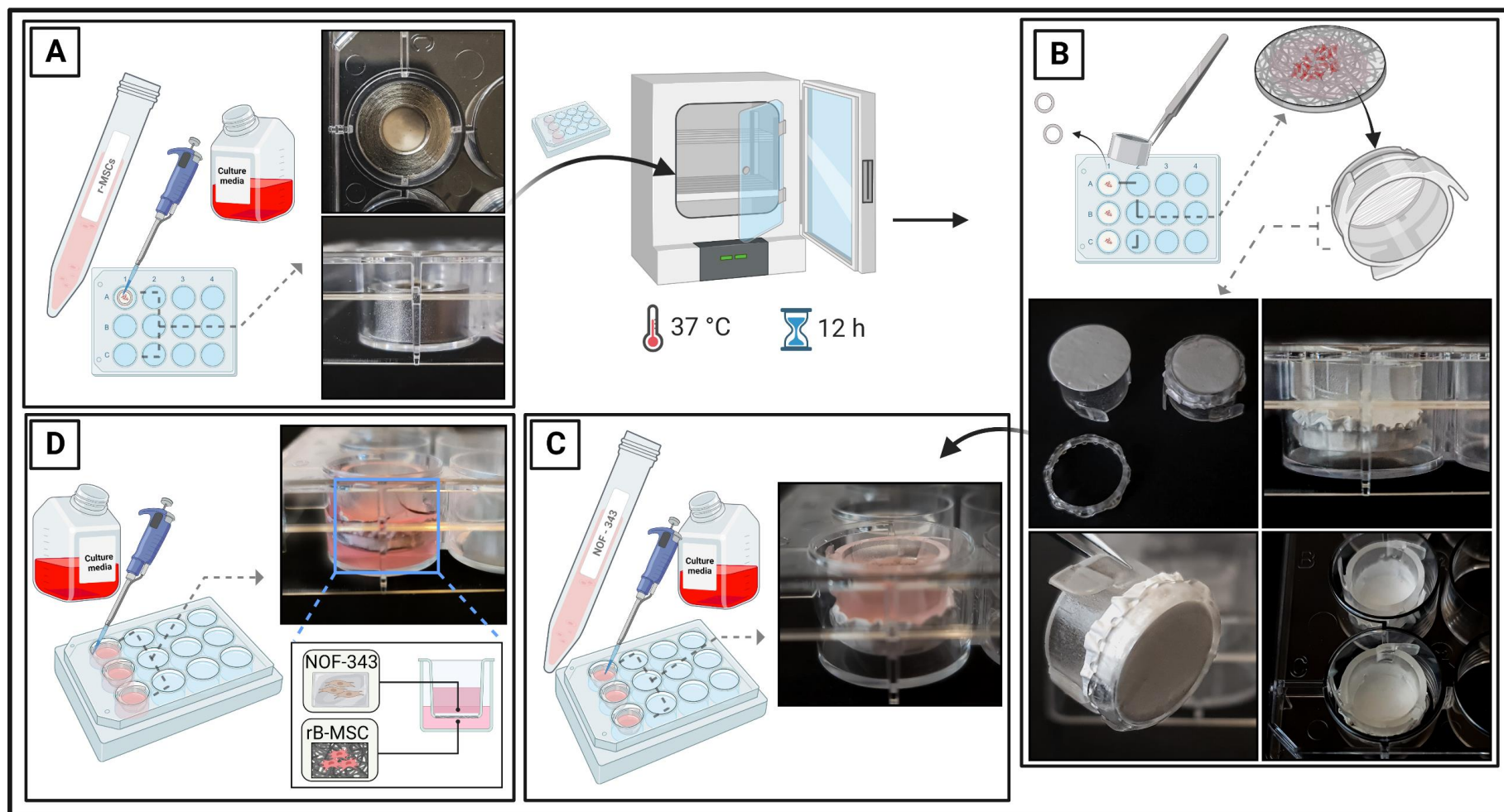
Figure 3-16 Overall schematic illustration of the process of co-culture between rBMSCs and fibroblasts on the fabricated bilayer membrane. Begin by culture rBMSCs in 12 well plates on the fibrous layer face of the bilayer membrane with steel rings (a); After 12 hours of incubation, the bilayer membrane was transferred to the cell-crown inserts with the fibrous layer facing outward (b). On the smooth layer of the bilayer membrane (C), fibroblasts were cultured, and the relevant cell culture media was carefully pipetted into and around the insert (C-D).

3.4.9 Cell attachment and proliferation assays

3.4.9.1 Cell Migration assay

The effect of Floreon and Floreon/ceramic scaffolds on cell migration was determined by the scratch cell migration assay. Scratch assays evaluate cell migration by first growing a cell monolayer to confluence in a multiwall assay plate, then making a scratch - a zone devoid of cells inside a monolayer - into which cells can grow, and finally, reconstruction of the scratched area is monitored to quantify cell migration. The experimental procedure involved the presence of scaffolds following the methodology outlined by Liang, Park and Guan, (2007) and Zadeh *et al.*, (2019). Initially, a 24-well plate was seeded with 50,000 cells per well and incubated at 37 °C in 5% CO_2 for 24 hours. The monolayer was then scratched vertically through the middle using a sterile 200 µl pipet tip. Subsequently, the membranes were attached to a CellCrown insert (Scaffdex, Sigma-Aldrich, Poole, UK) and then gently placed into the 24-well plate to avoid contact with the bottom. Finally, light microscope photographs were taken at 0,12, 24, and 36 hours to evaluate the wound closure rate (Leica, Motic).

To quantify the wound closure rate, the wound size was measured using Image J software (National Institutes of Health, USA). The initial wound area was determined to be 1165.5 mm^2. To ensure accuracy, the data were normalised using Prism software, with three samples per each type of scaffold used, and each sample measured three times. The wound closure rate was determined using the following equation:

$$\textbf{wound closure rate } (\%) = \frac{(A0-At)}{A0} \times 100 \qquad \textbf{Equation 3-4}$$

where A0 represents the initial wound area and At represents the wound area at the specified time.

3.4.9.2 Live/Dead Assay

In order to analyse the viability of the cells that were previously seeded on fabricated membranes in a 24-well plate (as described in section 3.4.7), a live/dead assay was performed using a live/dead imaging kit (LIVE/DEAD® Viability/Cytotoxicity Kit, Invitrogen™, UK).

The assay was based on the use of the acetoxymethyl-ester of calcein (Calcein-AM) and ethidium homodimer-1 (EthD-1) (Poole, Brookes and Clover, 1993; Lau, Evans and Case, 1994; Vaughan *et al.*, 1995). Calcein AM fluoresces green and indicates intracellular esterase

activity (live cells), while the ethidium homodimer-1 stain is red and binds to exposed DNA, indicating loss of membrane integrity (dead cells). At the required time points, the assay was performed by aspirating the culture media from the well of each sample, rinsing the seeded membrane with sterilised D-PBS, and addition of 100 µL of the live-dead solution was added to each well. The solution of Calcein-AM and EthD-1 was prepared by diluting 20 µL of 2 mM EthD-1 and 5 µL of 4 mM Calcein-AM from the LIVE/ DEAD® reagents in a 10 mL of culture media. The resulting working dye was then vortexed to ensure thorough mixing, and a final concentration of 4 µM EthD-1 and 2 µM calcein AM was achieved. After adding the live dead solution, the well-plate was then covered with aluminum foil to protect from light damage and incubated in a humidified atmosphere of 95% air, 5% CO_2 at 37 °C for 20 minutes. After incubation, the live/dead solution was aspirated from each well, and each sample was washed with DPBS and imaged with a fluorescent microscope (Axioplan 2, ZEISS). To accurately quantify the percentage of dead cells on each membrane type, the number of dead cells was determined using the Cell Counter plugin in ImageJ software (National Institutes of Health, USA). To ensure accuracy, three samples were analysed for each scaffold type, and each sample was measured three times. The resulting data was expressed as the mean percentage of dead cells ± standard deviation. This allowed for a comprehensive analysis of the viability of cells on each type of scaffold.

3.4.9.3   Presto Blue Assay

The PrestoBlue assay is another colorimetric approach that may be utilised for determining the total number of viable cells present in a given culture. The PrestoBlue™ Cell Viability Reagent (Invitrogen Thermofisher, UK) is a solution that is based on resazurin and that quantitatively measures cell proliferation by using the reducing ability of living cells. When cells are alive and healthy, they preserve a reducing environment within the cytosol of their nucleus. As the PB reagent enters a live cell, it is converted to resorufin, a red and highly fluorescent substance. The fluctuation in the cell's fluorescence and/or absorbance can be used to determine the health of the cell. Cells that are metabolically active constantly convert the PB reagent. The indicator dye cannot be reduced by non-viable cells; hence, they are unable to produce a change in signal.

A PrestoBlue® assay was carried out using a 10 v/v % dilution of the PB reagent in culture media; 600 µl of the PrestoBlue® media solution was added to each well, according to

the manufacturer's instructions. The 24-well plate was incubated in a humidified atmosphere of 95% air, 5% CO_2 at 37 °C. After incubating for 1 hour, 200 µL was taken out of each well and transferred to a 96-well plate. Negative controls consisting of only the cell culture medium were added to account for background signal. The fluorescence of the samples was measured using a fluorescent plate reader (Infinite M200, Tecan) with excitation and emission wavelengths of 560 nm and 590 nm, respectively. After subtracting the readings of the no-cell controls, the relative fluorescence of each treatment group was measured. PB measurements were performed in triplicate on days 1, 3, 7, 14, and 21.

3.4.9.4   PicoGreen assay

To assess the ability of the cells to proliferate on the scaffolds, the DNA content of the cell/scaffold constructs was measured using a fluorescent Quant-iT™ PicoGreen® dsDNA reagent assay kit (Invitrogen, UK). This was used as a measure of total cell number through the binding of a fluorescent dye to double-stranded DNA in the cells.

On days 7,14 and 21, cell-seeded scaffolds were washed with PBS several times (5 minutes each) and placed in a bijou that contained a known volume of cell digestion buffer; this was made using 10% TE buffer (10 mM Tris-HCL, 1 mM ethylenediaminetetraacetic acid (EDTA), pH 7.5, 1:20) in distilled water. Samples were individually left at 4 °C for 12 hours in the cell digestion buffer. Samples were then sonicated for 2 minutes before being freeze-thawed 3 times by placing them at -80 °C for 2 hours and finally at 37 °C in a dry incubator for 15 minutes. This step was repeated three times. The lysed cell solutions were transferred to 1.5ml eppendorfs before being vortexed for 15 seconds and then centrifuged for 5 minutes at 10,000 rpm.

50 µl of cell lysate from each sample and 50 µl of distilled water were added to a black 96-well plate. The DNA standard curve solutions were prepared according to Table 3-6 and 100 µl of each solution was pipetted in triplicate into separate wells. Then, 100 µl of picogreen working solution (PicoGreen concentrated dye and TE buffer (1:200)) were added to each well (test samples and standard curve wells) using a multichannel pipette before the plate was wrapped in foil and left at room temperature for 5 min. Fluorescence intensity was recorded using a fluorescence reader TECAN (Magellan V7.2 software, Infinite M200) using 485 nm excitation and 528 nm emission.

Table 3-6 Range and concentration of PicoGreen standards.

3.4.9.5 Total Protein content

Concentration of DNA (ng/mL) when PG reagent is added	Volume of DNA stock (µl)	Volume of TE buffer (µl)
1000	1000	0
500	500	50
250	250	100
100	100	250
50	50	500
0	0	1000

Total protein quantity of cells seeded on the scaffolds was measured using the BCA protein assay to assess the effect of scaffolds on NOF/r-MSC protein deposition capability.

Cell lysate for protein evaluation was taken from the same cell solution used to extract total DNA using the same extraction techniques (see 3.4.9.5). To measure the purified protein concentration, the Pierce™ (BCA) Protein Assay kit (Thermo Scientific, UK) was used. The working reagent was created by combining reagents A and B in a 49:1 ratio. The standards were made as shown in Table 3-7. In a 96-well plate, 10 µl of the samples and standards were added in triplicate. Each well was treated with 200 µl of the working reagent. The plate was wrapped in foil, and the reaction was allowed to proceed at 37°C for 30 minutes. Using a Tecan plate reader, the optical density of the samples was then determined at 562 nm (Magellan V7.2 software, Infinite M200). The absorbance of the samples was applied to the standard curve equation to calculate the protein concentration of the samples.

Table 3-7 Range and concentration of (BCA) standards.

vial	Volume of Diluent (µl)	Volume and source of BCA (µl)	Final BCA Concentration (µl/mL)
A	0	300 of Stock	2000
B	125	375 of Stock	1500
C	325	325 of Stock	1000
D	175	175 of vial B dilution	750
E	325	325 of vial C dilution	500
F	325	325 of vial E dilution	250
G	325	325 of vial F dilution	125
H	400	100 of vial G dilution	25
I	400	0	0= Blank

3.4.9.6   Alkaline phosphatase activity

Alkaline phosphatase (ALP) has been shown to be a biochemical indicator for osteogenic differentiation, and its concentration was determined spectroscopically at 405 nm using p-nitrophenyl phosphate (Sigma-Aldrich) as a substrate.

After 21 days of growth of r-MSC on studied electrospun membranes in basal and osteogenic medium (StemPro Osteogenesis Differentiation Kit, Gibco, A1007201), the cell-scaffolds were washed three times with PBS, and the cells were lysed according to the procedure described in Section 3.4.9.4. The ALP Activity Assay Substrate (p-nitrophenyl phosphate) was prepared by dissolving 6.6 mg of pNPP in 1 ml of distilled water and wrapping it in foil. 10µl /20µl of each sample (for osteogenic and basal cultures, respectively) were put on a 96-well plate followed by an ALP buffer to achieve a total volume of 240 µl (230 / 220 µl respectively). To activate the reaction, 10 µl of ALP Activity Assay Substrate was added, and samples were incubated at 37 °C for 30 minutes before absorbance was read at 405 nm. Results were compared with a standard curve of concentrations that was prepared as shown in Table 3-8.

Table 3-8 Range and concentration of pNPP standards.

Concentration of pNP (nmole/mL)	Volume of stock/ previous dilution (mL)	Volume of ALP buffer (mL)
250	0.05 of stock	1.95
100	0.8 of previous dilution	1.2
50	1	1
10	04	1.6
0	0	1

3.4.9.7 Imaging of cell cultures on membranes

- **Scanning electron microscopy**

SEM was used to evaluate the influence of the studied membranes on cell morphology and growth. In order to prepare samples for scanning electron microscopy, a hexamethyldisilazane (HMDS) staining protocol was used. To begin this process, samples were washed three times with PBS to remove the medium. Following this, the samples were fixed with 2.5% glutaraldehyde in PBS for 60 minutes. After this incubation period, the samples were washed three more times in PBS. Later, the samples were washed once again, but this time with distilled water. Next, the samples were dehydrated through a series of graded acetone solutions, starting at 70%, 80%, 85%, 95% and ending at 100% vol/vol. After dehydration, and still inside the fume cupboard, the samples were dried to a critical point using 50/50 hexamethyldisilazane and ethanol, followed by washing them twice in 100% hexamethyldisilazane. After the samples had been treated with HMDS, the HMDS was taken off and they were allowed to air dry in the fume hood for an hour. After the samples were dried, they were gold-coated for imaging.

- **Immunofluorescence**

In order to study the morphology of the cells attached to the studied membranes, the cell nucleus and actin filaments were stained with DAPI and phalloidin TRITC (Merck Millipore, Darmstadt, Germany) and imaged under fluorescent microscopy. After 3, 7, and 14 days of culture, samples were washed three times with 1x buffer (0.005% Tween-20 in PBS) for 5 minutes to remove any residual media before being fixed by immersion in 4% paraformaldehyde in PBS at room temperature for 20 minutes. After rinsing twice with a wash buffer, the samples were permeabilised with 0.1% Triton X-100 in 1X PBS for 10 minutes at room temperature, followed by washing twice with a wash buffer. The samples were immersed in a blocked solution (1% bovine serum albumin (BSA) in PBS) for 30 min at room temperature, then were again washed once with 1x wash buffer. Final solutions of phalloidin-TRITC and DAPI (4′, 6-diamidino-2-phenylindole dihydrochloride) (Sigma-Aldrich) were made in PBS just before the incubation process (phalloidin-TRITC, 1:700; and DAPI, 1:1000). The samples were first incubated in a foil with phalloidin-TRITC for 45 minutes at room temperature to stain the actin filaments of the cytoskeleton. After three washes with 1x wash buffer (5–10 minutes per wash), samples were incubated for 15 minutes with DAPI to dye the cells' nuclei. The samples were washed again three times with 1x wash buffer (5–10 minutes per wash) before being kept in PBS for imaging with a Zeiss LSM 510 confocal microscope.

3.4.9.8 Histology analysis

The histological stain H&E was chosen to identify cell nuclei to determine if the bilayer membrane, prepared as described in Section 3.2.5, contained cells and also to study cell location and barrier layer efficiency. After 3 days of culture, samples were washed three times in PBS for one minute before being fixed in 3.7% formaldehyde solution for 50 minutes and immersed in 1% sucrose solution for 30 minutes before being embedded in an optimal cutting temperature compound (OCT) (Fisher). Using a cryostat (NX 70 HOMVPD Cryostar, Thermo Fisher Scientific, Waltham, MA, USA) at -24°C, samples were thinly sectioned at 5m thickness and mounted on Superfrost Plus ® slides (Thermo Fisher Scientific, #4951PLUS, Germany). The slides were then washed in water for one minute to eliminate any residual cryostat optimal cutting temperature compound (OCT) medium before being stained with hematoxylin and eosin (H&E). Images of stained slices were obtained using the 10X and 20X objectives of a light microscope (Leica, Motic) with 10X and 20X objectives. The Motic Tek software (Motic, Kowloon, Hong Kong) was used to capture the images. Image J (NIH, USA) software was used to scale the images that had been saved.

3.5 Statistical analysis

All quantitative values are given with a mean ± standard deviation (SD). Through an ANOVA test coupled with Tukey's HSD post hoc analyses, statistically significant differences were determined throughout the experiments. The significance of the findings is signalled by using (∗) symbols, where

(∗) indicates that significant differences have been recorded while the value of p is less than 0.05.

(∗∗) indicates that very significant differences have been recorded while the value of p is less than 0.01.

(∗∗∗) indicates that extremely significant differences have been recorded while the value of p is less than 0.005.

All obtained data were analysed using GraphPad Prism software (version 7.04)

.

CHAPTER 4:

RESULTS AND DISCUSSION

Chapter 4: Results and Discussion

This chapter is divided into three sections; Section I is related to the thin films/ membranes (Surface layer) and their complete characterisation; Section II is about electrospun porous scaffolds (Core layer) and complete characterisation of random mats. Section III presents results related to the bilayer membranes. Each section of this chapter contains a brief introduction and then description of the results.

4.1 Section I: Fabrication and characterisation of fibrous membrane

The characterisation of Floreon membranes that have been created by an electrospinning technique in order to act as a functional bone regeneration membrane will be discussed in the following section. The effect of introducing bioceramics (HA and $CaSiO_3$) at different concentrations (5%, 10%, and 20% by weight) was investigated. These findings were compared to those obtained by using PLA membranes.

The following flowchart (Figure 4-1) summarises the tests carried out to assess the characteristics of fibrous membranes. This involved investigating the properties of the raw materials that were utilised in the fabrication of the membranes, followed by studying the physical and chemical properties, as well as the biocompatibility of the membranes that were made.
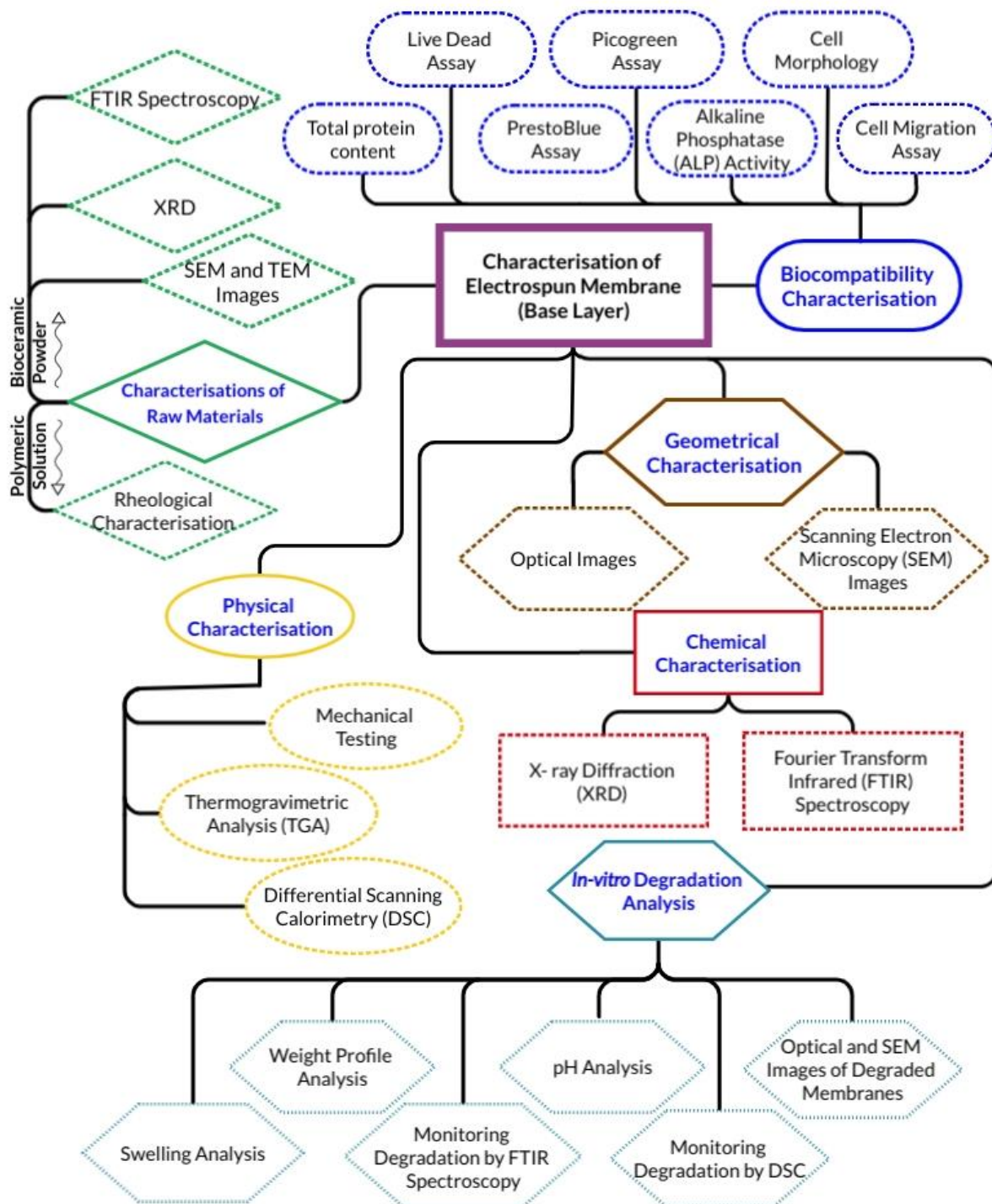
Figure 4-1 a flowchart illustrating the characteristics tests performed on the electrospun fibrous membrane.

4.1.1 Characterisation of Raw Materials

4.1.1.1 Bioceramic HA and CaSiO₃ Powder

• SEM and TEM Observations

Scanning Electron Microscopy (SEM) and Transmission Electron Microscopy (TEM) and are used to obtain a very high-resolution image in order to determine the surface morphology and the size of bioceramics particles. Figure 4-2 depicts SEM and TEM micrographs of hydroxyapatite and Calcium Silicate particles.

Figure 4-2 (A,B) and (D,E) show SEM images of hydroxyapatite and calcium silicate particles at two different magnifications. Hydroxyapatite has an average particle diameter of 1.03 μm ± 0.25 SD and the length was 3.44 μm ± 1.45 SD, whereas $CaSiO_3$ has a particle diameter of 2.80 μm ± 1.05 SD and the length was 6.13 μm ± 2.11 SD. Images taken at 10 μm show that the texture of hydroxyapatite powder is considerably smoother than that of calcium silicate powder.

Figure 4-2 (c and f) illustrates the detailed structure and orientation of two bioceramics at 200 nm resolution, as determined by transmission electron microscopy (TEM). As observed in Figure 4-2 (C), the hydroxyapatite particles are scattered and a bit lighter than the calcium silicate powder particles in Figure 4-2 (F). The bright and dark contrast appear so in the micrographs due to differentiative abilities of Hydroxyapatite and Calcium Silicate to diffract the electron beam. The contrast is darker if the material is thick because the beam interacts more in that case.

Hydroxyapatite (HA)   **Calcium Silicate (CaSiO₃)**
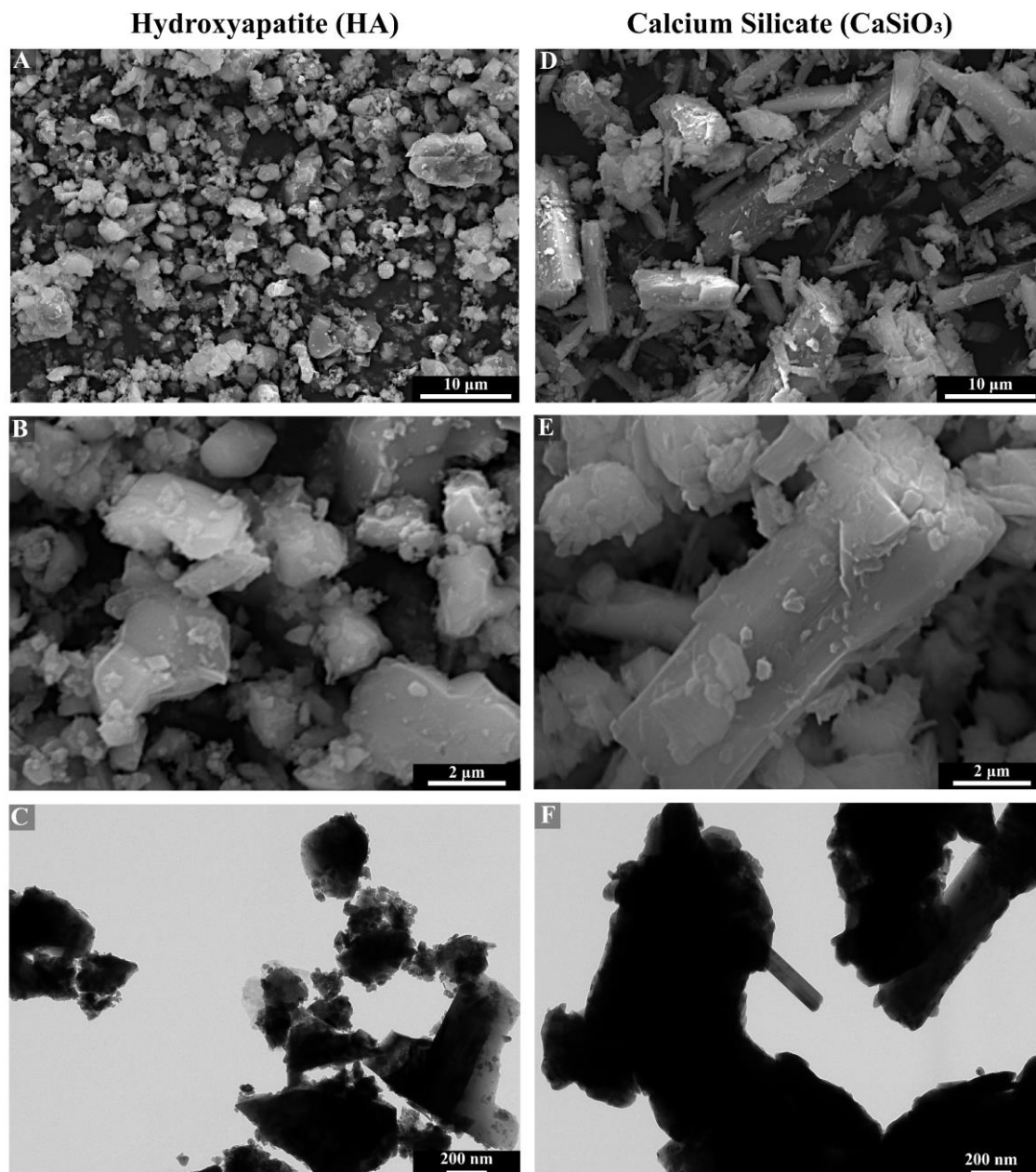
Figure 4-2 The morphology of HA and CaSiO$_3$ particles using SEM (A, B, D, and E) and TEM (C and F).

Although adequate morphology, microstructure, physical and mechanical properties are important issues for guided bone regeneration, osteoconductivity is also crucial (Wang *et al.*, 2005). In order to create a GBR membrane with osteoconductive properties, incorporation of bioceramics into the structure of GBR membranes is key. In this research, HA and CaSiO$_3$ were incorporated as bioceramics in the structure of the GBR layer.

As detailed in the methods section (section 3.3), the bioceramic materials were studied with SEM and TEM, and their particle dimension was compared with that provided by the manufacturer. SEM images of CS (CaSiO$_3$) revealed aggregated sphere-shaped particles with an average particle size of 2.797 μm, this was confirmed by the manufacturer (NYCO Minerals), as it showed that the size of these particles ranged between 2-23 μm (NYCO Minerals, 2002). The findings in the present study align with the results reported by Chrysafi *et al.,* as their SEM analysis of the CS material revealed the presence of crystallite and spherical 2CaO.SiO$_2$ particles with an average particle size ranging from 1 to 3 μm. Although the particle sizes are similar to ours, the synthesised particles used in these reported studies had spherical, smooth, dense, and a few crystallite morphologies that formed agglomerates (Wan *et al.*, 2005; Chrysafi, Perraki and Kakali, 2007).

- **X-ray diffraction (XRD) analysis**

The XRD oatterns were collected using a continuous scan mode and 2θ angle from 5 to 50 degrees. represents XRD pattern of HA and CaSiO$_3$.

Figure 4-3 illustrates x-ray diffraction patterns for hydroxyapatite and calcium silicate particles. The graph plotted for Hydroxyapatite has the sharp peaks at angles 25° plane (201), 32° plane (211), 32.5° plane (112), 33° plane (300), and 50° plane (213) indicating larger crystallites here. While the graph plotted for Calcium Silicate has the greater peaks are at angles 11° plane (200), 23.8° plane (440), 25.5° plane (102), 26.5° plane (202), 29° plane (202) and 30° plane (320). This difference in peaks for both materials describe the level of crystalline structure of each HA and CaSiO$_3$. The smaller and broader peaks show smaller crystallites in the material. Based on the Scherrer equation calculation for the greatest peaks as 32° plane (211) (for hydroxyapatite) and 23.8° plane (440) as well as 26.5° plane (202) (for calcium silicate). Based on the results obtained, it can be concluded that hydroxyapatite and calcium silicate possess similar levels of crystallinity. The incorporation of these materials into the combinations investigated in this study could potentially enhance their crystallisation properties.
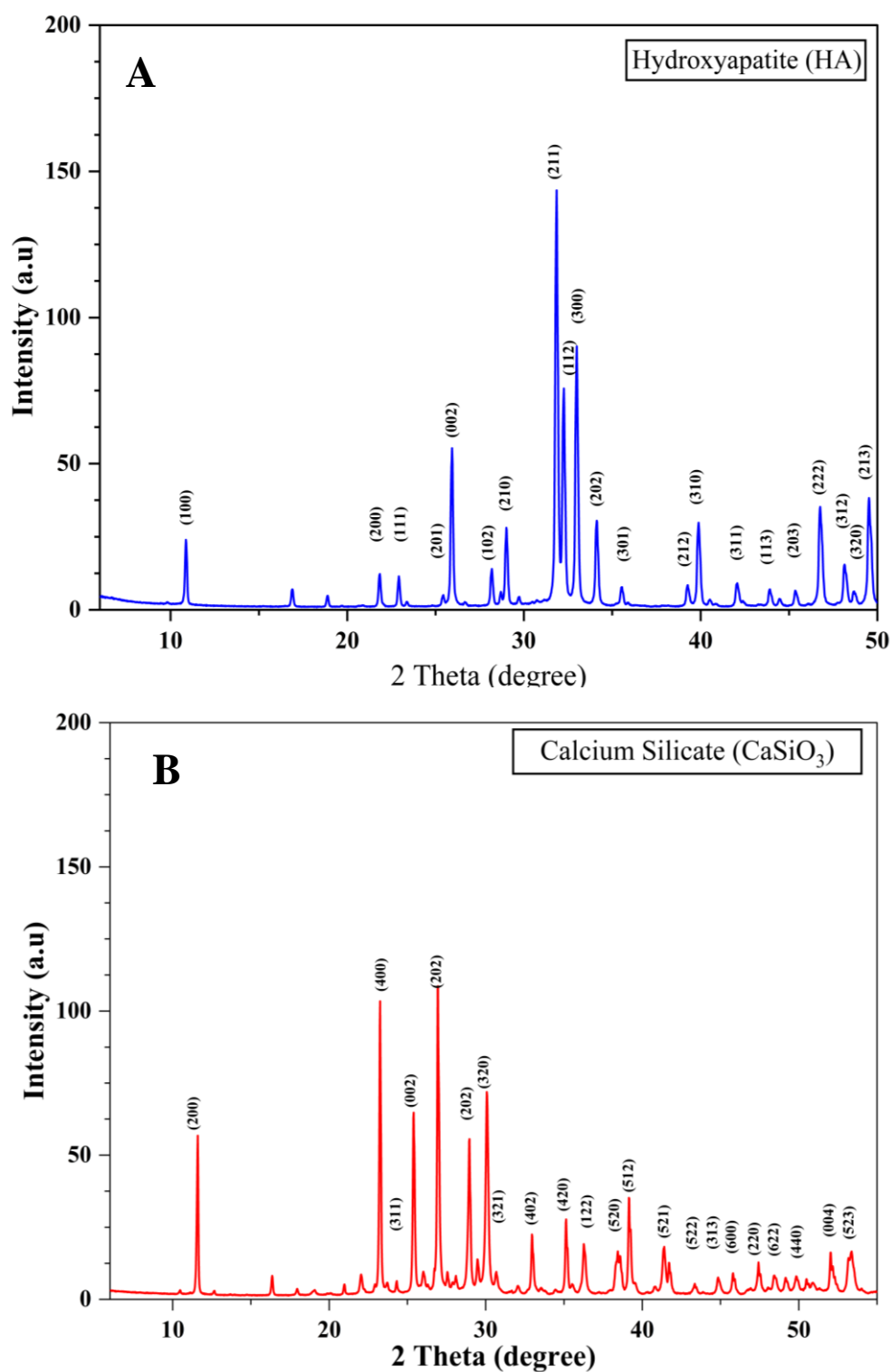
Figure 4-3 XRD for (a) Hydroxyapatite and (b) Calcium Silicate particles

X-ray diffraction (XRD) is a highly valuable analytical technique that enables the investigation of the atomic structure of materials via the elastic scattering of X-rays from the electron clouds of individual atoms. The dynamical theory of diffraction provides a theoretical framework for describing the scattering of X-rays from crystals (Selvan, Rachel and Gajendran, 2021). By comparing the lattice parameters, crystal structures, and crystallinity values of nanoparticles to known values, XRD can accurately identify the compounds present within them. In this study, XRD was employed to investigate the crystalline structure of bioceramics in order to evaluate the effect of bioceramic addition on Floreon and PLA membranes. The aim was to determine whether the incorporation of bioceramics would compromise the structural integrity of the membranes and to obtain a comprehensive understanding of the underlying mechanisms. The XRD pattern showed characteristic peaks which were consistent with the peaks given for HA and $CaSiO_3$ by the International Diffraction Data Centre, thus validating the XRD data values. Several previous studies have shown the crystalline nature of HA (Kaygili *et al.*, 2016) and $CaSiO_3$ (Palaniraja *et al.*, 2017). The strongest reflections of HA were detected at 25º (201), 32° (211), 32.5° (112), 33° (300), and 50° (213). On the other hand, $CaSiO_3$ showed sharp peaks at 11° (200), 23.8° (440), 25.5° (102), 26.5° (202), 29° (202) and 30° (320). The X-ray diffraction peaks for both $CaSiO_3$ and HA show that the materials crystallised successfully. This observation is consistent with those reported by Yuan-Ling Lee et al. and S A Manafi et al. (Manafi *et al.*, 2008; Lee *et al.*, 2017).

- ## **Fourier Transform Infra-Red (FT-IR) analysis**

Figure 4-4 shows the FTIR results of HA and $CaSiO_3$.The spectra were measured at a resolution of 4 cm-1, and a total of 128 scans in the spectral region of 4000 - 400 cm-1 were recorded. Prior to obtaining sample spectra, a carbon sample's background spectrum was produced.

FT-IR spectra of $CaSiO_3$ revealed bond bending modes at 460 cm^{-1} for O-Si-O and Si-O-Si bonds, bond stretching modes at 800 cm^{-1} for O-Si-O bonds, and bond stretching modes for Si-O-Ca bonds with non-bridging oxygen at 950 cm^{-1}. At 1080 cm^{-1}, symmetric stretching vibrations of Si–O–Si bonds were detected, followed by vibrations of the NO_3^- ion were at 1380 cm^{-1}, while vibrations of H_2O+ were found at 1630 cm^{-1}. However, the O-Si-O vibration causes the absorption bands to appear between 750 and 1170 cm^{-1}, while the Si-O vibration causes the absorption bands between 415 and 600 cm^{-1}. The release of water molecules that had been trapped within the solid matrix may be responsible for the drop in the band at 3445 cm^{-1} that occurs with increasing calcination temperature. The FT-IR spectrum of hydroxyapatite showed that the bending modes of PO_4^{3-} and OH^- lie in between 600 to 700 cm^{-1} range. However, vibrations of CO_3^{2-} and OH^- were observed at 1480 cm^{-1} and 1990 cm^{-1}

respectively. The absorption band of hydroxyapatite present in the range of 750–1170 cm^{-1} is due to vibrations of PO_4^{3-}.
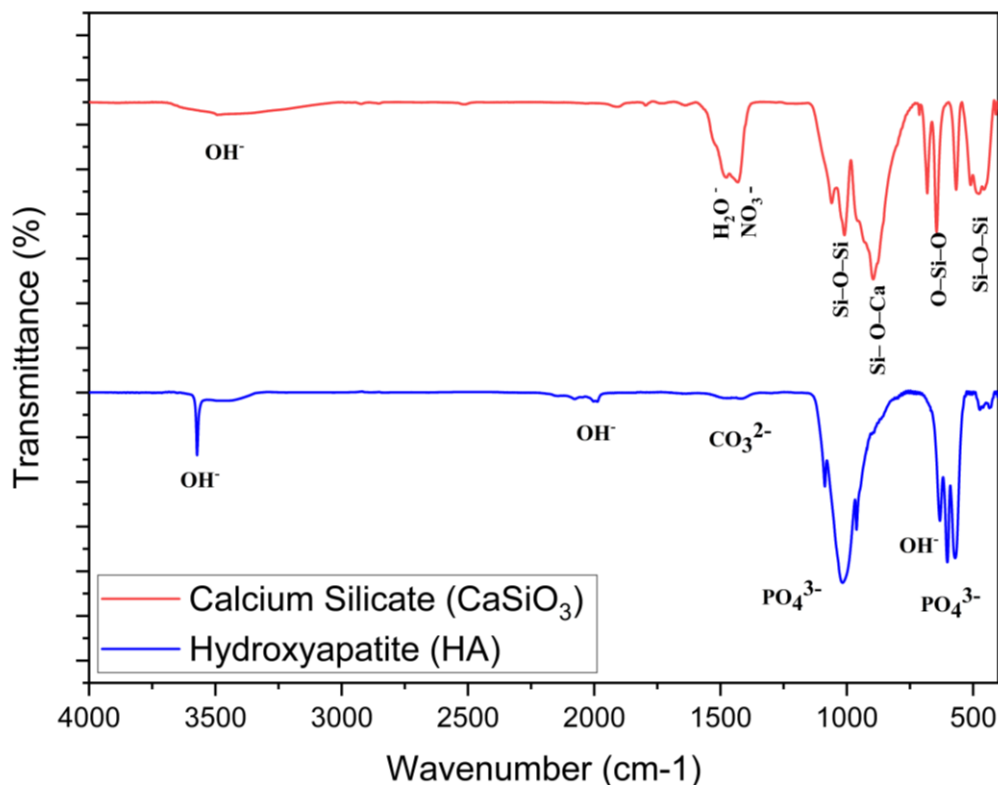
Figure 4-4 FTIR spectra of Hydroxyapatite and Calcium Silicate particles.

The FTIR of HA and CS is shown in Figure 4-4 and demonstrates the appearance of phosphate and/or SiO2 bands at 600, 1080, and 750 cm^{-1}. According to Kim et al., the bands of calcium silicate that were assigned to the symmetric stretching vibration of Si-O-Si bands appeared at 1080 cm^{-1}(Kim *et al.*, 2008). Additionally, CS's FT-IR spectrum reveals the presence of Si-O bands that are stretching and bending at wavelengths of 800-1000 and 400-600 cm^{-1}, respectively. Other groups have also observed this result, which is linked to the presence of modifier oxides in the silica network (Laudisio and Branda, 2001; Chrysafi, Perraki and Kakali, 2007).

4.1.1.2 Viscosity of polymeric solutions

To explore the relationship between the viscosity and the obtained mats, the complex viscosity of PLA and Floreon solutions containing different concentrations of HA and $CaSiO_3$ particles were measured as the function of frequency. Figure 4-5 and Figure 4-6 show the values of the complex viscosity η * for the solutions with including of HA and $CaSiO_3$ bioceramic particles correspondingly. As expected, the viscosity of solutions increased as more bioceramic particles were added; this was observed for both HA and $CaSiO_3$. The viscosity of the FLO/$CaSiO_3$ (20% wt) and FLO/HA (20% wt) solutions was higher than that of the Floreon solution at the higher frequency investigated, especially prior to the last quarter of the test. The control group also demonstrated the same relationship, with 10% HA or $CaSiO_3$ added to PLA increasing viscosity. Throughout the majority of the test, the viscosity of PLA and Floreon solutions was comparable, and the viscosity of all solutions decreases slightly as the shear rate increases.
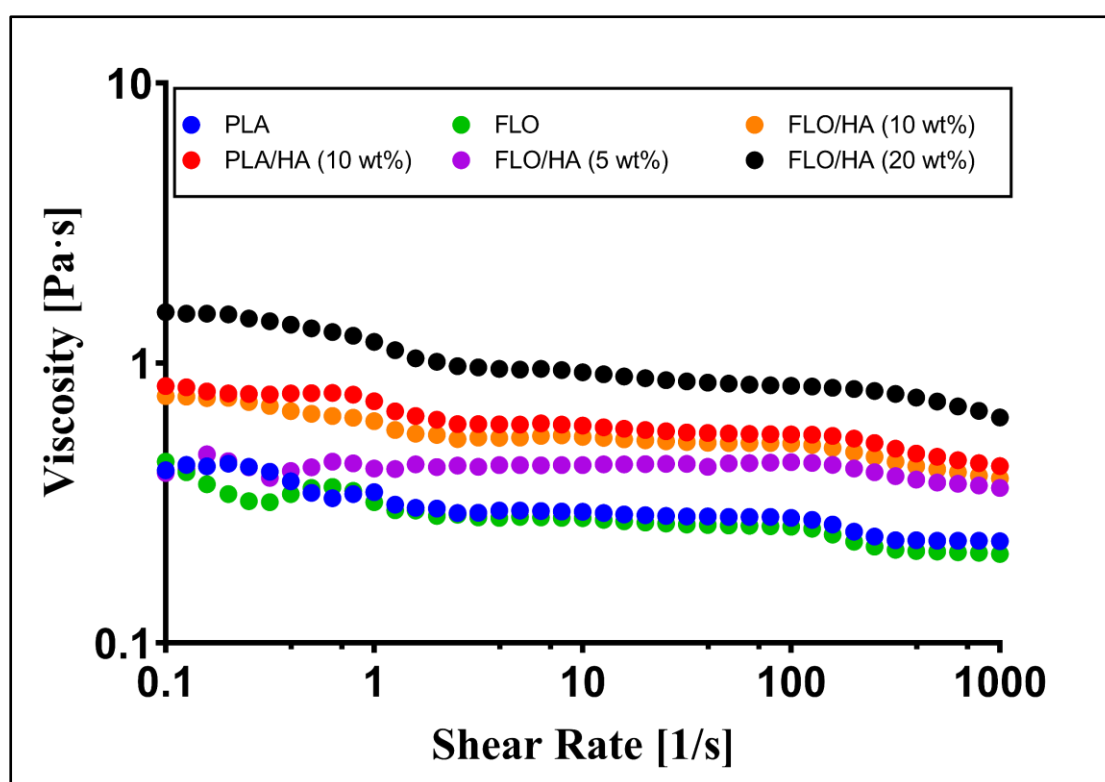
Figure 4-5 Complex viscosity (η *) of PLA, Floreon and their blends with different concentrations of Hydroxyapatite particles.
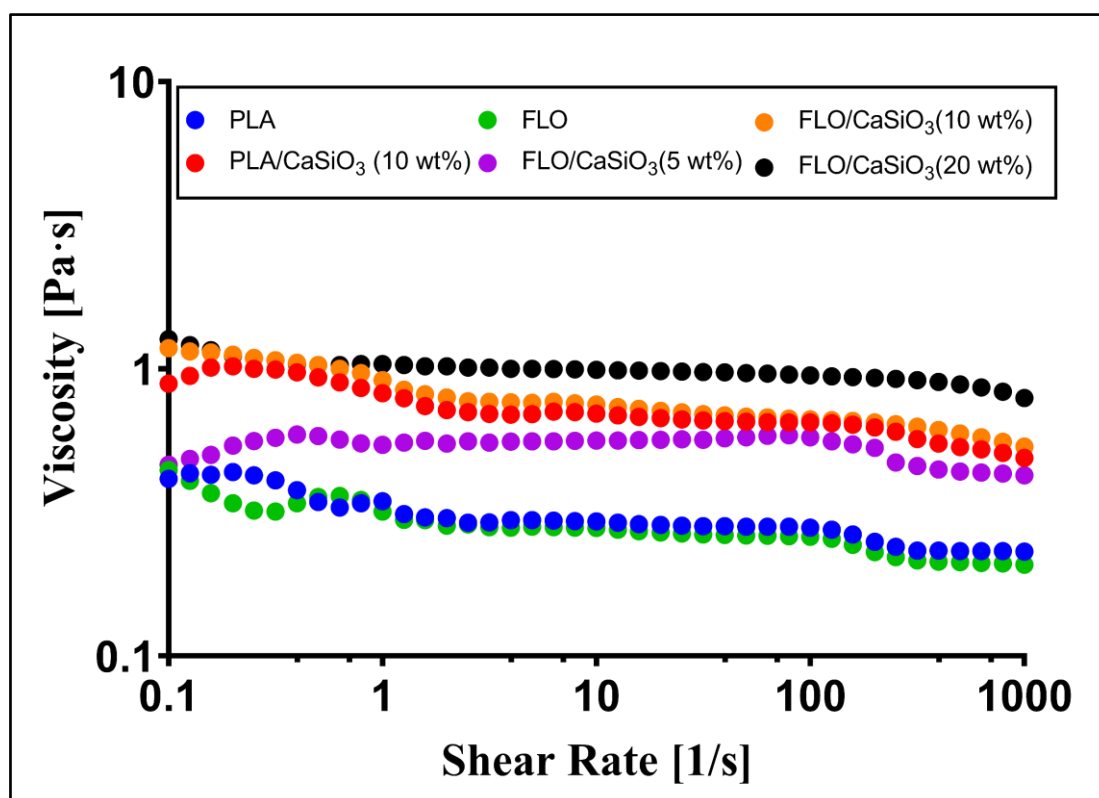
Figure 4-6 Complex viscosity (η *) of PLA, Floreon and their blends with different concentrations of Calcium Silicate particles.

The bioceramics were analysed as powders and were added to the constructs. The concentration of HA and $CaSiO_3$ had an important effect on microfibre morphologies. Three concentrations of bioceramic in solution (5%, 10%, and 20%) were studied at this stage. The untreated solutions of PLA and Floreon were prepared to have a low viscosity. The viscosity of the solution increased with the incorporation of HA and $CaSiO_3$ particles. The Floreon/$CaSiO_3$ (20% wt) and Floreon/HA (20% wt) solutions appeared to have higher viscosities compared to lower concentrations (Figure 4-5 and 6). It was reported that the incorporation of HA increased the solution viscosity in their studies (Hassan and Sultana, 2017). They observed that as the HA concentration increased, the PCL fibre's diameter also increased. It should be noted that larger diameter fibres are produced when the viscosity of the solution is further increased. This is because a polymer's chain entanglement and stress relaxation time increase with increasing viscosity. Due to these circumstances, the electrospinning process solution was ejected from a jet without it breaking up, which resulted in a larger fibre diameter (Wutticharoenmongkol, Pavasant and Supaphol, 2007; Sun *et al.*, 2014).

4.1.2 Characterisation of fibrous membranes: SEM

The basic aim to perform scanning electron microscopy is to dig deep into the structure of membrane and the texture of surface with and without adding the proposed bio-ceramic materials. Figure 4-7 through Figure 4-9 show SEM micrographs of PLA and Floreon fibrous membranes with various concentrations of Hydroxyapatite and Calcium Silicate particles. All the images were scaled at 20µm and 10µm.

At both investigated magnifications, it is observed that both PLA and Floreon membranes are homogeneous and free of beads or tiny crystalline particles. The PLA/HA and Floreon/HA membranes, on the other hand, as can be seen in Figures 4.3.2-3 and 4.3.2-1, contain smaller beads or crystals, the abundance of which varies depending on the concentration of the bioceramics that were added. Similarly, PLA/CaSiO$_3$ and Floreon/CaSiO$_3$ membranes can be observed to have smaller beads and smaller particles embedded in between the fibres. These particles can be clearly seen in the images scaled at 5µm.

The images also allowed for the visualisation of surface roughness in all groups and how it varies with the addition of bioceramic particles.
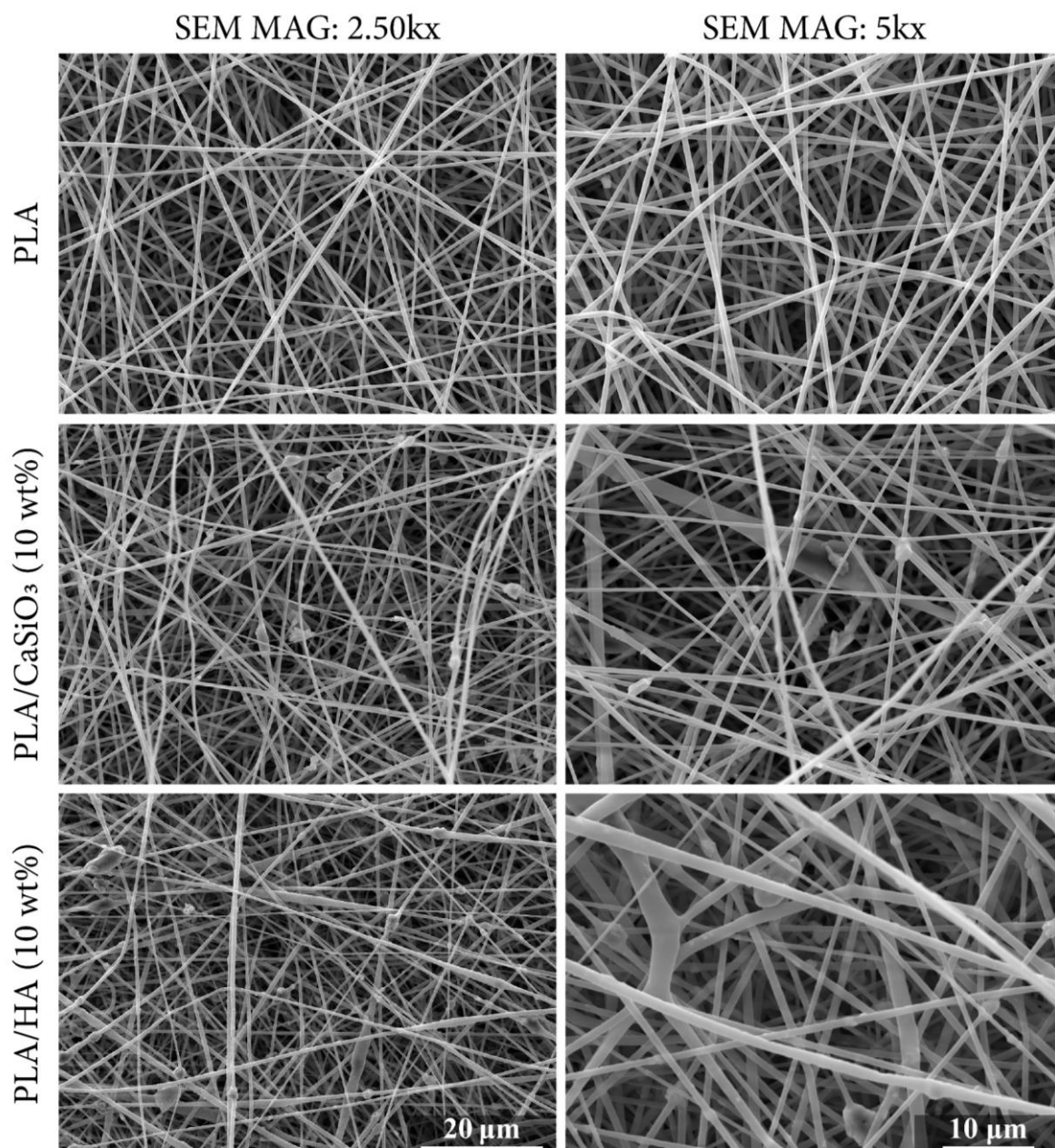
Figure 4-7 SEM micrographs of electrospun PLA fibrous membranes containing 10 wt% of HA and CaSiO3, the micrographs in the left column are scaled at 20 µm, while those in the right column are scaled at 10 µm.
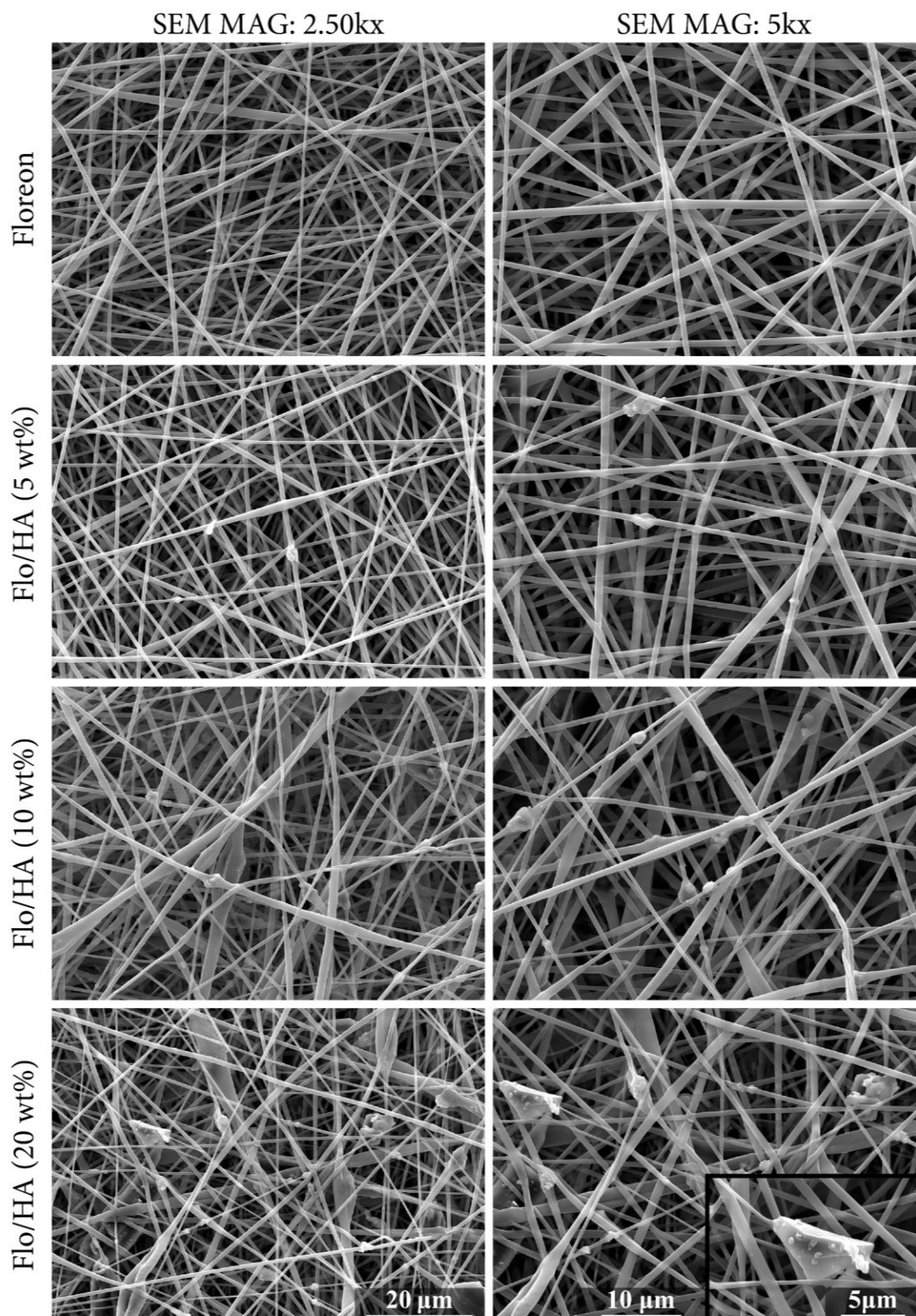
Figure 4-8 SEM micrographs of electrospun Floreon fibrous membranes containing different concentrations (5,10 and 20 wt%) of HA, the micrographs in the left column are scaled at 20 µm, while those in the right column are scaled at 10 µm. The lower right corner image is a zoomed-in view, scaled at 5 µm.
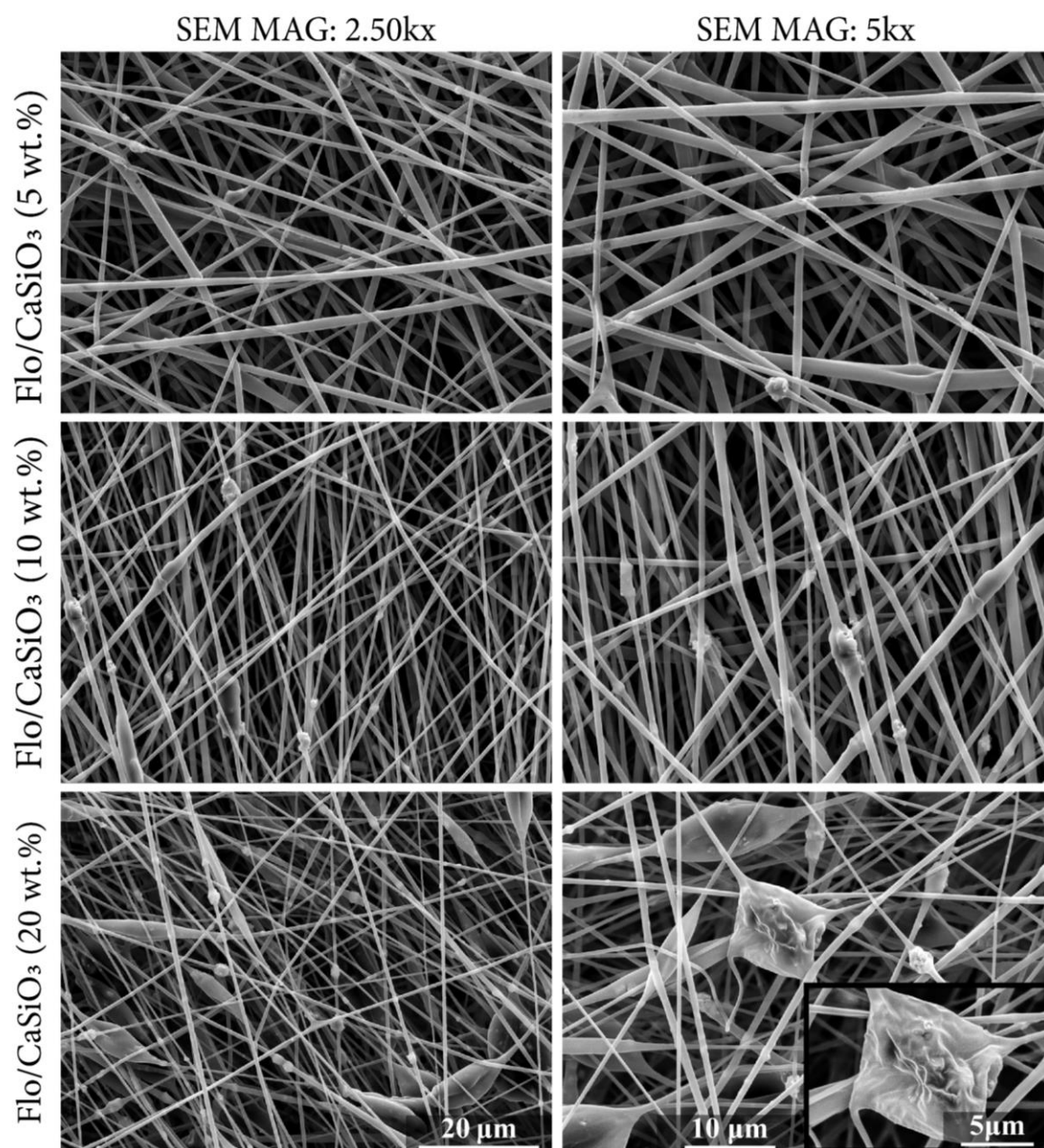
Figure 4-9 SEM micrographs of electrospun Floreon fibrous membranes containing different concentrations (5,10 and 20 wt%) of $CaSiO_3$, the micrographs in the left column are scaled at 20 µm, while those in the right column are scaled at 10 µm. The lower right corner image is a zoomed-in view, scaled at 5 µm.

4.1.3 TEM of fibrous membranes

To explore the distribution of HA /CaSiO$_3$ particles in fibrous PLA /Floreon membranes, TEM images of films containing varying concentrations of bioceramics were investigated. The TEM images of the corresponding PLA/Floreon membranes are displayed in Figure 4-10 to Figure 4-12.

It is demonstrated that the particles of HA/CaSiO$_3$ formed more agglomerates that were well adhered to the fibres and that the particles were not evenly distributed. It is also illustrated that the varying concentrations of ceramic added can affect the degree of particle agglomeration.
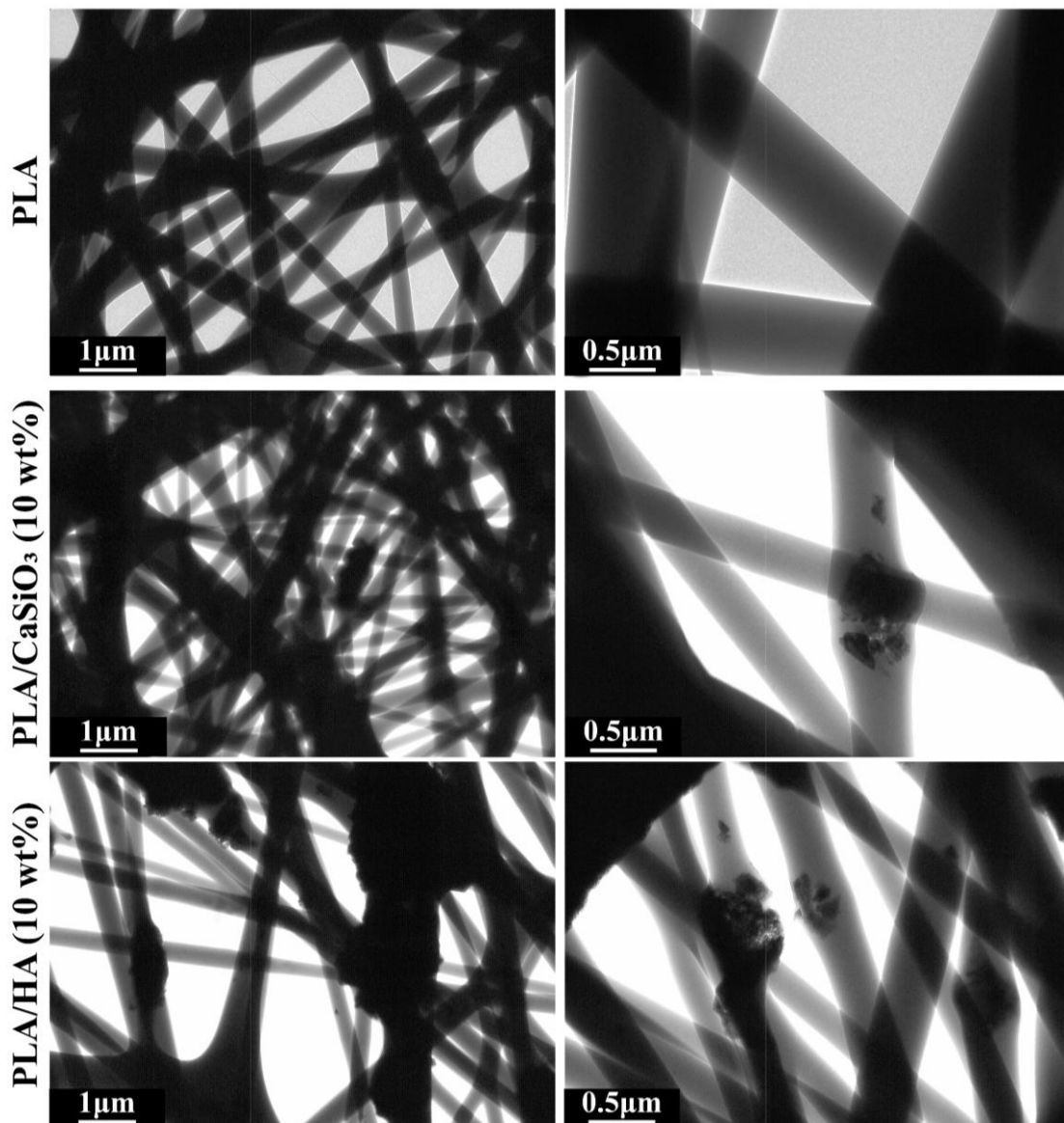
Figure 4-10 TEM micrographs of electrospun PLA fibrous membranes containing 10 wt% of HA and CaSiO$_3$, all images scaled at 1 and 0.5 µm.
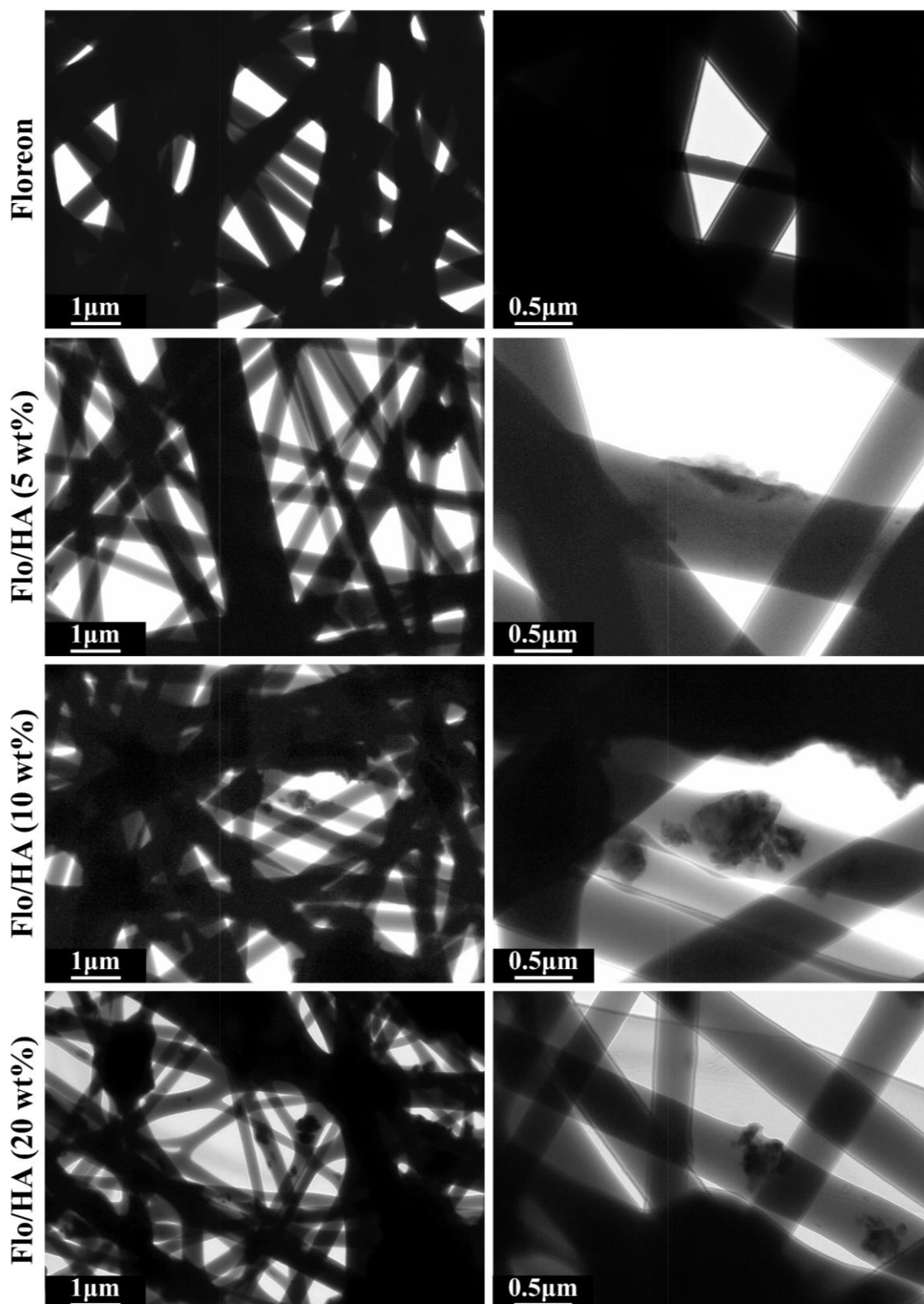
Figure 4-11 TEM micrographs of electrospun Floreon fibrous membranes containing different concentrations (5,10 and 20 wt%) of HA, all images scaled at 1 and 0.5 µm.
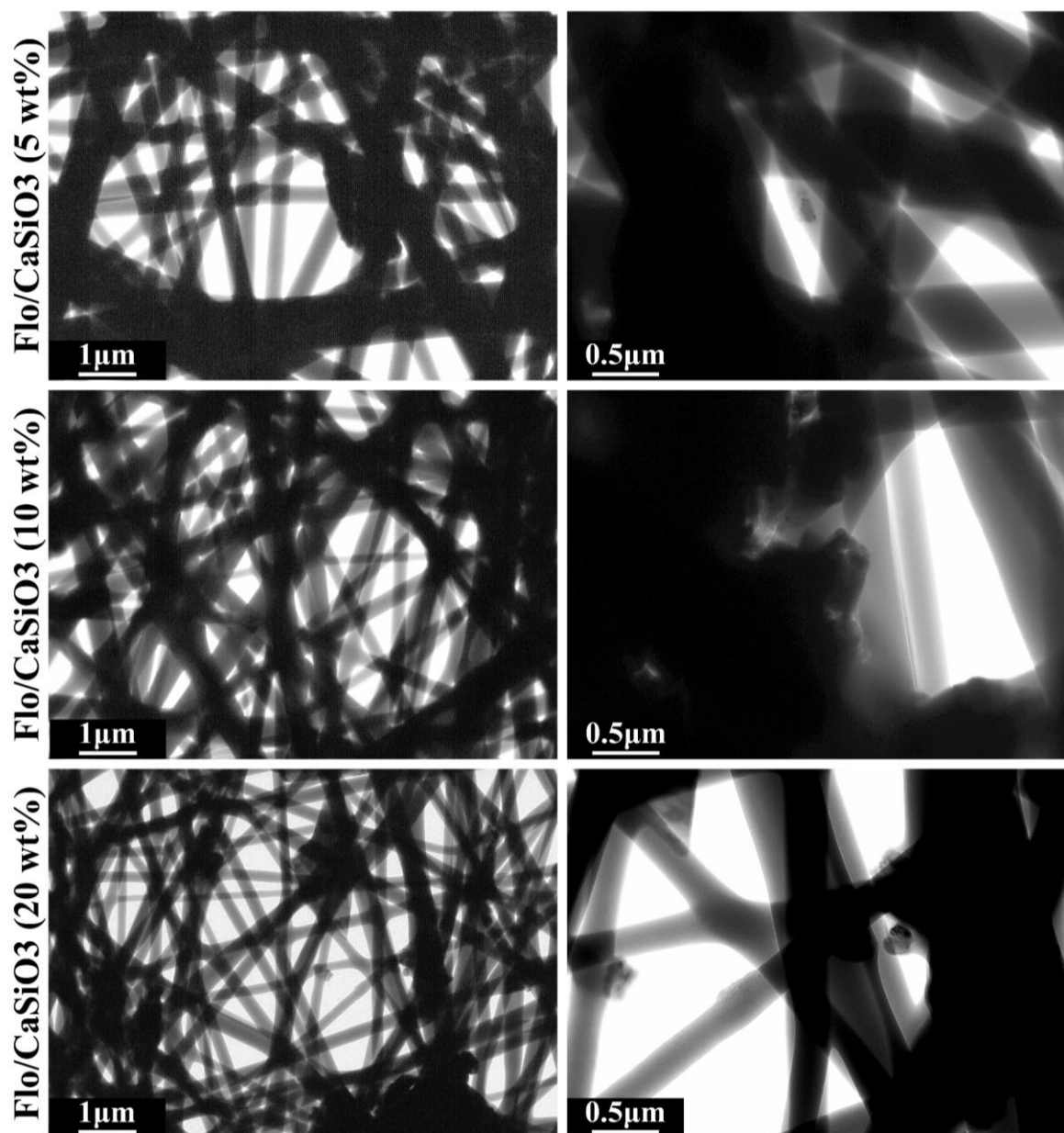
Figure 4-12 TEM micrographs of electrospun Floreon fibrous membranes containing different concentrations (5,10 and 20 wt%) of CaSiO$_3$, all images scaled at 1 and 0.5 µm.

To examine the morphological structure of Floreon and PLA constructs, SEM and TEM studies were undertaken. The SEM images for the Floreon and PLA membranes at various HA and CaSiO$_3$ concentrations are shown in Figure 4-7 to -9. TEM images, on the other hand, investigated the level of HA/CaSiO$_3$ particle agglomeration (Figure 4-10, -11, and -12). Here it was shown that pure PLA and Floreon exhibited homogeneous membrane structures free of beads. The elevation of HA and CaSiO$_3$ concentrations promoted the production of tiny beads into PLA and Floreon membranes. PLA showed the same activity at 10% wt of HA and CaSiO$_3$, whereas Floreon showed the maximum small beads at 20% wt of HA and CaSiO$_3$. For

HA-PLA, and CaSiO$_3$-PLA composites containing high CS and/HA concentration, SEM revealed aggregated spherical-shaped CS (CaSiO$_3$) particles, as shown in Fig. 5c and d, respectively, demonstrating substantial CS content. This finding is consistent with that of Chrysafi et al., who showed CS crystallites and spherical CaSiO$_3$ particles in the SEM of their CS material. The produced particles were round, smooth, dense, and had few crystallite morphologies that formed agglomerates (Wan et al., 2005; Chrysafi, Perraki and Kakali, 2007).

4.1.4 Fibre diameter distribution

The results were obtained by performing electron microscopy, and then ImageJ was used to measure the diameters of the fibres, which were then histogrammed according to frequency by including the mean diameter ± standard deviation for each sample. Figure 4-13 demonstrates that the average diameter of PLA and Floreon scaffolds increases with the addition of hydroxyapatite, whereas the average diameter of Floreon scaffolds decreases slightly as the weight percentage of HA increases from 10% to 20%.
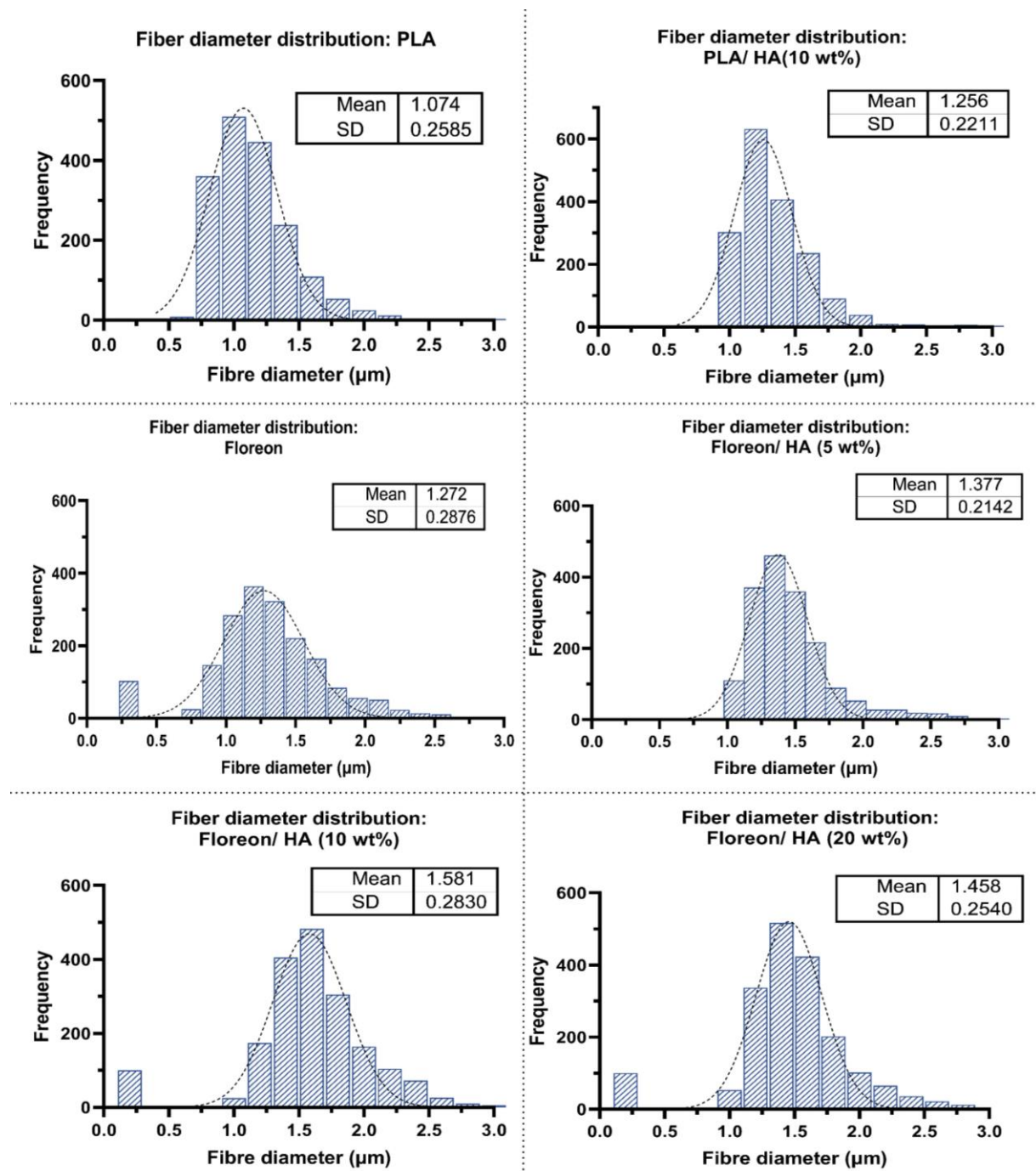
Figure 4-13 Fiber diameter distribution of PLA and Floreon fibrous membranes containing different concentrations of HA.

The same outcomes as those previously stated were obtained when Calcium Silicate was added to Floreon and PLA scaffolds (Figure 4-14). As $CaSiO_3$ was added, the average fiber diameter of PLA and Floreon increased, but it decreased slightly when the concentration was raised from 10% to 20%.
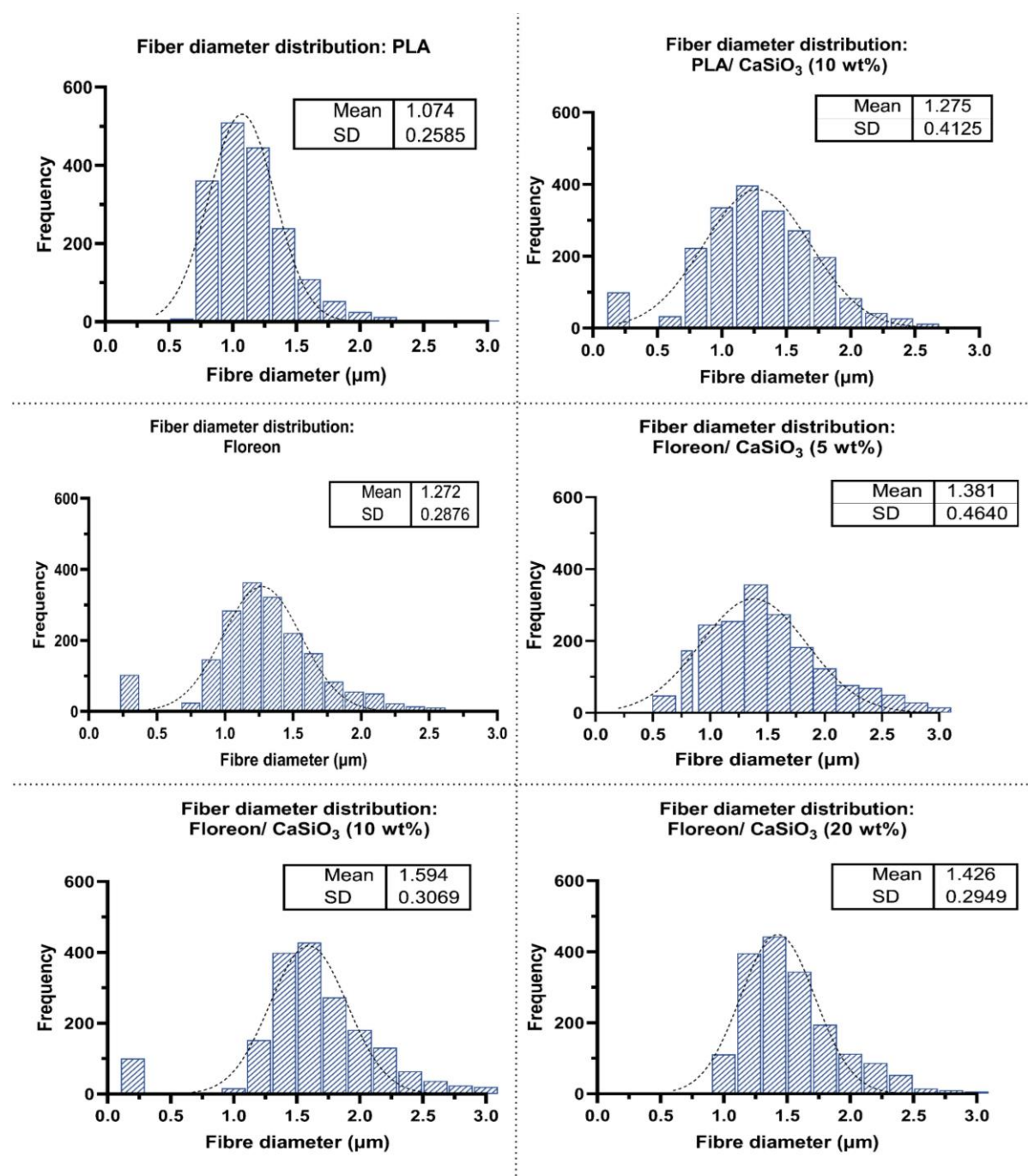
Figure 4-14 Fiber diameter distribution of PLA and Floreon fibrous membranes containing different concentrations of $CaSiO_3$.
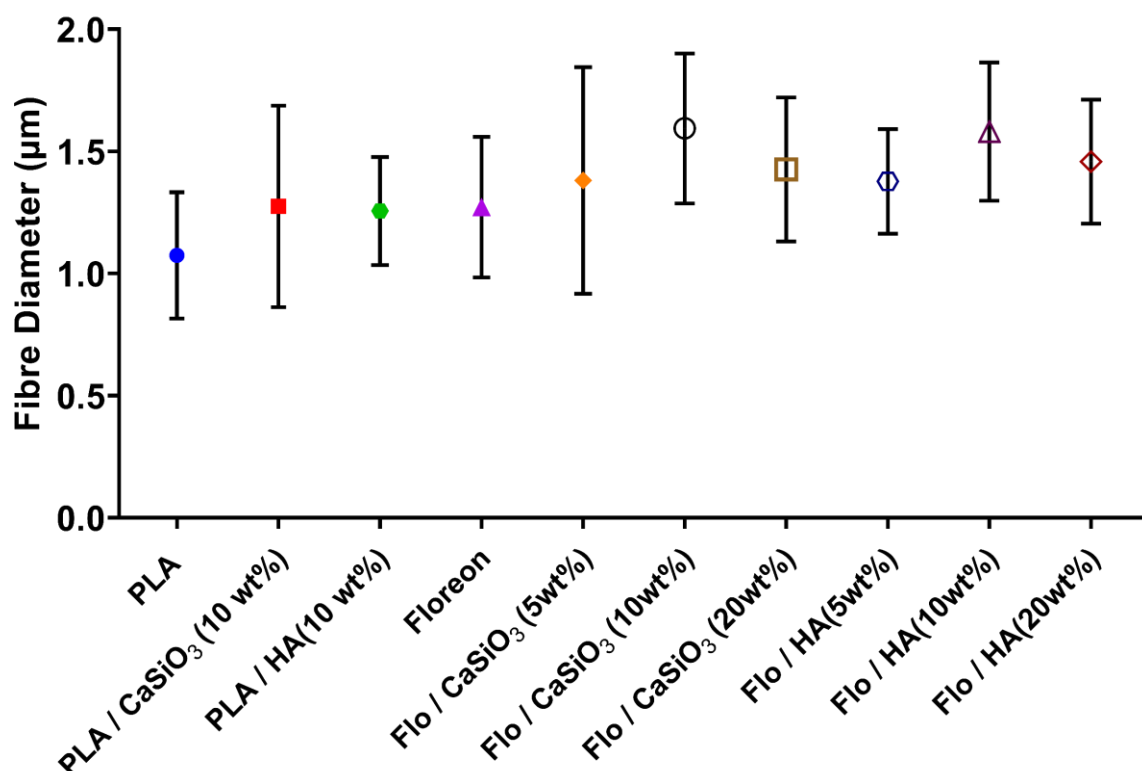
Figure 4-15 Fiber diameter distribution of PLA and Floreon fibrous membranes containing different concentrations of HA and CaSiO₃.

Overall, the morphology of the electrospun microfibers was controlled by the concentration and viscosity of the solution. The morphology of manufactured microfibres, specifically the fibre diameter (Figure 4-13 - 15) and uniform size, might have an impact on cell adhesion. The ability to apply manufactured microfibres with a smaller diameter for the replacement of bone tissue may be advantageous. According to additional studies, osteoblast differentiation is improved by using microfibres with a lower diameter and no beads (Sisson et al., 2010). In Figure 4-13 and 14, the bioceramics had an impact on the mean diameter of PLA and Floreon. PLA and Floreon diameter increased at 5%w and 10%w of HA and CaSiO₃, nevertheless, diameter decreased at 20%w of HA and CaSiO₃, which has been shown in previous studies (Akpan et al., 2019; Herrero-Herrero et al., 2021).

4.1.5 Pore size distribution and porosity

The porosity and pore size distribution of the PLA/Floreon films were evaluated using the mercury porosimetry technique. The membrane's porosity was calculated by dividing the pore size by the total membrane volume. This approach is based on the membrane absorption of a specific material under pressure.

The results are graphically represented in the Figure 4-16 to Figure 4-18 for PLA and Floreon and other membranes with HA and $CaSiO_3$. The graphs tell the cumulative pore area and cumulative intrusion measured against pressure. The Table 4-1 gives all the values numerically.

According to results, it is concluded that HA or $CaSiO_3$ effectively increase the percent porosity of the membrane when its concentration is increased. This indicated that bioceramics (HA and $CaSiO_3$) show the positive effect on the pore size distribution of Floreon membrane. Similar effects were reported in the PLA. As described in the table, Flo/$CaSiO_3$ (20% wt.) has the highest percent porosity with highest intrusion volume pore area. While Floreon has least porosity as well as intrusion volume and pore area. However, the porosity of Flo/HA is comparable to that of Flo/$CaSiO_3$ for the same concentration ratios.
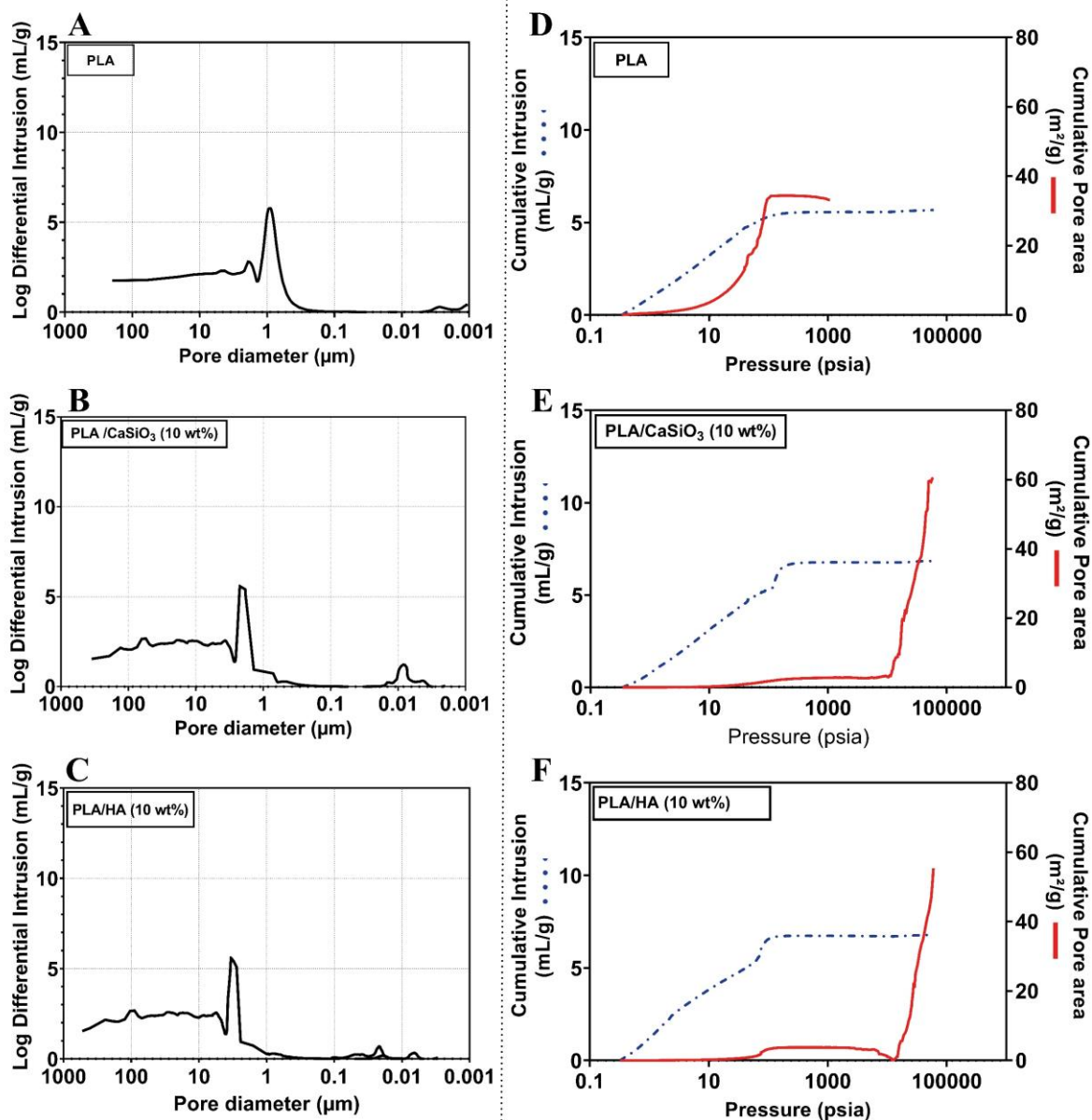
Figure 4-16 Differential (A-C) and cumulative (D-F) intrusion curves as a function of pore diameters measured by mercury intrusion porosimetry for PLA films containing 10 wt% of HA and CaSiO₃.
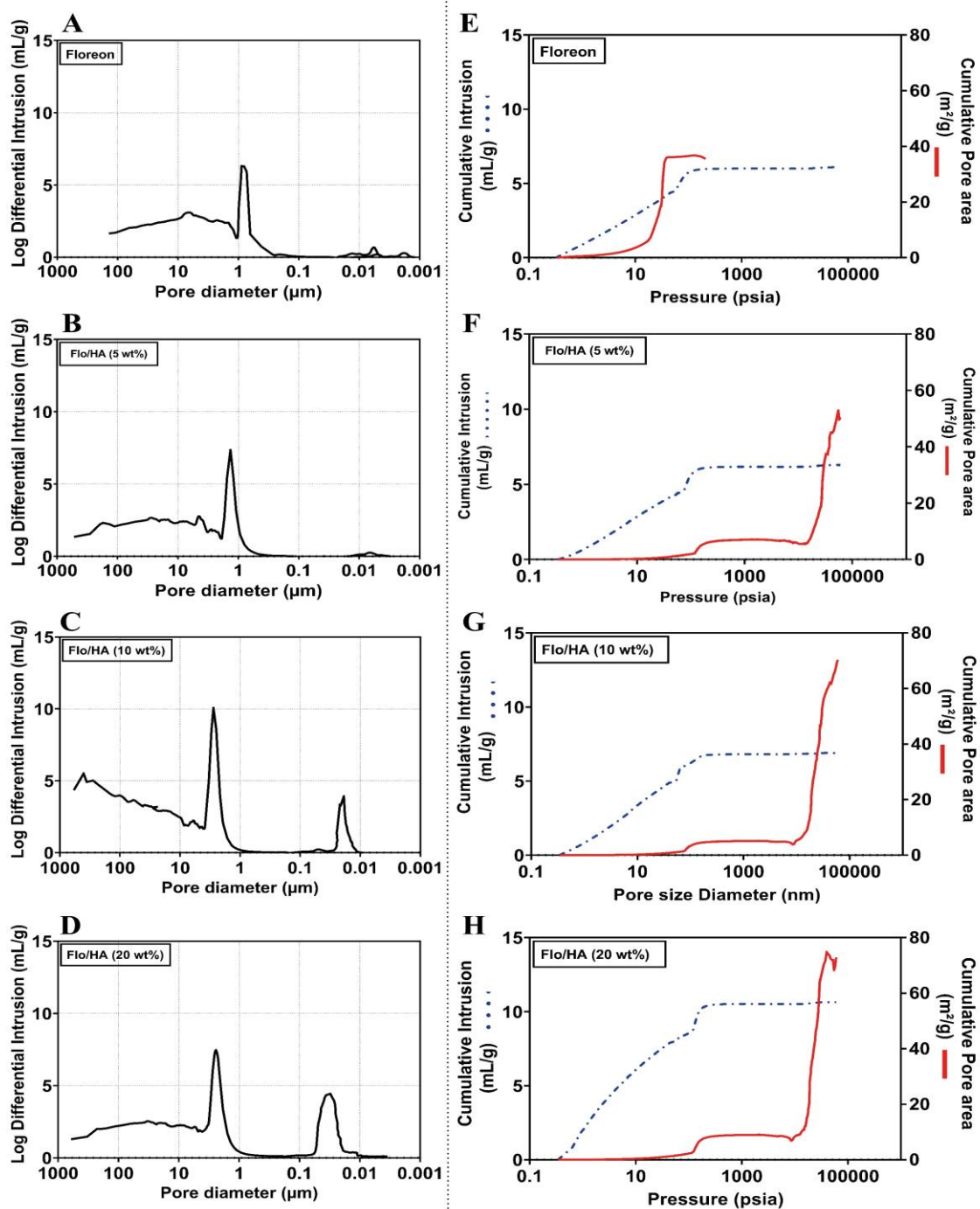
Figure 4-17 Differential (A-D) and cumulative (E-H) intrusion curves as a function of pore diameters measured by mercury intrusion porosimetry for Floreon films containing different concentrations (5,10 and 20 wt%) of HA.
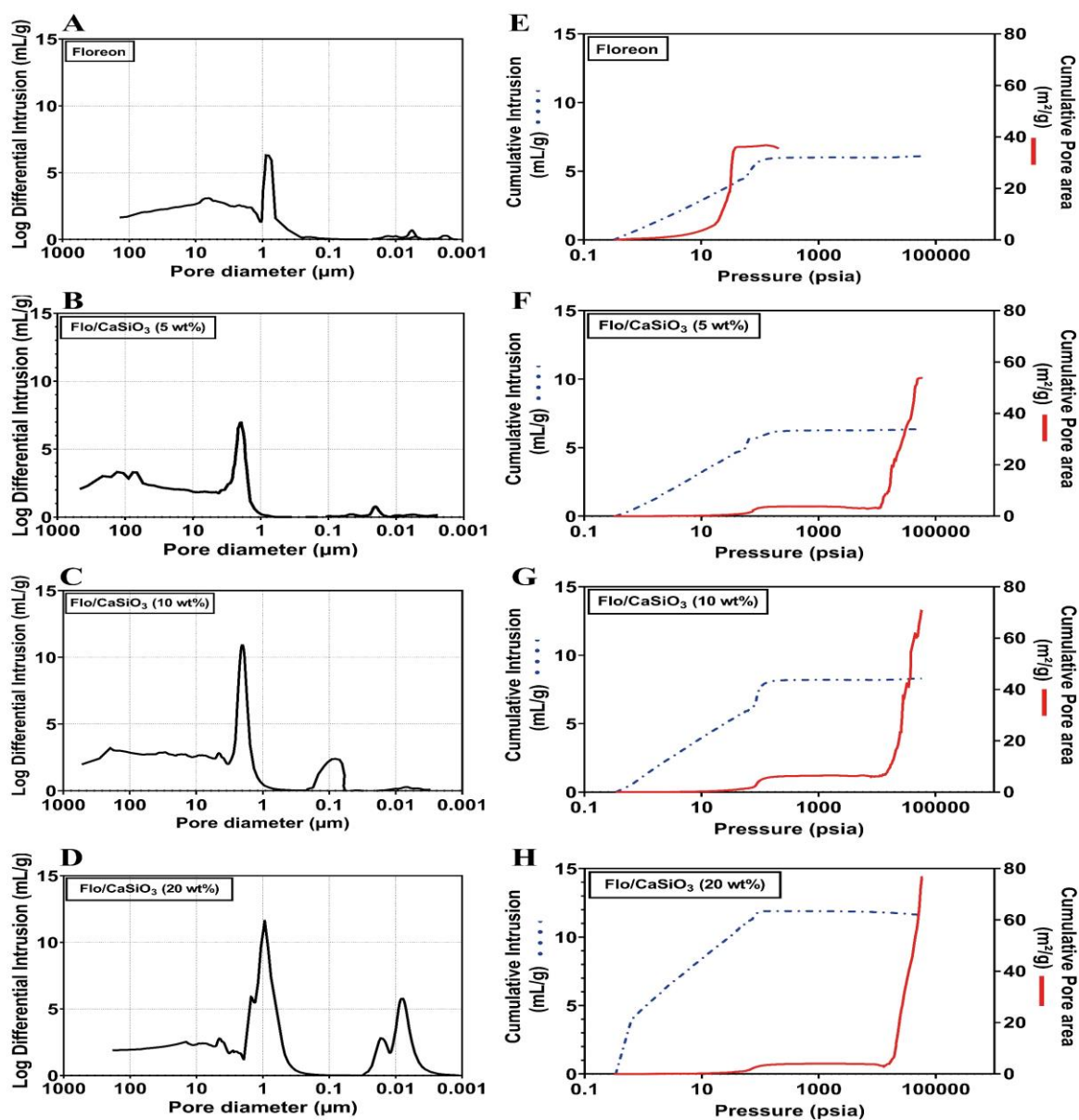
Figure 4-18 Differential (A-D) and cumulative (E-H) intrusion curves as a function of pore diameters measured by mercury intrusion porosimetry for Floreon films containing different concentrations (5,10 and 20 wt%) of CaSiO$_3$.

Table 4-1 Relevant output data of mercury intrusion porosimetry analysis.

Content	Total Intrusion Volume mL/g	Total Pore Area m²/g	Porosity %
PLA	5.67	34.86	75.4
PLA/HA (10 wt%)	6.79	55.36	82.77
PLA/CaSiO$_3$ (10 wt%)	6.84	60.49	82.82
Floreon	6.12	36.67	69.77
Flo/HA (5wt%)	6.29	50.43	78.5
Flo/HA (10wt%)	6.89	70.3	83.23
Flo/HA (20wt%)	10.65	72.9	86.3
Flo/CaSiO$_3$ (5 wt%)	6.34	53.93	81.03
Flo/CaSiO$_3$ (10 wt%)	8.3	70.35	83.3
Flo/CaSiO$_3$ (20 wt%)	11.92	76.86	89.37

Pore size, distribution, porosity, and interconnectivity are critical parameters affecting cellular attachment, ingrowth, and nutrient and waste transport within a scaffold, as demonstrated in Figures 4-16, 17, and 18, and Table 4-1. The present study revealed that an increase in the concentration of HA or CaSiO$_3$ led to a corresponding rise in the percentage of porosity of the membrane. This finding suggests that these bioceramics have the potential to promote biological growth when employed as a biomaterial within the human body (Chen and Liu, 2016). Floreon exhibited the largest percentage of porosity and intrusion volume at 20%w of CaSiO$_3$ and HA, whereas PLA has shown increased porosity at 10%w of bioceramics. Previous studies showed that pore size affects the mechanical and biological properties of the scaffold. If the pore size is too large, the scaffold will be mechanically unstable; conversely, if the pore size is too small, cell migration would be limited (Okamoto *et al.*, 2006). Porosity and interconnectivity are essential for cellular infiltration and proliferation. With poor interconnectivity, proliferation is limited due to the space and nutrient diffusion constraints (Son and Kim, 2009).

4.1.6 X-Ray diffraction (XRD) analysis

X-ray Diffraction Analysis was performed to get the detailed crystallographic structure, chemical composition, and physical properties of PLA and Floreon membranes before and after the addition of hydroxyapatite and calcium silicate in different concentrations.

Figure 4-19 and Figure 4-20 provide the detailed graphs plotted for different prepared films and compared to the XRD analysis results of hydroxyapatite and calcium silicate that were covered earlier in section 4.1.1.1 .

The graphs below demonstrate that a very broad scattering reflection, located at approximately $2\theta=17^{\circ}$, was observed in the XRD spectrum of PLA, indicating that PLA has an amorphous structure. Whereas XRD patterns of Floreon show that it is a semi-crystalline polymer with two distinct diffraction peaks that have been reported at $2\theta=21^{\circ}$ and $2\theta=23^{\circ}$. The addition of hydroxyapatite and calcium silicate particles increases the number and sharpness of the Bragg peaks.
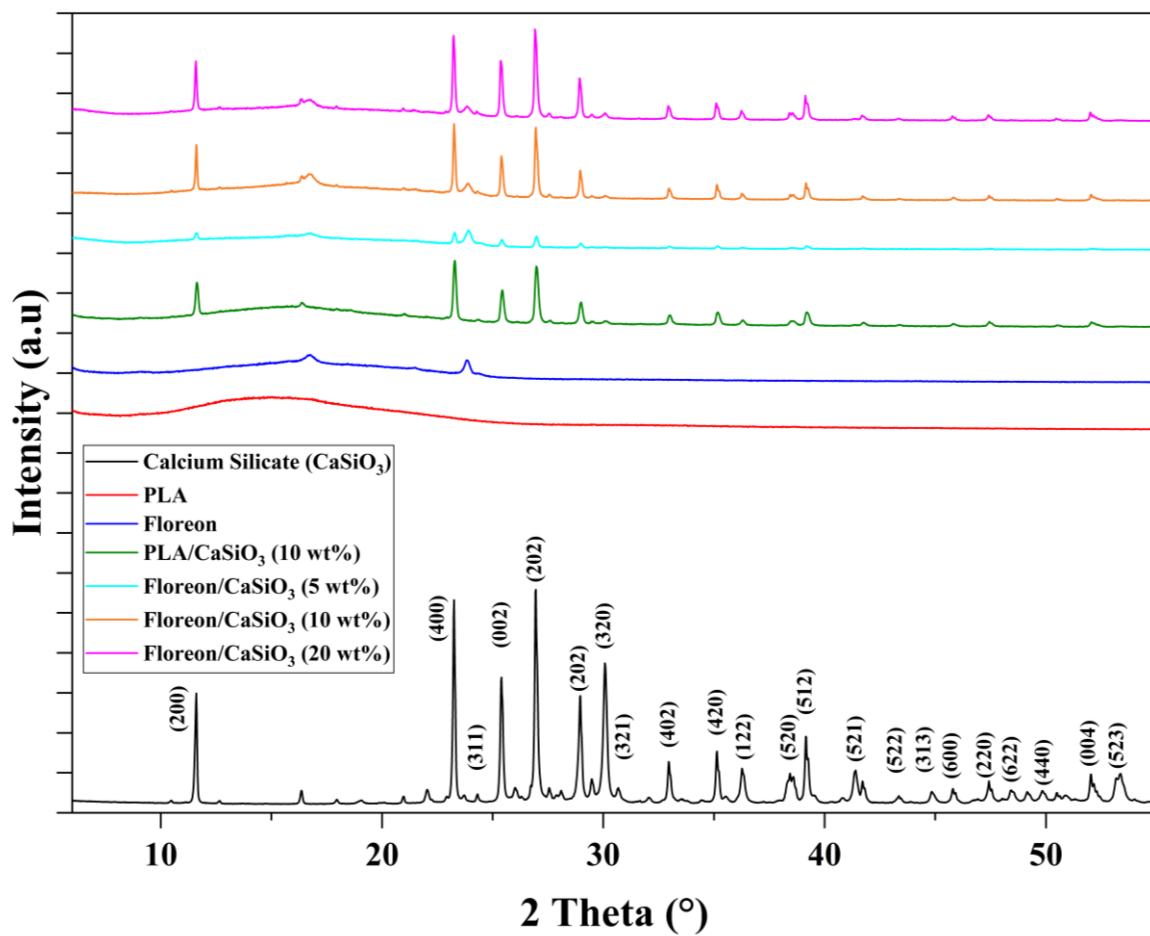
Figure 4-19 X-ray diffraction patterns of PLA and Floreon fibrous membranes containing different concentrations of $CaSiO_3$.
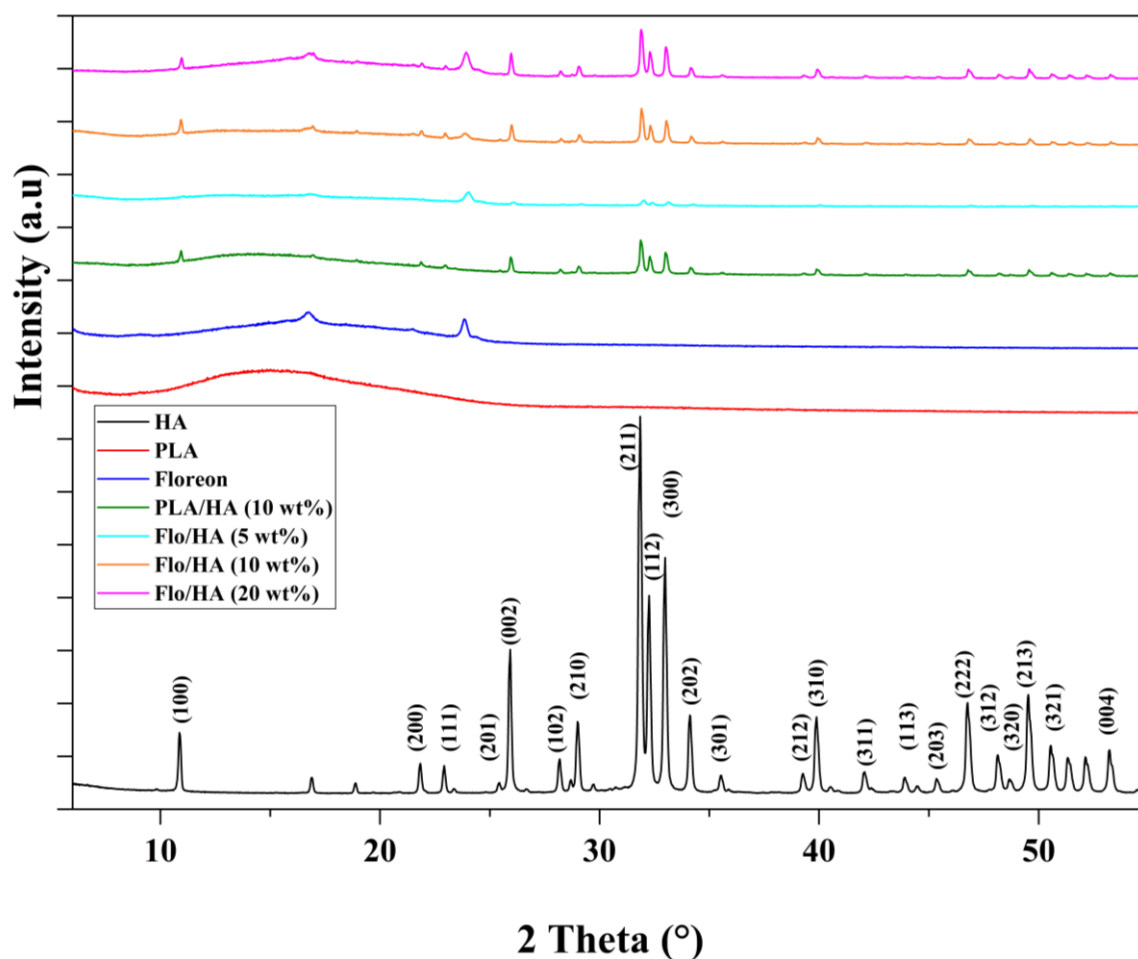
Figure 4-20 X-ray diffraction patterns of PLA and Floreon fibrous membranes containing different concentrations of HA.

As shown in the above plots, the incorporation of $CaSiO_3$ into the Floreon and PLA films, added in varying concentrations, results in a different number of crystallites present in the films. With increasing concentrations of ceramic particles, a noticeable increase can be seen in the crystallite peaks' intensity and numbers of peaks. The same kinds of outcomes were observed with hydroxyapatite-based films, as can be seen in Figure 4-20

The investigation focused on the effects of bioceramics on both Floreon and PLA membranes, given that bioceramics alone have a crystalline structure. Of particular relevance to the present study is the significance of the crystalline structure in determining the softness or brittleness of the GBR membrane. This is crucial since these features play a critical role in cell adhesion and function in vivo (Palomino-Durand, Pauthe and Gand, 2021). The XRD of PLA and Floreon showed different peaks at various concentrations of HA and CaSiO3 (Figure

4-19 and 20). The X-ray patterns of PLA and Floreon membranes had distinctive major peaks at 2θ=17o, showing the amorphous structure of PLA, and 2θ=21o and 2θ=23o for Floreon, suggesting a semi-crystalline polymer. The number of crystallite in the films varied based on the amount of HA/CaSiO3 added to Floreon and PLA membranes. The maximum crystallite peak intensity and number were seen with high concentrations (20%w) of HA and CaSiO3. According to the literature, these diffractions could be linked to the PLA's crystal. The PCL pattern, meanwhile, exhibits peaks that are approximately at 2θ=23 (Sun et al., 2014). The structure generated in the PLA is amorphous since there are no crystal peaks, whereas the addition of PCL caused crystallisation (Fang et al., 2010; Zhang et al., 2016; Wang et al., 2021).

The findings of Silverajah et al., are in agreement with the study's findings. PLA was mixed with epoxidised palm oil using the melt blend method (EPO) by Silverajah et al. The mixture of PLA/1 wt% EPO showed no crystal peaks, indicating the creation of an amorphous structure (Giita Silverajah et al., 2012). Work by Lu et al., revealed amorphous PLA in a PLA/PCL blend, which is distinguished by an indistinct peak with a low absorption intensity. This is because the PLA and PCL molecules underwent varying degrees of deformation throughout the sample fabrication (electrospinning) procedure. The PLA and PCL peaks in the mixed diffraction pattern of PLA/PCL are dominated by broad amorphous phase peaks with low absorption intensity (Lu, Chen and Zhang, 2016). PLA and Floreon (PLA/PCL blend) experienced a rapid increase in crystallinity and a relatively less amorphous shape after the addition of low weight HA and CaSiO3 (Zhang et al., 2018; Pandey and Sakurai, 2021). Additionally, a poor crystallinity level might hasten the rate of deterioration (Lu, Chen and Zhang, 2016).

4.1.7 Fourier Transform Infra-Red (FT-IR) analysis

The FTIR spectra of PLA and Floreon scaffolds filled with HA or $CaSiO_3$ at varying concentrations are shown in Figure 4-21, Figure 4-22 and Figure 4-23. The spectral features identified from the FTIR spectra of HA and $CaSiO_3$ particles were compared to the literature and the assignments of the detected peaks were discussed in section 4.1.1.1, while the spectral features of PLA and Floreon scaffolds are summarised in Table 4-2. The table describe the different phenomena as asymmetrical stretching, symmetrical stretching and rocking at different bonds in the molecules with their corresponding wave number derived from the FT-IR spectra.

As can be seen from the FTIR spectra, all membranes exhibit comparable patterns of vibrational peaks, such as the peak at 752 cm^{-1} associated with the α-methyl rocking vibration and the peak at 864 cm^{-1} related with the ester ($O-CH-CH_3$). the peak at about 1080 and 1180 cm^{-1} associated with the stretching vibration of C-O-C; the peak at around 1363 cm^{-1} associated with the CH symmetric bending vibration; and the peak at around 1452 cm^{-1} related with the CH_3 antisymmetric. The peak associated with the carbonyl C=O stretching vibration can be found at 1755 cm^{-1} as there was only one for PLA, while another appeared for Floreon at 1726 cm^{-1} due to the presence of PCL in its structure; the symmetric stretching vibration of CH_3 in saturated hydrocarbons can be found at 2943 cm^{-1}, and the antisymmetric stretching vibration can be detected at 2993 cm^{-1}.

As expected, the spectra of PLA/HA and Floreon/HA shows the typical bands associated with PLA or Floreon with HA, confirming the successful synthesis of composite membranes. The PLA/ $CaSiO_3$ and Floreon/ $CaSiO_3$ composite membranes displayed the same characteristics, demonstrating the successful inclusion of both components within the fibres.
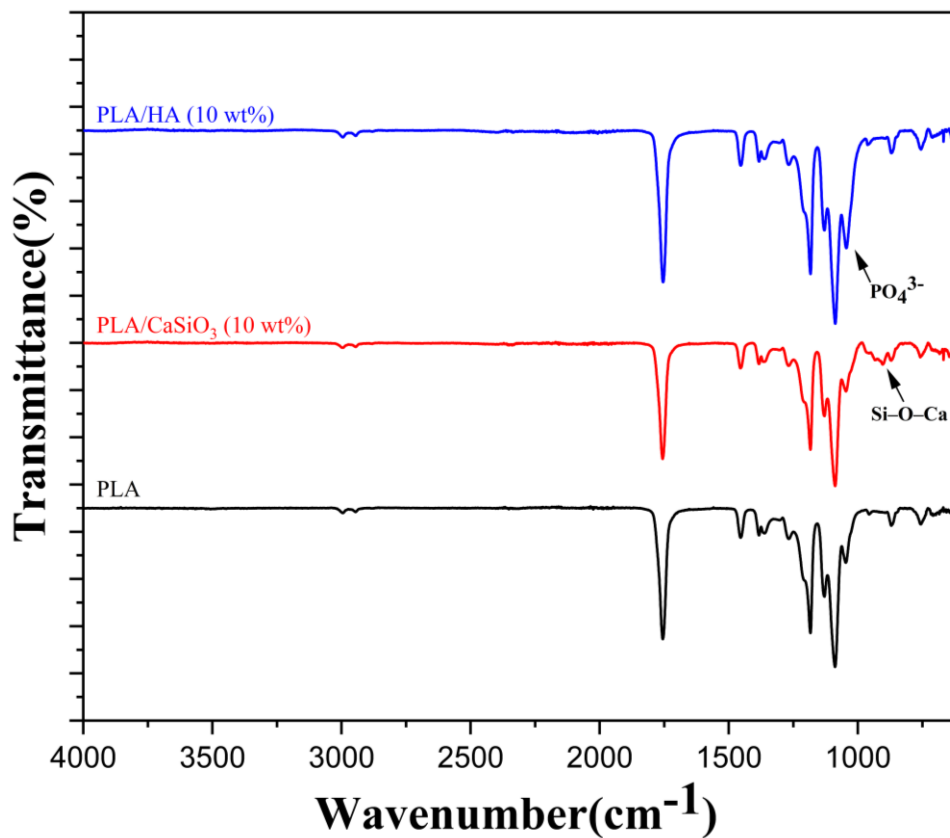
Figure 4-21 FTIR spectra of PLA films containing 10 wt% of HA and CaSiO$_3$.
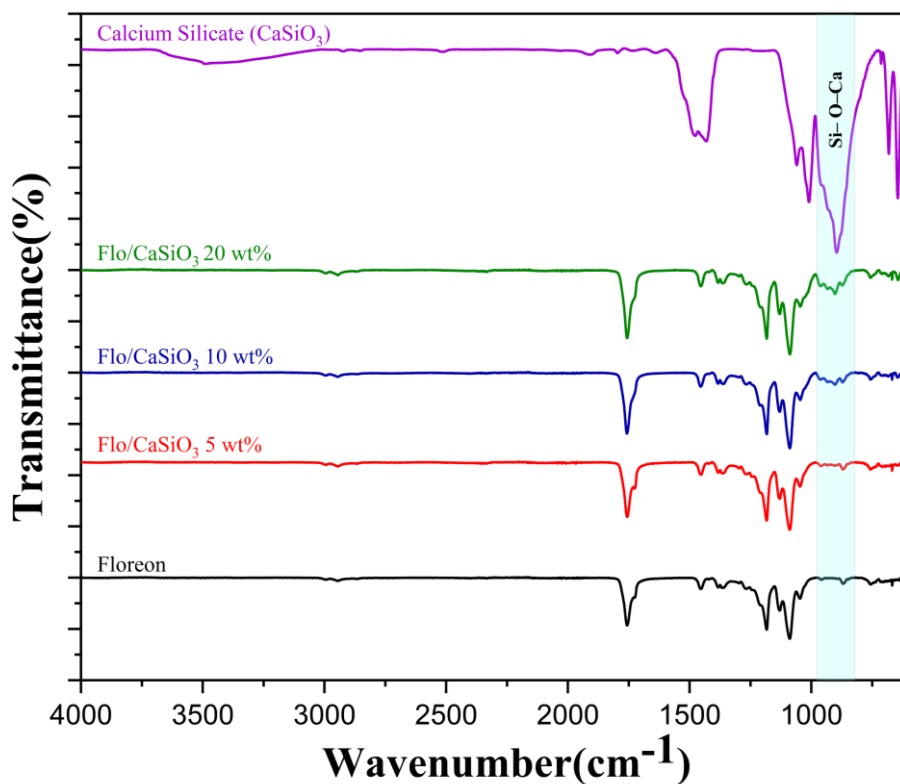
Figure 4-22 FTIR spectra of Floreon membranes containing different concentrations (5,10 and 20 wt%) of CaSiO$_3$.
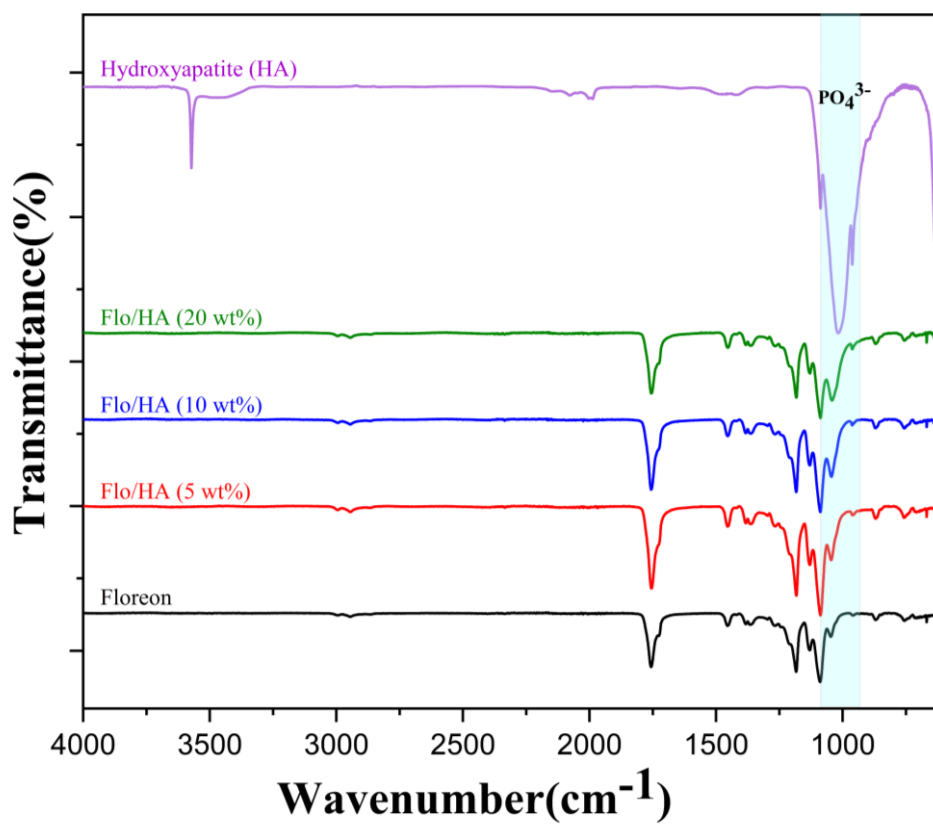
Figure 4-23 FTIR spectra of Floreon membranes containing different concentrations (5,10 and 20 wt%) of HA.

Table 4-2 Assignments of spectral features identified from the FTIR spectra of PLA and Floreon fibrous membranes containing different concentrations of Hydroxyapatite and Calcium Silicate particles.

Wavenumber (cm-1)	Polymer	Assignment	Abbreviation
2993	PLA / Floreon	Asymmetrical stretching	$v_{as}(CH_2)$
2943		Symmetrical stretching	$v_s(CH_2)$
1755		Stretching	$v(O=C)$
1726	Only Floreon	Stretching	$v(O=C)$
1450	PLA / Floreon	Asymmetrical scissoring	$\delta_{as}(CH_3)$
1360		Symmetrical scissoring	$\delta_s(CH_3)$
1182		Asymmetrical stretching + twisting	$v_{as}(C–O) + \tau(CH_3)$
1086		Symmetrical stretching	$v_s(C–O–C)$
1045		Symmetrical stretching	$v_s(C-CH_3)$
868		Stretching	$v_s(C-COO)$
752		Rocking	$\rho(CH2)$

In this study, Fourier transform infrared spectroscopy (FTIR) was employed to determine the composition of PLA and Floreon membranes following treatment with bioceramics. This analytical technique facilitated the assessment of the blending process between the polymer and bioceramics, representing a crucial initial step towards understanding the resulting structural implications. The primary objective of this investigation was to identify the optimal composition of the bioceramic-polymer blend in terms of structural properties prior to subjecting the compounds to biocompatibility testing. Figure 4-21, 22, and 23 show the FTIR of PLA and Floreon composites with HA and $CaSiO_3$ at various concentrations and indicates the appearance of phosphate and/or SiO_2 bands in the all composites (Table 4-2).The FTIR spectrum of the PLA and Floreon composites shows the presence of symmetric stretching vibration of Si-O-Si bands and appeared at 1080 cm^{-1}.Other researchers have also noticed this phenomenon, which they have attributed to the presence of modifier oxides in the silica network (Laudisio and Branda, 2001). According to Kim et al., the produced calcium silicate bands were attributed to the symmetric stretching vibration of Si-O-Si bands and appeared at 1080 cm^{-1} (Kim *et al.*, 2008). PLA exhibited the carbonyl C=O stretching vibration at 1755 cm^{-1} while Floreon (PLA /PCL blend) showed the carbonyl C=O stretching vibration at 1726

cm^{-1}. Hadi et al., reported that the carbonyl stretching vibration (C=O) band which ranged from 1781 to 1690 cm^{-1}, with a maximum at approximately 1730 cm^{-1} (Hadi *et al.*, 2020).

4.1.8 Differential scanning calorimetry (DSC)

DSC analysis was performed to study the thermal responses of the various electrospun systems; the thermal parameters obtained from the first heating scan are depicted in graphs (Figure 4-24 - Figure 4-26) and summarised in Table 4-3. The graphs are formed between Temperature and Heat Flow for all types of membranes and membrane scaffolds with different ceramic particles. The tables give glass transition temperature, crystallisation temperature and melting temperature for all the membranes. It can be deduced from all of the available data that increasing the concentration of HA and calcium silicate particles in Floreon and PLA membrane scaffolds causes the melting temperature to decrease. On the other hand, crystallisation temperature and glass transition temperature both rise as a result of the increased concentration.

Table 4-3 DSC results for of PLA and Floreon fibrous membranes containing different concentrations of Hydroxyapatite and Calcium Silicate particles.

Samples	Glass transition temperature	Crystallisation temperature	Melting temperature
	(Tg) (°C)	(Tc) (°C)	(Tm) (°C)
PLA	59.0	80.0	150.7
PLA/HA (10 wt%)	62.1	87.7	150.0
PLA/CaSiO$_3$ (10 wt%)	61.6	82.3	149.7
Floreon	58.3	73.4	150.9
Floreon/HA (5 wt%)	58.8	81.0	150.7
Floreon/HA (10 wt%)	59.5	83.8	150.4
Floreon/HA (20 wt%)	59.3	87.1	150.0
Floreon/CaSiO$_3$ (5 wt%)	57.0	79.4	150.8
Floreon/CaSiO$_3$ (10 wt%)	59.5	83.8	150.4
Floreon/CaSiO$_3$ (20 wt%)	62.4	92.4	148.7

Note: Calculations were repeated for three sets of samples. The standard deviation for the Tc, Tg, and Tm values was less than 0.5 %.
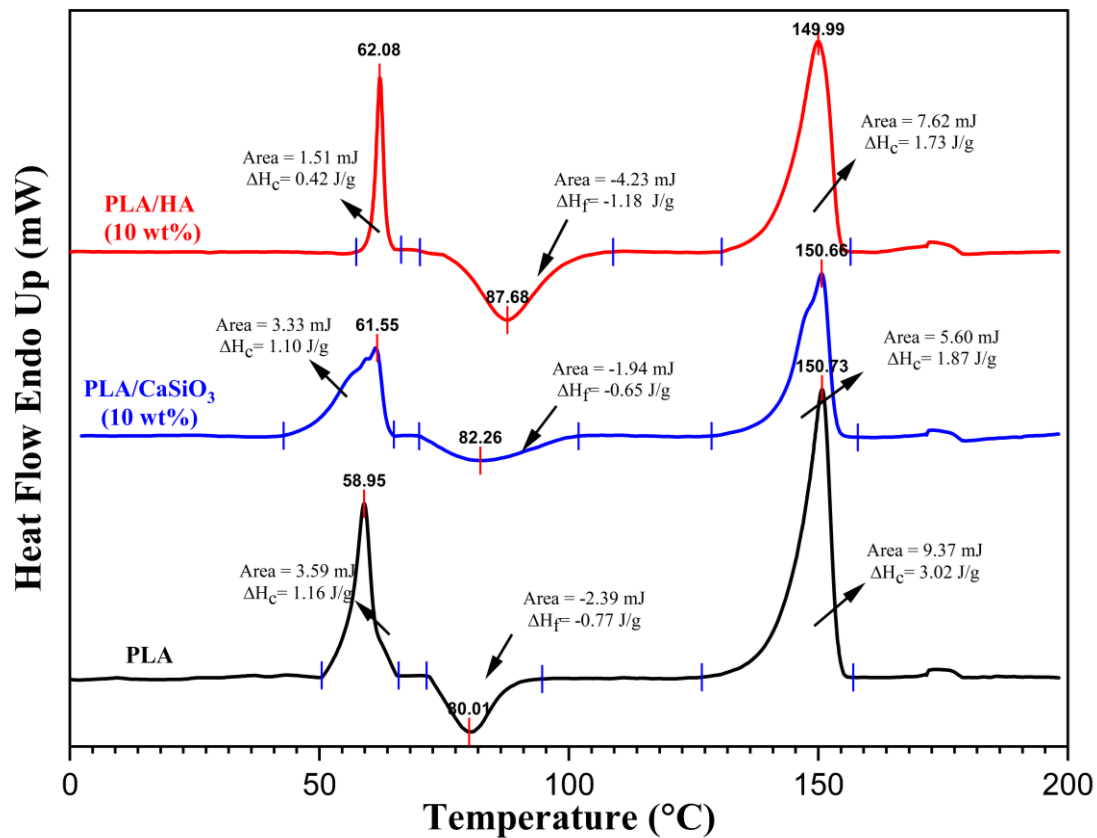
Figure 4-24 DSC thermograms of PLA films containing 10 wt% of HA and CaSiO$_3$.
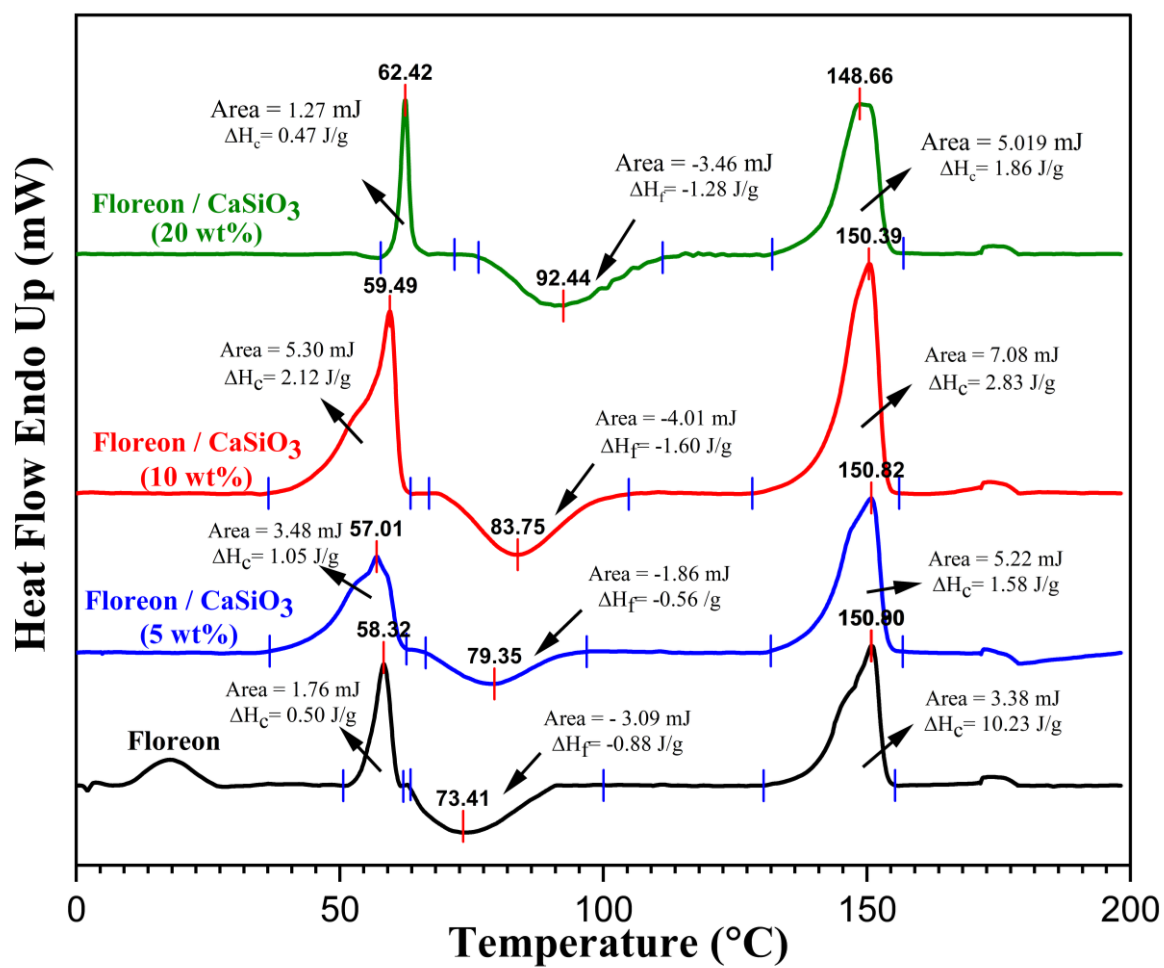
Figure 4-25 DSC thermograms of Floreon membranes containing different concentrations (5,10 and 20 wt%) of HA.
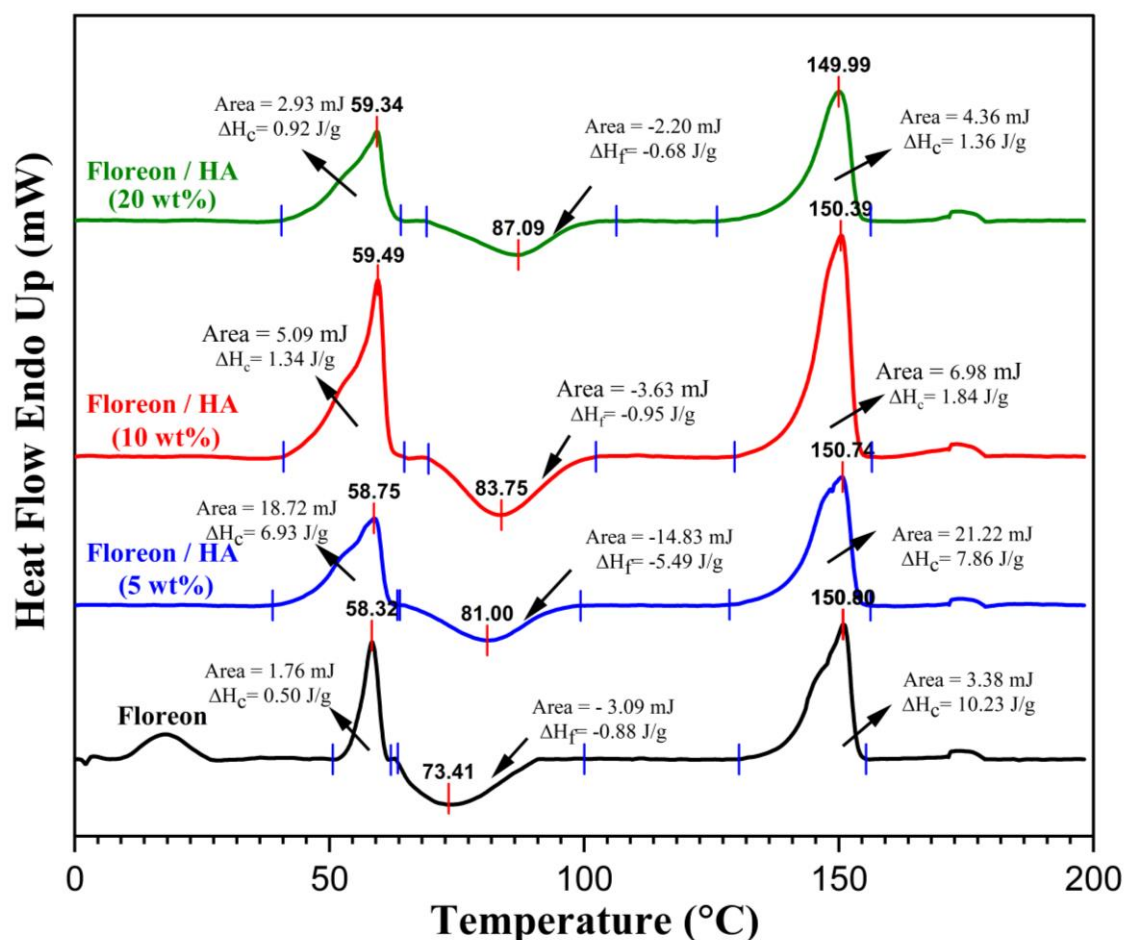
Figure 4-26 DSC thermograms of Floreon membranes containing different concentrations (5,10 and 20 wt%) of CaSiO₃.

Thermal properties are associated with a material-dependent response when heat is supplied to a solid body, a liquid, or a gas. This response might be a temperature increase, a phase transition, a change of length or volume, an initiation of a chemical reaction or the change of some other physical or chemical quantity (Buck and Rudtsch, 2011). The thermal properties of PLA and Floreon and their composites were studied, and the DSC results are shown in Figure 4-24, 25, and 26 and Table 4-3. DSC thermograms of PLA films containing 10 wt% of HA and CaSiO₃ (Figure 4-23) explored the crystallisation behaviour of PLA and PLA/HA or PLA/CaSiO₃ composite membranes, the crystallisation temperature (Tc) and crystallisation enthalpies (ΔHc), and other calculated parameters (Table 4-5). The Tc value increased from 80.01 for the plain PLA, 87.68 for the 10% wt HA, and 82.26 for the PLA with 10% wt CaSiO₃. The similar patterns of thermal response for the plain Floreon and Floreon with HA (5% wt, 10% wt, and 20% wt) or Floreon with CaSiO₃ (5% wt, 10% wt, and 20% wt) were observed.

159

Apart from 5% wt loading, Tc increased with an increase in HA and $CaSiO_3$ loading. This showed that higher Tc values translate to a stronger interfacial interaction of the bioceramics with the polymer (Jiang *et al.*, 2010). The second heating curves in Figures 4-24, to -25 show that the PLA and Floreon membranes with bioceramics undergo a melting transition with the endothermic peaks (Tm). The inclusion of HA and $CaSiO_3$ within the PLA and Floreon did not significantly affect Tm and Tg values. The fact that a crystallisation peak appears at temperatures only above Tg, indicates that a large number of crystal nuclei had already formed in the glass (Hernández Sánchez *et al.*, 2005). Note that the PLA's and FLO's degrading mechanisms cause the crystallinity to rise. The amorphous phase, which develops in the polymer's outer layer, is well recognised for being particularly vulnerable to water absorption and degrading quickly. As a result, an increase in crystallinity is seen in the samples after a specific period of degradation, which leads to a decrease in the amount of the amorphous phase.

4.1.9 Thermogravimetric Analysis – TGA

The thermal stability of PLA and Floreon scaffolds containing HA or $CaSiO_3$ at various concentrations was determined by performing TGA and the derivative thermogravimetric (DTG). These tests characterised the change in thermal stability of membranes upon addition of bioceramics. The fraction of volatile components in the membranes was also judged by this test as it indicates weight loss when a sample is constantly heated. Figure 4-27 to Figure 4-29 are showing the results for TGA and DTG. The TGA and DTG curves were used to determine the membranes' thermal properties, such as the initial weight loss temperature (T_i), at which 5% of the membranes' weight is degraded, and the temperature of maximum thermal degradation rate (T_d).

In Figure 4-27 , the graphs show that PLA, PLA/HA and PLA/$CaSiO_3$ began to degrade at 329.0, 317. 8 and 319.6 °C, respectively. Following that, the membranes degraded quickly, with maximum degradation seen at 346.2 °C for PLA. A two-step degradation profile (T_{d1} and $T_{d2)}$ was exhibited for the PLA/HA and PLA/$CaSiO_3$ at 348.2, 379.9 °C and 350.4, 380.2 °C, respectively. After reaching 400°C the slope becomes almost linear. Another point based on graphs below is that PLA/HA shows less weight loss among all while PLA is least thermal stable with large weight loss. This suggests that the presence of HA and $CaSiO_3$ particles in the PLA membranes could result in enhanced thermal stability of the membrane.

In Figure 4-28, similarly Floreon membrane and Floreon/$CaSiO_3$ membranes are compared at different concentrations of $CaSiO_3$ (5%, 10%, and 20%). Among all of the materials, Floreon/$CaSiO_3$ has more residual mass at above 400°C, hence it is thermally more stable. Finally, in the Figure 4-29 the same comparison is made for Floreon and Floreon/HA membranes with different concentrations of hydroxyapatite. The results are almost the same as in the previous case. The results are quantitatively reported in Table 4-4.

We can therefore draw the conclusion that the thermal stability of PLA and Floreon membranes improves as more hydroxyapatite and calcium silicate are added.

A

B
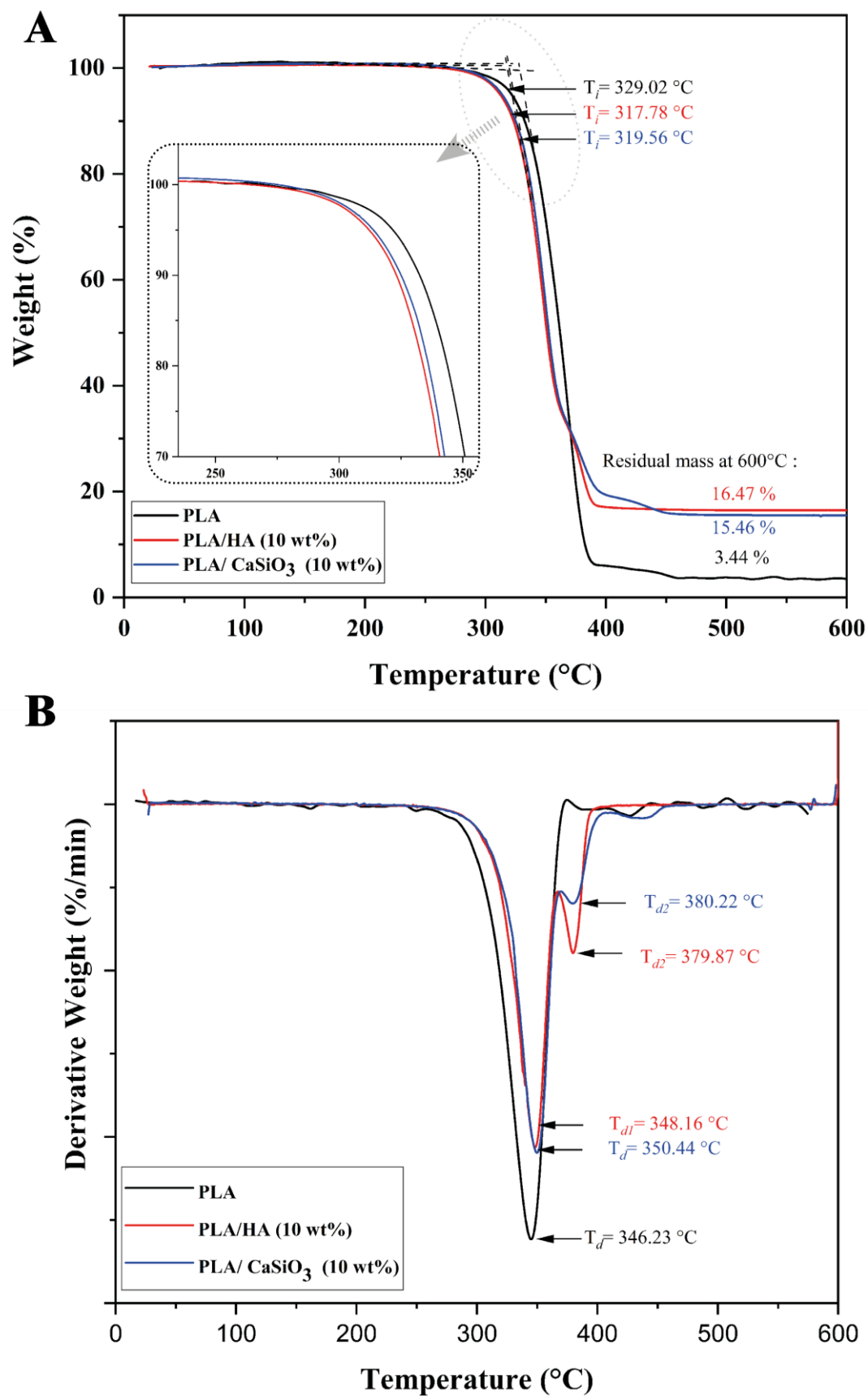
Figure 4-27 TGA (a) and DTG (b) curves of electrospun membranes prepared from PLA containing 10 wt% of HA and CaSiO₃.

A

B
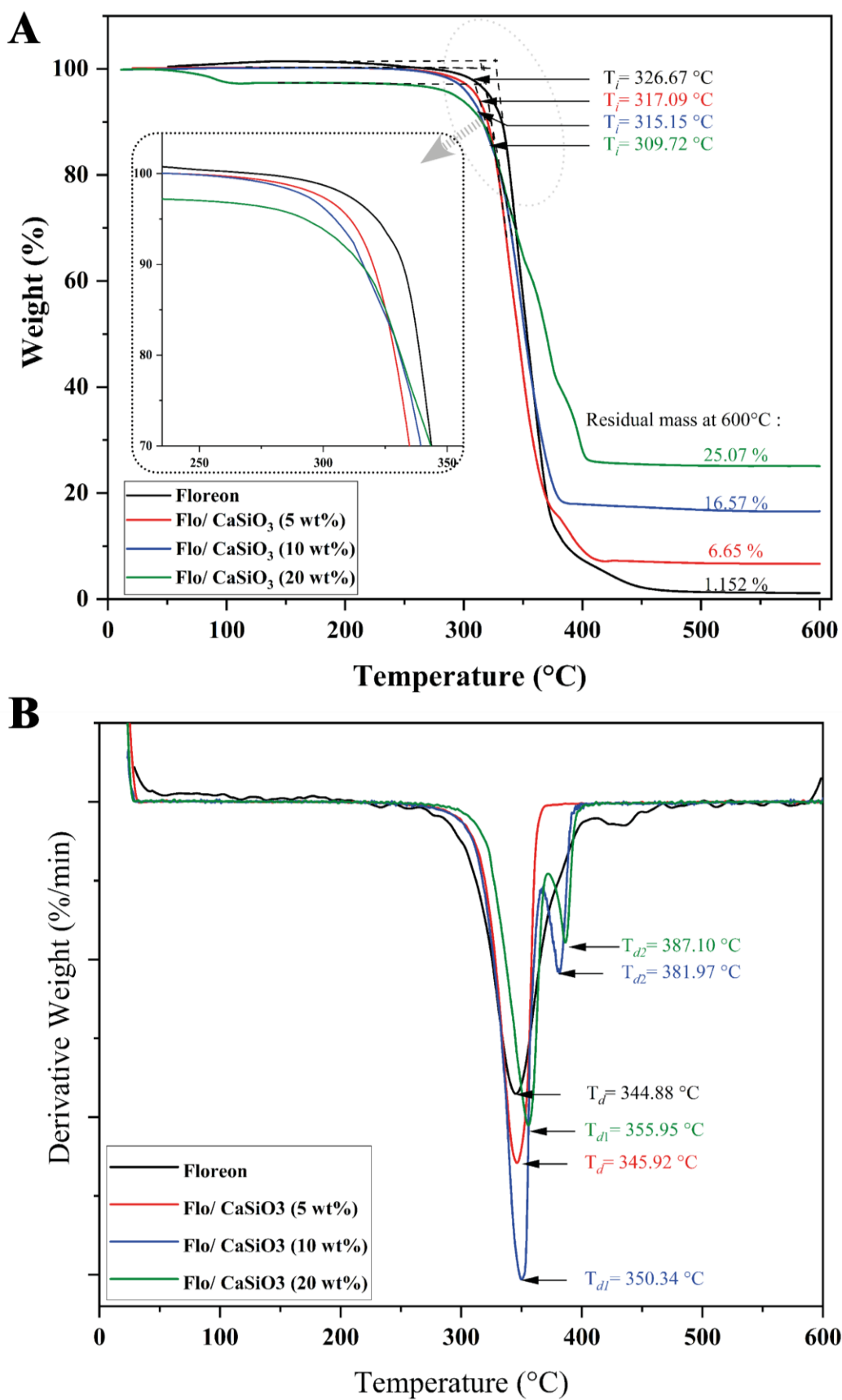
Figure 4-28 TGA (a) and DTG (b) curves of electrospun membranes prepared from Floreon containing different concentrations (5,10 and 20 wt%) of $CaSiO_3$.

A

B
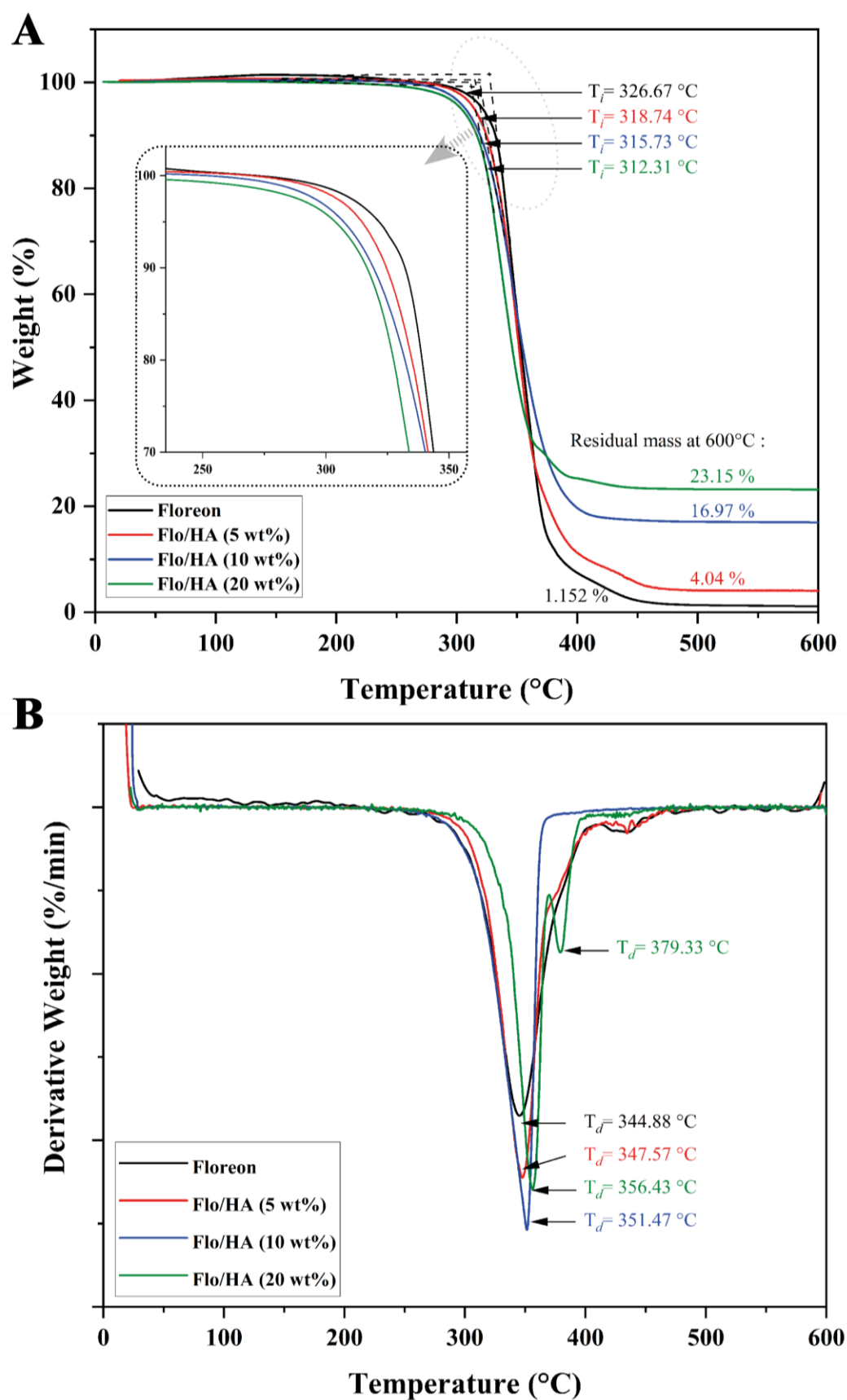
Figure 4-29 TGA (a) and DTG (b) curves of electrospun membranes prepared from Floreon containing different concentrations (5,10 and 20 wt%) of HA.

Table 4-4 Main parameters of TGA and DTG data for PLA and Floreon fibrous membranes containing different concentrations of Hydroxyapatite and Calcium Silicate particles.

	$T_{5\%}$ (°C)	T_d (°C)	Residual mass at 600 °C (%)
PLA	329.0	346.2	3.4
PLA/HA (10 wt%)	317.8	348.2 - 379.9	16.5
PLA/CaSiO$_3$ (10 wt%)	319.6	350.4 - 380.2	15.5
Floreon	326.7	344.9	1.2
Floreon/HA (5 wt%)	318.7	347.6	4.0
Floreon/HA (10 wt%)	315.7	351.5	17.0
Floreon/HA (20 wt%)	312.3	356.4 - 379.3	23.2
Floreon/CaSiO$_3$ (5 wt%)	317.1	345.9	6.7
Floreon/CaSiO$_3$ (10 wt%)	315.2	350.3 - 382.0	16.6
Floreon/CaSiO$_3$	309.7	356.0 - 387.1	25.1

Note: Calculations were repeated for three sets of samples. The standard deviation for the T5%, Td, and residual mass values was less than 0.5 %.

The TGA analysis has proven to be a suitable method to investigate thermal degradation of polymeric systems (Blumstein, 1997; Hatakeyama and Quinn, 1999). The knowledge of the degradation mechanism was needed in order to optimise the processing of the polymer mats. The threshold decomposition temperature gives information about the highest processing temperature that can be employed, whereas the study of the kinetics of the decomposition process helps in the identification of the decomposition mechanisms (Blumstein, 1997). Figures 4-27, 28, and 29 show the TGA and DTG data obtained for the PLA and Floreon samples at various heating rates. The process of thermal degradation may be divided into three stages. The first stage is a small level of weight loss, which may be associated with the loss of moisture in the samples. The second stage is the main decomposition stage (300–390 ∘C), where most organic materials decompose, and maximum weight loss occurs. The third stage is the carbonisation stage, with a slight weight loss, in which some carbonaceous fractions undergo further decomposition (Xu *et al.*, 2018). A major weight loss process was observed between 300∘C and 400∘C. No dehydration was found around 100∘C due to the hydrophobic nature of the polymer. It has been demonstrated that aldehyde is formed during degradation of PLA pellets (Zou *et al.*, 2009). The study also found by FTIR, that absorption bands at 1750 cm^{-1} (corresponding to the C=O stretching vibrations) can be observed in the pure polymer and until the end of the degradation.

4.1.10 Wettability of fibrous membranes

This study measured the water contact angle to describe the wettability of electrospun fibrous scaffolds and their impact on cell attachment, adhesion, and proliferation, all of which are crucial to the scaffolds' biological performances.

The results, including contact angle measurements and images, are shown in Figure 4-30 and Figure 4-31, respectively. Electrospun Scaffolds fabricated from PLA or Floreon polymer solutions displayed extremely high water-contact angles ($135.5° \pm 2.4$ SD and $132.7° \pm 3.1$ SD, respectively), which were significantly greater than those of polymeric films filled with HA or $CaSiO_3$ at varying concentrations. Composite scaffolds, which included HA or $CaSiO_3$ particles at concentrations up to 10wt%, showed a smaller water contact angle compared to their plain polymer films. By raising the ceramic concentration to 20 wt%, scaffolds displayed good wettability with a water contact angle of $90.9° \pm 2.8$ SD for Floreon containing 20wt% HA and $91.3° \pm 1.6$ SD for Floreon containing 20% $CaSiO_3$. In conclusion, the fibrous scaffolds were all hydrophobic, and the water contact angle of biofunctionalised scaffolds reduced gradually as the amount of HA or $CaSiO_3$ particles increased.
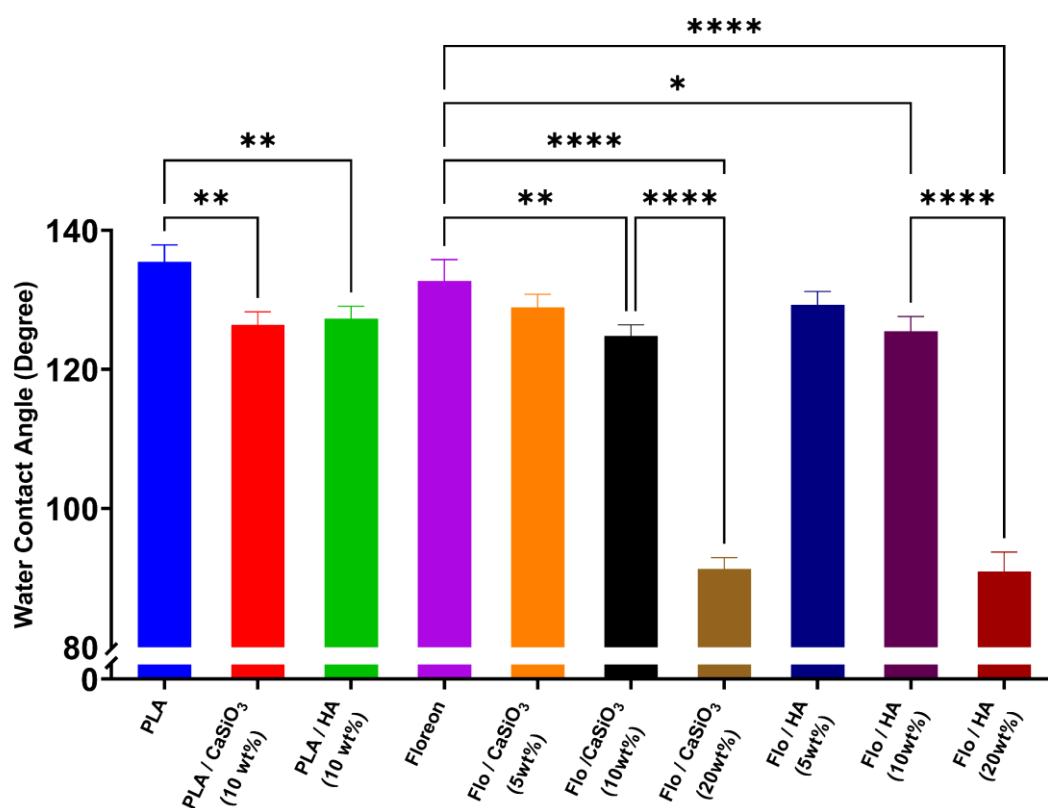
Figure 4-30 Water contact angle measurement of PLA and Floreon fibrous membranes containing different concentrations of Hydroxyapatite and Calcium Silicate particles. Data represented n=3, mean

± STDV following One-way ANOVA statistical analysis with Tukey comparison test. **** p < 0.0001 , *** p < 0.001, ** p < 0.01, * p < 0.05.
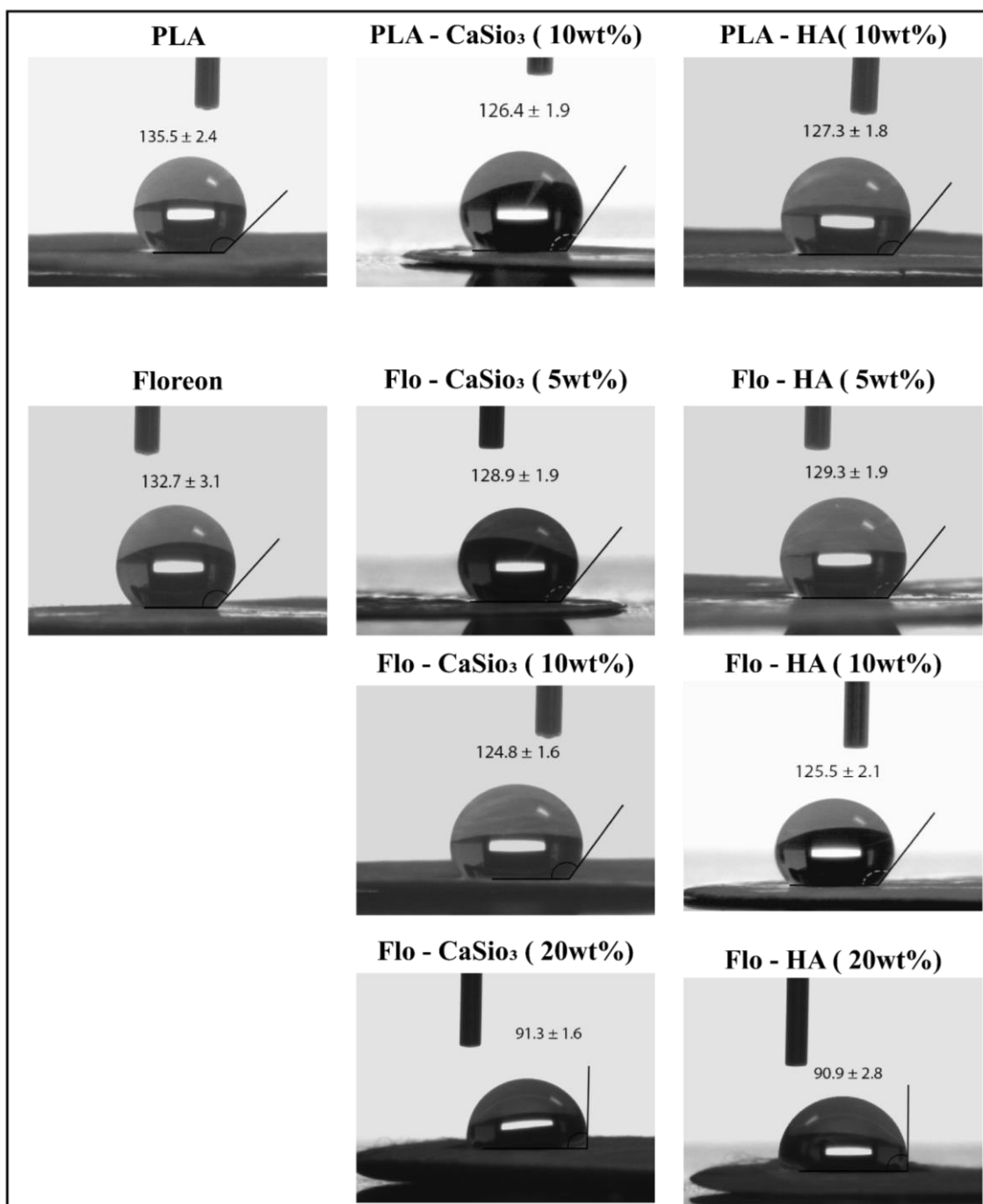
Figure 4-31 Water contact angle photos of PLA and Floreon fibrous membranes containing different concentrations of Hydroxyapatite and Calcium Silicate particles.

Membrane wettability plays an important role in aiding in the permeability of water filtration membranes (Chang *et al.*, 2020). Figures 4-30 and 31 show the water angle test result. Since PLA and Floreon are hydrophobic polymers, hydrophilic bioceramics (HA and $CaSiO_3$) with oxygenated functional groups were expected to enhance the membrane's wettability to contribute toward membrane permeability performance (Kobayashi *et al.*, 2012). The incorporation of HA and $CaSiO_3$ into PLA and Floreon membranes resulted in a significant ($p<0.05$) decrease in the water contact angle. Figure 4.1-30 show a decreasing trend in Floreon with HA/$CaSiO_3$ loading up to 20% wt. Compared with PLA scaffolds, the hydrophilicity of the Floreon and 20% wt $CaSiO_3$ scaffold surface improved significantly, evidenced by a decrease in Floreon from 132.7° to 91.3°.

4.1.11   Mechanical characterisation of fibrous membranes

The mechanical properties of fibrous membranes are highlighted in this part. Figure 4-32 and Figure 4-33 display the mechanical characteristics of PLA and Floreon scaffolds filled with HA or $CaSiO_3$ at varying concentrations, including ultimate tensile strength, stiffness, and percent of total elongation. The ultimate tensile strength of membranes is measured using a tensile tester that records tensile stress vs strain (i.e., extension per original length) until failure or rupture (Figure 4-32). Consequently, it is the greatest stress a membrane can withstand before permanently deforming or rupturing. It was shown that the ultimate tensile strength of Floreon membrane was much greater than that of comparable PLA films.

It was found that the tensile strength of scaffolds increases when 10% wt. of HA or $CaSiO_3$ was introduced; this was observed for both systems (PLA and Floreon). When the concentration of HA or $CaSiO_3$ was increased to 20%, however, the ultimate tensile strength clearly decreases, falling below that of Floreon membrane.

The stiffness of the membrane is the ability of a film to resist the force causing deformation. The film stiffness increased when HA and $CaSiO_3$ are added at a concentration of 10 wt% but decreases when the concentration is further increased to 20% wt.

A film's percent elongation indicates how much the film can be stretched before it breaks as a percentage of its original dimensions. Plain PLA and Floreon films exhibited the highest elongation percent, while the addition of ceramic particles reduced these values gradually. There were no obvious differences between the mechanical properties of pure Floreon films and those that had 5 percent of ceramic particles of either type added.

Table 4-5 provides numerical data to determine the membranes' mechanical properties.
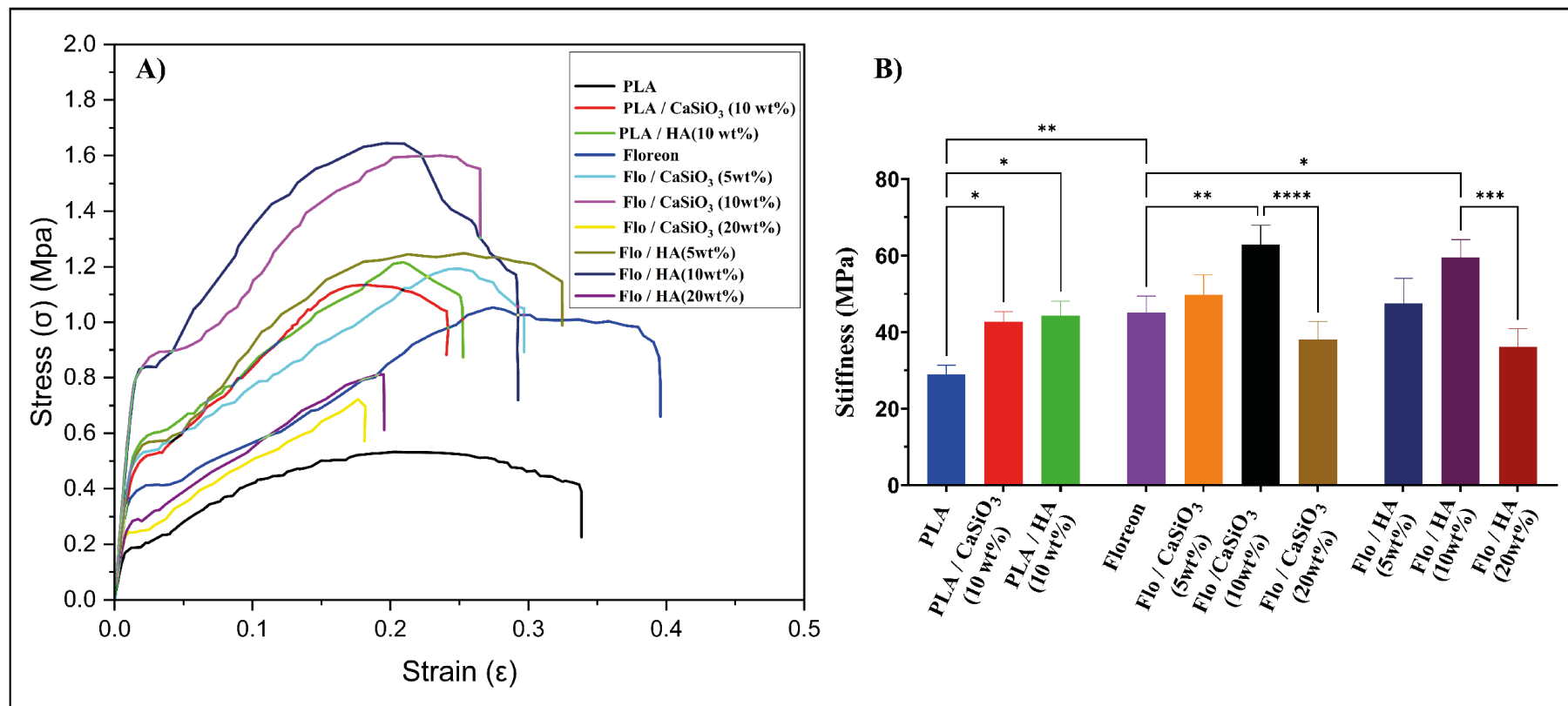
Figure 4-32 Stress-strain Curve(A); and Stiffness (B) of PLA and Floreon fibrous membranes containing different concentrations of Hydroxyapatite and Calcium Silicate particles. Data represented n=6, mean ± STDV following One-way ANOVA statistical analysis with Tukey comparison test. **** $p < 0.0001$, *** $p < 0.001$, ** $p < 0.01$, * $p < 0.05$.
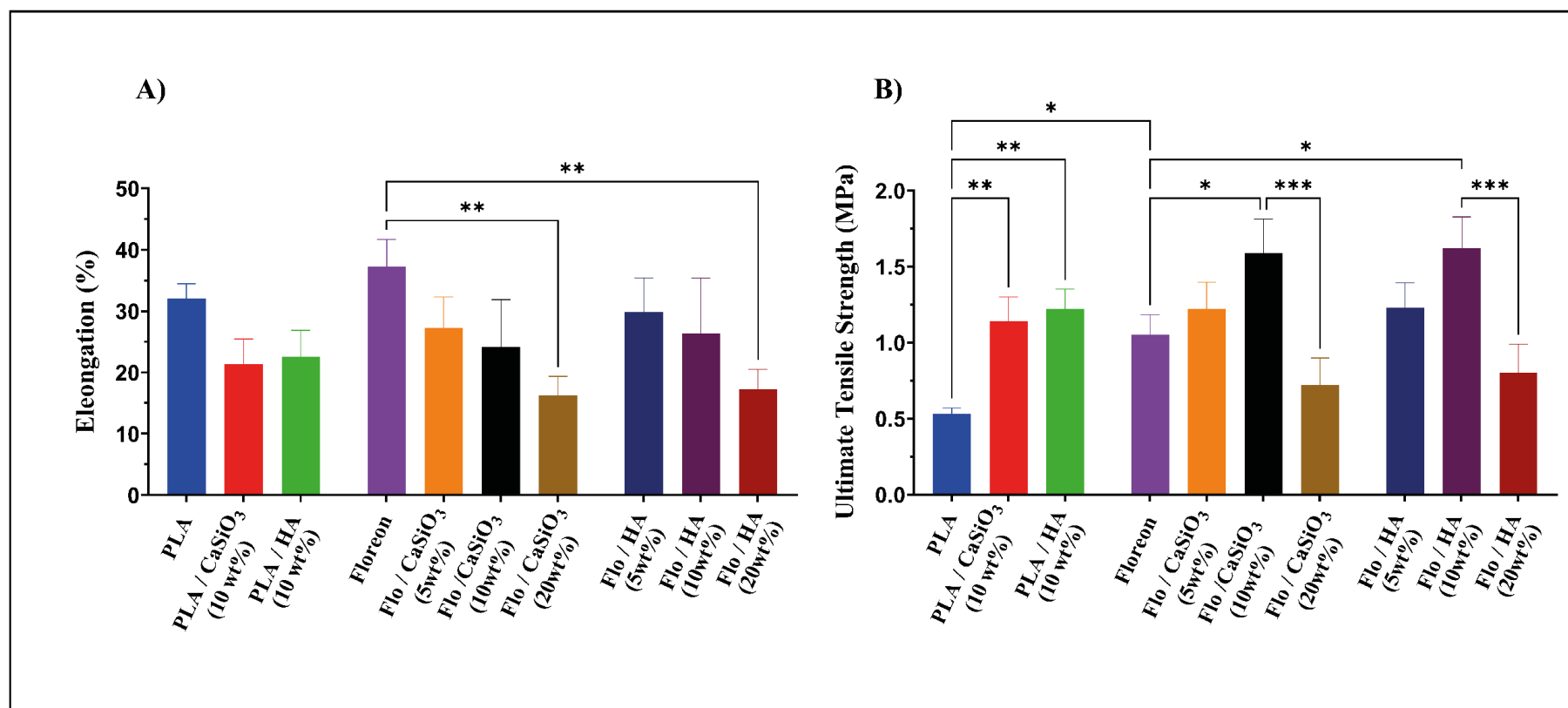
Figure 4-33 Percent Elongation (A); and Ultimate tensile strength Stiffness (B) of PLA and Floreon fibrous membranes containing different concentrations of Hydroxyapatite and Calcium Silicate particles.Data represented n=6, mean ± STDV following One-way ANOVA statistical analysis with Tukey comparison test. **** $p < 0.0001$, *** $p < 0.001$, ** $p < 0.01$, * $p < 0.05$.

Table 4-5 Tensile properties of PLA and Floreon scaffolds with different concentration of Hydroxyapatite and Calcium Silicate particles. To calculate the Ultimate tensile strength (MPa), Stiffness (MPa) and Elongation at break (%), Values shown are mean ± SD where n=6.

Membranes	Ultimate Tensile Strength (MPa)		Stiffness (MPa)		Percent Elongation (%)	
	Mean	SD	Mean	SD	Mean	SD
PLA	0.5	0.10	28.9	2.4	32.0	2.4
PLA / CaSiO$_3$ (10 wt%)	1.1	0.2	42.6	2.7	21.4	4.1
PLA / HA (10 wt%)	1.2	0.1	44.3	3.8	22.5	4.4
Floreon	1.1	0.1	45.1	4.2	37.2	4.4
Flo / CaSiO$_3$ (5wt%)	1.2	0.2	49.7	5.2	27.3	5.1
Flo / CaSiO$_3$ (10wt%)	1.6	0.2	62.8	5.1	24.1	7.7
Flo / CaSiO$_3$ (20wt%)	0.7	0.2	38.1	4.6	16.2	3.1
Flo / HA (5wt%)	1.2	0.2	47.5	6.5	29.9	5.5
Flo / HA (10wt%)	1.6	0.2	59.6	4.6	26.4	9.0
Flo / HA (20wt%)	0.8	0.2	36.1	4.7	17.3	3.2

The mechanical properties of the scaffolds are a very important parameter to characterise when using materials for tissue engineering because the scaffold needs to withstand stress incurred during *in vitro* culture and *in vivo* implantation (Birhanu *et al.*, 2018). The stress–strain curves are shown in Figures 4-32. The main parameters obtained for the different obtained membranes are displayed in Table 4-5 and Figures 4-32 and 33. The mechanical properties of scaffolds are important factors determining their *in vivo* performance for bone regeneration in the long term (Prasadh and Wong, 2018). They typically undergo different mechanical stress such as compression and tension from surrounding bone tissues, affecting their stability and integration properties (Little, Bawolin and Chen, 2011).

Therefore, the mechanical properties of scaffolds should be tailored to match the native bone to be repaired (Prasadh and Wong, 2018). After surface modification, the mechanical behaviour of scaffolds should be characterised before implantation to avoid possible implant failure. In the present study, the tensile was carried out for all scaffolds to determine the

changes in their mechanical properties before and after surface modification. Regarding tensile tests, although there was no statistical significance among all groups, the tensile modulus increased slightly after surface modification and reached its highest level at 10% wt in the PLA and Floreon group and reduced to 0.8 MPa at 20% wt for Floreon. Concerning the strain at break, with this type of morphological configuration, a very strong reduction is detected with respect to the membranes of PLA and Floreon. The stiffness of the membrane is the ability of a film to resist the force causing deforming. The film stiffness increased when HA and $CaSiO_3$ were added at a concentration of 10 wt% but decreased when the concentration was further increased to 20% wt. A film's percent elongation indicates how much the film can be stretched before it breaks as a percentage of its original dimensions. Unmodified PLA and Floreon films exhibited the highest elongation percent, while the addition of ceramic particles reduced these values gradually. There were no obvious differences between the mechanical properties of pure Floreon films and those that had 5% of ceramic particles of either type added (Rahim and Rasidi, 2020).

Many research teams worldwide have investigated the effect of adding ceramic particles of nano and micro sizes to electrospun polymeric scaffolds on their physicochemical and biological properties. Evidence from these studies suggests that incorporating these particles into a scaffold improved its thermal and mechanical properties and boosted its bioactivity (Sui *et al.*, 2007; Sonseca *et al.*, 2012; Rajzer *et al.*, 2014; Chen *et al.*, 2015). However, Kareem, (2020), pointed out that increasing ceramic particle concentrations in electrospun polymeric scaffolds causes filler agglomeration within the fibres and the formation of nano- and micro-cracks in the fibres during scaffold processing, which can have a negative impact on the scaffolds' mechanical properties (Kareem and Tanner, 2020). The study showed that the mechanical properties of Floreon were altered when 20% HA or $CaSiO_3$ were added to the composition.

4.1.12   *In-vitro*-degradation and bioactivity studies of nanofibers films

4.1.12.1 *In-vitro* degradation analysis

- **Weight profile analysis**

Figure 4-34 and Figure 4-35 illustrate the trend of the remaining weight percentage of Floreon and PLA membranes prepared by electrospinning process with the addition of different concentrations of bioceramic (HA and $CaSiO_3$) during 24 weeks of immersion in SBF. Table 0-1-Appendix shows levels of significance for differences in residual weight percentage between the analysed samples.

Tukey's test revealed that the addition of 10% HA or $CaSiO_3$ to Floreon and PLA nanofibers considerably increased the biodegradation rate compared to blank PLA and Floreon throughout the 24 weeks of immersion in SBF. However, the 5% increase did not significantly affect the biodegradation rate, particularly during the first 16 weeks of the study. The biodegradation rate of nanofibers containing 20% HA or $CaSiO_3$ was significantly faster than that of nanofibers containing 10% bioceramic. There was no significant difference in biodegradation rates between Floreon and PLA, even when bioceramics were added to the blend.
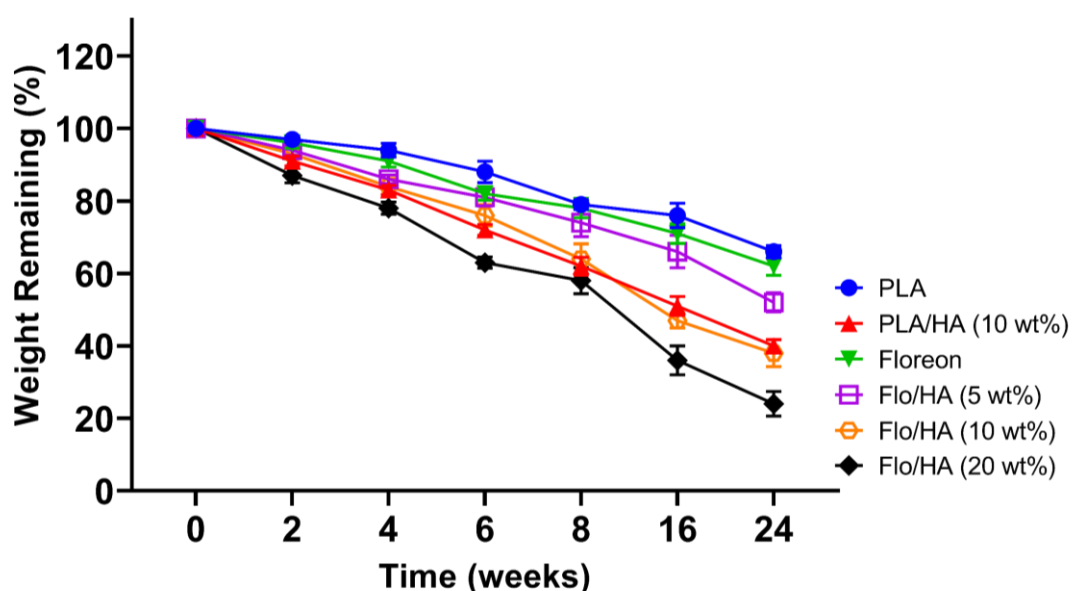
Figure 4-34 Weight loss behaviour of Floreon and Floreon-based HA nanofiber mats with different concentrations (5,10 and 20 wt%) during 24 weeks of immersion in SBF, compared to PLA and PLA/HA at 10 wt%.
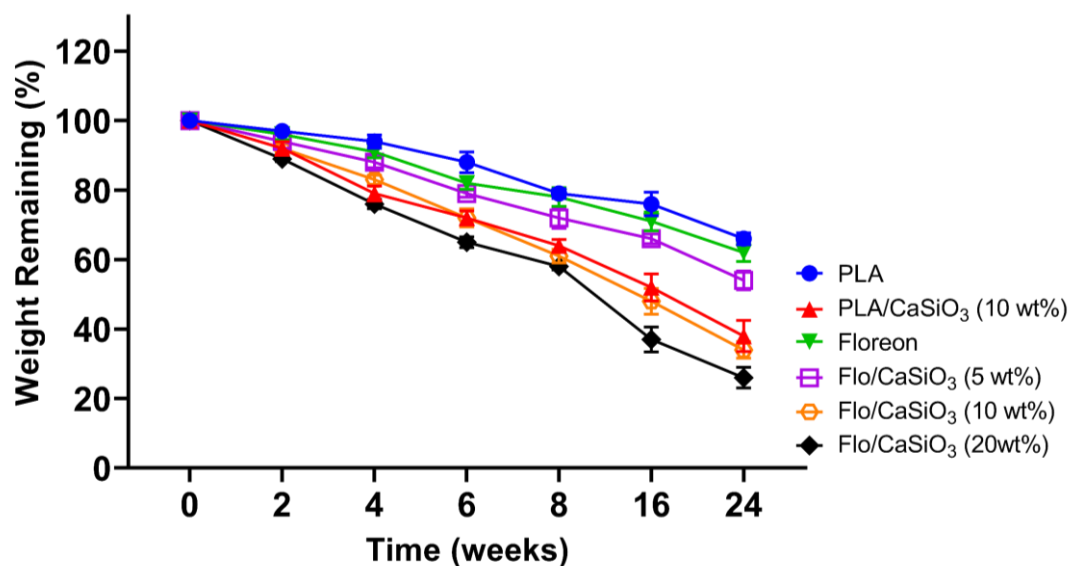
Figure 4-35 Weight loss behaviour of Floreon and Floreon-based $CaSiO_3$ nanofiber mats with different concentrations (5,10 and 20 wt%) during 24 weeks of immersion in SBF, compared to PLA and PLA/ $CaSiO_3$ at 10 wt%.

In general, hydrophilic polymers are more prone to hydrolysis and subsequent hydrolytic degradation than to hydrophobic polymers (Padsalgikar, 2017). There were no significant differences between the behaviour of HA microfibres and $CaSiO_3$ microfibres for both Floreon and PLA. Figure 4-34 showed weight loss behaviour of Floreon and Floreon-based HA microfibre mats with different concentrations (5,10 and 20 wt%) during 24 weeks of immersion in SBF, compared to PLA and PLA/HA at 10 wt%. Figure 4-35 showed weight loss behaviour of Floreon and Floreon-based $CaSiO_3$ fibrous mats with different concentrations (5, 10, and 20 wt%) during 24 weeks of immersion in SBF, compared to PLA and PLA/$CaSiO_3$ at 10 wt%. The weight loss was seen as faster in Floreon/ HA (20 wt.%) than that of all membranes. However, it was seen that concentrations of low (5 wt%), medium (10 wt%), and high (20 wt%)] of both HA and $CaSiO_3$ affected the degradation of films and weight loss. The weight percentage (wt%) was directly proportional to the weight loss. Weight loss was continuous but it was faster between 8-16 weeks. Sanchez and colleagues conducted a similar investigation on the biodegradation potential of HA and $CaSiO_3$ composites and discovered that following immersion in SBF solution, the samples lost weight for 4 days. They also reported that initial fast Ca2+ release from the specimens to the solution happens as a result of early weight loss (Sanchez *et al.*, 2021). A comparable investigation was carried out by Jeong et al. wherein weight loss was attributed to the breakdown of ester bonds. The process involves the attack of water molecules on the ester bonds, leading to the cleavage of lengthy polymer backbone

chains (Jeong *et al.*, 2017). The cleavage of ester linkages through hydrolysis generates hydroxyl and carboxylic acid groups, leading to a reduction in polymer molecular weight (Choi *et al.*, 2020). In the present study, the degradation induced by the fluid was monitored by measuring the weight of the membranes immersed in simulated body fluid (SBF) for a duration of up to 24 weeks. No dramatic difference was observed between Floreon and PLA. Rickel *et al.*, reported that the molecular weight of electrospun fibres decreased significantly by applying higher dosage, concluding that this effect seems to be dose-dependent (Rickel *et al.*, 2021). They described that the weight loss did not affect the morphology of the electrospun fibres up to (20 wt%), although a little narrowing of the fibre's diameter was noted. The structural integrity of Floreon fibres following the application of low, medium, and high doses of HA and $CaSiO_3$ was assessed in the present study. The results indicate that the application of these doses did not have any discernible impact on the structural integrity of the fibres. As such, these findings suggest that an appropriate dosage of HA and $CaSiO_3$ could be used in future applications of the Floreon and PLA structure within the field of engineering.

Electrospun polymers with high molecular weight like that used in the present study have long in this regard, a strong decrease in the molecular weight of fibres containing HA and $CaSiO_3$ (20 wt%) was observed in comparison with the low dose samples immersed in SBF, compared with the controls. Wu and Wang studied the effect of polymer Mw on PLGA degradation (Belabbes *et al.*, 2022). PLGA 75/25 extruded rods (Mw: 166,630; 241,450; 66,946; 31,403, and 10,876) were immersed in the buffer solutions for 72 days. Average Mw as a function of time during degradation for PLGA samples with the same composition and different Mw gives the constant of the degradation rate (k) of each sample. The absolute value of the degradation reaction rate increased with the rising Mw of the polymers. In fact, the degradation process was hypothesised to occur in three phases: (i) first, slow hydration of the polymers occurs within the first week; (ii) second, fast degradation rate occurs within the second and the fifth weeks and (iii) third, biodegradation rate slows down. The weight was also measured as a function of SBF incubation time. In general, Floreon, PLA, and their co-polymers undergo bulk degradation: polymer weight falls owing to hydrolysis of polymer ester linkages, resulting in shorter polymer chains (Eldrehmy *et al.*, 2022).

- **Water uptake analysis**

Figure 4-36 andFigure 4-37 show the trend of the water uptake percentage of electrospun Floreon and PLA membranes with the addition of various concentrations of bioceramic (HA and CaSiO$_3$) during 24 weeks of immersion in SBF. Table 0-2-Appendix illustrates degrees of significance changes in water uptake percentage between samples that have been analysed.

During 24 weeks of SBF immersion, the addition of 10 percent HA or CaSiO$_3$ to Floreon and PLA nanofibers dramatically increased the rate of water absorption compared to Floreon and PLA nanofibers without additives. However, the 5% increase had no significant effect on water absorption, particularly in the first six weeks of the incubation period. The adsorption rate of nanofibers containing 20% HA or CaSiO$_3$ was much greater than that of nanofibers containing 10% bioceramic. Even with the addition of bioceramics, there was no noticeable difference in adsorption rates between Floreon and PLA.
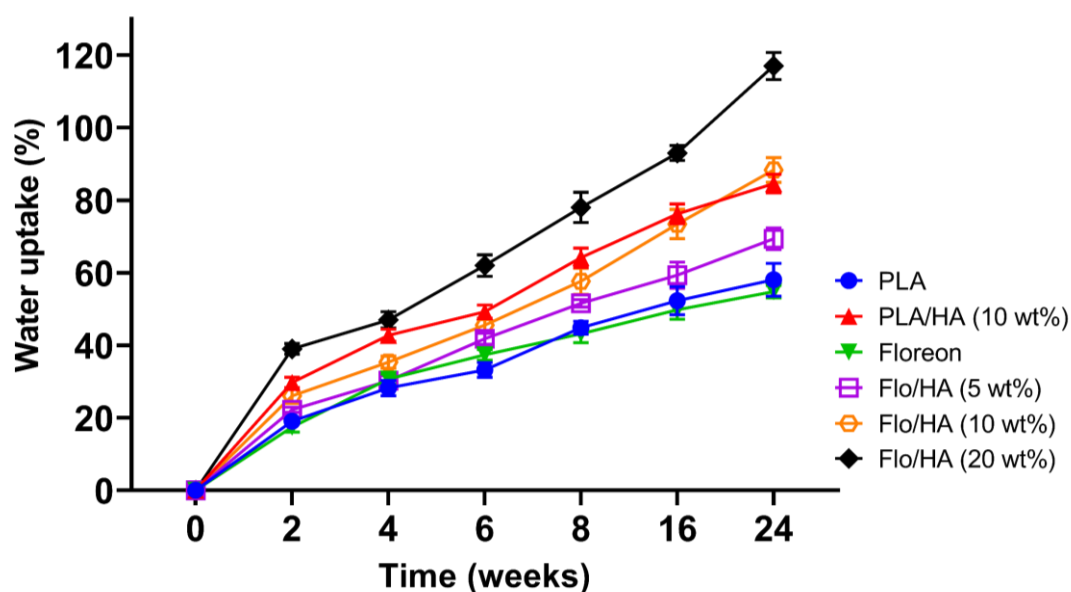
Figure 4-36 Water uptake of Floreon and Floreon-based HA nanofiber mats with different concentrations (5,10 and 20 wt%) during 24 weeks of immersion in SBF, compared to PLA and PLA/HA at 10 wt%.
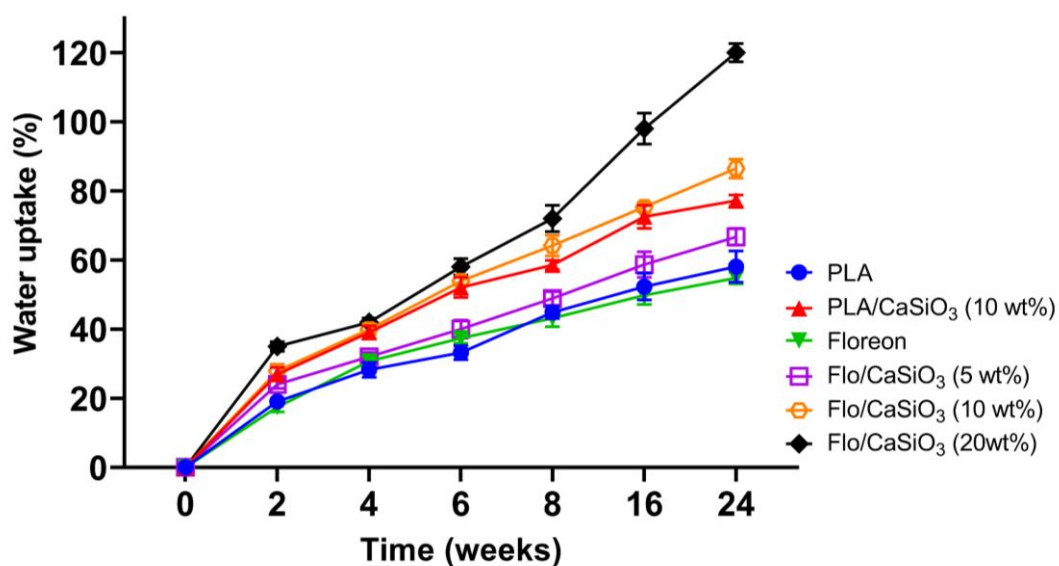
Figure 4-37 Water uptake of Floreon and Floreon-based CaSiO₃ nanofiber mats with different concentrations (5,10 and 20 wt%) during 24 weeks of immersion in SBF, compared to PLA and PLA/ CaSiO₃ at 10 wt%.

Water is absorbed by most polymers, but a change of properties is induced only in specific types of polymers. Water is considered to be present in the free volume and active only when attached to polymer chains by hydrogen bonds. Figure 4-36 showed water uptake of Floreon and Floreon-based HA fibrous mats with different concentrations (5, 10, and 20 wt%) during 24 weeks of immersion in SBF, compared to PLA and PLA/HA at 10 wt%. Figure 4-37 shows water uptake of Floreon and Floreon-based CaSiO₃ fibrous mats with different concentrations (5, 10, and 20 wt%) during 24 weeks of immersion in SBF, compared to PLA and PLA/CaSiO₃ at 10 wt%). The water uptake was higher in Floreon/ HA (20 wt%) than that of all treatments. There were no significant differences between the behaviour of HA microfibres and CaSiO₃ microfibres for both Floreon and PLA. However, it was seen that concentrations (low [5 wt%], medium [10 wt%], and high [20 wt%]) of both HA and CaSiO₃ in combination with PLA and Floreon affected the degradation of films and caused more surface wettability. The weight percentage (wt%) was directly proportional to the water uptake. Water uptake was continuous, but it was faster between 8-16 weeks, similar to previous studies (Nica *et al.*, 2022).

- **FTIR Spectroscopy for degraded membranes**

Figure 4-38 to Figure 4-40 depict the Fourier-transform infrared (FTIR) spectra of non-degraded (week 0) and degraded (weeks 12 and 24) electrospun Floreon and PLA films that were immersed in SBF and mixed with various concentrations of bioceramic particles (HA

and CaSiO$_3$). The selected spectral features and corresponding peak assignments were summarised in Table 4-8 in the preceding section, where the inter-group differences were analysed. This section will focus on the intra-group alterations observed during the degradation process. In all samples, it was found that the peak intensities had changed over time, which is the most notable finding. Particularly, in week 0 two small peaks appear at 2995 and 2944 cm-1, which belong to a CH bond in a PLA monomer, were employed for internal normalisation, these peaks disappear in case of week 12 and week 24, peak at 1749 represent –C=O– carbonyl linkage in ester, this peak was strong in week 0 but it is medium in other weeks, small peaks at 1452 and two peaks at 1360 and 1382 corresponds to −CH− deformation (including sym and asym bend), Peaks at 1268, 1180, 1129, 1080, and 1043 are due to −C−O− stretch. A small peak at 868 represents −C−C− stretch, peak around 755 corresponds to –CH2− groups.

All of these peaks were at their most intense before being immersed in SBF (week 0). However, their intensity decreased in weeks 12 and 24.
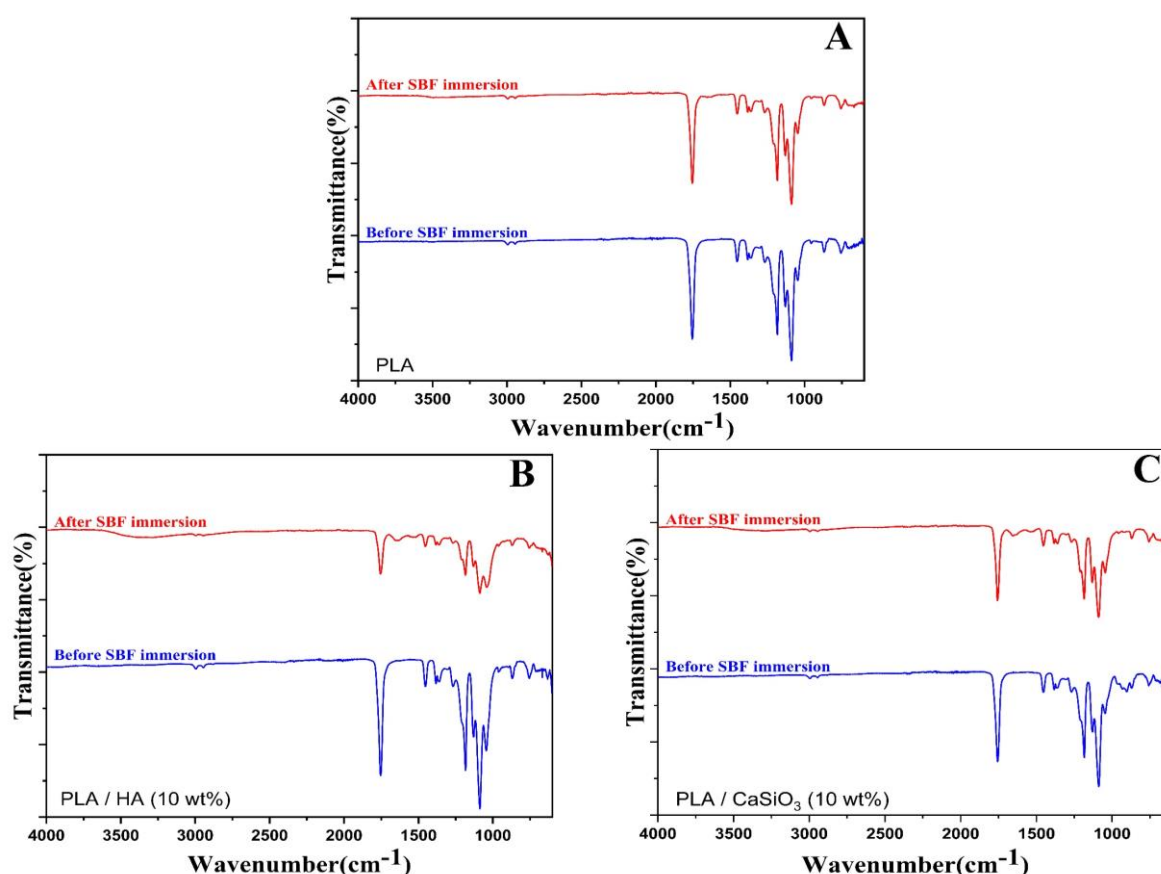
Figure 4-38 FTIR spectroscopy of (a) PLA, (b) PLA/HA-10 wt% and (c) PLA/CaSiO$_3$-10 wt% nanofiber mats during 24 weeks of immersion in SBF.
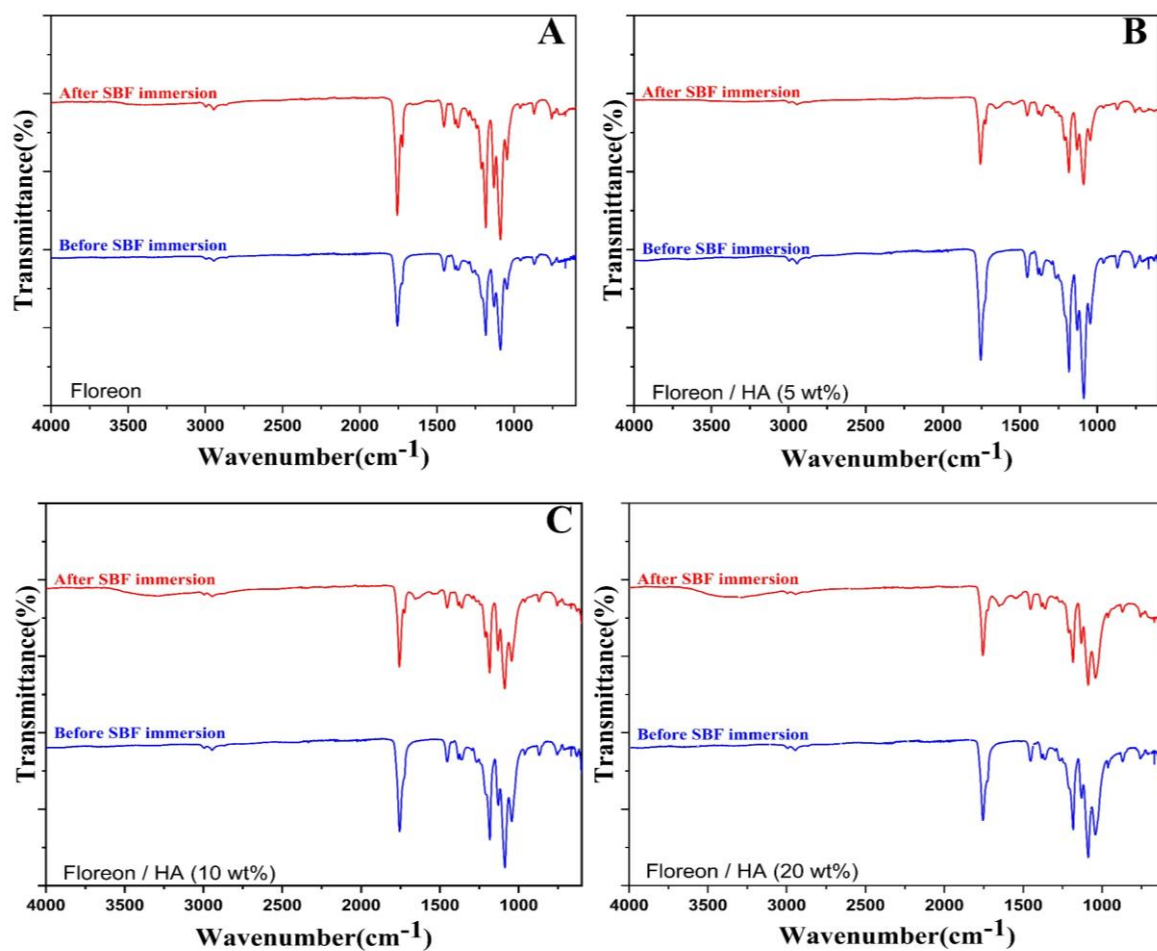
Figure 4-39 FTIR spectroscopy of (a) Floreon, (b) Flo/HA-5 wt%, (c) Flo/HA-10 wt% and (d) Flo/HA-20 wt% nanofiber mats during 24 weeks of immersion in SBF.
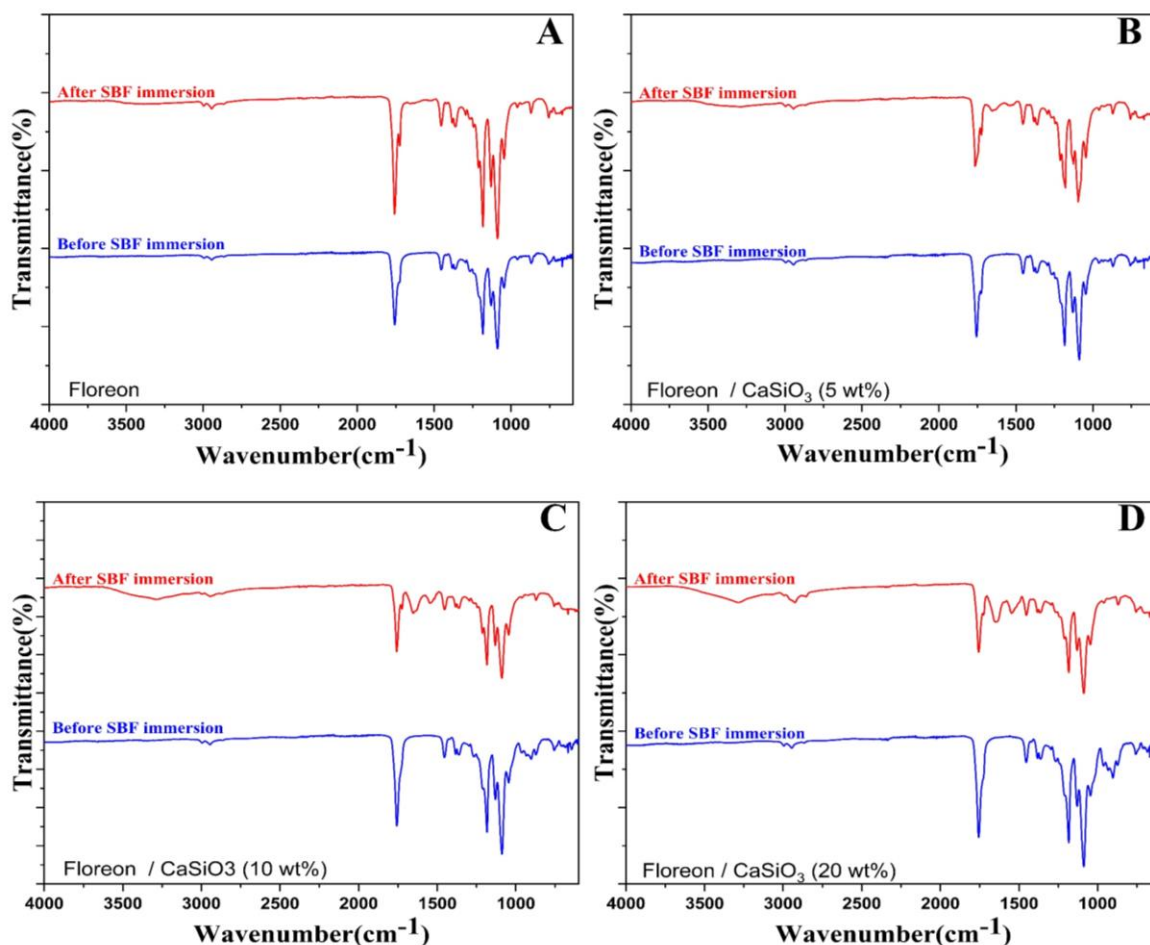
Figure 4-40 FTIR spectroscopy of (a) Floreon, (b) Flo/CaSiO$_3$-5 wt%, (c) Flo/CaSiO$_3$-10 wt% and (d) Flo/CaSiO$_3$-20 wt% nanofiber mats during 24 weeks of immersion in SBF.

FTIR spectroscopy was used to identify changes of typical chemical functional groups of the fibres. FTIR presents typical vibrational modes in the infrared region like aliphatic C-H stretching modes (3000–2850 cm−1), carbonyl C=O stretching modes (1850–1650 cm−1), CH3/CH2 symmetric angular deformation (1500–1250 cm−1) and ester C–O asymmetric stretching modes (1300–1000 cm−1) (Patricio *et al.*, 2013; Aldemir Dikici *et al.*, 2019).

Figure 4-38 showed FTIR spectroscopy of (a) PLA, (b) PLA/HA-10 wt% and (c) PLA/CaSiO$_3$-10 wt% microfibre mats during 24 weeks of immersion in SBF. Figure 4-39 and 40 showed the FTIR spectroscopy of Floreon fibrous films with addition of bioceramic particles in various concentrations during 24 weeks of immersion in SBF.

At week 0, peaks appear at 2995 and 2944 cm^{-1} that belong to a CH bond in a PLA monomer. A peak at 1749 represents -C=O carbonyl linkage. The peak at 1452 and peak at 1360 and 1382 correspond to CH deformation. A peak at 868 relates to CC stretch, whereas a peak around 755 refers to -CH$_2$ groups. Lee et al., studied the degradation process of PLGA

(50:50) microfibres immersed in PBS solution and found an asymmetric stretching mode of O=C–ONa groups polymers 2020, 12, 1853 13 of 19 at 1600 cm^{-1} is attributed to a mixture of acidic oligomers from the PLGA degradation and sodium ions from PBS, which could explain the band at 1610 cm^{-1} (Lee *et al.*, 2022).

These changes or slight shifts in intensity and peaks were correlated to degraded scaffolds. Initial destruction was related to the destruction of the pyranose ring. Another significant change noted was at the peak corresponding to saccharide structure at 755 cm^{-1} that flattened out at the end of 24 weeks. The band found at 1715 cm^{-1} seems to be related to the hydrogen bond in water, coordinated with the polymer carbonyl group (C=O) from a shift on C=O vibration modes (Chor *et al.*, 2020). These results indicate a polymer chemical change probably due to the hydrolysis degradation of PLA and Floreon immersed in SBF solution. The band found at 1715 cm^{-1} seems to be related to the hydrogen bond in water, coordinated with the polymer carbonyl group (C=O) from a shift on C=O vibration modes.

It has been reported by Yang and colleagues that when lysozymes were used to assess degradation of chitin and CH, characteristic peaks were not reduced; they attributed this to the low hydrolytic activity of lysozyme relative to the high DD of CH matrix. In the same study a quantitative assessment of hydrolysis was carried out using the 1110 cm^{-1} peak of HA and 1072cm^{-1} (pyranose ring) peak of CH. Correlations between absorbance ratios of pyranose of CH to the phosphate of HA were taken to be indicative of CH matrix remaining after lysozyme degradation by enzymatic hydrolysis. However, spectral data collected from the bottom surface of HA membrane in this study showed that some HA was lost. This was observed as the symmetric and asymmetric vibrations of phosphate and hydroxyl peaks visible in the spectra collected from the bottom surface showed decrease in intensity which could be indicative of the HA being resorbed or losing its bond with CH. Although this loss of HA was relatively very small, some similar studies conducted on CaSiO$_3$ degradation have ignored this amount (Yang *et al.*, 2020).

A short review of CaSiO$_3$ and HA composites by Yunos et al., states that the bio-resorption of HA is dependent on several factors, such as chemical, physical and biological conditions affecting bioceramic integrity (Mohamad Yunos, Bretcanu and Boccaccini, 2008).

- **DSC analysis for degraded membranes**

Figure 4-41 to Figure 4-43 and Table 4-6 display the thermal behaviours of electrospun Floreon and PLA films mixed with various concentrations of bioceramic (HA and CaSiO$_3$) before and after immersion in SBF for 24 weeks. It can be seen that the thermodynamic properties (Tg, Tc, and Tm) of films immersed in SBF changed over time. After 24 weeks of immersion, the crystallisation temperature (Tc) decreased for all samples, whereas the glass transition temperature (Tg) increased for all samples with the exception of those treated with 20% CaSiO$_3$. Regarding the melting temperature (Tm), it was observed that the degrees of PLA and Floreon blank films dropped, whereas the degrees of bioceramic-added films increased after immersion.

Table 4-6 Thermal properties of Floreon and Floreon-based ceramics composite with different concentrations (5,10, and 20%) before and after 24 weeks of SBF immersion compared to PLA and PLA/ceramics 10%.

Samples	Before immersion			After SBF immersion		
	Glass transition temperature (Tg) (°C)	Crystallisation temperature (Tc) (°C)	Melting temperature (Tm)(°C)	Glass transition temperature (Tg) (°C)	Crystallisation temperature (Tc) (°C)	Melting temperature (Tm)(°C)
PLA	59.0	80.0	150.7	61.0	79.9	149.5
PLA/HA (10 wt%)	62.1	87.7	150.0	64.5	84.4	151.2
PLA/CaSiO$_3$ (10 wt%)	61.6	82.3	149.7	63.4	82.2	150.7
Floreon	58.3	73.4	151	60.2	72.1	150.3
Floreon/HA (5 wt%)	58.7	81	150.8	59.7	76.4	151.0
Floreon/HA (10 wt%)	59.5	83.8	150.4	59.7	80.5	151.2
Floreon/HA (20 wt%)	59.3	87.1	150	59.9	84.5	150.7
Floreon/CaSiO$_3$ (5 wt%)	57.0	79.4	150.9	59.8	78.6	151.0
Floreon/CaSiO$_3$ (10 wt%)	59.5	83.8	150.3	59.9	79.6	151.6
Floreon/CaSiO$_3$ (20 wt%)	62.4	92.4	148.7	58.8	71.6	148.7
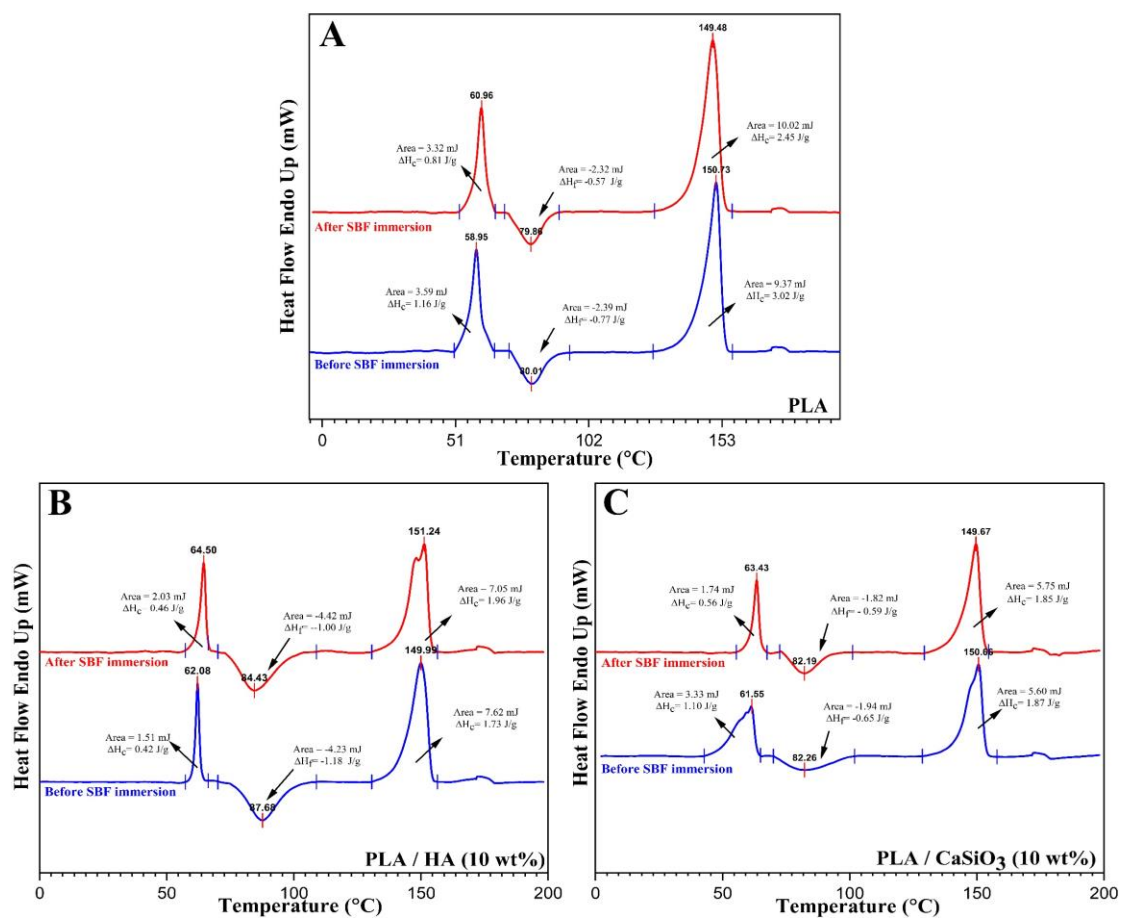
Figure 4-41 DSC thermogram of (a) PLA, (b) PLA/HA-10 wt% and (c) PLA/CaSiO₃-10 wt% nanofiber mats before and after SBF immersion for 24 weeks.
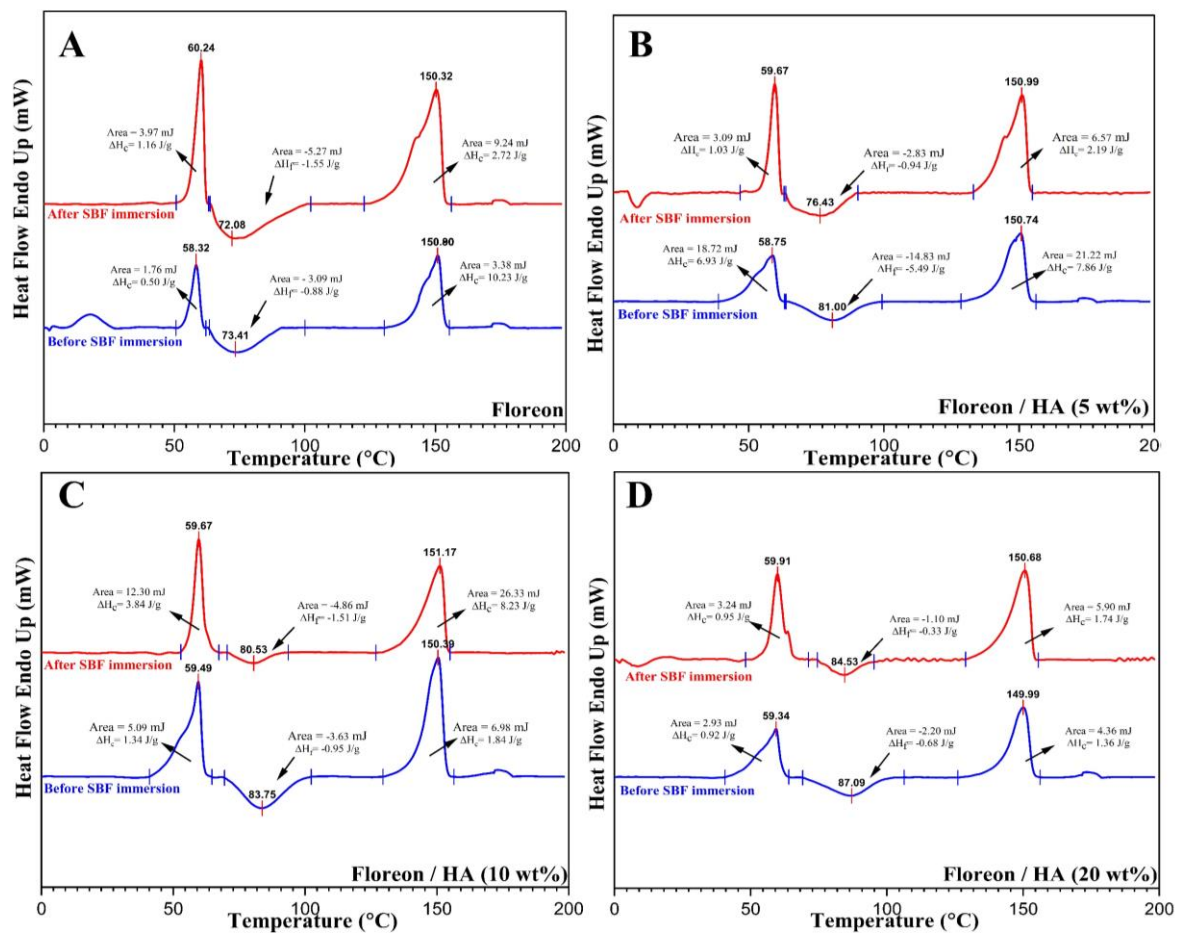
Figure 4-42 DSC thermogram of (a) Floreon, (b) Flo/HA-5 wt%, (c) Flo/HA-10 wt% and (d) Flo/HA-20 wt% nanofiber mats before and after SBF immersion for 24 weeks.
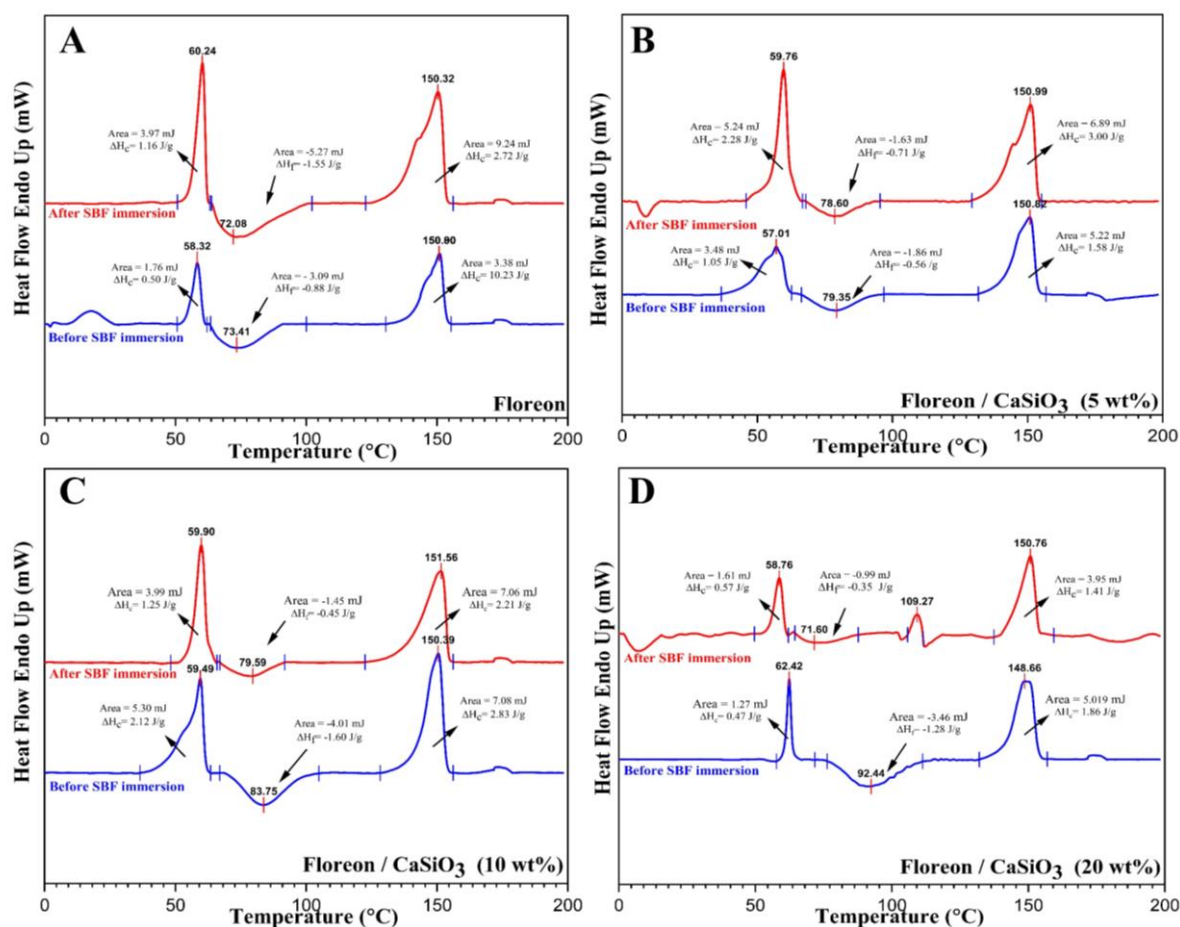
Figure 4-43 DSC thermogram of (a) Floreon, (b) Flo/CaSiO$_3$-5 wt%, (c) Flo/CaSiO$_3$-10 wt% and (d) Flo/CaSiO$_3$-20 wt% nanofiber mats before and after SBF immersion for 24 weeks.

It can be seen that the thermodynamic properties (Tg, Tc, and Tm) of films immersed in SBF changed over time. After 24 weeks of immersion, the crystallisation temperature (Tc) decreased for all samples, whereas the glass transition temperature (Tg) increased for all samples with the exception of those treated with 20% CaSiO$_3$. Regarding the melting temperature (Tm), it was observed that the degrees of PLA and Floreon blank films dropped, whereas these degrees increased for the bioceramic-added films after immersion.

It is noticeable that the peak's intensity increased with immersion time for all peaks. Polymer glass transition temperature is a function of different parameters among which the polymer Mw. It is a reversible step change in molecular mobility, from a rigid glassy state to a mobile rubbery state. This change is linked to the free volume associated with the polymer chain ends. When the Mw decreases, more chain ends are present and more free volume is generated. The polymer chains have, therefore, more space to move and the rubbery state is reached earlier i.e., at a lower temperature (Wang *et al.*, 2021).

As demonstrated by a decrease in Tg observed by DSC analyses of Floreon and PLA with different doses of HA and CaSiO$_3$ in comparison with the respective controls, a plasticisation (water absorption by the polymer chains) probably occurred in the bulk material depending on the immersion time. Li *et al*. have previously reported that a decrease in Tg was related to an initial process of degradation irradiated and irradiated caused by mass loss (Li and Chang, 2013). Effectively, the thermal analyses performed in this study indicate a similar trend of decreasing Mw in Floreon and PLA with concentrations of HA and CaSiO$_3$ in the SBF solutions, compared with controls. This event is compatible with cleavage of the covalent bonds in the polymer backbone.

In general, fibres without ceramics immersed in the SBF presented a higher degree of crystallinity in ceramics mixed fibres, suggesting that a fluid-induced crystallisation had higher influence over the higher Mw fibres. The higher degree of crystallinity may be associated with preferential degradation and solubilisation of the amorphous phase, increasing the crystalline phase (Alsharif *et al.*, 2020). As observed for the controlled/blank PLA and Floreon membranes immersed in SBF for 24 weeks, fibres with concentrations of HA and CaSiO$_3$ immersed in SBF showed the endothermic event before Tg that can probably be due to a relaxation process of highly oriented chain domains induced by SBF. So far, no report on enthalpic relaxation process at temperatures higher than Tg (more than 20 °C in some cases) were reported for electrospun fibres, and other investigations must be carried out to clear the origin of this transition.

- **Optical Images for degraded membranes**

Figure 4-44 to Figure 4-46 show optical images of Floreon and Floreon-based ceramics composites with varying concentrations (5, 10, and 20%) recorded at different time points from week 0 to week 24, compared to PLA and PLA/ceramics 10 wt %. The rate of biodegradation was accelerated by the presence of ceramics in the film, and this rate increases as the concentration of ceramics in the film increases. This is consistent with the prior findings from the remaining weight evaluation.
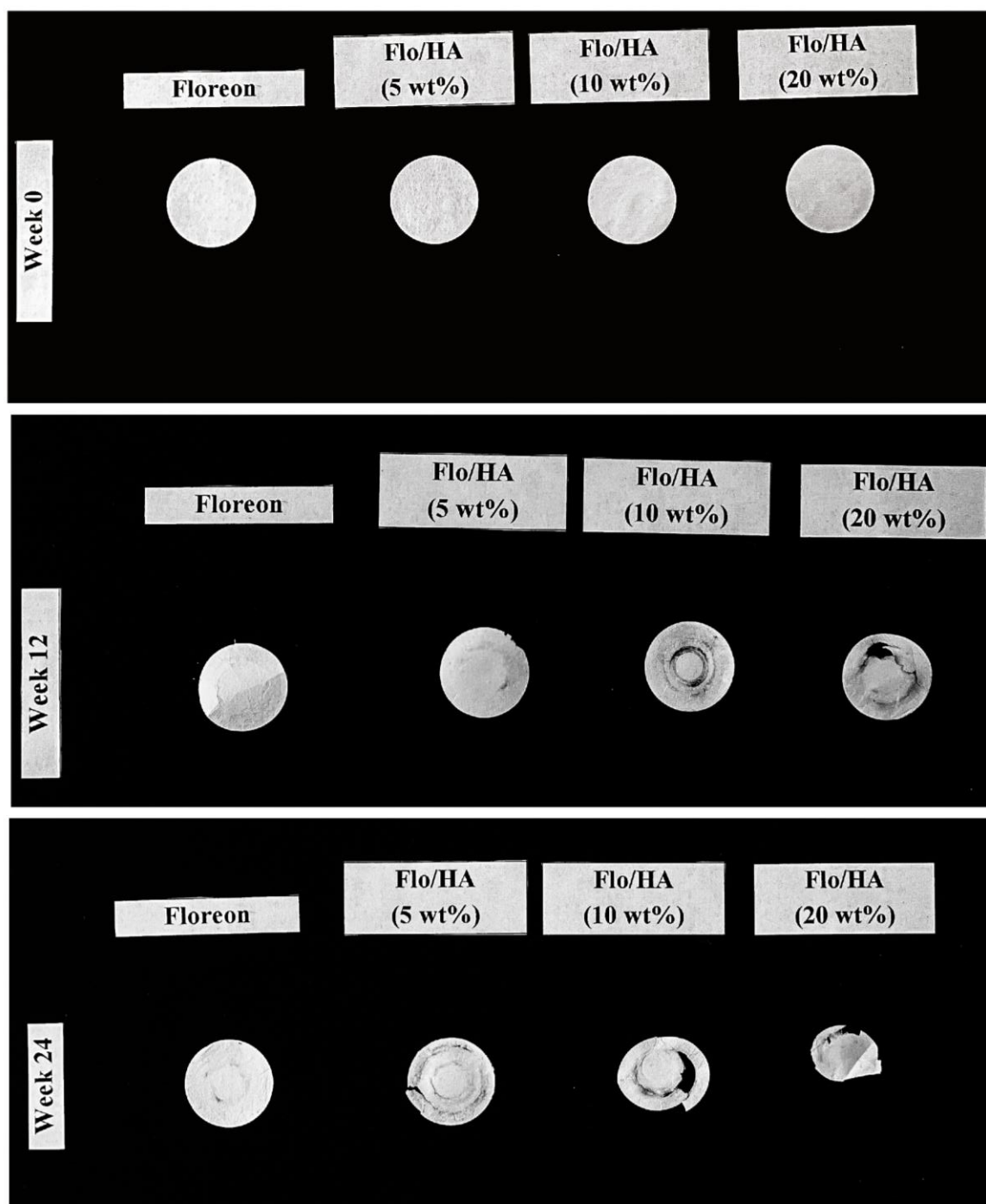
Figure 4-44 Optical Images of Floreon, Flo/HA-5 wt%, Flo/HA-10 wt% and Flo/HA-20 wt% nanofiber mats after degradation study at week 0, 12 and 24. Samples were selected out of three at each time point.
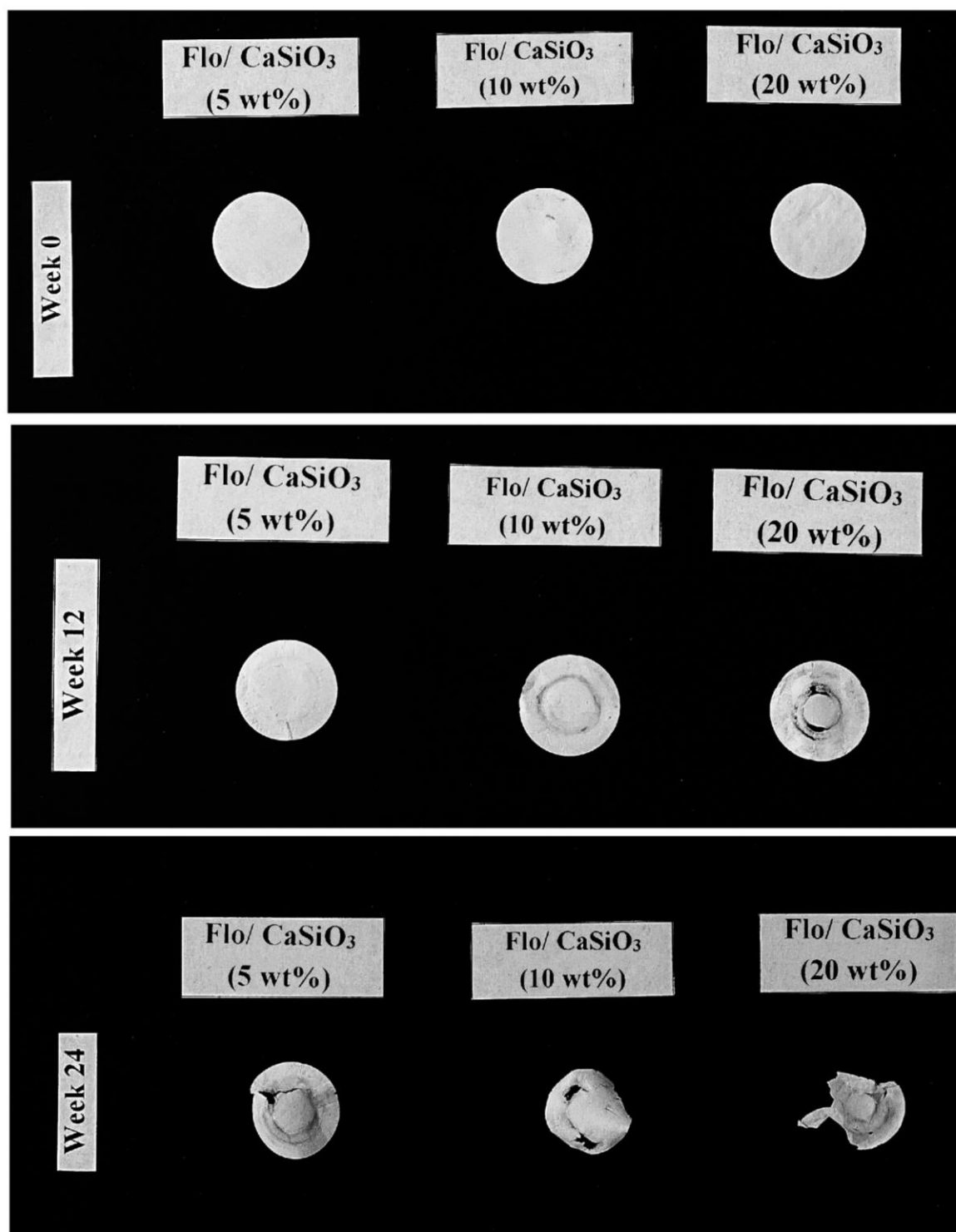
Figure 4-45 Optical Images of Floreon, Flo/CaSiO3-5 wt%, Flo/CaSiO3-10 wt% and Flo/CaSiO3-20 wt% nanofiber mats after degradation study at week 0, 12 and 24. Samples were selected out of three at each time point.
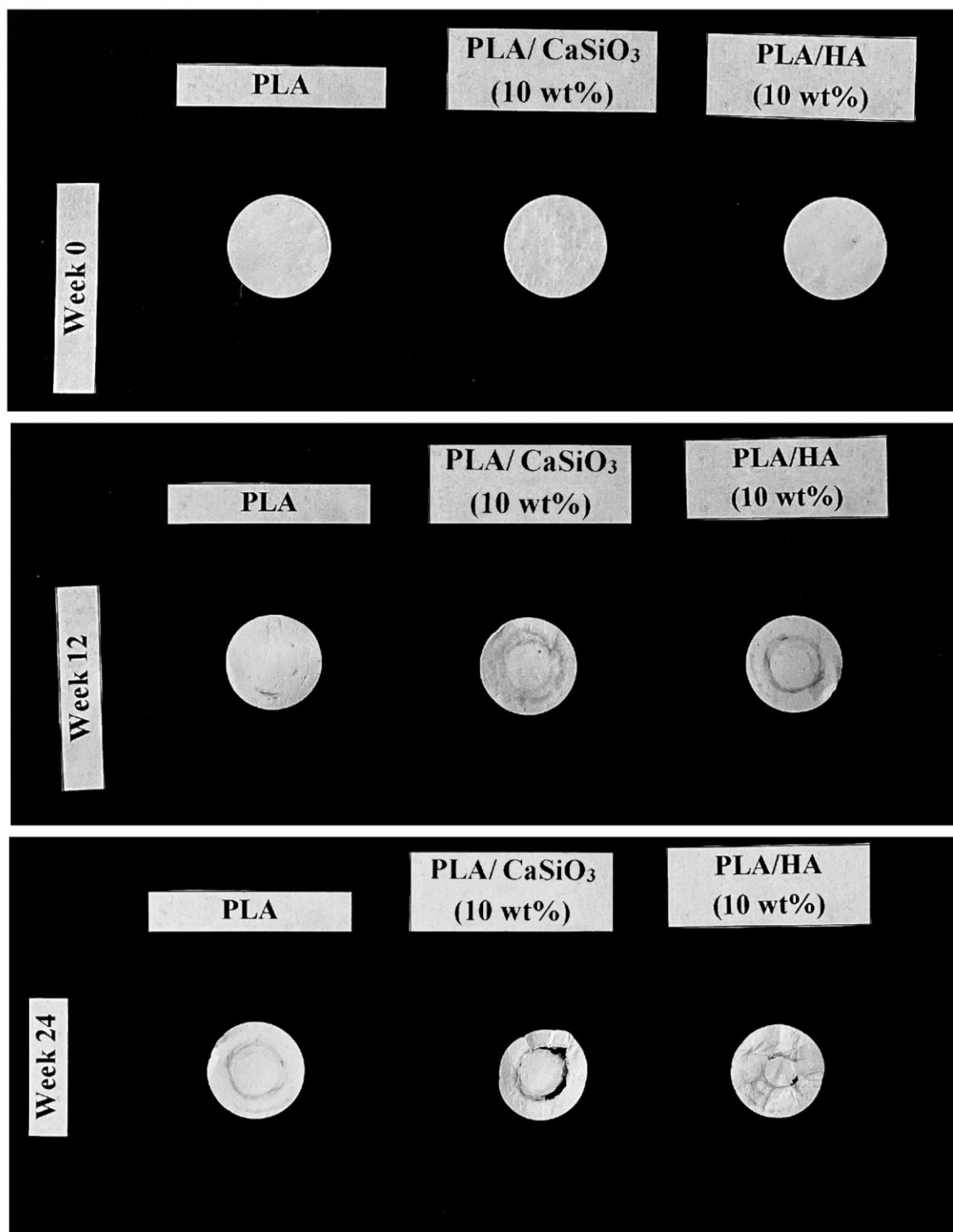
Figure 4-46 Optical Images of Floreon, Flo/CaSiO₃-5 wt%, Flo/CaSiO₃-10 wt% and Flo/CaSiO₃-20 wt% nanofiber mats after degradation study at week 0, 12 and 24. Samples were selected out of three at each time point.

Figure 4-44 to Figure 4-46 show optical images of Floreon and Floreon-based ceramics composites with varying concentrations (5, 10, and 20%) recorded at different time points from week 0 to week 24, compared to PLA and PLA/ceramics 10 wt%. The rate of biodegradation was increased by increasing the doses of HA and $CaSiO_3$ ceramics. In both cases of HA and $CaSiO_3$, during week 0, there were no significant changes in images. But during week 24 the curling rate was very high, and films were degraded completely.

Because the ester linkages are cleaved randomly along the polymer backbone, relatively few water-soluble fragments form initially. The reduction in molecular weight produces an increase in hydrophilicity but not necessarily changes in physical properties or mass (Payne, McKeown and Jones, 2019). In short, breakage of ester bonds is the biggest reason for curling of Floreon membranes. The scaffold collapses and breakdown products are released when the size of the polymer fragments gets small enough that the mechanical characteristics of the scaffold are dramatically reduced. A similar study was conducted by Zan and colleagues which revealed that Mw declined modestly with degradation time. Water diffused into the polymer due to the plasticising impact of the water molecules is another cause that may contribute to a reduction in material glass transition. A decrease in molecular weight increases hydrophilicity but does not always result in changes in physical qualities or mass (Zan *et al.*, 2022). Another factor that may lead to the decrease of material glass transition is the water diffused into the polymer, due to the plasticising effect of the water molecules (You, Noonan and Coates, 2020).

A study by Monsees *et al.*, has reported a comparative result of HA with magnesium and titanium coatings (Monsees *et al.*, 2017). The severity of the effects of the degradation processes is strongly influenced by environmental factors as well as the level of thermal treatment applied to the ceramic material. Similarly, in this investigation, the presence of ceramics in the film increased biodegradation, and this rate rises as the concentration of ceramics in the film increases. This indicates that increase in concentration of ceramics are positively correlated with the degradation of films.

4.1.12.2 Bioactivity analysis

- **Scanning electron microscopy**

Figure 4-47 to Figure 4-49 show SEM images obtained to study the biodegradation and bioactivity of nanofiber films immersed in SPF over 24 weeks. Regarding the degradation behaviour, a change in the nanofibers' size and shape was noticed with time for all samples.

Regarding the bioactivity of the nanofibers, apatite precipitation was observed on the ceramic-containing films, and its presence became progressively more prominent as the immersion period increased. The surface of Floreon with 5% bioceramic nanofibers was not observed to be coated with Apatite , however, the addition of 10% and 20% bioceramics caused a biological apatite to precipitate visibly, with a higher rise after 24 weeks as most of the fibres were covered by a cauliflower-like nano-textured layer.
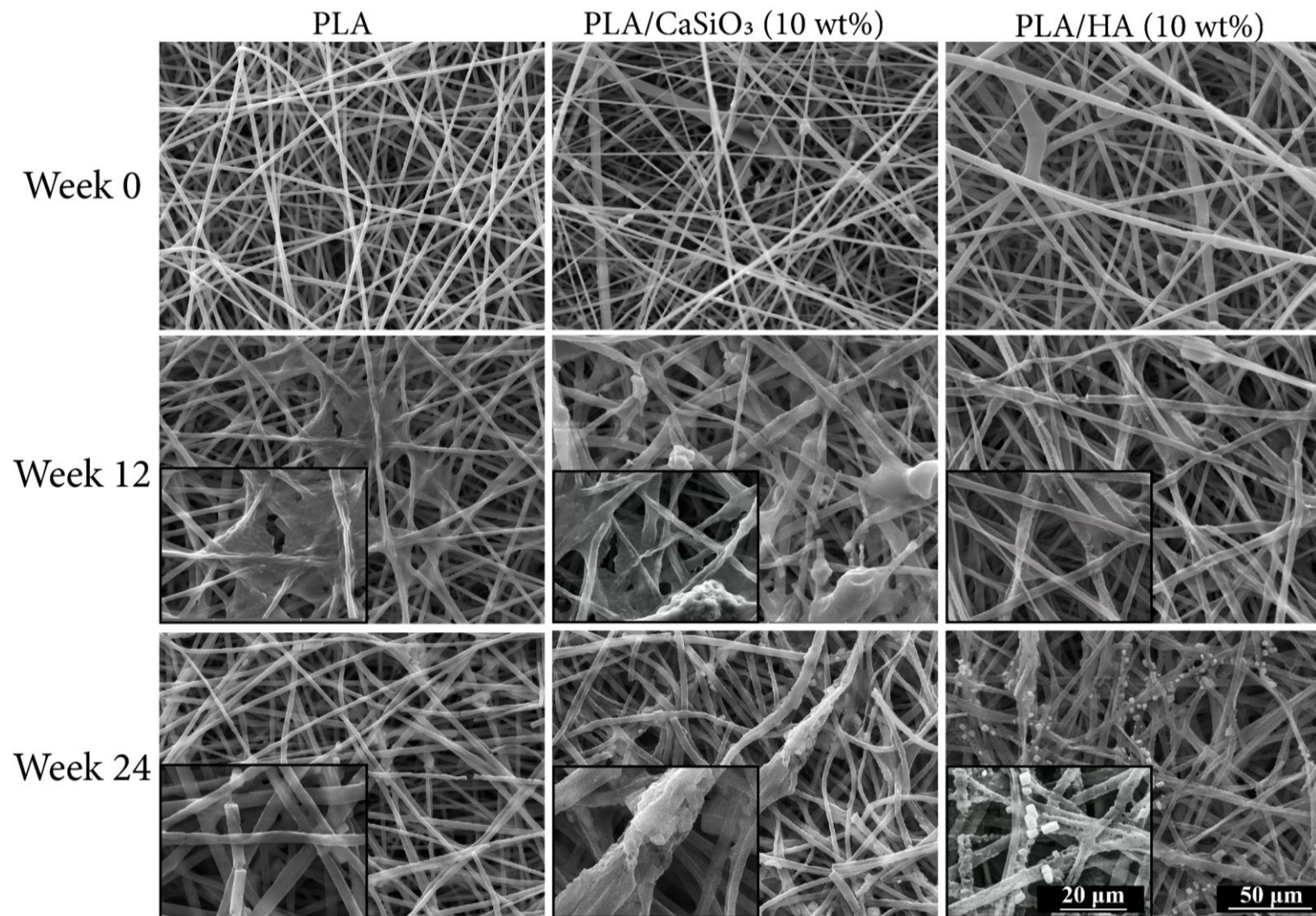
Figure 4-47 SEM images of PLA, PLA/CaSiO₃ -10 wt% and PLA/HA-10 wt% nanofiber mats after degradation study at week 0,12 and 24. Samples were selected out of three at each time point. All images were scaled to different magnifications, with the larger images in the main panels scaled at 50 µm and the smaller zoomed micrographs in the lower left corners scaled at 20 µm.
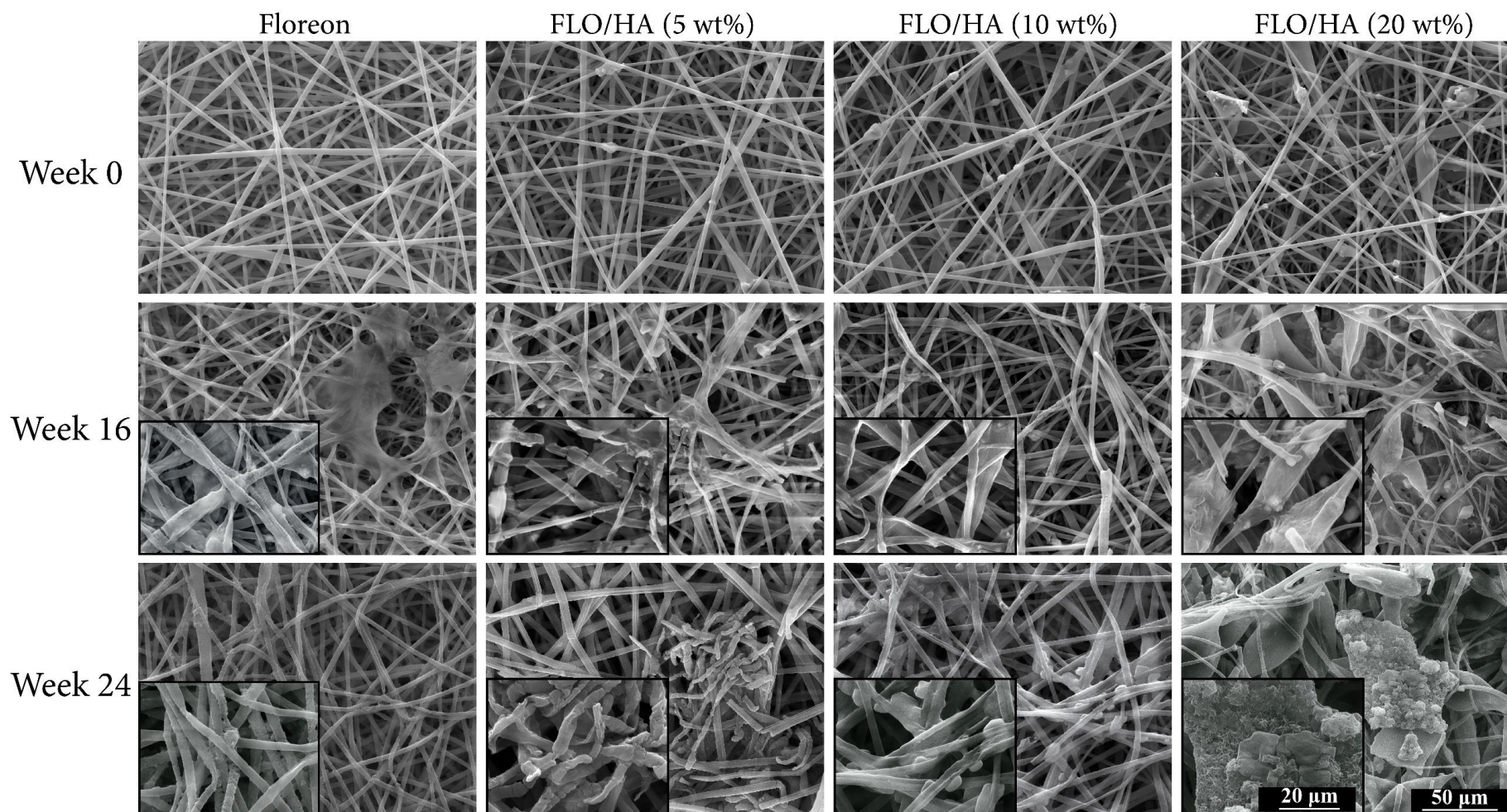
Figure 4-48 SEM images of Floreon, Flo/HA-5 wt%, Flo/HA-10 wt% and Flo/HA-20 wt% nanofiber mats after degradation study at week 0, 12 and 24. Samples were selected out of three at each time point. All images were scaled to different magnifications, with the larger images in the main panels scaled at 50 μm and the smaller zoomed micrographs in the lower left corners scaled at 20 μm.
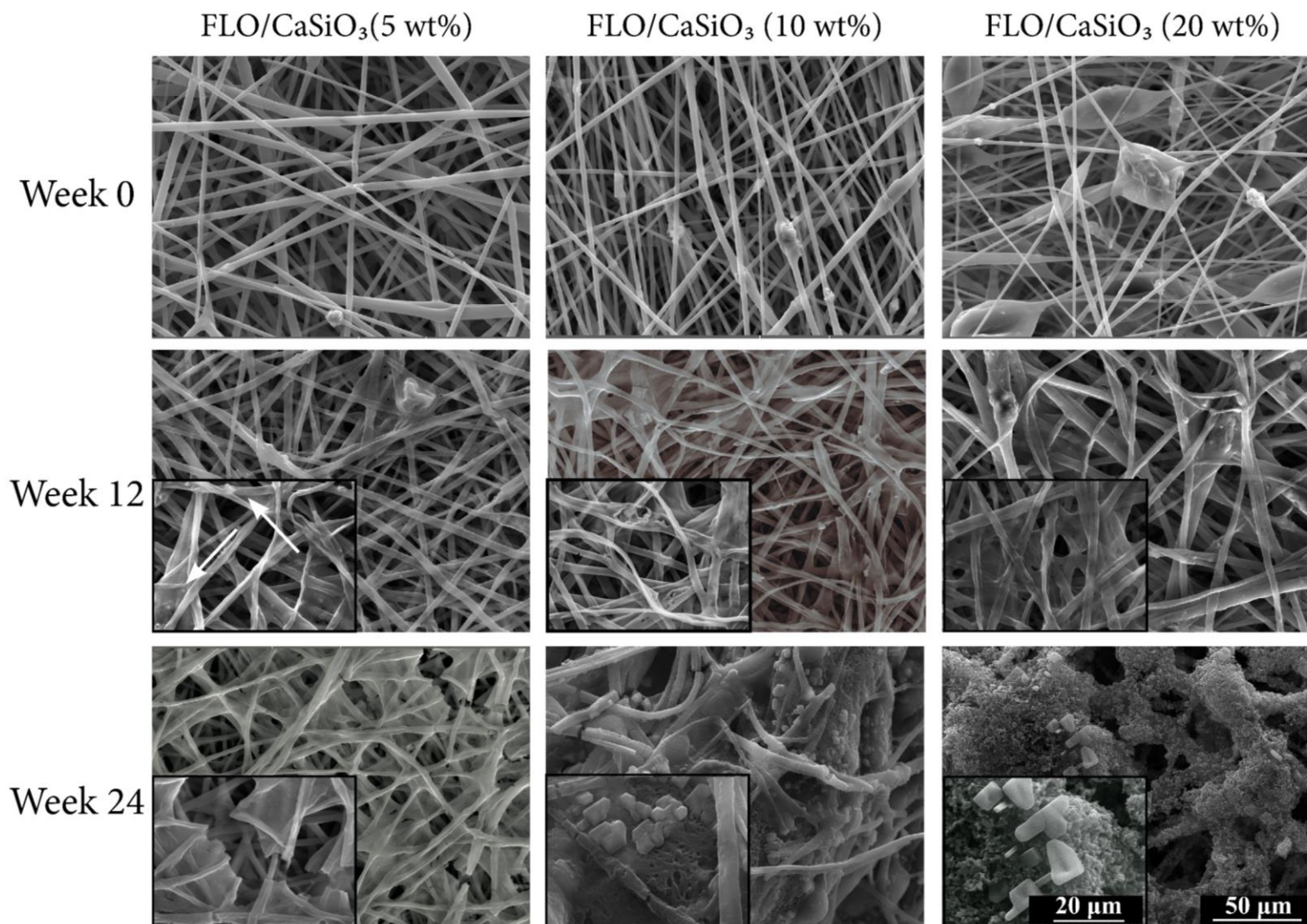
Figure 4-49 SEM images of Flo/CaSiO₃-5 wt%, Flo/CaSiO₃-10 wt% and Flo/CaSiO₃-20 wt% nanofiber mats after degradation study at week 0, 12 and 24. Samples were selected out of three at each time point. All images were scaled to different magnifications, with the larger images in the main panels scaled at 50 µm and the smaller zoomed micrographs in the lower left corners scaled at 20 µm.

SEM examination facilitated the acquisition of valuable qualitative morphological data pertaining to the appearance of the fibers under different treatment conditions. Here, an initial phase of degradation was shown following 16 weeks of immersion in SBF. Concerning the bioactivity of the microfibres, apatite precipitation was found on the ceramic-containing films, and its presence became more obvious as the immersion period increased. The surface of Floreon containing 5% bioceramic microfibres was not observed to be coated with apatite; however, the addition of 10% and 20% bioceramics caused apatite to precipitate visibly, with a higher rise after 24 weeks as the majority of the fibres were coated with a cauliflower-like apatites layer.

Normally, apatite does not develop rapidly on synthetic polymers until their surfaces are activated. This was also observed in the present study, as the untreated Floreon and PLA microfibres exhibited no apatite after the incubation period. (Kokubo, 1998; Chen, Chu and Hsiao, 2006). The addition of HA or $CaSiO_3$ caused the microfibres to precipitate apatite. Two mechanisms account for the ceramic particles' effect: (a) the nanoparticles' dissolution and the release of their calcium content, and (b) the presence of the nanoparticles on the surface acting as a nucleation site for apatite production and development (Kokubo, 1998). On the surface of ceramic based membranes, apatite layers were discovered and this boosted biocompatibility and provided a suitable substratum for cell attachment, adhesion, and dissemination (Madhumathi *et al.*, 2009).

Degradation is a process influenced by fluid-induced relaxation of oriented polymer backbone chains. Regarding Floreon/HA and Floreon/$CaSiO_3$ (5%, 10% and 20%), diameters of membrane fibres immersed in SBF at 24 weeks were smaller relative to 7 days and 15 weeks, suggesting that the thinner diameters at 24 weeks are compatible with an initial process of fibre's degradation. Swelled fibres were also observed at 15 days after immersion in SBF (Lee *et al.*, 2022), which could be induced by fluid absorption into the fibre structure. Another important event was the formation of cracks along the fibres immersed in SBF, probably due to the beginning of erosion induced by polymer degradation. In all cases diameter was reduced with immersion of day*s.*

In vitro bioactivity studies were performed to determine whether or not the CH membranes with incorporated ceramics were able to promote the formation of a carbonated apatite layer on the bottom surface (ceramic-enriched) of the membranes. These studies were based on the morphological and structural changes that occurred in the membranes. HA has

been found to stimulate the formation of a bone-like apatite layer at its surface when exposed to SBF (Fathi, Hanifi and Mortazavi, 2008). Regarding the microfibres' bioactivity, apatite precipitation was seen on the ceramic-containing films, and its presence was shown to be progressively more pronounced the longer the immersion period. The surface of Floreon with 5% bioceramic microfibres was coated with a biological apatite after 12 weeks, whereas the addition of 10% and 20% bioceramics caused apatite to precipitate visibly, with a greater increase after 24 weeks as most of the fibres were covered by an apatites layer. layer resembling a cauliflower.

Despite the fact that scaffolds incorporating ceramic particles were more bioactive than non-filled scaffolds, the amount of apatite synthesis was often lower than anticipated and the apatite layer did not cover the whole surface of the fibres, particularly at 5% and 10%, as previously reported (Rajzer *et al.*, 2014; Hassan and Sultana, 2017; Da Silva *et al.*, 2018). The number of ceramic particles utilised in this study is a possible contributor to the observed variation in apatite formation rate. Material dissolution and the release of calcium and phosphate ions from the implant's surface, followed by the precipitation of a biological apatite layer, are thought to be related to the bioactivity of calcium phosphate materials at different rates (Porter *et al.*, 2004).

- **pH analysis**

Figure 4-50 Figure 4-51 illustrate the change in pH levels of SBF containing electrospun Floreon and PLA films with varying concentrations of bioceramic (HA and $CaSiO_3$) throughout the degradation period. The degrees of significant differences in the pH measurements of SBF between samples are listed in Table 0-3 -Appendix.

The pH profile of Floreon and PLA membranes shows a similar trend over the degradation period. The initial pH of the SBF was 7.40. The pH value dropped from 7.40 to 7.10 ± 0.02SD by the end of the second week. Thereafter, slight stability is observed, and by the end of week 24, the pH of Floreon membranes was 6.01±0.13SD and that of PLA was 6.00±0.16SD. After gradually adding bioceramics, the rate of pH reduction decreased steadily with increasing concentration. Although no difference was found when 5% $CaSiO_3$ was added to blank Floreon, it was noticed when the same concentration of HA was added. The pH of films containing 10 % bioceramics decreased steadily during the immersion period until it reached

approximately 6.40 at week 24. The pH of the SBF solution containing Floreon with 20% bioceramics decreased gradually over the first 16 weeks with minimal variation. Flo/CaSiO$_3$ (20 %) had a pH of 6.57± 0.08SD, while Flo/HA (20 %) had a pH of 6.72± 0.09SD. At week 24, the pH profiles of Flo/CaSiO$_3$ (20 %) and Flo/HA (20 %) changed very slightly, with pH values of 6.54± 0.12SD and 6.65±0.11SD, respectively.
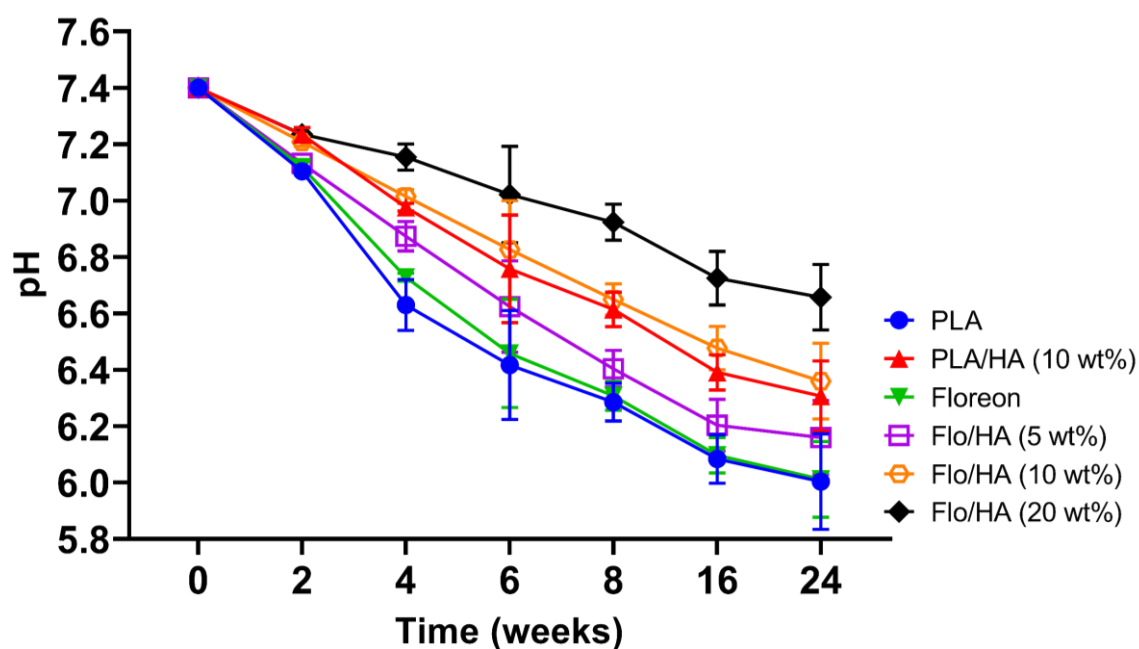
Figure 4-50 Change in pH of Floreon and Floreon-based HA nanofiber mats with different concentrations (5,10 and 20 wt%) during 24 weeks of immersion in SBF, compared to PLA and PLA/HA at 10 wt%.
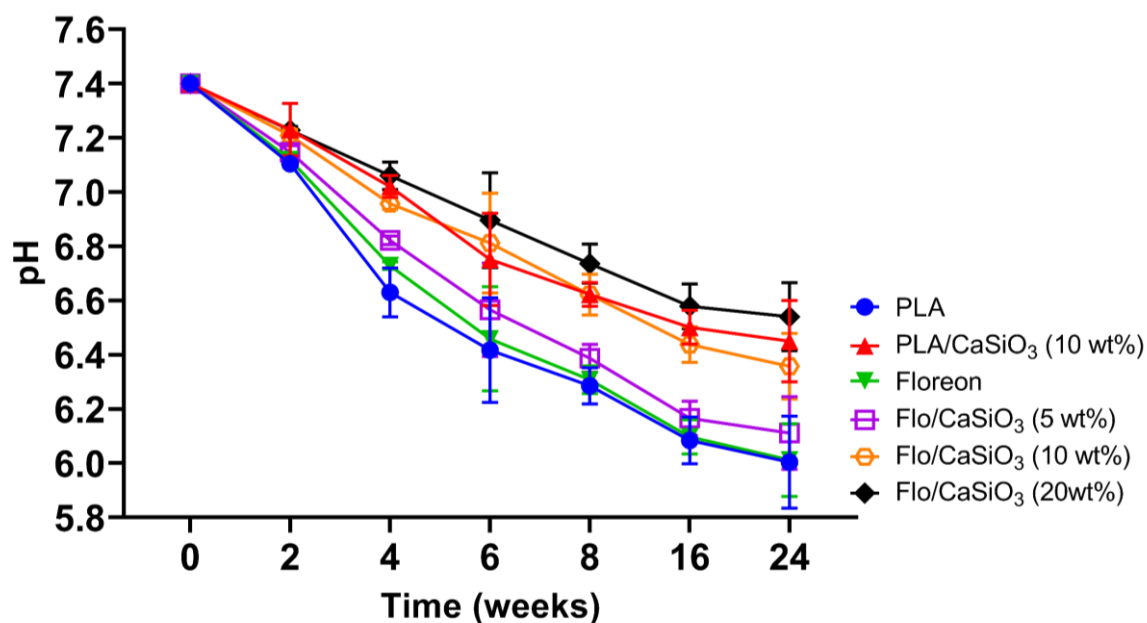
Figure 4-51 Change in pH of Floreon and Floreon-based CaSiO₃ nanofiber mats with different concentrations (5,10 and 20 wt%) during 24 weeks of immersion in SBF, compared to PLA and PLA/CaSiO₃ at 10 wt%.

In both PLA and Floreon groups final lowest pH was found in PLA and Highest pH was found in high treatment (20 wt%). Overall, it was found that pH of blank PLA was lower than that of blank Floreon. However, a similar dose (% wt) of HA and $CaSiO_3$ was more effective with a combination of Floreon as compared to PLA to reduce pH. There was a significant reduction in pH but it was faster between 8-16 weeks. Over the degrading period, the pH profiles of Floreon and PLA membranes show a similar pattern. The SBF's original pH was 7.40. By the conclusion of the second week, the pH had reduced from 7.40 to 7.10. Following on, there was some stability, and by the end of week 24, the pH of Floreon membranes was 6.01 and PLA was 6.00. The rate of pH decreased continuously with increasing concentration after progressively adding bioceramics. Although there was no difference when 5% $CaSiO_3$ was added to blank Floreon, it was noted when the same concentration of HA was applied. During the immersion period, the pH of films containing 10% bio ceramics fell progressively until it reached roughly 6.40 at week 24. The pH of the Floreon-containing SBF solution with 20% bio ceramics progressively fell throughout the first 16 weeks with negligible change. The pH of Floreon/CaSiO₃ (20%) was 6.57, while the pH of Floreon/HA (20%) was 6.72. The pH profiles of Floreon/CaSiO₃ (20%) and Floreon/HA (20%) altered very significantly at week 24, with pH values of 6.54 and 6.65, respectively. Similar study was conducted by Sanchez and colleagues on the pH of CH and HA composites over 21 days indicated that the pH values

decreased with increased CH. They also stated that this was due to the complex formation between CH and HA, which caused the solubility to be dependent on the buffering conditions. They also assessed the amount of Ca ions released in PBS medium at pH 7.4 to identify the type of biodegradation of composites. They discovered an increase in Ca ion release from composite membranes as compared to virgin HA media, which they attributed to the less stable nature of CH macromolecules causing Ca release from composite structures (Sanchez *et al.*, 2021).

Furthermore, the presence of OH− enhances the rate of degradation for PLA, triggering the nucleophilic attack at electron deficient carbonyl carbons. This is different from acid catalysed reactions, where H+ reacts with water to form a hydronium ion, which is then attracted to negative carbonyl oxygens. The carbonyl carbon becomes electrophilic attracting water so as to initiate hydrolysis. However, due to the limited charge concentration to make carbonyls, the use of the simulation enabled a carbon negative alkali attack to be observed that are viable for hydrolytic degradation in alkali rather than acidic conditions (Jem and Tan, 2020; Vaid *et al.*, 2021).

It is well established that pH plays a crucial role in the process of wound healing. According to the findings of comprehensive research on the relationship between pH and the process of wound healing that was carried out by Schneider et al., (2007) proper healing of a chronic wound needs an environment that is acidic (Schneider *et al.*, 2007). The pH values were observed to drop with increasing CH, according to the findings of research carried out by Murugan and Ramakrishna (2004) on assessing the pH of CH and HA composites over a period of 1000 hours (Murugan and Ramakrishna, 2004). They also noted that this was because the solubility was dependent on the buffering conditions because of the complex formation that occurred between CH and HA. This was due to the fact that CH and HA formed together. In addition to this, they found out the characteristics of the biodegradability of the composites by measuring the quantity of calcium ions that were released into the PBS medium at a pH of 7.4. They observed a greater release of Ca ions from composite membranes in comparison to virgin HA medium, which they attributed to the less stable nature of CH macromolecules, which triggered the release of Ca from composite structures. This was found to be the case when they compared the two types of media (Murugan and Ramakrishna, 2004). The researchers did not disclose in their study whether or not the degradation solution was replaced every two to three days to imitate physiological circumstances. Zhang et al., (2010) reported the pH changes of virgin CH during the course of 16 weeks of degradation in PBS (Zhang *et al.*, 2010). They

found that the pH value ranged anywhere from 7.4 to 7.8 during this time. It is possible that the breakdown products of CH, including amino sugars, are to blame for this (Zhang and Cui, 2012). In the current investigation, the addition of lysozyme resulted in a more alkaline pH of around 8 by the time the incubation period was completed.

In a previous study (Cortes *et al.*, 2005), it was found that the pH of SBF increased over time when bioactive glass and $CaSiO_3$ were in contact with the metal substrate. During the initial five days of immersion, the pH of SBF decreased moderately, possibly due to the partial breakdown of HA when immersed in SBF, leading to a drop in pH. After seven days in SBF, peaks corresponding to the alloying elements and peaks of lower intensity attributed to HA were observed in samples treated with wollastonite. Conversely, in samples treated with bioactive glass or HA, no peaks related to HA were detected after seven days of immersion. In the current investigation yielded similar outcomes, with the pH of the membranes increasing from 7.1 to 7.4 after being incubated in SBF with Floreon (20% wt) for a period of 24 weeks. These results suggest that the presence of bioceramics in the membranes may have influenced the pH levels in the SBF solution.

4.1.13   *In vitro* Biocompatibility

The following are the findings of a different *in vitro* characterisation of PLA and Floreon fibrous scaffolds containing varying concentrations of HA or $CaSiO_3$ particles.

4.1.13.1 Cell Migration

As the initial step of the *in vitro* examination, the migration of rat mesenchymal stem cells was studied. This was performed in the presence of the fibrous membranes. A thin "wound" is formed by scratching confluent cells with the tip of a pipette. Cells near the wound's edge polarise and migrate inside the wound. It is important to highlight this assay was performed indirectly, the scaffold was present in the well, but the cells were not seeded on it, the scratching was done on cells grown on tissue culture plastic. To measure the wound size accurately, the Image J software was used. The initial wound area was determined to be 1165.5 mm^2 at the 0-hour point. To ensure accuracy, the data were normalised using Prism software, with three samples per each type of scaffold used, and each sample measured three times.

The most reliable way of analysis is time-lapse imaging to visualise the extent of their growth and the effect of the membrane on wound closure. Figure 4-52 to Figure 4-54 show the micrographs taken after 12, 24 and 36 hours of the MSCs migration. The results of a cell migration assay are shown graphically in Figure 4-55 and Figure 4-56.

As with the control group, the results indicate that the percentage of wound closure in the presence of various membranes increases over time. Compared to membranes made of plain PLA or Floreon, membranes incorporating ceramic particles promote the migration of mesenchymal cells. These graphs also reveal an important relationship between the concentration of calcium silicate or hydroxyapatite in fibrous scaffolds and the rate at which wounds are healed: the higher the concentration, the faster the wounds are closed.
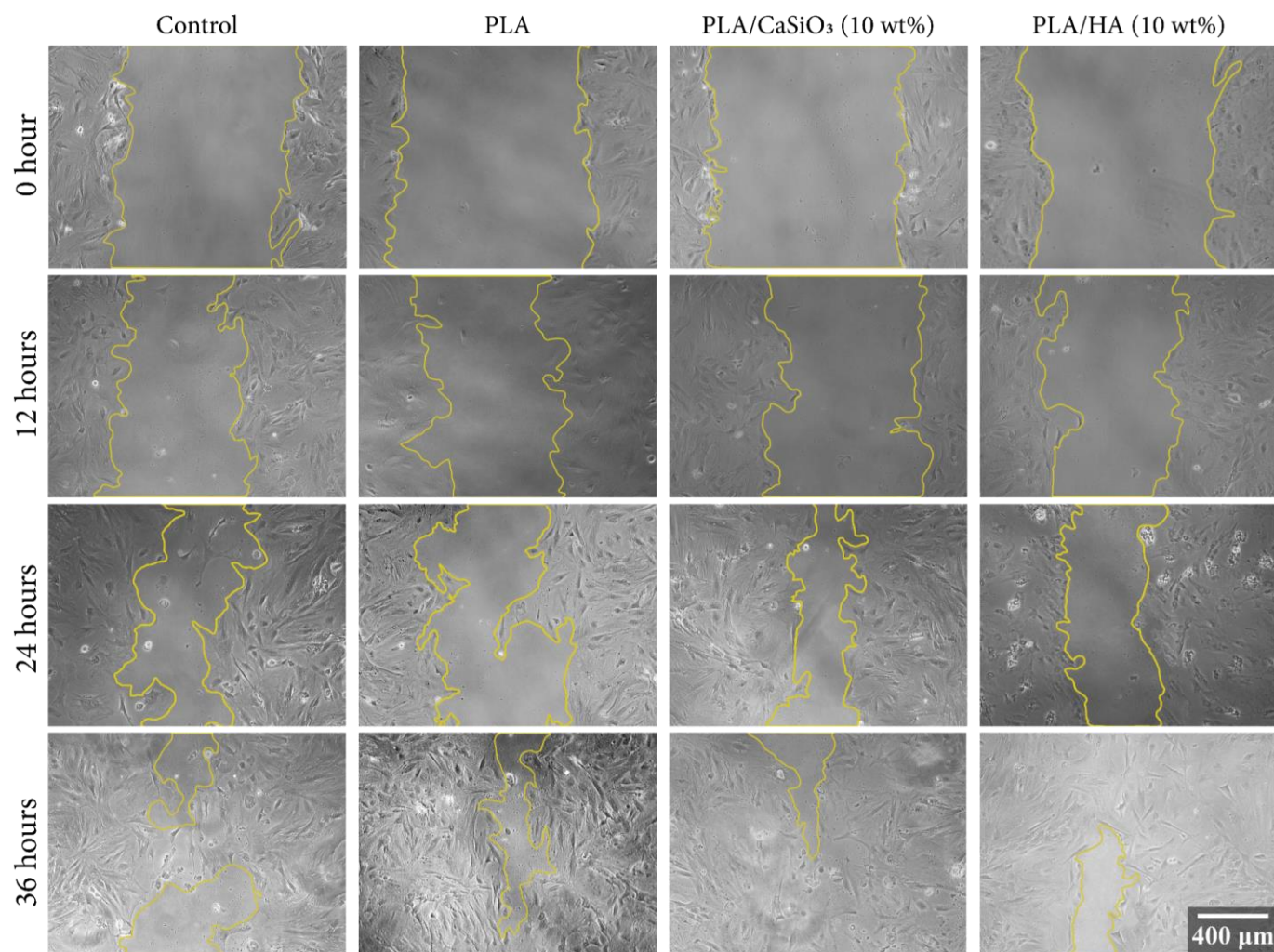
Figure 4-52 Microscope analysis revealing wound closure of rat MSCs (rMSCs) incubated in the presence of electrospun PLA membranes containing 10 wt% of HA and CaSiO₃ at different time points. All images were scaled at 400μm.
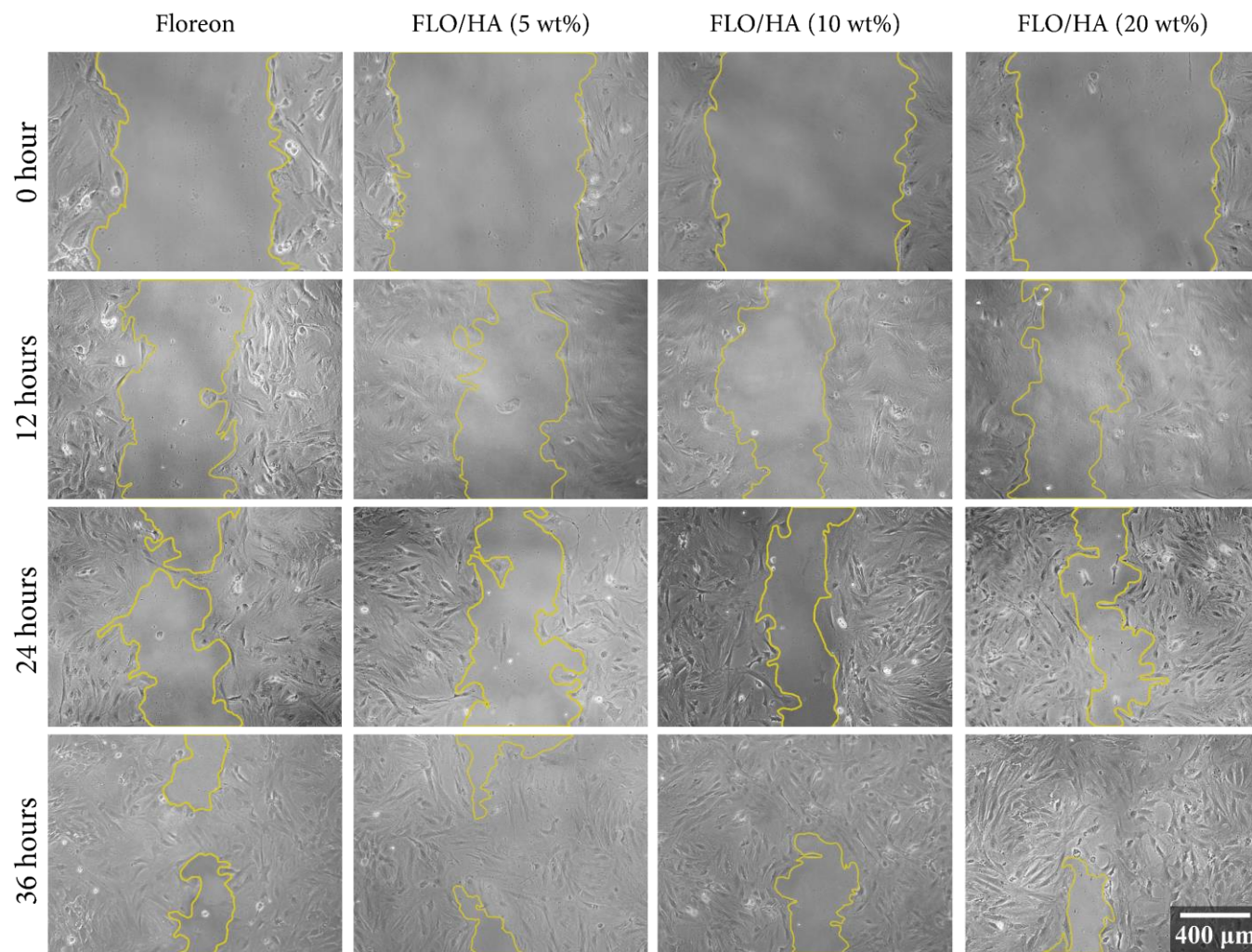
Figure 4-53 Microscope analysis revealing wound closure of rat MSCs (rMSCs) incubated in the presence of electrospun Floreon membranes containing different concentrations (5,10 and 20 wt%) of HA at different time points. All images were scaled at 400μm.
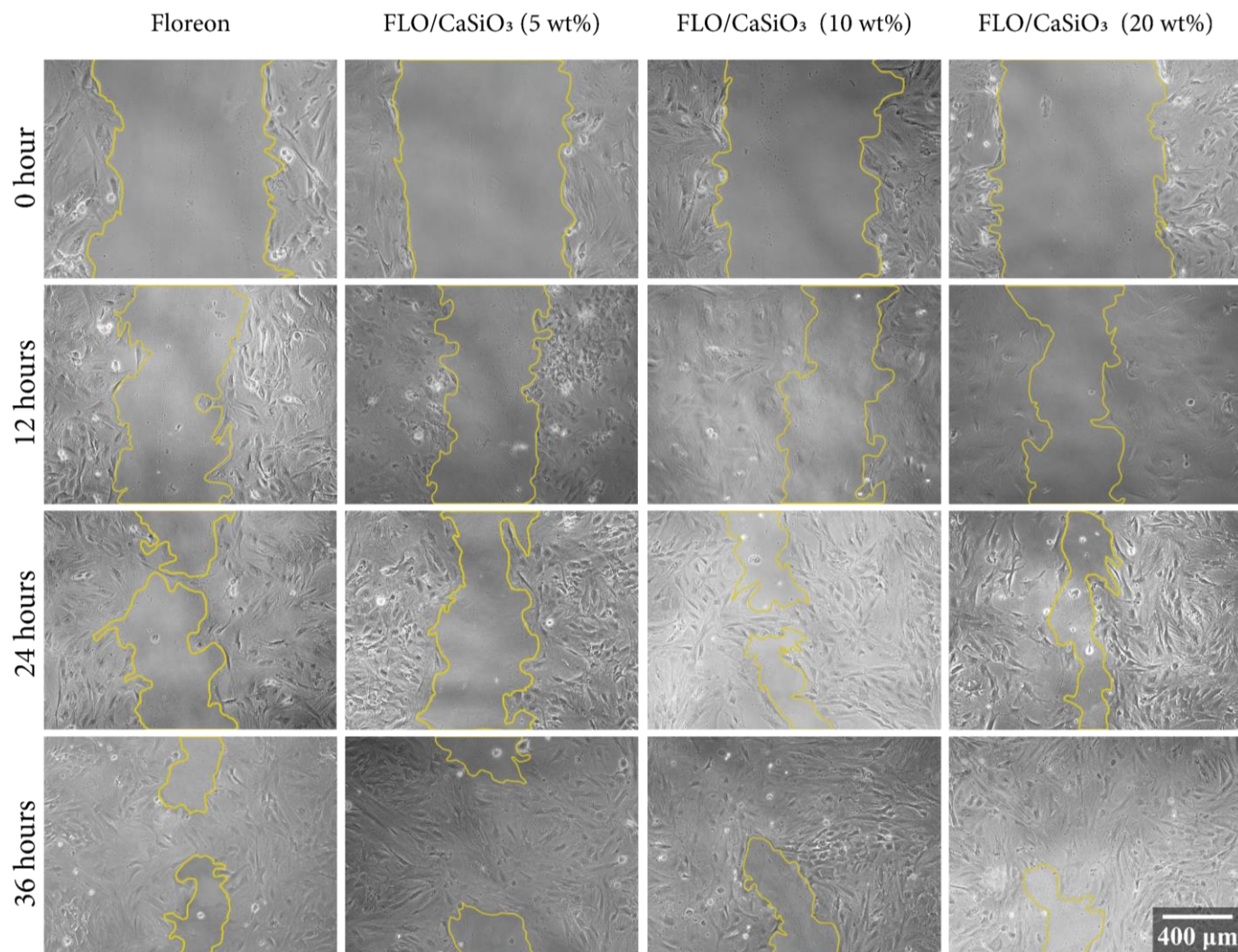
Figure 4-54 Microscope analysis revealing wound closure of rat MSCs (rMSCs) incubated in the presence of electrospun Floreon membranes containing different concentrations (5,10 and 20 wt%) of CaSiO₃ at different time points. All images were scaled at 400μm.
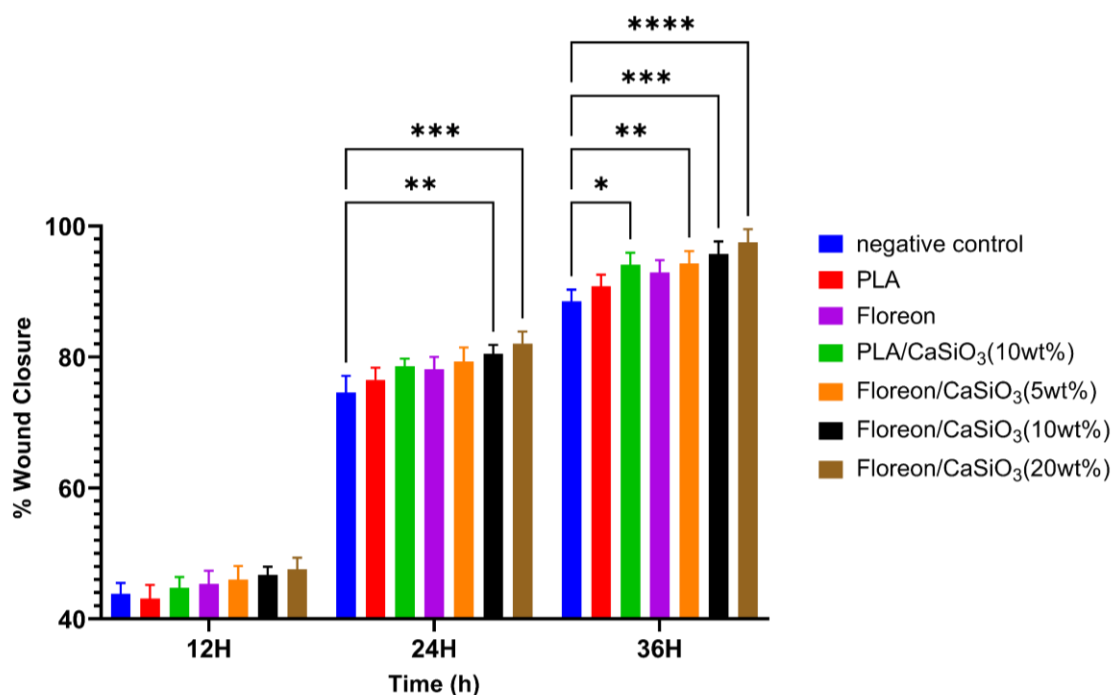
Figure 4-55 Ratios of wound closure in rat MSCs (rMSCs) incubated with the presence of PLA and Floreon fibrous membranes containing different concentrations of $CaSiO_3$. Data represented n=3, mean $\pm$ STDV following Two-way ANOVA statistical analysis with Tukey comparison test. **** $p < 0.0001$, *** $p < 0.001$, ** $p < 0.01$, * $p < 0.05$.
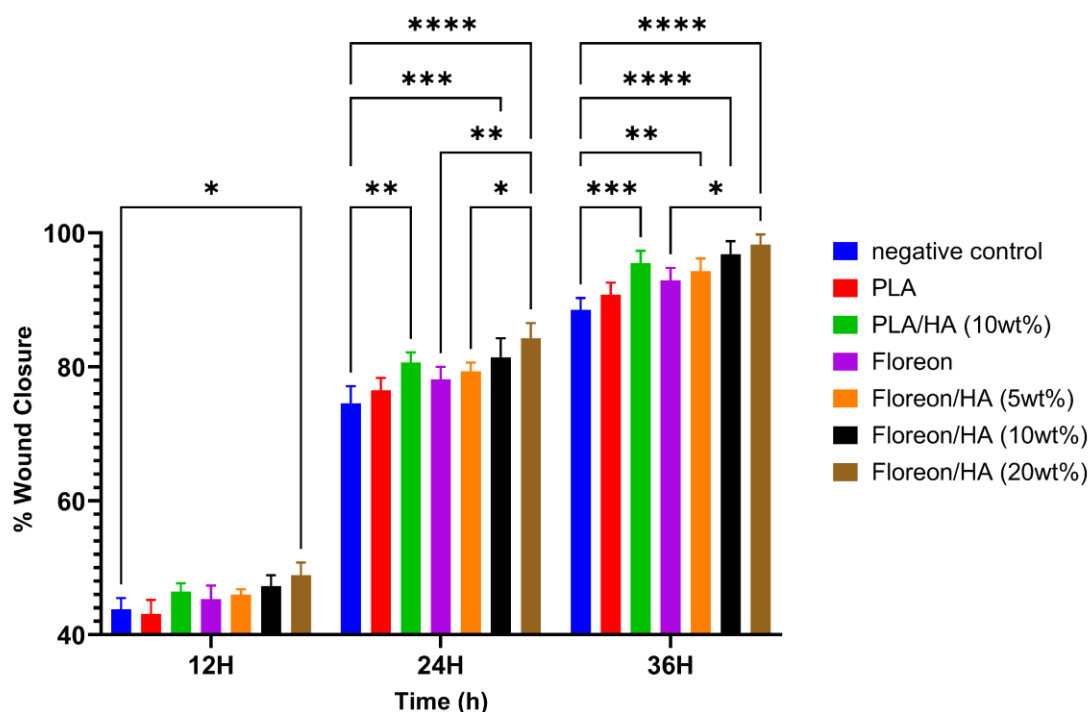
Figure 4-56 Ratios of wound closure in rat MSCs (rMSCs) incubated with the presence of PLA and Floreon fibrous membranes containing different concentrations of HA. Data represented n=3, mean $\pm$ STDV following Two-way ANOVA statistical analysis with Tukey comparison test. **** $p < 0.0001$, *** $p < 0.001$, ** $p < 0.01$, * $p < 0.05$.

The initial stage of the in vitro investigation involved studying the migration of rat Mesenchymal Stem Cells (rMSCs). These cells were selected as they constitute a primary cell type that has been previously optimised for bone regeneration studies, as demonstrated by Ramos-Rodriguez *et al.*, (2022). rMSCs were cultured as a 2D monolayer on an untreated surface as the control, and the cells were able to successfully cover the wound area. Compared to the control, cells cultured on both untreated PLA and Floreon scaffolds showed a greater percentage of wound closure. Furthermore, the addition of both HA or $CaSiO_3$ promoted wound closure which was statistically significant compared to the control. These graphs also reveal an important relationship between the concentration of calcium silicate or hydroxyapatite in fibrous scaffolds and the rate at which wounds are healed: the higher the concentration, the faster the wounds are closed.

When evaluating the wound size of electrospun PLA membranes containing HA or $CaSiO_3$ and comparing them to pure electrospun PLA membranes and the control group, it was observed that both electrospun PLA membranes containing bioceramics exhibited the smallest wound size and significantly improved scratch healing relative to the untreated electrospun PLA membrane and control groups. This is evidenced in Figure 4-52, where the wound size area was found to be the lowest in the groups containing electrospun PLA membranes with HA or $CaSiO_3$ after 36 hours, indicating a higher rate of cell migration compared to the electrospun PLA membrane and control group. Figure 4-53 demonstrates the wound closure due to cell migration in electrospun Floreon membranes containing different concentrations (5,10 and 20 wt%) of HA at different time points.

When examining the impact of incorporating different concentrations (5, 10, and 20 wt%) of HA in electrospun Floreon membranes, it is evident that the wound size is smaller in membranes containing HA after 36 hours, indicating a higher cell migration rate compared to simple electrospun Floreon membranes. Moreover, a positive correlation was observed between the concentration of HA in the electrospun Floreon membrane and the rate of wound closure, highlighting the crucial role of HA in promoting cell migration. This is illustrated in Figure 4-53, which depicts the wound closure in electrospun Floreon membranes containing various concentrations of $CaSiO_3$ at different time intervals, as well as in simple electrospun Floreon membranes. It is evident that the electrospun Floreon membranes containing different concentrations of $CaSiO_3$ exhibited smaller wound sizes and significantly improved scratch healing compared to the simple electrospun Floreon membrane. It was clear from Figure 4-54 that the area of wound size is lower in the Floreon membranes containing $CaSiO_3$ after 36 hrs,

which shows higher cell migration rate in these groups as compared to simple electrospun Floreon membrane. It was also shown that higher the concentration of $CaSiO_3$ in the electrospun Floreon membrane, the higher is the wound closure due to higher cell migration rate. The area of wound was measured from microscopic images by using ImageJ software and then compared and graphs are formed to easily compare and evaluate the percentage of wound closure as was shown in Figure 4-55 and Figure 4-56.

These results are in line with previous findings that Floreon films with ceramic content had a minimal change in pH compared to those without ceramics. which maintaining a neutral pH, as discovered during the bioactivity study when the Floreon and PLA films were immersed in SBF during the study period. Mackenzie et al., (1961) reported that the optimal pH range for mammalian cell growth was 7.38 to 7.87 (Mackenzie, Mackenzie and Beck, 1961). On the alkaline side of the optimal pH range, cell growth fell precipitously, whereas it declined gradually on the acidic side. In another study that investigated the growth and mineralisation of human BMSCs in a pH range of 6.3-8.5, the researchers found that the optimal activity level of BMSCs occurred at a pH of 8.0 (Fliefel *et al.*, 2016).

This study further evaluated its effect by combining PLA and Floreon membrane with different concentrations of HA and $CaSiO_3$ bioceramics and found that these bioceramics containing membranes showed better wound healing as compared to simple membranes. These results are also supported by various studies. A study reported that HA Influence the proliferation, wound healing, migration of cells. The influence of HA on cells migration to recover the wound was checked. It was found that group of cells treated with HA covers large area of wound as compared to the untreated cells during the same time (Ghose *et al.*, 2018). In the same study, cell migration was also evaluated, and it was found that the number of migrated cells in the HA treated group was higher than the untreated control group (Ghose *et al.*, 2018). As compared with HA, wollastonite shows higher bioactivity, and osteoinductivity (Li and Chang, 2013). Moreover, Ca and Si ions released by wollastonite have a synergistic effect on the cell growth and migration (Mao *et al.*, 2017). Therefore, it can be concluded that the addition of wollastonite or HA into PLA or Floreon membrane stimulates the cell migration and growth and the PLA + $CaSiO_3$ or PLA + HA as well as Floreon + $CaSiO_3$ or Floreon + HA composites are biocompatible.

4.1.13.2 Cell proliferation: Presto Blue assay

A PrestoBlue is a resazurin-based metabolic assay that was used to evaluate the proliferation rates and viability of MSCs after 7, 14, 21, and 27 days of incubation in different fibrous membrane mediums. Figure 4-57 and Figure 4-58 show the cellular metabolic activity measured by Presto Blue assay on PLA and Floreon fibrous scaffolds with various concentrations of HA or $CaSiO_3$ particles.

There was no significant difference in cellular metabolic activity between scaffolds made of plain PLA and Floreon. However it is clear that incubation with bioceramic particles has an effect on the cells' metabolic activity. The PrestoBlue assay reported a higher cellular metabolic activity in membranes containing 10 and 20 wt% $CaSiO_3$ particles (Figure 4-57), similar to the behaviour seen in membranes containing HA (Figure 4-58). Therefore, the proposed Floreon-based blend showed promising properties as a potential membrane *in vitro* culture system without negatively affecting cellular response during 21 days of incubation.
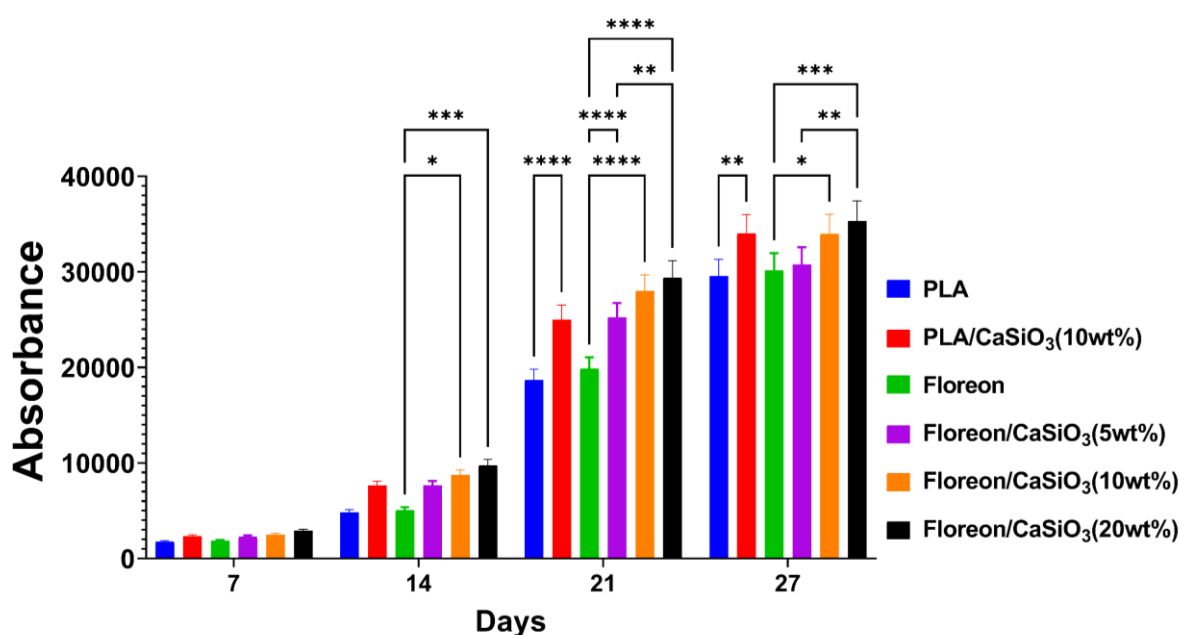
Figure 4-57 The PrestoBlue ® assay performed for viability of rat MSCs (rMSCs) seeded over PLA and Floreon fibrous membranes containing different concentrations of $CaSiO_3$. Data represented n=3, mean ± STDV following Two-way ANOVA statistical analysis with Tukey comparison test. **** $p < 0.0001$, *** $p < 0.001$, ** $p < 0.01$, * $p < 0.05$.
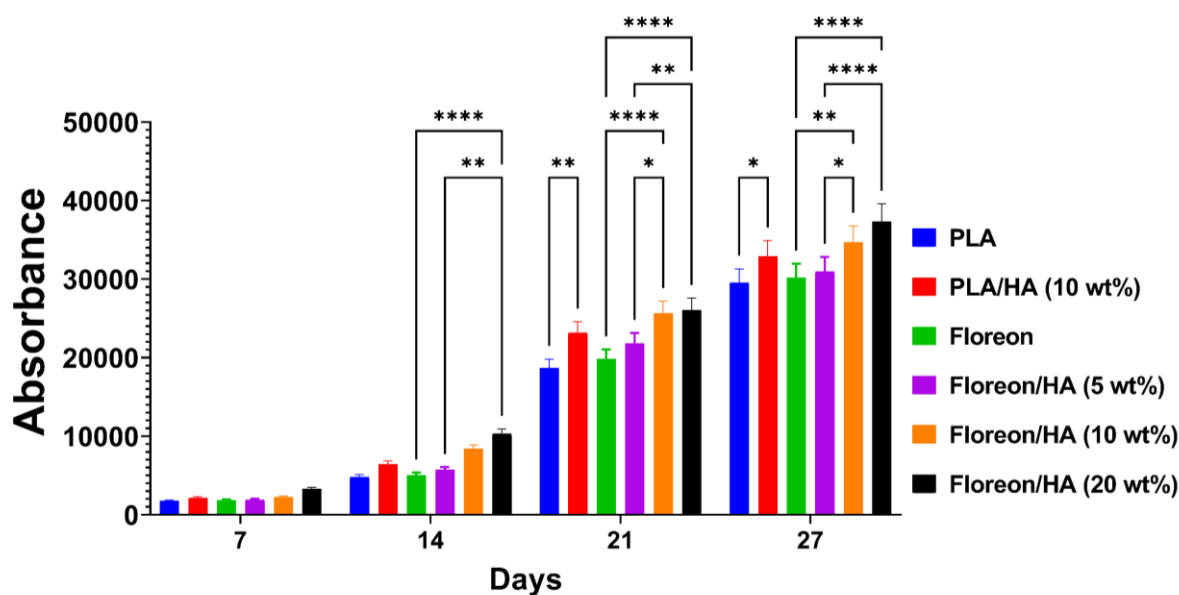
Figure 4-58 The PrestoBlue ® assay performed for viability of rat MSCs (rMSCs) seeded over PLA and Floreon fibrous membranes containing different concentrations of HA. Data represented n=3, mean $\pm$ STDV following Two-way ANOVA statistical analysis with Tukey comparison test. **** $p < 0.0001$, *** $p < 0.001$, ** $p < 0.01$, * $p < 0.05$.

The PrestoBlue assay reported a higher cellular metabolic activity in membranes containing 10 and 20 wt% $CaSiO_3$ particles (Figure 4-57), similar to the behaviour seen in membranes containing HA (Figure 4-58). Therefore, the proposed Floreon-based blend showed promising properties as a potential membrane culture system *in vitro* without negatively affecting cellular response during 21 days of incubation.

Although the data regarding increased cell proliferation is visually clear and statistically significant, this does affect the interpretation of the wound closure assay because the closure that was witnessed could be the result of cells growing faster to occupy the empty space as opposed to actual cell migration. It is important to determine whether the rMSCs can migrate further distances on the membrane surface because the proliferation data suggests that the cells may grow faster and eventually cover the membrane area as opposed to cells migrating during bone formation. Figure 4-57 demonstrates the cell proliferation on PLA membrane, Floreon membrane, and PLA as well as Floreon membranes containing different concentrations of $CaSiO_3$ at different days. It is evident that Floreon and PLA membranes containing $CaSiO_3$ shows higher cell proliferation at different days as compared to other groups. It was also evident that the higher the concentration of $CaSiO_3$ in the electrospun membrane, the higher the cell proliferation. Figure 4-58 depicts the cell proliferation rate in PLA membrane, Floreon

membrane, and PLA and Floreon membranes with varying concentrations of HA over a period of several days. From these results, it is clear that PLA and Floreon membrane containing HA show higher cell proliferation at different days as compared to other groups. It is also evaluated that the higher the concentration of HA in the electrospun PLA and Floreon membrane, the higher the rate of cell proliferation.

These results of Presto Blue assay supported the results of wound healing assay. A study reported that PLA + HA membranes showed higher proliferation and cell adhesion as compared to the PLA as well as PLA + BG scaffolds (Alksne *et al.*, 2020). In another study, cell migration and proliferation were assessed by culturing osteoblasts on the PHBV membrane, PHBV membrane with 10% $CaSiO_3$ and PHBV membrane with 20% $CaSiO_3$. It was reported that the osteoblasts cultured on PHBV membrane with 20% $CaSiO_3$ showed more proliferation and differentiation rate than those on the pure PHBV substrates and the Si and Ca containing ionic products of wollastonite in the composites might be the reason for this stimulatory effect (Li, Zhai and Chang, 2008).

4.1.13.3 live dead assay

The live-dead test is a commonly used method for labelling cells. Calcein-AM stains living cells with a green fluorescence, whereas EthD-1 stains dead cells with a red fluorescence.

Figure 4-59 to Figure 4-63 illustrate that cell death was notably low in the LIVE/DEAD experiment. On day 3, the cells were firmly attached to the fibrous scaffolds. The number of dead cells was lower on bioceramic particle-containing scaffolds compared to those on untreated polymeric films.

The LIVE/DEAD experiment on days 7 and 14 demonstrated that the cells had branched and linked networks in addition to exhibiting good morphology, indicating an enhanced proliferation rate. In addition, it was clear that raising the concentration of HA or $CaSiO_3$ from 5 to 10 and then to 20 wt% improved cell viability, adhesion, and proliferation of MSCs on the surface of their membranes, as compared to plain PLA or Floreon films.
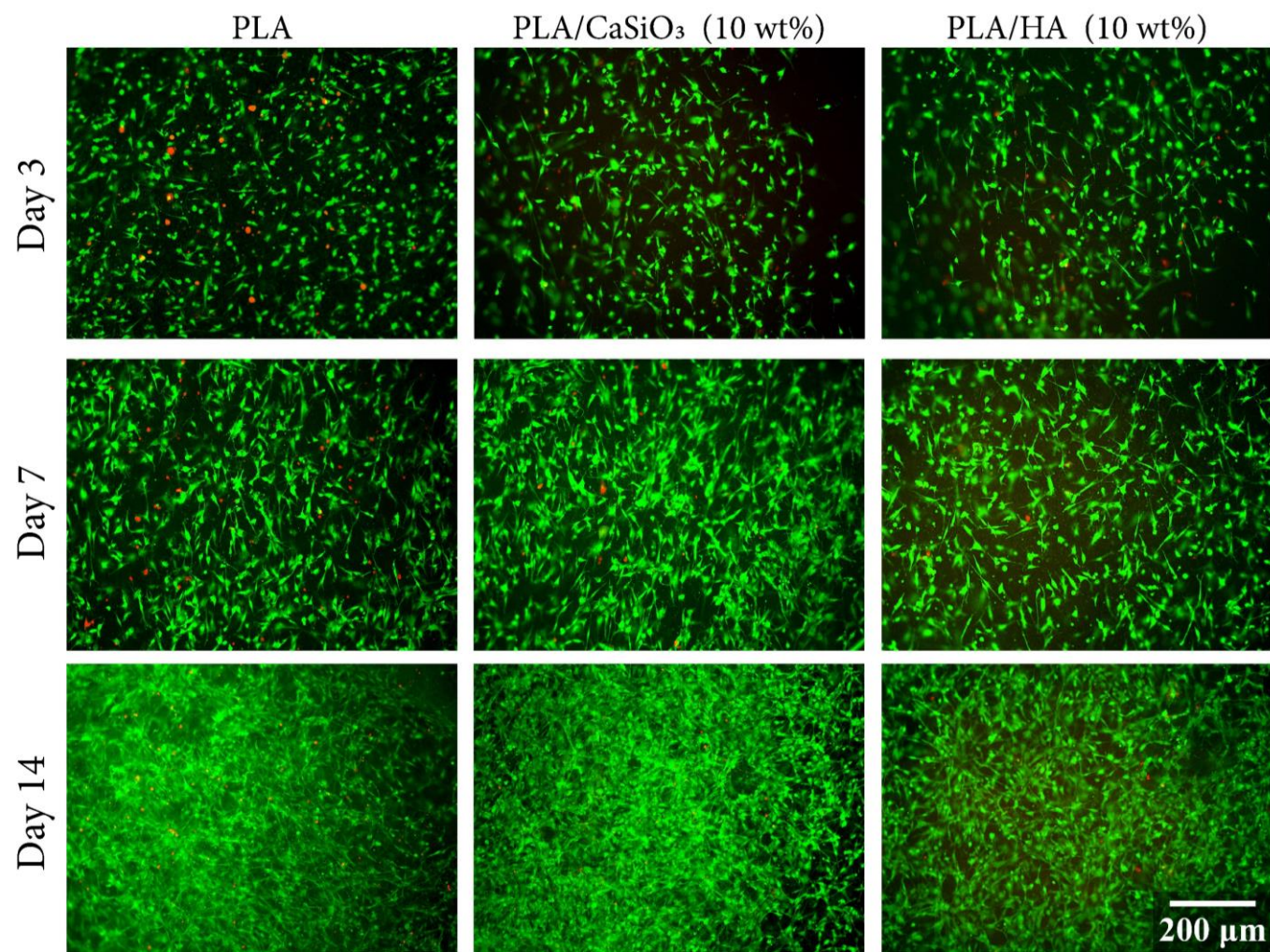
Figure 4-59 Fluorescence images of rat MSCs(rMSCs) viability seeded over electrospun PLA fibrous membranes containing 10 wt% of HA and CaSiO₃, after 3, 7, and 14 days of culture. All images were scaled at 200 µm.
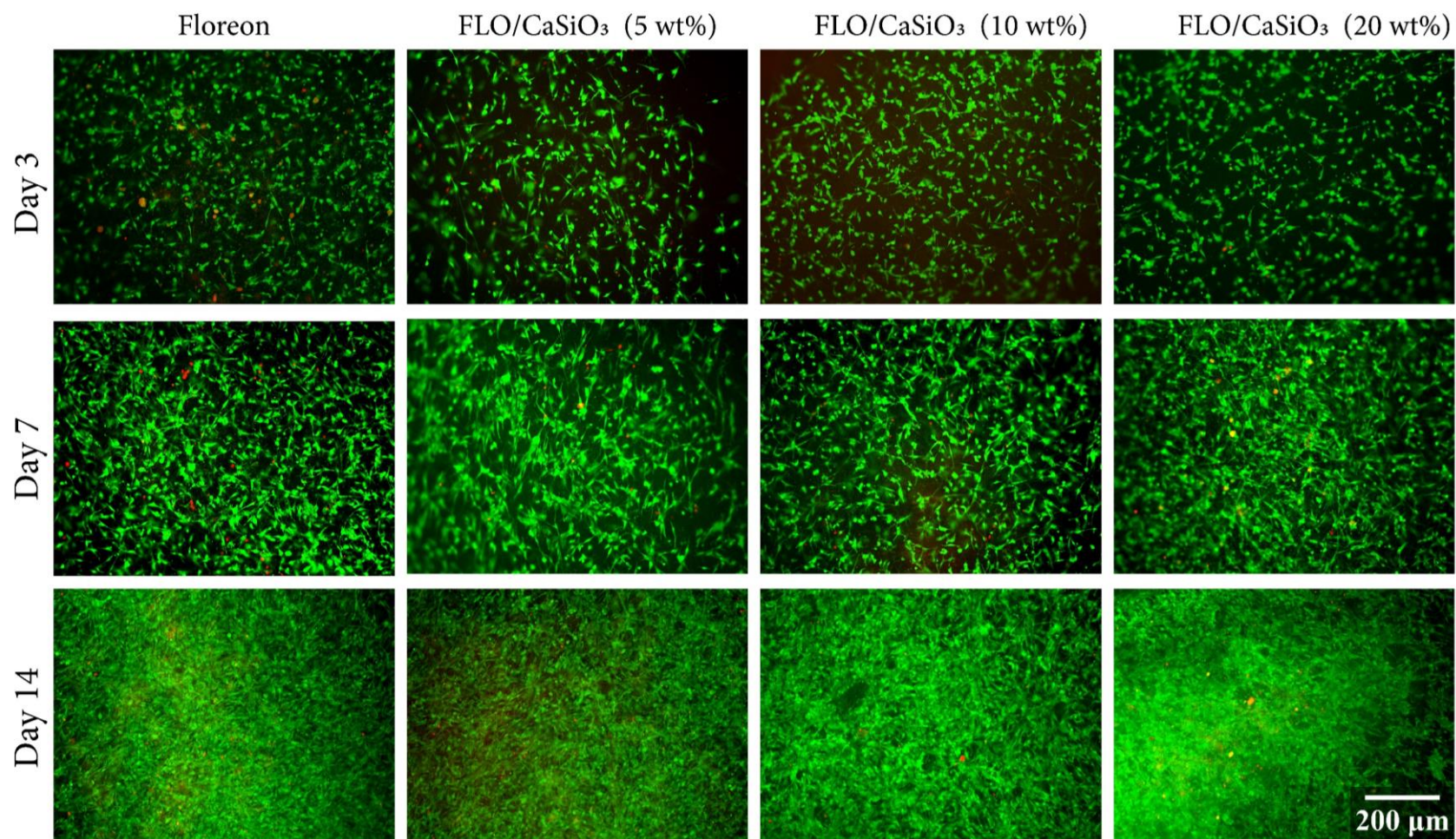
Figure 4-60 Fluorescence images of rat MSCs(rMSCs) viability seeded over electrospun Floreon membranes containing different concentrations (5,10 and 20 wt%) of CaSiO$_3$, after 3, 7, and 14 days of culture. All images were scaled at 200 µm.

Figure 4-61 Fluorescence images of rat MSCs(rMSCs) viability seeded over electrospun Floreon membranes containing different concentrations (5,10 and 20 wt%) of HA, after 3, 7 and 14 days of culture. All images were scaled at 200 μm.
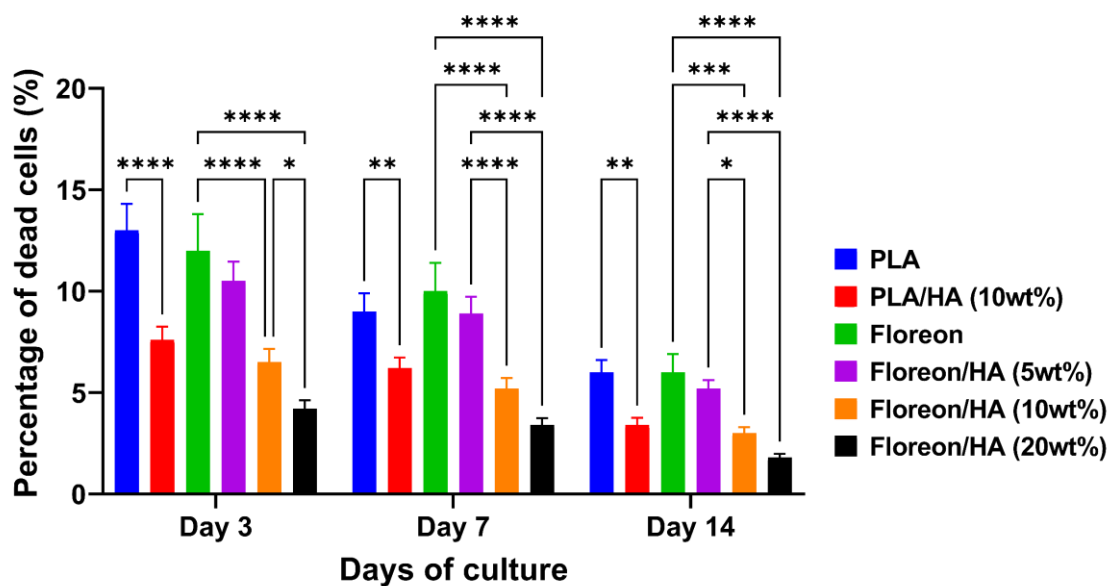
Figure 4-62 Quantitative analysis of the percent of dead cells within each cellular scaffold on days 3, 7, and 14. The data is presented as mean-standard deviation (n = 3). Following two-way ANOVA statistical analysis with the Tukey comparison test, there was a significant difference between PLA and Floreon fibrous membranes containing different concentrations of HA within the same culture condition and time point (*$p < 0.05$; **$p < 0.01$; ***p 0.001 and ****p 0.0001).
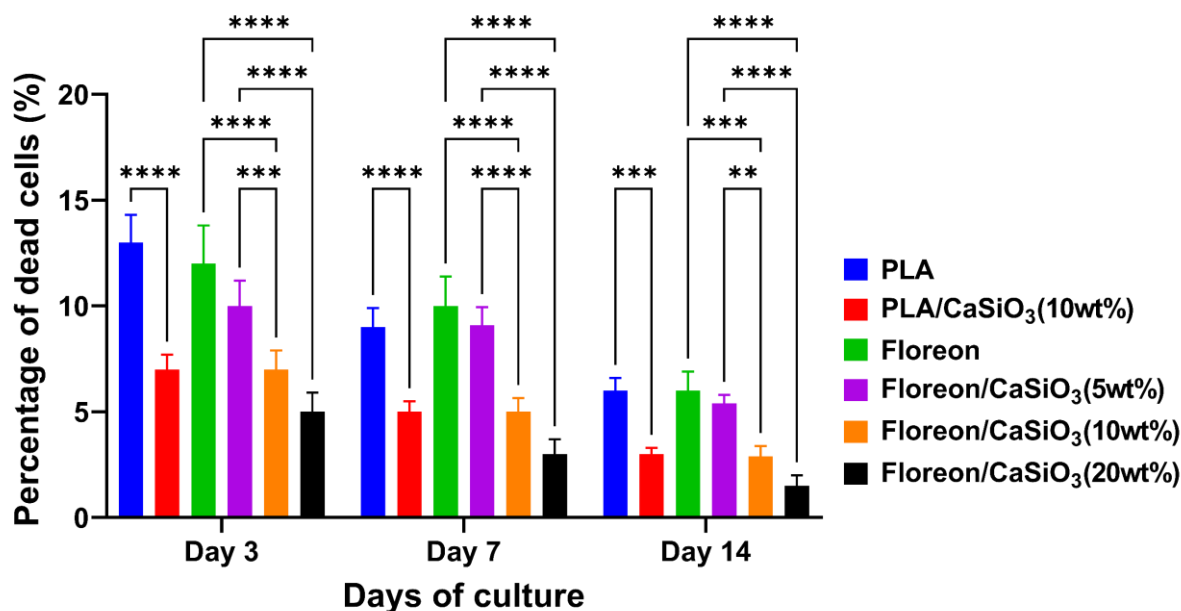
Figure 4-63 Quantitative analysis of the percent of dead cells within each cellular scaffold on days 3, 7, and 14. The data is presented as mean-standard deviation (n = 3). Following two-way ANOVA statistical analysis with the Tukey comparison test, there was a significant difference between PLA and Floreon fibrous membranes containing different concentrations of $CaSiO_3$ within the same culture condition and time point (*$p < 0.05$; **$p < 0.01$; ***p 0.001 and ****p 0.0001).

214

The number of dead cells was lower on bioceramic particle-containing scaffolds compared to those on untreated polymeric films. In addition, it was clear that raising the concentration of HA or $CaSiO_3$ from 5 to 10 and then to 20 wt% in both types of bioceramics improved cell viability, adhesion, and proliferation of rMSCs on the surface of their membranes, as compared to plain PLA or Floreon films. This was a particularly important finding that rMSCs have a preferred surface to adhere to and this also corresponds to increased proliferation. It is also important to note that at the later time points with higher cell confluency, there were few dead cells present suggesting that rMSCs do prefer growth on the Floreon membranes containing bioceramics.

The observation that there were fewer dead rMSCs could be because stem cells are more resistant to cell death compared with differentiated cells and perhaps the scaffolds promote a more stem-like profile of the rMSCs (Baykan et al., 2015). The findings are in line with a study which shows high cell viability of BMSC on the PLA/HA composite scaffolds. In this study, a LIVE/DEAD assay was performed to show cell viability after 1-, 3-, 5- and 7-days culturing on PLA/HA scaffold. High live-cell density of BMSCs cultured on PLA/HA composite scaffold was reported (Tu et al., 2020). In another study, LIVE/DEAD assay was performed to evaluate cell viability after culturing on PCL/HA scaffold and it was found that less number of dead cells was present in the group cultured on PCL/HA composite scaffold as compared to simple PCL scaffolds (Zhang et al., 2014). It was also reported that the osteoblasts cultured on PHBV membrane with 20% $CaSiO_3$ showed more proliferation than those on the pure PHBV substrates due to Si and Ca containing ionic products of wollastonite (Li, Zhai and Chang, 2008).

4.1.13.4 Total protein content

This experiment was conducted to determine the total protein content of the cells in various scaffolds. The results were achieved using the bicinchoninic acid (BCA) assay. It is a colorimetric assay using BCA reagent. After adding the reagent to the lysed cell solution, the sample is incubated at a specific temperature and for a specific time in order not to ruin the sample. The absorption rate of the sample was measured using a spectrophotometer and then the protein content was calculated, keeping in view calibration standards.

Figure 4-64 and Figure 4-65 depict the results as protein concentration versus culture duration. All PLA and Floreon scaffolds, filled with HA or $CaSiO_3$ at different concentrations, show a statistically significant increase in protein content over the incubation time. Figure 4-64 demonstrates that PLA and Floreon membranes have the lowest protein concentration, while Floreon/$CaSiO_3$ (20% wt) scaffolds have the highest protein concentration. As the amount of $CaSiO_3$ increases from 5% to 10% and then to 20%, the concentration of protein in the sample goes up in a linear manner.

Similarly, Figure 4-65 demonstrates that the membranes containing HA had a higher protein concentration than the other scaffolds, as it was observed that the protein concentration of the sample increased directly with the increase of HA concentration. There were no significant differences found between PLA and Floreon, or between Floreon and a version of it that had 5% of either type of bioceramic particle (HA or $CaSiO_3$).
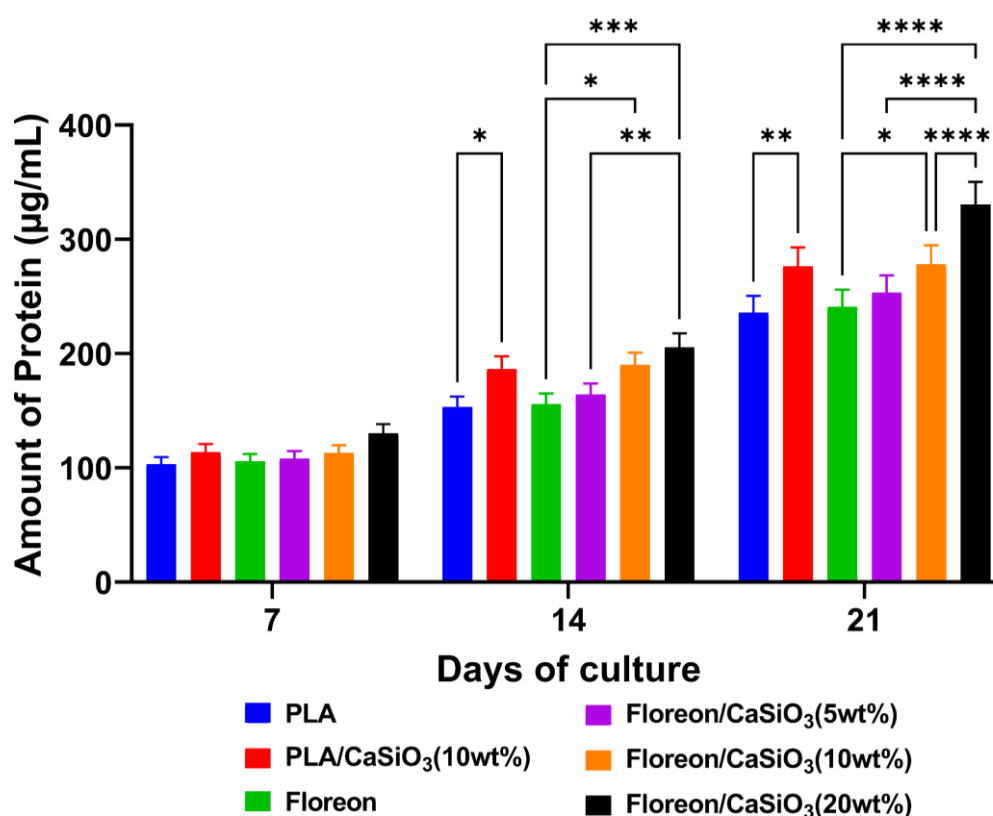
Figure 4-64 Protein concentration in cellular scaffolds on days 7, 14, and 21. The amount of protein is expressed as mean-SD (n = 3). Significant difference between PLA and Floreon fibrous membranes containing different concentrations of $CaSiO_3$ within the same culture condition and time point (*p < 0.05; **p < 0.01; ***p 0.001 and ****p 0.0001).
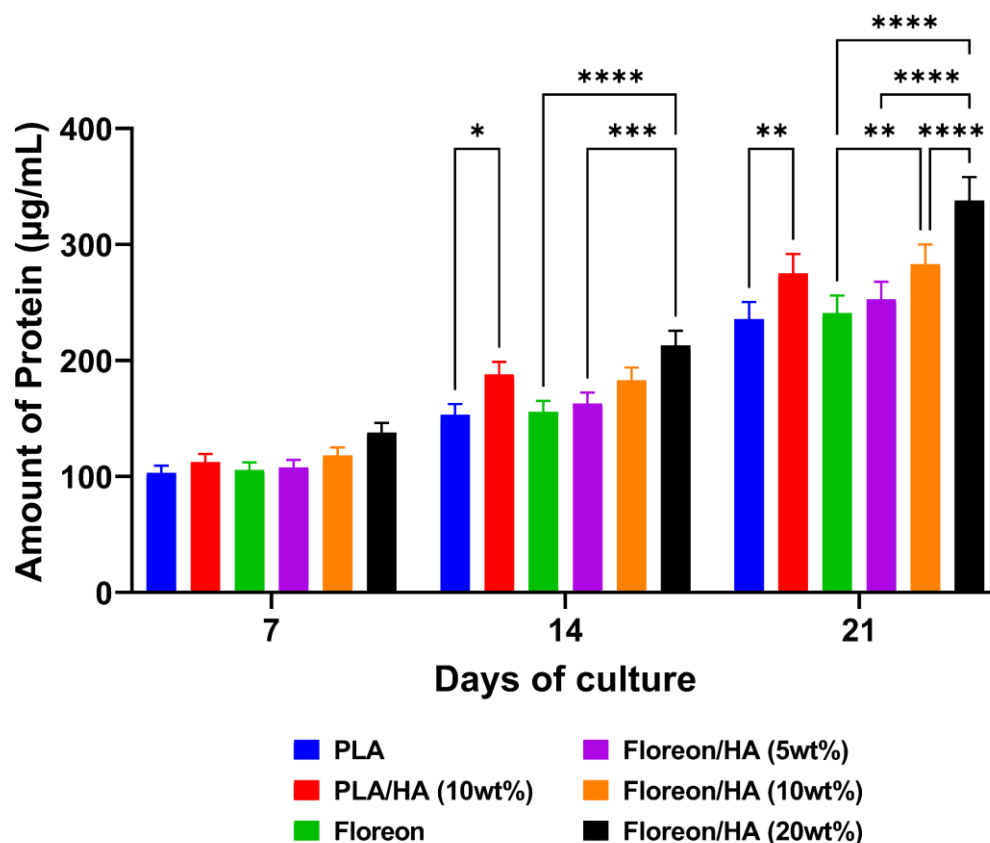
Figure 4-65 Protein concentration in cellular scaffolds on days 7, 14, and 21. The amount of protein is expressed as mean-SD (n = 3). Significant difference between PLA and Floreon fibrous membranes containing different concentrations of HA within the same culture condition and time point (*p < 0.05; **p < 0.01; ***p 0.001 and ****p 0.0001).

While these findings were statistically significant, it should be considered that increased cell proliferation is likely to have been attributed to total protein concentration increases, particularly over the longer cell culture duration. However, the LIVE/DEAD assay does suggest that fewer r-MSC cells die when cultured with the bioceramic treated scaffolds which will certainly influence the findings of the BCA assay. Figure 4-64 and Figure 4-65 present the results as protein concentration versus cell culture duration. All PLA and Floreon scaffolds, treated with HA or $CaSiO_3$ at different concentrations, show a statistically significant increase in protein content over the incubation time. It is also demonstrated that higher the concentration of HA or $CaSiO_3$ in the electrospun PLA and Floreon membrane, the higher is the protein content due to higher cell proliferation rate.

These findings are supported by a similar published study which reported that protein content of calcium phosphate containing PLA membranes was slightly higher than the content shown by unmodified PLA membranes (Maia-Pinto *et al.*, 2020). In another study, it was reported that cells proliferate more rapidly on the HA containing PLGA scaffolds as compared

to simple PLGA scaffolds (Haider, Gupta and Kang, 2014). It is also reported that $CaSiO_3$ provided an adequate environment for cell growth and proliferation and were characterised as biocompatible and promising as bone implant material (Jagadale *et al.*, 2013). The increase in cell proliferation and cell growth relates in high protein content.

4.1.13.5 PicoGreen assay

This test was performed to provide a quantitative analysis of double-stranded DNA in rat mesenchymal stromal cells cultured on various fibrous scaffolds. Pico green is a fluorescent dye used to stain DNA in order to make it fluorescent specifically and a part of other proteins, having a maximum emission wavelength of 590 nm. Using a fluorospectrometer, the fluorescence activity was measured, and the findings are shown in Figure 4-66 andFigure 4-67.

 Figure 4-66 demonstrates that DNA concentrations in all membranes and membrane scaffolds significantly rise with time, with the lowest quantities found after 7 days and the highest concentrations found after 21 days. Additionally, it has been proven that PLA and Floreon membranes have the lowest DNA concentration, while Floreon/$CaSiO_3$ (20% wt) scaffolds have the highest DNA concentration. As the concentration of $CaSiO_3$ increases from 5% to 10% and then to 20%, the concentration of DNA increases correspondingly.

Similarly, Figure 4-67 demonstrates that DNA concentration is lowest in PLA and Floreon membranes, whereas it increases with an increase in HA quantity, indicating that Floreon/HA (20% wt) has the highest DNA concentration of all the scaffolds. The DNA concentration difference between plain Floreon and Floreon/$CaSiO_3$ (5% wt.) or Floreon/HA (5% wt.) is negligible, hence no significant difference can be observed.
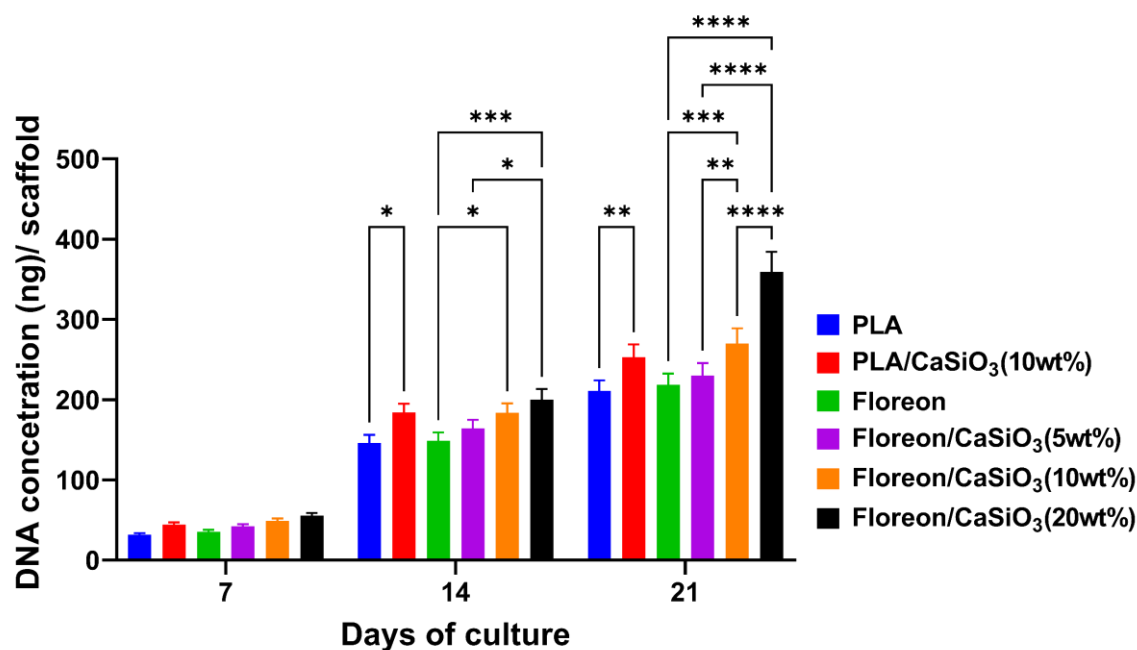
Figure 4-66 Quantification of dsDNA in cellular scaffolds by PicoGreen assay on days 7, 14, and 21. The amount of DNA is expressed as mean-SD (n = 3). Significant difference between PLA and Floreon fibrous membranes containing different concentrations of $CaSiO_3$ within the same culture condition and time point (*p < 0.05; **p < 0.01; ***p 0.001 and ****p 0.0001).
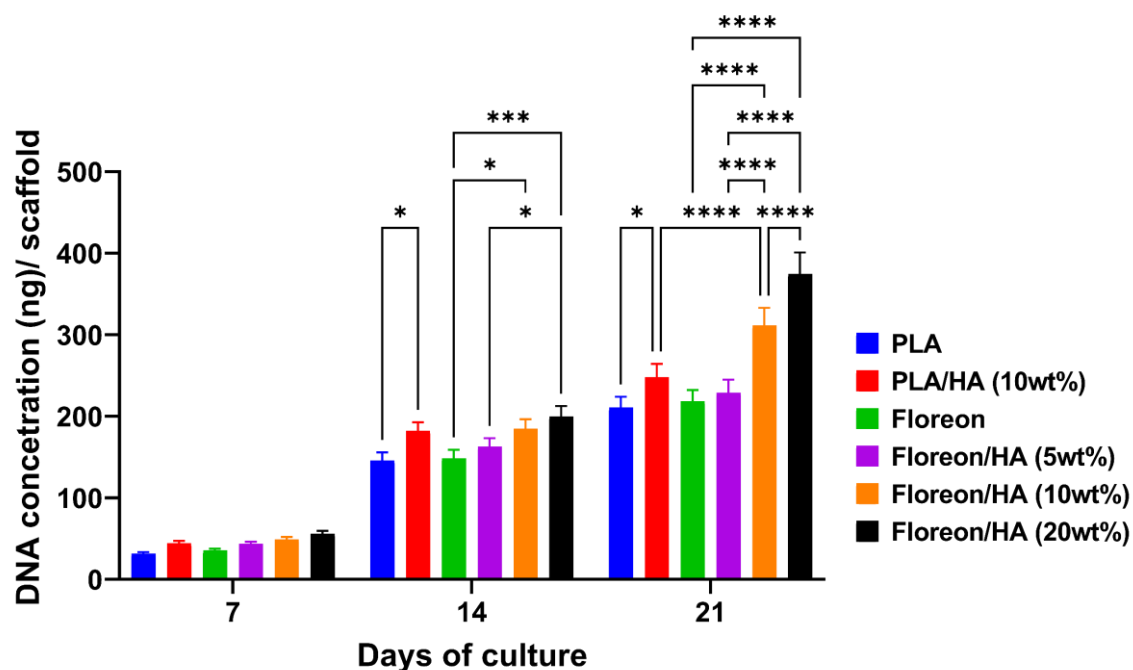
Figure 4-67 Quantification of dsDNA in cellular scaffolds by PicoGreen assay on days 7, 14, and 21. The amount of DNA is expressed as mean-SD (n = 3). Significant difference between PLA and Floreon fibrous membranes containing different concentrations of HA within the same culture condition and time point (*p < 0.05; **p < 0.01; ***p 0.001 and ****p 0.0001).

These findings tie in with the BCA assay which shows that total protein was increased in cells cultured on Floreon with HA and $CaSiO_3$. The PicoGreen assay showed a similar trend with more DNA present in the bioceramic treated surfaces with the exception that HA was more effective than $CaSiO_3$ treatment.

These findings are supported by the study in which DNA content was checked between HA containing TCP-PCL scaffolds group and simple PCL scaffold group. It was reported in the study that the HA containing TCP-PCL scaffolds group contained a significantly higher amount of DNA, which was thought to be equivalent to the number of cells, as compared to the simple PCL scaffolds group on day 21. Even though the PCL scaffold started off with more cells than the HA/TCP-PCL scaffold on day 2, after 21 days of culture, the HA/TCP-PCL scaffold had significantly more cells than the PCL scaffold (Chen et al., 2015). In a related study conducted in this research laboratory, no significant difference in the DNA quantity was observed between the $CaSiO_3$ containing Floreon membrane group and the control group of simple Floreon membrane (Ramos-Rodriguez *et al.*, 2022).

4.1.13.6 Cell Differentiation: Alkaline Phosphatase (ALP) Activity

The ALP activity (indicating osteoblast phenotype) of rMSCs grown in both basal medium (BM) and osteogenic medium (OS) was measured on day 21 of the culture (Figure 4-68 and Figure 4-69). As expected, the ALP levels of rMSCs that were grown in OS conditions were steadily and significantly higher than those of BM-cultured cells, no matter what type of scaffold was used. It was noted that there was no difference between the ALP activity of cells cultured on Floreon films and those cultured on PLA films using the same media. However, a distinct rise in ALP activity was found in cells cultured on scaffolds with the addition of bioceramic at different concentrations; the activity increased as the amount of HA or $CaSiO_3$ particles steadily increased. These findings suggest that, as hypothesised earlier, the addition of ceramic particles to the membrane structure stimulates osteogenesis in rMSCs making the scaffold a relevant platform for bone regeneration applications. This was especially clear when an OS medium that boosted ALP activity very much was used.
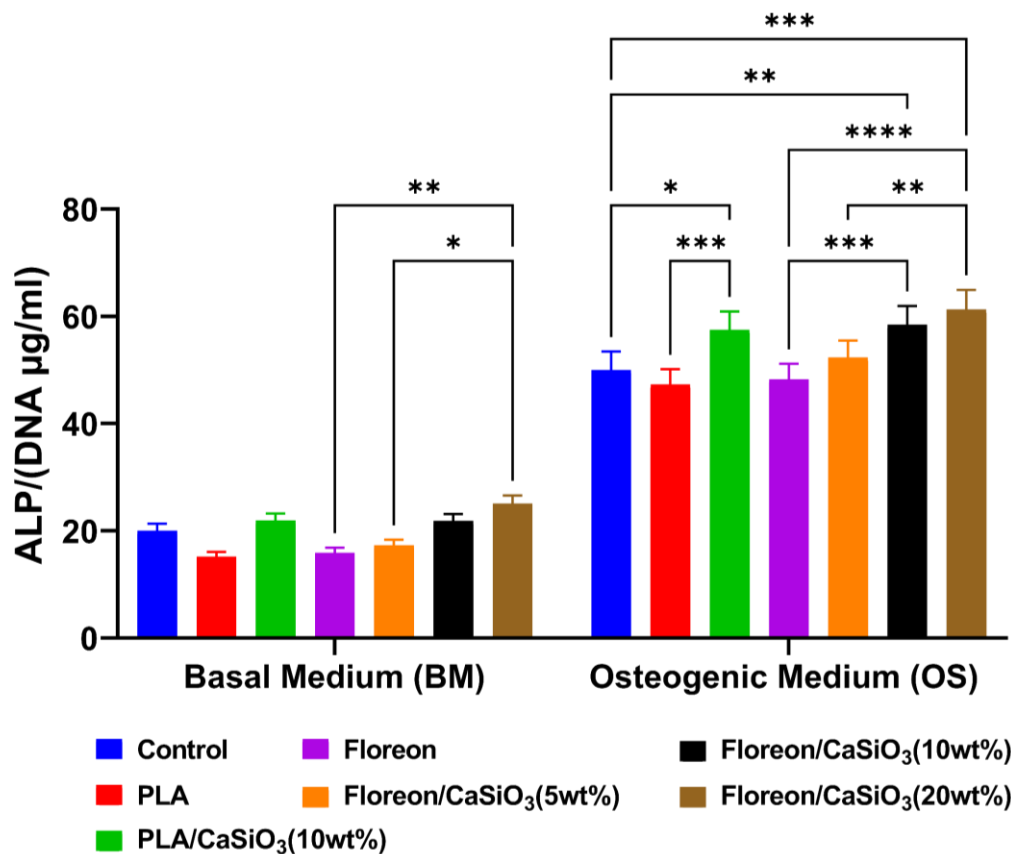
Figure 4-68 Alkaline phosphatase (ALP) activity of rat MSCs (rMSCs) after 21 days of culture in basal medium (BM) and osteogenic medium (OS) on PLA and Floreon fibrous membranes containing different concentrations of $CaSiO_3$ as well as control samples. The amount of ALP is expressed as mean-SD (n = 3). Significant difference between fibrous membranes within the same culture condition and time point (*p < 0.05; **p < 0.01; ***p 0.001 and ****p 0.0001).
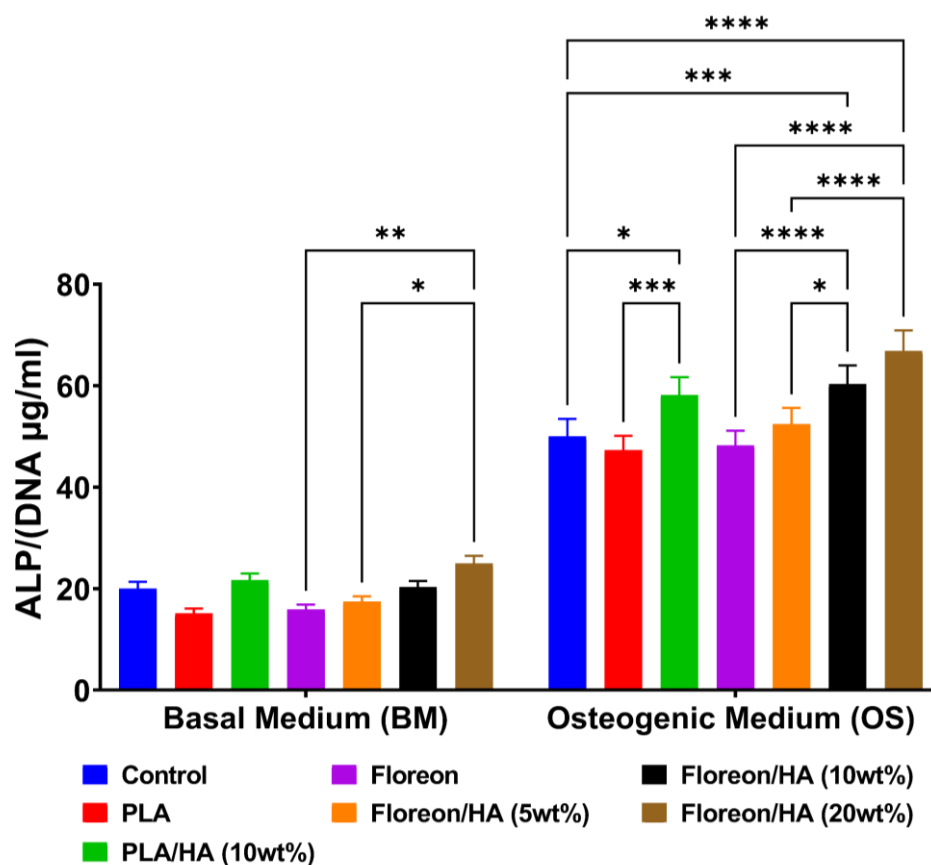
Figure 4-69 Alkaline phosphatase (ALP) activity of rat MSCs (rMSCs) after 21 days of culture in basal medium (BM) and osteogenic medium (OS) on PLA and Floreon fibrous membranes containing different concentrations of HA as well as control samples. The amount of ALP is expressed as mean-SD (n = 3). Significant difference between fibrous membranes within the same culture condition and time point (*p < 0.05; **p < 0.01; ***p 0.001 and ****p 0.0001).

The ALP activity, which is an indicator of rMSCs differentiation towards an osteoblast phenotype (Li *et al.*, 2019). As expected, the ALP levels of rMSCs that were grown in OS conditions were steadily and significantly higher than those of BM-cultured cells, no matter what type of scaffold was used. It was noted that there was no difference between the ALP activity of cells cultured on Floreon scaffolds and cells cultured on PLA films using the same media. This finding was supported by Sandrine and colleagues' study of the ALP activity of three cell types differentiated on various substrates in basal and osteogenic cell culture media, which found that, over time and across all three substrates, the ALP activity was significantly higher in osteogenic media than in basal media (Lavenus *et al.*, 2011).

However, a distinct rise in ALP activity was found in cells cultured on scaffolds with the addition of bioceramics; the activity increased as the amount of HA or $CaSiO_3$ particles steadily increased. These findings suggest that the addition of ceramic particles to the membrane structure stimulates osteoblast differentiation in rMSCs. This was especially clear when an OS medium that boosted ALP activity was used. These findings were recorded after 21 days of culture; however, it would be interesting to determine from which day ALP activity begins to increase and define the moment from which differentiation begins in relation to the scaffold used. Time constraints did not allow the use of immunocytochemistry labelling but it would have been interesting to identify what differentiation markers were shown by the cell on each type of scaffold.

These findings are in line with a study which demonstrated high ALP activity in the HA containing PLA groups as compared to simple PLA scaffold group (Grottkau *et al.*, 2020). Some previous studies also used $CaSiO_3$ as the active agent for regeneration of bone tissue in the polymer scaffolds. The $CaSiO_3$ addition has been linked with the enhanced formation of bone, producing superior or equal results to the tricalcium phosphate (Wu *et al.*, 2008, 2012; Tcacencu *et al.*, 2018; Qian *et al.*, 2019). This is thought to be a consequence of the bioceramic's Si ions, which are known to promote osteoblast proliferation and differentiation as well as angiogenesis (Nair *et al.*, 2009; Wang *et al.*, 2013).

4.1.13.7 Cell morphology

Cell morphology describes the structure of the cells in the culture. This section performs two different analyses to describe the cell morphology.

• **Cell morphology analysis by Fluorescence Imaging:**

In order to study the cell morphology and microfilament structure, the F-actin and nucleus of rat mesenchymal stem cells were stained with Phalloidin (stains actin, red) and DAPI (stains nucleus, blue) and then images were taken using a fluorescent microscope. Figure 4-70 to Figure 4-72 show representative fluorescence images of rMSCs growing on the PLA and Floreon fibrous scaffolds filled with HA or $CaSiO_3$ at varying concentrations after 3, 7, and 14 days of culture. It was observed on the third day of incubation that many rMSCs had already attached and showed initial spreading, as evidenced by small round cells on all fibrous scaffolds. The cells were randomly distributed when cultured on fibrous membranes and displayed a pyramidal shape with randomly oriented actin filaments 7 days after seeding. This was seen in all the membranes.

The fluorescent images of rMSCs cultured on the fibrous scaffolds after 14 days demonstrated similar responses regardless of the type of polymer used. The cells had attached, proliferated, and formed a cell sheet that covered the entire surface. There were no differences in cell shape, which clearly resembled their characteristic rMSCs morphology. The cascade of the cellular response on the Floreon membranes was similar to that of the cells seeded on the PLA films. It is therefore suggested that rMSCs can attach and proliferate on Floreon as well as on the control group (PLA).
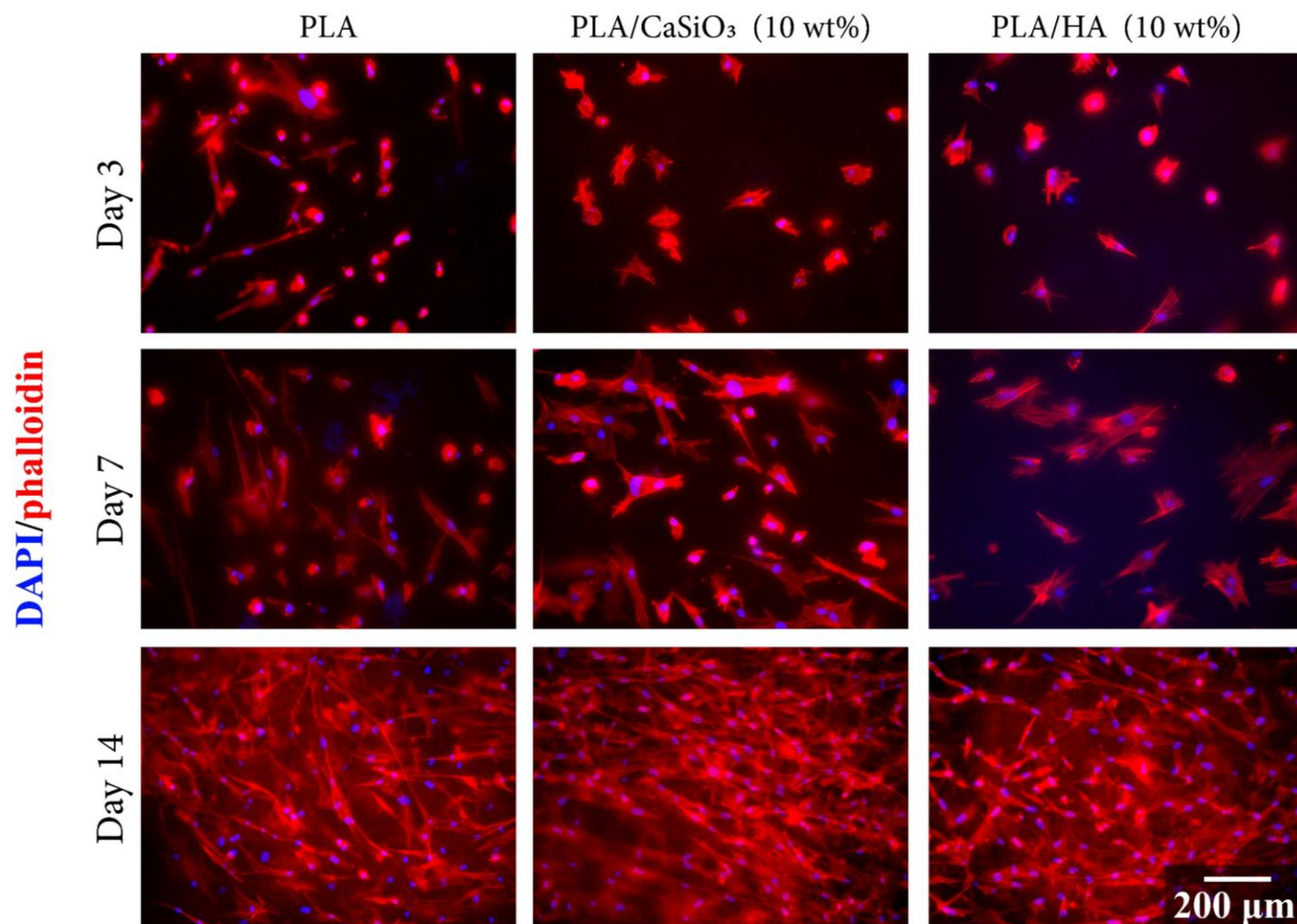
Figure 4-70 Phalloidin labelled F-actin (red), DAPI nuclear staining (blue) and overlaid fluorescent image of immunostained cellular components (merged) for the images of rat MSCs(rMSCs) seeded over electrospun PLA fibrous membranes containing 10 wt% of HA and CaSiO$_3$, after 3, 7, and 14 days of culture. All images were scaled at 200 µm.

225
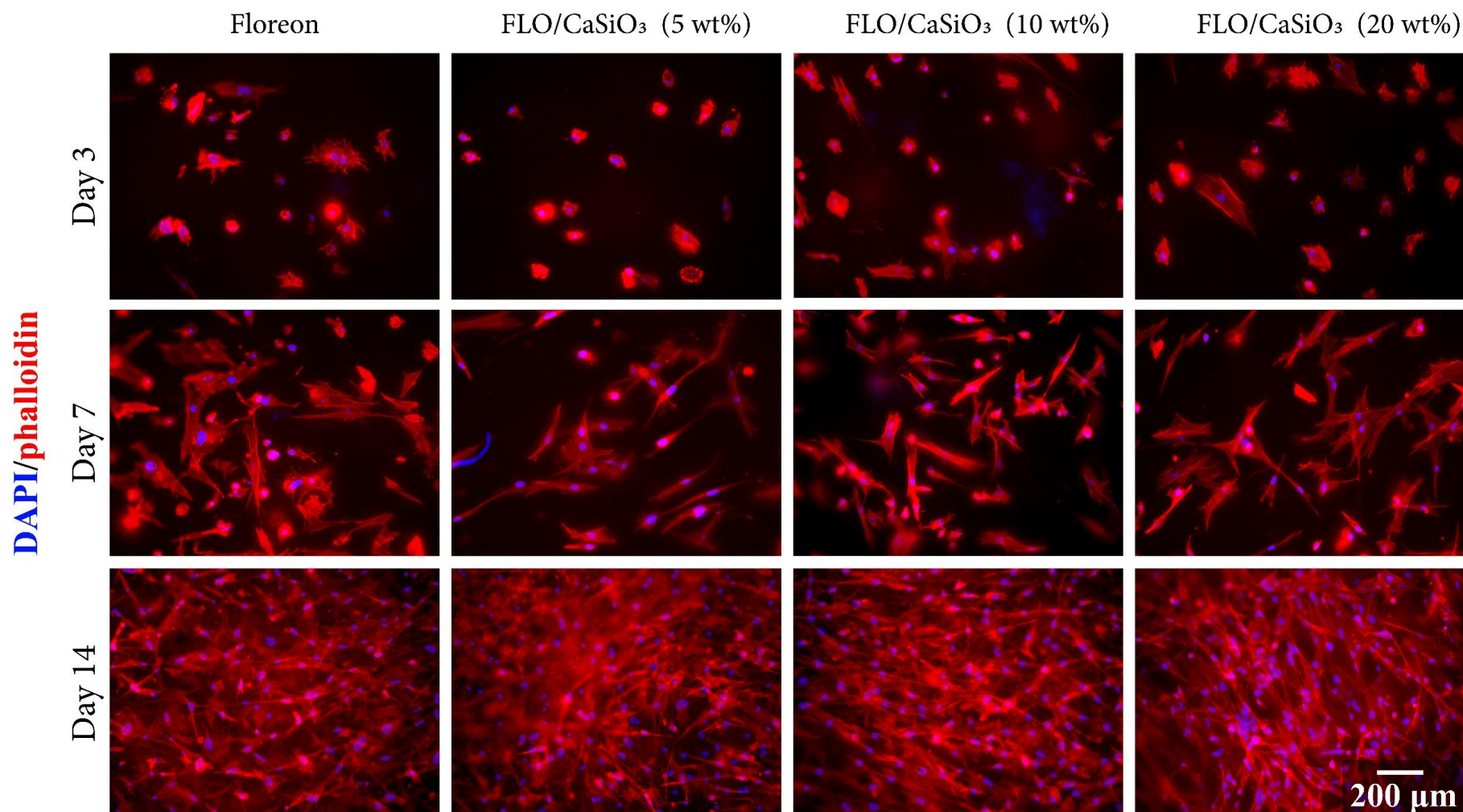
Figure 4-71 Phalloidin labelled F-actin (red), DAPI nuclear staining (blue) and overlaid fluorescent image of immunostained cellular components (merged) for the images of rat MSCs(rMSCs) seeded over electrospun Floreon membranes containing different concentrations (5,10 and 20 wt%) of CaSiO₃, after 3, 7, and 14 days of culture. All images were scaled at 200 μm.
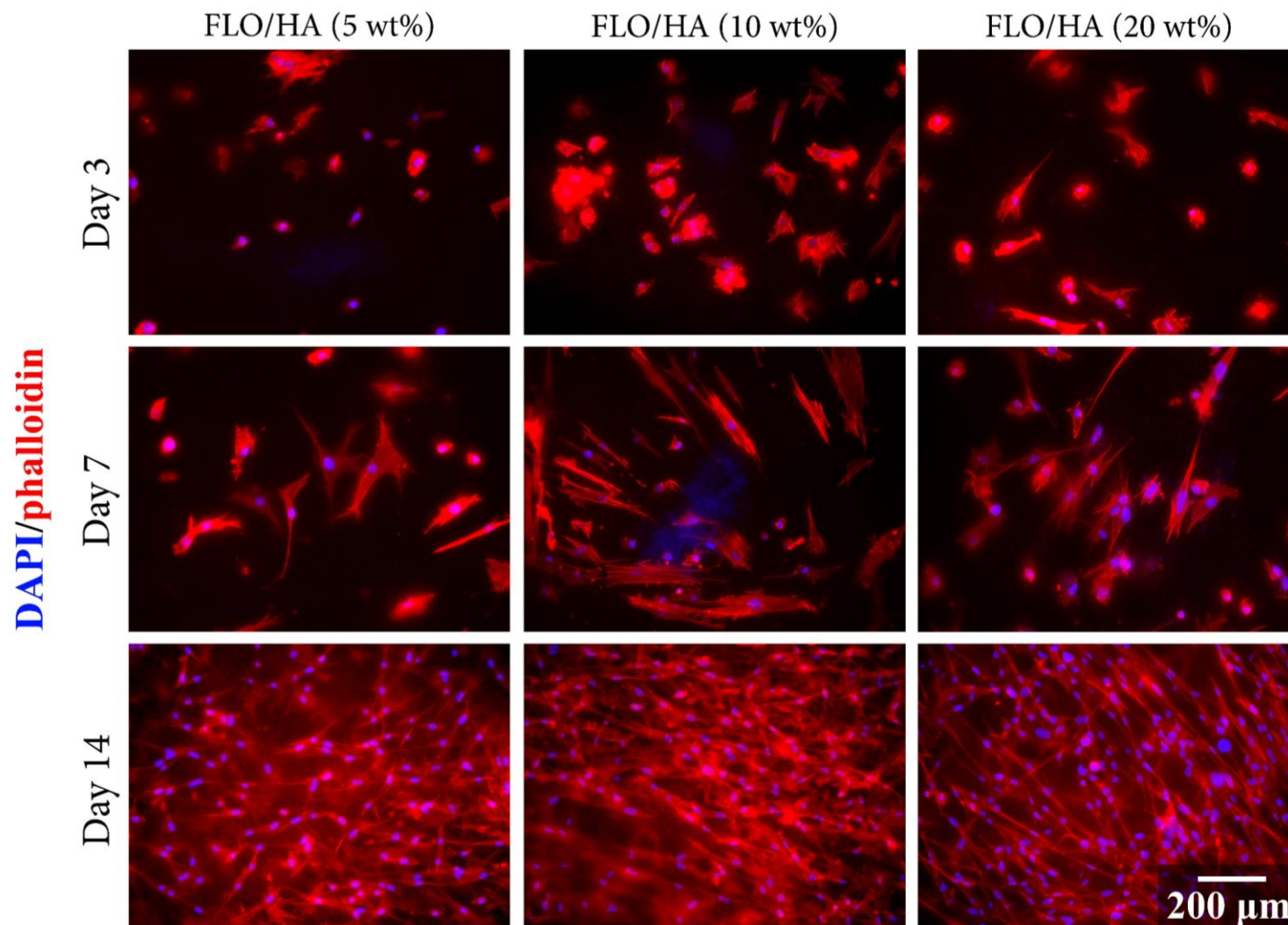
Figure 4-72 Phalloidin labelled F-actin (red), DAPI nuclear staining (blue) and overlaid fluorescent image of immunostained cellular components (merged) for the images of rat MSCs(rMSCs) seeded over electrospun Floreon membranes containing different concentrations (5,10 and 20 wt%) of HA, after 3, 7, and 14 days of culture. All images were scaled at 200 µm.

In order to study the cell morphology and microfilament structure, F-actin and nucleus of rMSCs were stained with phalloidin (stains actin red) and DAPI (stains the nucleus blue) and images then taken using a fluorescent microscope. Figure 4-70 to Figure 4-72 show representative fluorescence images of rMSCs growing on the PLA and Floreon fibrous scaffolds with HA or $CaSiO_3$ at varying concentrations after 3, 7, and 14 days of culture. It was observed on the third day of incubation that rMSCs had attached and showed signs of initial spreading, as evidenced by larger and flatter cells.

The findings of this study revealed that, on day 3, rMSCs seeded on both PLA and Floreon displayed a rounded and compact phenotype. However, by day 7, there was a notable transition towards a more stretched and flattened morphology, which was supported by an increase in F-actin expression. At day 14 when the cells had become mostly confluent, the rMSCs become more elongated which could be due to the restricted culture area. At day 3, the cells appeared more motile and therefore, less adherent to the scaffold. Interestingly, with the addition of HA or $CaSiO_3$, rMSCs appeared to become larger and more adherent at day 7 than without any bioceramic. The cells were randomly distributed when cultured on fibrous membranes and displayed a pyramid-like shape with randomly oriented actin filaments 7 days after seeding. This was seen in all the membranes.

The fluorescent images of rMSCs cultured on the fibrous scaffolds after 14 days demonstrated similar responses regardless of the type of polymer used. The cells had attached, proliferated, and formed a cell layer that covered the entire surface. There were no differences in cell shape between the scaffold conditions, which clearly resembled their characteristic rMSCs morphology. The cascade of the cellular response on the Floreon membranes was similar to that of the cells seeded on the PLA films. It is therefore suggested that rMSCs can attach and proliferate on Floreon as well as on the control group (PLA).

As described earlier that ALP activity was also increased under the same scaffold conditions, the observed F-actin staining could be due to the promoted osteoblast differentiation. These observations could also be due to increased rMSC proliferation. It is interesting to note that at day 3 there are some very rounded cells, which could be due to the cells being very loosely attached to the scaffold and possibly Floreon, even amoeboid-like. Amoeboid cells are not well understood but are found in very aggressive melanoma and indicative of invasiveness, and perhaps rMSCs at day 3 are more migratory than at day 7 (Maiques and Sanz-Moreno, 2022).

The figures also show that the in vitro viability as well as proliferation of cells are also not affected when they are cultured on the PLA, Floreon or $CaSiO_3$ or HA containing PLA or Floreon membranes and their results are comparable to one another. The morphology of the cells is also not affected by PLA, Floreon or $CaSiO_3$ or HA containing PLA or Floreon membranes. These results are supported by the study conducted in this research laboratory which reported that the in vitro viability as well as proliferation of fibroblast is not affected when they are cultured on the Floreon or $CaSiO_3$ containing Floreon and that Floreon results are comparable to the PLA and TCP controls (Ramos-Rodriguez *et al.*, 2022).

- **Cell morphology analysis by SEM Imaging:**

A scanning electron microscopy was utilised in order to observe the morphological features of cells in relation to the structure of the fibrous scaffolds. Figure 4-73 to Figure 4-75 illustrate the integration of the cells after three days of the cell culture on PLA or Floreon scaffolds that were modified with HA or $CaSiO_3$ at varying concentrations. The images were taken at different magnifications (10k, 5k, and 3k times).

All scaffolds displayed structural integrity and a three-dimensional shape following seeding with rMSCs, and their interconnected pores were beneficial for the adhesion, migration and proliferation rate of the cells. Figure 4-74 illustrates that, similar to what was seen with the PLA membrane (the control group), cells spread and attached to the surface of the Floreon membrane to produce a lamellar structure, and they stretched further into the pores.

These observations indicate that the Floreon membranes provide ample space for cell growth. The rMSCs adhered and spread on the Floreon fibres, penetrated through the pores, and proliferated across the surface. Furthermore, the cells extended in the direction of the fibre orientation, creating a three-dimensional and multicellular network in accordance with the scaffold architecture.

Lastly, it was evident that the rate of proliferation and expansion of rMSCs and the extracellular matrix (ECM) on scaffolds containing bioceramic particles (HA or $CaSiO_3$) increased with increasing concentrations of these particles in the membrane structure.
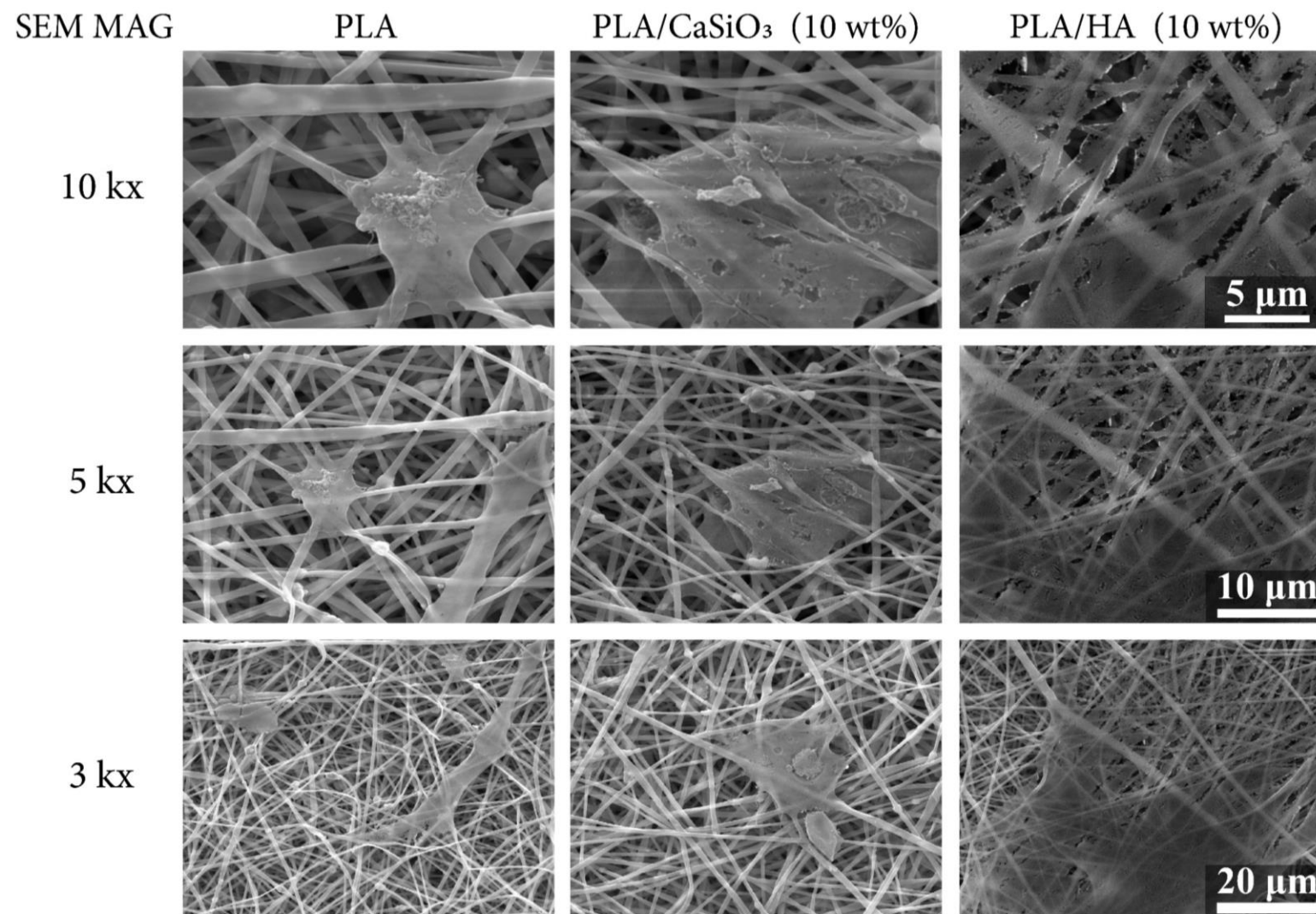
Figure 4-73 SEM micrographs of rat MSCs(rMSCs) seeded over electrospun PLA fibrous membranes containing 10 wt% of HA and CaSiO₃, after 3 days of culture. The images depict different levels of magnification, with the top row scaled at 5 µm, the middle row at 10 µm, and the bottom row at 20 µm.
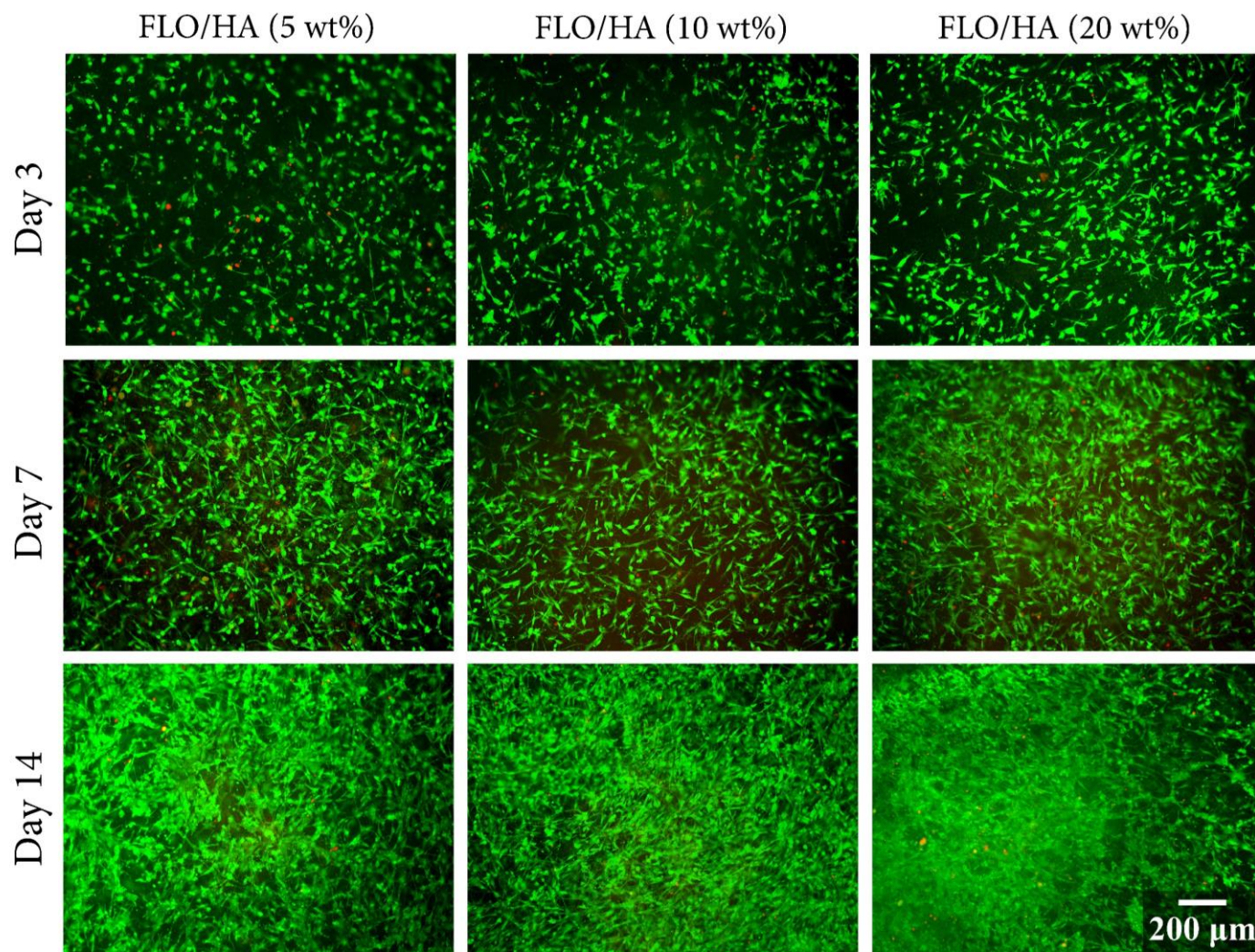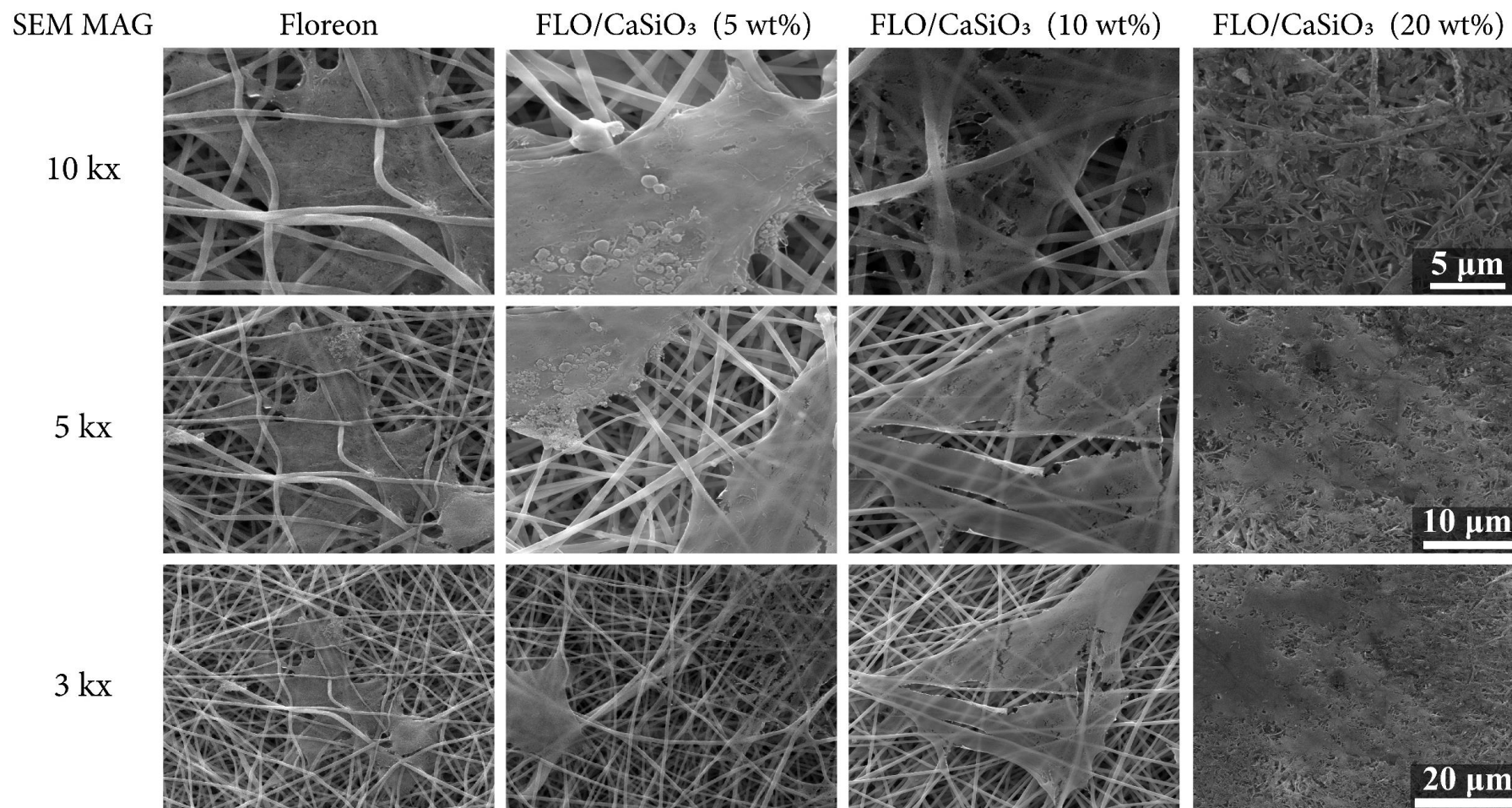
Figure 4-74 SEM micrographs of rat MSCs(rMSCs) seeded over electrospun Floreon membranes containing different concentrations (5,10 and 20 wt%) of $CaSiO_3$, after 3days of culture. The images depict different levels of magnification, with the top row scaled at 5 µm, the middle row at 10 µm, and the bottom row at 20 µm.
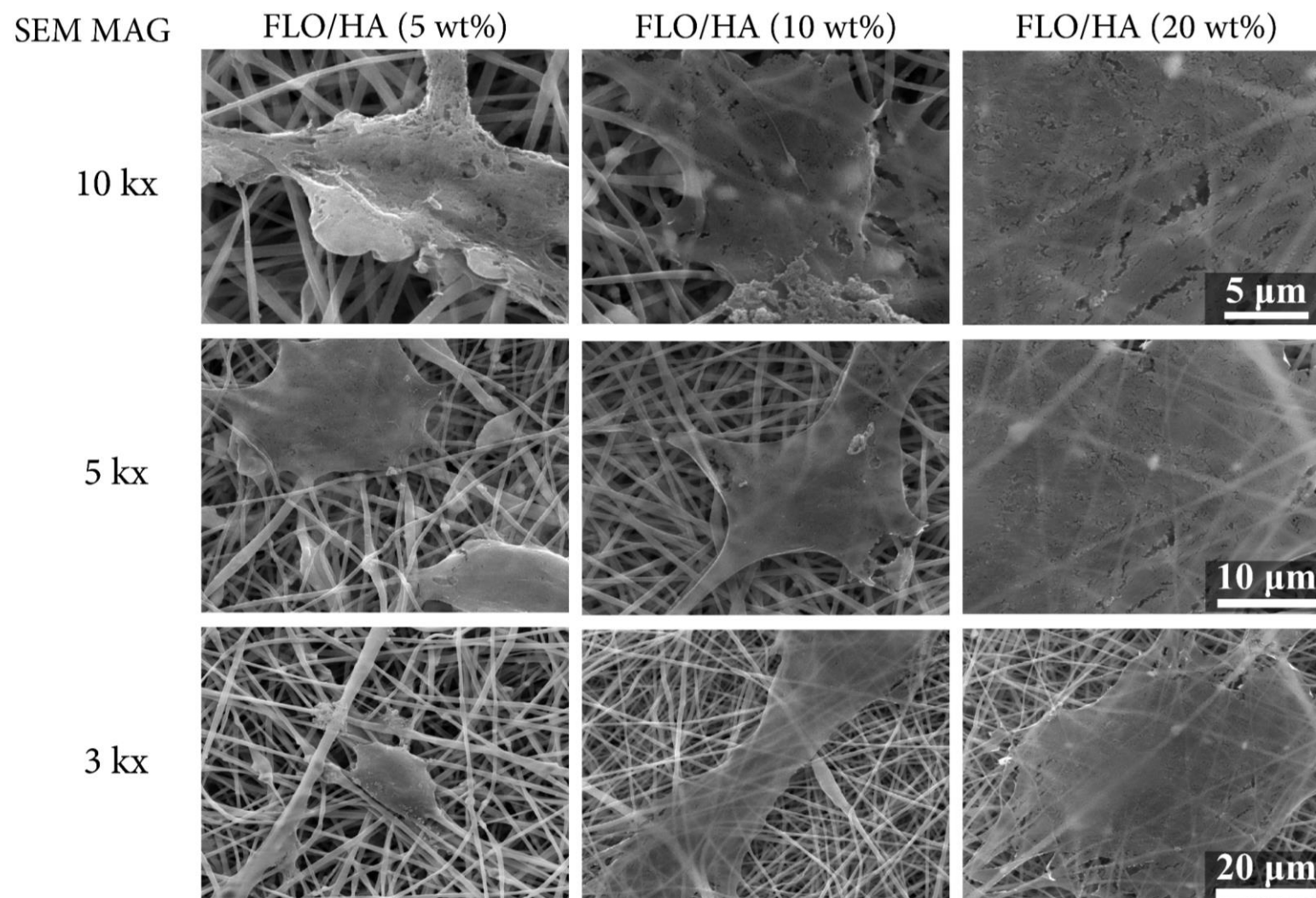
Figure 4-75 SEM micrographs of rat MSCs(rMSCs) seeded over electrospun Floreon membranes containing different concentrations (5,10 and 20 wt%) of HA, after 3 days of culture. The images depict different levels of magnification, with the top row scaled at 5 µm, the middle row at 10 µm, and the bottom row at 20 µm.

The rMSCs cultured on PLA and $CaSiO_3$ scaffolds were observed with a SEM to reveal the scaffold pores made by the electrospinning technique. All scaffolds displayed structural integrity and a 3-dimensional shape following seeding with rMSCs, and their interconnected pores appeared to be beneficial for the adhesion, migration, and proliferation rate of the cells.

Cells were seen attached to the Floreon scaffold to produce a lamellar structure. Furthermore, rMSCs stretch along and in the direction of the fibres which presents the possibility of directing cells towards a specified location based on the fibre direction. The findings also indicate that Floreon scaffold provides spaces for cells to grow.

For the subsequent functioning of the cell, the initial cell attachment is crucial. A study by Lee and colleagues describes the observation that the attachment of osteoblasts on membrane with the 0.2-8 micrometre pores and found that cells were fully adhered and spread on the surface with 0.2-1 micrometre pores, whereas cells became spherical with few filopodia and lamellipodia on the membrane with larger micropores (Lee *et al.*, 2004). Additionally, it was demonstrated that PLLA scaffolds with fibres (50–500nm) improve protein adsorption, which aids in cell adhesion (Woo, Chen and Ma, 2003). It was also demonstrated that the osteoblasts adhered and multiplied more successfully on the uneven surface (0.81 micrometre pore size) than they did on the smooth one (Hatano *et al.*, 1999). As a result, the scaffold's design and pore size affect cellular migration and proliferation inside it.

The rMSCs were observed to adhere and spread on the Floreon fibres, penetrate through the pores, and proliferate across the surface. Finally, it was evident that the rate of proliferation and expansion of rMSCs on scaffolds containing bioceramic particles (HA or $CaSiO_3$) increased as the concentration of these particles in the membrane structure increased.

4.2   Section II: Fabrication and charactarisation of thin membrane

The following findings concern the characterisation of Floreon and PLA thin films using two different methods, namely solvent casting and spin coating techniques, to serve as a surface layer of the functionally graded guided tissue regenerative membrane.

The following flowchart (Figure 4-76) summarises the tests conducted to investigate the properties of thin films. This involved examining the properties of the materials utilised and the physical and chemical features of the membranes that were manufactured, as well as their biocompatibility.
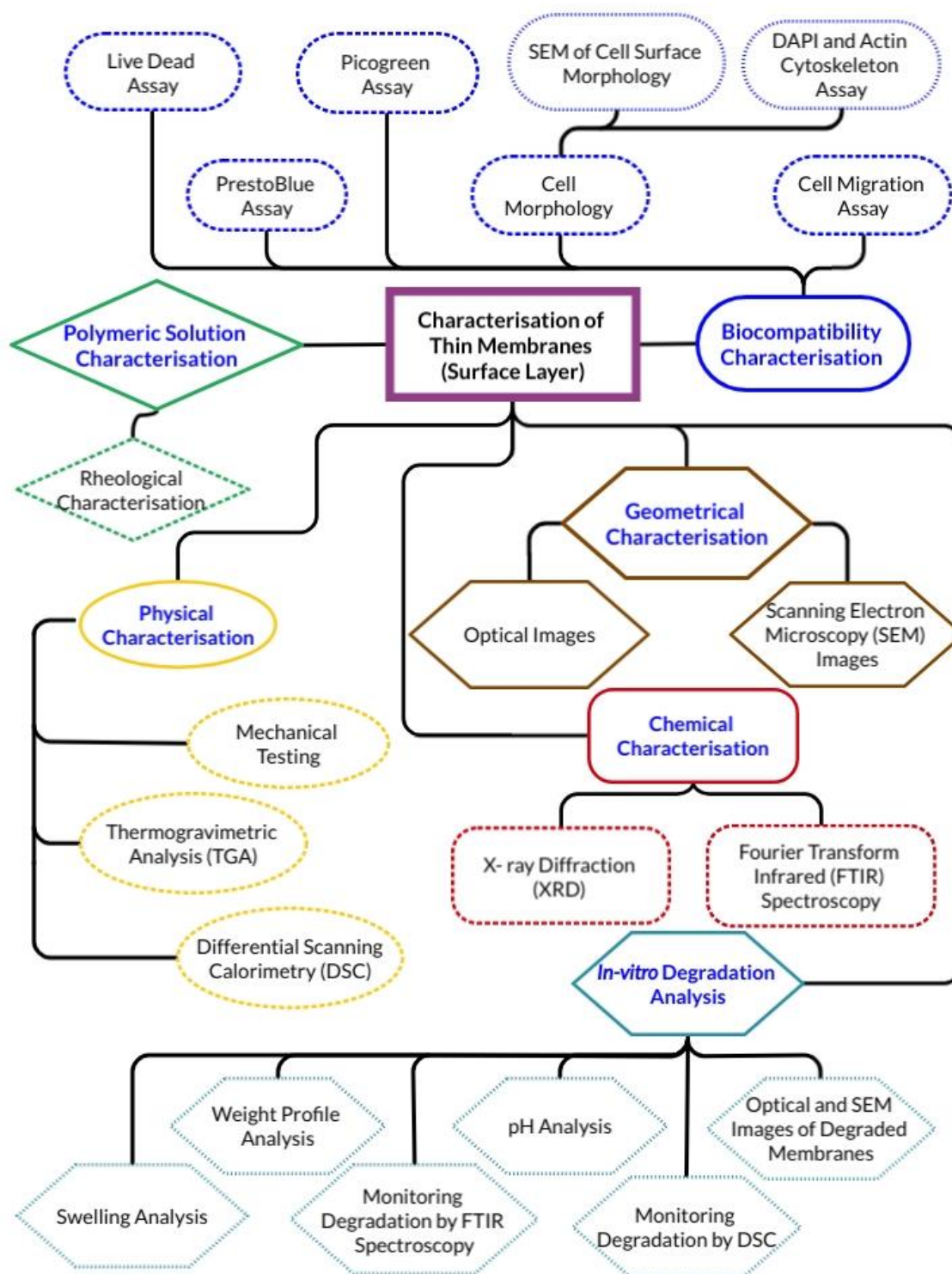
Figure 4-76 a flowchart illustrating the characteristics tests performed on the thin Floreon and PLA films manufactured by solvent casting and spin coating processes.

4.2.1 Characterisation of the polymeric solution:Viscosity evaluation

In order to evaluate the correlation between the viscosity of the initial polymer-solvent solution and the physical properties of the obtained mats, the complex viscosity of PLA, as well as Floreon solutions, were measured as a function of frequency. Figure 4-77 shows the values of the complex viscosity $\eta *$ for the PLA (black line) and Floreon (red line). As expected, Floreon solution showed higher viscosity if compared with PLA solution at the higher frequency investigated, especially before the last quarter of the test.
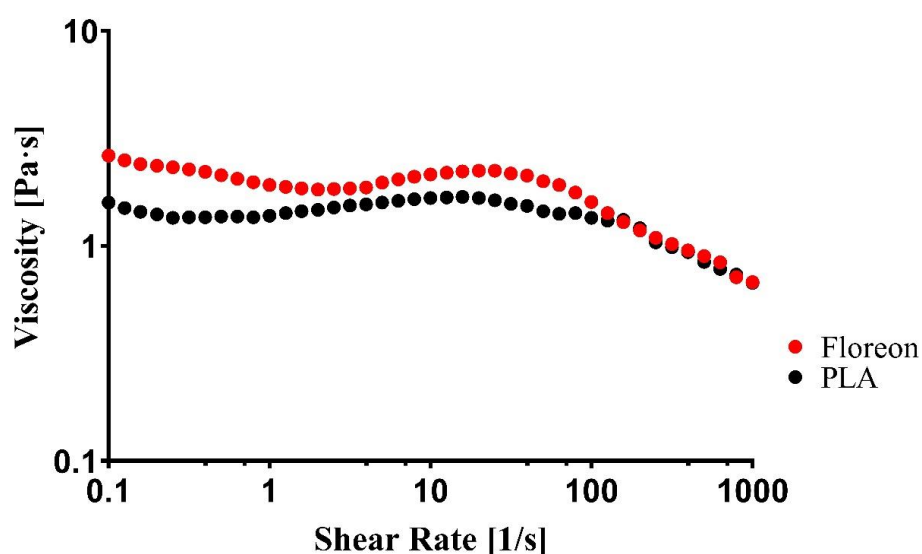
Figure 4-77 Complex viscosity of PLA (black line) Floreon (red line).

In terms of rheology, the measurement of the complex viscosities of Floreon and PLA compounds as a function of frequency indicated that: (a) the Floreon compound has a slightly higher viscosity than plain PLA, and that (b) both are exhibiting shear thinning behaviours (Figure 4.2-4). In Figure 4-77, The viscosity of the PLA solution is increased with the incorporation of PCL polymer. The study findings indicate that the optimal morphology and synergistic effects in the mechanical performance of the systems can be achieved through melt-mixing of the polymers with the optimised composition of PLA/PCL (80/20 by weight) (Ostafinska *et al.*, 2015).

4.2.2 Geometrical Characterisation: Optical Images of membranes

Optical images of prepared membranes of Floreon and PLA fabricated using casting and spin coating techniques are shown in Figure 4-78 and Figure 4-79. Plain PLA membranes presented a transparent nature shown when using both manufacturing methods. The amount of PCL used in a given Floreon compositions had a noticeable effect on the film's colour. On visual examination, all films of all types and by all manufacturing methods were smooth and shiny and had flexibility while bending. There were more wrinkles and other imperfections in the Floreon membranes than in the PLA ones.
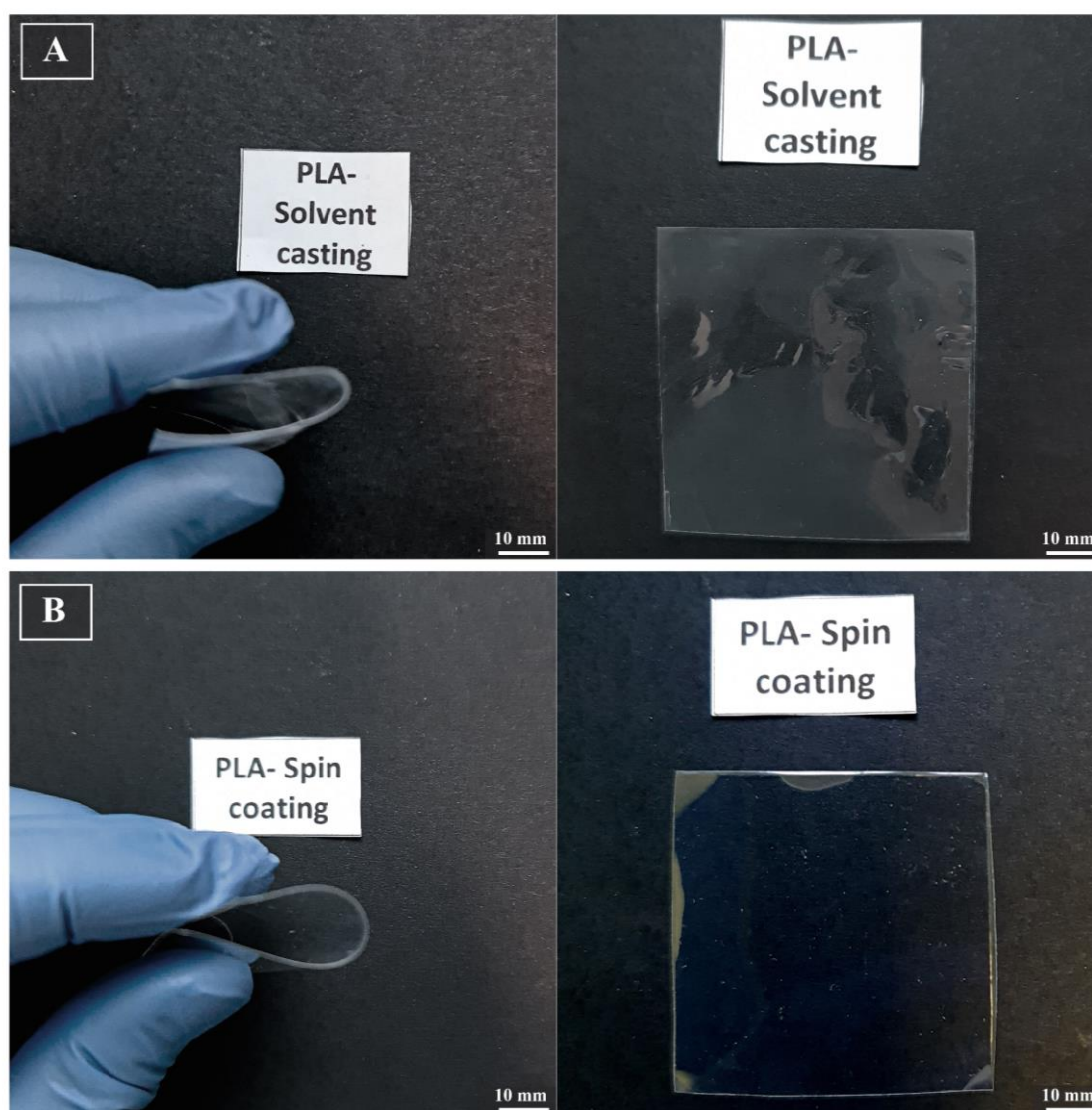
Figure 4-78 Macroscopic view of a fabricated PLA membranes (a) PLA -casting technique (b) PLA -spin coating technique. Images taken with a DSLR S5600 with Macro lens (Nikon), inset image shows the handling properties of the as prepared membrane while bending.
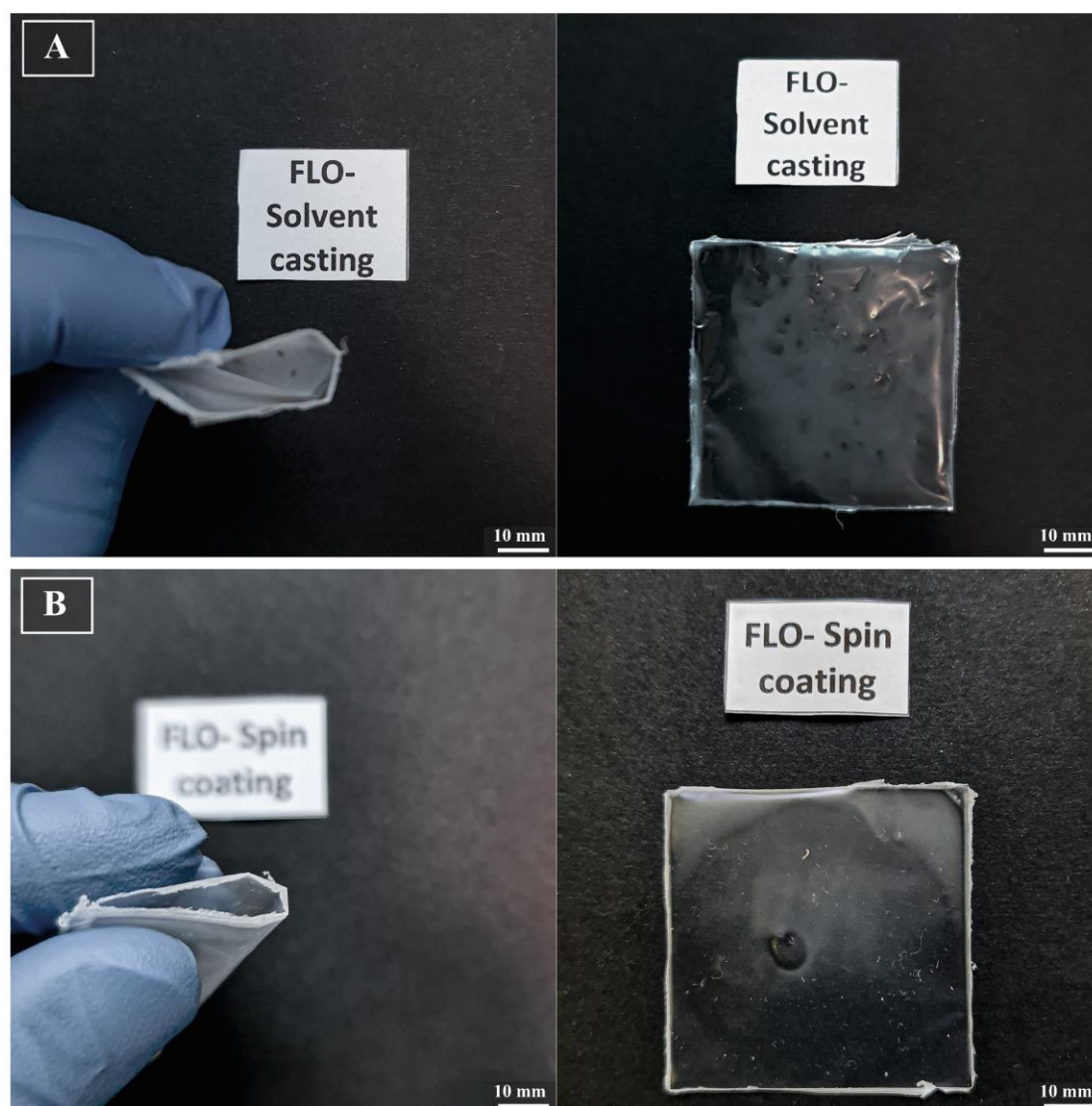
Figure 4-79 Macroscopic view of a fabricated Floreon membranes (a) Floreon -casting technique (b) Floreon-spin coating technique. Images taken with a DSLR S5600 with Macro lens (Nikon), inset image shows the handling properties of the as prepared membrane while bending.

Smooth PLA membranes demonstrated a transparent nature when produced with either approach. Balla et al have reported the similar properties of synthesised PLA (Balla *et al.*, 2021). As the amount of PCL increased for a particular Floreon composition, a visible shift in the colour of the Floreon films could be seen. Upon closer inspection, all membrane types produced appeared to be glossy, smooth, and flexible when bent. Floreon films displayed obvious flaws including wrinkling, which may have been caused by solvent evaporation during casting (Magalhães *et al.*, 2010).

4.2.3 Scanning electron microscopy (SEM) of Thin Membranes

Figure 4-80 depicts SEM micrographs of PLA and Floreon taken at two magnifications (3 and 10 kx). It can be seen that Spin-coated PLA and Floreon films showed smooth surface, whereas solvent-casted PLA and Floreon showed signs of surface waviness and ridges.
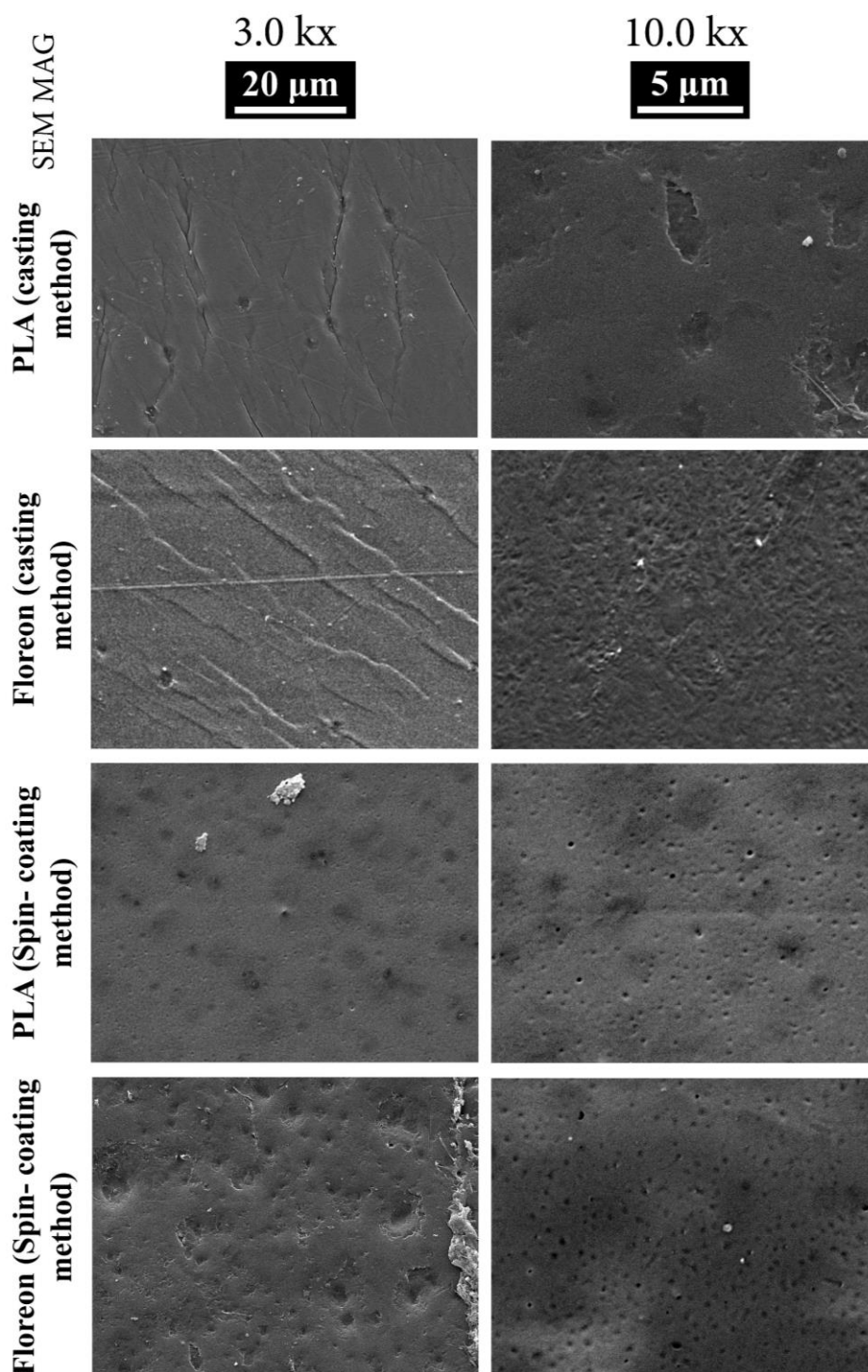
Figure 4-80 SEM performed on PLA and Floreon films fabricated using both techniques, the micrographs in the left column are scaled at 20 µm, while those in the right column are scaled at 5µm.

Figure 4-80 displays SEM images of PLA and Floreon. As can be seen, solvent-casted PLA and Floreon films had surface waviness and ridges, but spin-coated PLA and Floreon films had smooth surfaces. During the solvent casting process, the solvent evaporates, leading to these observed characteristics (Magalhães *et al.*, 2010).

4.2.4 Pore size distribution and porosity

The total amount of mercury that permeated each membrane sample when pressure was applied is shown in Figure 4-81 (A); referring to the spin-coated films made of both PLA or Floreon (red lines), they obtained a greater volume of mercury, indicating that their porosity is higher than that produced by the solvent casting method (blue line). It was also found that there is no difference between membranes produced using the same technique.

The same finding was also confirmed in Figure 4-81 (B), which displayed the volume of mercury intruded into each gram of sample as a function of pore diameter is presented graphically. The spin coating process produced more porous films than the casting method. These results are numerically summarised in Table 4-7.

Table 4-7 Most important output data of mercury intrusion porosimetry analysis.

Content	Total Intrusion Volume mL/g	Total Pore Area m²/g	Porosity %
PLA (casting method)	0.26	34.07	24.18
Floreon (casting method)	0.29	32.71	35.51
PLA (Spin -Coating method)	0.42	30.40	34.70
Floreon (Spin -Coating method)	0.45	28.08	41.82
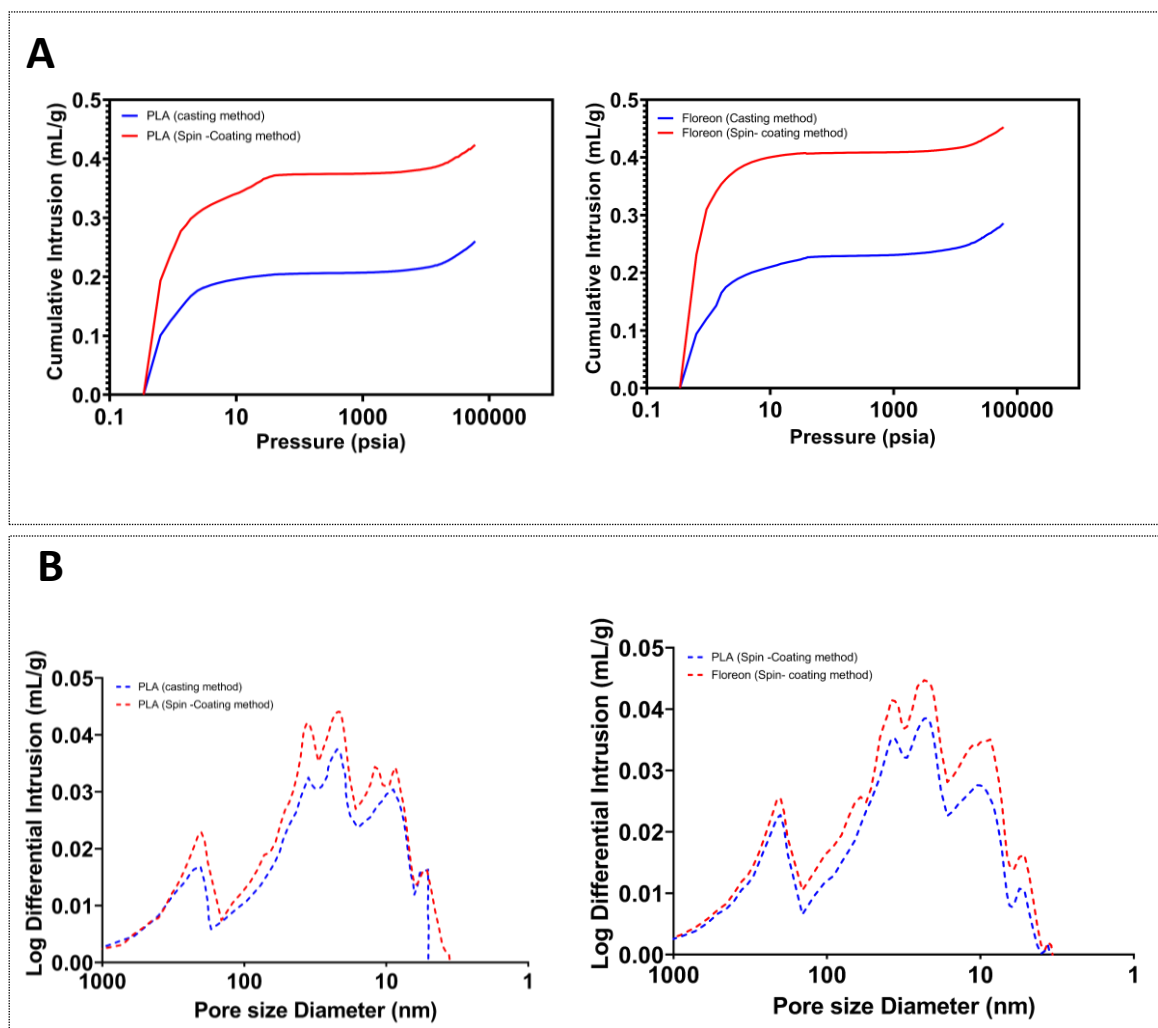
Figure 4-81 Cumulative (A) and differential (B) intrusion curves as a function of pore diameter measured by mercury intrusion porosimetry.

The SEM images of the created films revealed what the MIP results validated; Table 4-7 provides a summary of these results. The maximum total pore area and smallest pore characteristic lengths were found in the cast PLA and Floreon films. Regarding spin-coated films created with both materials, their porosity was equivalent between themselves, 34.70% for PLA and 41.82% for Floreon membranes, although noticeably higher than cast films (24.18%, PLA, and 35.51% for Floreon). Previous research by Zhang XL et al. (2008) and Ulbricht (2006) delved into the utilisation of solvent-casting methods for polymer synthesis. The studies demonstrated that nanostructures can be induced from a polymer solution when initially dissolved in a good solvent and subjected to solvent evaporation, cooling, or exposure to non-solvents, such as water. Such processes have been shown to induce porosity in a wide range of polymers, including commercially available ones, and have the capacity to generate sub-100 nm pores, which is consistent with the observations made in the

present study. For instance, PCL dissolved in a mixture of dioxane and 2-methoxyethanol can generate a nanostructured film when cast and subsequently submerged in water (Ulbricht, 2006; Zhang *et al.*, 2008). Other studies demonstrated that this process is compatible with a variety of polymers but generally produces irregular structures (Krause *et al.*, 2002; Reverchon, Volpe and Caputo, 2003; Tomasko *et al.*, 2003; Merlet *et al.*, 2007)

4.2.5 X-Ray diffraction (XRD) analysis

X-ray diffraction (XRD) patterns of plain PLA and Floreon membranes have been recorded. As shown in Figure 4-82, only a broad diffuse scattering reflection, located at around17°2θ, was found in the XRD spectrum of plain PLA, indicating an amorphous structure of PLA. For Floreon mats, XRD patterns show that all diffraction peaks correspond to Floreon, which is a semicrystalline polymer with two distinct diffraction peaks reported at ~21 and ~23°2θ.
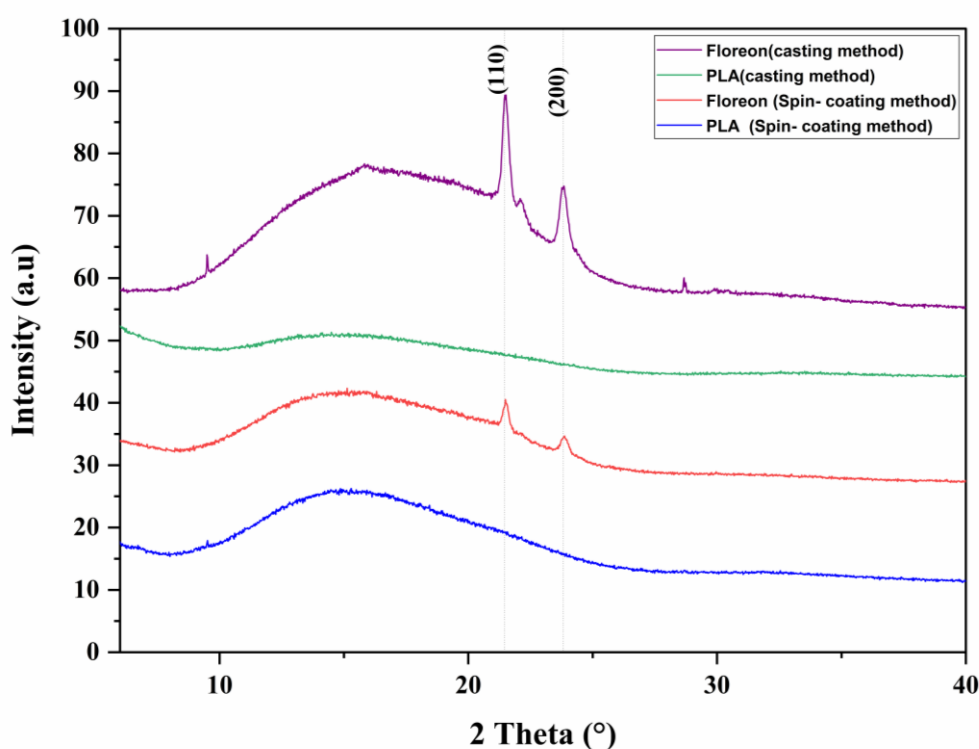
Figure 4-82 X-ray diffraction patterns of PLA and Floreon membranes prepared via spin-coating and solvent-casting methods.

The XRD spectrum of plain PLA contained a single broad scattering reflection at approximately $2\theta = 17°$, which showed that PLA has an amorphous structure. Wan Ishak et al., showed the influence of amorphous cellulose on mechanical, thermal, and hydrolytic

degradation of PLA biocomposites. They reported a broad XRD peak at $2\theta=21°$, which indicates that the cellulose I structure was transformed into an amorphous one due to incorporation of PLA (Wan Ishak, Rosli and Ahmad, 2020), and also reported by others (Avolio *et al.*, 2012; Zhang *et al.*, 2014). XRD diffraction peaks at approximately $2\theta=21^0$ and 23^0 indicated the semi-crystalline polymer of Floreon. According to Correale (2004), most semi-crystalline polymers can be arbitrarily divided into two categories: those which readily crystallise into highly ordered structures, and those that do not (Correale, Murthy and Minor, 2004). Diffractometer scans from the first class of polymers have well resolved crystalline peaks, and therefore, the scan can be fitted with an amorphous halo and crystalline peaks reliably and reproducibly over a wide range of crystallinities without imposing any special constraints in the least-squares procedure. Amorphous crystalline polymers have some benefits over semi-crystalline polymers in the context of GBR membranes as they are easier to thermoform. However, amorphous crystalline polymers contain hydrocarbons that make the material more sensitive to stress cracks and if used for periodontitis (Kroeze *et al.*, 2009; Djukic *et al.*, 2020), likely to suffer from mechanical wear. Furthermore, these polymers have less chemical resistance than semi-crystalline polymers, which would be a concern *in vivo* (Palomino-Durand, Pauthe and Gand, 2021).

4.2.6 Fourier Transform Infra-Red (FT-IR) analysis

FTIR experiments were conducted to investigate the chemical interactions between PLA and PCL in the Floreon membranes that manufactured by solvent casting and spin coating. Similar spectra were obtained for PLA membranes. Peak assignments for these polymers can be found in Figure 4-83 and Table 4-8.

As can be seen from the FTIR spectra, all membranes exhibit comparable patterns of vibrational peaks, such as the peak at 752 cm^{-1} associated with the α-methyl rocking vibration and the peak at 868 cm^{-1} related with the ester (O-CH-CH$_3$). the peak at about 1086 and 1182 cm^{-1} associated with the stretching vibration of C-O-C; the peak at around 1360 cm^{-1} associated with the CH symmetric bending vibration; and the peak at around 1450 cm^{-1} related with the CH$_3$ antisymmetric. The peak associated with the carbonyl C=O stretching vibration can be found at 1755 cm^{-1} as there was only one for PLA, while another appeared for Floreon at 1726 cm^{-1} due to the presence of PCL in its structure; the symmetric stretching vibration of CH$_3$ in saturated hydrocarbons can be found at 2943 cm^{-1}, and the antisymmetric stretching vibration can be detected at 2993 cm^{-1}.
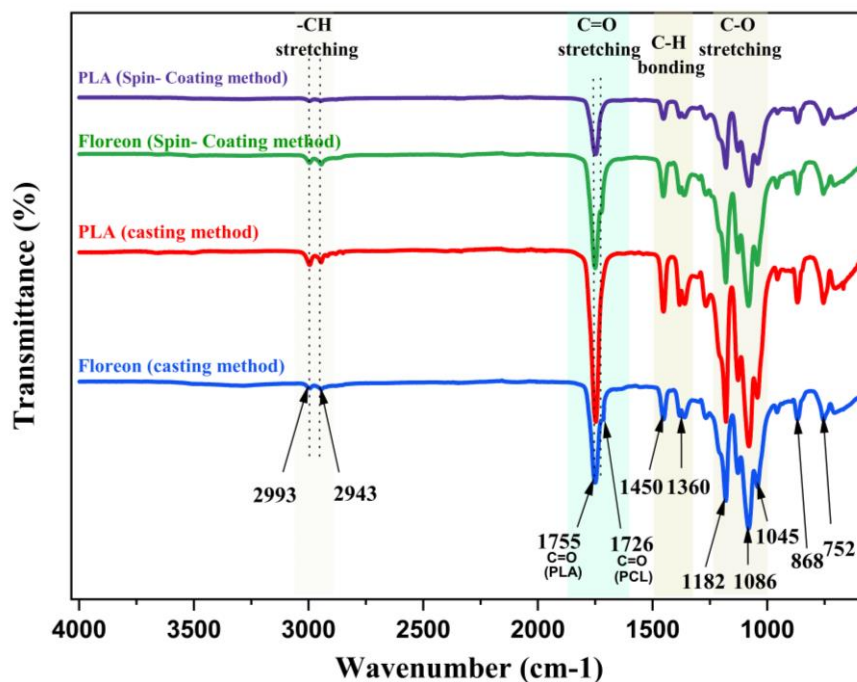
Figure 4-83 FTIR spectra of PLA and Floreon membranes prepared by solvent casting and spin-coating techniques.

Table 4-8 Assignments of spectral features identified from the FTIR spectra of PLA and Floreon membranes.

Wavenumber (cm-1)	Polymer	Assignment	Abbreviation
2993	PLA / Floreon	Asymmetrical stretching	$v_{as}(CH_2)$
2943		Symmetrical stretching	$v_s(CH_2)$
1755		Stretching	$v(O=C)$
1726	Floreon	Stretching	$v(O=C)$
1450	PLA / Floreon	Asymmetrical scissoring	$\delta_{as}(CH_3)$
1360		Symmetrical scissoring	$\delta_s(CH_3)$
1182		Asymmetrical stretching + twisting	$v_{as}(C–O) + \tau(CH_3)$
1086		Symmetrical stretching	$v_s(C–O–C)$
1045		Symmetrical stretching	$v_s(C\text{-}CH_3)$
868		Stretching	$v_s(C\text{-}COO)$
752		Rocking	$\rho(CH_2)$

All membranes showed the similar patterns of vibrational peaks except with the carbonyl C=O stretching vibration. It was found at 1755 cm^{-1} for PLA, and at 1726 cm^{-1} for Floreon due to the presence of PCL. Recently, Prajongtat et al., reported that the C=O stretching bands of PLA and PCL still appeared at the same wave numbers observed for pure PLA and pure PCL, and their intensities increased with increasing amounts of PLA and PCL in the membranes, respectively, implying that no chemical reaction occurred between PLA and PCL in the blended material and the structural properties of both polymers remained the same after blending (Prajongtat *et al.*, 2019). In this study, it was shown that there are no chemical changes in Floreon membranes, which were prepared by solvent casting and spin-coating methods.

4.2.7 Differential scanning calorimetry (DSC)

The differential scanning calorimeter (DSC) was used to evaluate the thermal behaviour of PLA-based membranes and Floreon-based films, and the results are presented in Figure 4-84 and Table 4-9 respectively.

Crystallisation temperatures of PLA were observed to be approximately 121 and 117°C for cast membranes and spin-coated membranes, respectively, which were slightly higher than those of Floreon-based membranes. The glass transition temperatures of the cast Floreon films were around 61°C, which was almost similar to those of the casted PLA films. In contrast to the spin-coated films, the PLA films had a higher Tg of 62.5 °C than the Floreon, which was found to have two peaks of Tg values at 59.2 and 61.4 °C.

All Floreon films were found to have melting temperatures between 149.6 and 151.1 °C, for cast and spin-coated films, respectively, whereas PLA films had melting temperatures between 148.6 and 149.2 °C, for spin-coated and cast films, respectively.
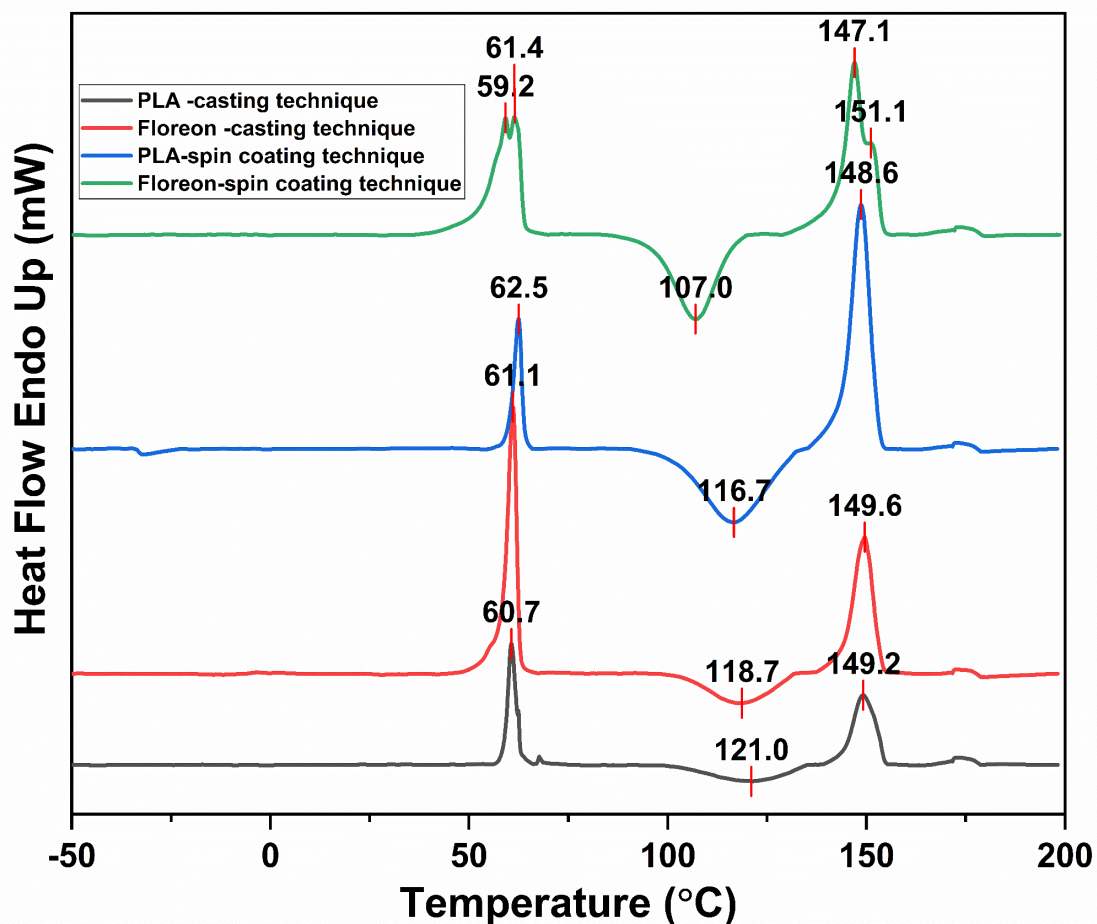
Figure 4-84 DSC thermograms of Spin-coated and solvent-casted membranes for PLA- based films (a) and Floreon- based films (b).

Table 4-9 DSC results for PLA and Floreon films fabricated using both techniques.

	Glass transition temperature (Tg) (°C)	Crystallisation temperature (Tc) (°C)	Melting temperature (Tm)(°C)
PLA (casting method)	60.7	121.0	149.2
Floreon (casting method)	61.1	118.7	149.6
PLA (spin-coating method)	62.5	116.7	148.6
Floreon (spin-coating method)	59.2 - 61.4	107.0	147.1 – 151.1

Note: Calculations were repeated for three sets of samples. The standard deviation for the Tc, Tg, and Tm values was less than 0.5 %.

The temperature shifts occurred as a result of the disruption of the composition and crystalline structure of Floreon compared to PLA. The reduction in the crystallisation and glass temperatures after the introduction of PCL into the structure of Floreon was reported in many studies (Dell'Erba *et al.*, 2001; Can *et al.*, 2011). The presence of PCL has been reported for the melt-blended PLLA/PCL samples in several other works (Dell'Erba *et al.*, 2001; Maglio *et al.*, 2004; Can *et al.*, 2011) and is attributed to the enhancement of PLLA melting temperature and crystallisation rate (by dynamic experiments), which likely occurs through the increase in nucleation rate (Dell'Erba *et al.*, 2001). Nauman et al. demonstrated a correlation between Tm and Young's modulus, a measure of the strength of atomic bonds, in a recent review. In general, a higher melting temperature corresponds with a greater modulus, and vice versa. They determined that the post-heat treatment of the films helps to improve their thermal properties, which in turn increases the Young's modulus (Nauman, Lubineau and Alharbi, 2021)

4.2.8 Thermogravimetric Analysis – TGA

Thermo-gravimetric analysis (TGA) is one of the most effective means of evaluating the thermal degradation performance and thermal stability of materials. The thermal stability of all membranes was studied via TGA and the derivative thermogravimetric (DTG).

Figure 4-85 depicts the TGA (a) and DTG (b) analysis of PLA and Floreon manufactured via solvent casting and spin coating. The TGA and DTG curves were used to determine the membranes' thermal properties, such as the initial weight loss temperature (T_i), at which 5% of the membranes' weight is degraded, and the temperature of maximum thermal degradation rate (T_{max}). As can be seen in Figure 4-85 , the cast PLA membrane started degrading at 340.9°C and had maximum degradation at 371.1°C. in contrast, the Floreon cast-film exhibited a different thermal behaviour, with a beginning 5% weight loss temperature of 328.0°C and a maximum thermal degradation temperature of 359.8°C, indicating that the Floreon membranes are more stable under heat.

The same response was observed throughout the spin-coated films. The degradation of PLA and Floreon began at 338.0°C and 326.8°C, respectively, and hit its peak at 365.9°C and 361.6°C. In both the PLA and Floreon manufacturing methods, the residual mass of the PLA films was greater than that of the Floreon films.
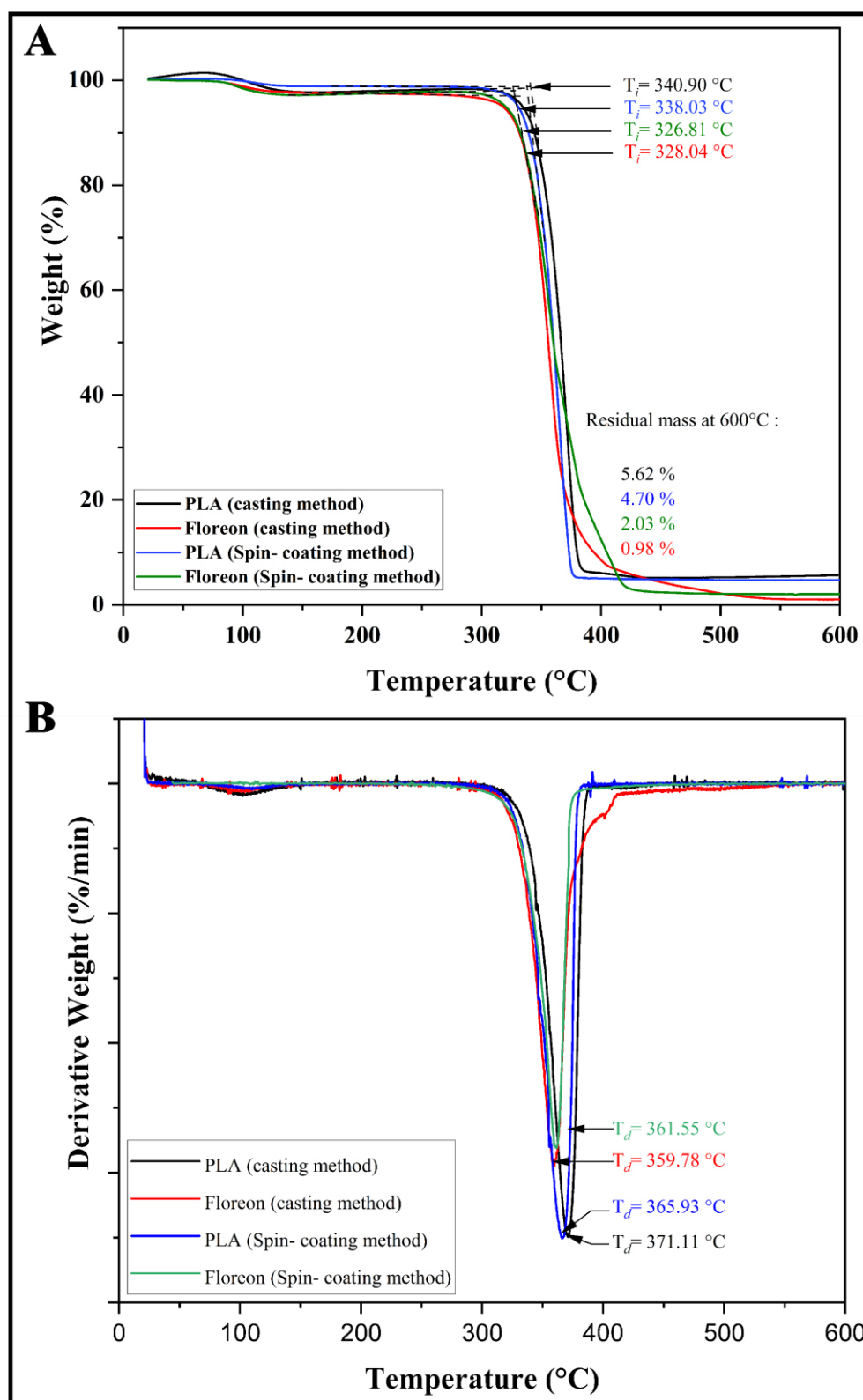
Figure 4-85 TGA and DTG data for pure PLA and Floreon prepared via solvent casting (a) and spin coating (b) techniques.

In both the PLA and Floreon manufacturing methods, the residual mass of the PLA films were greater than that of the Floreon films. Previous research has indicated that optimal thermal stability for membranes is achieved at a PCL concentration of 60%. Notably, pure PLA membranes (0% PCL) exhibit a single-step decomposition (Tmax), while those made from pure PCL exhibit multi-step decomposition (Hoidy et al., 2010). However, this study found that Floreon is thermally more stable than PLA, which has the potential to be beneficial in the context of manufacturing processes.

4.2.9 Wettability of thin membranes

Polymer surfaces were assessed to determine surface wettability, and hydrophobic / hydrophilic characteristics, by measuring the water contact angle. Figure 4-86 and Figure 4-87 show the water contact angles recorded for spin-coated and solvent-cast membranes for PLA and Floreon- based films

Overall, Spin-coated films had a lower water contact angle, compared to solvent-casted membranes, indicating a more hydrophilic nature and higher wettability. solvent-casted PLA, solvent-casted Floreon, Spin-coated PLA and Spin-coated Floreon all recorded water contact angles below 90° indicating that all the polymers were hydrophilic. Water contact angles of solvent-casted film for PLA and Floreon- based films were 78.4° ± 0.2SD and 69.9° ± 1.7SD, compared to Spin-coated film for PLA and Floreon- based films, which were 68.5° ± 2.1SD and 57.0° ± 1.3SD respectively. Although Spin-coated films were hydrophilic, and had higher surface wettability, no significant difference was detected between PLA and Floreon.
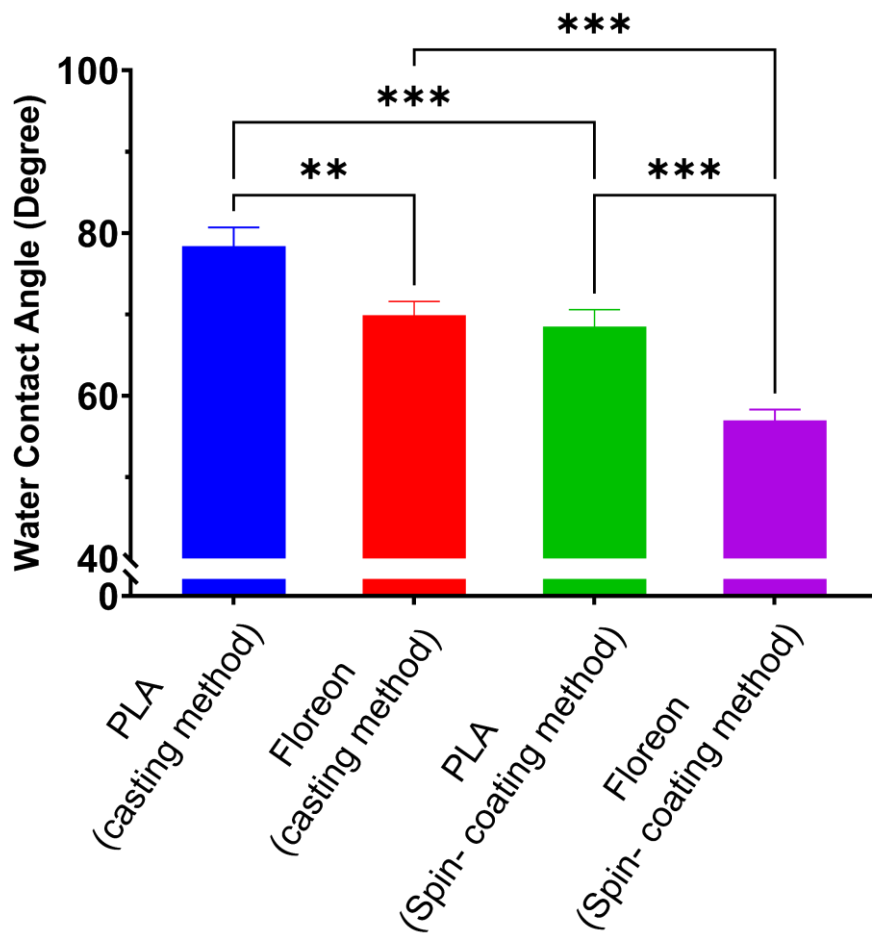
Figure 4-86 Water contact angle measurement of Spin-coated and solvent-casted membranes for PLA and Floreon- based films. Data represented n=3, mean ± STDV following One-way ANOVA statistical analysis with Tukey comparison test. **** $p < 0.0001$, *** $p < 0.001$, ** $p < 0.01$, * $p < 0.05$.
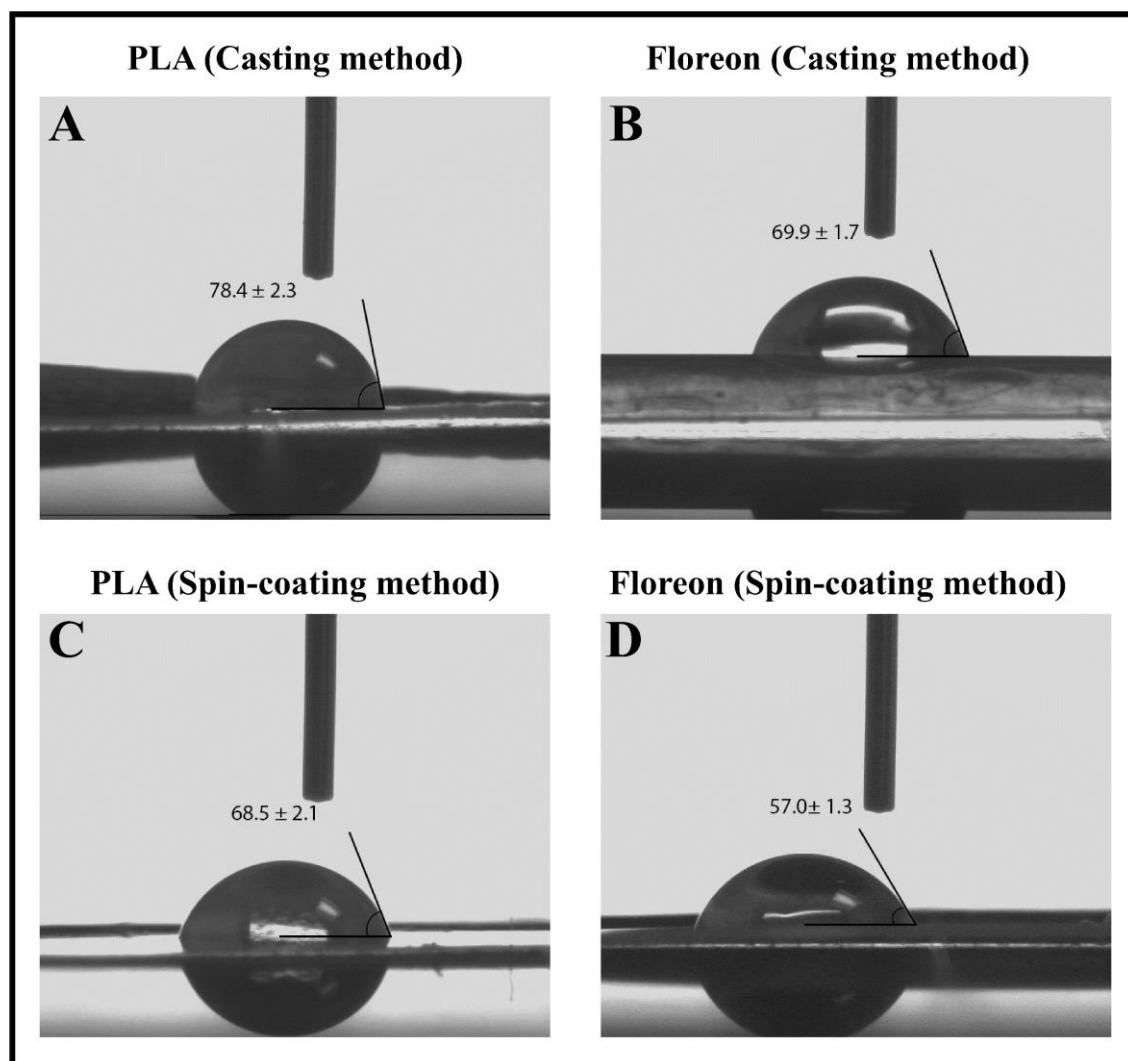
Figure 4-87 The water contact angle photos of the cast PLA (a) and Floreon (b) membranes and the spin-coated PLA (c) and Floreon (d) membranes.

By measuring the water contact angle, polymer surfaces were evaluated to determine their surface wettability and hydrophobic/hydrophilic properties. In general, compared to solvent-casted membranes, spin-coated films showed a lower water contact angle, indicating a more hydrophilic nature and high wettability. All four types of polymers—solvent-cast PLA, solvent-cast Floreon, spin-coated PLA, and spin-coated Floreon—recorded water contact angles that were less than 90 degrees, showing that they were all hydrophilic. The water contact angles for spin-coated and solvent-cast membranes for PLA and Floreon-based films are shown in Figure 4-86and Figure 4-87. Floreon was more hydrophilic than PLA and the reason for this was because of changes in the chemical structure and Mw (Masutani and Kimura, 2014).

Floreon is made specifically for the engineering of bone tissue. The PCL in Floreon is a biodegradable polyester (others include PGA and PLLA), with a glass transition temperature of 60 °C and melting temperatures between 59 and 64 °C (above body temperature). Thus, the semi-crystalline PCL achieves a rubbery state at physiological temperature, giving it its high toughness and good mechanical characteristics (high strength, elasticity depending on its molecular weight) (Bezwada *et al.*, 1995).

4.2.10 Mechanical characterisation of Thin Membranes

Mechanical Tension tests were performed on spin-coated and solvent-cast membranes prepared by PLA and Floreon, and the resulting values are shown in Table 4-10 and Figure 4-88.

According to the data, Floreon samples have a higher ultimate tensile strength than PLA films. This was seen with both preparation methods. The spin-coated Floreon membrane has the highest stress value of all membranes at 2.491 MPa, followed by the cast Floreon membrane at 1.700 MPa, followed by the spin-coated and cast PLA membranes with stress values of 1.487 and 1.200 MPa, respectively. Although the PLA films exhibited slightly greater elongation than the Floreon films, the stiffness of the Floreon films was more than twice that of PLA, regardless of the manufacturing method used. In conclusion, Floreon has ideal mechanical properties when compared to PLA, which makes it a promising material for medical applications,specifically for bone tissue engineering.

Table 4-10 Tensile properties of Spin-coated and solvent-casted membranes prepared by PLA and Floreon. To calculate the Ultimate tensile strength (MPa), Stiffness (MPa) and Elongation at break (%), Values shown are mean ± SD where n=6.

Membranes	Ultimate Tensile Strength (MPa)		Stiffness (MPa)		Percent Elongation (%)	
	Mean	SD	Mean	SD	Mean	SD
PLA (casting method)	1.20	0.14	47.59	5.71	9.06	1.09
Floreon (Casting method)	1.70	0.17	75.93	7.39	8.49	0.83
PLA (Spin- coating method)	1.49	0.19	52.88	6.79	14.64	1.88
Floreon (Spin- coating method)	2.49	0.24	93.13	9.03	13.52	1.31
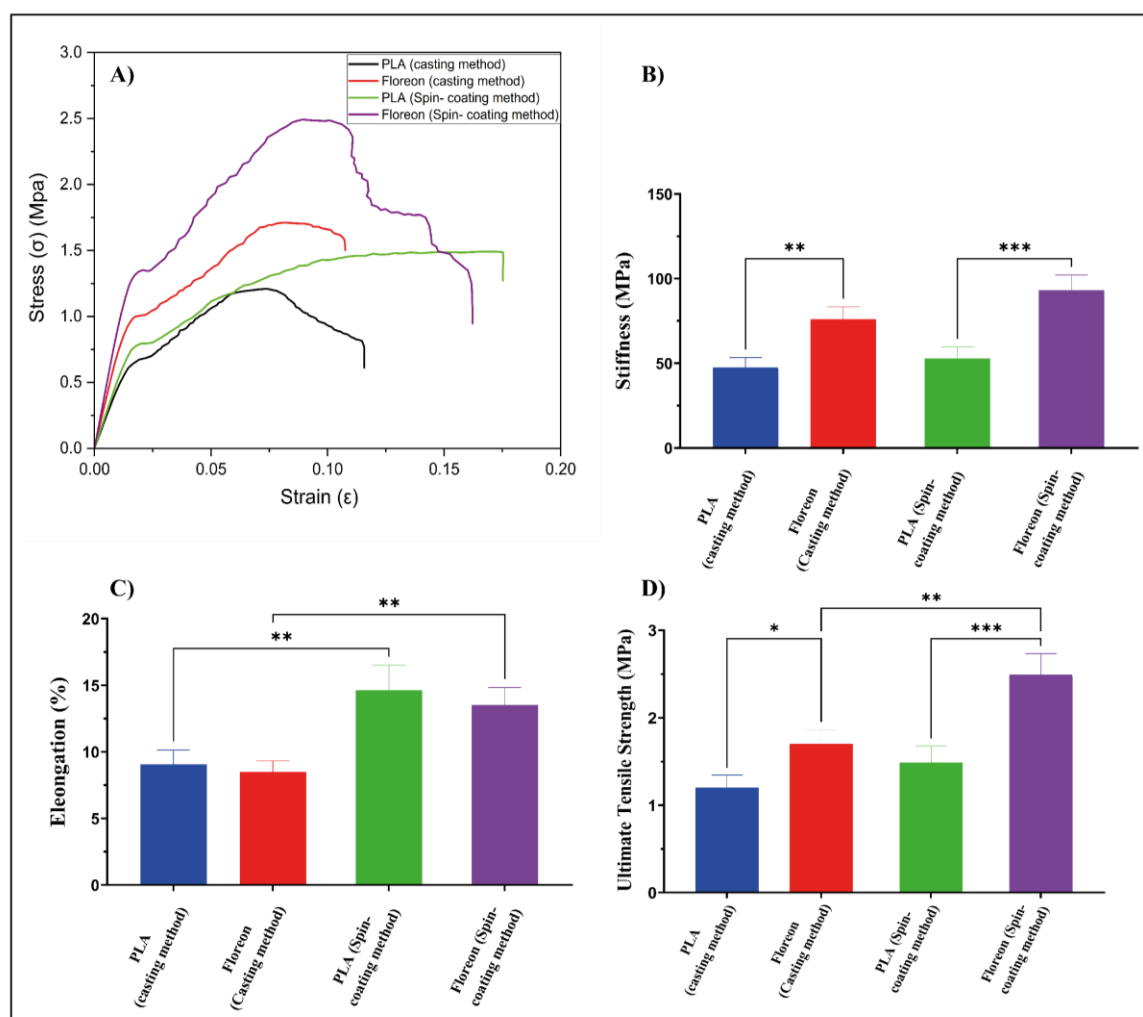
Figure 4-88 Stress strain Curve(A); Stiffness (B); Percent Elongation (C); and Ultimate tensile strength (UTS) (D) of various membranes prepared by Spin-coating and solvent-casting techniques. Data represented n=6, mean ± STDV following One-way ANOVA statistical analysis with Tukey comparison test. **** $p < 0.0001$, *** $p < 0.001$, ** $p < 0.01$, * $p < 0.05$.

The mechanical properties of spin-coated and solvent-coated membranes composed of Pure PLA and PLA/PCL blend (Floreon) were evaluated to assess their suitability for bone tissue engineering. The study revealed that spin-coated PLA and Floreon membranes exhibited superior mechanical performance compared to the cast PLA/Floreon membranes. Specifically, spin-coated membranes demonstrated higher stiffness, ultimate tensile strength, and elongation percentage compared to their cast counterparts. However, there was no significant difference in the elongation percentage between the Floreon and PLA regardless of the fabrication method used. It was observed that the porosity and pore area of these membranes had significant influence on the tensile mechanical properties. As have been mentioned before that the spin coated films have lower total pore area than those of cast membranes and the spin coated Floreon films showed with the lowest pore area (see section 4.2.4).

Similar findings were found in other investigations (Sawalha, Schroën and Boom, 2008; Aouadja *et al.*, 2022). They discovered that the tensile and fatigue properties are the main mechanical behaviours impacted by porosity formation. The elastic modulus, yield strength, ultimate tensile strength, and ductility are all greatly impacted by the creation of pores. It has been discovered that pore size and open porosity are related to a material's strength (Aouadja *et al.*, 2022).

While PLA is a promising material for biomedical applications, it exhibits weak durability. Recent research suggests that incorporating PCL into PLA can improve the impact strength of the resulting blend beyond that of the individual components. The results are shown in Figure 4-88 and Table 4-10. Several studies reported that the mechanical properties of PLA can be tuned from rigid to ductile by the addition of PCL (Tsuji and Ikada, 1998; Jelcic, Holjevac-Grguric and Rek, 2005; Yeh *et al.*, 2009). In conclusion, Floreon is a promising material for medical applications because it has better mechanical qualities than PLA.

4.2.11   *In-vitro*-degradation and bioactivity studies of thin film

4.2.11.1 *In-vitro* degradation analysis

- **Weight profile analysis**

Figure 4-89 shows the trend in the percentage weight remaining of Floreon and PLA membranes made by solvent casting and spin-coating for up to 24 weeks. Table 0-4 -Appendix provides levels of significance for differences in remaining weight between samples created by different methods.

Stable membrane profiles may be seen up to week 8 for PLA and Floreon membranes with both approaches, with no notable difference. Between the 16th and 24th week, the residual weight percent of spin-coated and cast Floreon films falls, with a total weight remaining of between 73 and 77% after the study period. When comparing the two methods of fabricating the Floreon membrane, no significant differences could be identified.
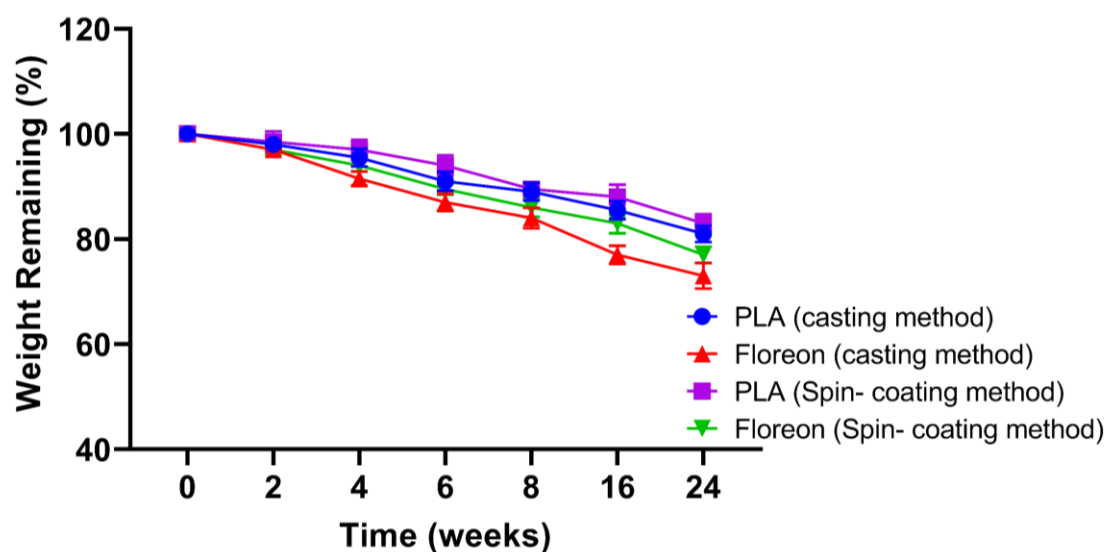
Figure 4-89 Weight loss profile of PLA and Floreon films fabricated using both techniques during 24 weeks of immersion in SBF.

Both fabrication methods and polymeric materials had a greater effect on the weight loss behaviour. Overall, the weight loss effect of the casting method was much higher than that of spin coating method, which correlates with other published studies (Hosseini, Ghaderi and Gómez-Guillén, 2021). A possible reason for these findings could be weak solvent–solute

interaction caused by the both solvent-casting and spin-coating methods techniques (Zhang *et al.*, 2016).

During 16th to 24th week, weight reduced more rapidly. But the decrease in weight was the same for Floreon and PLA. The rate of hydrolysis depends on factors such as the size, the monomer composition and degree of crystallinity of the polymer (Laycock, B., Nikolić, M., Colwell, J.M., Gauthier, E., Halley, P., Bottle, S. and George, 2017). For instance, non-porous structures undergo degradation more rapidly than porous ones, because the latter facilitate dissolving and spread of the degradation products throughout the aqueous medium, thus discouraging self-catalysis behaviour (Payne, McKeown and Jones, 2019). This decrease in weight was due to the breakage of ester linkages. Water molecules attack the ester linkages, breaking long polymer backbone chains into shorter ones (Onuma and Serruys, 2011). Ester linkage cleaving by hydrolysis results in hydroxyl and carboxylic acid groups formation, resulting in a decrease in the polymer molecular weight (MW) (Zan *et al.*, 2022). Because the ester linkages are cleaved randomly along the polymer backbone, relatively few water-soluble fragments form initially (Onuma and Serruys, 2011). The reduction in molecular weight produces an increase in hydrophilicity but not necessarily changes in physical properties or mass (Laycock, B., Nikolić, M., Colwell, J.M., Gauthier, E., Halley, P., Bottle, S. and George, 2017).

Molecular weight was also monitored as a function of incubation time in SBF. In general, a bulk degradation process occurs for Floreon, PLA, and their copolymers: polymer molecular weight decreases due to the hydrolysis of polymer ester bonds, forming shorter polymer chains (Luo and Zhou, 2022). When the size of the polymer fragments becomes small enough so that scaffold mechanical properties are significantly decreased, scaffold collapses and degradation products are released. This behaviour was in agreement with total weight data, which showed that both total weights slightly decreased as a function of degradation time.

- **Water uptake analysis**

Figure 4-90 shows the trend in the water uptake of Floreon and PLA membranes made by solvent casting and spin-coating for up to 24 weeks. Table 0-5-Appendix provides levels of significance for differences in water uptake between samples created by different methods.

As for the water absorption rate, the change in chemical composition of Floreon led to a considerable rise in the water absorption rate, which was found between weeks 8 and 24 in the various used manufacturing techniques. When comparing the two methods of fabricating the Floreon membrane, no significant differences could be identified.
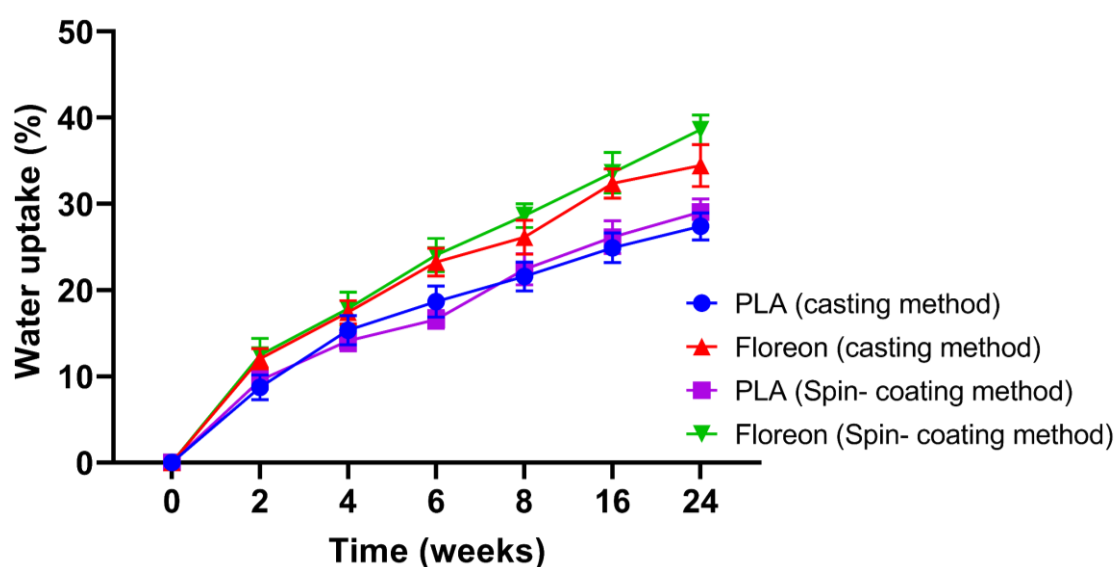
Figure 4-90 Water uptake of PLA and Floreon films fabricated using both techniques during 24 weeks of immersion in SBF.

Spin coating technique was more effective for water uptake of Floreon films. In the start, the effect of the spin coating method was low but it became more effective later as compared to solvent casting method. for PLA films. Overall, Floreon films absorb more water as compared to PLA films. Similar results were found in Lunkong studies (Lukong, Ukoba and Jen, 2022). The reduction in molecular weight produces an increase in hydrophilicity but not necessarily changes in physical properties or mass (Laycock, B., Nikolić, M., Colwell, J.M., Gauthier, E., Halley, P., Bottle, S. and George, 2017). The rate of hydrolysis depends on factors such as the size, the monomer composition and degree of crystallinity of the polymer (Laycock, B., Nikolić, M., Colwell, J.M., Gauthier, E., Halley, P., Bottle, S. and George, 2017). For

instance, non-porous structures undergo degradation more rapidly than porous ones, because the latter facilitate dissolving and spread of the degradation products throughout the aqueous medium, thus discouraging self-catalysis behaviour (Odelius *et al.*, 2011).

- **FTIR analysis**

Figure 4-91 to Figure 4-94 show FTIR spectra obtained from non-degraded (week 0) and degraded (12th and 24th week) Floreon and PLA membranes produced by solvent casting and spin-coating. In the previous section, Table 4-4 summarised the spectral features identified from the FTIR spectra of the membranes and the assignments of the observed peaks.

The peaks are shown to have changed throughout time. Particularly, in week 0 two small peaks appear at 2995 and 2944 cm-1, which belong to a CH bond in a PLA monomer, were employed for internal normalisation, these peaks disappear in case of week 12 and week 24, peak at 1749 represent –C=O– carbonyl linkage in ester, this peak is strong in week 0 but it is medium in other weeks, small peaks at 1452 and two peaks at 1360 and 1382 corresponds to −CH− deformation (including sym and asym bend), Peaks at 1268, 1180, 1129, 1080, and 1043 are due to −C−O− stretch. A small peak at 868 represents −C−C− stretch, peak around 755 corresponds to –CH2− groups. Before immersion in SBF (week 0), the intensity of all these peaks was at its highest. However, in weeks 12 and 24, their intensity decreased.

Figure 4-91 FTIR spectroscopy of cast PLA membrane at week 0, 12 and 24 of immersion in SBF.
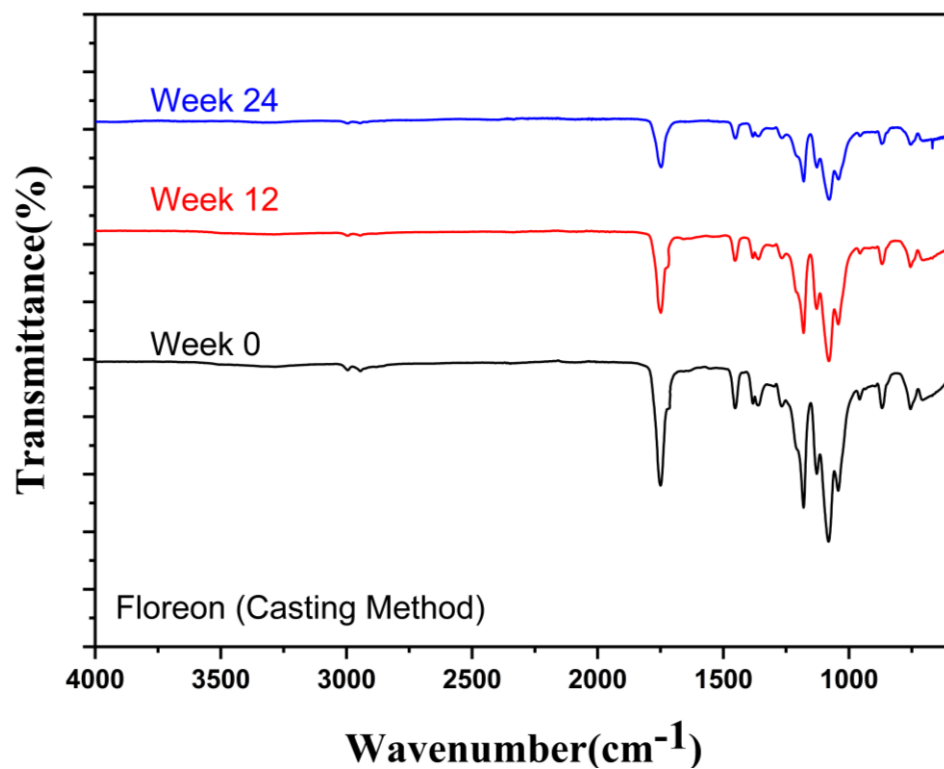
Figure 4-92 FTIR spectroscopy of cast Floreon membrane at week 0, 12 and 24 of immersion in SBF.
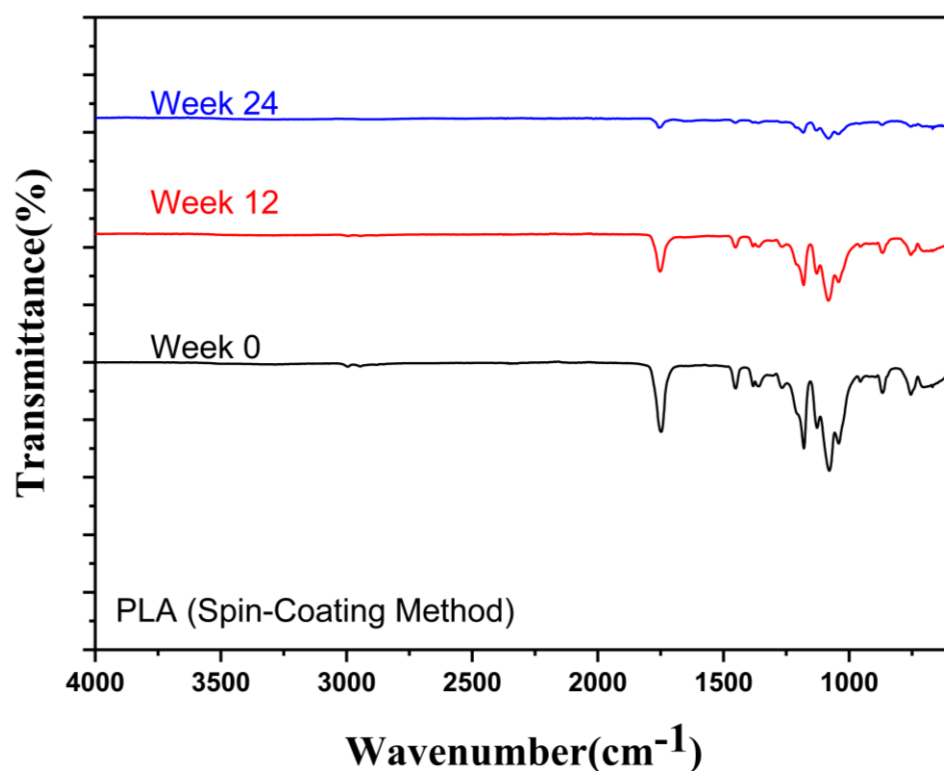
Figure 4-93 FTIR spectroscopy of spin-coated PLA membrane at week 0, 12 and 24 of immersion in SBF.
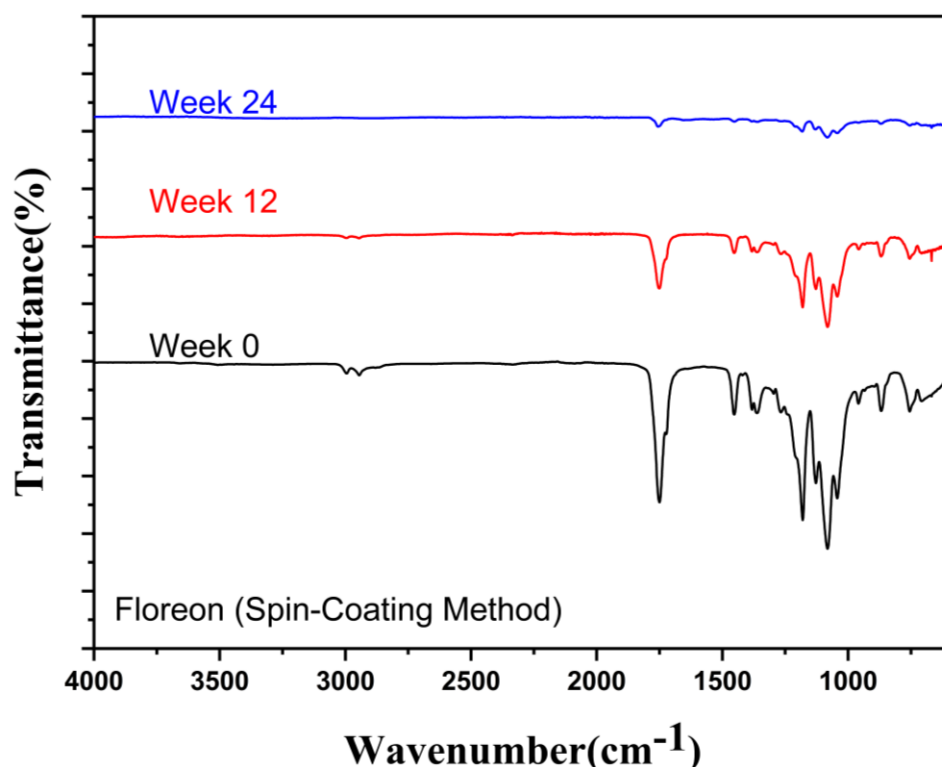
Figure 4-94 FTIR spectroscopy of spin-coated Floreon membrane at week 0, 12 and 24 of immersion in SBF.

The peaks are shown to decrease in intensity as the materials degrade overall time due to the breakdown of the crosslinks in the polymeric used in this study. Lee *et al.* have demonstrated that under acidic conditions, asymmetric stretching of O=C–ONa groups can occur, which is consistent with the band observed at 1610 cm−1 in the FTIR analysis of this study (Li *et al.*, 2021).

Particularly, in week 0 two small peaks appear at 2995 and 2944 cm-1, which belong to a CH bond in a PLA monomer, were employed for internal normalisation, these peaks disappear in case of week 12 and week 24, peak at 1749 represent –C=O− carbonyl linkage in ester, this peak is strong in week 0 but it is medium in other weeks, small peaks at 1452 and two peaks at 1360 and 1382 corresponds to −CH− deformation (including symmetric and asymmetric bend), peaks at 1268, 1180, 1129, 1080, and 1043 are due to −C−O− stretch. A small peak at 868 represents −C−C− stretch, peak around 755 corresponds to –CH2− groups. Before immersion in SBF (week 0), the intensity of all these peaks was at its highest. However, in weeks 12 and 24, their intensity decreases.

The ester bond was confirmed by the presence of absorption bands in the 1044-1184 cm-1 interval region, assigned to the C–O–C ether group stretching. Finally, the bands at

approximately 865 cm^{-1} arose from the stretching vibration of the C-C bond (Curvello, Raghuwanshi and Garnier, 2019). Characteristic peaks of polyesters could be observed in all the analysed samples, namely, the strong absorption band at about 1750 cm^{-1} attributed to the stretching vibration of C=O bond and the absorption bands in the 1000-1184 cm^{-1} interval region related to the ester bond (C–O– C ether group stretching) (Zhu *et al.*, 2012). Moreover, similar results were explained by Peers and colleagues, where a peak between 3400 cm^{-1} and 3600 cm^{-1} appeared attributed to the presence of terminal –OH groups and to an increased amount of absorbed water (Peers, Montembault and Ladavière, 2020). However, the typical absorption band of CHS sulfonate groups (S=O stretching at around 1230 cm^{-1}) was not detected in FTIR-ATR spectra of LbL coated Blend samples, as it was masked by the intense C=O bending and C-O-C stretching bands of polymers, in the 1300-1000 cm^{-1} wavenumber region (Bomkamp *et al.*, 2022). FTIR-ATR results suggested that multilayer deposition of CHS and CH polyelectrolytes on aminolysed samples was successful peak at 1025 cm^{-1} was due to δ3 of phosphate mode, a peak at 940 cm^{-1} corresponded to δ1 of phosphate and band at 853 cm^{-1} was attributed to P-OH stretching vibration. The observed peaks in this study were found to partially overlap with the typical absorption bands of DSP, as reported by Dejob *et al.* (2022). While these findings provide some validation for the peaks observed during the degradation experiments, they also suggest that the membrane is prone to structural changes. It is important to note that when considering the use of the membrane *in vivo*, the dynamic microenvironment, which is subject to changes depending on cell behaviour, must be taken into account. Additionally, the oral environment, which contains salivary enzymes that were not tested in this study, presents a unique set of challenges and should be considered in future research (Rai *et al.*, 2012).

- **DSC analysis**

The thermal behaviours of non-degraded (week 0) and degraded (12th and 24th week) Floreon and PLA membranes produced by solvent casting and spin-coating were evaluated by DSC, as illustrated in Figure 4-95 to Figure 4-98 and Table 4-11. It can be seen that the thermodynamic properties, including Tg, Tc, and Tm, of the films immersed in SBF exhibited temporal changes. The Tc of the films gradually decreased, while Tg and Tm increased with the emergence of new peaks. Moreover, the intensity of the peaks increased over time, as observed for all peaks.

Table 4-11 Thermal properties of PLA and Floreon films made using both processes during 0, 12, and 24 weeks of immersion in SBF.

Samples	Week	(Tg) (°C)	(Tc) (°C)	(Tm₁) (°C)	(Tm₂) (°C)
PLA (casting method)	0	60.7	121	149.2	-
	12	63.2	108.2	146.7	153.3
	24	64.7	104.7	146.1	153.5
Floreon (Casting method	0	61.1	118.7	149.6	-
	12	63.7	107	146	152.7
	24	63.7	103	145.6	153
PLA (Spin- coating method)	0	62.5	116.7	148.6	-
	12	64.1	108.7	146.7	153
	24	64.9	104.9	146	153.3
Floreon (Spin- coating method)	0	60.9	107.0	147	151
	12	62.4	91.3	151	-
	24	61.8	89.4	151.2	-
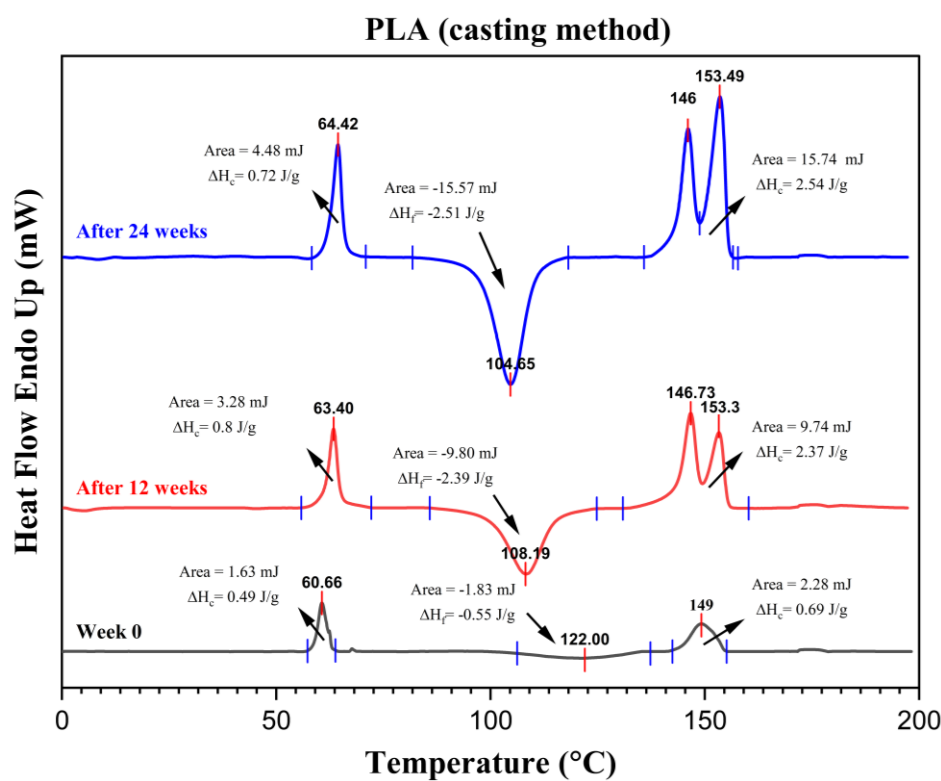
Figure 4-95 DSC thermogram of cast PLA membrane at week 0, 12 and 24 of immersion in SBF.
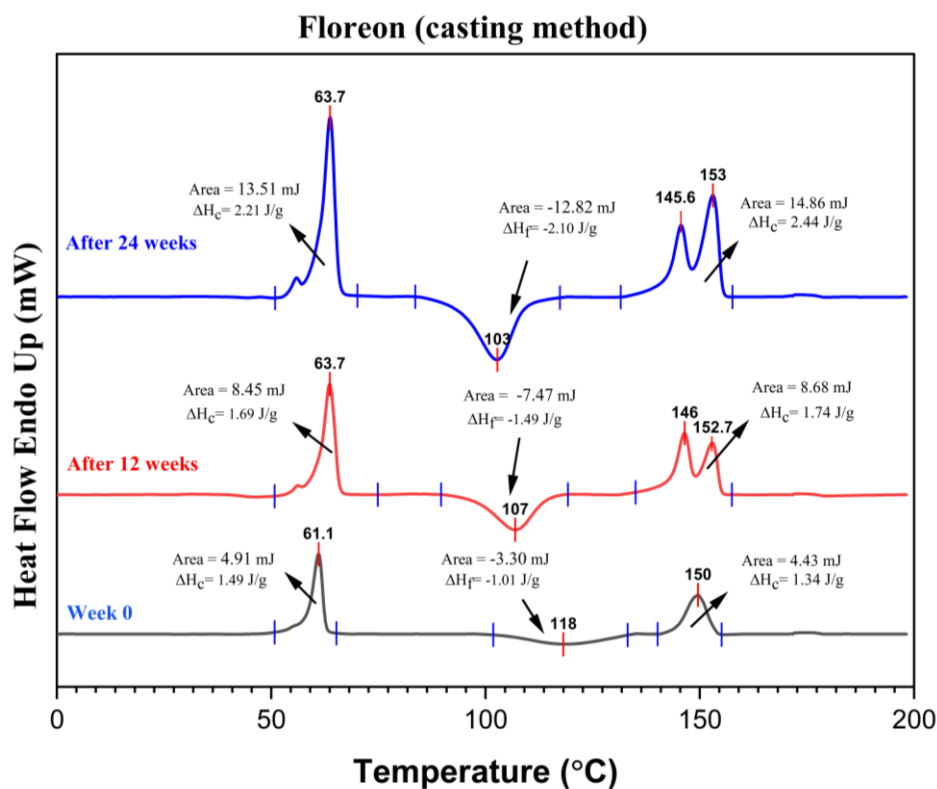
Figure 4-96 DSC thermogram of cast Floreon membrane at week 0, 12 and 24 of immersion in SBF.
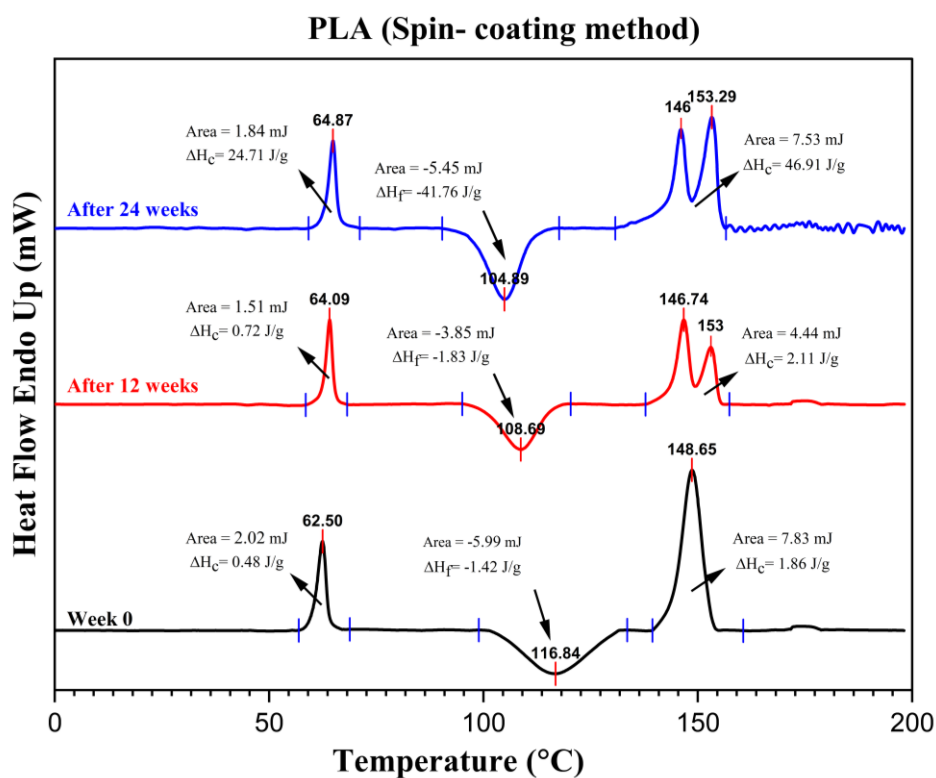
Figure 4-97 DSC thermogram of spin-coated PLA membrane at week 0, 12 and 24 of immersion in SBF.

Figure 4-98 DSC thermogram of spin-coated Floreon membrane at week 0, 12 and 24 of immersion in SBF.

In this study, both Floreon and PLA exhibited a rise in Tc temperature using both techniques, while Tm and Tg decreased in all films using both methods. However, the spin-coating technique increased Tm1. These changes led to softening and loss of film shape. It is noticeable that the peak's intensity increased with immersion time for all peaks. Polymer glass transition temperature is a function of different parameters among which the polymer molecular weight. It is a reversible step change in molecular mobility, from a rigid glassy state to a mobile rubbery state. This change is linked to the free volume associated with the polymer chain ends. When the molecular weight decreases, more chain ends are present and more free volume is generated. The polymer chains have, therefore, more space to move and the rubbery state is reached earlier, ie, at a lower temperature (Li et al., 2021). In the context of using the membrane in vivo, as the weight decreases (through degradation), the membrane becomes more flexible and likely to become irregular. Whether this is important depends on how long the membrane is required to remain stable, which could depend on the amount of GBM required. In terms of GBM, once cells have established themselves through early proliferation, the scaffold may become redundant in which case, deformity of the membrane may not have effect, but this needs further elucidation.

264

- **Optical Images**

Figure 4-99 illustrates optical images of PLA and Floreon membranes captured at each time point from week 0 to week 24. It can be seen that the Floreon membranes have a tendency to curl up.
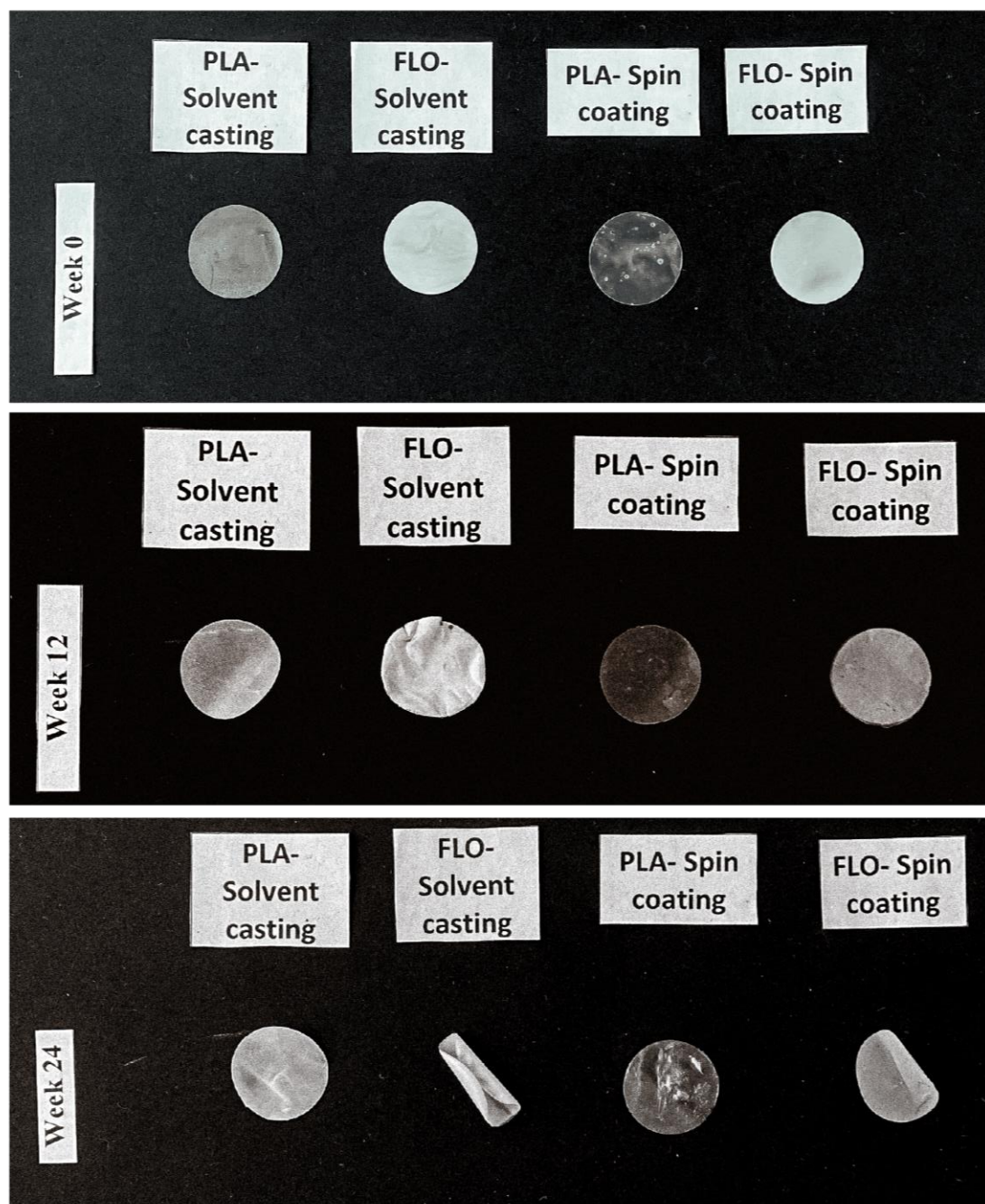
Figure 4-99 Optical Images of Floreon and PLA membranes produced by solvent casting and spin-coating after degradation study at week 0, 12 and 24. Samples were selected out of three at each time point.

265

Optical Images Figure 4-99 illustrates optical images of PLA and Floreon membranes captured at each time point from week 0 to week 24. During week 0, very little or no effect was seen in both PLA and Floreon films. In this week both techniques were not affected for both films and did not curl any film. During the 12th week, PLA films show little curling as compared to Floreon films. The solvent casting technique shows more curling in PLA films as compared to the Floreon films. Also spin coating was more effective for PLA films than that of Floreon films.

During the 24th week, it can be seen that the Floreon membranes have a tendency to curl up. The comparative analysis of both techniques revealed that Floreon films demonstrated more curling than PLA films. Additionally, when evaluating the effectiveness of the two techniques for a specific film, it became apparent that solvent casting was more effective than spin coating. This can be attributed to the random cleavage of ester linkages along the polymer backbone, which leads to the initial formation of relatively few water-soluble fragments (Onuma and Serruys, 2011). The reduction in molecular weight produces an increase in hydrophilicity but not necessarily changes in physical properties or mass (Laycock, B., Nikolić, M., Colwell, J.M., Gauthier, E., Halley, P., Bottle, S. and George, 2017). Although not explicitly shown by FTIR, breakage of ester bonds is likely the reason for curling of Floreon membranes.

4.2.11.2 Bioactivity analysis

- **Scanning electron microscopy**

Figure 4-100 displays the SEM images of Floreon and PLA membranes fabricated through solvent casting and spin-coating methods after 0, 12, and 24 weeks of immersion in SBF. The absence of apatite formation on the immersed films was noted, even after 24 weeks. Nevertheless, the findings revealed that the degradation duration significantly influenced pore sizes and porosities of the scaffolds. In this investigation, Floreon scaffolds created using both techniques exhibited higher porosity and more uniform pore distribution compared to PLA scaffolds.
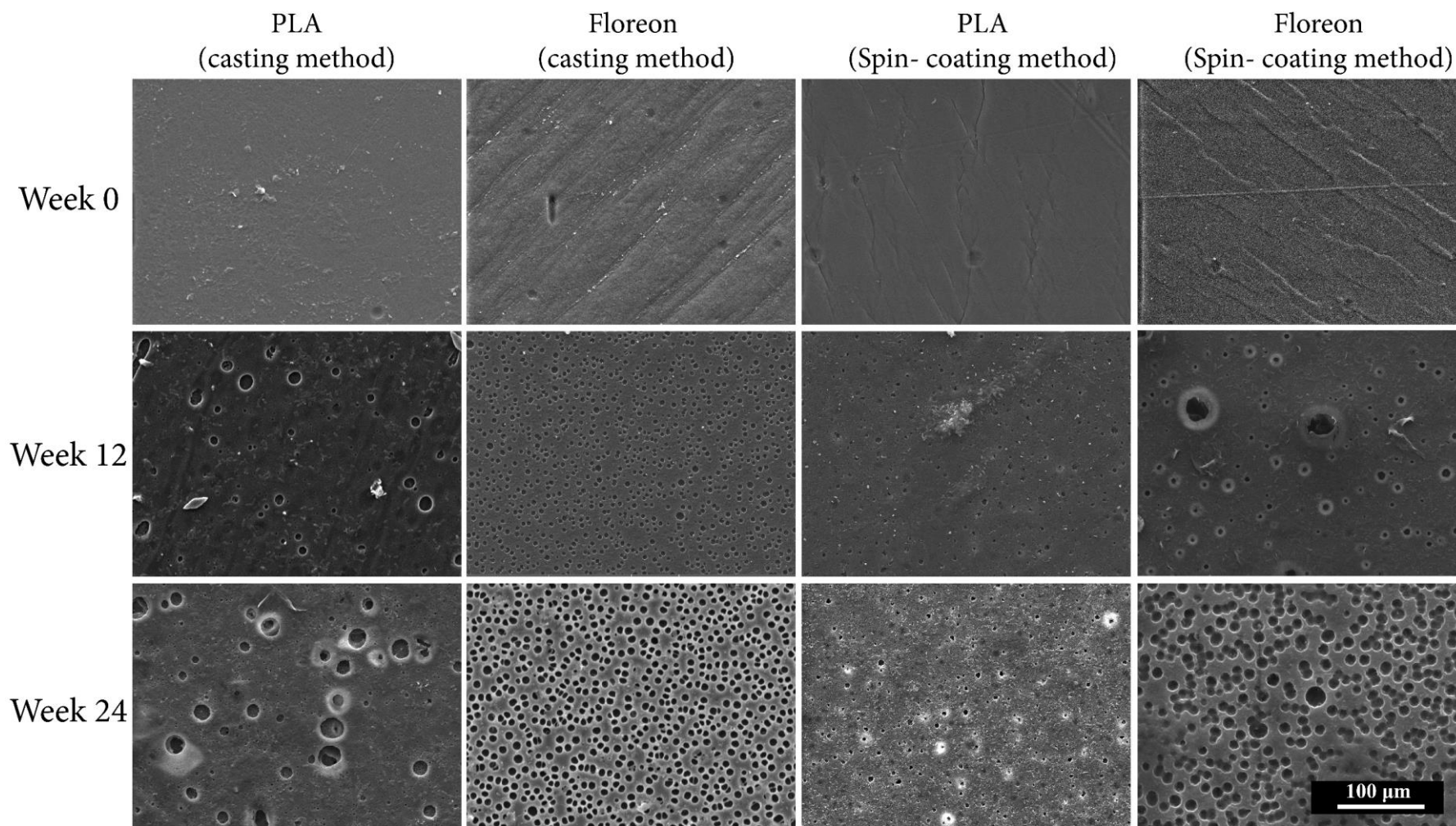
Figure 4-100 SEM images of Floreon and PLA membranes fabricated by solvent casting and spin-coating techniques at weeks 0. 12 and 24 of immersion in SBF. All images were scaled at 100 μm.

SEM analysis was conducted on porous membrane surfaces to assess the influence of composition and cross-linking on sample morphology. At week 0, no notable difference was observed between Floreon and PLA films regarding degradation. However, as the weeks progressed, the solvent-casting approach resulted in more pronounced degradation of Floreon films in comparison to PLA films. Furthermore, the spin-coating method also caused more degradation in Floreon films than in PLA films, indicating a more substantial impact of solvent-casting compared to spin-coating. Floreon films exhibited larger pore sizes and increased surface degradation. During the 12th week, PLA-casting films showed lowest pores but the diameter of pore was greater as compared to the Floreon-casting films. But PLA-spin coated films showed more pores with small pore size as compared to the Floreon spin-coated films. Similar results were seen during the 24th week but the number of pores and pore size were increased. The physical characteristics of a scaffold can be described as porosity (Yuan, Ding and Wen, 2019). Pore interconnectivity was required for access to nutrients and transport of waste products (Kim et al., 2021). Spin-coating techniques and casting techniques caused surfaces to degrade and become rough, breaking ester bonds thus, causing more porosity and greater pore size with time (Koh, Zhang and He, 2018).

- **pH analysis**

The Change in the pH levels of SBF containing the Floreon and PLA films were tracked before and during the 24 weeks of incubation at 37°C, and these results are illustrated in Figure 4-101. Table 0-6 - Appendix provides levels of significance for differences in pH levels between samples created by different methods. The initial pH of the SBF was 7.40, however, it decreased over time. During the 24-week incubation period, the pH of the SBF containing the Floreon films changed minimally, maintaining a neutral pH. After 24 weeks, the pH of PLA sheets made using both production methods had the lowest pH at around 6.45. However, the spin-coated Floreon film had the greatest pH, at $6.61 \pm 0.02SD$.
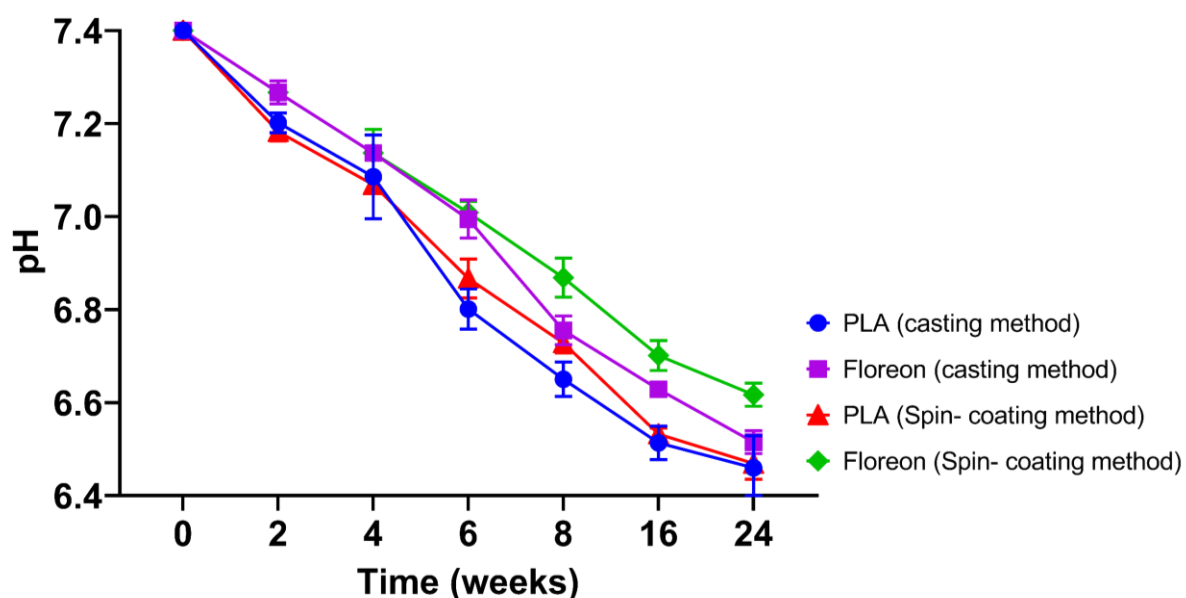
Figure 4-101 Change in pH of Floreon and PLA films fabricated by solvent casting and spin-coating techniques incubated for 24 weeks in SBF.

The change in the pH levels of SBF containing the Floreon and PLA films were tracked before and during the 24 weeks of incubation at 37°C, and these results are illustrated in Figure 4-101. The initial pH of the SBF was 7.40, however, the pH decreased over time. During the 24-week incubation period, the pH of the SBF containing the Floreon films changed minimally, maintaining a neutral pH. After 24 weeks, the pH of PLA sheets made using both production methods had the lowest pH at around 6.45. This alternate change in pH was also reported in other work in the literature (Yang et al., 2021). As degradation time increases, the Mw decrease leads to a reduction in physical properties and the formation of water-soluble fragments that decrease local pH. These water-soluble fragments diffuse away from the polymer and are ultimately hydrolysed to lactic acid, which are processed through normal metabolic pathways.

4.2.12   *In vitro* **Biocompatibility**

4.2.12.1 Cell Migration

The scratch-wound assay was used to assess the basic variables of cell migration, including speed, durability, and polarity. The wound size was measured using Image J, where at the start point (0-hour), it was around 1165.5 mm^2. The wound closure rate was measured at different times using time-lapse imaging produced using a light microscope. For each type of scaffold, three samples were tested, and each sample was measured three times. The specifics of this examination procedure were already outlined in Section 3.4.9.1.

A comparison of the scratch healing rate on NOFs in the presence of cast or spin-coated films was carried out and is presented in Figure 4-102 and Figure 4-103. The results reveal that the healing rate during the first 12 and 24 hours was comparable across all samples, and was similar to that of the negative control. However, a slight difference was observed between Floreon and PLA films on the third day of incubation, irrespective of their method of manufacture.
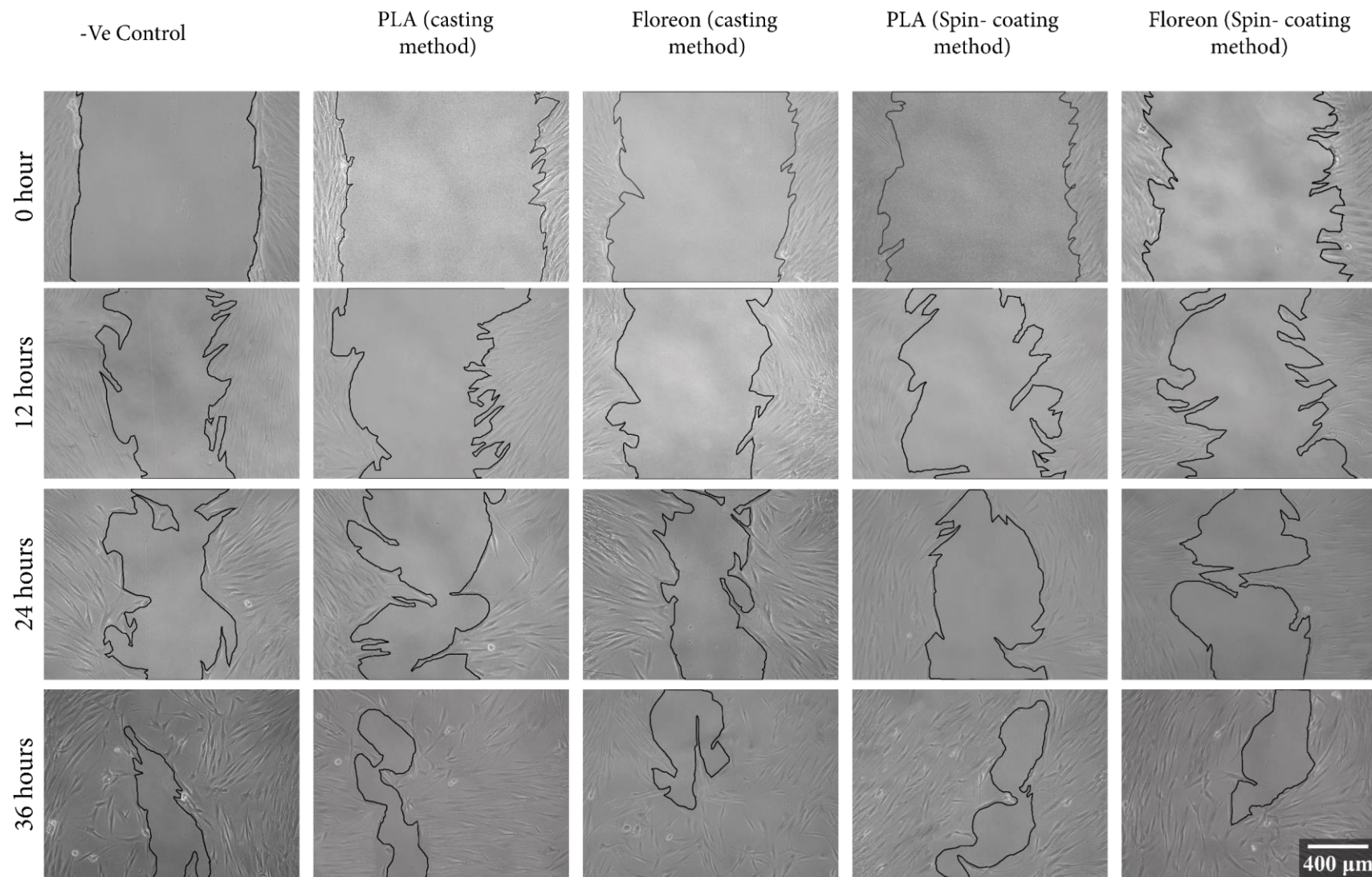
Figure 4-102 Images from a scratch assay experiment at different time points. All images were scaled at 400 µm.
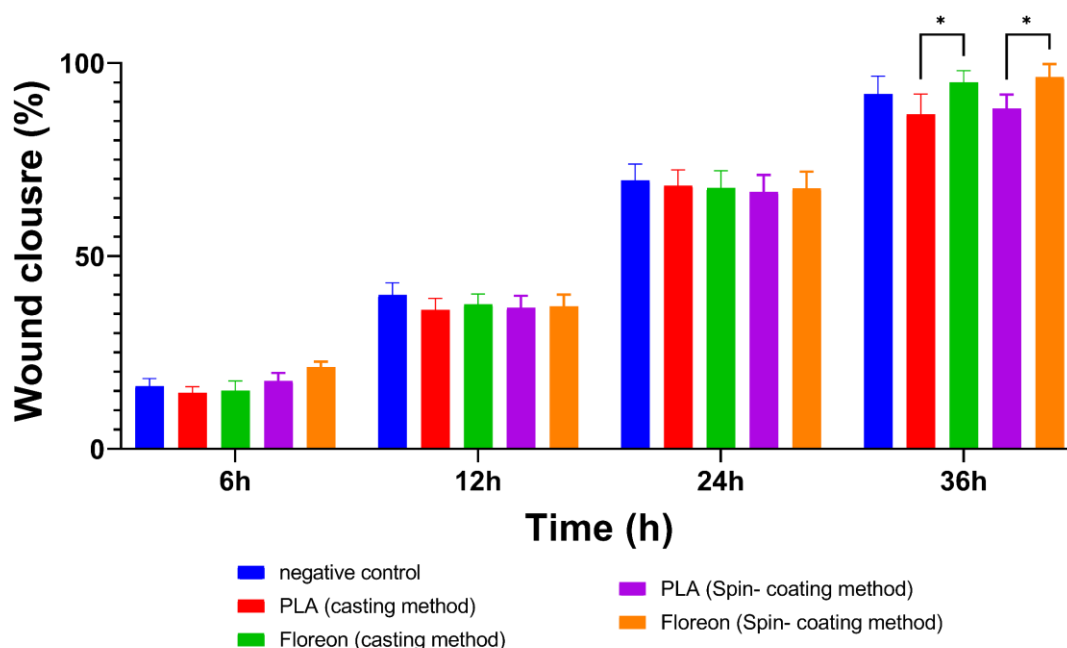
Figure 4-103 Closure area (%) of Normal Oral Fibroblast cells in the presence of PLA and Floreon membranes fabricated using two various methods and at different time points. Data represented n=3, mean ± STDV following Two -way ANOVA statistical analysis with Tukey comparison test. **** $p < 0.0001$, *** $p < 0.001$, ** $p < 0.01$, * $p < 0.05$. Data = mean ± SD.

As a standalone material or in copolymers with the other polymers like polyglycolic acid and polycaprolactone, PLA is biocompatible. Different membrane fabrication techniques or the use of composite membranes can modify the physical qualities of PLA membrane (Da Silva et al., 2018). PCL and PL are two examples of bioresorbable polyesters used in the production of Floreon, which is a combination of sustainable biobased polymers (Ramos-Rodriguez et al., 2022). The wound healing scratch test can be performed to determine the influence of materials or drugs on the in vitro acceleration or retardation of wound healing (Liang, Park and Guan, 2007). The approach used in this study has been applied in a variety of other studies (Augustine et al., 2019; Zadeh et al., 2019). The most reliable method of this analysis is time-lapse imaging produced using a light microscope at different times to measure the wound closure rate.

When examining the scratch healing rate on NOFs in the presence of cast or spun-coated films, as presented in Figure 4-102 and Figure 4-103, it can be observed that the healing rate during the first 12 and 24 hours was consistent across all samples, and similar to that of the negative control. However, on the third day of incubation, there was a slight variation observed

between the Floreon and PLA films, irrespective of their method of manufacture. It could be because the pH of the Floreon films changed minimally, maintaining a neutral pH, as discovered during the bioactivity study when the Floreon and PLA films were immersed in SBF during the study period. Mackenzie et al. (1961) reported that the optimal pH range for mammalian cell growth was 7.38 to 7.87 (Mackenzie, Mackenzie and Beck, 1961). On the alkaline side of the optimal pH range, cell growth fell precipitously, whereas it declined gradually on the acidic side. In another study that investigated the growth and mineralisation of human BMSCs in a pH range of 6.3-8.5, the researchers found that the optimal activity level of BMSCs occurred at a pH of 8.0 (Fliefel et al., 2016).

4.2.12.2 Cell proliferation: Presto Blue assay

PrestoBlue is a resazurin-based metabolic test that was used to measure the proliferation rate of fibroblasts and cytotoxicity of seeded membranes. The metabolic activity of living cells permits resazurin to be converted into an easily measurable component; the rate of resazurin conversion correlates directly with the number of viable cells existing in the culture. Cell proliferation was measured at various time intervals (1, 3, 7, 14, and 21 days, after the seeding) and plotted in Figure 4-104.

According to the results, the metabolic activity of NOFs cells was significantly higher on spin-coated films made with both materials than on cast films. This became obvious after the seventh day of incubation. There was no significant difference between the two materials, Floreon and PLA, during the culture period, with the exception of a slight difference between the spin-coated Foreon and PLA films on the fourteenth day.
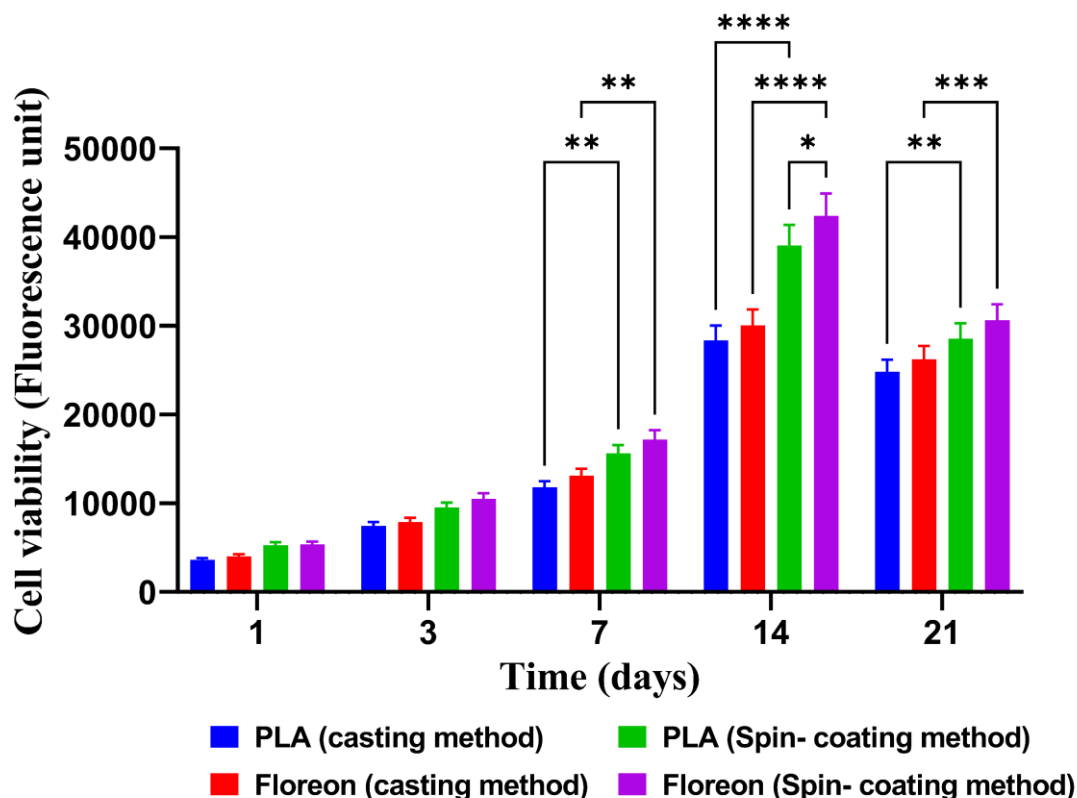
Figure 4-104 The PrestoBlue ® assay performed for viability Fibroblast seeded over Floreon membranes fabricated via two different techniques for different times, compared with PLA membranes. Data represented n=3, mean ± STDV following Two-way ANOVA statistical analysis with Tukey comparison test. **** $p < 0.0001$, *** $p < 0.001$, ** $p < 0.01$, * $p < 0.05$. Data = mean ± SD.

The process of a cell growing and dividing to form two daughter cells is known as cell proliferation (Grewal and Edgar, 2003). Cytotoxicity, cell viability and cell proliferation can be measured by Presto Blue assay. A PrestoBlue is a resazurin-based metabolic test that can be used to measure the proliferation rate of fibroblasts and cytotoxicity of seeded membranes. The reducing environment of live cells, which upon entering, transforms non fluorescent resazurin solution into the highly fluorescent resorufin, can be used to measure cell proliferation. Metabolic activity of living cells permits resazurin to be converted into an easily measurable component; the rate of resazurin conversion correlates directly with the number of viable cells existing in the culture (Riss *et al.*, 2016).

The mitochondrial activity in resazurin-based Presto Blue test converts the nonfluorescent blue resazurin to fluorescent pink resorufin (O'brien *et al.*, 2000; Quent *et al.*, 2010). This non-toxic water-soluble dye has been proven to be an effective instrument to measure cell viability and proliferation and allows for continuous cell culture monitoring (Gloeckner, Jonuleit and

Lemke, 2001; Jiao and Cui, 2007; Zhou *et al.*, 2013). The quantity of resorufin produced when cells are incubated with the resazurin is directly proportional to the number of live cells, which may be measured colorimetrically or fluorometrically. Fluorescence detection is the preferred technique for reaching a high degree of sensitivity (Riss *et al.*, 2016).

Cell proliferation was measured by PrestoBlue assay at various time points (1,3,7,14, and 21 days, after the seeding) and plotted in Figure 4-104. It was observed that the rate of proliferation increased with the passage of time till day 14 in all the membranes and after day 14, the rate of proliferation decreased. It was also observed that both the PLA and Floreon spin-coated films showed superior proliferation ability compared to the PLA and Floreon cast films; this tendency was validated for cells seeded on spin-coated scaffolds, particularly on day 14. Furthermore, membranes produced by Floreon (by either spin-coating method or casting method) had significantly higher cell proliferation than those produced by PLA.

So, Floreon membranes prepared by spin-coating method have highest cell viability as well as cell proliferation as compared to other membranes used in this assay. Hence the cell proliferation and cell viability rate are not negatively affected by Floreon and PLA membranes. This finding is in line with another study in which proliferation and viability of fibroblast *in vitro* was checked after culturing on Floreon, PLA, and TCP membranes. It was reported in the study conducted previously in this research laboratory that proliferation and viability is not affected when cells are cultured on Floreon, PLA, and TCP membranes for periods up to 18 days (Ramos-Rodriguez *et al.*, 2022).

After the 7 and 14 days of the static cell culture on Floreon and PLA scaffolds, cell viability and proliferation were evaluated. The findings showed that, regardless of the substance, all scaffolds may support cell adhesion and proliferation. Due to PLA's increased hydrophilic properties, the addition of PLA to the PCL matrix obviously improves cell attachment and proliferation (Patricio *et al.*, 2013).

It is also noteworthy to notice from a biological perspective that the PCL/PLA mix (Floreon) production process has a significant impact on fibroblast adhesion and proliferation. On PCL/PLA scaffolds made using the spin-coating process, a higher rate of cell proliferation was seen. This high cell proliferation rate in spin-coated membranes was due to the highly porous structure of PLA and Floreon membranes prepared by spin-coating method while lower in flat structured PLA and Floreon membranes prepared by solvent casting method. This is supported by a study which reported that the 3D PGSU scaffolds have the capacity to promote cell

proliferation due to their optimal porous structure and porosity. It was reported that the smaller pore size and less porosity of the scaffolds had a negative impact on cell penetration and proliferation. It was revealed that the PGSU-5% scaffolds' high porosity and medium to large pore sizes encouraged tissue development and cell proliferation (Samourides *et al.*, 2020).

Due to the flat surface of scaffolds, which hinders cell attachment, and the uneven distribution of PLA inside the PCL matrix, the low biological performance of the PCL/PLA scaffold mix created by solvent casting is likely caused by these factors. Based on the integrity of plasma membrane and the esterase activity, the live dead assay is a rapid and simple two-colour experiment to detect the viability of the cells in a population (Wang *et al.*, 2021). The staining solution for the LIVE/DEAD assay is a combination of two fluorescent dyes that distinguish between living and dead cells. Green colour indicates healthy, alive cells (Krause *et al.*, 2008). It is membrane permeable and non-fluorescent until the ubiquitous intracellular esterases remove the ester groups and make the molecule fluorescent (Stiefel *et al.*, 2015).

4.2.12.3 live dead assay

The live-dead test is a frequently employed method of cell labelling. The calcein-stained slices of living tissue show green fluorescence when their cytoplasm is excited. Ethidium homodimer dye (EthD), which binds to the DNA of dead cells and emits a red fluorescence, is used to identify dead cells.

Figure 4-105 and Figure 4-106 show the live-dead assay of the investigated membranes, in which it is evident that there are fewer red dots indicating dead cells in spin-coated membranes created by PLA and Floreon to those of cast membranes. Figure 4-106 demonstrates that spin-coated films had a lower percentage of dead cells than the cast group, suggesting that Floreon material is biocompatible as PLA.
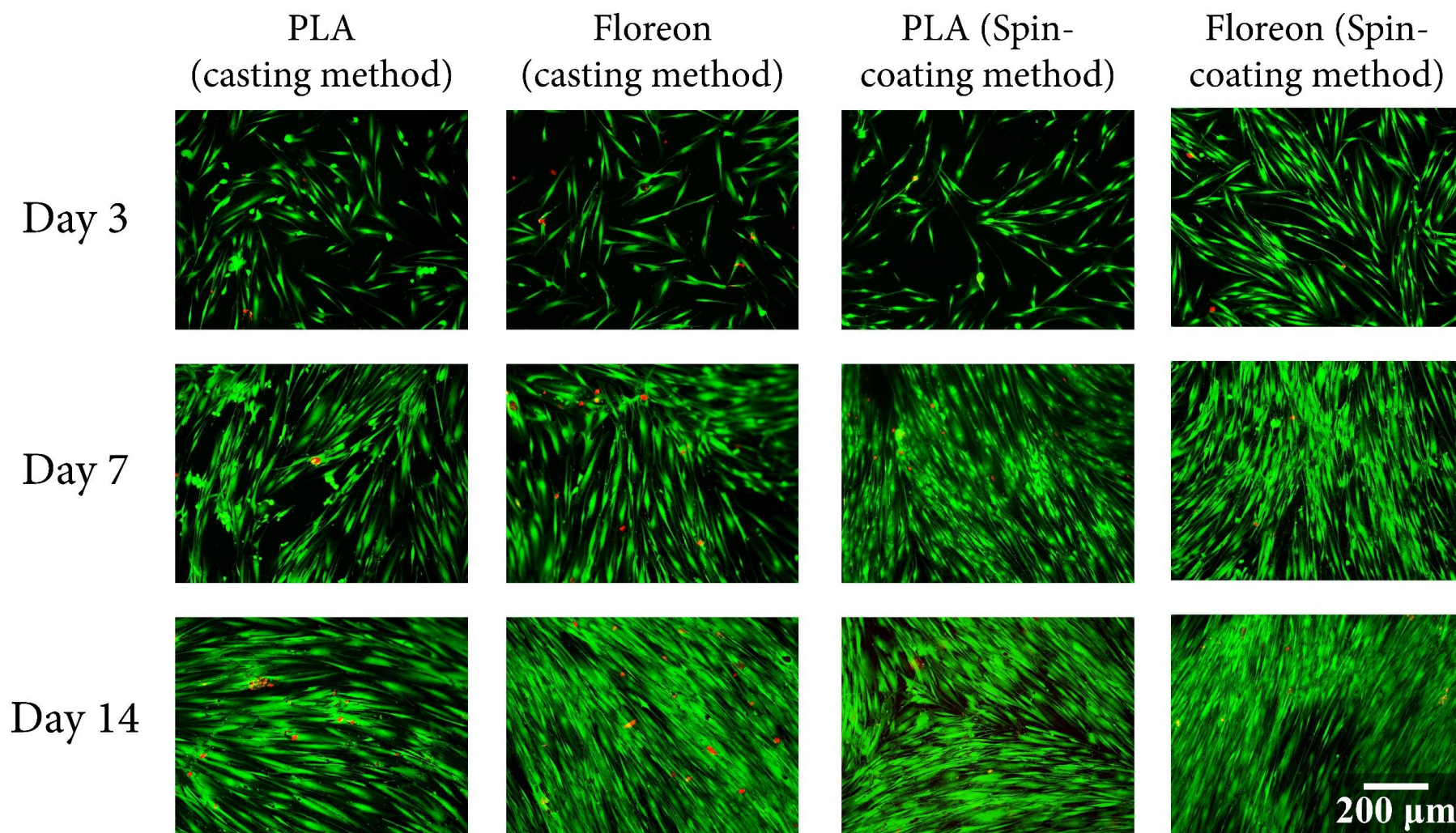
Figure 4-105 Fluorescence images of fibroblast cell viability in the PLA and Floreon membranes were fabricated using two various methods on day3,7 and 14. All images were scaled at 200 µm.
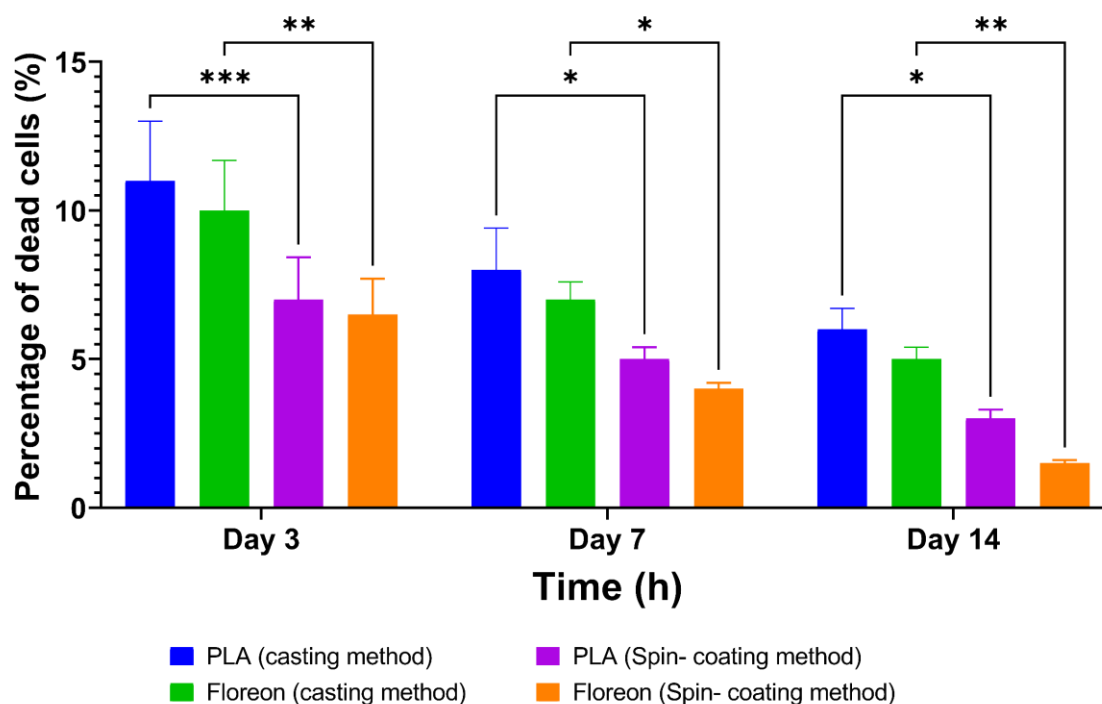
Figure 4-106 Quantitative analysis of the percent of dead cells within each scaffolds fabricated using two various methods in different experimental periods. Data represented n=3, mean ± standard deviation following Two-way ANOVA statistical analysis with Tukey comparison test. **** $p < 0.0001$, *** $p < 0.001$, ** $p < 0.01$, * $p < 0.05$.

This assay is a frequently employed method of cell staining. The calcein-stained cells show green fluorescence when their cytoplasm is excited. Ethidium homodimer dye (EthD), which binds to the DNA of dead cells and emits a red fluorescence, is utilised to identify dead cells (Krause *et al.*, 2008). This assay is safer for detection of cell viability (Wang *et al.*, 2021). In contrast to Trypan blue exclusion, which is frequently used to distinguish between living and dead cells, this test is more sensitive. Due to intense fluorescence of both dyes when they come into contact with either living (for calcein-AM) or dead (for ethidium homodimer-1) cells, this low-cost test is extremely sensitive (Krause *et al.*, 2008). Because both dyes are almost completely non-fluorescent before interacting with the cells, background levels are minimal.

Figure 4-106 shows the live-dead assay of the investigated membranes, in which it is evident that there are fewer red dots indicating dead cells in spin-coated membranes created by PLA and Floreon to those of cast membranes. Cell viability was measured at various time intervals (3, 7, and 14 days, after the seeding). It was observed that the number of live cells increased with the passage of time in all the membranes. It can also be seen that both the PLA and Floreon spin-coated films showed greater numbers of green live cells compared to the PLA and Floreon cast films. Furthermore, membranes produced by Floreon (by either spin-coating method or

casting method) had significantly higher live cells than those produced by PLA and very less number of red dead cells. This enables us to conclude that Floreon and PLA material is biocompatible and has greater than 95 % living cell ratios. Among the spin-coating and casting methods of membrane preparation, membranes formed by spin coating method have more live cells and less dead cells as compared to membranes formed by casting method. This high number of viable cells in membranes prepared by spin-coated method was due to the highly porous structure while higher dead cells in PLA and Floreon membranes prepared by solvent casting method due to its smooth surface. This is supported by a study which reported that the osteoblasts adhere and proliferate more successfully on the porous surface (0.81 micrometre pore size) than they did on the smooth one (Hatano *et al.*, 1999).

Biocompatibility of various membranes has also been reported by live dead assay in previous studies. In a study, cell viability and cell proliferation was checked and compared between PCL and PLA/PCL blend scaffolds and it was reported that PLA/PCL blend scaffold have high cell viability and cell proliferation as compared to PCL scaffold (Patricio *et al.*, 2013). This study is in line with the results of the live and dead assay of the investigation. In another study, human dermal fibroblast cells and MSCs were stained using live-dead staining. Fluorescent microscopy was used to detect emission on days 3 and 7. On day 7 and on modified PCL-P membranes, there were significantly more living cells visible than on day 3 and on unmodified PCL membranes (Nguyen *et al.*, 2019).

4.2.12.4 PicoGreen assay

PicoGreen® DNA quantification assay was utilised to determine the number of fibroblasts present on PLA and Floreon films in culture. The assay utilised fluorescence to measure the quantity of dsDNA contained in each sample. A standard curve was then used to infer the number of cells present. The standard curve was constructed by fitting a second-order polynomial to the fluorescence values generated from known amounts of λDNA (0-1,000 ng/ml DNA) to the fluorescence data. The R^2 value for the fitted curve was 0.99, which indicates a great agreement with the data.
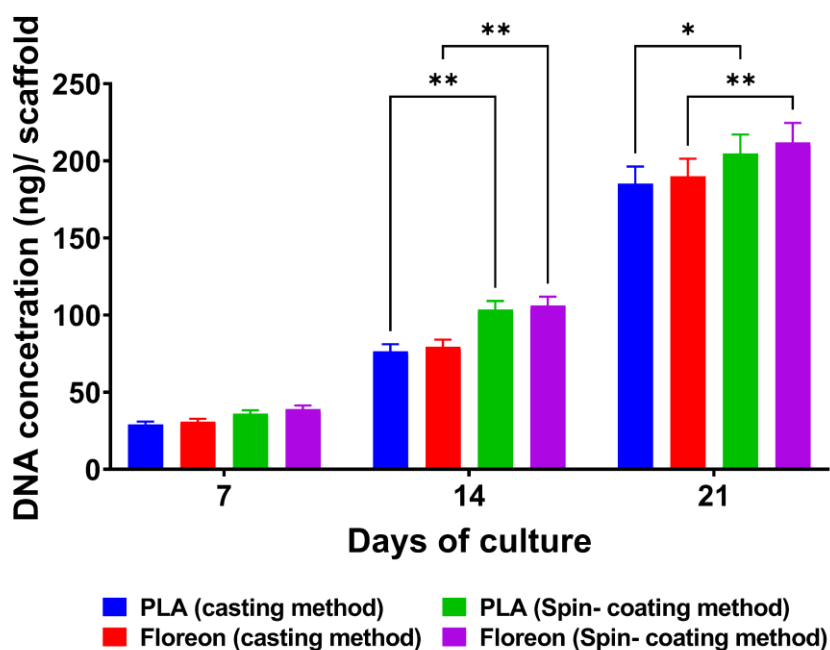
Figure 4-107 PicoGreen results for PLA and Floreon membranes were fabricated using two various methods in different experimental periods. Data represented n=3, mean ± standard deviation following Two-way ANOVA statistical analysis with Tukey comparison test. **** $p < 0.0001$, *** $p < 0.001$, ** $p < 0.01$, * $p < 0.05$.

For 7, 14, and 21 days, fibroblasts were grown on PLA and Floreon membranes produced using solvent casting and spin coating processes. Figure 4-107 demonstrates the results for each time point. Throughout the period of the investigation, the amount of fluorescence was seen to rise. Moreover, it shows that cell proliferation was significantly greater on spin-coated films than on cast membranes. However, the concentration of dsDNA in PLA and Floreon films was comparable in both prepared methods used. In conclusion, the total quantity of cellular dsDNA assessed by the PicoGreen assay is in strong agreement with the PrestoBlue test results.

The main difference between DNA quantity of PLA and Floreon membranes is due to their manufacturing method. The PLA and Floreon membranes prepared by spin-coating method are highly porous while PLA and Floreon membranes prepared by solvent casting method are comparatively smooth. Due to the high porous structure of PLA and Floreon membranes prepared by the spin-coating method, cells adhere and proliferate rapidly. As a result, more DNA quantity was obtained in PLA and Floreon membranes prepared by spin-coating method. This is supported by a study which reported that the PGSU scaffolds promote cell proliferation due to their optimal porous structure and porosity. It was revealed that the PGSU-5% scaffolds' high porosity and medium to large pore sizes encouraged tissue development and cell

proliferation (Samourides *et al.*, 2020). Numerous studies validate the picogreen assay's DNA quantitation. In a research, the quantification of DNA, which was considered to be proportional to the number of cells, showed the progression of cell proliferation in the scaffolds. Within different time points, the PCL scaffold's DNA content does not alter noticeably while the number of cells for the HA/TCP-PCL scaffold dramatically increased on day 21 compared to prior time points. The HA/TCP-PCL scaffold had much more cells than PCL scaffold after 21 days of culture, despite the fact that the PCL scaffold had more cells on day 2 than HA/TCP-PCL scaffold did (Chen *et al.*, 2015).

The PicroGreen test revealed in a different investigation that there were no differences in cell proliferation between groups at days 1 or 18. This suggests that the membrane's effects on cell metabolism in human dermal fibroblasts were limited to those of PLA, FLM, or FLM + W (Ramos-Rodriguez *et al.*, 2022). In one study, a PicoGreen test was used to calculate the DNA values in the scaffolds and compare the rates of cell proliferation in samples with and without MNPs. On the first day of cultivation, it was evident that cultivation on scaffolds containing MNPs produced a substantially larger amount of the DNA. Over the course of seven days, static cell growth on PCL scaffold was observed (Daňková *et al.*, 2015).

4.2.12.5 Total protein content

The BCA protein test, which uses the bicinchoninic acid (BCA) reagent, is a simple and efficient method for quantifying protein. To evaluate cell activity, a test for total protein concentration was done. As depicted in Figure 4-108, the results for all studied membranes are as follows, it reveals that the total protein content of all groups increases with increasing incubation time. It was also observed that the total protein secretion of spin-coated membranes was greater than that of cast membranes, regardless of the type of material. There was no noticeable difference between Floreon and PLA membranes, suggesting that Floreon membranes are comparable to the control group.
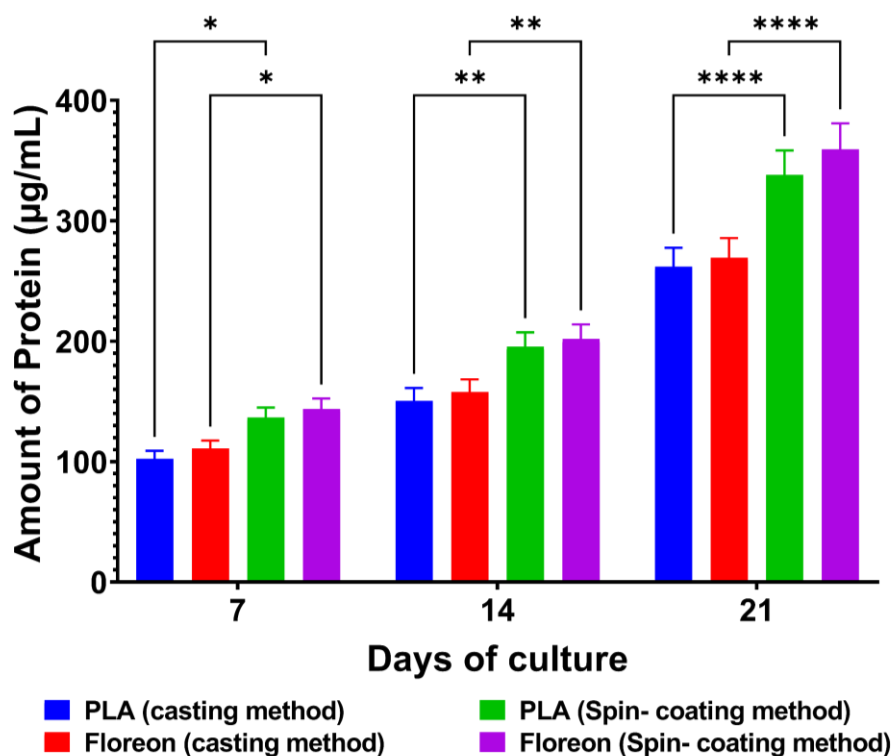
Figure 4-108 Protein concentration for PLA and Floreon membranes were fabricated using two various methods in different experimental periods. Data represented n=3, mean ± STDV following Two-way ANOVA statistical analysis with Tukey comparison test. **** $p < 0.0001$, *** $p < 0.001$, ** $p < 0.01$, * $p < 0.05$.

Cell activity (total protein content) was measured at various time intervals (7, 14, and 21 days, after the seeding). It was observed that the amount of protein increased with the passage of time in all the membranes. It was also observed that both the PLA and Floreon spin-coated films showed higher protein content compared to the PLA and Floreon cast membranes. Furthermore, the total protein content is the same between PLA and Floreon membranes prepared by the same method. These findings are supported by other studies which show that PLA membranes and PLA complex membranes did not negatively affect cell activity (Patricio *et al.*, 2013). In one study, the total protein content of the cells seeded on 10%-HA and 10%-CaSiO$_3$ membranes were not significantly different from each other measured by BCA assay after 1 and 2 weeks of culture (Oldinski *et al.*, 2011). In another study, total protein content was calculated by BCA assay from the cells seeded on different EB scaffolds (Goh, Olsen and Banerjee, 2013).

Hence the cell activity is not affected by Floreon and PLA membrane which is in strong agreement with the total quantity of cellular dsDNA assessed by the PicoGreen assay and the PrestoBlue test results.

4.2.12.6 Cell morphology

- **Cell morphology analysis by Fluorescence Staining of the Actin Cytoskeleton:**

In order to study the cell morphology and microfilament structure, the actin filaments and nucleus were stained with Phalloidin and DAPI, respectively. The fluorescent images shown in Figure 4-109 are indicative of the fibroblasts that have grown on the respective membranes after 3, 7, and 14 days of culture.

Initially, when fibroblasts were cultured on cast/coated-spun membranes made with PLA or Floreon materials, the microfilaments seemed disorganised and spread in all directions. After 14 days of growth, the microfilaments of fibroblasts on these four types of membranes showed partial localised alignment but no uniform anisotropic cell structure.

Although there was no difference in cell behaviour and morphology between Floreon and PLA membranes regardless of fabrication method, the cell spreading area was larger on the Floreon mat than on the PLA mat by day 14.
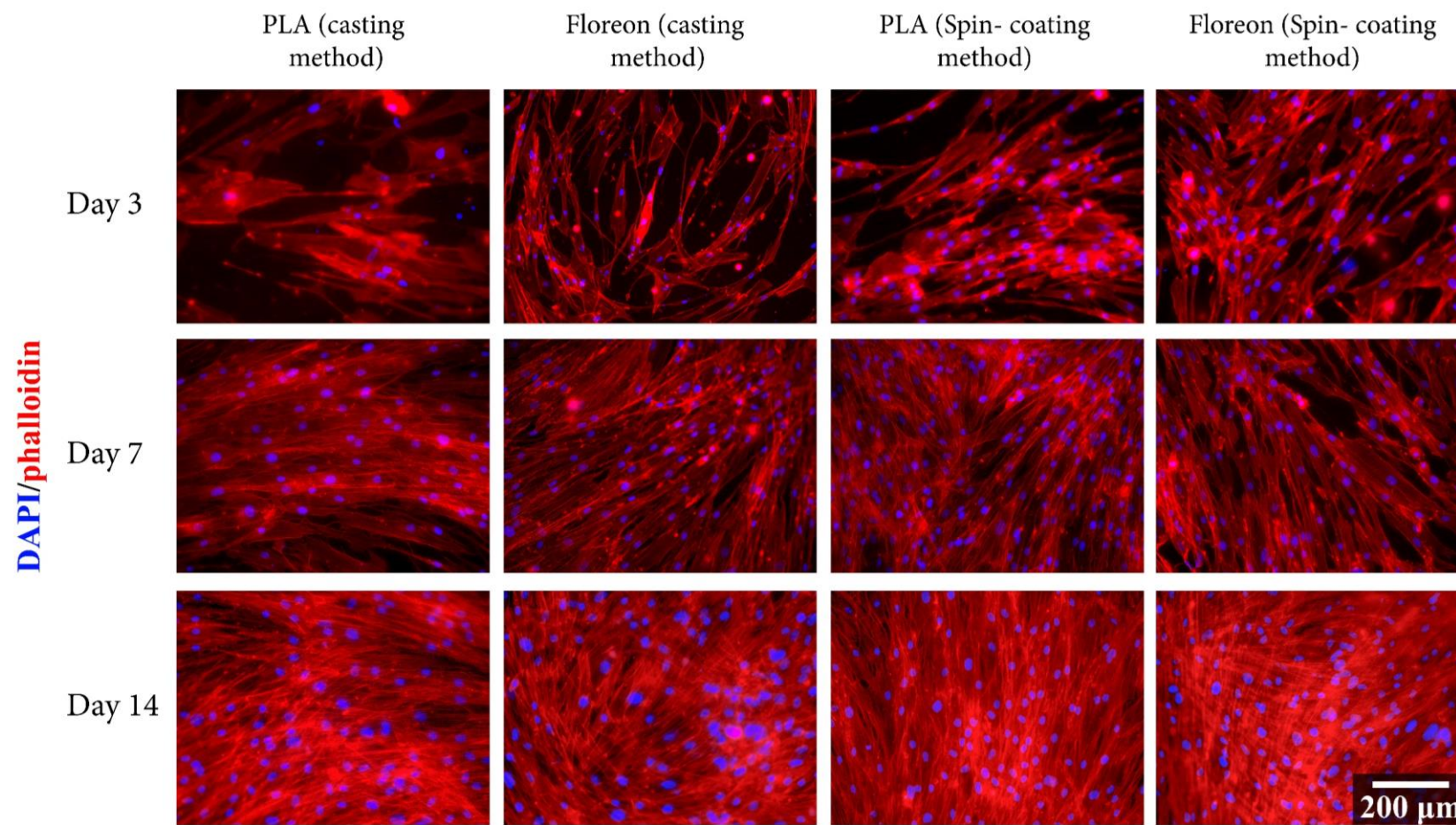
Figure 4-109 Phalloidin labelled F-actin (red), DAPI nuclear staining (blue) and overlaid fluorescent image of immunostained cellular components (merged) for the normal oral fibroblasts on PLA (control) and Floreon membranes. All images were scaled at 200 µm.

Cell morphology plays a significant role in determining its phenotype and is essential for controlling how the cell behaves. One of the most prevalent proteins in cells is actin, and actin filaments may easily be marked using fluorescent versions of the naturally occurring protein phalloidin (Small *et al.*, 1999). A highly specific bicyclic peptide called phalloidin is used to stain actin filaments (also known as F-actin). It binds to all types of actin filaments in a wide variety of animal and plant species (Pozhvanov, 2018). For fluorescence microscopy visualisation of filamentous actin structures in fixed mammalian cells, F-Actin Stain is a simple probe-based approach. Major cytoskeleton constituent F-actin participates in essential cellular activities such cell division, morphogenesis, and migration (Ballestrem, Wehrle-Haller and Imhof, 1998).

For marking DNA with fluorescence microscopy, use DAPI Staining Solution, a fluorescent stain. DAPI (4',6-diamidino-2-phenylindole) is a well-known fluorescent chemical that emits blue light and is frequently used for nuclear staining (Kim Törnqvist, 2010). The A/T-rich dsDNA sequences in the minor groove are bound by DAPI, which enters cell membranes and selectively stains nuclei (Ali *et al.*, 2018). F-actin and nuclei were stained with phalloidin and DAPI respectively, to examine the cell shape and microfilament structure.

The fluorescent images shown in Figure 4-109 are indicative of the fibroblasts that have grown on the respective membranes after 3, 7, and 14 days of culture. Initially, when fibroblasts were cultured on cast/coated-spun membranes made with PLA or Floreon materials, the microfilaments seemed disorganised and spread in all directions. After 14 days of growth, the microfilaments of fibroblasts on these four types of membranes showed partial localised alignment but no uniform anisotropic cell structure. This is because fibroblasts are spindle shaped and retain this shape even when densely packed whereas, stem cells for example are plastic in their phenotype and can aggregate into tightly packed spherical colonies under certain circumstances.

The main difference between PLA and Floreon membranes is their manufacturing method which affects cell spreading and cell morphology. The PLA and Floreon membranes prepared by the spin-coating method are highly porous while PLA and Floreon membranes prepared by solvent casting method are comparatively smooth. Due to the high porous structure of PLA and Floreon membranes prepared by spin-coating methods, cells adhere and proliferate rapidly. As a result, the cell spreading area was larger on the Floreon mat than on the PLA mat by day 14. This indicates that the newly synthesised Floreon membranes are biocompatible.

In a previous investigation carried out in this research laboratory, the cell morphology and spreading of fibroblasts were examined on the 18th day after seeding. Fluorescence microscopy, with DAPI (blue) and phalloidin-TRITC (red) staining to visualise the nucleus and cytoskeleton, respectively, was utilised to evaluate the cells on PLA membrane, Floreon membrane, and Floreon and wollastonite mixed membranes. The results indicated that all of the membranes under study were biocompatible for fibroblasts (Ramos-Rodriguez *et al.*, 2022).

In a different investigation, phalloidin-rhodamine fluorescent dye was used to analyse the cell spreading and morphology under a microscope on days 1, 7, and 21. The cells on the PCL scaffolds showed a nonspread shape and were evenly dispersed on the first day. In contrast, the PCL-MNPs scaffolds' cells were widely dispersed, suggesting improved initial cell adherence. On day 7, the PCL scaffold's cells were dispersed and separated into tiny colonies. The cells on the PCL-MNPs scaffold were dispersed across the scaffold in bigger colonies. Throughout the study time, the number of cells steadily grew, however on the PCL-MNPs scaffolds; the cell layer was fully confluent. On day 21, the cells on the PCL were grouped into enormous colonies and displayed a well-distributed morphology, showing that the PCL was biocompatible. The cell layer, however, was not completely confluent (Daňková *et al.*, 2015).

- **Cell morphology analysis by SEM:**

The SEM was used to evaluate the cell morphology of the dehydrated samples following gold coating. Figure 4-110 shows the results of the SEM observation of the cell-seeded scaffolds. Particularly, after 3 days of cell seeding and culture, the SEM images revealed strong cell attachment of the normal oral fibroblast cells on the material surface, indicating that the cells are initially arranged in a monolayer, with very flattened cellular morphologies. In comparison to the control group consisting of PLA membranes, the Floreon mats demonstrated a higher degree of cell attachment, with fibroblasts being securely attached and spread across the surface.

Furthermore, it should be noted that the rate of proliferation and expansion of rMSCs and extracellular matrix (ECM) on scaffolds increased with time, indicating promising results for tissue engineering applications.
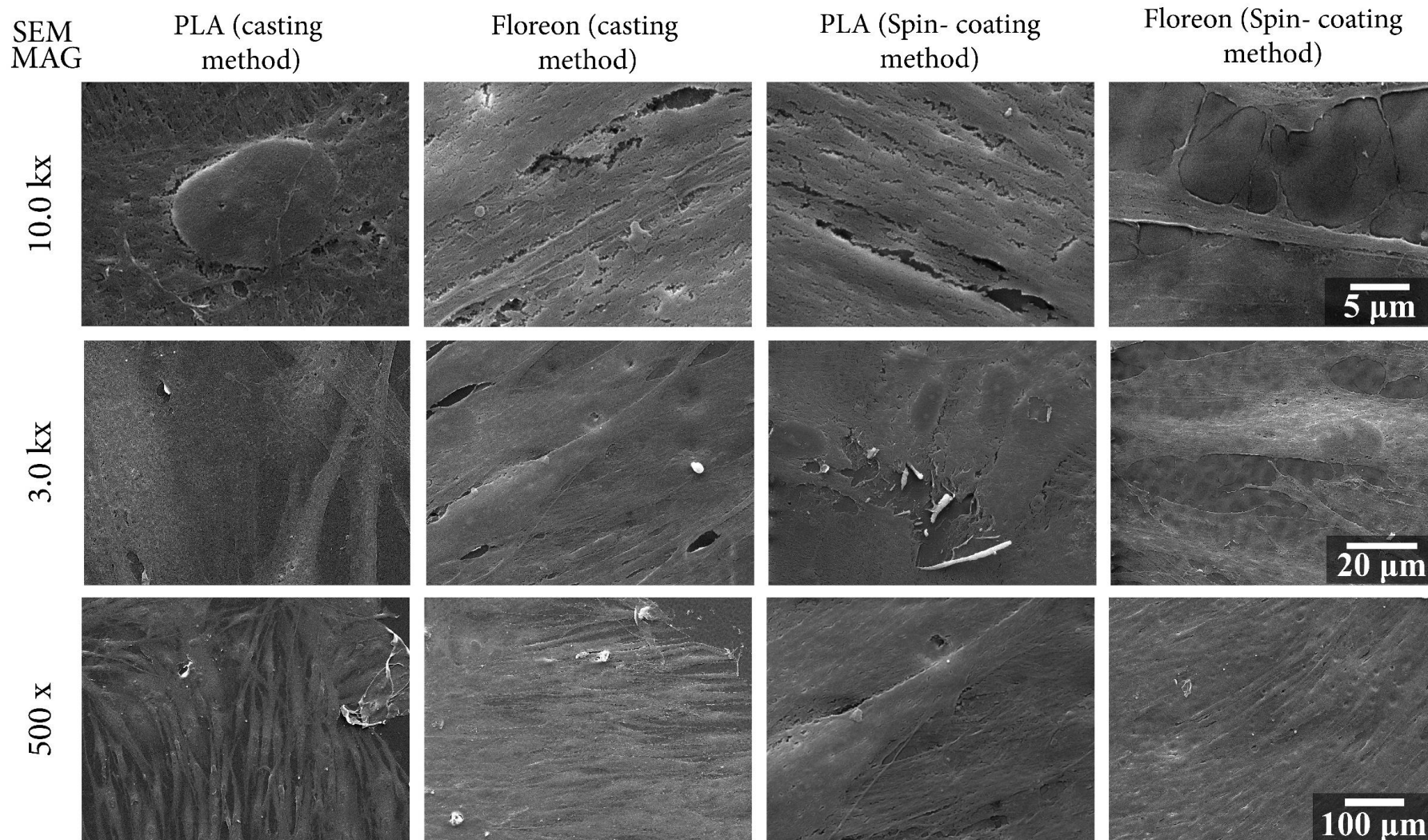
Figure 4-110 SEM micrographs of normal oral fibroblasts grown onto PLA (control) and Floreon membranes. The images depict different levels of magnification, with the top row scaled at 5 µm, the middle row at 20 µm, and the bottom row at 100 µm.

Images created by SEM can provide details about a material's surface composition and topography (Stachewicz *et al.*, 2019). In order to make the surface of samples conductive and prevent charging effects, gold, platinum, or other conductive elements are frequently nano sprayed onto the sample. Additional preparation measures are frequently needed to guarantee the sample is dry and capable of withstanding the low pressure (Murtey and Ramasamy, 2016). SEM has the benefit of qualitatively evaluating cell development on surface layers over physical approaches (Wang *et al.*, 2010). SEM can achieve resolutions up to roughly 1 nm (Smith, Smallwood and Macneil, 2010). SEM was used to evaluate the influence of studied membranes on cell morphology and growth. After the samples were prepared and dried, they were gold coated for imaging the cell culture on the membranes PLA and Floreon membranes prepared by casting method or spin coating method. Figure 4-109 shows the results of the SEM observation of the cell-seeded scaffolds. In particular, after 3 days of cell seeding and culture, the SEM images revealed strong cell attachment of the normal oral fibroblast cells on the material surface, indicating that the cells are initially arranged in a monolayer, with much flattened cellular morphologies. Compared to the control group (PLA membranes), the shape and amount of fibroblast cells on the surface of the Floreon mats indicated that fibroblasts were securely attached with the spreading of lamellipodia and filopodia.

In a prior study, scaffold-cell constructions cultivated for 24 hours with human osteoblast-like cells had their cell morphology examined by SEM. The scaffolds were poly (LLA-co-"-CL), poly(PLLA), and poly (LLA-co-DXO). As a control, cells were grown on TCPS. It was discovered that cells had adhered and disseminated effectively, were dispersed inside scaffolds, and had experienced significant migration (Idris *et al.*, 2010). Another study employed the SEM to examine the cell morphology of PCL and PCL/PLA scaffolds and found that all scaffolds had uniform pore distribution and well-defined internal geometry (Patricio *et al.*, 2013).

The present investigation provides further support for the biocompatibility of polyester membranes, such as PLA, PCL, and Floreon, as reported in earlier studies. Notably, this study is the first to explore the potential of Floreon polyester blends for tissue engineering applications, specifically in the context of periodontal therapy. The mechanical characteristics of Floreon membranes were analysed in detail, and their impact strength was found to be superior to that of PLA, rendering them suitable for use as periodontal scaffolds. The present work is notable for its use of fibroblasts to confirm the biocompatibility of Floreon material. Overall, this study underscores the biocompatibility and potential of the innovative and sustainable Floreon mixture as a platform for periodontal therapy.

4.3 Section III: Fabrication and characterisation of bilayer membrane

The following section evaluates the capability to fabricate bilayer films based on the results of the individual membrane properties examined in the previous sections. The prototype bilayer films were produced by electrospinning Floreon containing 10% bioceramic particles (HA and $CaSiO_3$) directly on top of smooth Floreon membranes manufactured using spin coating. The overarching objective of this multifunctional bi-layered device was to ensure that each layer effectively performs the function for which it was designed, as this was for the treatment of periodontal disease. The primary function of the electrospun membrane composed of Floreon and reinforced with relevant bioceramics was to facilitate the formation of new bone by facilitating the adherence of osteoblasts. While the smooth surface layer was produced from pure Floreon utilising spin coating technology, its primary purpose was to act as a physical barrier to ensure required mechanical performance and prevent connective tissue and epithelium interference during bone formation.

After being able to construct these bilayer films, as stated in Section 3.2.5, they were studied visually and under a scanning electron microscope (as detailed in the subsequent sections) and their mechanical properties were compared to those of monolayer films.

For the *in vitro* analysis of the bilayer membranes, fibroblast cells were grown on the smooth spin-coated membranes (that would serve as guided tissue regeneration membranes), and r-MSCs were grown on fibrous membranes (that would serve as guided bone regenerative membranes). The co-culture process was explained in detail in Section 3.4.8. After 14 days in culture, films were sectioned and examined under a scanning electron microscope and a histological microscope.

4.3.1 Optical images of fabricated bilayer membranes:

Optical image of the manufactured bilayer membrane, shown in Figure 4-111. Figure 4-111-A illustrates the cross-sectional topography of the bilayer construct, which was successfully fabricated via electrospinning Floreon with bioceramic particles onto a Floreon spin-coated film. For imaging purposes, the two layers were separated using tweezers, and Figure 4-111-B provides an interior view of the interface between the top and bottom layers. The presence of fibre bonds and effective interaction between the two layers is evident, indicating potential for load transfer between the layers and improved mechanical properties of the bilayer mats, as discussed in the mechanical analysis section. Figure 4-111-C and Figure 4-111-D showcase the top and bottom layers, respectively, and confirm the maintenance of structural integrity in both layers after the fabrication process.
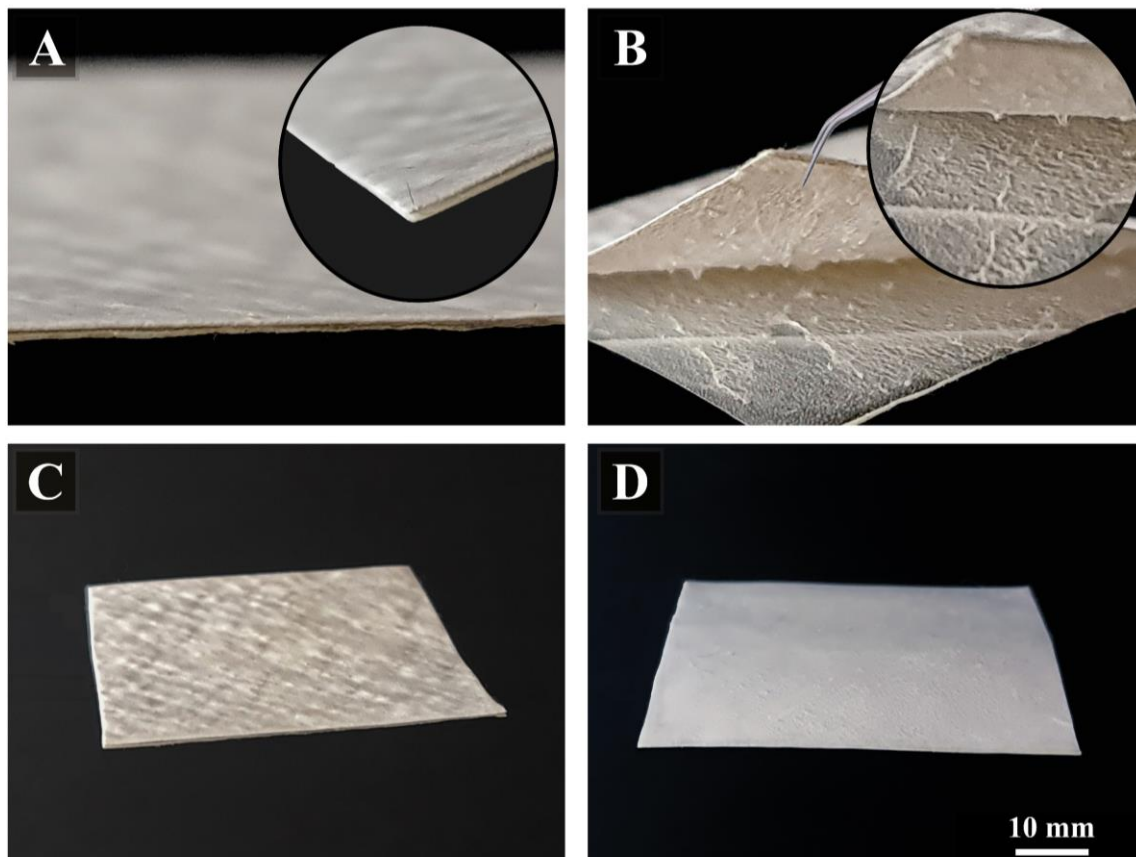
Figure 4-111 Photographs show the cross-section (a), internal (b), bottom (c), and top (d) views of a bilayer membrane after random fibres deposition over the spin-coated membrane. All images were scaled at 10 mm.

It is important to note that the main goal in creating this multifunctional, bilayered device, which was intended to treat periodontal disease, was to make sure that each layer effectively carried out the purpose for which it was created. The electrospun membrane made of Floreon and supplemented with pertinent bioceramics was designed primarily to aid in the production of new bone by promoting osteoblast adhesion. The smooth surface layer was created using spin coating technology from pure Floreon, but its main function was to act as a physical barrier to maintain the necessary mechanical performance and prevent interference from connective tissue and epithelium during bone formation. Periodontal membranes' fundamental properties should include biocompatibility, cell-occlusiveness, space-making, tissue integration, and clinical manageability (Gottlow, 1993; Scantlebury, 1993).

The requirement for surgical removal has been eliminated by the development of bioresorbable membranes. In maxillofacial, regenerative periodontal, and neurosurgery, such membranes have been thoroughly explored, primarily in animals but also in humans (Schmidmaier *et al.*, 2006; Retzepi and Donos, 2010). Recently, long bone lesions in the clinical context have also been repaired using commercially available bioresorbable membranes. They have been proven to improve bone healing, particularly in situations where there has been severe soft tissue loss or bone defects of more than 4 to 5 cm, where autologous bone grafting alone is not advised due to the risk of resorption (Klaue, Knothe and Masquelet, 1995), and they help secure the grafting material (Gielkens *et al.*, 2008). The morphological and topographical behaviour of the Floreon bilayer membranes was carried out using scanning electron microscopy (Czanderna, Madey and Powell, 2006).

4.3.2 Scanning Electron Microscopy (SEM) of fabricated bilayer membranes:

Figure 4-112 illustrates SEM micrographs of a bilayer template. The images show the morphological characteristics of the smooth top surface (Figure 4-112 A and B) and electrospun layers (Figure 4-112 C and D). The top surface has a flat profile with uneven small pores, whereas the bottom surface appeared as a uniform network of interconnected fibres with average diameters of 1.58 μm ± 0.28SD and 1.59 μm ± 0.306 SD, along with some beads for Floreon/Hydroxyapatite and Floreon/Calcium Silicate, respectively. The topography of the cross section at the interface (Figure 4-112 E and F) revealed how tightly the two layers are connected in a homogenous pattern, as some uneven pores were observed.
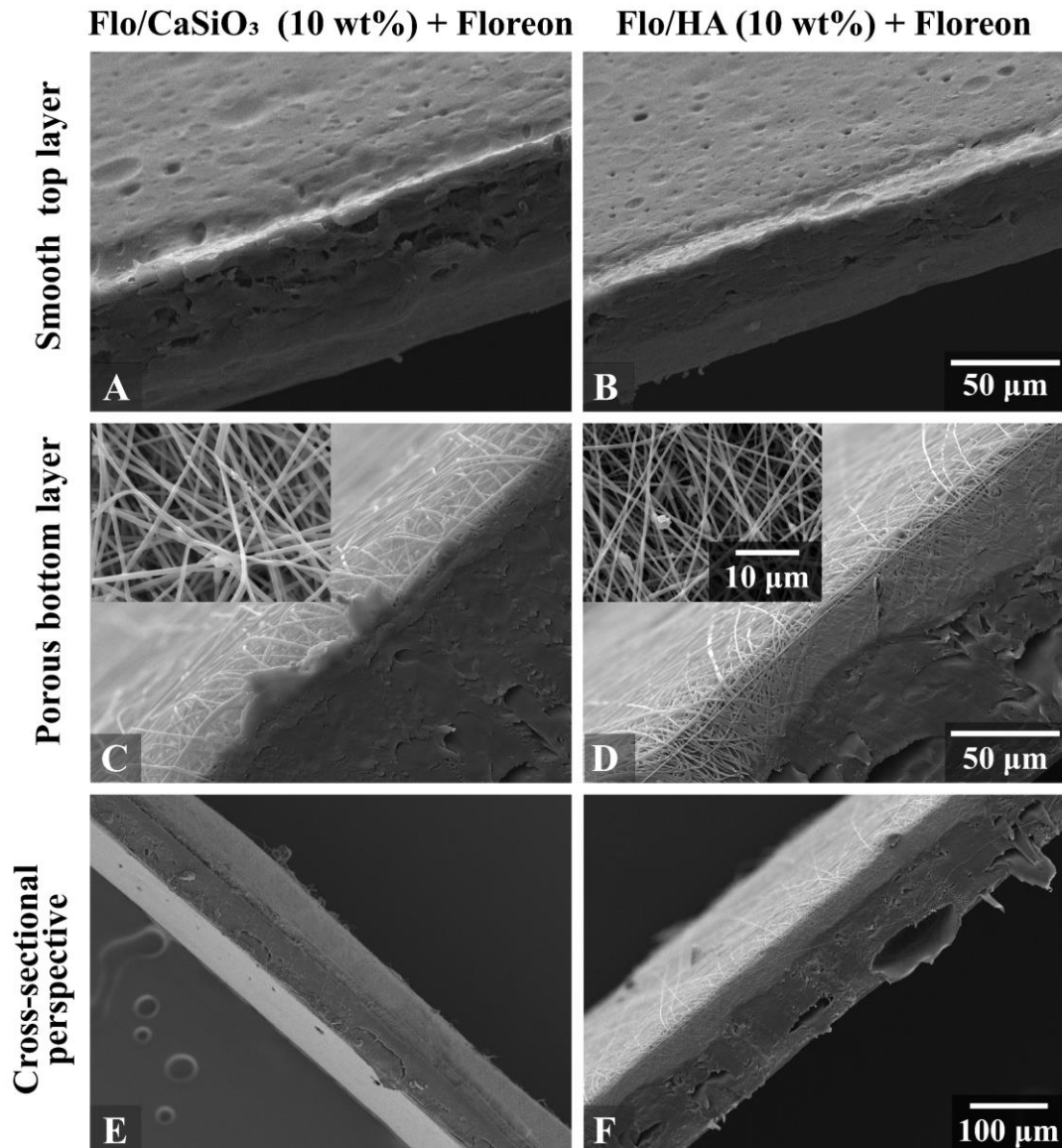
Figure 4-112 SEM analysis of Top, Bottom (scaled at 50µm) and Cross-sectional (scaled at 100µm) surfaces to observe the morphological features of electrospun Floreon with CaSiO₃/spin coated Floreon membrane (left images) and electrospun Floreon with HA/spin coated Floreon membrane (right images). INSET image shows a more magnified section of the bottom's surface, with a 10 μm scale bar.

In the topographical analysis, the figures illustrated the homogeneous pattern of electrospun Floreon membranes. Several studies have shown that the diameter of PLA/PCL blended microfibres is modified due to their surface modification with the incorporated chemicals (Lee *et al.*, 2003; Can-Herrera, Oliva and Cervantes-Uc, 2022; Haroosh *et al.*, 2022).

Although both polymers, PLA and PCL, have distinctive individual characteristics, merging the two can result in a new biodegradable material with well-balanced qualities. However, this method has the drawback that both substances are hydrophobic. This flaw was addressed by using

HA and CaSiO$_3$ surface modification to electrospun PCL/PLA blends of varied weight ratios (Fang *et al.*, 2010; Gupta *et al.*, 2018; Can-Herrera, Oliva and Cervantes-Uc, 2022).

Spectroscopic and microscopic methods were used to characterise the alterations the microfibres underwent, and the water contact angle (WCA) was also established. The findings revealed an increase in roughness and a decrease in WCA values when the PCL content was predominant in the blend after treatment. Nevertheless, morphological alterations were not observed in the electrospun PCL/PLA blends. The surface properties of the PCL/PLA scaffold mixes can be enhanced through HA and CaSiO$_3$ modification and fine-tuning of the component concentrations.

4.3.3 Mechanical characterisation of fabricated bilayer membranes:

Figure 4-113-A shows the typical stress–strain curves for the bilayer mats under uniaxial tension. The ultimate tensile strength, stiffness, and percentage of elongation at failure are calculated from the curves and plotted in Figure 4-113 (B,C and D) and listed in

Table 4-12. The figure also shows the tensile stress–strain curves of single layers of spin-coated Floreon film and Floreon/ceramic fibrous mats for comparison.

As it can be seen in the figure, the tensile strength of the spin-coated Floreon single layer is 1.59 MPa, which is about 90% greater than that of the electrospun Floreon/ceramic single layers (1.59 for Floreon/CaSiO$_3$ and 1.62 for Floreon/HA fibrous film). Thus, the addition of a spin-coated layer to the fibrous mat increased the maximum tensile strength of the bilayer mats by approximately 43.9% for bilayer Floreon-Floreon/CaSiO$_3$ membranes compared to fibrous Floreon/CaSiO$_3$ films and by 13.2% for bilayer Floreon-Floreon/HA membranes compared to fibrous Floreon/HA films. This increase is a result of the significant physical connection that exists between these two layers (see Figure 4-113-D), which helps for stress to be transferred over the interface and improves the membranes' capacity to resist deformation (stiffness).
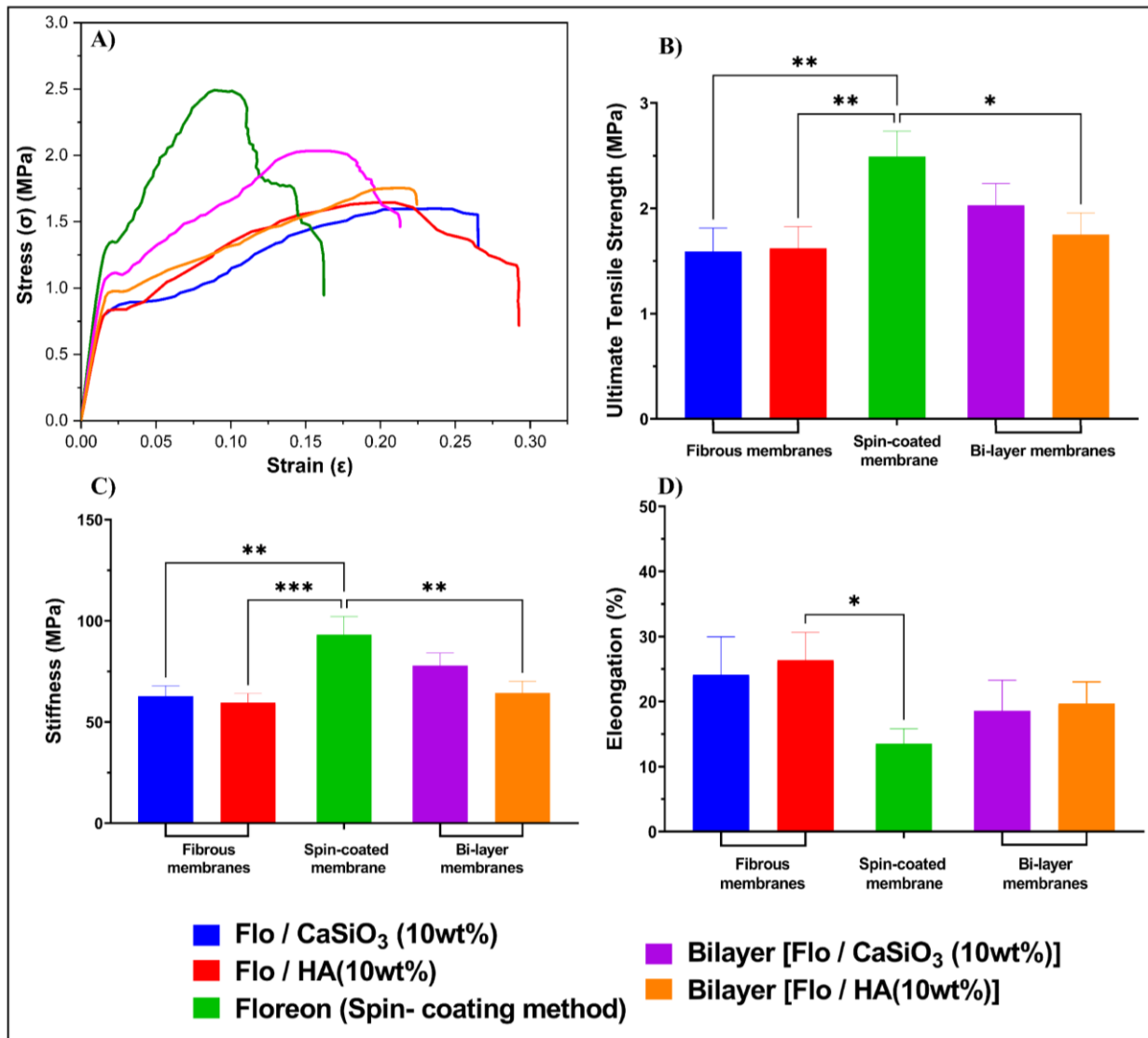
Figure 4-113 Stress-strain curve (A), ultimate tensile strength (B), stiffness (C), and percent elongation (D) of bilayer membranes formed by the deposition of Floreon random fibres over a Floreon spin-coated membrane are shown. The fibrous films were made of Floreon with 10 wt.% of Hydroxyapatite and Calcium Silicate particles. The outcome was compared to the performance of monolayer membranes. Data represented n=6, mean ± STDV following One-way ANOVA statistical analysis with Tukey comparison test. **** $p < 0.0001$, *** $p < 0.001$, ** $p < 0.01$, * $p < 0.05$.

Table 4-12 Tensile properties of the prepared bilayer films compared to those of monolayer films. To calculate the Ultimate tensile strength (MPa), Stiffness (MPa) and Elongation at break (%), the Values shown are mean ± SD where n=6.

Membranes	Ultimate Tensile Strength (MPa)		Stiffness (MPa)		Percent Elongation (%)	
	Mean	SD	Mean	SD	Mean	SD
Floreon (Spin- coating method)	2.49	0.24	93.13	9.03	13.52	1.31
Flo / CaSiO₃ (10wt%)	1.59	0.19	62.78	5.12	24.13	7.74
Flo / HA (10wt%)	1.62	0.21	59.55	4.60	26.35	9.00
Bilayer [Flo / CaSiO₃ (10wt%)]	2.03	0.23	77.92	3.80	18.56	5.05
Bilayer [Flo / HA (10wt%)]	1.75	0.20	64.37	3.53	19.67	6.02

The majority of the published research on membranes is concentrated on the processing of membranes (Khayet, Matsuura and Mengual, 2005; Susanto and Ulbricht, 2009), surface modification and antifouling qualities (Rahimpour and Madaeni, 2007; Vatanpour *et al.*, 2011). The physical and mechanical characteristics of a fibrous membrane have recently been explored using molecular dynamics (Cohen-Tanugi and Grossman, 2012, 2014). However, there are few reports of experimental studies of the mechanical properties of porous membranes under complicated loading modes with bioceramics. In this study, the mechanical properties measured from a stress–strain curve and corresponding calculations (ultimate tensile strength, stiffness, and percentage of elongation) were measured, including differences in Floreon classes. The experimental outputs are shown in Figure 4-113 and Table 4-12. The ultimate tensile strength of the spin-coated single layered Floreon was less than the spin-coated bilayer Floreon with bioceramics (10% wt). Although the spin-coated layer showed the best mechanical properties, the bilayer membranes were better than the single electrospun membrane, which was successful in enhancing the mechanical properties of the main layer.

According to previous reports on the material tensile strength, high ultimate tensile strengths make good, fitted materials for applications (Audic, Fourcade and Chaufer, 2007; Aly *et al.*, 2016; Hahn *et al.*, 2017). Stiffness of membrane *in vivo* is important for tissue biological functions, and the alteration of stiffness often relates to tissue dysfunction (Burg, Porter and Kellam, 2000; Lu *et al.*, 2003; Augustine *et al.*, 2019). The proliferation of rMSCs and NOFs cells in the bilayered architecture of the scaffold also depends on the stiffness and % elongation (Bružauskaitė *et al.*, 2016; Marei *et al.*, 2016; Xue *et al.*, 2017). The results indicate that the bilayered scaffold

constructed with Floreon, 10% HA, and CaSiO3 displayed more favorable outcomes compared to the single-layered Floreon scaffold.

4.3.4 Cell morphology and growth on scaffold surface:

The bilayered architecture of the scaffold was designed to fulfil its criteria as a future GBR membrane, which are to repair bone defects and prevent in-growth of soft tissue to the bone defects. Therefore, the functional properties of fibrous layers were assessed by growing rat-mesenchymal stem cells (r-MSCs), while normal oral fibroblasts (NOFs) were used on the compact spin-coated films. Differences in morphology and composition of the scaffolds influenced the migration and proliferation of r-MSCs and NOF cells in distinct ways.

After a seven-day incubation period, the adhesion, migration, and proliferation of fibroblast cells on spin-coated films were examined using SEM imaging and H&E staining, as depicted in Figure 4-114 and Figure 4-115, respectively. It can be seen in Figure 4-114(A and B) that the presence of small, uneven pores on the scaffold surfaces was found to facilitate cell growth and adherence, resulting in even cellular coverage. Importantly, the spin-coated membrane acted as a barrier, preventing cell penetration. In contrast, fibrous scaffolds were found to enhance the growth and proliferation of MSCs, as well as promote cellular infiltration, filling the inter-fiber spaces. This is evident in the magnified image presented in Figure 4-114 (C and D).
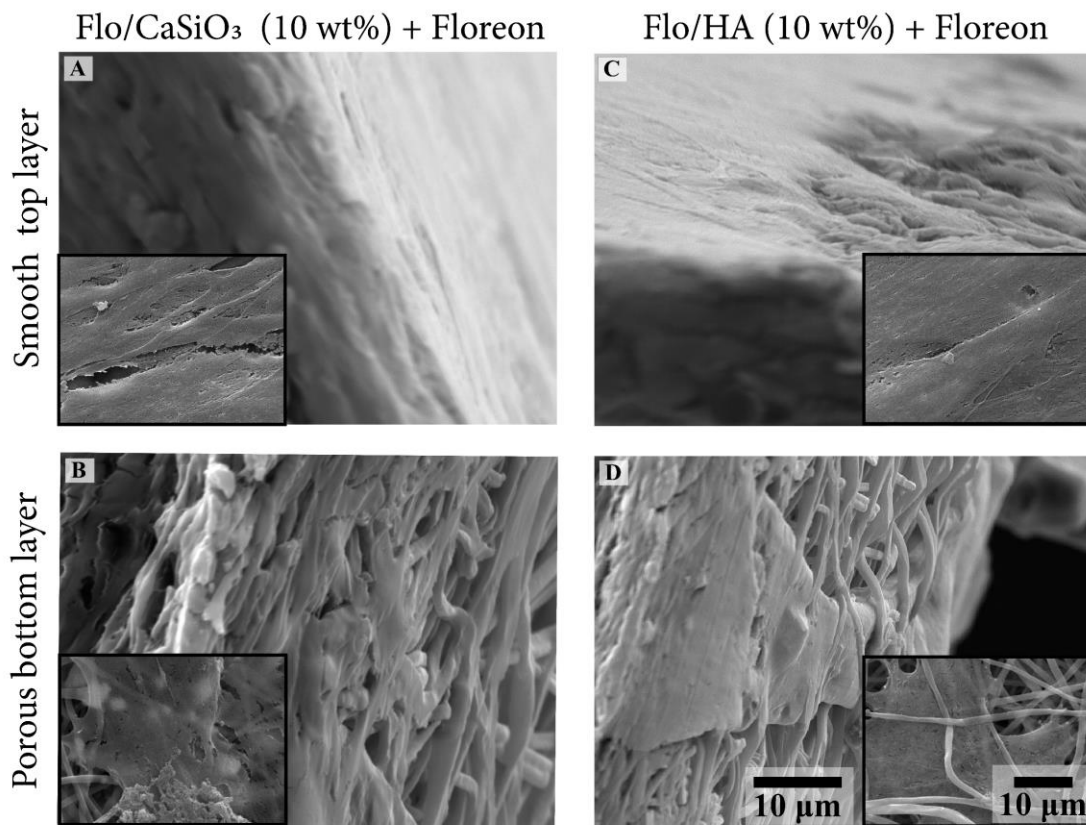
Figure 4-114 Cross-sectional SEM images of the bilayer films that had NOFs on the smooth membrane (A and C) and r-MSCs on the fibrous membrane (B and D) and then cultured for 7 days. The images on the left (A and B) show Floreon with 10% calcium silicate particles over a spin-coated Floreon membrane, while the images on the right (C and D) show Floreon with 10% hydroxyapatite particles over a spin-coated Floreon membrane. INSET image shows a more magnified section of the film's surface. The scale bar in all images is 10 μm

To monitor cellular migration and proliferation within the scaffold, cross-sections of cell-seeded films were stained with Hematoxylin and Eosin (H&E) to assess cellular migration and proliferation. It was clear that MSCs had infiltrated the scaffold, since cells were distributed throughout the interior and cells had stuck to the fibre structures denoted by the arrows (Figure 4-115 - B). However, as highlighted above, when NOF cells were seeded onto spin-coated films, they adhered and moved only on the surfaces, without penetrating the membrane (Figure 4-115 -A). Studying the H&E images, it became even clearer that the smaller pore size and compact architecture provided by the spin-coated layer stopped NOF cells' ingrowth into the fibrous layer making it an ideal barrier membrane prototype.
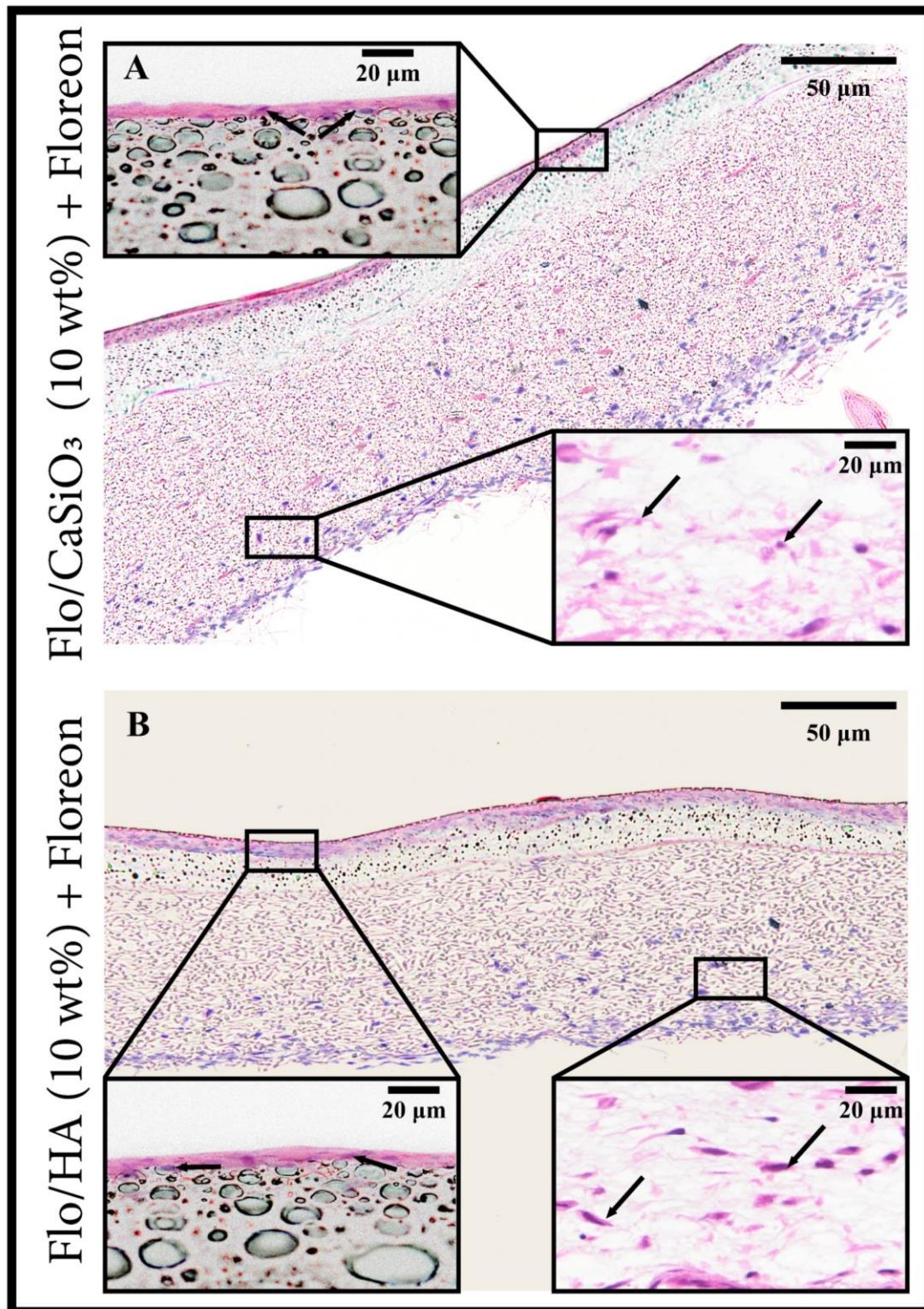
Figure 4-115 Hematoxylin and eosin staining indicating the histology of the prepared bilayer films seeded with r-MSCs on the fibrous membrane and NOFs on the smooth membrane and then cultured for 7 days; (A) Floreon with 10% hydroxyapatite particles deposition over a spin-coated Floreon membrane (scaled at 50 and 20 µm). ; (B) Floreon with 10% calcium silicate particles over a spin-coated Floreon membrane(scaled at 50 and 20 µm).

The interaction of cells with the extracellular matrix (ECM) profoundly regulates the spontaneous regeneration process of human tissues (Ehrbar *et al.*, 2007; Liu *et al.*, 2017). Recent research has examined how the physical characteristics of the extracellular matrix (ECM), specifically porosity, topography, and hierarchical 3D architecture, affect cellular processes and extrapolated guidelines for designing structures for efficient tissue regeneration (Li, Xiao and Liu, 2017; Lin *et al.*, 2018).

Electrospinning is one of the technologies that is frequently used to create ECM-mimicking structures, namely, to duplicate the fibrillar architecture of ECM (Khorshidi *et al.*, 2016). By regulating and adjusting the process parameters, it is possible to modify the topographical properties and induce porosity in electrospun microfibres. Similar alterations can be made to alter the ultimate structure of the fibrous network, including fibre alignment and patterning (Bhardwaj and Kundu, 2010; Binan *et al.*, 2014).

In this study, modified Floreon (PLA/PCL80/20) microfibers were produced using the electrospinning method with a composition of 10% wt HA and $CaSiO_3$, and were applied onto pure Floreon through a spin-coating process. Ramos-Rodriguez et al., found that the Floreon blend has proven to be a promising material to be used in bone tissue regeneration as shows an impact strength in the same range of that shown by native bone (just under 10 kJ/m2), and supports an improvement in osteogenic activity when modified with wollastonite (Ramos-Rodriguez *et al.*, 2022).

According to mechanical features analysis of this scaffold, the bilayered Floreon membranes with 10% HA and $CaSiO_3$ were a good choice for the GBR membrane. r-MSCs were employed to grow on the membrane to examine the functional qualities of the fibrous layers, whereas normal oral fibroblasts (NOFs) were applied to the compact spin-coated films. The MSCs that regenerate and differentiate into bone, cartilage, and fat become the cells that make up each of these tissues. This research helped us to find out the best membrane for GBR. SEM analysis (Figure 4-114) showed that the rMSCs cells stuck to the scaffold fibres and dispersed throughout the interior, in contrast to the NOFs, which were unable to grow into spin-coated membrane. Similar behaviour from MSCs has been observed in earlier research (Xue *et al.*, 2017). The spin-coated Floreon membrane can therefore be a beneficial support to heal bone defects and stop the ingrowth of soft tissue into the bone flaws.

The dense layer of the bilayer membranes exhibited appropriate pore sizes and an asymmetric pore structure that allow fibroblast to adhere to its surface, both of which are great indicators of the membranes' capacity to inhibit fibroblast infiltration. Pore sizes on the GTR side were smaller than

those seen in earlier membrane investigations (Rad *et al.*, 2017). H&E-stained pictures confirmed that the electrospun layer was porous, demonstrating its ability to permit osteoblast migration and nutrient permeability. The porosity of the electrospun layer was around 83% as were measured (see section 4.2.4).

Since the interface between layers is often difficult in several multilayer applications due to their distinct properties and lack of adhesion, research on tri-layer membranes seeking a functionally graded structure has been conducted (Liao *et al.*, 2005; Sun *et al.*, 2019). However, this study showed that a bilayer membrane with a well-adhered interface can be fabricated and that this type of membrane shows outstanding performance in terms of mechanical behaviour, morphological properties and bone regenerating ability with calcium phosphates enhancing osteoblast adhesion and migration.

CHAPTER 5:

GENERAL DISCUSSION

Chapter 5: General Discussion

Periodontal diseases are highly prevalent and can affect up to 90% of the worldwide population (Armitage, 2004; Jordan, 2004). These diseases may be of developmental, inflammatory, traumatic, neoplastic, genetic, or of metabolic origin (Armitage, 2004). However, periodontal disease usually refers to the common inflammatory disorders gingivitis and periodontitis, which are caused by pathogenic microorganisms in the biofilm or dental plaque, and form adjacent to the teeth on a daily basis (Albandar and Rams, 2002). The most common type of periodontal disease is gingivitis which is easily treatable with good oral hygiene. Worldwide, 50–90% of adults are affected by gingivitis (Albandar and Rams, 2002).

Periodontitis is characterised by inflammation that penetrates deep into the tissue causing the loss of alveolar bone and supporting connective tissue. Between the gingiva and tooth root, soft tissue pockets or deepening fissures develop as a result. In addition to occasional pain and discomfort, severe periodontitis can cause teeth to become loose, thus hindering chewing. Furthermore, both periodontitis and gingivitis patients are susceptible to developing oral cancer, of which periodontitis patients are at a higher risk than gingivitis patients (Wen *et al.*, 2014). Depending on the individual treatment goal, many non-surgical and surgical procedures are used to treat gingivitis and periodontitis (Albandar and Rams, 2002). The diverse periodontal therapy approaches seek to: (1) lessen and/or completely eradicate inflammation in tissue caused by bacterial plaque; (2) repair defects or anatomical issues caused by the disease; and (3) regenerate new periodontal tissue (Wang *et al.*, 2005; Sculean, Nikolidakis and Schwarz, 2008).

Since the mid-1980s, a variety of therapies have been developed to stimulate periodontal regeneration, including guided tissue/bone regeneration (GTR/GBR), root surface biomodification, bone replacement grafts, and the infusion of growth factors or gene therapies (Ramseier *et al.*, 2012). Among them, GTR and GBR have been identified as the most promising treatments and have been used extensively in clinical treatment (Nyman *et al.*, 1982; Villar and Cochran, 2010).

Periodontitis GTR/GBR treatments involve surgically implanting a regeneration membrane with the primary goal of aiding the renewal of damaged periodontal tissue underlying the teeth. The epithelial and gingival connective tissues frequently migrate quickly into the area of damage, inhibiting periodontal regeneration (Nyman *et al.*, 1982). In these treatments, the regeneration membrane is crucial because it serves as a barrier to stop epithelial and gingival connective cells from developing into periodontal defects and a friendly environment to encourage osteoblasts and periodontal ligament cells to migrate and multiply within the damaged area (Bottino *et al.*, 2012).

Barrier membranes must meet a number of fundamental criteria in order to improve clinical outcomes in dental implantology including good biocompatibility and biodegradability, suitable adhesiveness between the membrane and surrounding bone tissues to prevent membrane movement, high flexibility to facilitate surgery, and sufficient mechanical strength to maintain their barrier function for bone regeneration (Jianqi *et al.*, 2002; Oh *et al.*, 2006). Additionally, GTR/GBR procedures can be further improved by utilising a bioactive membrane that can accelerate bone development, while limiting the impact of bacterial contamination on the efficacy of the regenerative process (Jeon *et al.*, 2007).

The regeneration of periodontal tissue remains a challenge and over the past decades, GBR/GTR strategies using bioresorbable or non-resorbable dental membranes have been employed for regeneration of maxillofacial bone defects and treatment of periodontal tissue by mimicking the extracellular matrix and facilitating cell adhesion, proliferation, and differentiation (Soheilifar *et al.*, 2014). Currently, non-resorbable and resorbable membranes are widely available for guided tissue regeneration/ guided bone regeneration procedures in periodontal diseases. However, the use of biodegradable synthetic polymers such as polylactic acid (PLA), poly(D,L-lactide-co-glycolide) (PLGA), and poly(D,L-lactide-co-caprolactone) (PLCL) in constructing these membranes presents certain limitations such as poor mechanical properties, early or late absorption, and reduced capacity to maintain space, among others. To address these drawbacks, the potential of Floreon, a sustainable polymer blend composed of bioresorbable polyesters like PLA and polycaprolactone (PCL), was explored in this study for the first time in GTR/GBR applications. Several studies have shown that the addition of ceramic components into polymeric matrices that mimic the composition of real bone can enhance the osteoconductive and osteoinductive properties of bone constructs (Amini, Laurencin and Nukavarapu, 2012).

The aim of this research was to design and produce a bioactive Floreon-based membrane suitable for GTR/GBR techniques with improved mechanical properties and the ability to promote bone regeneration through osteoconductive and osteoinductive properties. To achieve this objective, bioceramics such as Hydroxyapatite (HA) and calcium silicate ($CaSiO_3$) were integrated into the polyester blend to enhance the functionality of the Floreon membrane. Prior research has established that $CaSiO_3$ can stimulate bone regeneration through the release of biologically relevant Si, similarly to tricalcium phosphate-based materials (Liu et al., 2017; Tcacencu et al., 2018; Qian et al., 2019). The project is divided into three main sections for discussion: fabrication and characterization of the fibrous membrane, fabrication and characterization of the smooth membrane, and fabrication and characterization of the bilayer membrane.

The initial task of this study was to manufacture and characterise individual membranes fabricated from Floreon and subsequently compare them to PLA membranes, which served as the control. The production processes were also compared, specifically focusing on solvent-coating and spin-coating. A comprehensive analysis of various physical properties was conducted to evaluate the efficacy of the membranes. The results indicated that Floreon membranes exhibited superior performance compared to PLA membranes across multiple criteria. To further optimise the suitability of the Floreon electrospun membranes for guided tissue and guided bone regeneration, bioceramics were incorporated. The structural integrity of these membranes was verified through validation procedures, and the results were consistent with prior research findings (Ramos-Rodriguez *et al.,* 2022).

Additionally, an optimised composition of Floreon/PLA with HA/CaSiO3 was formulated and the viscosity of the resulting solution was examined. The viscosity of the Floreon solution was found to be significantly higher than that of the PLA solution, as corroborated by prior investigations (Sreekumar, Al-Harthi and De, 2012; Bartczak and Galeski, 2014). Visual comparison of various Floreon compositions revealed that the addition of PCL that was used to form the thin layer, had a noticeable effect on the colour of the membrane. Additionally, compared to PLA membranes, Floreon membranes had more wrinkles and imperfections. Also, FTIR analysis showed that both PLA and Floreon exhibited comparable vibrational peak patterns with an additional peak observed with Floreon at 1726 cm-1 (because of the PCL used in its membrane).

Scanning electron microscopy (SEM) analysis revealed that spin-coated PLA and Floreon membranes possessed a smooth surface, while the solvent-casting method produced membranes with surface waviness and ridges. Moreover, the spin-coating method resulted in the formation of more porous membranes than the solvent-casting method, which is an essential feature for promoting cell adhesion. In order to optimise the pore size of the membrane scaffolds, previous studies have emphasized the importance of balancing mechanistic stability with cell migration. Specifically, Cao et al. (2010) and Atesok et al. (2016) have highlighted the need for a pore size that is neither too large nor too small. The highest level of porosity was achieved with a Floreon/CaSiO3 (20% wt) composite, which exhibited the highest crystallinity properties. This observation is consistent with earlier reports indicating that increasing the bioceramic concentration promotes higher crystallinity (Zhang et al., 2018; Pandey and Sakurai, 2021).

The crystallisation temperature of PLA was slightly higher than Floreon-based membranes, whereas the glass transition temperature of solvent-cast Floreon membranes was higher than PLA

membranes. In comparison, spin-coated PLA films had the highest Tg but it should be noted that all solvent-cast membranes had a higher melting point than spin-coated membranes. XRD analysis of the plain PLA structure revealed an amorphous form whereas Floreon has a semi-crystalline structure.

The thermal response of the membrane was examined, and it was found that an increase in bioceramic concentration promoted an increase in Tc, thus strengthening the interfacial interaction of the bioceramic with the polymer. However, increased bioceramic concentration had no effect on Tm and Tg values (Jiang *et al.*, 2010). The Floreon membranes demonstrated a lower onset temperature of degradation compared to PLA films and exhibited a lower maximum thermal degradation, indicating that they are more stable under heat. The thermal degradation of the scaffolds was assessed using TGA analysis, and no dehydration was observed at temperatures above approximately 100°C.

The wettability of the scaffold was also evaluated, and it was observed that both HA and $CaSiO_3$ improved the membrane wettability of PLA, with greater enhancement observed in Floreon membranes compared to PLA. Additionally, spin-coated membranes exhibited lower water contact angles than solvent-cast membranes, indicating higher hydrophilicity and wettability resulting from the spin-coating process. Although spin-coated films were more hydrophilic and exhibited higher surface wettability, no significant difference was detected between PLA and Floreon. The optimal wettability performance was observed with Floreon/$CaSiO_3$ (20% wt), which also displayed the highest level of hydrophilicity.

The mechanical properties of the scaffolds were evaluated for their potential *in vivo* performance (Prasadh and Wong, 2018). This is critical as the membrane must retain functionality under mechanical stresses, particularly with regards to interacting cells (Little, Bawolin and Chen, 2011). The tensile characteristics of the scaffolds were assessed under stress, and it was found that the addition of bioceramics increased stiffness compared to the absence of bioceramics, although the highest concentrations decreased stiffness. Furthermore, the addition of bioceramics reduced the elongation capacity of the scaffold. Although PLA membranes exhibited slightly greater elongation than Floreon membranes, the stiffness of the Floreon films was more than twice that of PLA, regardless of whether the membrane was solvent-coated or spin-coated. Moreover, Floreon membranes exhibited the highest tensile strength when spin-coated. The addition of a spin-coated layer to the fibrous layer increased the maximum tensile strength of the bilayer compared to fibrous membranes alone. This increase resulted from the significant physical connection between these

two layers, which also facilitated stress transfer across the interface, thereby enhancing the membranes' capacity to resist deformation. The relevance of these findings to fibroblast or rMSC migration and the potential impact on GTR/GBR were not evaluated.

Previous research has shown that HA and $CaSiO_3$ microfibres can undergo changes due to exposure to hydrolytic fluids (Calvino, 2022). However, significant differences in microfibres were not observed when applied to PLA or Floreon. The weight loss of the scaffolds was consistent but faster between 8 and 16 weeks, consistent with previous studies (Nica *et al.*, 2022), but different from other studies reporting an initial weight loss for 4 days (Sanchez *et al.*, 2021). This weight loss is attributed to Ca^{2+} release (Sanchez *et al.*, 2021), ester bond breaks (Jeong *et al.*, 2017), or the production of hydroxyl and carboxylic acid groups (Choi *et al.*, 2020). The residual weight percentage of spin-coated and solvent-cast PLA membranes was higher than Floreon membranes, but there were no major differences between the two methods used to produce either Floreon or PLA membranes. It should be noted that the effects of these chemical changes on cells in the presence of the scaffolds require extensive testing, as Ca^{2+} affects many cellular processes, including cell-to-cell signalling, apoptosis, innate immunity, transcription, and motility (Clapham, 2007). Although scaffold integrity may be compromised, the release of Ca^{2+} may prove beneficial in the context of GTR/GBR. Notably, the concentration of HA and $CaSiO_3$ did not affect the structural integrity of the microfibres. Water uptake is an important consideration, with Floreon/HA showing a higher water uptake (20% wt) that alters the hydrophilicity of the membrane. Spin-coated films were found to be more effective for water uptake than solvent-cast membranes. While the water absorption rate of spin-coated and solvent-cast Floreon membranes was higher than that of PLA, there were no major differences between the two production methods.

The structural changes that occur during scaffold degradation were analyzed in detail using Fourier transform infrared (FTIR) analysis. The various changes that occur during the degradation process, including the loss of hydroxyapatite (HA) from the fibers, have been previously observed by Yang *et al.* (2020). However, it has also been shown that HA and $CaSiO3$ can be reabsorbed under specific conditions (Nguyen and Thao, 2022). The analysis showed changes in fiber diameter with respect to the number of days immersed in simulated body fluid (SBF). Furthermore, cracks that appeared to be due to erosion were observed. In addition, the Floreon membranes curled up under these conditions, and scanning electron microscopy (SEM) revealed no indication of apatite formation on the membranes immersed in SBF. While the importance of scaffold pore size has been described, it should be noted that there were considerable changes to the porosity after scaffold-mediated degradation, which became more severe with time, particularly with Floreon scaffolds.

In all samples, it was found that the FTIR peak intensities decreased over time due to immersion in SBF. Furthermore, DSC analysis showed that after 24 weeks of immersion, Tc decreased for all samples, while Tg and Tm increased, evidenced by the emergence of new peaks of which the intensity of peaks increased in proportion to the length of immersion time.

Other changes were observed, including a tendency for Floreon membranes to curl up. As noted previously, comprehending the influence of scaffold property variations on cellular behavior would be advantageous. Previous studies have linked surface bioactivity to the alterations observed on membrane surfaces instead of the molecular changes that occur within cells. Furthermore, considering that cells exist in different morphologies and states depending on their functions, it is essential to investigate the direct bioactivity of membranes on cells.

Changes in pH were observed as the scaffolds degraded, with a notable increase in rate between 8 and 16 weeks, coinciding with the period of rapid weight loss. Regarding the production method, the pH of SBF-containing spin-coated and solvent-cast Floreon membranes was higher compared to PLA membranes. The pH continued to decrease up to week 24 and was further reduced with the addition of bioceramics. It would be important to determine if the changes to pH, weight loss, and Ca^{2+} among other factors could be related to each other. As mentioned earlier, the biological impact of Ca^{2+} is significant as the cell behaviour can change dramatically and the same can be applied to pH changes. Studies of wound healing have shown that cell proliferation is enhanced in alkaline conditions while a shift towards either alkaline or acidic conditions reduced cell migration (Kruse *et al.*, 2017). Furthermore, the study discussed herein has demonstrated that a highly acidic wound environment can impede wound closure and re-epithelialisation, whereas alkaline conditions do not appear to have such an effect. This observation is of particular importance given that the higher concentrations of bioceramics used in the study resulted in the lowest pH levels. While prior research has suggested that an acidic environment may promote enzyme functionality, which is an essential requirement for wound healing (Schneider *et al.*, 2007), it is vital to consider other factors that could impact the pH, such as the degradation of hydroxyapatite and the release of calcium ions (Murugan and Ramakrishna, 2004). Notably, the pH of simulated body fluid (SBF) is known to decrease moderately within the first five days, which is consistent with the findings of the present study (Cortes *et al.*, 2005). However, bioceramics and degradation significantly influenced the pH, and the highest pH was observed in Floreon (20% wt) incubated in SBF for 24 weeks. Furthermore, previous research has established the optimal pH range for mammalian cell growth to be 7.38 to 7.87, with pH 8 being the ideal pH for the growth and mineralisation of bone marrow stromal cells (BMSCs) (Mackenzie, Mackenzie and Beck, 1961; Fliefel *et al.*, 2016). This suggests that

maintaining an appropriate pH level is crucial for wound healing and cell growth, and thus should be carefully monitored in biomedical research.

After an evaluation of the suitability of the Floreon/bioceramic combination as a scaffold, the scaffold's interaction with rMSCs was examined. The results revealed that the Floreon scaffold with either HA or $CaSiO_3$ provides a favorable environment for rMSCs, promoting successful adhesion and proliferation rates that surpass those observed under control conditions. It is noteworthy that the Floreon scaffold outperforms PLA, and the incorporation of both HA and $CaSiO_3$ enhances cell migration, as demonstrated by the wound closure assay and cell adhesion. The PrestoBlue cell proliferation assay showed that the addition of HA or $CaSiO_3$ at increasing concentration, increased proliferation and these results were mirrored for PicoGreen and total protein assays, showing higher concentrations of DNA and protein, respectively. More specifically, the metabolic activity of fibroblasts was significantly higher on spin-coated membranes made with both materials than on solvent-cast membranes.

There was a slight difference between the spin-coated Floreon and PLA membranes on day 14 where cells attached to Floreon had a higher metabolic activity. The spin-coated membranes had a lower percentage of dead cells and significantly higher cell proliferation than solvent-cast membranes, although the concentration of dsDNA in PLA and Floreon membranes were comparable for each production method. The total protein secretion from cells cultured on spin-coated membranes was greater than solvent-cast membranes, regardless of the type of material. The metabolic activity of fibroblasts were significantly higher on spin-coated PLA and Floreon membranes compared to solvent-cast scaffolds. Furthermore, ALP activity was also increased in rMSCs under the same scaffold conditions.

Regarding the impact of bioceramics on cells, existing research has demonstrated that cells treated with hydroxyapatite (HA) exhibit a greater ability to spread over a wound area and migrate compared to untreated cells (Ghose *et al.*, 2018). Similarly, other bioceramics like wollastonite have demonstrated higher bioactivity and osteoinductivity when compared to untreated membranes (Li and Chang, 2013). In light of these findings, observation using scanning electron microscopy (SEM) indicated that there was no significant difference in cell morphology between Floreon and polylactic acid (PLA) membranes, regardless of the fabrication method. However, by day 14, cell area spread was greater on Floreon membranes compared to PLA membranes. Additionally, the shape and number of fibroblasts on the surface of the Floreon membrane indicate a secure cell attachment, as evidenced by visible spreading of lamellipodia and filopodia, when compared to PLA membranes.

The bilayer membranes exhibited the appropriate pore structure that allows fibroblasts to adhere to its surface with pore sizes shown to be smaller than those seen in earlier membrane investigations (Jafari *et al.*, 2017). H&E-staining confirmed that the electrospun layer was porous, which demonstrates its ability to permit osteoblast migration whilst allowing for nutrient permeability. Furthermore, the bilayer membrane shows excellent performance in terms of mechanical behaviour, morphological properties, and bone regeneration ability with calcium phosphates that enhance cell adhesion and migration.

In essence, the data presents a positive biocompatibility outcome for the Floreon scaffolds to fibroblasts and rMSCs; however, it is important to consider that some results could be because of increased cell proliferation such as the increase in total protein and DNA, likely to be higher because of the greater number of cells, or faster wound closure due to proliferation rather than the individual cell capacity to migrate further. For both instances, individual cell tracking and marker specificity would be needed to be explored in the future. To better understand whether the individual rMSCs did migrate, live cell tracking could be performed with a time-lapse microscope. It is also important to consider the way in which the rMSCs migrate in relation to cell density. Mesenchymal stem cells can migrate collectively or individually (De Pascalis C, 2017) and this will affect tissue and bone regeneration. This also relates to how rMSCs behave in terms of their stemness and how the scaffold and bioceramics may affect differentiation and as such, it should be considered how stem and differentiation markers are altered by cell interaction to Floreon as well as HA and CaSiO$_3$. This could be investigated by Floreon cytometry, western blot, or qPCR at selected timepoints of increasing cell density.

A particularly important consideration should be rMSC epithelial-to-mesenchymal transition (EMT) and the reverse process of mesenchymal-to-epithelial transition (MET). Although rMSCs are not epithelial by nature, epithelial characteristics are important for osteoblast growth and overall bone generation and is characterised by a loss of stem cell markers in MSCs such as CD44 (Hanna, Mir and Andre, 2018; Larrouture *et al.*, 2021). The PrestoBlue assay shows greater proliferation which is a characteristic of stem cells and MET, and suggests the suppression of EMT-mediated migration. Similar to wound healing in the skin upon which the wound closure assay was formulated, a number of keratinocytes will undergo EMT to fill the empty space after which they will revert to an epithelial form, which corresponds to upregulated proliferation (Nourian Dehkordi A, Mirahmadi Babaheydari F, Chehelgerdi M, 2019). Furthermore, stem cells are thought to be plastic therefore, rMSC transitioning between phenotypes could be characterised further (Zhang *et al.*, 2014). It would also be useful to determine how the expression of markers changes over time as

the cells become more confluent. As mentioned earlier, with higher cell density the EMT markers would be reduced while proliferation increases towards the Hayflick limit.

While the results generally show successful biocompatibility of rMSCs to the scaffolds particularly Floreon with HA or $CaSiO_3$, there are a few questions that arise. A study by Amer and colleagues tested the adhesion of human MSCs to smooth, dimpled, and angular surfaces and found that the cells were more adherent to the textured surfaces (Amer *et al.*, 2021). The study also showed that ALP activity was higher in cells attached to the textured surfaces which validates the findings in this study. More importantly, Amer *et al*. (2021) demonstrated that textured scaffolds improved the attachment of human MSCs and induced bone regeneration in vivo when implanted in mice. Based on the present study's findings, it can be inferred that the Floreon-based model tested in this study could serve as an effective GBR membrane. Nevertheless, it is crucial to consider the gene profiling results obtained by Amer and colleagues, which revealed significantly different metabolic and genetic profiles of MSCs attached to smooth and textured membranes. This variation is likely attributed to the MSCs' adhesion profile to different surfaces, which could significantly contribute to the observed outcomes in this study.

As discussed earlier, and inferred by the study by Amer and colleagues (Amer *et al.*, 2021), the attachment and overall cell phenotype will affect the characteristics of the rMSCs. As such, it would be beneficial to study this in more detail to further optimise GBR when using a Floreon scaffold. Firstly, it would be useful to determine at which density and time point rMSCs are most migratory, which is likely to be when the cell density is lowest and before there is secure attachment to the scaffold. Given that rMSCs were shown to migrate in the direction of the scaffold fibres, this could open a window of opportunity to direct rMSCs to a very specific area for GBR. The profile of the cells at this point would be that of reduced proliferation and potentially identifiable by the upregulation of EMT cells. Secondly, it would be beneficial to identify when rMSCs start to adhere to the scaffold. This is likely to be when the cells begin to increase proliferation and could be identified by an increase in MET markers. Furthermore, this may coincide with increased ALP activity, which would suggest rMSC cell differentiation to osteoblasts. Regarding the culture of rMSCs in BM and OS media, it was expected that ALP activity would be greater in OS media than BM media however, the effect OS media has on other factors that could affect GBR are not known. The findings of this study suggest that promoting osteoblast differentiation using Floreon with either HA and CaSiO3 can potentially benefit the guided bone regeneration (GBR) process. However, it remains unclear if this approach has any effect on epithelial-to-mesenchymal transition (EMT) or cell adhesion.

As such, it would be useful to further define the profile of rMSCs cultured with both BM and OS media for proliferation, protein and DNA level, cell migration, and phenotype. Then, OS media should be removed to see how the differentiated osteoblasts behave in relation to proliferation and cell viability from the treatment standpoint, as the viability of the cells needs to be maintained without OS media.

The present study culminated in the development of a bilayered membrane, which underwent extensive testing with both NOFs and rMSCs. Following meticulous experimentation, the optimal membrane was identified to be Floreon with 10% HA or CaSiO3, fabricated utilising electrospinning and spin-coating techniques. The membrane's distinct properties were found to facilitate rMSC cell adhesion, proliferation, and migration, while also preventing NOFs from crossing the membrane barrier. Through SEM analysis, a high degree of rMSC integration with the scaffold was observed, with cells infiltrating the inter-fibre gaps. This is a fundamental aspect of in vivo use, as it would allow for MSC migration and subsequent differentiation, without interference from fibroblasts in the affected area. Although the study successfully demonstrated the scaffold's in vivo suitability under the given experimental conditions, additional layers of information could enhance GBR optimization, such as examining the microenvironmental changes.

The co-culture of rMSCs with NOFs could have been tested at different densities to determine what the optimal ratio of each cell type should be. Given that cells cultured on the membranes migrate and proliferate more, it would be useful to know rMSCs interact with NOFs via paracrine signalling for example. Furthermore, profiling the secreted component from cells is also something to consider as excessive or uncontrollable growth could elicit an unwanted immune response. To expand on this, it would be useful to characterise rMSCs and/or osteoblasts once the cells have become confluent. At this point it would be expected that GBR would be occurring therefore, learning the cellular profile of these changes would allow for better optimisation and use of the Floreon scaffold.

Ultimately, this study showed that a bilayer membrane with a well-adhered interface can be fabricated and that this type of membrane shows outstanding performance in terms of mechanical behaviour, morphological properties and bone regenerating ability with calcium phosphates enhancing osteoblast adhesion and migration.

CHAPTER 6:

CONCLUSIONS AND FUTURE WORK

Chapter 6: Conclusions and Future Work

Conclusions

The aim of this project was to deliver a functional periodontal bilayer membrane. For the membrane to be functional, individual layers needed to be carefully designed and tested. The primary function of the spin-coated membrane composed of Floreon reinforced with relevant bioceramics, was to facilitate the formation of new bone by assisting the adherence of mesenchymal stromal cells. While the smooth, thin surface layer was produced from pure Floreon utilising spin-coating technology and its primary purpose was to act as a physical barrier to ensure the required mechanical performance and prevent connective tissue and epithelium interference during bone formation. The results demonstrated the successful fabrication of a bilayer construct by electrospinning Floreon with bioceramic particles over a Floreon spin-coated film.

This study has achieved several significant milestones in the field of GTR/GBR treatments, including:

- Identification of a suitable Floreon/HA and Floreon/CaSiO3 membrane polymer composition for in vivo GBR use, resulting in the fabrication of a scaffold with a compact, smooth top surface and a uniform, fibrous bottom surface. The membrane was fabricated by spin-coating of the fibrous layer to increase the maximum tensile strength of the bilayer, creating a physical connection between the two layers that improved their capacity to resist deformation.

- Identification of an optimal bioceramic and Floreon composition that allows for rMSC cell adherence. The degradation properties that include pH level changes and precipitation of a biological apatite layer serve as important findings that can be used in future optimisations of the scaffold, particularly in vivo once the full extent of these scaffold property changes are realised in rMSCs.

- Assessment of stiffness and structural changes provide information about possible treatment duration and when coupled with rMSC proliferation and differentiation profiles, could become vital for creating full treatment plans, which could also negate the effects of scaffold degradation, if GTR/GBR occurs faster.

- Presence of small and irregular pores on the scaffold surfaces facilitated cell adhesion and growth, resulting in even cellular coverage. Notably, the spin-coated membrane served as a barrier and prevented interference from fibroblasts, ultimately promoting rMSC growth. Additionally, the fibrous scaffolds exhibited increased rMSC cell growth, proliferation, and migration.

- Observance of rMSC infiltration of the scaffold and attachment to the fibre structures, while fibroblasts were only able to adhere and move on the surfaces of spin-coated films without penetrating the membrane. These findings represent significant advancements in the field of GTR/GBR treatments and hold promise for future applications.

It has been established that the surface pattern, pore size, and incorporation of bioceramics into Floreon significantly influence rMSC cell adherence and migration. Additionally, the scaffold material affects cellular biology, including proliferation and morphology. These findings demonstrate the intricacy of scaffold biosuitability and emphasise the need for additional considerations in cell biology. As part of improving the GTR/GBR process, characterisation of cellular behaviour is crucial for optimising the regeneration process. A better understanding of how factors such as Ca^{2+} affect specific cell types can lead to the development of improved GTR/GBR approaches beyond scaffold properties.

The study presents an optimised and characterised prototype Floreon membrane that has undergone successful in vitro testing using fibroblasts and rMSCs. The bilayer membrane, with a well-adhered interface, demonstrates excellent mechanical behaviour, morphological properties, and bone regeneration abilities. These findings provide a basis for the development of a biofunctional and sustainable periodontal therapy platform.

Future work

This study focused primarily on the optimisation and characterisation of the bilayer membrane, with a partial examination of its biological performance. Given the opportunity for further investigation, a comprehensive characterisation of cell performance on the Floreon scaffolds would be beneficial. This could involve RNA sequencing to profile the specific cellular changes that occur, ideally at different timepoints. As previously mentioned, the epithelial-mesenchymal transition (EMT) phase of rMSCs occurs early in the wound healing process, after which the cells undergo proliferation and differentiation. It is hypothesised that the genetic changes occurring during this process, and the molecular mechanisms affected by the scaffold, could be observed through RNA sequencing. Such information would aid in the optimization of cell performance, potentially through the identification of supplements that promote guided bone regeneration. This would be particularly valuable in the field of stem cell biology, as it would allow for the control and optimisation of cell migration and differentiation at various stages.

Immunofluorescence would provide very useful information regarding cell differentiation across the construct which could be studied using relevant markers including CD105, CD73 and CD9. Fibroblast on the top layer could be labelled using Vimentin.

Scaffold degradation revealed a number of changes including the release of Ca2+ and a change in pH levels. A simple experiment would be to collect the products of degradation and test the effects on cells directly, again comparing early and late degradation products. By identifying the individual products (possibly by mass spectrometry) and profiling cellular changes allows for another layer of optimisation, which could be as simple as adjusting the pH at different timepoints to affect cell behaviour. Another factor to consider is the production of free radicals from degradation and the possible effects on cell behaviour. Similarly, it would be interesting to understand if degraded scaffolds retain their cell adherence and migration properties, which would help us to understand the longevity of the scaffolds and if it is possible to perhaps refresh older scaffolds with treatments that help the GTR/GBR process even when the scaffold has become compromised.

Based on the observations made, it was found that the addition of bioceramics has a significant impact on cellular interaction, but it compromises the stiffness and elongation of the scaffold. Hence, it is imperative to investigate the behaviour of cells on the stressed and damaged scaffolds. Additionally, it is important to determine if the scaffolds can be repaired and how this could affect the ongoing guided tissue regeneration (GTR) or guided bone regeneration (GBR) process. A more comprehensive study on biocompatibility and cell behaviour, coupled with the optimisation of the

prototypes, would be necessary to establish the ideal scenario. This would involve an in vivo study to obtain key data on the performance of the membranes in a physiologically relevant environment.

Covid-19 Impact Statement

In March 2020, the COVID-19 pandemic caused by the novel coronavirus emerged as a global health crisis, leading to nationwide and global lockdowns in an effort to contain its spread. The University of Sheffield was among the institutions that were affected by this pandemic, with the majority of its campuses being closed. This had a significant impact on the postgraduate research researchers (PGRs) who were conducting research at the university.

The closure of the University of Sheffield campuses meant that many PGRs were unable to continue their research work as planned, resulting in significant delays and disruptions. Although the university campuses started to reopen in June 2020, they had to implement various regulations and restrictions to ensure the safety of their staff and students. This included limiting laboratory access to 10 hours per week, which further impacted the research activities of PGRs.

As a result, I had to modify their research objectives to account for the disruption caused by the pandemic and the associated restrictions. Some objectives that were previously outlined as future work could not be achieved due to the limited access to laboratory facilities, and the need to adhere to safety protocols.

Despite the challenges posed by the pandemic, I persevered and conducted extensive testing during these difficult times, adapting to new working conditions and modifying my research objectives to account for the disruption caused by the pandemic and the associated restrictions. This experience has underscored the importance of contingency planning and risk management in research activities, which will enable researchers to be better equipped to handle unexpected disruptions in the future.

CHAPTER 7:

REFERENCES AND APPENDIX

Chapter 7: References and Appendix

References

Aaboe, M., Pinholt, E.M. and Hjorting-Hansen, E. (1995) 'Healing of experimentally created defects: a review', *British Journal of Oral and Maxillofacial Surgery*, 33(5), pp. 312–318.

Abdelaal, O.A.M. and Darwish, S.M.H. (2013) 'Review of rapid prototyping techniques for tissue engineering scaffolds fabrication', in *Characterization and Development of Biosystems and Biomaterials*. Springer, pp. 33–54.

Abdollahi, S., Ma, A.C.C. and Cerruti, M. (2013) 'Surface transformations of Bioglass 45S5 during scaffold synthesis for bone tissue engineering', *Langmuir*, 29(5), pp. 1466–1474.

Abe, G.L. *et al.* (2020) 'Fabrication of novel poly (lactic acid/caprolactone) bilayer membrane for GBR application', *Dental Materials*, 36(5), pp. 626–634.

Agarwal, S., Wendorff, J.H. and Greiner, A. (2009) 'Progress in the field of electrospinning for tissue engineering applications', *Advanced Materials*, 21(32-33), pp. 3343–3351.

Agrawal, C.M. *et al.* (2000) 'The use of the vibrating particle technique to fabricate highly porous and permeable biodegradable scaffolds', in *Synthetic Bioabsorbable Polymers for Implants*. ASTM International.

Agrawal, C.M., Parr, J.E. and Lin, S.T. (2000) 'Synthetic bioabsorbable polymers for implants', in. American Society for Testing and Materials West Conshohocken, PA.

Akpan, E.I. *et al.* (2019) 'Electrospun porous bio-fibre mat based on polylactide/natural fibre particles', *Arab Journal of Basic and Applied Sciences*, 26(1), pp. 225–235.

Albandar, J.M. and Rams, T.E. (2002) 'Global epidemiology of periodontal diseases: an overview', *Periodontology 2000*, 29(1), pp. 7–10.

Aldemir Dikici, B. *et al.* (2019) 'A novel bilayer polycaprolactone membrane for guided bone regeneration: combining electrospinning and emulsion templating', *Materials*, 12(16), p. 2643.

Ali, M.S. *et al.* (2018) 'Comprehensive exploration of the anticancer activities of procaine and its binding with calf thymus DNA: a multi spectroscopic and molecular modelling study', *RSC advances*, 8(17), pp. 9083–9093.

Alizadeh, M. *et al.* (2013) 'Microstructure and characteristic properties of gelatin/chitosan scaffold prepared by a combined freeze-drying/leaching method', *Materials Science and Engineering: C*,

33(7), pp. 3958–3967.

Aljohani, W. *et al.* (2018) 'Bioprinting and its applications in tissue engineering and regenerative medicine', *International journal of biological macromolecules*, 107, pp. 261–275.

Alksne, M. *et al.* (2020) 'In vitro comparison of 3D printed polylactic acid/hydroxyapatite and polylactic acid/bioglass composite scaffolds: Insights into materials for bone regeneration', *Journal of the mechanical behavior of biomedical materials*, 104, p. 103641.

Alsharif, N. *et al.* (2020) 'Physiologically relevant mechanics of biodegradable polyester nanoparticles', *Nano Lett.*, 20(10), pp. 7536–7542. Available at: https://doi.org/10.1021/acs.nanolett.0c03004.

Alvarez-Fernandez, A. *et al.* (2020) 'Structural characterization of mesoporous thin film architectures: a tutorial overview', *ACS applied materials & interfaces*, 12(5), pp. 5195–5208.

Aly, I.H.M. *et al.* (2016) 'Preparation and characterization of wollastonite/titanium oxide nanofiber bioceramic composite as a future implant material', *Ceramics International*, 42(10), pp. 11525–11534.

Amer, M.H. *et al.* (2021) 'Designing topographically textured microparticles for induction and modulation of osteogenesis in mesenchymal stem cell engineering', *Biomaterials*, 266, p. 120450. Available at: https://doi.org/https://doi.org/10.1016/j.biomaterials.2020.120450.

Amini, A.R., Laurencin, C.T. and Nukavarapu, S.P. (2012) 'Bone tissue engineering: recent advances and challenges', *Critical Reviews™ in Biomedical Engineering*, 40(5).

An, J. *et al.* (2015) 'Design and 3D printing of scaffolds and tissues', *Engineering*, 1(2), pp. 261–268.

Aouadja, F. *et al.* (2022) 'Fabrication and properties of novel porous ceramic membrane supports from the (Sig) diatomite and alumina mixtures', *Boletín de la Sociedad Española de Cerámica y Vidrio*, 61(5), pp. 531–540.

Araujo, M.G., Berglundh, T. and Lindhe, J. (1998) 'GTR treatment of degree III furcation defects with 2 different resorbable barriers an experimental study in dogs', *Journal of clinical periodontology*, 25(3), pp. 253–259.

Armitage, G.C. (2004) 'Periodontal diagnoses and classification of periodontal diseases', *Periodontology 2000*, 34(1), pp. 9–21.

Atesok, K. *et al.* (2016) 'Multilayer scaffolds in orthopaedic tissue engineering', *Knee Surgery, Sports Traumatology, Arthroscopy*, 24(7), pp. 2365–2373.

Audic, J.-L., Fourcade, F. and Chaufer, B. (2007) 'Biodegradable material obtained from renewable resource: Plasticized sodium caseinate films', in *Thermodynamics, Solubility and Environmental Issues*. Elsevier, pp. 369–382.

Augustine, R. *et al.* (2019) 'CTGF loaded electrospun dual porous core-shell membrane for diabetic wound healing'.

Avolio, R. *et al.* (2012) 'A multitechnique approach to assess the effect of ball milling on cellulose', *Carbohydrate Polymers*, 87(1), pp. 265–273.

Balla, E. *et al.* (2021) 'Poly (lactic Acid): A versatile biobased polymer for the future with multifunctional properties—From monomer synthesis, polymerization techniques and molecular weight increase to PLA applications', *Polymers*, 13(11), p. 1822.

Ballestrem, C., Wehrle-Haller, B. and Imhof, B.A. (1998) 'Actin dynamics in living mammalian cells', *Journal of cell science*, 111(12), pp. 1649–1658.

Barber, H.D. *et al.* (2007) 'Using a dense PTFE membrane without primary closure to achieve bone and tissue regeneration', *Journal of Oral and Maxillofacial Surgery*, 65(4), pp. 748–752.

Bartczak, Z. and Galeski, A. (2014) 'Polymer Blends Handbook'. Springer Dordrecht, The Netherlands:

Bartee, B.K. (1995) 'The use of high-density polytetrafluoroethylene membrane to treat osseous defects: clinical reports', *Implant dentistry*, 4(1), pp. 21–31.

Basile, M.A. *et al.* (2015) 'Functionalized PCL/HA nanocomposites as microporous membranes for bone regeneration', *Materials Science and Engineering: C*, 48, pp. 457–468.

Baykan, B. *et al.* (2015) 'Migraine incidence in 5 years: a population-based prospective longitudinal study in Turkey', *The journal of headache and pain*, 16(1), pp. 1–10.

Becker, W. *et al.* (1991) 'Guided tissue regeneration for implants placed into extraction sockets: A study in dogs', *Journal of Periodontology*, 62(11), pp. 703–709.

Becker, W. *et al.* (2001) 'A longitudinal study comparing scaling, osseous surgery, and modified Widman procedures: results after 5 years', *Journal of periodontology*, 72(12), pp. 1675–1684.

Behring, J. *et al.* (2008) 'Toward guided tissue and bone regeneration: morphology, attachment, proliferation, and migration of cells cultured on collagen barrier membranes. A systematic review', *Odontology*, 96(1), pp. 1–11.

Belabbes, K. *et al.* (2022) 'Creation of a stable nanofibrillar scaffold composed of star-shaped PLA network using sol-gel process during electrospinning', *Molecules*, 27(13), p. 4154. Available at: https://doi.org/10.3390/molecules27134154.

Berkovitz, B.K.B., Holland, G.R. and Moxham, B.J. (2017) *Oral Anatomy, Histology and Embryology E-Book*. Elsevier Health Sciences.

Bezwada, R.S. *et al.* (1995) 'Monocryl® suture, a new ultra-pliable absorbable monofilament suture', *Biomaterials*, 16(15), pp. 1141–1148.

Bhardwaj, N. and Kundu, S.C. (2010) 'Electrospinning: a fascinating fiber fabrication technique', *Biotechnology advances*, 28(3), pp. 325–347.

Bhattarai, D. *et al.* (2018) 'A review on properties of natural and synthetic based electrospun fibrous materials for bone tissue engineering', *Membranes*, 8(3), p. 62.

Bianco, A. *et al.* (2007) 'Thermal stability and sintering behaviour of hydroxyapatite nanopowders', *Journal of thermal analysis and calorimetry*, 88(1), pp. 237–243.

Bianco, A. *et al.* (2009) 'Electrospun poly (ε-caprolactone)/Ca-deficient hydroxyapatite nanohybrids: microstructure, mechanical properties and cell response by murine embryonic stem cells', *Mater Sci Eng C*, 29(6), pp. 2063–2071.

Bikiaris, D.N. *et al.* (2007) 'Miscibility and enzymatic degradation studies of poly (ε-caprolactone)/poly (propylene succinate) blends', *European polymer journal*, 43(6), pp. 2491–2503.

Bilir, A. *et al.* (2007) 'Biocompatibility of different barrier membranes in cultures of human CRL 11372 osteoblast-like cells: an immunohistochemical study', *Clinical Oral Implants Research*, 18(1), pp. 46–52.

Binan, L. *et al.* (2014) 'Differentiation of neuronal stem cells into motor neurons using electrospun poly-L-lactic acid/gelatin scaffold', *Biomaterials*, 35(2), pp. 664–674.

Birhanu, G. *et al.* (2018) 'An improved surface for enhanced stem cell proliferation and osteogenic differentiation using electrospun composite PLLA/P123 scaffold', *Artif. Cells Nanomed.*

Biotechnol., 46(6), pp. 1274–1281. Available at: https://doi.org/10.1080/21691401.2017.1367928.

Blumstein, R.B. (1997) 'Thermal Characterization of Polymeric Materials. Volumes 1 and 2 Edited by Edith A. Turi (Polytechnic University, New York). Academic Press: San Diego. 1997. xxiv+ 2420 pp. ISBN 0-12-703783-7.' ACS Publications.

Bomkamp, C. *et al.* (2022) 'Scaffolding biomaterials for 3D cultivated meat: Prospects and challenges', *Advanced Science*, 9(3), p. 2102908.

Boncler, M. *et al.* (2014) 'Comparison of PrestoBlue and MTT assays of cellular viability in the assessment of anti-proliferative effects of plant extracts on human endothelial cells', *Journal of pharmacological and toxicological methods*, 69(1), pp. 9–16.

Bosshardt, D.D. and Sculean, A. (2009) 'Does periodontal tissue regeneration really work?', *Periodontology 2000*, 51(1), pp. 208–219.

Bottino, M.C. *et al.* (2009) 'Freeze-dried acellular dermal matrix graft: effects of rehydration on physical, chemical, and mechanical properties', *Dental Materials*, 25(9), pp. 1109–1115.

Bottino, M.C. *et al.* (2010) 'Acellular dermal matrix graft: synergistic effect of rehydration and natural crosslinking on mechanical properties', *Journal of Biomedical Materials Research Part B: Applied Biomaterials*, 95(2), pp. 276–282.

Bottino, M.C. *et al.* (2012) 'Recent advances in the development of GTR/GBR membranes for periodontal regeneration—a materials perspective', *Dental materials*, 28(7), pp. 703–721.

Bottino, M.C., Thomas, V. and Janowski, G.M. (2011) 'A novel spatially designed and functionally graded electrospun membrane for periodontal regeneration', *Acta biomaterialia*, 7(1), pp. 216–224.

Boyko, G.A., Melcher, A.H. and Brunette, D.M. (1981) 'Formation of new periodontalligament by periodontal ligament cells implanted in vivo after culture in vitro: A preliminary study of transplanted roots in the dog', *Journal of periodontal research*, 16(1), pp. 73–88.

Braghirolli, D.I., Steffens, D. and Pranke, P. (2014) 'Electrospinning for regenerative medicine: a review of the main topics', *Drug discovery today*, 19(6), pp. 743–753.

Bružauskaitė, I. *et al.* (2016) 'Scaffolds and cells for tissue regeneration: different scaffold pore sizes—different cell effects', *Cytotechnology*, 68(3), pp. 355–369.

Brydone, A.S., Meek, D. and Maclaine, S. (2010) 'Bone grafting, orthopaedic biomaterials, and the clinical need for bone engineering', *Proceedings of the Institution of Mechanical Engineers, Part*

H: Journal of Engineering in Medicine, 224(12), pp. 1329–1343.

Buck, W. and Rudtsch, S. (2011) 'Thermal properties', in *Springer handbook of metrology and testing*. Springer, pp. 453–483.

Burg, K.J.L., Porter, S. and Kellam, J.F. (2000) 'Biomaterial developments for bone tissue engineering', *Biomaterials*, 21(23), pp. 2347–2359.

Buser, D. *et al.* (1993) 'Localized ridge augmentation using guided bone regeneration. I. Surgical procedure in the maxilla.', *International Journal of Periodontics & Restorative Dentistry*, 13(1).

Calvino, C. (2022) 'Photocycloadditions for the Design of Reversible Photopolymerizations', *Chimia*, 76(10), p. 816.

Camargo, P.M. *et al.* (2002) 'Platelet-rich plasma and bovine porous bone mineral combined with guided tissue regeneration in the treatment of intrabony defects in humans', *Journal of Periodontal Research*, 37(4), pp. 300–306.

Can-Herrera, L.A., Oliva, A.I. and Cervantes-Uc, J.M. (2022) 'Enhancement of chemical, physical, and surface properties of electrospun PCL/PLA blends by means of air plasma treatment', *Polymer Engineering & Science*, 62(5), pp. 1608–1618.

Can, E. *et al.* (2011) 'Investigation of PLLA/PCL blends and paclitaxel release profiles', *Aaps Pharmscitech*, 12(4), pp. 1442–1453.

Canullo, L. and Malagnino, V.A. (2008) 'Vertical Ridge Augmentation Around Implants by e-PTFE Titanium-Reinforced Membrane and Bovine Bone Matrix: A 24-to 54-Month Study of 10 Consecutive Cases.', *International Journal of Oral & Maxillofacial Implants*, 23(5).

Cao, H. *et al.* (2010) 'Solid freeform fabrication of three-dimensional scaffolds for engineering replacement tissues and organs', *Biomaterials*, 7(3), pp. 303–315.

Cao, H. and Kuboyama, N. (2010) 'A biodegradable porous composite scaffold of PGA/β-TCP for bone tissue engineering', *Bone*, 46(2), pp. 386–395.

Cascone, M.G. *et al.* (2001) 'Bioartificial polymeric materials based on polysaccharides', *Journal of Biomaterials Science, Polymer Edition*, 12(3), pp. 267–281.

Ten Cate, A.R. and Nanci, A. (2013) *Ten Cate's oral histology: development, structure, and function*. Elsevier.

Catelas, I. *et al.* (2006) 'Human mesenchymal stem cell proliferation and osteogenic differentiation in fibrin gels in vitro', *Tissue engineering*, 12(8), pp. 2385–2396.

El Chaar, E. and Abitbol, T. (2023) 'Overview of Gingival Tissue and Periodontium', *Practical Techniques in Periodontics and Implant Dentistry*, p. 3.

Chang, H. *et al.* (2020) 'A critical review of membrane wettability in membrane distillation from the perspective of interfacial interactions', *Environmental Science & Technology*, 55(3), pp. 1395–1418.

Chang, P.-C. and Lim, L.P. (2012) 'Interrelationships of periodontitis and diabetes: A review of the current literature', *Journal of Dental Sciences*, 7(3), pp. 272–282.

Chen, B. *et al.* (2015) 'Fabrication of polylactic acid/polyethylene glycol (PLA/PEG) porous scaffold by supercritical CO 2 foaming and particle leaching', *Polymer Engineering & Science*, 55(6), pp. 1339–1348.

Chen, F.-M. and Liu, X. (2016) 'Advancing biomaterials of human origin for tissue engineering', *Progress in polymer science*, 53, pp. 86–168.

Chen, F. *et al.* (2006) 'Enhancement of periodontal tissue regeneration by locally controlled delivery of insulin-like growth factor-I from dextran–co-gelatin microspheres', *Journal of Controlled Release*, 114(2), pp. 209–222.

Chen, J., Chu, B. and Hsiao, B.S. (2006) 'Mineralization of hydroxyapatite in electrospun nanofibrous poly (L-lactic acid) scaffolds', *Journal of Biomedical Materials Research Part A: An Official Journal of The Society for Biomaterials, The Japanese Society for Biomaterials, and The Australian Society for Biomaterials and the Korean Society for Biomaterials*, 79(2), pp. 307–317.

Chen, Y.-W. *et al.* (2008) 'Periodontitis may increase the risk of peripheral arterial disease', *European Journal of Vascular and Endovascular Surgery*, 35(2), pp. 153–158.

Chen, Z. *et al.* (2001) 'Structure of poly (ferrocenyldimethylsilane) in electrospun nanofibers', *Macromolecules*, 34(18), pp. 6156–6158.

Cheung, H.-Y. *et al.* (2007) 'A critical review on polymer-based bio-engineered materials for scaffold development', *Composites Part B: Engineering*, 38(3), pp. 291–300.

Choi, S.-W. *et al.* (2020) 'Human tonsil-derived mesenchymal stem cells-loaded hydroxyapatite-chitosan patch for mastoid obliteration', *ACS Applied Bio Materials*, 3(2), pp. 1008–1017.

Chor, A. *et al.* (2020) 'In vitro degradation of electrospun poly (lactic-co-glycolic acid)(PLGA) for oral mucosa regeneration', *Polymers*, 12(8), p. 1853.

Christenson, E.M. *et al.* (2007) 'Nanobiomaterial applications in orthopedics', *Journal of orthopaedic research*, 25(1), pp. 11–22.

Chrysafi, R., Perraki, T. and Kakali, G. (2007) 'Sol–gel preparation of 2CaO· SiO2', *Journal of the European Ceramic Society*, 27(2–3), pp. 1707–1710.

Ciardelli, G. *et al.* (2005) 'Blends of poly-(ε-caprolactone) and polysaccharides in tissue engineering applications', *Biomacromolecules*, 6(4), pp. 1961–1976.

Clapham, D.E. (2007) 'Calcium signaling', *Cell*, 131(6), pp. 1047–1058.

Cohen-Tanugi, D. and Grossman, J.C. (2012) 'Water desalination across nanoporous graphene', *Nano letters*, 12(7), pp. 3602–3608.

Cohen-Tanugi, D. and Grossman, J.C. (2014) 'Mechanical strength of nanoporous graphene as a desalination membrane', *Nano letters*, 14(11), pp. 6171–6178.

Conn, R.E. *et al.* (1995) 'Safety assessment of polylactide (PLA) for use as a food-contact polymer', *Food and Chemical Toxicology*, 33(4), pp. 273–283.

Correale, S., Murthy, N.S. and Minor, H. (2004) *XRD analysis of the amorphous phase in semicrystalline polymer fibers.*

Cortellini, P., Prato, G.P. and Tonetti, M.S. (1996) 'Periodontal regeneration of human intrabony defects with bioresorbable membranes. A controlled clinical trial', *Journal of Periodontology*, 67(3), pp. 217–223.

Cortes, D.A. *et al.* (2005) 'Biomimetic apatite formation on a CoCrMo alloy by using wollastonite, bioactive glass or hydroxyapatite', *Journal of Materials Science*, 40(13), pp. 3509–3515.

Curvello, R., Raghuwanshi, V.S. and Garnier, G. (2019) 'Engineering nanocellulose hydrogels for biomedical applications', *Advances in colloid and interface science*, 267, pp. 47–61.

Czanderna, A.W., Madey, T.E. and Powell, C.J. (2006) *Beam effects, surface topography, and depth profiling in surface analysis*. Springer Science & Business Media.

Damien, E. and Revell, P.A. (2004) 'Coralline hydroxyapatite bone graft substitute: a review of experimental studies and biomedical applications', *Journal of Applied Biomaterials and*

Biomechanics, 2(2), pp. 65–73.

Daňková, J. *et al.* (2015) 'Highly efficient mesenchymal stem cell proliferation on poly-ε-caprolactone nanofibers with embedded magnetic nanoparticles', *International journal of nanomedicine*, 10, p. 7307.

Darby, I.B. and Morris, K.H. (2013) 'A systematic review of the use of growth factors in human periodontal regeneration', *Journal of periodontology*, 84(4), pp. 465–476.

Datta, P. *et al.* (2017) 'Bone tissue bioprinting for craniofacial reconstruction', *Biotechnology and bioengineering*, 114(11), pp. 2424–2431.

Deas, D.E. *et al.* (2016) 'Scaling and root planing vs. conservative surgery in the treatment of chronic periodontitis', *Periodontology 2000*, 71(1), pp. 128–139.

Dehghani, F. and Annabi, N. (2011) 'Engineering porous scaffolds using gas-based techniques', *Current opinion in biotechnology*, 22(5), pp. 661–666.

Dejob, L. *et al.* (2022) 'Nitrate-Free Synthesis and Electrospinning of Carbonated Hydroxyapatite Coatings on TA6V Implants', *Advanced Materials Interfaces*, 9(17), p. 2102342.

Dell'Erba, R. *et al.* (2001) 'Immiscible polymer blends of semicrystalline biocompatible components: thermal properties and phase morphology analysis of PLLA/PCL blends', *Polymer*, 42(18), pp. 7831–7840. Available at: https://doi.org/https://doi.org/10.1016/S0032-3861(01)00269-5.

Dewey, M.J. *et al.* (2021) 'Glycosaminoglycan content of a mineralized collagen scaffold promotes mesenchymal stem cell secretion of factors to modulate angiogenesis and monocyte differentiation', *Materialia*, 18, p. 101149.

Dhruvakumar, D., Arun Kumar, K. V and Ayilavarapu, S. (2019) *Hand Book on Bone Regeneration: Materials, Techniques and Procedures: From Research to Clinical Practice*. Notion Press.

Djukic, S. *et al.* (2020) 'Mechanical properties of amorphous and semi-crystalline semi-aromatic polyamides', *Heliyon*, 6(4), p. e03857.

Dong, Y. *et al.* (2010) 'Distinctive degradation behaviors of electrospun polyglycolide, poly (dl-lactide-co-glycolide), and poly (l-lactide-co-ε-caprolactone) nanofibers cultured with/without porcine smooth muscle cells', *Tissue Engineering Part A*, 16(1), pp. 283–298.

Donos, N., Kostopoulos, L. and Karring, T. (2002) 'Alveolar ridge augmentation using a resorbable copolymer membrane and autogenous bone grafts: an experimental study in the rat', *Clinical Oral Implants Research*, 13(2), pp. 203–213.

Ehrbar, M. *et al.* (2007) 'Enzymatic formation of modular cell-instructive fibrin analogs for tissue engineering', *Biomaterials*, 28(26), pp. 3856–3866.

Eldrehmy, E.H. *et al.* (2022) 'Hydroxyapatite-based bio-ceramic of ternary nanocomposites containing cuprous oxide/graphene oxide for biomedical applications', *Diamond and Related Materials*, p. 109121.

Elgali, I. *et al.* (2017) 'Guided bone regeneration: materials and biological mechanisms revisited', *European journal of oral sciences*, 125(5), pp. 315–337.

Eltom, A., Zhong, G. and Muhammad, A. (2019) 'Scaffold Techniques and Designs in Tissue Engineering Functions and Purposes: A Review', *Advances in Materials Science and Engineering*, 2019.

EU-Commission (2012) 'Regulation of the European Parliament and of the Council on medical devices, and amending Directive 2001/83/EC, Regulation (EC) No 178/2002 and Regulation (EC) No 1223/2009'.

Fabbri, P. *et al.* (2010) 'Highly porous polycaprolactone-45S5 Bioglass® scaffolds for bone tissue engineering', *Composites Science and Technology*, 70(13), pp. 1869–1878.

Fang, R. *et al.* (2010) 'Electrospun PCL/PLA/HA based nanofibers as scaffold for osteoblast-like cells', *Journal of nanoscience and nanotechnology*, 10(11), pp. 7747–7751.

Fathi, M.H., Hanifi, A. and Mortazavi, V. (2008) 'Preparation and bioactivity evaluation of bone-like hydroxyapatite nanopowder', *Journal of materials processing technology*, 202(1–3), pp. 536–542.

Felipe, M.E.M.C. *et al.* (2007) 'Comparison of two surgical procedures for use of the acellular dermal matrix graft in the treatment of gingival recessions: A randomized controlled clinical study', *Journal of periodontology*, 78(7), pp. 1209–1217.

Feng, B. *et al.* (2012) 'Acetic-acid-mediated miscibility toward electrospinning homogeneous composite nanofibers of GT/PCL', *Biomacromolecules*, 13(12), pp. 3917–3925.

Feng, Y. *et al.* (2021) 'Three-dimensional ordered magnetic macroporous metal-organic

frameworks for enzyme immobilization', *Journal of Colloid and Interface Science*, 590, pp. 436–445.

Ferraz, M.P., Monteiro, F.J. and Manuel, C.M. (2004) 'Hydroxyapatite nanoparticles: a review of preparation methodologies', *Journal of Applied Biomaterials and Biomechanics*, 2(2), pp. 74–80.

Fliefel, R. *et al.* (2016) 'Mesenchymal stem cell proliferation and mineralization but not osteogenic differentiation are strongly affected by extracellular pH', *Journal of Cranio-Maxillofacial Surgery*, 44(6), pp. 715–724.

Floreon (2017) *Floreon 3D today announced that they are looking for strategic partnerships in the 3D filament market. The company has proven technology for the enhancement of PLA for 3D printing.*

Floreon (2018) *Limited Floreon-Transforming Packaging"Floreon." [Online]. Available:* Available at: https://www.floreon.com/home/#Why_PLA?

Floreon 3D (2014) *"Floreon 3D." [Online]. Available:* Available at: http://www.floreon3d.com/.

Fontana, F. *et al.* (2008) 'Clinical and Histologic Evaluation of Allogeneic Bone Matrix Versus Autogenous Bone Chips Associated with Titanium-Reinforced e-PTFE Membrane for Vertical Ridge Augmentation: A Prospective Pilot Study.', *International Journal of Oral & Maxillofacial Implants*, 23(6).

Gao, Y. *et al.* (2022) 'Advances in modification methods based on biodegradable membranes in guided bone/tissue regeneration: a review', *Polymers*, 14(5), p. 871.

Garlotta, D. (2001) 'A literature review of poly (lactic acid)', *Journal of Polymers and the Environment*, 9(2), pp. 63–84.

Geckil, H. *et al.* (2010) 'Engineering hydrogels as extracellular matrix mimics', *Nanomedicine*, 5(3), pp. 469–484.

Georgiou, G. *et al.* (2007) 'Polylactic acid–phosphate glass composite foams as scaffolds for bone tissue engineering', *Journal of Biomedical Materials Research Part B: Applied Biomaterials: An Official Journal of The Society for Biomaterials, The Japanese Society for Biomaterials, and The Australian Society for Biomaterials and the Korean Society for Biomaterials*, 80(2), pp. 322–331.

Gestrelius, S., Lyngstadaas, S.P. and Hammarström, L. (2000) 'Emdogain–periodontal regeneration based on biomimicry', *Clinical oral investigations*, 4(2), pp. 120–125.

Ghose, S. *et al.* (2018) 'Dynamic Hyaluronan drives liver endothelial cells towards angiogenesis', *BMC cancer*, 18(1), pp. 1–13.

Giannobile, W. V (2014) 'Commentary: treatment of periodontitis: destroyed periodontal tissues can be regenerated under certain conditions'.

Gielkens, P.F.M. *et al.* (2008) 'Vivosorb®, Bio-Gide®, and Gore-Tex® as barrier membranes in rat mandibular defects: an evaluation by microradiography and micro-CT', *Clinical oral implants research*, 19(5), pp. 516–521.

Giita Silverajah, V.S. *et al.* (2012) 'A comparative study on the mechanical, thermal and morphological characterization of poly (lactic acid)/epoxidized palm oil blend', *International journal of molecular sciences*, 13(5), pp. 5878–5898.

Gloeckner, H., Jonuleit, T. and Lemke, H.-D. (2001) 'Monitoring of cell viability and cell growth in a hollow-fiber bioreactor by use of the dye Alamar Blue™', *Journal of immunological methods*, 252(1–2), pp. 131–138.

Goh, S.-K., Olsen, P. and Banerjee, I. (2013) 'Extracellular matrix aggregates from differentiating embryoid bodies as a scaffold to support ESC proliferation and differentiation', *Plos one*, 8(4), p. e61856.

Gorustovich, A.A., Roether, J.A. and Boccaccini, A.R. (2010) 'Effect of bioactive glasses on angiogenesis: a review of in vitro and in vivo evidences', *Tissue Engineering Part B: Reviews*, 16(2), pp. 199–207.

Gottlow, J. *et al.* (1984) 'New attachment formation as the result of controlled tissue regeneration', *Journal of clinical periodontology*, 11(8), pp. 494–503.

Gottlow, J. *et al.* (1986) 'New attachment formation in the human periodontium by guided tissue regeneration Case reports', *Journal of clinical periodontology*, 13(6), pp. 604–616.

Gottlow, J. (1993) 'Guided tissue regeneration using bioresorbable and non-resorbable devices: initial healing and long-term results', *Journal of periodontology*, 64, pp. 1157–1165.

Grandin, H.M., Gemperli, A.C. and Dard, M. (2011) 'Enamel matrix derivative: a review of cellular effects in vitro and a model of molecular arrangement and functioning', *Tissue Engineering Part B: Reviews*, 18(3), pp. 181–202.

Grewal, S.S. and Edgar, B.A. (2003) 'Controlling cell division in yeast and animals: does size

matter?', *Journal of biology*, 2(1), pp. 1–4.

Grottkau, B.E. *et al.* (2020) 'Rapid fabrication of anatomically-shaped bone scaffolds using indirect 3D printing and perfusion techniques', *International Journal of Molecular Sciences*, 21(1), p. 315.

Guo, Y. *et al.* (2022) 'Sustained Delivery of Methylsulfonylmethane from Biodegradable Scaffolds Enhances Efficient Bone Regeneration', *International Journal of Nanomedicine*, pp. 4829–4842.

Gupta, A. *et al.* (2018) 'Functionalized chitosan mediated stereocomplexation of poly (lactic acid): Influence on crystallization, oxygen permeability, wettability and biocompatibility behavior', *Polymer*, 142, pp. 196–208.

Gupta, B., Revagade, N. and Hilborn, J. (2007) 'Poly (lactic acid) fiber: An overview', *Progress in polymer science*, 32(4), pp. 455–482.

Gupta, D. *et al.* (2009) 'Aligned and random nanofibrous substrate for the in vitro culture of Schwann cells for neural tissue engineering', *Acta biomaterialia*, 5(7), pp. 2560–2569.

Hadi, N.A. *et al.* (2020) 'Characterization and stability of short-chain fatty acids modified starch Pickering emulsions', *Carbohydrate polymers*, 240, p. 116264.

Hahn, E.N. *et al.* (2017) 'On the ultimate tensile strength of tantalum', *Acta Materialia*, 126, pp. 313–328.

Haider, A., Gupta, K.C. and Kang, I.-K. (2014) 'Morphological effects of HA on the cell compatibility of electrospun HA/PLGA composite nanofiber scaffolds', *BioMed research international*, 2014.

Hanna, H., Mir, L.M. and Andre, F.M. (2018) 'In vitro osteoblastic differentiation of mesenchymal stem cells generates cell layers with distinct properties', *Stem Cell Research & Therapy*, 9(1), p. 203. Available at: https://doi.org/10.1186/s13287-018-0942-x.

Hao, L. *et al.* (2015) 'Deficiency of cathepsin K prevents inflammation and bone erosion in rheumatoid arthritis and periodontitis and reveals its shared osteoimmune role', *FEBS Letters*, 589(12), pp. 1331–1339. Available at: https://doi.org/https://doi.org/10.1016/j.febslet.2015.04.008.

Haroosh, H.J. *et al.* (2022) 'Morphological Structures and Drug Release Effect of Multiple Electrospun Nanofibre Membrane Systems Based on PLA, PCL, and PCL/Magnetic Nanoparticle Composites', *Journal of Nanomaterials*, 2022.

Haschtmann, D. *et al.* (2006) 'Establishment of a novel intervertebral disc/endplate culture model:

analysis of an ex vivo in vitro whole-organ rabbit culture system', *Spine*, 31(25), pp. 2918–2925.

Hassan, M.I. and Sultana, N. (2017) 'Characterization, drug loading and antibacterial activity of nanohydroxyapatite/polycaprolactone (nHA/PCL) electrospun membrane', *3 Biotech*, 7(4), pp. 1–9.

Hatakeyama, T. and Quinn, F.X. (1999) *Thermal analysis: fundamentals and applications to polymer science*. [sl].

Hatano, K. *et al.* (1999) 'Effect of surface roughness on proliferation and alkaline phosphatase expression of rat calvarial cells cultured on polystyrene', *Bone*, 25(4), pp. 439–445.

Hearnden, V. *et al.* (2009) 'Diffusion studies of nanometer polymersomes across tissue engineered human oral mucosa', *Pharmaceutical research*, 26(7), pp. 1718–1728.

Hekmati, A.H. *et al.* (2014) 'Effect of nanofiber diameter on water absorption properties and pore size of polyamide-6 electrospun nanoweb', *Textile Research Journal*, 84(19), pp. 2045–2055.

Hernández Sánchez, F. *et al.* (2005) 'Influence of low-temperature nucleation on the crystallization process of poly (L-lactide)', *Biomacromolecules*, 6(6), pp. 3283–3290.

Herrero-Herrero, M. *et al.* (2021) 'Influence of chemistry and fiber diameter of electrospun PLA, PCL and their blend membranes, intended as cell supports, on their biological behavior', *Polymer Testing*, 103, p. 107364.

Hoidy, W.H. *et al.* (2010) 'Preparation and characterization of polylactic acid/polycaprolactone clay nanocomposites', *Journal of Applied sciences*, 10(2), pp. 97–106.

Hosseini, S.F., Ghaderi, J. and Gómez-Guillén, M.C. (2021) 'trans-Cinnamaldehyde-doped quadripartite biopolymeric films: Rheological behavior of film-forming solutions and biofunctional performance of films', *Food Hydrocolloids*, 112, p. 106339.

Hou, L. *et al.* (2004) 'Polymer-assisted regeneration therapy with Atrisorb® barriers in human periodontal intrabony defects', *Journal of clinical periodontology*, 31(1), pp. 68–74.

Huang, L. *et al.* (2000) 'Generation of synthetic elastin-mimetic small diameter fibers and fiber networks', *Macromolecules*, 33(8), pp. 2989–2997.

Huang, W. *et al.* (2010) 'PHBV microspheres–PLGA matrix composite scaffold for bone tissue engineering', *Biomaterials*, 31(15), pp. 4278–4285.

Hunter, K.T. and Ma, T. (2013) 'In vitro evaluation of hydroxyapatite–chitosan–gelatin composite membrane in guided tissue regeneration', *Journal of Biomedical Materials Research Part A*, 101(4), pp. 1016–1025.

Hutmacher, D.W. (2000) 'Scaffolds in tissue engineering bone and cartilage', in *The biomaterials: Silver jubilee compendium*. Elsevier, pp. 175–189.

Iacopino, A.M. (2001) 'Periodontitis and diabetes interrelationships: role of inflammation', *Annals of periodontology*, 6(1), pp. 125–137.

Idris, S.B. *et al.* (2010) 'Biocompatibility of polyester scaffolds with fibroblasts and osteoblast-like cells for bone tissue engineering', *Journal of bioactive and compatible polymers*, 25(6), pp. 567–583.

Institution, B.S. (1999) 'TS EN ISO 13934-1: Textiles-Tensile Properties of Fabrics–Part 1: Determination of Maximum Force and Elongation at Maximum Force Using the Strip Method', *British Standard: Brussels, Belgium* [Preprint].

Institution, B.S. (2013) 'Textiles-Tensile properties of fabrics-Part 1: Determination of maximum force and elongation at maximum force using the strip method'.

Iso, B. and STANDARD, B. (2009) 'Biological evaluation of medical devices', *Part*, 1, p. 10993.

Izquierdo-Barba, I. *et al.* (2008) 'High-performance mesoporous bioceramics mimicking bone mineralization', *Chemistry of Materials*, 20(9), pp. 3191–3198.

Jacobs, V., Anandjiwala, R.D. and Maaza, M. (2010) 'The influence of electrospinning parameters on the structural morphology and diameter of electrospun nanofibers', *Journal of applied polymer science*, 115(5), pp. 3130–3136.

Jafari, M. *et al.* (2017) 'Polymeric scaffolds in tissue engineering: a literature review', *Journal of Biomedical Materials Research Part B: Applied Biomaterials*, 105(2), pp. 431–459.

Jagadale, P.N. *et al.* (2013) 'Synthesis and characterization of nanostructured CaSiO3 biomaterial', *Materials Science-Poland*, 31(2), pp. 269–275.

Jamuna-Thevi, K. *et al.* (2014) 'Triple-layered PLGA/nanoapatite/lauric acid graded composite membrane for periodontal guided bone regeneration', *Materials Science and Engineering: C*, 43, pp. 253–263.

Jang, J.-H., Castano, O. and Kim, H.-W. (2009) 'Electrospun materials as potential platforms for

bone tissue engineering', *Advanced drug delivery reviews*, 61(12), pp. 1065–1083.

Javed, F. *et al.* (2011) 'Significance of the platelet-derived growth factor in periodontal tissue regeneration', *Archives of oral biology*, 56(12), pp. 1476–1484.

Jelcic, Z., Holjevac-Grguric, T. and Rek, V. (2005) 'Mechanical properties and fractal morphology of high-impact polystyrene/poly (styrene-b-butadiene-b-styrene) blends', *Polymer degradation and stability*, 90(2), pp. 295–302.

Jem, K.J. and Tan, B. (2020) 'The development and challenges of poly (lactic acid) and poly (glycolic acid)', *Advanced Industrial and Engineering Polymer Research*, 3(2), pp. 60–70.

Jeon, O. *et al.* (2007) 'Enhancement of ectopic bone formation by bone morphogenetic protein-2 released from a heparin-conjugated poly (L-lactic-co-glycolic acid) scaffold', *Biomaterials*, 28(17), pp. 2763–2771.

Jeong, K. *et al.* (2017) 'In vivo study on the biocompatibility of chitosan–hydroxyapatite film depending on degree of deacetylation', *Journal of Biomedical Materials Research Part A*, 105(6), pp. 1637–1645.

Ji, W. *et al.* (2013) 'Incorporation of stromal cell-derived factor-1α in PCL/gelatin electrospun membranes for guided bone regeneration', *Biomaterials*, 34(3), pp. 735–745.

Jiang, L. *et al.* (2010) 'Preparation and characterization of graphene/poly (vinyl alcohol) nanocomposites', *Journal of Applied Polymer Science*, 118(1), pp. 275–279.

Jiang, T. *et al.* (2015) 'Electrospinning of polymer nanofibers for tissue regeneration', *Progress in polymer Science*, 46, pp. 1–24.

Jianqi, H. *et al.* (2002) 'Comparison of calcium alginate film with collagen membrane for guided bone regeneration in mandibular defects in rabbits', *Journal of oral and maxillofacial surgery*, 60(12), pp. 1449–1454.

Jiao, Y.-P. and Cui, F.-Z. (2007) 'Surface modification of polyester biomaterials for tissue engineering', *Biomedical materials*, 2(4), pp. R24–R24.

Johnson, T. *et al.* (2010) 'Fabrication of highly porous tissue-engineering scaffolds using selective spherical porogens', *Bio-medical materials and engineering*, 20(2), pp. 107–118.

Jordan, R.C.K. (2004) 'Diagnosis of periodontal manifestations of systemic diseases', *Periodontology 2000*, 34(1), pp. 217–229.

Jovanovic, S.A. and Nevins, M. (1995) 'Bone formation utilizing titanium-reinforced barrier membranes.', *International Journal of Periodontics & Restorative Dentistry*, 15(1).

Kareem, M.M. and Tanner, K.E. (2020) 'Optimising micro-hydroxyapatite reinforced poly (lactide acid) electrospun scaffolds for bone tissue engineering', *Journal of Materials Science: Materials in Medicine*, 31(4), pp. 1–13.

Karring, T. (2000) 'Regenerative periodontal therapy.', *Journal of the International Academy of Periodontology*, 2(4), pp. 101–109.

Kaygili, O. *et al.* (2016) 'The effect of simulating body fluid on the structural properties of hydroxyapatite synthesized in the presence of citric acid', *Progress in Biomaterials*, 5(3), pp. 173–182.

Kedem, S. *et al.* (2005) 'Composite polymer nanofibers with carbon nanotubes and titanium dioxide particles', *Langmuir*, 21(12), pp. 5600–5604.

Khan, A.S. *et al.* (2008) 'Preparation and characterization of a novel bioactive restorative composite based on covalently coupled polyurethane–nanohydroxyapatite fibres', *Acta Biomaterialia*, 4(5), pp. 1275–1287.

Khayet, M., Matsuura, T. and Mengual, J.I. (2005) 'Porous hydrophobic/hydrophilic composite membranes: Estimation of the hydrophobic-layer thickness', *Journal of Membrane Science*, 266(1–2), pp. 68–79.

Khorshidi, S. *et al.* (2016) 'A review of key challenges of electrospun scaffolds for tissue-engineering applications', *Journal of tissue engineering and regenerative medicine*, 10(9), pp. 715–738.

Kim, H.-S. *et al.* (2021) '3D macroporous biocomposites with a microfibrous topographical cue enhance new bone formation through activation of the MAPK signaling pathways', *Journal of Industrial and Engineering Chemistry*, 104, pp. 478–490.

Kim, I.Y. *et al.* (2008) 'Preparation of bioactive spherical particles in the CaO–SiO2 system through sol–gel processing under coexistence of poly (ethylene glycol)', *Journal of the European Ceramic Society*, 28(8), pp. 1595–1602.

Kim, J.Y. *et al.* (2009) 'Cell adhesion and proliferation evaluation of SFF-based biodegradable scaffolds fabricated using a multi-head deposition system', *Biofabrication*, 1(1), p. 15002.

Kim, K.-H. *et al.* (2005) 'Biological efficacy of silk fibroin nanofiber membranes for guided bone regeneration', *Journal of biotechnology*, 120(3), pp. 327–339.

Kim, K. *et al.* (2003) 'Control of degradation rate and hydrophilicity in electrospun non-woven poly (D, L-lactide) nanofiber scaffolds for biomedical applications', *Biomaterials*, 24(27), pp. 4977–4985.

Kim, S. *et al.* (2005) 'Chitosan/gelatin–based films crosslinked by proanthocyanidin', *Journal of Biomedical Materials Research Part B: Applied Biomaterials: An Official Journal of The Society for Biomaterials, The Japanese Society for Biomaterials, and The Australian Society for Biomaterials and the Korean Society for Biomaterials*, 75(2), pp. 442–450.

Kim Törnqvist, C. (2010) 'QUEMESA'.

Kinane, D.F., Stathopoulou, P.G. and Papapanou, P.N. (2017) 'Periodontal diseases', *Nature reviews Disease primers*, 3(1), pp. 1–14.

Klaue, K., Knothe, U. and Masquelet, A. (1995) 'Effet biologique des membranes à corps étranger induites in situ sur la consolidation des greffes d'os spongieux', *Rev Chir Orthop Suppl*, 70(e rkunion annuelle), pp. 109–110.

Kluge, J.A. and Mauck, R.L. (2011) 'Synthetic/biopolymer nanofibrous composites as dynamic tissue engineering scaffolds', *Biomedical applications of polymeric nanofibers*, pp. 101–130.

Kobayashi, M. *et al.* (2012) 'Wettability and antifouling behavior on the surfaces of superhydrophilic polymer brushes', *Langmuir*, 28(18), pp. 7212–7222.

Koh, J.J., Zhang, X. and He, C. (2018) 'Fully biodegradable Poly (lactic acid)/Starch blends: A review of toughening strategies', *International Journal of biological macromolecules*, 109, pp. 99–113.

Kokubo, T. *et al.* (1990) 'Solutions able to reproduce in vivo surface-structure changes in bioactive glass-ceramic A-W3', *Journal of Biomedical Materials Research*, 24(6), pp. 721–734. Available at: https://doi.org/10.1002/jbm.820240607.

Kokubo, T. (1991) 'Bioactive glass ceramics: properties and applications', *Biomaterials*, 12(2), pp. 155–163.

Kokubo, T. (1998) 'Apatite formation on surfaces of ceramics, metals and polymers in body environment', *Acta materialia*, 46(7), pp. 2519–2527.

Kokubo, T. and Takadama, H. (2006) 'How useful is SBF in predicting in vivo bone bioactivity?', *Biomaterials*, 27(15), pp. 2907–2915.

Könönen, E., Gursoy, M. and Gursoy, U.K. (2019) 'Periodontitis: a multifaceted disease of tooth-supporting tissues', *Journal of clinical medicine*, 8(8), p. 1135.

Koo, K.-T. *et al.* (2008) 'Histopathological observations of a polylactic acid-based device intended for guided bone/tissue regeneration'.

Krause, B. *et al.* (2002) 'Open nanoporous morphologies from polymeric blends by carbon dioxide foaming', *Macromolecules*, 35(5), pp. 1738–1745.

Krause, M. *et al.* (2008) 'Localizing and identifying living bacteria in an abiotic environment by a combination of Raman and fluorescence microscopy', *Analytical chemistry*, 80(22), pp. 8568–8575.

Kroeze, R.J. *et al.* (2009) 'Biodegradable polymers in bone tissue engineering', *Materials*, 2(3), pp. 833–856.

Kruse, C.R. *et al.* (2017) 'The effect of pH on cell viability, cell migration, cell proliferation, wound closure, and wound reepithelialization: In vitro and in vivo study', *Wound Repair and Regeneration*, 25(2), pp. 260–269.

Ku, Y. *et al.* (2009) 'Chitosan/poly (l-lactic acid) multilayered membrane for guided tissue regeneration', *Journal of Biomedical Materials Research Part A: An Official Journal of The Society for Biomaterials, The Japanese Society for Biomaterials, and The Australian Society for Biomaterials and the Korean Society for Biomaterials*, 90(3), pp. 766–772.

Kumbar, S.G. *et al.* (2008) 'Electrospun nanofiber scaffolds: engineering soft tissues', *Biomedical materials*, 3(3), p. 34002.

Kwon, I.K., Kidoaki, S. and Matsuda, T. (2005) 'Electrospun nano-to microfiber fabrics made of biodegradable copolyesters: structural characteristics, mechanical properties and cell adhesion potential', *Biomaterials*, 26(18), pp. 3929–3939.

Kwon, T., Lamster, I.B. and Levin, L. (2021) 'Current concepts in the management of periodontitis', *International dental journal*, 71(6), pp. 462–476.

Lang, H. *et al.* (1995) 'Formation of differentiated tissues in vivo by periodontal cell populations cultured in vitro', *Journal of dental research*, 74(5), pp. 1219–1225.

Larrouture, Q.C. *et al.* (2021) 'Growth and mineralization of osteoblasts from mesenchymal stem

cells on microporous membranes: Epithelial-like growth with transmembrane resistance and pH gradient', *Biochemical and Biophysical Research Communications*, 580, pp. 14–19. Available at: https://doi.org/https://doi.org/10.1016/j.bbrc.2021.09.075.

Lau, K.R., Evans, R.L. and Case, R.M. (1994) 'Intracellular Cl− concentration in striated intralobular ducts from rabbit mandibular salivary glands', *Pflügers Archiv*, 427(1), pp. 24–32.

Laudisio, G. and Branda, F. (2001) 'Sol–gel synthesis and crystallisation of 3CaO· 2SiO2 glassy powders', *Thermochimica Acta*, 370(1–2), pp. 119–124.

Lavenus, S. *et al.* (2011) 'Behaviour of mesenchymal stem cells, fibroblasts and osteoblasts on smooth surfaces', *Acta biomaterialia*, 7(4), pp. 1525–1534.

Laycock, B., Nikolić, M., Colwell, J.M., Gauthier, E., Halley, P., Bottle, S. and George, G. (2017) 'Lifetime prediction of biodegradable polymers', *Progress in Polymer Science*, 71, pp. 144–189.

LAYPORT, C. (2010) *Periodontal Disease*. Available at: http://www.drcindylayport.com/index.asp?N=Periodontist-Tigard-OR-Periodontal-Disease&C=139&P=2299.

Leal, A.I. *et al.* (2013) 'Asymmetric PDLLA membranes containing Bioglass® for guided tissue regeneration: Characterization and in vitro biological behavior', *Dental Materials*, 29(4), pp. 427–436.

Lee, C.-H. *et al.* (2022) 'Hybrid Core–Shell Nanofibrous Scaffolds/Stents Deliver Angiotensin II Receptor Blocker to Treat Diabetic Artery Disease', *ACS Applied Polymer Materials* [Preprint].

Lee, C.H. *et al.* (2016) 'Mechanical properties of kenaf fibre reinforced floreon biocomposites with magnesium hydroxide filler', *Journal of Mechanical Engineering and Sciences*, 10(3), pp. 2234–2248.

Lee, C.H., Sapuan, S.M. and Hassan, M.R. (2018) 'Thermal analysis of kenaf fiber reinforced floreon biocomposites with magnesium hydroxide flame retardant filler', *Polymer Composites*, 39(3), pp. 869–875.

Lee, H.-S. *et al.* (2019) 'Past, present, and future of regeneration therapy in oral and periodontal tissue: A review', *Applied Sciences*, 9(6), p. 1046.

Lee, J.W., Kim, J.Y. and Cho, D.-W. (2010) 'Solid free-form fabrication technology and its application to bone tissue engineering', *International journal of stem cells*, 3(2), p. 85.

Lee, K.H. *et al.* (2003) 'Characterization of nano-structured poly (ε-caprolactone) nonwoven mats via electrospinning', *polymer*, 44(4), pp. 1287–1294.

Lee, S.J. *et al.* (2004) 'Response of MG63 osteoblast-like cells onto polycarbonate membrane surfaces with different micropore sizes', *Biomaterials*, 25(19), pp. 4699–4707.

Lee, Y.-L. *et al.* (2017) 'Hydration behaviors of calcium silicate-based biomaterials', *Journal of the Formosan Medical Association*, 116(6), pp. 424–431.

Lemmons, M. and Beebe, D. (2019) 'Oral anatomy and physiology', *Wiggs's veterinary dentistry: Principles and practice*, pp. 1–24.

Leong, K.F., Cheah, C.M. and Chua, C.K. (2003) 'Solid freeform fabrication of three-dimensional scaffolds for engineering replacement tissues and organs', *Biomaterials*, 24(13), pp. 2363–2378. Available at: https://doi.org/10.1016/S0142-9612(03)00030-9.

Li, H. and Chang, J. (2005) 'In vitro degradation of porous degradable and bioactive PHBV/wollastonite composite scaffolds', *Polymer Degradation and Stability*, 87(2), pp. 301–307.

Li, H. and Chang, J. (2013) 'Stimulation of proangiogenesis by calcium silicate bioactive ceramic', *Acta biomaterialia*, 9(2), pp. 5379–5389.

Li, H., Zhai, W. and Chang, J. (2008) 'In vitro biocompatibility assessment of PHBV/Wollastonite composites', *Journal of Materials Science: Materials in Medicine*, 19(1), pp. 67–73.

Li, L. *et al.* (2019) 'Enhanced bone tissue regeneration of a biomimetic cellular scaffold with co-cultured MSCs-derived osteogenic and angiogenic cells', *Cell proliferation*, 52(5), p. e12658.

Li, W.-J., Mauck, R.L. and Tuan, R.S. (2005) 'Electrospun nanofibrous scaffolds: production, characterization, and applications for tissue engineering and drug delivery', *Journal of Biomedical Nanotechnology*, 1(3), pp. 259–275.

Li, W. *et al.* (2002) 'Electrospun nanofibrous structure: a novel scaffold for tissue engineering', *Journal of Biomedical Materials Research: An Official Journal of The Society for Biomaterials, The Japanese Society for Biomaterials, and The Australian Society for Biomaterials and the Korean Society for Biomaterials*, 60(4), pp. 613–621.

Li, W. *et al.* (2003) 'Biological response of chondrocytes cultured in three-dimensional nanofibrous poly (ε-caprolactone) scaffolds', *Journal of Biomedical Materials Research Part A: An Official Journal of The Society for Biomaterials, The Japanese Society for Biomaterials, and The Australian*

Society for Biomaterials and the Korean Society for Biomaterials, 67(4), pp. 1105–1114.

Li, W. *et al.* (2015) 'Multifunctional chitosan-45S5 bioactive glass-poly (3-hydroxybutyrate-co-3-hydroxyvalerate) microsphere composite membranes for guided tissue/bone regeneration', *ACS applied materials & interfaces*, 7(37), pp. 20845–20854.

Li, W. *et al.* (2021) 'Chemically modified and conjugated antimicrobial peptides against superbugs', *Chemical Society Reviews*, 50(8), pp. 4932–4973.

Li, X. and Chang, J. (2005) 'Preparation and characterization of bioactive collagen/wollastonite composite scaffolds', *Journal of Materials Science: Materials in Medicine*, 16(4), pp. 361–365.

Li, Y., Xiao, Y. and Liu, C. (2017) 'The horizon of materiobiology: a perspective on material-guided cell behaviors and tissue engineering', *Chemical reviews*, 117(5), pp. 4376–4421.

Liang, C.-C., Park, A.Y. and Guan, J.-L. (2007) 'In vitro scratch assay: a convenient and inexpensive method for analysis of cell migration in vitro', *Nature protocols*, 2(2), pp. 329–333.

Liang, H.-Q. *et al.* (2013) 'Polar polymer membranes via thermally induced phase separation using a universal crystallizable diluent', *Journal of membrane science*, 446, pp. 482–491.

Liang, Y., Luan, X. and Liu, X. (2020) 'Recent advances in periodontal regeneration: A biomaterial perspective', *Bioactive materials*, 5(2), pp. 297–308.

Liao, C. *et al.* (2002) 'Fabrication of porous biodegradable polymer scaffolds using a solvent merging/particulate leaching method', *Journal of Biomedical Materials Research: An Official Journal of The Society for Biomaterials, The Japanese Society for Biomaterials, and The Australian Society for Biomaterials and the Korean Society for Biomaterials*, 59(4), pp. 676–681.

Liao, S. *et al.* (2005) 'A three-layered nano-carbonated hydroxyapatite/collagen/PLGA composite membrane for guided tissue regeneration', *Biomaterials*, 26(36), pp. 7564–7571.

Lin, J. *et al.* (2018) 'Cell-material interactions in tendon tissue engineering', *Acta biomaterialia*, 70, pp. 1–11.

Lin, W., McCulloch, C.A.G. and Cho, M. (1994) 'Differentiation of periodontal ligament fibroblasts into osteoblasts during socket healing after tooth extraction in the rat', *The Anatomical Record*, 240(4), pp. 492–506.

Lindfors, L.T. *et al.* (2010) 'Guided bone regeneration using a titanium-reinforced ePTFE membrane and particulate autogenous bone: the effect of smoking and membrane exposure', *Oral*

Surgery, Oral Medicine, Oral Pathology, Oral Radiology, and Endodontology, 109(6), pp. 825–830.

Linh, N.T.B., Min, Y.K. and Lee, B.-T. (2013) 'Fabrication and in vitro evaluations with osteoblast-like MG-63 cells of porous hyaluronic acid-gelatin blend scaffold for bone tissue engineering applications', *Journal of Materials Science*, 48(12), pp. 4233–4242.

Little, C.J., Bawolin, N.K. and Chen, X. (2011) 'Mechanical properties of natural cartilage and tissue-engineered constructs', *Tissue Engineering Part B: Reviews*, 17(4), pp. 213–227.

Liu, H., Slamovich, E.B. and Webster, T.J. (2005) 'Increased osteoblast functions on nanophase titania dispersed in poly-lactic-co-glycolic acid composites', *Nanotechnology*, 16(7), pp. S601–S601.

Liu, J. and Kerns, D.G. (2014) 'Suppl 1: Mechanisms of guided bone regeneration: A review', *The open dentistry journal*, 8, p. 56.

Liu, X. *et al.* (2018) 'A comparison of in vitro cytotoxicity assays in medical device regulatory studies', *Regulatory toxicology and pharmacology*, 97, pp. 24–32.

Liu, X. and Ma, P.X. (2004) 'Polymeric scaffolds for bone tissue engineering', *Annals of biomedical engineering*, 32(3), pp. 477–486.

Liu, Y. *et al.* (2017) 'Synergetic effect of topological cue and periodic mechanical tension-stress on osteogenic differentiation of rat bone mesenchymal stem cells', *Colloids and Surfaces B: Biointerfaces*, 154, pp. 1–9.

Loh, Q.L. and Choong, C. (2013) 'Three-dimensional scaffolds for tissue engineering applications: role of porosity and pore size'.

Lu, H.H. *et al.* (2003) 'Three-dimensional, bioactive, biodegradable, polymer–bioactive glass composite scaffolds with improved mechanical properties support collagen synthesis and mineralization of human osteoblast-like cells in vitro', *Journal of Biomedical Materials Research Part A: An Official Journal of The Society for Biomaterials, The Japanese Society for Biomaterials, and The Australian Society for Biomaterials and the Korean Society for Biomaterials*, 64(3), pp. 465–474.

Lu, Y., Chen, Y.-C. and Zhang, P.-H. (2016) 'Preparation and characterisation of polylactic acid (PLA)/polycaprolactone (PCL) composite microfibre membranes', *Fibres & Textiles in Eastern Europe* [Preprint].

Lukong, V.T., Ukoba, K. and Jen, T.-C. (2022) 'Review of self-cleaning TiO2 thin films deposited with spin coating', *The International Journal of Advanced Manufacturing Technology*, pp. 1–22.

Luo, Y. and Zhou, T. (2022) 'Connecting the dots: Targeting the microbiome in drug toxicity', *Medicinal Research Reviews*, 42(1), pp. 83–111.

Mackenzie, C.G., Mackenzie, J.B. and Beck, P. (1961) 'The effect of pH on growth, protein synthesis, and lipid-rich particles of cultured mammalian cells', *The Journal of Cell Biology*, 9(1), pp. 141–156.

Madhumathi, K. *et al.* (2009) 'Preparation and characterization of novel β-chitin–hydroxyapatite composite membranes for tissue engineering applications', *International journal of biological macromolecules*, 44(1), pp. 1–5.

Madhuri, S.V. (2016) 'Membranes for Periodontal Regeneration', *Int. J. Pharm. Sci. Invent*, 5, pp. 19–24.

Magalhães, R. *et al.* (2010) 'The role of solvent evaporation in the microstructure of electroactive β-poly (vinylidene fluoride) membranes obtained by isothermal crystallization', *Soft Materials*, 9(1), pp. 1–14.

Maglio, G. *et al.* (2004) 'Immiscible Poly (l-lactide)/Poly (ε-caprolactone) Blends: Influence of the Addition of a Poly (l-lactide)-Poly (oxyethylene) Block Copolymer on Thermal Behavior and Morphology', *Macromolecular chemistry and physics*, 205(7), pp. 946–950.

Maia-Pinto, M.O.C. *et al.* (2020) 'Biomimetic mineralization on 3D printed PLA scaffolds: on the response of human primary osteoblasts spheroids and in vivo implantation', *Polymers*, 13(1), p. 74.

Maiques, O. and Sanz-Moreno, V. (2022) 'Location, location, location: Melanoma cells "living at the edge"', *Experimental Dermatology*, 31(1), pp. 82–88.

Maksoud, M.A. (2001) 'Immediate implants in fresh posterior extraction sockets: report of two cases', *Journal of Oral Implantology*, 27(3), pp. 123–126.

Malli Sureshbabu, N. *et al.* (2019) 'Concentrated growth factors as an ingenious biomaterial in regeneration of bony defects after periapical surgery: a report of two cases', *Case reports in dentistry*, 2019.

Manafi, S.A. *et al.* (2008) 'Synthesis of nano-hydroxyapatite under a sonochemical/hydrothermal condition', *Biomedical Materials*, 3(2), p. 025002.

Maniatopoulos, C., Sodek, J. and Melcher, A.H. (1988) 'Bone formation in vitro by stromal cells obtained from bone marrow of young adult rats', *Cell and tissue research*, 254(2), pp. 317–330.

Mao, L. *et al.* (2017) 'The synergistic effects of Sr and Si bioactive ions on osteogenesis, osteoclastogenesis and angiogenesis for osteoporotic bone regeneration', *Acta Biomaterialia*, 61, pp. 217–232.

Marei, N.H. *et al.* (2016) 'Mesenchymal stem cells growth and proliferation enhancement using PLA vs PCL based nanofibrous scaffolds', *International journal of biological macromolecules*, 93, pp. 9–19.

Marra, K.G. *et al.* (1999) 'In vitro analysis of biodegradable polymer blend/hydroxyapatite composites for bone tissue engineering', *Journal of Biomedical Materials Research: An Official Journal of The Society for Biomaterials, The Japanese Society for Biomaterials, and The Australian Society for Biomaterials and the Korean Society for Biomaterials*, 47(3), pp. 324–335.

Masutani, K. and Kimura, Y. (2014) 'PLA synthesis. From the monomer to the polymer'.

McAllister, B.S. and Haghighat, K. (2007) 'Bone augmentation techniques', *Journal of periodontology*, 78(3), pp. 377–396.

McClellan, S.J. and Franses, E.I. (2005) 'Adsorption of bovine serum albumin at solid/aqueous interfaces', *Colloids and Surfaces A: Physicochemical and Engineering Aspects*, 260(1–3), pp. 265–275.

Meek, M.F. *et al.* (2004) 'In vitro degradation and biocompatibility of poly (dl-lactide-ϵ-caprolactone) nerve guides', *Journal of Biomedical Materials Research Part A: An Official Journal of The Society for Biomaterials, The Japanese Society for Biomaterials, and The Australian Society for Biomaterials and the Korean Society for Biomaterials*, 68(1), pp. 43–51.

Melamed, M.R., Kamentsky, L.A. and Boyse, E.A. (1969) 'Cytotoxic test automation: a live-dead cell differential counter', *Science*, 163(3864), pp. 285–286.

Melcher, A.H. (1976) 'On the repair potential of periodontal tissues.', *Journal of periodontology*, 47(5), pp. 256–260. Available at: https://doi.org/10.1902/jop.1976.47.5.256.

Mellonig, J.T. (1992) 'Autogenous and allogeneic bone grafts in periodontal therapy', *Critical Reviews in Oral Biology & Medicine*, 3(4), pp. 333–352.

Merlet, S. *et al.* (2007) 'Preparation and characterization of nanocellular poly (phenylquinoxaline)

foams. A new approach to nanoporous high-performance polymers', *Macromolecules*, 40(6), pp. 2070–2078.

Merolli, A. *et al.* (2001) 'Bone response to polymers based on poly-lactic acid and having different degradation times', *Journal of Materials Science: Materials in Medicine*, 12(9), pp. 775–778.

Mikos, A.G. and Temenoff, J.S. (2000) 'Formation of highly porous biodegradable scaffolds for tissue engineering', *Electronic Journal of Biotechnology*, 3(2), pp. 23–24.

Miller, N. *et al.* (1996) 'Resorption rates of 2 commercially available bioresorbable membranes: a histomorphometric study in a rabbit model', *Journal of clinical periodontology*, 23(12), pp. 1051–1059.

Miron, R.J. and Zhang, Y.F. (2012) 'Osteoinduction: a review of old concepts with new standards', *Journal of dental research*, 91(8), pp. 736–744.

Mohamad Yunos, D., Bretcanu, O. and Boccaccini, A.R. (2008) 'Polymer-bioceramic composites for tissue engineering scaffolds', *Journal of Materials Science*, 43(13), pp. 4433–4442.

Monsees, T.K. *et al.* (2017) 'Biodegradable ceramics consisting of hydroxyapatite for orthopaedic implants', *Coatings*, 7(11), p. 184.

Mota, J. *et al.* (2012) 'Chitosan/bioactive glass nanoparticle composite membranes for periodontal regeneration', *Acta biomaterialia*, 8(11), pp. 4173–4180.

Murphy, K.G. and Gunsolley, J.C. (2003) 'Guided tissue regeneration for the treatment of periodontal intrabony and furcation defects. A systematic review', *Annals of periodontology*, 8(1), pp. 266–302.

Murtey, M. Das and Ramasamy, P. (2016) 'Sample preparations for scanning electron microscopy–life sciences', *Modern electron microscopy in physical and life sciences*, 2.

Murugan, R. and Ramakrishna, S. (2004) 'Bioresorbable composite bone paste using polysaccharide based nano hydroxyapatite', *Biomaterials*, 25(17), pp. 3829–3835.

Murugan, R. and Ramakrishna, S. (2005) 'Development of nanocomposites for bone grafting', *Composites science and technology*, 65(15–16), pp. 2385–2406.

Nair, K. *et al.* (2009) 'Characterization of cell viability during bioprinting processes', *Biotechnology Journal: Healthcare Nutrition Technology*, 4(8), pp. 1168–1177.

Nair, L.S. and Laurencin, C.T. (2007) 'Biodegradable polymers as biomaterials', *Progress in Polymer Science (Oxford)*, 32(8–9), pp. 762–798. Available at: https://doi.org/10.1016/j.progpolymsci.2007.05.017.

Nauman, S., Lubineau, G. and Alharbi, H.F. (2021) 'Post processing strategies for the enhancement of mechanical properties of enms (Electrospun nanofibrous membranes): A review', *Membranes*, 11(1), p. 39.

Needleman, I. *et al.* (2002) 'A systematic review of guided tissue regeneration for periodontal infrabony defects', *J. Periodont. Res.*, 37(5), pp. 380–388. Available at: https://doi.org/10.1034/j.1600-0765.2002.01369.x.

Needleman, I. *et al.* (2006) 'Guided tissue regeneration for periodontal infra-bony defects', *Cochrane Database of Systematic Reviews* [Preprint], (2).

Nevins, M. *et al.* (2005) 'Platelet-derived growth factor stimulates bone fill and rate of attachment level gain: Results of a large multicenter randomized controlled trial', *Journal of periodontology*, 76(12), pp. 2205–2215.

Newman, M.G. *et al.* (2018) *Newman and Carranza's Clinical periodontology E-book*. Elsevier Health Sciences.

Nguyen, H.T. and Thao, P.T.B. (2022) 'Ferroelectric nanocomposites from potassium dihydrogen phosphate with oxidised multi-walled carbon nanotubes: preparation, composition effects, structure, ferroelectricity and electrical properties', *Philosophical Magazine*, 102(23), pp. 2444–2458.

Nguyen, L.T.B. *et al.* (2019) 'Development of thermo-responsive polycaprolactone macrocarriers conjugated with Poly (N-isopropyl acrylamide) for cell culture', *Scientific reports*, 9(1), pp. 1–11.

Nica, S.L. *et al.* (2022) 'MWCNTs Composites-Based on New Chemically Modified Polysulfone Matrix for Biomedical Applications', *Nanomaterials*, 12(9), p. 1502.

Nourian Dehkordi A, Mirahmadi Babaheydari F, Chehelgerdi M, R.D.S. (2019) 'Skin tissue engineering: wound healing based on stem-cell-based therapeutic strategies.', *Stem Cell Res Ther.*, 10(1), p. 111.

Nuñez, J. *et al.* (2019) 'Cellular therapy in periodontal regeneration', *Periodontology 2000*, 79(1), pp. 107–116.

NYCO Minerals, I. (2002) *Nyco NYAD® MD400 Wollastonite*. Available at:

https://www.matweb.com/search/DataSheet.aspx?MatGUID=f186945bea6d447ab87b18a8e6743c09 (Accessed: 15 December 2022).

Nyman, S. *et al.* (1982) 'The regenerative potential of the periodontal ligament: An experimental study in the monkey', *Journal of clinical periodontology*, 9(3), pp. 257–265.

Nyman, S. *et al.* (1990) 'Bone regeneration adjacent to titanium dental implants using guided tissue regeneration: a report of two cases.', *International Journal of Oral & Maxillofacial Implants*, 5(1).

O'brien, J. *et al.* (2000) 'Investigation of the Alamar Blue (resazurin) fluorescent dye for the assessment of mammalian cell cytotoxicity', *European journal of biochemistry*, 267(17), pp. 5421–5426.

Obiechina, N. (2011) *Understanding Periodontitis: A Comprehensive Guide to Periodontal Disease for Dentists, Dental Hygienists and Dental Patients*. AuthorHouse.

Odelius, K. *et al.* (2011) 'Porosity and pore size regulate the degradation product profile of polylactide', *Biomacromolecules*, 12(4), pp. 1250–1258.

Oh, S.H. *et al.* (2006) 'Asymmetrically porous PLGA/Pluronic F127 membrane for effective guided bone regeneration', *Journal of Biomaterials Science, Polymer Edition*, 17(12), pp. 1375–1387.

Okamoto, M. *et al.* (2006) 'Influence of the porosity of hydroxyapatite ceramics on in vitro and in vivo bone formation by cultured rat bone marrow stromal cells', *Journal of materials science: Materials in medicine*, 17(4), pp. 327–336.

Oldinski, R.A. *et al.* (2011) 'Dynamic mechanical analysis and biomineralization of hyaluronan–polyethylene copolymers for potential use in osteochondral defect repair', *Acta biomaterialia*, 7(3), pp. 1184–1191.

Onuma, Y. and Serruys, P.W. (2011) 'Bioresorbable scaffold: the advent of a new era in percutaneous coronary and peripheral revascularization?', *Circulation*, 123(7), pp. 779–797.

OpenStax College - Anatomy & Physiology, C.W. site. (2013) *The structure of alveolar bone and different Types of bone cells*, *Wikimedia Commons*. Available at: https://commons.wikimedia.org/wiki/File:604_Bone_cells.jpg#/media/File:604_Bone_cells.jpg.

Ostafinska, A. *et al.* (2015) 'Synergistic effects in mechanical properties of PLA/PCL blends with optimized composition, processing, and morphology', *RSC advances*, 5(120), pp. 98971–98982.

Owen, G.R. *et al.* (2010) 'An in vitro study of plasticized poly (lactic-co-glycolic acid) films as

possible guided tissue regeneration membranes: Material properties and drug release kinetics', *Journal of biomedical materials research Part A*, 95(3), pp. 857–869.

Ozbolat, I.T., Peng, W. and Ozbolat, V. (2016) 'Application areas of 3D bioprinting', *Drug discovery today*, 21(8), pp. 1257–1271.

Ozbolat, I.T. and Yu, Y. (2013) 'Bioprinting toward organ fabrication: challenges and future trends', *IEEE Transactions on Biomedical Engineering*, 60(3), pp. 691–699.

Padsalgikar, A.D. (2017) '4 - Biological Properties of Plastics', in A.D.B.T.-P. in M.D. for C.A. Padsalgikar (ed.) *Plastics Design Library*. William Andrew Publishing, pp. 83–102. Available at: https://doi.org/https://doi.org/10.1016/B978-0-323-35885-9.00004-7.

Page, R.C. (1991) 'The role of inflammatory mediators in the pathogenesis of periodontal disease', *Journal of periodontal research*, 26(3), pp. 230–242.

Palaniraja, J. *et al.* (2017) 'Synthesis of calcium silicate nanoparticles and its catalytic application in Friedlander reaction', *Inorganic and Nano-Metal Chemistry*, 47(6), pp. 946–949.

Palomino-Durand, C., Pauthe, E. and Gand, A. (2021) 'Fibronectin-Enriched Biomaterials, Biofunctionalization, and Proactivity: A Review', *Applied Sciences*, 11(24), p. 12111.

Palumbo, A. (2011) 'The anatomy and physiology of the healthy periodontium', in *Gingival Diseases-Their Aetiology, Prevention and Treatment*. IntechOpen.

Pandey, A.K. and Sakurai, S. (2021) 'Recent Developments in the Crystallization of PLLA-Based Blends, Block Copolymers, and Nanocomposites', *Crystallization and Applications* [Preprint].

Park, C.H. *et al.* (2010) 'Biomimetic hybrid scaffolds for engineering human tooth-ligament interfaces', *Biomaterials*, 31(23), pp. 5945–5952.

De Pascalis C, E.-M.S. (2017) 'Single and collective cell migration: the mechanics of adhesions', *Mol Biol Cell.*, 28(14), pp. 1833–1846. Available at: https://doi.org/10.1091/mbc.E17-03-0134.

Patricio, T. *et al.* (2013) 'Characterisation of PCL and PCL/PLA scaffolds for tissue engineering', *Procedia Cirp*, 5, pp. 110–114.

Pawlina, W. and Ross, M.H. (2018) *Histology: a text and atlas: with correlated cell and molecular biology*. Lippincott Williams & Wilkins.

Payne, J., McKeown, P. and Jones, M.D. (2019) 'A circular economy approach to plastic waste',

Polymer Degradation and Stability, 165, pp. 170–181.

Peers, S., Montembault, A. and Ladavière, C. (2020) 'Chitosan hydrogels for sustained drug delivery', *Journal of Controlled Release*, 326, pp. 150–163.

Persson, G.R. *et al.* (2011) 'Prediction of hip and hand fractures in older persons with or without a diagnosis of periodontitis', *Bone*, 48(3), pp. 552–556.

Peter, M., Binulal, N.S., *et al.* (2010) 'Novel biodegradable chitosan–gelatin/nano-bioactive glass ceramic composite scaffolds for alveolar bone tissue engineering', *Chemical engineering journal*, 158(2), pp. 353–361.

Peter, M., Ganesh, N., *et al.* (2010) 'Preparation and characterization of chitosan–gelatin/nanohydroxyapatite composite scaffolds for tissue engineering applications', *Carbohydrate polymers*, 80(3), pp. 687–694.

Pham, Q.P., Sharma, U. and Mikos, A.G. (2006a) 'Electrospinning of polymeric nanofibers for tissue engineering applications: a review', *Tissue engineering*, 12(5), pp. 1197–1211.

Pham, Q.P., Sharma, U. and Mikos, A.G. (2006b) 'Electrospun poly (ε-caprolactone) microfiber and multilayer nanofiber/microfiber scaffolds: characterization of scaffolds and measurement of cellular infiltration', *Biomacromolecules*, 7(10), pp. 2796–2805.

Pighinelli, L. and Kucharska, M. (2013) 'Chitosan–hydroxyapatite composites', *Carbohydrate polymers*, 93(1), pp. 256–262.

Pitaru, S., McCulloch, C.A.G. and Narayanan, S.A. (1994) 'Cellular origins and differentiation control mechanisms during periodontal development and wound healing', *Journal of periodontal research*, 29(2), pp. 81–94.

Place, E.S. *et al.* (2009) 'Synthetic polymer scaffolds for tissue engineering', *Chemical society reviews*, 38(4), pp. 1139–1151.

Plan, A.S. (2011) 'Advancing regulatory science at FDA', *Washington DC: FDA* [Preprint].

Pontoriero, R., Wennström, J. and Lindhe, J. (1999) 'The use of barrier membranes and enamel matrix proteins in the treatment of angular bone defects. A prospective controlled clinical study.', *Journal of Clinical Periodontology*, 26(12), p. 833.

Poole, C.A., Brookes, N.H. and Clover, G.M. (1993) 'Keratocyte networks visualised in the living cornea using vital dyes', *Journal of cell science*, 106(2), pp. 685–691.

Porter, A.E. *et al.* (2004) 'Effect of sintered silicate-substituted hydroxyapatite on remodelling processes at the bone–implant interface', *Biomaterials*, 25(16), pp. 3303–3314.

Pozhvanov, G. (2018) 'Visualization and analysis of actin cytoskeleton organization in plants', *Biological Communications*, 63(1), pp. 59–69.

Prajongtat, P. *et al.* (2019) 'Moisture-resistant electrospun polymer membranes for efficient and stable fully printable perovskite solar cells prepared in humid air', *ACS applied materials & interfaces*, 11(31), pp. 27677–27685.

Prasadh, S. and Wong, R.C.W. (2018) 'Unraveling the mechanical strength of biomaterials used as a bone scaffold in oral and maxillofacial defects', *Oral Science International*, 15(2), pp. 48–55.

Price, D.M., Hourston, D.J. and Dumont, F. (2000) 'Thermogravimetry of polymers', *Encyclopedia of analytical chemistry*, pp. 8094–8105.

Puppi, D. *et al.* (2010) 'Polymeric materials for bone and cartilage repair', *Progress in polymer Science*, 35(4), pp. 403–440.

Qasim, S.B. *et al.* (2015) 'Freeze gelated porous membranes for periodontal tissue regeneration', *Acta biomaterialia*, 23, pp. 317–328.

Qian, G. *et al.* (2019) 'Novel strategy to accelerate bone regeneration of calcium phosphate cement by incorporating 3D plotted poly (lactic-co-glycolic acid) network and bioactive wollastonite', *Advanced Healthcare Materials*, 8(9), p. 1801325.

Quent, V.M.C. *et al.* (2010) 'Discrepancies between metabolic activity and DNA content as tool to assess cell proliferation in cancer research', *Journal of cellular and molecular medicine*, 14(4), pp. 1003–1013.

Rad, M.M. *et al.* (2017) 'Fabrication and characterization of two-layered nanofibrous membrane for guided bone and tissue regeneration application', *Materials Science and Engineering: C*, 80, pp. 75–87.

Rahim, N.A.M. and Rasidi, M.S.M. (2020) 'Mechanical Properties of Porous Polylactic Acid (PLA) Via Salt Leaching Method', in *IOP Conference Series: Materials Science and Engineering*. IOP Publishing, p. 012124.

Rahimpour, A. and Madaeni, S.S. (2007) 'Polyethersulfone (PES)/cellulose acetate phthalate (CAP) blend ultrafiltration membranes: preparation, morphology, performance and antifouling properties',

Journal of Membrane Science, 305(1–2), pp. 299–312.

Rai, R. *et al.* (2012) 'Synthesis, properties and biomedical applications of poly(glycerol sebacate) (PGS): A review', *Progress in Polymer Science*, 37(8), pp. 1051–1078. Available at: https://doi.org/https://doi.org/10.1016/j.progpolymsci.2012.02.001.

Rajzer, I. *et al.* (2014) 'Bioactive nanocomposite PLDL/nano-hydroxyapatite electrospun membranes for bone tissue engineering', *Journal of Materials Science: Materials in Medicine*, 25(5), pp. 1239–1247.

Ramakrishna, S. (2005) *An introduction to electrospinning and nanofibers*. World Scientific.

Ramakrishna, S. *et al.* (2006) 'Electrospun nanofibers: solving global issues', *Materials today*, 9(3), pp. 40–50.

Ramos-Rodriguez, D.H. *et al.* (2022) 'Demonstrating the Potential of Using Bio-Based Sustainable Polyester Blends for Bone Tissue Engineering Applications', *Bioengineering*, 9(4), p. 163.

Ramseier, C.A. *et al.* (2012) 'Advanced reconstructive technologies for periodontal tissue repair', *Periodontology 2000*, 59(1), pp. 185–202.

Reddy, M.S.B. *et al.* (2021) 'A comparative review of natural and synthetic biopolymer composite scaffolds', *Polymers*, 13(7), p. 1105.

Requicha, J.F. *et al.* (2014) 'A tissue engineering approach for periodontal regeneration based on a biodegradable double-layer scaffold and adipose-derived stem cells', *Tissue Engineering Part A*, 20(17–18), pp. 2483–2492.

Requicha, J.F. *et al.* (2016) 'Design and characterization of a biodegradable double-layer scaffold aimed at periodontal tissue-engineering applications', *Journal of tissue engineering and regenerative medicine*, 10(5), pp. 392–403.

Retzepi, M. and Donos, N. (2010) 'Guided bone regeneration: biological principle and therapeutic applications', *Clinical oral implants research*, 21(6), pp. 567–576.

Reverchon, E., Volpe, M.C. and Caputo, G. (2003) 'Supercritical fluid processing of polymers: composite particles and porous materials elaboration', *Current Opinion in Solid State and Materials Science*, 7(4–5), pp. 391–397.

Rezwan, K. *et al.* (2006) 'Biodegradable and bioactive porous polymer/inorganic composite scaffolds for bone tissue engineering', *Biomaterials*, 27(18), pp. 3413–3431.

Richardson, C.R. *et al.* (1999) 'Clinical evaluation of Bio-Oss®: a bovine-derived xenograft for the treatment of periodontal osseous defects in humans', *Journal of clinical periodontology*, 26(7), pp. 421–428.

Rickel, A.P. *et al.* (2021) 'Electrospun nanofiber scaffold for vascular tissue engineering', *Materials Science and Engineering: C*, 129, p. 112373.

Riss, T.L. *et al.* (2016) 'Cell viability assays', *Assay Guidance Manual [Internet]* [Preprint].

Rokkanen, P.U. *et al.* (2000) 'Bioabsorbable fixation in orthopaedic surgery and traumatology', *Biomaterials*, 21(24), pp. 2607–2613.

Rose, L.F. *et al.* (2004) 'Periodontics: Medicine', *Surgery and Implants*, pp. 254–258.

Roseti, L. *et al.* (2017) 'Scaffolds for bone tissue engineering: state of the art and new perspectives', *Materials Science and Engineering: C*, 78, pp. 1246–1262.

Rowe, M.J. *et al.* (2016) 'Dimensionally stable and bioactive membrane for guided bone regeneration: An in vitro study', *Journal of Biomedical Materials Research Part B: Applied Biomaterials*, 104(3), pp. 594–605.

Sam, G. and Pillai, B.R.M. (2014) 'Evolution of barrier membranes in periodontal regeneration-"are the third generation membranes really here?', *Journal of clinical and diagnostic research: JCDR*, 8(12), pp. ZE14–ZE14.

Samourides, A. *et al.* (2020) 'The effect of porous structure on the cell proliferation, tissue ingrowth and angiogenic properties of poly (glycerol sebacate urethane) scaffolds', *Materials Science and Engineering: C*, 108, p. 110384.

Sanchez, A.G. *et al.* (2021) 'Chitosan-hydroxyapatite-MWCNTs nanocomposite patch for bone tissue engineering applications', *Materials Today Communications*, 28, p. 102615.

De Sanctis, M. and Zucchelli, G. (1996) 'Guided tissue regeneration with a resorbable barrier membrane (Vicryl) for the management of buccal recession: a case report.', *International Journal of Periodontics & Restorative Dentistry*, 16(5).

Santocildes-Romero, M.E. *et al.* (2015) 'The osteogenic response of mesenchymal stromal cells to strontium-substituted bioactive glasses', *Journal of tissue engineering and regenerative medicine*, 9(5), pp. 619–631.

Sawalha, H., Schroën, K. and Boom, R. (2008) 'Mechanical properties and porosity of polylactide

for biomedical applications', *Journal of applied polymer science*, 107(1), pp. 82–93.

Scantlebury, T. V (1993) '1982-1992: A decade of technology development for guided tissue regeneration', *Journal of periodontology*, 64, pp. 1129–1137.

Schenk, R.K. *et al.* (1994) 'Healing pattern of bone regeneration in membrane-protected defects: a histologic study in the canine mandible.', *International journal of oral & maxillofacial implants*, 9(1).

Schmidlin, P.R. *et al.* (2013) 'Evaluation of moldable, in situ hardening calcium phosphate bone graft substitutes', *Clinical Oral Implants Research*, 24(2), pp. 149–157.

Schmidmaier, G. *et al.* (2006) 'Biodegradable polylactide membranes for bone defect coverage: biocompatibility testing, radiological and histological evaluation in a sheep model', *Clinical oral implants research*, 17(4), pp. 439–444.

Schneider, L.A. *et al.* (2007) 'Influence of pH on wound-healing: a new perspective for wound-therapy?', *Archives of dermatological research*, 298(9), pp. 413–420.

Schwarz, F. *et al.* (2006) 'Angiogenesis pattern of native and cross-linked collagen membranes: An immunohistochemical study in the rat', *Clinical oral implants research*, 17(4), pp. 403–409.

Sculean, A., Nikolidakis, D. and Schwarz, F. (2008) 'Regeneration of periodontal tissues: combinations of barrier membranes and grafting materials–biological foundation and preclinical evidence: a systematic review', *Journal of clinical periodontology*, 35, pp. 106–116.

Sela, M.N. *et al.* (2003) 'Enzymatic degradation of collagen-guided tissue regeneration membranes by periodontal bacteria', *Clinical oral implants research*, 14(3), pp. 263–268.

Selvan, G.A., Rachel, S. and Gajendran, T. (2021) 'Chapter 13 - Several assorted characterization methods of nanoparticles', in R.P. Kumar and B.B.T.-N. Bharathiraja (eds). Academic Press, pp. 301–308. Available at: https://doi.org/https://doi.org/10.1016/B978-0-12-822401-4.00040-4.

Sheikh, Z. *et al.* (2016) 'Protein adsorption capability on polyurethane and modified-polyurethane membrane for periodontal guided tissue regeneration applications', *Materials Science and Engineering: C*, 68, pp. 267–275.

Shenoy, S.L. *et al.* (2005) 'Role of chain entanglements on fiber formation during electrospinning of polymer solutions: good solvent, non-specific polymer–polymer interaction limit', *Polymer*, 46(10), pp. 3372–3384.

Sherman, P.R. *et al.* (1990) 'The effectiveness of subgingival scaling and root planing I. Clinical detection of residual calculus', *Journal of periodontology*, 61(1), pp. 3–8.

Shi, R. *et al.* (2014) 'Structure, physical properties, biocompatibility and in vitro/vivo degradation behavior of anti-infective polycaprolactone-based electrospun membranes for guided tissue/bone regeneration', *Polymer degradation and stability*, 109, pp. 293–306.

Shim, J.-H. *et al.* (2013) 'Fabrication of blended polycaprolactone/poly (lactic-co-glycolic acid)/β-tricalcium phosphate thin membrane using solid freeform fabrication technology for guided bone regeneration', *Tissue Engineering Part A*, 19(3–4), pp. 317–328.

Shim, J.-H. *et al.* (2014) 'Efficacy of rhBMP-2 loaded PCL/PLGA/β-TCP guided bone regeneration membrane fabricated by 3D printing technology for reconstruction of calvaria defects in rabbit', *Biomedical materials*, 9(6), p. 65006.

Sill, T.J. and von Recum, H.A. (2008) 'Electrospinning: applications in drug delivery and tissue engineering', *Biomaterials*, 29(13), pp. 1989–2006.

Da Silva, D. *et al.* (2018) 'Biocompatibility, biodegradation and excretion of polylactic acid (PLA) in medical implants and theranostic systems', *Chemical Engineering Journal*, 340, pp. 9–14.

Sinha, V.R. *et al.* (2004) 'Poly-ϵ-caprolactone microspheres and nanospheres: an overview', *International journal of pharmaceutics*, 278(1), pp. 1–23.

Sisson, K. *et al.* (2010) 'Fiber diameters control osteoblastic cell migration and differentiation in electrospun gelatin', *Journal of biomedical materials research Part A*, 94(4), pp. 1312–1320.

Slavkin, H.C. and Bartold, P.M. (2006) 'Challenges and potential in tissue engineering', *Periodontology 2000*, 41(1), pp. 9–15.

Small, J. *et al.* (1999) 'Visualising the actin cytoskeleton', *Microscopy research and technique*, 47(1), pp. 3–17.

De Smit, M.J. *et al.* (2011) 'Rheumatoid arthritis and periodontitis; a possible link via citrullination', *Anaerobe*, 17(4), pp. 196–200.

Smith, L.E., Smallwood, R. and Macneil, S. (2010) 'A comparison of imaging methodologies for 3D tissue engineering', *Microscopy research and technique*, 73(12), pp. 1123–1133.

Soheilifar, Sara *et al.* (2014) 'Barrier membrane, a device for regeneration: properties and applications'.

Son, J. and Kim, G. (2009) 'Three-dimensional plotter technology for fabricating polymeric scaffolds with micro-grooved surfaces', *Journal of Biomaterials Science, Polymer Edition*, 20(14), pp. 2089–2101.

Sonseca, A. *et al.* (2012) 'Electrospinning of biodegradable polylactide/hydroxyapatite nanofibers: study on the morphology, crystallinity structure and thermal stability', *Polymer degradation and stability*, 97(10), pp. 2052–2059.

Sreekumar, P.A., Al-Harthi, M.A. and De, S.K. (2012) 'Studies on compatibility of biodegradable starch/polyvinyl alcohol blends', *Polymer Engineering & Science*, 52(10), pp. 2167–2172.

Stachewicz, U. *et al.* (2019) 'Pore shape and size dependence on cell growth into electrospun fiber scaffolds for tissue engineering: 2D and 3D analyses using SEM and FIB-SEM tomography', *Materials Science and Engineering: C*, 95, pp. 397–408.

Standardization, I.O. for (2018) 'ISO 527-3:2018 Plastics — Determination of tensile properties — Part 3: Test conditions for films and sheets'. Available at: https://www.iso.org/standard/70307.html.

Stepaniuk, K. (2019) 'Periodontology', *Wiggs's Veterinary Dentistry: Principles and Practice*, pp. 81–108.

Stevens, B. *et al.* (2008) 'A review of materials, fabrication methods, and strategies used to enhance bone regeneration in engineered bone tissues', *Journal of Biomedical Materials Research Part B: Applied Biomaterials: An Official Journal of The Society for Biomaterials, The Japanese Society for Biomaterials, and The Australian Society for Biomaterials and the Korean Society for Biomaterials*, 85(2), pp. 573–582.

Stiefel, P. *et al.* (2015) 'Critical aspects of using bacterial cell viability assays with the fluorophores SYTO9 and propidium iodide', *BMC Microbiology*, 15(1), p. 36. Available at: https://doi.org/10.1186/s12866-015-0376-x.

Sui, G. *et al.* (2007) 'Poly-L-lactic acid/hydroxyapatite hybrid membrane for bone tissue regeneration', *Journal of Biomedical Materials Research Part A: An Official Journal of The Society for Biomaterials, The Japanese Society for Biomaterials, and The Australian Society for Biomaterials and the Korean Society for Biomaterials*, 82(2), pp. 445–454.

Sulaiman, S. Bin *et al.* (2013) 'Tricalcium phosphate/hydroxyapatite (TCP-HA) bone scaffold as potential candidate for the formation of tissue engineered bone', *The Indian journal of medical research*, 137(6), p. 1093.

Sun, B. *et al.* (2014) 'Advances in three-dimensional nanofibrous macrostructures via electrospinning', *Progress in Polymer Science*, 39(5), pp. 862–890.

Sun, F. *et al.* (2019) 'Development of biomimetic trilayer fibrous membranes for guided bone regeneration', *Journal of Materials Chemistry B*, 7(4), pp. 665–675.

Sun, F., Zhou, H. and Lee, J. (2011) 'Various preparation methods of highly porous hydroxyapatite/polymer nanoscale biocomposites for bone regeneration', *Acta biomaterialia*, 7(11), pp. 3813–3828.

Sundararaghavan, H.G. *et al.* (2008) 'Genipin-induced changes in collagen gels: Correlation of mechanical properties to fluorescence', *Journal of Biomedical Materials Research Part A: An Official Journal of The Society for Biomaterials, The Japanese Society for Biomaterials, and The Australian Society for Biomaterials and the Korean Society for Biomaterials*, 87(2), pp. 308–320.

Susanto, H. and Ulbricht, M. (2009) 'Characteristics, performance and stability of polyethersulfone ultrafiltration membranes prepared by phase separation method using different macromolecular additives', *Journal of Membrane Science*, 327(1–2), pp. 125–135.

Taba Jr, M. *et al.* (2005) 'Current concepts in periodontal bioengineering', *Orthodontics & craniofacial research*, 8(4), pp. 292–302.

Taguchi, Y. *et al.* (2005) 'A histological evaluation for guided bone regeneration induced by a collagenous membrane', *Biomaterials*, 26(31), pp. 6158–6166.

Takata, T., Miyauchi, M. and Wang, H. (2001) 'Migration of osteoblastic cells on various guided bone regeneration membranes', *Clinical oral implants research*, 12(4), pp. 332–338.

Tang, Y. *et al.* (2016) 'Fabrication of PLGA/HA (core)-collagen/amoxicillin (shell) nanofiber membranes through coaxial electrospinning for guided tissue regeneration', *Composites Science and Technology*, 125, pp. 100–107.

Tcacencu, I. *et al.* (2018) 'Osseointegration of porous apatite-wollastonite and poly (lactic acid) composite structures created using 3D printing techniques', *Materials Science and Engineering: C*, 90, pp. 1–7.

Templeton, A.C. *et al.* (2000) 'Solvent refractive index and core charge influences on the surface plasmon absorbance of alkanethiolate monolayer-protected gold clusters', *The Journal of Physical Chemistry B*, 104(3), pp. 564–570.

Teng, S. *et al.* (2008) 'Three-layered membranes of collagen/hydroxyapatite and chitosan for guided bone regeneration', *Journal of Biomedical Materials Research Part B: Applied Biomaterials: An Official Journal of The Society for Biomaterials, The Japanese Society for Biomaterials, and The Australian Society for Biomaterials and the Korean Society for Biomaterials*, 87(1), pp. 132–138.

Thein-Han, W.W. and Kitiyanant, Y. (2007) 'Chitosan scaffolds for in vitro buffalo embryonic stem-like cell culture: An approach to tissue engineering', *Journal of Biomedical Materials Research Part B: Applied Biomaterials: An Official Journal of The Society for Biomaterials, The Japanese Society for Biomaterials, and The Australian Society for Biomaterials and the Korean Society for Biomaterials*, 80(1), pp. 92–101.

Thoma, D.S. *et al.* (2009) 'Evaluation of a new biodegradable membrane to prevent gingival ingrowth into mandibular bone defects in minipigs', *Clinical Oral Implants Research*, 20(1), pp. 7–16.

Thomas, V. *et al.* (2007) 'Nanostructured biocomposite scaffolds based on collagen coelectrospun with nanohydroxyapatite', *Biomacromolecules*, 8(2), pp. 631–637.

Tomasko, D.L. *et al.* (2003) 'Supercritical fluid applications in polymer nanocomposites', *Current Opinion in Solid State and Materials Science*, 7(4–5), pp. 407–412.

Tsioufis, C. *et al.* (2011) 'Periodontitis and blood pressure: the concept of dental hypertension', *Atherosclerosis*, 219(1), pp. 1–9.

Tsuji, H. and Ikada, Y. (1998) 'Blends of aliphatic polyesters. II. Hydrolysis of solution-cast blends from poly (L-lactide) and poly (E-caprolactone) in phosphate-buffered solution', *Journal of applied polymer science*, 67(3), pp. 405–415.

Tu, C. *et al.* (2020) 'Effects of electromagnetic fields treatment on rat critical-sized calvarial defects with a 3D-printed composite scaffold', *Stem Cell Research & Therapy*, 11(1), pp. 1–14.

Ulbricht, M. (2006) 'Advanced functional polymer membranes', *Polymer*, 47(7), pp. 2217–2262.

Urist, M.R. (1965) 'Bone: formation by autoinduction', *Science*, 150(3698), pp. 893–899.

Vaid, R. *et al.* (2021) 'Hydrolytic Degradation of Polylactic Acid Fibers as a Function of pH and Exposure Time', *Molecules*, 26(24), p. 7554.

Vaquette, C. and Cooper-White, J. (2013) 'A simple method for fabricating 3-D multilayered composite scaffolds', *Acta biomaterialia*, 9(1), pp. 4599–4608.

Vatanpour, V. *et al.* (2011) 'Fabrication and characterization of novel antifouling nanofiltration membrane prepared from oxidized multiwalled carbon nanotube/polyethersulfone nanocomposite', *Journal of membrane science*, 375(1–2), pp. 284–294.

Vaughan, P.J. *et al.* (1995) 'Thrombin receptor activation protects neurons and astrocytes from cell death produced by environmental insults', *Journal of Neuroscience*, 15(7), pp. 5389–5401.

Villar, C.C. and Cochran, D.L. (2010) 'Regeneration of periodontal tissues: guided tissue regeneration', *Dental Clinics*, 54(1), pp. 73–92.

Vlachos, N. *et al.* (2006) 'Applications of Fourier transform-infrared spectroscopy to edible oils', *Analytica chimica acta*, 573, pp. 459–465.

Wan Ishak, W.H., Rosli, N.A. and Ahmad, I. (2020) 'Influence of amorphous cellulose on mechanical, thermal, and hydrolytic degradation of poly (lactic acid) biocomposites', *Scientific Reports*, 10(1), pp. 1–13.

Wan, X. *et al.* (2005) 'Preparation and in vitro bioactivities of calcium silicate nanophase materials', *Materials Science and Engineering: C*, 25(4), pp. 455–461.

Wang, C. *et al.* (2013) 'Osteogenesis and angiogenesis induced by porous β-CaSiO3/PDLGA composite scaffold via activation of AMPK/ERK1/2 and PI3K/Akt pathways', *Biomaterials*, 34(1), pp. 64–77.

Wang, H.-L. and MacNeil, R.L. (1998) 'Guided tissue regeneration. Absorbable barriers.', *Dental Clinics of North America*, 42(3), pp. 505–522.

Wang, H. and Greenwell, H. (2001) 'Surgical periodontal therapy', *Periodontology 2000*, 25(1), pp. 89–99.

Wang, H.B. *et al.* (2010) 'Varying the diameter of aligned electrospun fibers alters neurite outgrowth and Schwann cell migration', *Acta biomaterialia*, 6(8), pp. 2970–2978.

Wang, H.L. *et al.* (2005) 'Position Paper: Periodontal Regeneration', *Journal of Periodontology*, 76(9), pp. 1601–1622. Available at: https://doi.org/https://doi.org/10.1902/jop.2005.76.9.1601.

Wang, L. *et al.* (2021) 'Fabrication of a novel Three-Dimensional porous PCL/PLA tissue engineering scaffold with high connectivity for endothelial cell migration', *European Polymer Journal*, 161, p. 110834.

Wang, X. *et al.* (2015) 'Fabrication of nano-structured calcium silicate coatings with enhanced

stability, bioactivity and osteogenic and angiogenic activity', *Colloids and Surfaces B: Biointerfaces*, 126, pp. 358–366.

Wang, X., Ding, B. and Li, B. (2013) 'Biomimetic electrospun nanofibrous structures for tissue engineering', *Materials today*, 16(6), pp. 229–241.

Wen, B.-W. *et al.* (2014) 'Cancer risk among gingivitis and periodontitis patients: a nationwide cohort study', *QJM: An International Journal of Medicine*, 107(4), pp. 283–290.

Wikesjö, U.M.E. *et al.* (1991) 'Early healing events at the dentin-connective tissue interface. Light and transmission electron microscopy observations', *Journal of periodontology*, 62(1), pp. 5–14.

Wikesjö, U.M.E. *et al.* (2009) 'Bone morphogenetic proteins for periodontal and alveolar indications; biological observations–clinical implications', *Orthodontics & craniofacial research*, 12(3), pp. 263–270.

Wikesjö, U.M.E., Nilvéus, R.E. and Selvig, K.A. (1992) 'Significance of early healing events on periodontal repair: a review', *Journal of periodontology*, 63(3), pp. 158–165.

Williams, D.F. (2014) 'There is no such thing as a biocompatible material', *Biomaterials*, 35(38), pp. 10009–10014.

Woo, K.M., Chen, V.J. and Ma, P.X. (2003) 'Nano-fibrous scaffolding architecture selectively enhances protein adsorption contributing to cell attachment', *Journal of Biomedical Materials Research Part A: An Official Journal of The Society for Biomaterials, The Japanese Society for Biomaterials, and The Australian Society for Biomaterials and the Korean Society for Biomaterials*, 67(2), pp. 531–537.

Wu, C. *et al.* (2008) 'Improvement of mechanical and biological properties of porous CaSiO3 scaffolds by poly (D, L-lactic acid) modification', *Acta Biomaterialia*, 4(2), pp. 343–353.

Wu, C. *et al.* (2012) '3D-printing of highly uniform CaSiO 3 ceramic scaffolds: preparation, characterization and in vivo osteogenesis', *Journal of Materials Chemistry*, 22(24), pp. 12288–12295.

Wu, Q. *et al.* (2017) 'Deriving osteogenic cells from induced pluripotent stem cells for bone tissue engineering', *Tissue Engineering Part B: Reviews*, 23(1), pp. 1–8.

Wutticharoenmongkol, P., Pavasant, P. and Supaphol, P. (2007) 'Osteoblastic phenotype expression of MC3T3-E1 cultured on electrospun polycaprolactone fiber mats filled with hydroxyapatite

nanoparticles', *Biomacromolecules*, 8(8), pp. 2602–2610.

Xu, F. *et al.* (2018) 'Thermal degradation of typical plastics under high heating rate conditions by TG-FTIR: Pyrolysis behaviors and kinetic analysis', *Energy Conversion and Management*, 171, pp. 1106–1115.

Xu, H., Cui, W. and Chang, J. (2013) 'Fabrication of patterned PDLLA/PCL composite scaffold by electrospinning', *Journal of applied polymer science*, 127(3), pp. 1550–1554.

Xu, L. *et al.* (2012) 'Cellular retinol-binding protein 1 (CRBP-1) regulates osteogenenesis and adipogenesis of mesenchymal stem cells through inhibiting RXRα-induced β-catenin degradation', *The international journal of biochemistry & cell biology*, 44(4), pp. 612–619.

Xue, J. *et al.* (2013) 'Engineering ear-shaped cartilage using electrospun fibrous membranes of gelatin/polycaprolactone', *Biomaterials*, 34(11), pp. 2624–2631.

Xue, J., He, M., Liu, H., *et al.* (2014) 'Drug loaded homogeneous electrospun PCL/gelatin hybrid nanofiber structures for anti-infective tissue regeneration membranes', *Biomaterials*, 35(34), pp. 9395–9405.

Xue, J., He, M., Liang, Y., *et al.* (2014) 'Fabrication and evaluation of electrospun PCL–gelatin micro-/nanofiber membranes for anti-infective GTR implants', *Journal of Materials Chemistry B*, 2(39), pp. 6867–6877.

Xue, R. *et al.* (2017) 'Polycaprolactone nanofiber scaffold enhances the osteogenic differentiation potency of various human tissue-derived mesenchymal stem cells', *Stem cell research & therapy*, 8(1), pp. 1–9.

Xynos, I.D. *et al.* (2001) 'Gene-expression profiling of human osteoblasts following treatment with the ionic products of Bioglass® 45S5 dissolution', *Journal of Biomedical Materials Research: An Official Journal of The Society for Biomaterials, The Japanese Society for Biomaterials, and The Australian Society for Biomaterials and the Korean Society for Biomaterials*, 55(2), pp. 151–157.

Yan, X.Z. *et al.* (2014) 'The effect of enamel matrix derivative (emdogain®) on gene expression profiles of human primary alveolar bone cells', *Journal of tissue engineering and regenerative medicine*, 8(6), pp. 463–472.

Yang, F. *et al.* (2009) 'Development of an electrospun nano-apatite/PCL composite membrane for GTR/GBR application', *Acta biomaterialia*, 5(9), pp. 3295–3304.

Yang, L. *et al.* (2021) 'High-throughput methods in the discovery and study of biomaterials and materiobiology', *Chemical reviews*, 121(8), pp. 4561–4677.

Yang, Y. *et al.* (2020) 'Mg bone implant: Features, developments and perspectives', *Materials & Design*, 185, p. 108259.

Yeh, J.-T. *et al.* (2009) 'Study on the crystallization, miscibility, morphology, properties of poly (lactic acid)/poly (ε-caprolactone) blends', *Polymer-Plastics Technology and Engineering*, 48(6), pp. 571–578.

Yoo, C.-K. *et al.* (2016) 'Cell attachment and proliferation of osteoblast-like MG63 cells on silk fibroin membrane for guided bone regeneration', *Maxillofacial Plastic and Reconstructive Surgery*, 38(1), pp. 1–6.

Yoshimoto, I. *et al.* (2018) 'Development of layered PLGA membranes for periodontal tissue regeneration', *Dental Materials*, 34(3), pp. 538–550.

You, W., Noonan, K.J.T. and Coates, G.W. (2020) 'Alkaline-stable anion exchange membranes: A review of synthetic approaches', *Progress in Polymer Science*, 100, p. 101177.

Yuan, B., Zhou, S. and Chen, X. (2017) 'Rapid prototyping technology and its application in bone tissue engineering', *Journal of Zhejiang University-SCIENCE B*, 18(4), pp. 303–315.

Yuan, L., Ding, S. and Wen, C. (2019) 'Additive manufacturing technology for porous metal implant applications and triple minimal surface structures: A review', *Bioactive materials*, 4, pp. 56–70.

Yuan, X. *et al.* (2004) 'Morphology of ultrafine polysulfone fibers prepared by electrospinning', *Polymer international*, 53(11), pp. 1704–1710.

Yun, Y.-R. *et al.* (2010) 'Fibroblast growth factors: biology, function, and application for tissue regeneration', *Journal of tissue engineering*, 1(1), p. 218142.

Zadeh, K.M. *et al.* (2019) 'Electrospun polylactic acid/date palm polyphenol extract nanofibres for tissue engineering applications', *Emergent Materials*, 2(2), pp. 141–151.

Zafar, M. *et al.* (2016) 'Potential of electrospun nanofibers for biomedical and dental applications', *Materials*, 9(2), p. 73.

Zan, J. *et al.* (2022) 'Dilemma and breakthrough of biodegradable poly-l-lactic acid in bone tissue repair', *Journal of Materials Research and Technology* [Preprint].

Zeng, Q. *et al.* (2020) 'Reassessment of mercury intrusion porosimetry for characterizing the pore structure of cement-based porous materials by monitoring the mercury entrapments with X-ray computed tomography', *Cement and Concrete Composites*, 113, p. 103726.

Zhang, C. *et al.* (2018) 'Melt crystallization behavior and crystalline morphology of polylactide/poly (ε-caprolactone) blends compatibilized by lactide-caprolactone copolymer', *Polymers*, 10(11), p. 1181.

Zhang, E. *et al.* (2016) 'Electrospun PDLLA/PLGA composite membranes for potential application in guided tissue regeneration', *Materials Science and Engineering: C*, 58, pp. 278–285.

Zhang, K.-R. *et al.* (2019) 'Multifunctional bilayer nanocomposite guided bone regeneration membrane', *Matter*, 1(3), pp. 770–781.

Zhang, X. *et al.* (2008) 'A biodegradable, immunoprotective, dual nanoporous capsule for cell-based therapies', *Biomaterials*, 29(31), pp. 4253–4259.

Zhang, X. *et al.* (2014) 'Polymer-ceramic spiral structured scaffolds for bone tissue engineering: effect of hydroxyapatite composition on human fetal osteoblasts', *PloS one*, 9(1), p. e85871.

Zhang, Y. *et al.* (2010) 'Enhanced biomineralization in osteoblasts on a novel electrospun biocomposite nanofibrous substrate of hydroxyapatite/collagen/chitosan', *Tissue Engineering Part A*, 16(6), pp. 1949–1960.

Zhang, Z. and Cui, H. (2012) 'Biodegradability and biocompatibility study of poly (chitosan-g-lactic acid) scaffolds', *Molecules*, 17(3), pp. 3243–3258.

Zhao, R. *et al.* (2021) 'Bone grafts and substitutes in dentistry: A review of current trends and developments', *Molecules*, 26(10), p. 3007.

Zhao, S. *et al.* (2000) 'Histological evaluation of different biodegradable and non-biodegradable membranes implanted subcutaneously in rats', *Journal of Cranio-Maxillofacial Surgery*, 28(2), pp. 116–122.

Zhao, X. *et al.* (2015) 'A highly bioactive and biodegradable poly (glycerol sebacate)–silica glass hybrid elastomer with tailored mechanical properties for bone tissue regeneration', *Journal of Materials Chemistry B*, 3(16), pp. 3222–3233.

Zheng, R. *et al.* (2014) 'The influence of Gelatin/PCL ratio and 3-D construct shape of electrospun membranes on cartilage regeneration', *Biomaterials*, 35(1), pp. 152–164.

Zhou, X. *et al.* (2013) 'Noninvasive real-time monitoring by AlamarBlue® during in vitro culture of three-dimensional tissue-engineered bone constructs', *Tissue Engineering Part C: Methods*, 19(9), pp. 720–729.

Zhu, J. (2010) 'Bioactive modification of poly (ethylene glycol) hydrogels for tissue engineering', *Biomaterials*, 31(17), pp. 4639–4656.

Zhu, J. *et al.* (2012) 'Elastic chitosan conduits with multiple channels and well defined microstructure', *International journal of biological macromolecules*, 51(1–2), pp. 105–112.

Zou, H. *et al.* (2009) 'Thermal degradation of poly (lactic acid) measured by thermogravimetry coupled to Fourier transform infrared spectroscopy', *Journal of thermal analysis and calorimetry*, 97(3), pp. 929–935.

Zupancic, S. *et al.* (2015) 'Contribution of nanotechnology to improved treatment of periodontal disease', *Current pharmaceutical design*, 21(22), pp. 3257–3271.

Zussman, E., Yarin, A. and Weihs, D. (2002) 'A micro-aerodynamic decelerator based on permeable surfaces of nanofiber mats', *Experiments in Fluids*, 33(2), pp. 315–320.

Zwahlen, R.A. *et al.* (2009) 'Comparison of two resorbable membrane systems in bone regeneration after removal of wisdom teeth: a randomized-controlled clinical pilot study', *Clinical Oral Implants Research*, 20(10), pp. 1084–1091.

Appendix

Statistical analysis for chapter 4 – section (4.1.12)

Table 0-1 Statistical analysis of the weight loss of fibrous membranes immersed in SBF, comparing Floreon at concentrations of 5, 10, and 20% with those of PLA at different time points. ns = non-significant, * = $p < 0.05$, ** = $p < 0.01$, *** = $p < 0.001$.

week	Floreon vs PLA	Flo/HA (10 wt%) vs PLA /HA (10 wt%)	Flo/CaSiO$_3$ (10 wt%) vs PLA / CaSiO$_3$ (10 wt%)
2	ns	ns	ns
4	ns	ns	ns
6	ns	ns	ns
8	ns	ns	ns
16	ns	ns	ns
24	ns	ns	ns
week	Floreon vs Flo/HA (5wt%)	Floreon vs Flo/HA (10 wt%)	Floreon vs Flo/HA (20 wt%)
2	ns	ns	**
4	ns	ns	***
6	ns	ns	***
8	ns	***	***
16	ns	***	***
24	***	***	***
week	Flo/HA (5wt%) vs Flo/HA (10 wt%)	Flo/HA (10 wt%) vs Flo/HA (20 wt%)	Flo/HA (5 wt%) vs Flo/HA (20 wt%)
2	ns	ns	ns
4	ns	ns	ns
6	ns	***	***
8	***	ns	***
16	***	***	***
24	***	***	***
week	Floreon vs Flo/ CaSiO$_3$ (5wt%)	Floreon vs Flo/ CaSiO$_3$ (10 wt%)	Floreon vs Flo/ CaSiO$_3$ (20 wt%)
2	ns	ns	ns
4	ns	ns	***
6	ns	***	***
8	ns	***	***
16	ns	***	***
24	ns	***	***
week	Flo/CaSiO$_3$ (5wt%) vs Flo/ CaSiO$_3$ (10 wt%)	Flo/ CaSiO$_3$ (10 wt%) vs Flo/ CaSiO$_3$ (20 wt%)	Flo/ CaSiO$_3$ (5 wt%) vs Flo/ CaSiO$_3$ (20 wt%)
2	ns	ns	ns
4	ns	ns	***
6	ns	ns	***
8	***	ns	***
16	***	***	***
24	***	ns	***

Table 0-2 Statistical analysis of the water absorption of fibrous membranes immersed in SBF, comparing Floreon at concentrations of 5, 10, and 20% with those of PLA at different time points. ns = non-significant, * = p < 0.05, ** = p < 0.01, *** = p< 0.001.

week	Floreon vs PLA	Flo/HA (10 wt%) vs PLA /HA (10 wt%)	Flo/CaSiO$_3$ (10 wt%) vs PLA / CaSiO$_3$ (10 wt%)
2	ns	ns	ns
4	ns	ns	ns
6	ns	ns	ns
8	ns	ns	ns
16	ns	ns	ns
24	ns	ns	**
week	Floreon vs Flo/HA (5wt%)	Floreon vs Flo/HA (10 wt%)	Floreon vs Flo/HA (20 wt%)
2	ns	*	***
4	ns	ns	***
6	ns	*	***
8	*	***	***
16	**	***	***
24	***	***	***
week	Flo/HA (5wt%) vs Flo/HA (10 wt%)	Flo/HA (10 wt%) vs Flo/HA (20 wt%)	Flo/HA (5 wt%) vs Flo/HA (20 wt%)
2	ns	***	***
4	ns	***	***
6	ns	***	***
8	ns	***	***
16	***	***	***
24	***	***	***
week	Floreon vs Flo/ CaSiO$_3$ (5wt%)	Floreon vs Flo/ CaSiO$_3$ (10 wt%)	Floreon vs Flo/ CaSiO$_3$ (20 wt%)
2	ns	***	***
4	ns	**	***
6	ns	***	***
8	ns	***	***
16	**	***	***
24	***	***	***
week	Flo/CaSiO$_3$ (5wt%) vs Flo/ CaSiO$_3$ (10 wt%)	Flo/ CaSiO$_3$ (10 wt%) vs Flo/ CaSiO$_3$ (20 wt%)	Flo/ CaSiO$_3$ (5 wt%) vs Flo/ CaSiO$_3$ (20 wt%)
2	ns	ns	***
4	ns	ns	***
6	***	ns	***
8	***	ns	***
16	***	***	***
24	***	***	***

Table 0-3 Statistical analysis of the pH changes of SBF-containing fibrous membranes, comparing Floreon at concentrations of 5, 10, and 20% with those of PLA at different time points. ns = non-significant, * = p < 0.05, ** = p < 0.01, *** = p< 0.001.

week	Floreon vs PLA	Flo/HA (10 wt%) vs PLA /HA (10 wt%)	Flo/CaSiO$_3$ (10 wt%) vs PLA / CaSiO$_3$ (10 wt%)
2	ns	ns	ns
4	ns	ns	ns
6	ns	ns	ns
8	ns	ns	ns
16	ns	ns	ns
24	ns	ns	ns
week	Floreon vs Flo/HA (5wt%)	Floreon vs Flo/HA (10 wt%)	Floreon vs Flo/HA (20 wt%)
2	ns	ns	*
4	***	***	***
6	***	***	***
8	ns	***	***
16	ns	***	***
24	***	***	***
week	Flo/HA (5wt%) vs Flo/HA (10 wt%)	Flo/HA (10 wt%) vs Flo/HA (20 wt%)	Flo/HA (5 wt%) vs Flo/HA (20 wt%)
2	ns	ns	ns
4	***	***	***
6	***	***	***
8	***	***	***
16	***	***	***
24	***	***	***
week	Floreon vs Flo/ CaSiO$_3$ (5wt%)	Floreon vs Flo/ CaSiO$_3$ (10 wt%)	Floreon vs Flo/ CaSiO$_3$ (20 wt%)
2	ns	ns	ns
4	ns	***	***
6	ns	***	***
8	ns	***	***
16	ns	***	***
24	ns	***	***
week	Flo/CaSiO$_3$ (5wt%) vs Flo/ CaSiO$_3$ (10 wt%)	Flo/ CaSiO$_3$ (10 wt%) vs Flo/ CaSiO$_3$ (20 wt%)	Flo/ CaSiO$_3$ (5 wt%) vs Flo/ CaSiO$_3$ (20 wt%)
2	ns	ns	ns
4	**	ns	***
6	***	ns	***
8	***	*	***
16	***	***	***
24	***	***	***

Statistical analysis for chapter 4 – section (4.2.11)

Table 0-4 Statistical analysis of the weight loss of smooth membranes immersed in SBF, comparing Floreon to that of PLA at different time points. ns = non-significant, * = p < 0.05, ** = p < 0.01, *** = p< 0.001.

week	Cast Floreon membrane vs Cast PLA membrane	Spin-coated Floreon membrane vs Spin-coated PLA membrane	Cast Floreon membrane vs Spin-coated Floreon membrane	Cast PLA membrane vs Spin-coated PLA membrane
2	ns	ns	ns	ns
4	ns	ns	ns	ns
6	ns	ns	ns	ns
8	*	ns	ns	ns
16	***	*	**	ns
24	***	**	ns	ns

Table 0-5 Statistical analysis of the water absorption of smooth membranes immersed in SBF, comparing Floreon to that of PLA at different time points. ns = non-significant, * = p < 0.05, ** = p < 0.01, *** = p< 0.001.

week	Cast Floreon membrane vs Cast PLA membrane	Spin-coated Floreon membrane vs Spin-coated PLA membrane	Cast Floreon membrane vs Spin-coated Floreon membrane	Cast PLA membrane vs Spin-coated PLA membrane
2	ns	ns	ns	ns
4	ns	ns	ns	ns
6	ns	***	ns	ns
8	ns	**	ns	ns
16	***	***	ns	ns
24	***	***	ns	ns

Table 0-6 Statistical analysis of the pH changes of SBF-containing smooth membranes, comparing Floreon to that of PLA for different time points. ns = non-significant, * = $p < 0.05$, ** = $p < 0.01$, *** = $p < 0.001$.

week	Cast Floreon membrane vs Cast PLA membrane	Spin-coated Floreon membrane vs Spin-coated PLA membrane	Cast Floreon membrane vs Spin-coated Floreon membrane	Cast PLA membrane vs Spin-coated PLA membrane
2	ns	ns	ns	ns
4	ns	ns	ns	ns
6	***	**	ns	ns
8	ns	**	*	ns
16	*	***	ns	ns
24	ns	***	ns	ns

49 Spadina Ave. Suite 200
Toronto ON M5V 2J1 Canada
www.biorender.com

Confirmation of Publication and Licensing Rights
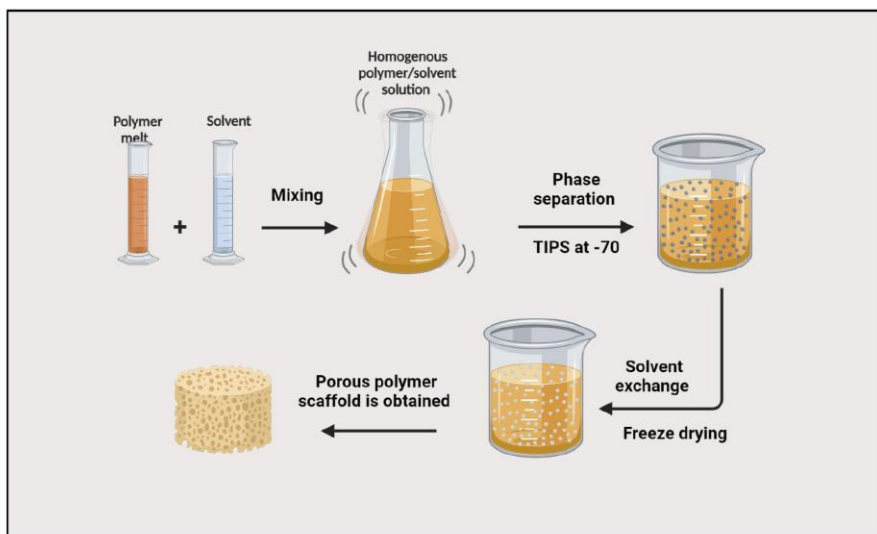
December 18th, 2022
Science Suite Inc.

Subscription: *Student Plan*
Agreement number: *TM24S6TRPQ*
Journal name: *The University of Sheffield*

To whom this may concern,

This document is to confirm that ALI ALQAHTANI has been granted a license to use the BioRender content, including icons, templates and other original artwork, appearing in the attached completed graphic pursuant to BioRender's Academic License Terms. This license permits BioRender content to be sublicensed for use in journal publications.

All rights and ownership of BioRender content are reserved by BioRender. All completed graphics must be accompanied by the following citation: "Created with BioRender.com".

BioRender content included in the completed graphic is not licensed for any commercial uses beyond publication in a journal. For any commercial use of this figure, users may, if allowed, recreate it in BioRender under an Industry BioRender Plan.

For any questions regarding this document, or other questions about publishing with BioRender refer to our BioRender Publication Guide, or contact BioRender Support at support@biorender.com.

Confirmation of Publication and Licensing Rights

December 18th, 2022
Science Suite Inc.

Subscription:	*Student Plan*
Agreement number:	*VJ24S6TZKK*
Journal name:	*The University of Sheffield*

To whom this may concern,

This document is to confirm that ALI ALQAHTANI has been granted a license to use the BioRender content, including icons, templates and other original artwork, appearing in the attached completed graphic pursuant to BioRender's Academic License Terms. This license permits BioRender content to be sublicensed for use in journal publications.

All rights and ownership of BioRender content are reserved by BioRender. All completed graphics must be accompanied by the following citation: "Created with BioRender.com".

BioRender content included in the completed graphic is not licensed for any commercial uses beyond publication in a journal. For any commercial use of this figure, users may, if allowed, recreate it in BioRender under an Industry BioRender Plan.

For any questions regarding this document, or other questions about publishing with BioRender refer to our BioRender Publication Guide, or contact BioRender Support at support@biorender.com.

49 Spadina Ave. Suite 200
Toronto ON M5V 2J1 Canada
www.biorender.com

Confirmation of Publication and Licensing Rights
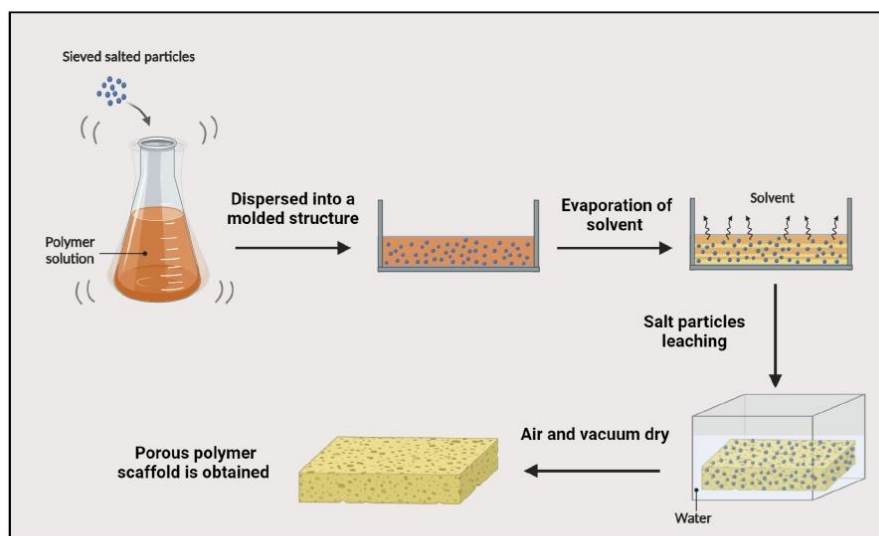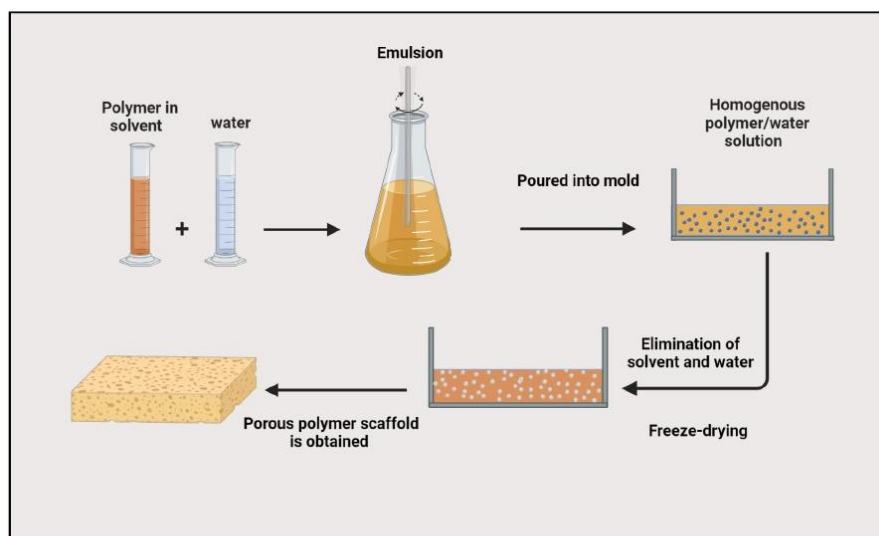
December 18th, 2022
Science Suite Inc.

Subscription: *Student Plan*
Agreement number: *SB24S6WURD*
Journal name: *The University of Sheffield*

To whom this may concern,

This document is to confirm that ALI ALQAHTANI has been granted a license to use the BioRender content, including icons, templates and other original artwork, appearing in the attached completed graphic pursuant to BioRender's Academic License Terms. This license permits BioRender content to be sublicensed for use in journal publications.

All rights and ownership of BioRender content are reserved by BioRender. All completed graphics must be accompanied by the following citation: "Created with BioRender.com".

BioRender content included in the completed graphic is not licensed for any commercial uses beyond publication in a journal. For any commercial use of this figure, users may, if allowed, recreate it in BioRender under an Industry BioRender Plan.

For any questions regarding this document, or other questions about publishing with BioRender refer to our BioRender Publication Guide, or contact BioRender Support at support@biorender.com.

49 Spadina Ave. Suite 200
Toronto ON M5V 2J1 Canada
www.biorender.com

Confirmation of Publication and Licensing Rights
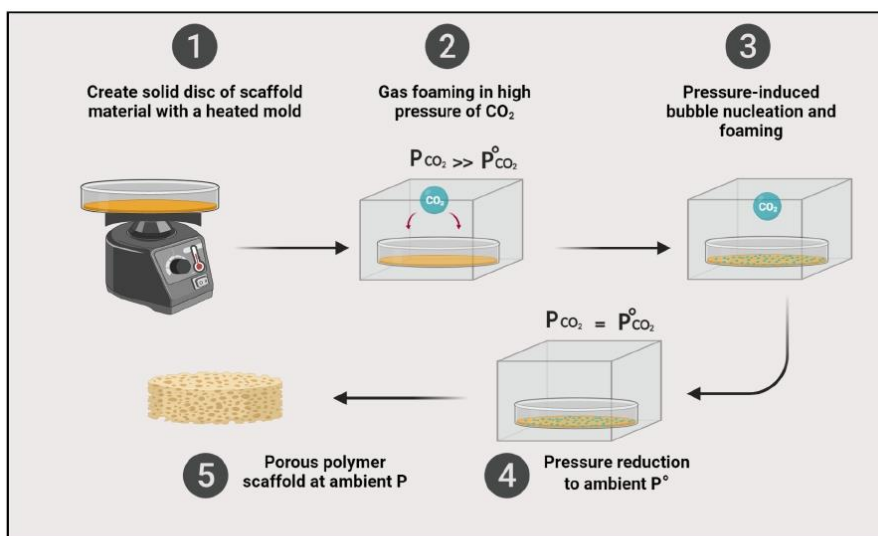
December 18th, 2022
Science Suite Inc.

Subscription: *Student Plan*
Agreement number: *RF24S6U3L3*
Journal name: *The University of Sheffield*

To whom this may concern,

This document is to confirm that ALI ALQAHTANI has been granted a license to use the BioRender content, including icons, templates and other original artwork, appearing in the attached completed graphic pursuant to BioRender's Academic License Terms. This license permits BioRender content to be sublicensed for use in journal publications.

All rights and ownership of BioRender content are reserved by BioRender. All completed graphics must be accompanied by the following citation: "Created with BioRender.com".

BioRender content included in the completed graphic is not licensed for any commercial uses beyond publication in a journal. For any commercial use of this figure, users may, if allowed, recreate it in BioRender under an Industry BioRender Plan.

For any questions regarding this document, or other questions about publishing with BioRender refer to our BioRender Publication Guide, or contact BioRender Support at support@biorender.com.

49 Spadina Ave. Suite 200
Toronto ON M5V 2J1 Canada
www.biorender.com

bio
RENDER

Confirmation of Publication and Licensing Rights

December 18th, 2022
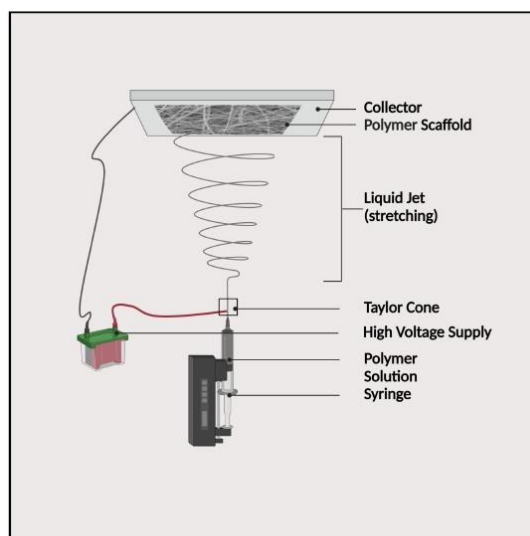**Science Suite Inc.**

Subscription: *Student Plan*
Agreement number: *CG24S6W0BX*
Journal name: *The University of Sheffield*

To whom this may concern,

This document is to confirm that ALI ALQAHTANI has been granted a license to use the BioRender content, including icons, templates and other original artwork, appearing in the attached completed graphic pursuant to BioRender's Academic License Terms. This license permits BioRender content to be sublicensed for use in journal publications.

All rights and ownership of BioRender content are reserved by BioRender. All completed graphics must be accompanied by the following citation: "Created with BioRender.com".

BioRender content included in the completed graphic is not licensed for any commercial uses beyond publication in a journal. For any commercial use of this figure, users may, if allowed, recreate it in BioRender under an Industry BioRender Plan.

For any questions regarding this document, or other questions about publishing with BioRender refer to our BioRender Publication Guide, or contact BioRender Support at support@biorender.com.

bio
RENDER

Confirmation of Publication and Licensing Rights

December 18th, 2022
Science Suite Inc.

Subscription: *Student Plan*
Agreement number: *ES24S6TV6V*
Journal name: *The University of Sheffield*

To whom this may concern,

This document is to confirm that ALI ALQAHTANI has been granted a license to use the BioRender content, including icons, templates and other original artwork, appearing in the attached completed graphic pursuant to BioRender's Academic License Terms. This license permits BioRender content to be sublicensed for use in journal publications.

All rights and ownership of BioRender content are reserved by BioRender. All completed graphics must be accompanied by the following citation: "Created with BioRender.com".

BioRender content included in the completed graphic is not licensed for any commercial uses beyond publication in a journal. For any commercial use of this figure, users may, if allowed, recreate it in BioRender under an Industry BioRender Plan.

For any questions regarding this document, or other questions about publishing with BioRender refer to our BioRender Publication Guide, or contact BioRender Support at support@biorender.com.

49 Spadina Ave. Suite 200
Toronto ON M5V 2J1 Canada
www.biorender.com

Confirmation of Publication and Licensing Rights

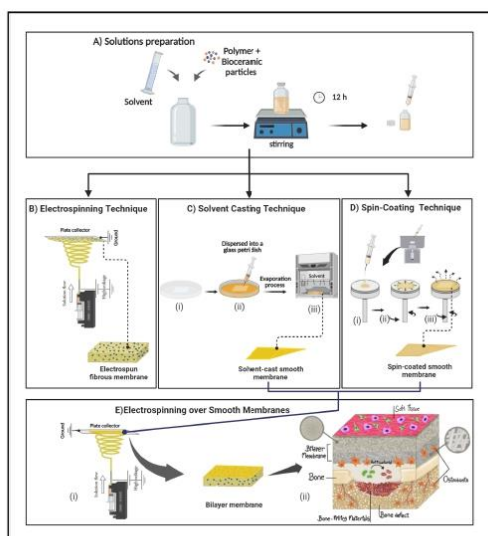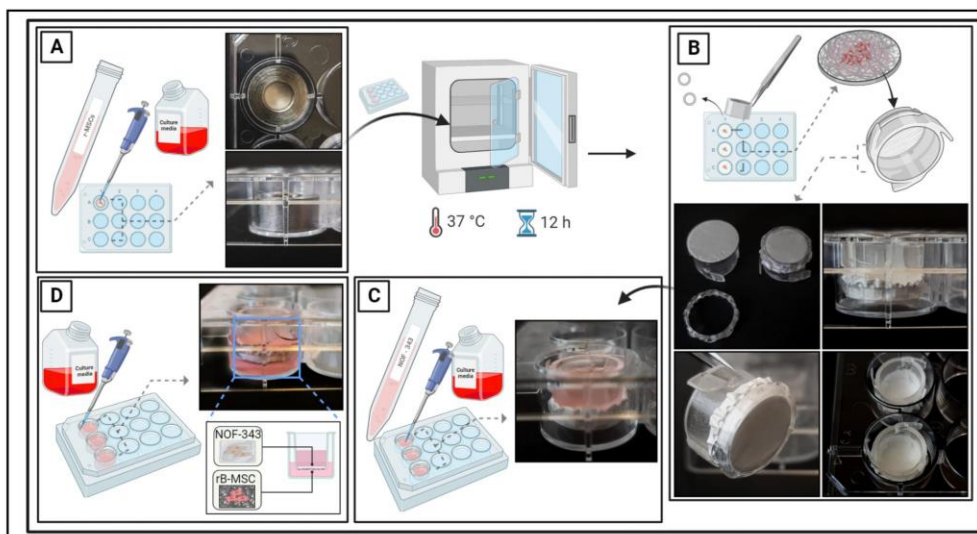**December 18th, 2022**
Science Suite Inc.

Subscription:	*Student Plan*
Agreement number:	*FT24S6TJEO*
Journal name:	*The University of Sheffield*

To whom this may concern,

This document is to confirm that ALI ALQAHTANI has been granted a license to use the BioRender content, including icons, templates and other original artwork, appearing in the attached completed graphic pursuant to BioRender's Academic License Terms. This license permits BioRender content to be sublicensed for use in journal publications.

All rights and ownership of BioRender content are reserved by BioRender. All completed graphics must be accompanied by the following citation: "Created with BioRender.com".

BioRender content included in the completed graphic is not licensed for any commercial uses beyond publication in a journal. For any commercial use of this figure, users may, if allowed, recreate it in BioRender under an Industry BioRender Plan.

For any questions regarding this document, or other questions about publishing with BioRender refer to our BioRender Publication Guide, or contact BioRender Support at support@biorender.com.